ENERGY- AND RESOURCE-SAVING TECHNOLOGIES OF DEVELOPING THE RAW-MATERIAL BASE OF MINING REGIONS

MULTI-AUTHORED MONOGRAPH

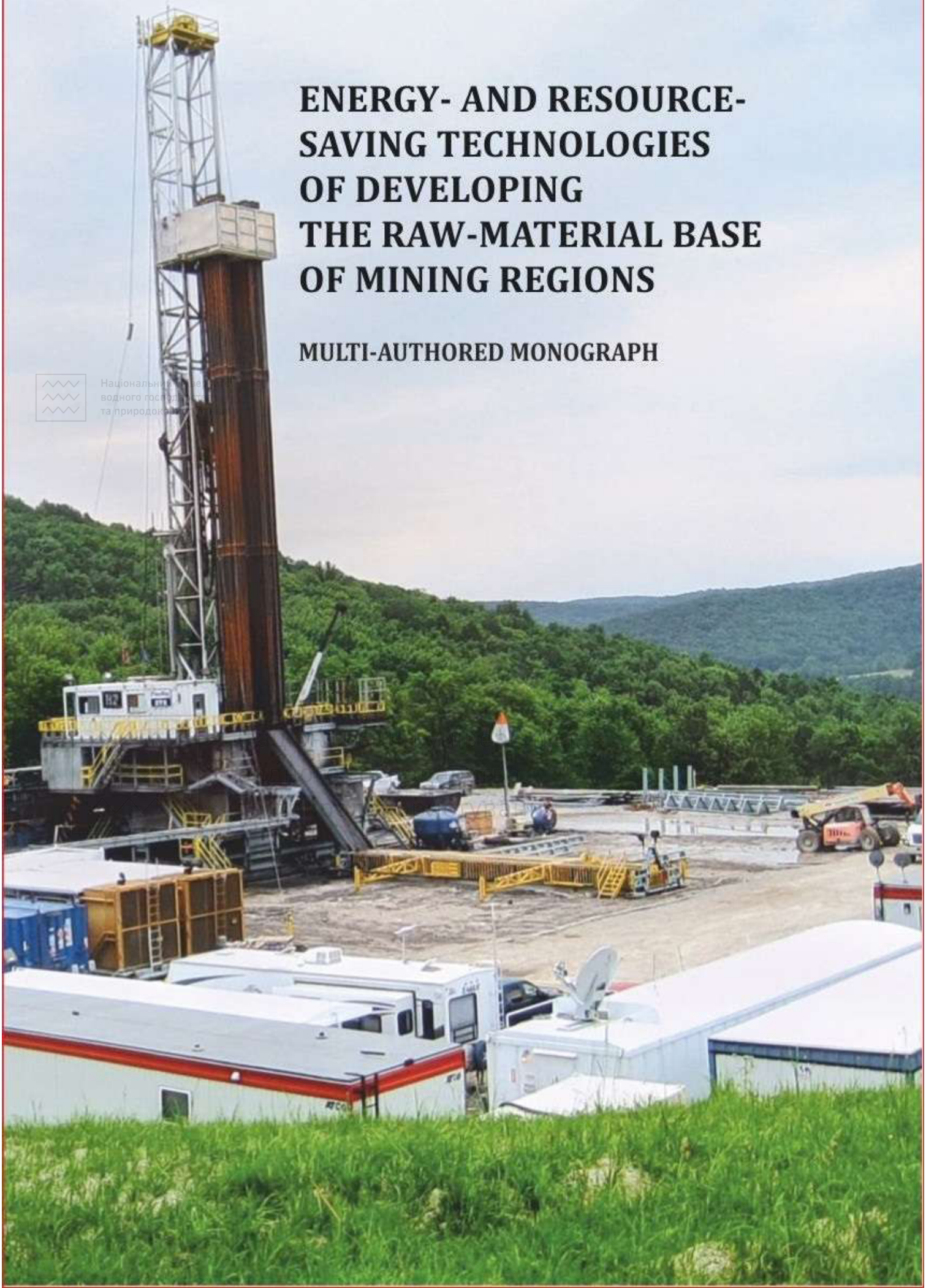

ENERGY- AND RESOURCE-SAVING TECHNOLOGIES OF DEVELOPING THE RAW-MATERIAL BASE OF MINING REGIONS

Multi-authored monograph

UNIVERSITAS Publishing
Petroșani, 2021

UDC 622.002 https://doi.org/10.31713/m1001

Recommended for publication by Board of Directors of the University of Petrosani, Minutes № 2163 as of March 25, 2021

Reviewers: ***Mihaela TODERAS***, Professor, Ph.D.Habil.Eng., Vice-Dean Faculty of Mines University of Petroșani, Romania

Khavalbolot KELGENBAI, Professor, Head of Department of Mineral Processing and Engineering of School of Geology and Mining at Mongolian University of Science and Technology, Mongolia

Dimitar ANASTASOV**,** Professor, Phd.Eng. Department of Mining of Mineral Deposits, University of Mining and Geology "St. Ivan Rilski", Bulgaria

Energy- and resource-saving technologies of developing the raw-material base of mining regions. Multi-authored monograph. – Petroșani, Romania: UNIVERSITAS Publishing, 2021. - 505 p.

ISBN 978-973-741-733-6

The monograph considers potential technological development of ore mining and processing industries through updating mining machines and technologies

The book is intended for a broad mining audience of scholars, practitioners, postgraduates and students.

UDC 622.002

PREFACE

We are glad to present the multi-authored monograph “Energy- and resource-saving technologies of developing the raw-material base of mining regions”

Present-day conditions require creating a scientific and methodological base for sustainable use of natural resources. The given monograph is aimed at dealing with these problems.

There are presented results of researches into various aspects of developing the mineral material complex.

The complete cycle of operations aimed at introducing energy- and resource-saving technologies from geological analysis of mineral resources to their processing and metal-roll production is under consideration.

Much attention is paid to implementation of technologies followed up by reclamation of disturbed lands and water balance in mining regions.

The multi-authored monograph is of great interest to mining scholars and young people mastering mining specialities at university.

The monograph editors appreciate the authors’ contribution to the given edition.

Co-editors,

Zinovii MALANCHUK - Doctor of Sciences (Engineering), Professor, Director Institute of Postgraduate Education, National University of Water and Environmental Engineering, Ukraine.

Maria LAZAR - Professor, Ph.D., Research Vice-Rector University of Petroșani, Romania.

Table of contents

https://doi.org/10.31713/m1002

INFORMATION TECHNOLOGIES IN HYDROMECHANICAL METHOD OF AMBER MINING

Malanchuk Z.R.
National University of Water and Environmental Engineering (NUWEE), Professor, Doctor of Technical Sciences, Professor, Department of Development of Deposits and Mining, Ukraine

Nadutyi V.P.
Institute of Geotechnical Mechanics named after M.S. Polyakova (IGM), Professor, Doctor of Technical Sciences, Professor, Department of mechanics of machines and processes of mineral processing, Ukraine

Korniyenko V.Ya.
National University of Water and Environmental Engineering (NUWEE), Professor, Doctor of Technical Sciences, Professor, Department of Development of Deposits and Mining, Ukraine

Malanchuk Ye.Z
National University of Water and Environmental Engineering (NUWEE), Professor, Doctor of Technical Sciences, Professor, Department of Automation and Computer Integrated Systems, Ukraine

Khrystyuk A.O.
National University of Water and Environmental Engineering (NUWEE), Ph.D., Associate Professor, Department of Automation and Computer Integrated Systems, Ukraine

Abstract

The analysis results of possibilities of use of modern information technologies at control of process of extraction of amber from sand deposits are resulted. The expediency and efficiency of using artificial neural networks in the control of hydromechanical extraction of amber from sand deposits is shown. The structure of

an artificial neural network which considers features of hydromechanical extraction of amber is offered.

Introduction

The object of research is the process of controlling the extraction of amber in the hydromechanical method of extraction from sand deposits.

Existing methods and technical means of implementing the management of the process of hydromechanical amber mining do not fully meet the requirements, namely, the existing control systems of mining facilities are reduced to ensuring the sustainability of certain parameters of the process. It is proved that the efficiency of hydromechanical mining plants, energy consumption, water, air consumption, as well as the amount of extracted useful component, directly depend on the duration of hydromechanical impact on the sand massif, ie the speed at which amber particles float to the surface. depends on a number of factors and technological parameters.

Today, amber mining requires the latest technologies and improvements in technical and technological means to intensify the mining process, which achieves higher productivity and efficiency, as well as reducing the negative environmental impact of the environment. The most effective is the introduction of modern automation tools in the process of amber mining, and in particular modern intelligent control methods that do not require significant modernization of existing technologies, but ensure the most efficient use of existing technological equipment, and have the prospect of improvement by ensuring high selection of optimal ratios of water and air consumption, and oscillation frequency of the working body.

1. Analysis of the process of hydromechanical amber extraction

The northern districts of Rivne region are characterized mainly by the occurrence of amber in sandy soils, which are characterized by the presence between the skeleton of the soil pores of water and air between them. Sandy soil becomes mobile when the balance between the soil skeleton and water pores is disturbed, and a slight influence of hydraulic flows can lead to the displacement of the massif and the transition of large masses of soil to a liquefied state. The transition of

water-saturated sands to the liquefied state causes the destruction of the structure of the sands and their compaction under the action of its own weight or external influences. When the sand is liquefied, the bearing capacity is lost completely or partially and the fluid state arises as a result of the destruction of the structure and displacement of the sand particles relative to each other, accompanied by the formation of a denser particle placement and reduced porosity. [1-4].

The phenomenon of liquefaction occurs when the destruction of the structure and the possibility of compaction of sand; full, or close to full, saturation of sand with water.

When conducting research amber sand deposit at the initial stage goes into a state of rarefaction, and then it is compacted. The duration of water-saturated sands in a rarefied state is much shorter than the time of soil compaction. In our opinion, and based on the analysis of literature sources, the compaction process is more studied than the liquefaction process, so experimental studies of the liquefaction process, the process of amber surface and the time of transition of sandy soil to compacted state require additional research. To create the necessary conditions for the surface of amber to investigate the parameters of vibration and the use of water and air when exposed to sand.

It is known from studies [5-8] that the movement of sand in the vibrating fluidized bed is not subject to the law of motion of particles in airless space. In addition to the force of gravity, the trajectory of the sand layer is significantly influenced by the parameters of the environment. When tossing, a vacuum is formed, when falling - an increase in medium pressure. The lower layers of sandy soil have a larger pressure drop than the upper ones, therefore, the air is displaced from below and compaction is carried out between the particles.

Thus, the vibrating fluidized bed of sandy soil behaves like a pump that pumps the gas-liquid mixture to the surface, capturing the particles of amber and transporting them to the top. The rate of particle rise from the bottom to the top depends on the vibrational excitation of the array, the vacuum of the medium, the saturation of air bubbles and the viscosity of the medium.

The pressure drop depends on the frequency and amplitude of the oscillator, the height of the layer, the particle size and humidity of

the sandy soil, as well as the coefficient of friction of the particles against each other. The intensity of the pumping action of the vibrating fluidized bed is characterized by three parameters: the pressure above and the vacuum under the vibrating fluidized bed, the pressure drop in the layer.

The creation of the vibro-boiling layer of the soil is influenced by the following parameters: 1) the amplitude of oscillations; 2) frequency of oscillations; 3) coercive force; 4) water pressure; 5) air pressure; 6) geometric location of oscillators.

The method of hydromechanical amber mining is implemented with the minimum amount of reclamation work required for overburden work, transportation costs, with a small amount of water supplied to the array under a pressure of 0.1-0.2 MPa. This confirms the high energy and economic efficiency of the method.

Experiments have shown that the amount of water is determined by the porosity of the soil in the treated area. When implementing the method of water filtration gradient outside the treated array can be neglected, because the process is transient.

The supply of air to the sand massif intensifies the process of amber rising. An increase in air flow above the rational leads to a decrease in the rate of ascent and the formation of channels through which air freely reaches the surface of the field and there is no vibration of the whole array.

When comparing the operation of the installation in different operating modes, the minimum density of 1600 kg/m^3 of sandy environment, which creates a vibrating agent, are observed with simultaneous water and air supply and water supply without air supply at a vibration frequency of 26-36 Hz.

During the operation of the installation, a certain working zone of the suspended soil and its boiling with the removal of solid pieces of amber in the surface layers of the soil mass was observed.

The rate of exit to the surface of amber depended on the intensity of the process, namely the action of oscillations of the working body, the supply of gas-air mixture and the physic-chemical properties of the soil.

The following was observed during experimental studies:

- the rate of amber float depends on the oscillation frequency of the working body, the amplitude and density of the medium and has its extremum;

- the density of the medium significantly affects the creation of conditions for rapid emergence of amber, which affects the productivity of the hydromechanical method of amber mining;

- there are values of parameters of oscillations and supply of air and water at which the suspended environment is not created, and there is no rise of amber on a field surface.

Intensify the process of amber mining is possible with the use of oscillations, supply to the soil mass of water, or water and air.

Creating the desired density of the medium depends on the supply of gas-liquid mixture, oscillation frequency and geometric parameters of the working body and its weight. The water supply affects the duration of the vacuum.

2. Main parameters of control systems

Synthesis of modern mining management systems requires the establishment of structural relationships between input and output parameters of the object, the correct choice of controlled parameters and control effects. Analyzing the results of research, we found that the main regulatory parameters in hydromechanical amber mining are water and air consumption, frequency and amplitude of oscillations of the working body, adjustable - the density of amber-containing medium and the rate of amber ascent. The main disturbing factor influencing the regulating and regulated parameters is the physical and geological properties of the formation. Based on this, we have developed and tested at the field a structural diagram of the relationship between the parameters of hydromechanical amber mining (fig. 1).

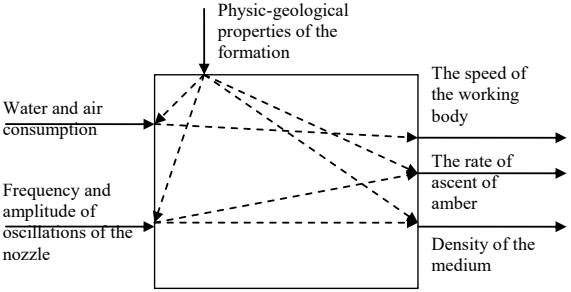

Fig. 1. Block diagram of hydromechanical amber mining management links

Coordination of the hydromechanical complex of amber mining is provided by the dispatching service, which is responsible for the tasks of direct production management: centralized management of individual production sites and facilities; control of technological process of extraction and transportation of amber, and also a condition of separate responsible knots, regulation (if necessary) of processes by remote change of installations of the regulators carrying out stabilization of giving of working agents: the centralized account of quantity of the received product, material and power expenses, etc.. It is most expedient to apply a one-stage structure of operative management of a complex at which management and control of all process is carried out from the uniform central dispatching point where the control and measuring equipment is established. The central control room receives all the necessary information about the flow of technological processes at different production sites.

When carrying out the main technological process (actual extraction) the stabilization of parameters of working agents should be provided. For this purpose, control valves and diaphragms are installed on the pipelines.

3. Hydromechanical amber mining control system based on fuzzy logic

The problem of ensuring the maximum extraction of amber is solved by adjusting the parameters of the hydromechanical extraction. Based on the conditions of resource conservation and efficient extraction of minerals necessary time (over time) coordination of the required frequency of oscillation of the working body and the supply of water and air.

Significant uneven distribution of mineral deposits and differences in deposits and unpredictability of deposit conditions virtually preclude the use of traditional methods of regulating the parameters of the mining plant to ensure efficient amber mining.

One of the effective ways to solve problems of object management with nonlinear multiparameter characteristics in conditions of complete or partial uncertainty is the use of fuzzy logic with neural network adaptation.

Fuzzy neural networks combine the advantages of neural networks and fuzzy output systems. Structurally, these are two separate mathematical devices.

Traditional formal-logical systems do not fully describe the nature of human reasoning and the course of thought as opposed to fuzzy logic, which makes it more natural.

Fuzzy control is a procedure or algorithm for obtaining fuzzy conclusions based on fuzzy conditions using the concepts of fuzzy logic.

When forming a control system based on fuzzy logic, we proceed primarily from the fact that the state of a complex dynamic system and the control effect of SAC are considered as linguistic variables that are evaluated by qualitative terms (means of natural language). Each term is considered as a fuzzy set and is formalized using the membership function.

The formation of the control effect is carried out on the basis of a set of rules that establish the relationship between the state of the dynamic system and the control effect in the automatic control system. Determination of the control effect is carried out by implementing the procedure of transition from the membership function to a specific numerical value, which is transmitted to the actuator.

The algorithm of operation of the control system based on fuzzy logic is shown in Fig. 2. The main stages can be implemented in different ways.

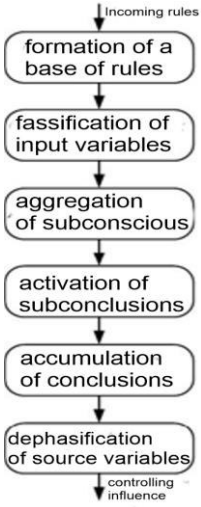

Fig. 2. General algorithm of fuzzy control system operation

Artificial neural networks are a set of models of biological neural networks, which are a network of elements - artificial neurons - interconnected by synaptic connections.

The basic element of neural networks, an artificial neuron (Fig. 3) has a group of synapses - unidirectional input connections connected to the outputs of other neurons, as well as an axon - the output channel through which the signal (excitation or inhibition) enters the synapses of subsequent neurons.

Each input is multiplied by a corresponding weight (weight) similar to the synaptic force, and all products are summed to determine the level of activation.

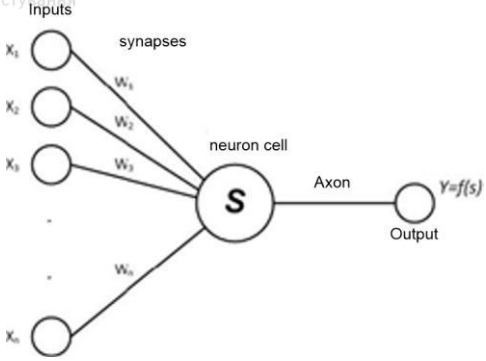

Fig. 3. Artificial neuron: $X_1,X_2,\ldots,X_n$ - inputs; $W_1,W_2,\ldots,Wn$ - synaptic scales; S - algebraic adder of weighted inputs; Y - output; $f(s)$ – nonlinear activation function

As an activation function, it is advisable to use a nonlinear activation function of S - similar type with saturation (sigmoid or logical function with saturation).

The neuron implements the scalar function of the vector argument. His mathematical model

$$S = \sum_{i=1}^{n} W_i X_i + b$$

where W_i - synapse weight (when i=1,2,…,n); b - offset value; S - the result of summation; X_i - component of the input vector (input signal) (when i=1,2,…,n); n - the number of neuron inputs.

The process of neural network functioning depends on the magnitude of synaptic weights. For a certain network structure (depending on the task), it is necessary to find the optimal value of all variable weights - this stage is called neural network training: the quality of the neural network to solve the tasks set before it depends on how well it is carried out.

As a result, the neural network generates an output signal (Y) in accordance with the input signal (X), implementing some function: $Y=g(X)$. If the network architecture is specified, the type of functional dependence is determined by the values of synaptic weights and network offsets.

There are many automatic control systems with fuzzy and neural network regulators, which significantly outperform traditional analogues when working with nonlinear and non-stationary objects

(processes), which include the process of hydromechanical extraction of amber.

The advantages of developments using fuzzy logic and neural networks are:

- work in conditions of uncertainty about the nature of the input signals;
- reliable operation with a large number of input variables compared to traditional systems.

Disadvantages of using neural networks:

- long training time;
- the complexity of the analysis of the structure of the "trained" network, respectively, the impossibility of its optimization;
- the impossibility of entering apriority (expert) information to accelerate network learning.

Disadvantages of systems using fuzzy logic:

- the impossibility of automatic acquisition of knowledge in the process of functioning;
- the need to split universal sets into separate domains creates a maximum number of input parameters.

To increase the productivity of control systems and managed objects (processes), it is necessary to eliminate these shortcomings. This can be achieved by creating hybrid neural networks, where conclusions are made on the basis of fuzzy logic, and the corresponding membership functions are adjusted using a neural network learning algorithm. Developed systems can not only use a priori information, but also receive new knowledge in the process of functioning [9-13].

That is, a fuzzy neural network is a neural network with clear signals, weights, and an activation function, but t-norms or other continuous operations are used to combine them.

To develop a system of operation of the installation for hydromechanical extraction of amber should use a static model, which can be obtained by numerical factorial experiment based on the regressive static characteristics of the object. That is, the functional dependence of the yield of amber on the perturbing action: the properties of the formation, the conditions of extraction under the action of the control factor and regulatory actions.

To study the control system of the amber mining plant on the basis of a neural network, three blocks of experimentally obtained data sets were used Training data, Testing data and Checking data. Using these data sets, the controller in the process of operation is adjusted to the variable parameters of the field and the operating conditions of the installation.

Conclusions

Thus, the analysis of technological parameters of amber extraction from sand deposits by hydromechanical method is carried out, which will ensure the minimum duration of impact on the array and reduce energy consumption and water consumption of extraction technology. The modern control system of the amber mining plant on the basis of fuzzy logic is considered.

In conducting the analysis, we took into account all the parameters of the amber mining plant, in particular the vibration frequency of the working body, water and air flow in the developed array. Ensuring the optimal ratio of these parameters by using a controller based on fuzzy logic will minimize energy consumption for the production process with the most efficient process.

Bibliography

1. **Malanchuk Z., Malanchuk E., Khrystyuk A**. Mathematical modeling of hydraulic mining from placer deposits of minerals / Mining of Mineral Deposits. National mining university, 2016. № 10. pp. 18–24. DOI: http://dx.doi.org/10.15407/mining10.02.013

2. **Malanchuk Z., Malanchuk E., Khrystyuk A**. Results of experimental studies of amber extraction by hydromechanical method in Ukraine / Eastern-European Journal of Enterprise Technologies, – 2016. Vol 3, №10(81). pp. 24–28. DOI: 10.15587/1729-4061.2016.72404

3. **Malanchuk Z.** Modeling the formation of high metal concentration zones in man-made deposits /**Malanchuk Z., Korniienko V., Malanchuk Ye., Soroka V., Vasylchuk O**. Mining of mineral deposits. ISSN 2415-3435, 2018, pp. 76-84 DOI: 10.15407/mining12.02.076.

4. **Malanchuk Z.** Results of experimental studies of amber extraction by hydromechanical method in Ukraine / [Z**. Malanchuk, V Korniyenko, Y. Malanchuk** and other.]. // Eastern European Journal of Enterprise Technologies. – 2016. – pp. 24–28. DOI: https://doi.org/10.15587/1729-4061.2016.72404.

5. **Malanchuk Z.** Examining features of the process of heavy metals distribution in technogenic placers at hydraulic mining / **Malanchuk Z., Malanchuk Ye., Korniyenko V., Ignatyuk I.** Eastern-European Journal of Enterprise Technologies ISSN 1729-3774, 2017, pp. 45-51 DOI:10.15587/1729-4061.2017.92638.

6. **Arens, V.** (2001). Physical and chemical geotechnology: text-book (p. 656). Moscow: State. Mining University Press.

7. **Khrystyuk A. O.** Analiz isnuyuchykh sposobiv ta tekhnolohichnykh zasobiv hidromonitornoho rozmyvu / Visnyk Inzhenernoyi akademiyi nauk. Kyyiv, 2015. Vyp. № 1. S. 236–240.

8. **Malanchuk Z., Malanchuk E., Khrystyuk A.** Simulation of the comminution process to complex processing of metal-bearing basalt raw material / Cambridge Journal of Education and Science, 2015. No 2 (14), July-December. pp. 542–549.

9. **Malanchuk YE. Z., Khrystyuk A. O.** Matematychne modelyuvannya protsesiv sverdlovynnoho hidrovydobutku rozsypnykh korysnykh kopalyn / Visnyk Inzhenernoyi akademiyi nauk. Kyyiv, 2015. Vyp. № 4. S. 187–194.

10. **Khomenko O.Ye.** Principles of rock pressure energy usage during underground mining of deposits **/ Khomenko, O.Ye.,Sudakov, A.K., Malanchuk, Z.R., Malanchuk, Ye.Z.** / Naukovyi Visnyk Natsionalnoho Hirnychoho Universytetu, National Mining University of Ukraine, ISBN: 2071-2227, 2017, pp 34–43.

11. **MalanchukZ.R.,MalanchukE.Z., KorniyenkoV.Ya.** Modern geotechnical methods of management of the process of amber extraction / Multi-authored monograph:"Innovative development of resource-saving technologies of mining of minerals" Publishsng house «St. Ivan Rilsky» Mining and Mining University of Geology (Sofia, Bulgaria). – 2018. –P. 80–103.

12. Malanchuk Z. Physico-Mechanical and Chemical Characteristics of Amber / [**Z. Malanchuk, V Moshynskyi, Y. Malanchuk** and other.]. // Solid State Phenomena. – 2018. – pp. 80–89. DOI: https://doi.org/10.4028/www.scientific.net/SSP.277.80.

13. **Malanchuk Z. R.** Results of studies on amber extraction by hydromechanical method / **Z. R. Malanchuk, V. Ya. Kornienko, E. Z. Malanchuk.** Mining of Mineral Deposits, 11(1), 2017, 93-99. DOI: http://doi.org/10.15407/mining11.01.093.

14. **Malanchyk Z., Korniyenko V.** Modern condition and prospects of extraction of amber in Ukraine / Proceedings of the 1st International Academic Congress “Fundamental and Applied Studies in the Pacific and Atlantic Oceans Countries”. (Japan, Tokyo, 25 October 2014). Volume II.“Tokyo University Press”.– 2014. – P. 318–321.

15. **Bulat A., Naduty V., Korniyenko V.** Substantiations of technological parameters of extraction of amber in Ukraine / American Journal of Scientific and Educational Research. – No.2. (5) (July-December). Volume II.“Columbia Press”.– New York. – 2014. – P. 591–597.

https://doi.org/10.31713/m1003

POSSIBILITIES TO RECOVER ALUMINUM FROM MINING WASTE DUMPS LOCATED IN JIU VALLEY. ECONOMIC, SOCIAL AND ENVIRONMENTAL OPPORTUNITIES

Faur F.
University of Petroşani, Faculty of Mining, Department of Environmental Engineering and Geology, Doctor of Engineering Sciences, Lecturer, Romania

Lazăr M.
University of Petroşani, Faculty of Mining, Department of Environmental Engineering and Geology, Doctor Habil. of Engineering Sciences, Professor, Vice-Rector for Scientific Research and International Relations, Romania

Apostu I.-M.
University of Petroşani, Faculty of Mining, Department of Environmental Engineering and Geology, Doctor of Engineering Sciences, Assistant Professor, Romania

Rada C.
University of Petroşani, Faculty of Mining, Department of Environmental Engineering and Geology, PhD Student of Engineering Sciences, Romania

Abstract

The exploitation of low-grade ore deposits or the recovery of useful minerals from old waste dumps and tailing ponds is considered as an interesting economic opportunity especially in the context in which we speak more and more of a reduction in availability of some mineral resources or depletion of conventional ore deposits. The exploitation of old waste dumps and tailing ponds is possible on the one hand due to progress in terms of processing technologies (process efficiency and by lowering the minimum useful content that can be recovered) and on the other by the rise in the demand and the price on the internal and international markets for some useful mineral substances.

This paper presents some considerations related to the opportunity to extract useful mineral substances, more precisely aluminum, contained in coal mining waste dumps from Jiu Valley (Romania), regarded in terms of economic, social and environmental benefits.

Keywords: waste dumps, bauxite, aluminum, sterile rocks, Jiu Valley

Introduction

The history of the southern part of Hunedoara County (Romania), known as the Jiu Valley, is definitely linked to the discovery and exploitation of coal deposits (hard coal) [9].

An inevitable consequence of coal mining and pro is the appearance of mining waste dumps (about 60 scattered along the Jiu Valley) in which important quantities of rocks, of different types (sandstones, marls, clays, etc.) are stored and which occupy appreciable areas of land [12]. Of course, in the 21st century these engineering structures are seen as environmental problems that must be solved in one way or another by mining operators.

Thus, in line with the objectives of modern mining, the operators and investors have begun to view these rock deposits not only as environmental issues, but also as possible sources of useful minerals, other than those originally mined in the area.

Although the chemical analyzes that demonstrate the presence of this element (aluminum) in a concentration that allows taking into account the possibility of recovery were performed on material from only two of the four active waste dumps, judging from their location (inside Petroşani mining basin) and similar geological conditions (including those related to the genesis of the carbonaceous deposit), it can be extrapolated that the material from the other two waste dumps is similar in terms of the aluminum content [8].

In this context, the present paper analyzes the opportunity to extract the aluminum ore (bauxite) (figure 1) contained in the four active coal mining waste dumps from Jiu Valley and further needed processing operations in order to obtain a salable product (99.7 % pure aluminum).

Fig. 1. Bauxite fragment (with calcite depositions) collected from Lonea I waste dump: *a* – front view; *b* – side view)

Given the presented aspects, the assessment of the total amount of aluminum that can be recovered and its economic value refers to the total volume of the bauxite stored in the four active waste dumps from Jiu Valley.

The origin of the material from sterile deposits

Due to productive activities conducted in the four mines that are sill operating in Jiu Valley (Lonea, Livezeni, Vulcan and Lupeni), results a relatively large amount of sterile rocks that are stored in four waste dumps located in valleys or on slopes (figure 2).

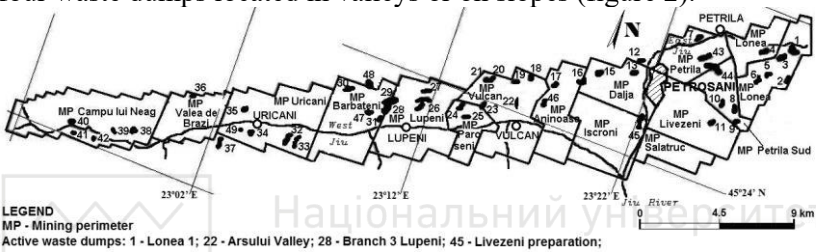

Fig. 2. Location of active waste dumps from Jiu Valley [13]

The mining mass from the dumps is composed of a heterogeneous mixture of soft rocks (such as clay or marls) and hard rocks (such as sandstones) with a pronounced unevenness of granulometry and physical and mechanical properties (figure 3*a-d*) [12].

a *b*

c *d*

Fig. 3. Details regarding the stored material: *a* – Lupeni; *b* - Arsului Valley; *c* - Livezeni and *d* – Lonea waste dumps

Since the four dumps are located in valleys and on inclined terrains, for their construction there were used conveyor systems (Lonea and Livezeni), dumping trucks (Vulcan) and funicular installations (Lupeni). Through them it was ensured the transport and deposition of the sterile rocks in the waste dumps. The dumps were constructed on different alignments and the discharge points were determined according to the configuration of the terrain on the respective alignments.

Description of the active waste dumps

In order to increase storage capacity, the material discharged from the transportation systems is generally pushed laterally by bulldozers, forming deposition platforms. The platforms width varies between 15 and 50 m at the top and between 50 and 150 m at the bottom (at the contact with the base natural terrain) [12, 13].

Dumps height varies between 3 and 4 m (in the contact areas with the inclined base terrains) and between 30 and 40 m (where the material is deposited on horizontal terrains). The slope angle, in situations where plastics leakage occurred has values of 7-8 degrees, but generally it is between 40 and 50 degrees [12, 13]. During the discharge or when the waste material is pushed by bulldozers a particle size-sorting takes place, the coarse material is deposited at the base of the dumps and, also, there is a tendency for the material to arrange itself at slope angles greater than the final one. If the base terrain has abrupt slopes, the flattening of the waste dumps slopes is more obvious and the material requires more space to expand.

At present there are four active waste dumps, belonging to the four underground mines that are currently in operation. However two of them (those belonging to Lonea and Lupeni mines) will soon be put into conservation. The other two (belonging to Livezeni and Vulcan mines) will be in operation at least until 2024. Although the waste dumps are considered to be stable or relatively stable, the isolated instability incidents involving these artificial engineering constructions exert a negative influence on the immediately surrounding terrains [13].

The total area of terrains occupied by the four waste dumps exceeds 14 ha and the volume of waste material stored is over 2.7 million m^3 (table 1).

Table 1

Active mining waste dumps from Jiu Valley

Waste dump	Mining Unit	Dump surface [m^2]	Designed capacity [m^3]	Used capacity [m^3]
Branch 3 Lupeni	Lupeni ME	62,700	2,000,000	1,360,108
Arsului Valley	Vulcan ME	17,500	1,200,000	367,918
Livezeni preparation	Livezeni ME	37,500	800,000	563,619
Lonea 1	Lonea ME	23,000	4,000,000	426,119
TOTAL	-	140,700	8,000,000	2,717,764

ME – mining exploitation

The laboratory analysis carried out over the years, regarding the physical characteristics of the dumped material, shows that the average volumetric density is of 1,820 kg/m^3 [13], which means that in the four active waste dumps the total stored quantity of sterile is of approx. 4,95 million *t*.

Chemical analysis of the waste rocks

To determine the chemical composition of the deposited material, samples were collected from two dumps (Lonea I waste dump – located in the eastern edge of Petroşani coal basin and Arsului Valley Vulcan waste dump - located in the center of the basin) and subjected to laboratory analysis using a S4 Pioneer spectrometer. The results of these tests are shown in table 2.

Table 2

Chemical composition of the waste material [7, 8]

No.	Parameter	Measuring unit	Determined value	
			Lonea I (Lonea ME)	Arsului Valley (Vulcan ME)
1	Volatile	%	69.60	60.00
2	Si	%	22.40	22.30
3	**Al**	**%**	**9.82**	**10.70**
4	Fe	%	3.04	2.37
5	K	%	2.33	2.20
6	Ca	%	0.69	0.52
7	Ti	%	0.60	0.51
8	Na	%	0.49	0.49
9	Mg	%	0.43	0.46
10	S	%	0.35	0.21
11	Ba	%	0.068	0.054
12	P	%	0.042	0.044
13	Mn	%	0.035	0.029
14	Cr	%	0.025	0.020
15	Sr	%	0.017	0.016
16	Ni	%	0.016	0.011
17	Zr	%	0.016	0.0137
18	Cl	%	0.011	0
19	Rb	%	0.011	0.011
20	V	%	0.010	0.013
21	Cu	%	0.010	0.008
22	Zn	%	0.008	0.0076
23	Pb	%	0.006	0
24	W	%	0.004	0
25	Ga	%	0.0034	0.022
26	Others	%	0.0061	0.0041

As shown in table 2, the aluminum content in the two waste dumps from Jiu Valley (which is extrapolated to be the same for the other two waste dumps, Livezeni and Lupeni) is in a considerable concentration, of approx. 10% on average, in other words, it can be recovered a theoretical amount of 0.495 million t of aluminum.

Recovery of aluminum on economic basis

The concentration that is found in the waste dump's material complies with the minimum average useful content for aluminum ore (6-8%) [3,4]. This led to the idea of analyzing the opportunity of

recovery and capitalization of this element from the four active dumps from Jiu Valley.

For the recovery of aluminum to be economically viable the following relationship (1) must be satisfied [5]

$$c_{med_{\min}} = \frac{P}{p \cdot \eta - M} \cdot \frac{1}{k \cdot m} \quad [\%] \qquad (1)$$

where

c_{medmin} - minimum average useful content %;

P - costs of mining and ore preparation USD/t;

p - the selling price of the metal USD/t;

η - efficiency of metallurgic extraction;

k - coefficient that during the appreciation of the advisability of operation has the value equal to 1;

M - all metallurgical processing costs USD/t;

m - extraction of metal in the concentrate %.

Since this paper assumes that only the primary processing will take place in Jiu Valley, separation of bauxite from the rest of waste rocks from the dumps in order to obtain a concentrate to be submitted later (in another location) for metallurgical processing and refining processes, not all the values of the parameters involved in relation (1) can be set.

However, the relationship can be simplified and some judgments can be made on the opportunity to recover aluminum from the active waste dumps, given the average price of 99.7% pure aluminum on the world market for the last 5 years (figure 4).

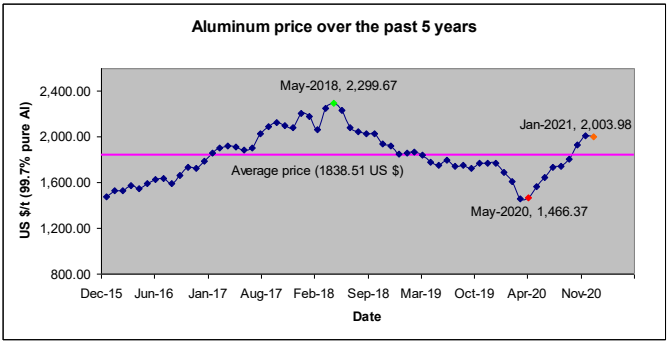

Fig. 4. Price per metric ton of aluminum (99.7% purity) [17]

As can be seen from figure 4, the price of aluminum on the international market has undergone significant variations in the last 5 years. If in May 2018 the price per ton of aluminum reached almost 2,300 USD, in May 2020 it recorded the lowest value in the analyzed time period, of only 1,466 USD/t.

Although the average value calculated for the price of aluminum is approx. 1,838 USD per ton, the authors believe that the period corresponding to 2020 should be eliminated, which would lead to an increase in the average price to approx. 1,875 USD per ton (value that will be considered representative further in the paper).

The sudden drop in price followed by an equally sudden rise from 2020 does not reflect the normal behavior of the world market, this variation being obviously a reaction to the restrictive measures adopted by most countries in the world in the effort to manage the crisis caused by the SARS-CoV-2 (COVID 19) pandemic.

Substituting the known values into relation (1), this becomes (2)

$$10 = \frac{P}{1875 \cdot \eta - M} \cdot \frac{1}{m} \quad [\%] \tag{2}$$

If we analyze relation (2), the minimum average useful content is constant and the cost of extraction and preparation is much lower than for operating a bauxite quarry (this cost decreases because we are not talking about an actual exploitation but an excavation and transport of the waste material from the dumps to a processing plant and therefore the largest share in this cost will be held by ore processing rather then mining).

As the other technological parameters depend on the performance of machines and equipments (and their value varies generally in known limits) we can say that the most important variables in determining the appropriateness of recovery of aluminum are the costs of metallurgical processing (especially the influence of the electricity price) and the selling price on the world market of aluminum.

So according to these variables it can be established the appropriate time to recover the aluminum contained in the dumps from Jiu Valley, meaning that they can be reprocessed in sequences, when the values of the variables mentioned satisfies equation (2) (or when the calculated minimum average useful content is below 10).

Primary processing

For processing the material from the active waste dumps from Jiu Valley, in order to separate the bauxite from the rest of the rocks, the technological flux shown in figure 5 is proposed.

The material (which can be assimilated with a low-grade ore) deposited in the waste dumps, with a granulometry up to 200 mm, is excavated and transported towards the processing plant by trucks.

Here, the material is subjected to a primary grinding stage, using an autogenous mill.

Primary crushed material obtained in the discharge of the autogenous mill is volumetrically classified at 3 and 1 mm on a vibrating screen with two superimposed filing surfaces, on which acts powerful jets of water (to remove clays) [10].

Refusal of the 3 mm surface is returned to the autogenous mill, while the refuse from the 1 mm surface (fraction ranging from 1 mm to 3 mm) is then subjected to the separation process in dense medium (first stage), obtaining a concentrate and a sludge. Fine fraction -1 mm is subject to hydrocyclonage at 0.3 mm separating the predominantly clayey slurry from the bauxite. Refusal product from the hydrocyclone (fraction between -1 and +0.3 mm) is driven to the second stage of separation in dense medium, obtaining a concentrate (which is united with the concentrate obtained in the first stage of separation in dense medium) and a sludge [8].

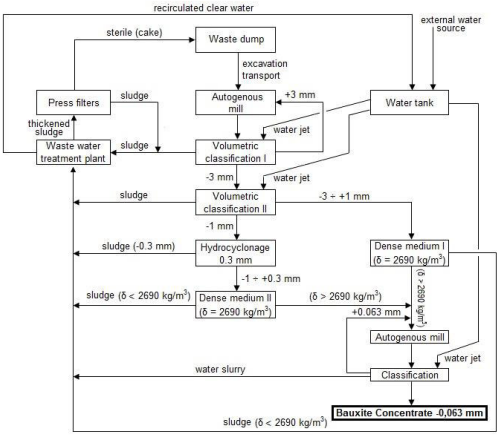

Fig. 5. Primary processing flux (modified after [8])

The second stage of grinding and advanced washing of bauxite is designed to bring the particle size to -0.063 mm, size necessary to obtain good extraction efficiencies in the Bayer process [10, 14, 15].

The sludge resulted from the primary and secondary volumetric classifications, hydrocyclonage and separation in dense medium as well as the water slurry resulted from the last classification is driven through the waste water treatment plant.

The thickened sludge goes into batteries of press filters. The resulted slurry is driven back to the waste water treatment plant and the sterile rocks (cakes) are transported back to the waste dump.

The resulting clear water will be recycled in the process.

Metallurgical extraction and refining

Bayer technology (alkaline process)

In this process, the aim is to convert aluminum hydroxides from bauxite ores to sodium aluminate. In Romania, this procedure is applied in metallurgical plants from Oradea, Slatina and Tulcea.

The following main steps can be distinguished in Bayer technology (figure 6): leaching, dilution, decomposition, and concentration [6].

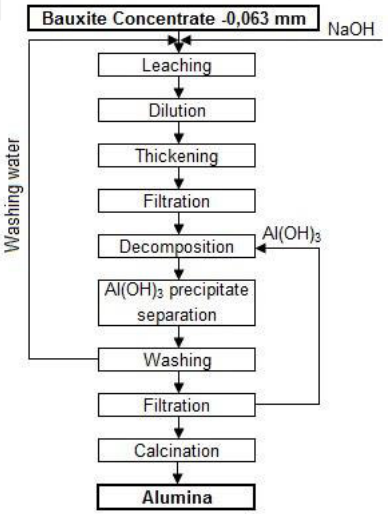

Fig. 6. Schematics of Bayer process [4]

Solubilization is performed with sodium hydroxide, in autoclaves, under pressure. In this stage reaction (3) takes place

$$Al_2O_3 . H_2O + 2\,NaOH = 2\,NaAlO_2 + 2\,H_2O . \quad (3)$$

The other compounds present in bauxite interact with alkaline solutions, forming sulfates, hydroxides, vanadates and phosphates that can be precipitated from recycled solutions, under different technological conditions [3].

The bauxite ore (already grounded to sizes less than 0.063 mm) is put in contact with a concentrated solution of sodium hydroxide and placed in autoclaves at temperatures of 150-250 °C.

From the autoclave, the slurry is passed into wet tanks and diluted, followed by a series of successive settlements and filtrations of the diluted solution to separate the sodium aluminate from the residue in suspension. The obtained solution is subjected to the decomposition operation. The most important feature of these solutions is the caustification ratio (4) - which is the molar ratio between alkaline oxides and alumina present in the solution [3, 4]

$$\alpha_k = \frac{Na_2O_k}{Al_2O_3} \quad (4)$$

The decomposition is carried out by slow cooling (in 70-80 hours to reach a temperature of 20 °C) during which the concentrated solution of sodium aluminate hydrolyzes, with the precipitation of $Al(OH)_3$ according to reaction (5) [3, 4]

$$NaAlO_2 + 2\,H_2O = NaOH + Al(OH)_3 \quad (5)$$

After filtration, the aluminum hydroxide is calcinated in rotary ovens at temperatures of 1,200 – 1,400°C. The purpose of calcination is to dehydrate the aluminum hydroxide as completely as possible and to obtain non-hygroscopic alumina according to reaction (6) [4, 15]

$$2\,Al(OH)_3 \rightarrow \gamma Al_2O_3 \rightarrow \alpha Al_2O_3 \quad (6)$$

Obtaining aluminum from alumina

It consists of electrolysis of alumina dissolved in a salt melt. The electrolysis medium is a melt of cryolite (mixture of aluminum and sodium fluoride) and calcium fluoride.

The alumina is mixed with the melt at a temperature of 940 - 960°C and decomposes releasing aluminum ions Al^{3+} and AlO_3^{3-} anions, according to reaction (7) [11, 14].

$$Al_2O_3 \rightarrow Al^{3+} + AlO_3^{3-} \quad (7)$$

The aluminum thus obtained is deposited on the bottom of the electrolysis bath, having a purity of 99.5-99.7% (which is also the purpose of this proposed project).

Along with aluminum, Cu,Si,Fe,Ti,Ca and non-metallic inclusions are deposited, which is why the product must be further subjected to electrolytic refining (after which 99.99% pure aluminum is obtained) [4,5,15].

Economic and social benefits

By leveraging all of the aluminum estimated to be present in the dumps of Jiu Valley, of 0.495 million t, at the average world market price of 1,875 USD/t results in a total revenue of 928,125,000 USD (this amount needs to balance all operating costs, wages and bring a decent profit).

Also, beyond the obvious economic benefits, we must consider the opportunity to solve some social problems that appeared in Jiu Valley since the mid-90's, when the coal mining exploitations (16 at the time) began to close, on the account of a so-called restructuring program [9] (currently only 4 mines being still in operation).

We are referring here at the problem of unemployment (the real unemployment rate in Jiu Valley is estimated to be almost double compared to the national one) and the lack of alternative jobs.

By reprocessing the four active waste dumps from Jiu Valley for the recovery of useful minerals (aluminum as proposed in this study) would create, at least for a period of time, jobs, which would largely address the people dismiss from the mining and mineral resources processing sectors.

Environmental benefits

To identify the environmental effects (benefits) it should be noted that the chemical analysis revealed the concentration of metallic aluminum in the active waste dumps to be of approx. 10% on average. This aluminum is actually present in bauxite and if we consider that in Romania the bauxites have an average content of

50% Al [16], results in a simple calculation that by reprocessing the four waste dumps (separation of bauxite from the rest of the rocks) the volume of stored material decreases by about 20%.

For a total volume of sterile approx. 2.72 million m^3 results a decrease by approx. 544,000 m^3, which by extrapolation leads to a decrease in the total area occupied by waste dumps of approx. 3 ha.

Another advantage from the point of view of environmental protection is represented by the reduction of the contamination risk with Al^{3+} of the adjacent natural terrains.

To explain this benefit we must take into consideration that in Jiu Valley operates a power plant (CET Paroşeni). This power plant produces electricity and hot water using coal (as the main fuel) extracted from the four still operating mines in the area. This clarification is necessary because the coal extracted from Jiu Valley has a relatively high sulfur content, sulfur that after the combustion process is released into the atmosphere in appreciable quantities in the form of SO_2 (although a desulphurization installation was put into operation a few years ago). Also, from combustion processes, results appreciable quantities of NO_x.

The two above-mentioned residual combustion gases are, as is known, responsible for the formation of acid precipitations. Once in contact with rocks from the waste dumps containing aluminum, the Al^{3+} ion is released. In turn it migrates into the soil and replaces calcium in its connections, resulting in a decrease of the intake of nutrients, with negative consequences in terms of plant resistance to insects, disease or excessive climate [1, 2].

Finally, recovery of aluminum from the waste dumps should be seen as an environmental protection action if we take into account the fact that it can provide a significant amount of this metal for the domestic market without requiring to put into service new conventional bauxite deposits, which certainly would generate a significant direct negative impact on the environment and would require a supplementary energy consumption.

Conclusions

Recovery of aluminum contained in the four active waste dumps from Jiu Valley is possible if we take into account the concentration of this element (10% minimum average useful content compared to 6

- 8% considered exploitable at present) and the significant reduction in operating costs compared to those claimed when operating a conventional bauxite quarry (basically we are talking about an excavation of waste dumps instead of complex mining operations in bauxite quarries).

To ensure the economic efficiency of the aluminum recovery process from the four considered waste dumps, their operation can be performed sequentially by considering the most important variables (price of electricity and aluminum) so that the relationship between the average minimum useful content and the mentioned variables is satisfied at any moment in time.

From an environmental perspective, the recovery of aluminum has advantages as it reduces the risk of soil contamination with aluminum ions in the vicinity of the waste dumps, the volume and the areas occupied by waste dumps are reduced and for a period of time we avoid to generate a negative impact on the environment (by not putting into exploitation conventional bauxite deposits).

Such an activity, of recovering aluminum from waste dumps is beneficial economically and socially by providing employment for a significant period of time for the residents of Jiu Valley and it complies with international policies on secondary resource exploitation, environmental protection and sustainable resource management.

References

1. **Andersson M.** Toxicity and tolerance of aluminum in vascular plants, Water, Air, & Soil Pollution. Vol. 39, No. 3–4, pp. 439–462. doi:10.1007/BF00279487, 1988.

2. **Apostu I.M., Faur F., Lazăr M.** Identification and assessment of the environmental impact generated by the implementation of Certej Mining Project, Research Journal of Agricultural Science, ISSN 2066-1843, Vol. 48, Nr. 4, pp. 254-264, 2016.

3. **Bădulescu C.** Preparation and metallurgical processing technologies of concentrates (in Romanian), Universitas Publishing House, ISBN 973-8035-15-5, 160 p., Petrosani, Romania, 2000.

4. **Bădulescu C.** Techniques and technologies in the metallurgical industry (in Romanian), Sitech Publishing House, ISBN 973-657-681-7, 236 p., Craiova, Romania, 2004.

5. **Craig W., Leonard A.** Manufacturing Engineering & Technology, Scientific e-Resources, ISBN 978-1-83947-242-8, 352 p., 2019.

6. **Drozdov A.** Aluminium: The Thirteenth Element, RUSAL Library, ISBN 978-5-91523-002-5, 232 p., 2007.

7. **Faur F.** The elaboration of an environmental monitoring system in Jiu's Valley (in Romanian), Doctoral Thesis, University of Petrosani, Romania, 164 p., 2009.

8. **Faur F., Lazăr M, Dunca E., Ciolea D.I.** Opportunity of recovery and capitalization of useful minerals from waste dumps in Jiu's Valley. Proceedings of the 13th SGEM GeoConference on Science and Technologies in Geology, Exploration and Mining, ISBN 978-954-91818-8-3/ISSN 1314-2704, Vol. 2, 595 - 602 pp., June 16-22, 2013, Albena, Bulgaria.

9. **Faur F., Marchiş D., Nistor C.M.** Evolution of the coal mining sector in Jiu Valley in terms of sustainable development and current socio-economic implications, Research Journal of Agricultural Science, ISSN 2066-1843, Vol. 49, Nr. 4, pp. 110-117, 2017.

10. **Fechete E.** Process for the preparation of diasporic bauxite ore (in Romanian), Invention Brevet, No. 116387, OSIM, Romania, 2001.

11. **Krausz S., Bădulescu C.** Technologies for preparation and metallurgical extraction of concentrates (in Romanian), Universitas Publishing House, 123 p., Petrosani, Romania, 2001.

12. **Lazăr M., Apostu I.M., Faur F.** Methodology for assessing the environmental risk due to mining waste dumps sliding - case study of Jiu Valley. Carpathian Journal of Earth and Environmental Sciences, ISSN 1842-4090, EISSN 1844-489X, Vol. 10, Issue 3, pp. 223-234, 2015.

13. **Lazăr M., Florea A., Faur F.** Research on load carrying capacity of base terrains of the waste dumps in Jiu Valley, Mining Revue, ISSN-L 1220-2053/ISSN 2247-8590, Vol. 20, No. 4, pp. 26-31, 2014.

14. **Lumley R.** Fundamentals of Aluminum Metallurgy: Production, Processing and Applications, Elsevier Science, ISBN 978-0-85709-025-6, 843 p., 2010.

15. **Polmear I.J.** Light Alloys: Metallurgy of the Light Metals (3 ed.), Butterworth-Heinemann, ISBN 978-0-340-63207-9, 362 p., 1995.

16. **Sîli N., Vesa E.M., Faur F., Apostu I.M.** Considerations regarding the evolution of the landscape in the area of the former bauxite quarries from Ohaba—Ponor, ISSN 2066-1843, Vol. 52, Nr. 4, pp. 123-132, 2020.

17. http://www.indexmundi.com/commodities/?commodity=aluminum

https://doi.org/10.31713/m1004

ALTERNATIVE DIRECTIONS OF PEAT USE

Moshynskyi V.S.
National University of Water and Environmental Engineering (NUWEE), Rector, Professor, Doctor of Sciences (Agricultural), Professor, Department of Land, Cadaster, Land Monitoring and Geoinformatics, Ukraine

Mohamed Tafsir Diallo
Polytechnic Institute of Gamal Abdel Nasser University of Conakry, Managing Director, Republic of Guinea

VasylchukO.Yu.
National University of Water and Environmental Engineering (NUWEE), Associate Professor, Department of Mining and Mining, Ukraine

Kucheruk M.O.
National University of Water and Environmental Engineering (NUWEE), Assistant, Department of Development of Deposits and Mining, Ukraine

Semeniuk V.V.
National University of Water and Environmental Engineering (NUWEE), Senior Lecturer,
Department of Development of Deposits and Mining, Ukraine

Summary
Peat extraction and processing in the world is a highly profitable and promising type of business. This section describes and discloses the essence of alternative uses of peat. The physical and chemical properties of peat are given. Emphasis is placed directly on the use of peat in the world and in Ukraine.

Introduction

Peat is a rock of plant origin, formed over thousands of years from under composed plant residues (grasses, mosses and wood), which due to high humidity and poor air access partially (about 50%) mineralized.

Peat deposits are common in all climatic zones and are in many countries. The most intensive accumulation of peat is characteristic of the northern hemisphere - Northern Europe, Western Siberia and

North America. The total area of peat deposits in the world is estimated at 176 million hectares. The modern wetland of the land is 4.5% of its total area, and the average annual growth of wetlands on the globe for the last 10 thousand years was 658 square kilometers. The largest reserves of peat are concentrated in the CIS countries (40.0%), Indonesia (13.6%), Finland (7.0%), Canada (7.0%), USA (7.0%), China (5, 4%) and Sweden (2.4%). World peat resources are estimated at 2 trillion tons, of which 770 billion tons are in the CIS, 510 - in Canada. Annual world production of peat is 26-28 million tons. Its largest volume is accounted for by Finland, Ireland (5.5 million tons each) and Germany - 4 million tons. On average, from one to two million tons per year are produced in the Russian Federation, Belarus, Canada and Sweden. In Scandinavia, a large proportion of peat is used as energy raw materials.

In Ukraine, most swamps are peat lands. The latter term is often used for drained marshes; sometimes under peat land understand the peat bog, especially when developing it. In the marshes of Ukraine lowland peat deposits prevail, in the Western Polissia and Carpathians mixed transitional types occur. Top and mixed top types of deposits are known in Western and Central Polissia, in the Carpathians. The most widespread peat deposits are in Rivne, Volyn, Chernihiv, Zhitomyr, Kyiv, Lviv regions. Tariffs of Rivne and Volyn regions reach 6.5%, while in Ternopil, Khmelnitsky, Vinnitsa, Cherkasy, Poltava, Sumy and Kharkiv regions it does not exceed 1.9% of the whole territory. Even less common are peat deposits in Mykolaiv, Zaporizhia, Dnipropetrovsk, Transcarpathian, Ivano-Frankivsk regions, where the degree of peat land does not exceed 0.1% [1].

The Ukrtorf concern produces up to 600,000 tons of peat annually, the vast majority of which (62%) is converted to fuel briquettes – a fairly efficient solid fuel with a lower combustion heat of about 15 MJ /kg, humidity up to 20% and ash content up to 23 %.[1]

The set of properties of peat differs sharply from other minerals. The chemical composition and properties of peat vary in a wide range depending on the type, species, degree of decomposition, acidity, ash content, etc. [2], so the directions of its use are extremely diverse.

The substance of peat contains partially decomposed plant residues, their decomposition products in the form of dark amorphous humic substance and a mineral part. In the natural state,

peat contains 85-95% water, and in the solid part - up to 50% of mineral compounds. The organic matter of peat contains 48-65% carbon, 4.7-7.3% hydrogen, 24.7-45.2% oxygen, 0.2-1.2% sulfur and 0.5-4.0% nitrogen [3]. Humus gives peat a dark color.

The elemental composition reflects the nature of the original plant material and the nature of its change during peat formation, as well as determines the botanical composition of peat, and nutritional conditions and the type of peat-forming plants determine the type of peat. Peat formed from plants of mainly atmospheric (oligotrophic) nutrition with a content of plant residues not less than 95% is called upland, and from plants of rich (eutrophic) nutrition, with a content of such plant residues not less than 95%, is called lowland. Peat, in which 10-90% of plant remains of one type and the rest - another, as well as there are remains of sphagnum mosses of mesotrophic type, is called transitional. Each type consists of subtypes: forest subtypes, forest-swamp and swamp, and the subtypes are divided into groups: tree, tree-grass, tree-moss, grass, grass-moss and moss. There are 20 species of lowland, 8 transitional and 12 upper peats. The level of biochemical decomposition of peat-forming plants is characterized by the degree of decomposition, which shows the proportion of unstructured peat that has lost the cellular structure of the substance. The degree of decomposition varies from 1 to 75%.

Depending on the geobotanical characteristics, the composition of peat changes significantly. During the transition from upper to lower peat, the content of nitrogen, humic acids and fulvic acids increases, while the number of components characteristic of plants (bitumen, water-soluble, hydrolyzed substances and cellulose) decreases by 1.5-3.0 times. In the component composition of the organic mass, the content of water-soluble substances is 1-5%, bitumen 2-10%, easily hydrolyzing compounds 20-40%, cellulose 4-10%, and humic acids 15-50% lignin 5-20%.

Peat is characterized by high moisture resistance in natural occurrence (88-96%), porosity up to 96-97% and a high coefficient of compressibility during compression tests [3]. The texture of peat is homogeneous, sometimes layered; the structure is usually fibrous or plastic. The color is yellow or brown to black. Weakly decomposed peat in the dry state has a low density (up to 0.3 g /

cm3), low thermal conductivity and high gas absorption capacity. Peat of high dispersion (after mechanical processing) forms dense pieces during drying with high mechanical strength and calorific value of 2650-3120 kcal/kg (at 40% humidity).

An important advantage of peat is its peculiar combustion. After all, peat fibers contain oxygen, so peat is able to burn without additional oxygen supply.

Peat is considered the first stage in the formation of fossil coal. It is used as fuel, building material, raw materials for the chemical industry, soil remediation agent, moisture absorber.

For greater clarity of the directions of use of peat in Ukraine and the world, this paper presents two schemes of integrated peat use in Fig.1. and Fig 2.

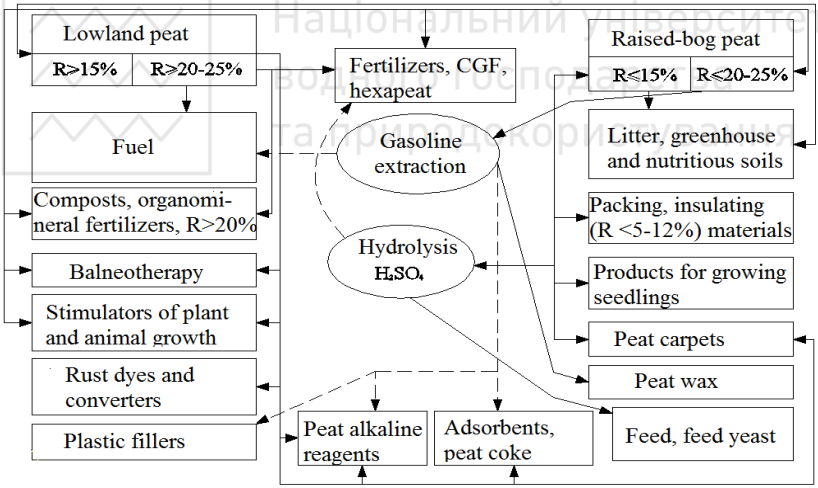

Fig. 1. Scheme of complex use of peat in Ukraine and the world
The solid line shows the areas of peat use, the dashed line shows the waste of the respective production

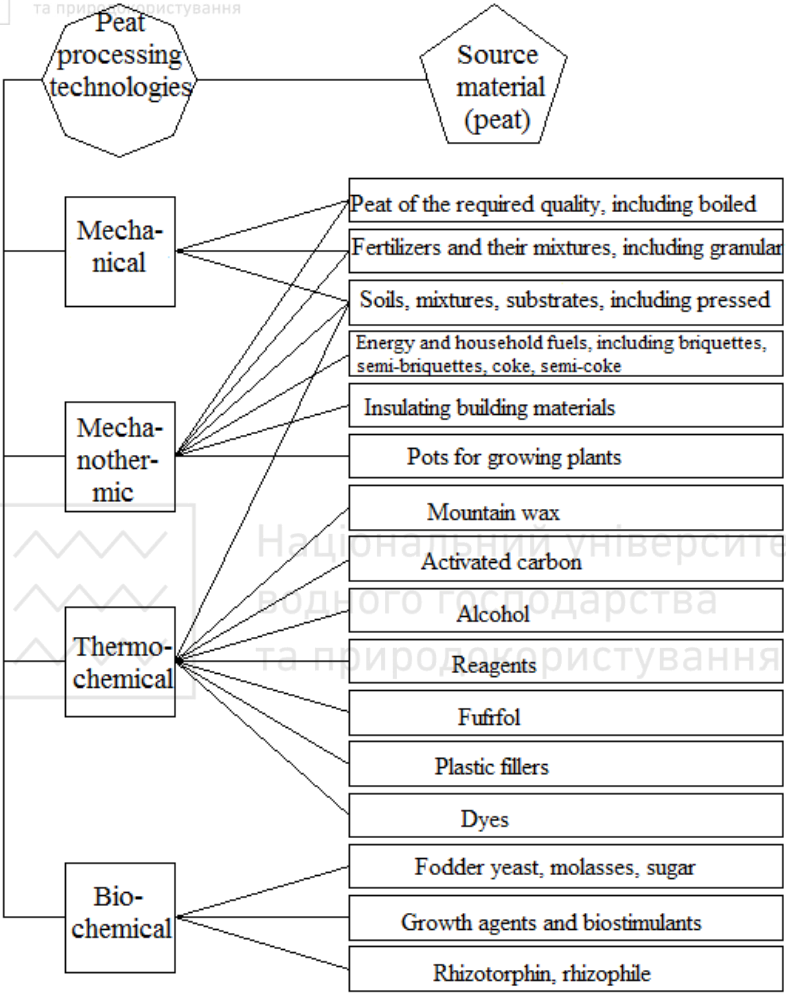

Fig. 2. Block diagram of peat processing technologies and its main products

The use of peat as fuel

Currently, about 500 peat deposits are being developed in Ukraine. Approximately 81% of peat extracted in Ukraine is used as fuel and 19% as fertilizer.

Despite the discovery of new energy sources, the use of peat as a fuel continues and will increase for energy and utilities in order to improve the fuel problems of today.

The use of peat as a fuel during its combustion is more environmentally friendly than coal, fuel oil and shale [4].

The main consumers of peat are agriculture and industrial and energy complex [5]. Previously, peat was commonly used as a household fuel, but over time it began to be widely used in industry and energy in the form of milling crumb, briquettes and pellets.

In small volumes (about 15 thousand tons) Ukraine exports peat products (mainly as fuel), and imports some varieties of peat (about 1700 tons).

Given the limited reserves of reised-bogpeat in Ukraine, as well as the situation on the fuel market in the country, we can agree with the statement that the main use of peat in modern conditions - the production of peat fuel (peat briquettes and lump peat) for public consumption [2].

The use of peat as a fuel is due to its composition: high carbon content, low sulfur content, harmful non-combustible residues and impurities. In fact, it is young coal. The main disadvantages of this type of fuel are: lower than coal energy value (heat of combustion) and the difficulty of combustion due to high moisture content (up to 65%).However, along with this peat has a number of advantages:

- low production costs;
- ecological purity of combustion (small percentage of sulfur);
- complete combustion (small residue and non-toxicity of ash);
- new combustion technologies that have appeared.

All this makes peat a promising local source of heat and electricity: cheaper than using coal and liquid fuels and more environmentally friendly.

The feasibility of introducing small thermal power plants on peat requires a more detailed study, based on the experience of Finland, where about 15% of electricity is produced by burning it [2].

The use of peat in agriculture

Agricultural direction is one of the main areas where peat is actively used. This is a great environment for growing all plants. Peat is used in the manufacture of various fertilizers, as well as substrates that are indispensable for plants grown in greenhouses. Peat is also

used to make lawn mixtures. Peat is added to the soil to improve its properties, it also has bactericidal and gas-absorbing properties, which heals the soil, destroys a certain amount of nitrates, and stimulates vegetation growth. Peat is not only a good basis for the production of various fertilizers, it is an ameliorant in the literal sense of the term, as it allows not only to introduce the necessary nutrients into the soil, but also to improve a number of properties of the fertile soil layer [6].

Peat contains humic acids, which stimulate the growth and development of plants, and amino acids needed to convert certain components of food into a form accessible to plants.

Peat has bactericidal and gas-absorbing properties, which are equally necessary for all types of soils. Peat heals the soil, reduces the content of nitrates in the product by 1.5-2 times, prevents the accumulation in plants of heavy metals and other harmful substances, weakens the effects of pesticides that enter the soil. Humus, which is formed in the soil during prolonged application of peat, prevents the leaching of easily soluble fertilizers.

To grow seedlings in greenhouses make special peat-humus pots, which is consist of a mixture of peat and rotted manure.

Advantages of peat and rationality of its use:

- Peat itself does not nourish plants, but helps them better absorb other fertilizers.
- The soil into which the peat has been applied becomes more structural, that is, one that consists of lumps and pores likes a sponge. This soil retains moisture, air and nutrients well.
- It makes sense to use peat only on poor, infertile or depleted soils.
- Peat is considered a natural antiseptic and inhibits the development of harmful fungi and bacteria.
- Peat (horse) can regulate the acidity of the soil, adjusting it to the needs of plants.

Peat is used as a litter for livestock and birds, because it retains and keeps heat, absorbs moisture and is very soft in texture. The ability of dry peat to absorb moisture and odors allows it to be used as bedding for livestock. One kilogram of light peat holds up to 20 liters of water. The resulting mixture can be composted without finishing. Another advantage of using peat for bedding is its

bactericidal properties: peat prevents many diseases in animals. Peat litter is more profitable than straw or sawdust: 1 ton of such litter later gives 5 tons of high-quality organic fertilizer.

Peat also purifies water from excess acidity, so it has found its application in the manufacture of filters for aquariums.

A large share of peat resources is used in agriculture. In countries such as Russia, Latvia, Belarus, Ukraine and some others, there are plants that produce mineral fertilizers based on peat. Peat soils used for growing vegetables, horticultural crops and rice crops have also been widely used [5].

The trend of peat production, namely, the direction, volume and pace, are determined not only by the resources of peat, but also, to a large extent, the needs for relevant products. Thus, in countries with cold climates, such as Russia, the Baltic countries, sphagnum peat is widely used as bedding, greenhouse and nutritious soils, as well as for the manufacture of micro greenhouses and micro districts.

In many countries of the world peat in the form of crumbs is used for packing of perishable products, vegetables and fruit at long transportations. In some countries, it is used to treat wastewater, land surface from petroleum products and as a raw material for the chemical and energy chemical industries [2].

Peat for breeding worms

In addition to horticulture and vegetable growing, the use of peat is gaining popularity in the cultivation of earthworms, manure, California worms and Dendroben worms for fishing.

The best food and habitat for the worm will be horse neutral peat, from which, as a result of the activity of worms, you can get compost. This environmentally friendly, natural organic fertilizer can then be used in the cultivation of vegetables, fruit trees and berry bushes.

Peat for breeding snails

A new area of application of peat is the breeding of snails. Previously, snails were kept at home in the terrarium as "pets", now their cultivation has grown to an industrial scale.

Peat with neutral acidity is used as litter in the cultivation of grape snails. Their meat can be eaten it contains a large percentage of protein. Peat is also used by mollusks as nests where they lay their eggs. Snail caviar is made from eggs. Snail caviar is a new delicacy

that is considered more valuable and, accordingly, more expensive than black and red fish caviar.

The use of peat in medicine

In medicine, peat is used for mud treatment and drug production. For general and local applications use lowland and upper peat of the increased degree of decomposition, in the form of raw or in the form of milling peat without any special long processing. The simplicity of the method of peat treatment with its high efficiency has made this method a very valuable treatment in practical medicine [5]. The health and therapeutic properties of peat have long been known. From ancient times in Greece peat baths were used to treat joint diseases and female reproductive disorders. Currently, peat-containing drugs are used to prevent and treat a wider range of injuries and diseases. Produce drugs for the treatment of eye diseases, burns and inflammatory processes.

Activated charcoal from peat is used to clean gases, air, medicines, food, etc.

The most valuable active ingredient in peat is unique macromolecular bonds, which are called humates (derived from the term "humus" - fertile).Among organic compounds, they occupy a special niche because they are formed by thermodynamic survivability, and not by genetic rules, as most. This explains the unique value of humates, their physiological activity and positive health effects.

The anti-infective properties of peat have been known since ancient times. Today, peat baths are widely used in health resorts in Western Europe, which use bactericidal and healing properties of peat.

Peat in the chemical industry

More than one hundred basic chemical products are obtained from peat: methyl and ethyl alcohol, combustible gases, phenol, wax, artificial wax, tar, coke, paraffin, lactic, acetic and oxalic acids, ammonia, plant growth stimulants, herbicides and much more. The fibers of the fluff, which are part of the peat, can be used in the manufacture of fabrics. Chemical products from peat are obtained by semi-coking, gasification, wet charring, and extraction. In terms of carbohydrate content and quality, peat is a raw material suitable for chemical and biochemical processing.

Coke, gas, briquettes, activated carbon, bitumen, wax, humic acids and other products are obtained from peat by thermal processing [7].

Peat processing products are used in mechanical engineering, furniture, printing and cosmetics industries, in the production of household chemicals [8].

The use of peat in construction

Peat can be used to grow peat carpets. Peat carpets are lawn-type coverings that are formed by the interweaving of fibrous root systems and the terrestrial part of grassy plants on a peat basis [9]. With the help of peat carpets strengthen the ditches of roads landscaping. Peat carpets are used to create decorative, sports and other types of lawns. In addition to decorative and aesthetic, sod coverings are of great economic importance, especially for strengthening the earthen slopes of roads and railways, in the construction of reclamation facilities, consolidation of river banks and reservoirs.

In many countries of the world are engaged in special cultivation of turf on both mineral (grass carpets) and peat-based (peat carpets).

Nowadays, it is quite effective to create a lawn with peat carpets from perennial grasses.

Creation of a turf covering on steep slopes by a method of sowing of seeds of grasses is inefficient as a considerable part of seeds is washed away by rains. Under such conditions, to protect the slopes from water and wind erosion, it is necessary to dramatically reduce the time of soil deforestation. To do this, it is best to use peat carpets, pre-grown (30-40 days) grown on a drained peat deposit.

The best basis for the cultivation of peat carpets is horse peat of the moss group, which has a high hydrolytic (H_g=101-175 mmol equivalent/100 grams of dry matter) and exchange $H_{exch.}$ (pH=2.5-4.7) acidity compared to ordinary soils (turf soil -1-2; podzol - 3-5 mmoll equivalent/100 grams of dry matter), which allows you to grow high quality carpets.

The technology of turf production is based on the creation of optimal conditions for the development of grasses, which form a peat turf from the roots, bases of shoots and green aboveground mass of the grass layer.

The mixture of seeds of perennial grasses is wrapped in a thin cultivated layer of peat deposit, which provides the necessary conditions for plant development. The interweaving of plant roots with peat fibers forms a strong peat base of the carpet. The layer of peat becomes an integral part of the finished turf. The penetration of plant roots into the deposit does not occur due to the high natural acidity of the lower layers of the peat deposit.

In Greenland, the Eskimos cut bricks out of peat, build a hut and cover it with snow. This house is suitable for living even during the polar winter.

A house built using peat retains heat much longer than wood or stone. In Norway, for centuries, peat covered the roofs of houses. Grass, flowers and even small trees grow on such roofs. The peat roof is very beautiful. It is durable, has good thermal and waterproofing properties. About 4-5 years ago in Ukraine began to use the roofs of high-rise buildings for private purposes. Every year in Ukraine the number of complexes with a rooftop lounge area grows.

The difference between the operated roof and the usual one is that the first one has a small slope in the range of 2-15 degrees. This decision prevents the formation of puddles after rain or in the spring, when the snow melts. Such a roof is created from several layers of material. This allows the roof to withstand heavy loads, not to collapse under the weight of the premises, furniture, greenery and people.

The first layer must be reinforced base, then laid vapor barrier and insulation, followed by a sloping floor screed, waterproofing and protective-separating layer. Only then does the roof appear on the coating in the form of soil with peat, non-slip tiles, wood, etc. (Fig. 3).

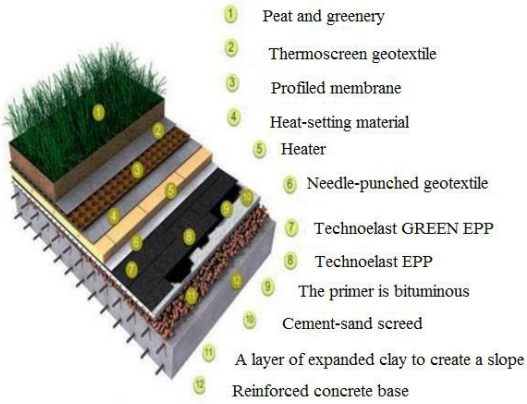

Fig. 3. The structure of the "green roof"

As the operated roof bears a significant load, in the process of its creation only durable and high-quality building materials are used. Otherwise, the roof will collapse and will not be able to withstand the constant impact of negative factors such as snow, rain, heat, etc. According to the type of roofing, the roof can be divided into 2 types for further use. Inversion - it has a layer of waterproofing located under the insulation. This option is suitable for those projects where plants are planned to be planted on the roof. As an additional layer, builders also use a drainage profiled membrane, fertile and filter layer. This promotes the full growth of flowers, shrubs and trees, and also protects the roots from the effects of changing weather. The second variety is traditional. In this operated roof, the waterproofing layer is located directly above the thermal insulation layer. This type of roof is easier to implement. It also does not require specific maintenance.

From certain types of peat, which are on the territory of Ukraine and meet certain requirements, which are given in table 1, it is possible to receive organic fertilizers, fuel, peat litter, heat-insulating plates, fodder yeast, activated carbon, metallurgical fuel, mining wax.

Table 1

Requirements for peat as a raw material for the manufacture of various products [1]

№	Type of products	Lowland peat	Horse and transitional peat
1	Fertilizer	R – from 15% A^c– to 35% CaO– from 10% P_2O_5 – from 1%	R – from 15% A^c– from 35%
2	Fuel	R – 10% and above A^c– to 35%	R – from 20% A^c – to 23%
3	Mountain wax	All types of peat Ac– to 10%, R – from 30%, the main criteria are the content of gasoline bitumen – 5%	
4	Yeast	-	R – from 35% A^c– to 6%
5	Activated carbon	-	R – from 35% A^c– to 6%
6	Litter	All types of peat R – from 15% - 20%, A^c– to 15%	
7	Pots and packing material	All types of peat R – from 10% to 25%, A^c– to 15%	

Unfortunately, in the presence of such diverse peat raw materials, over 80% of Ukraine's peat, regardless of its properties, is burned, while in the world more than 80% of peat is used in agriculture as a source of humus (Fig. 4) [1].

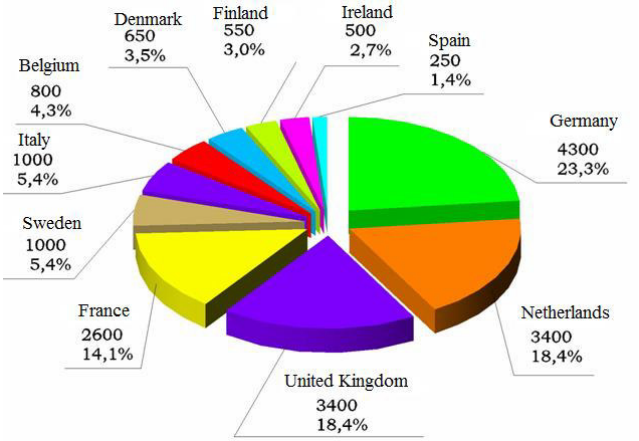

Fig. 4. Consumption of agricultural peat in Western Europe (thousand m^3). A total of 18,450,000 m^3

Peat is a complex polydisperse multicomponent system; its physical properties depend on the properties of individual parts, the relationships between them, and the degree of decomposition or dispersion of the solid part [10]. Weakly decomposed peat is an excellent filtering material and highly dispersed is used as an anti-filtration material. Peat absorbs and retains significant amounts of moisture, ammonia, cations (especially heavy metals).The filtration rate of peat varies within several orders of magnitude. Due to the variety of peat-forming plants and a wide range of peat accumulation conditions, the composition and properties of peat vary widely.

Conclusions

Areas of peat use are extremely diverse. The structure of peat resources, types of deposits and types of peat make them promising to use for different directions.

The future of intensive technologies for the use of peat in horticulture, horticulture, floriculture, balneology, production of peat carpets, plant and animal growth stimulants [2], rust converters, dyes, adsorbents for various purposes.

Analyzing the directions of peat use in the world, it is recommended that Ukraine pay attention to the introduction and use of alternative areas of peat.

References

1. **Moshynskyi, V.S.,Solvar, L.M., Semeniuk, V.V., Kucheruk, M.O.** (2018). Technology of production and processing of peat at enterprises of the Rivneregion. Petroşani, Romania: Monograph: «Resource-saving technologies of raw-material base development in mineral mining and processing». UNIVERSITAS Publishing. P. 34-52. Retrieved from http://ep3.nuwm.edu.ua/18346/1/2%20Moshynskyi%20VS%20%281%29.pdf

2. **Bodnaryuk, T.S**. (2008). Use of peat and peat deposits. Part 1. Rivne. 174 P.

3. **Saranchuk, V.I., Ilyashov, M.O., Oshovsky, V.V., Biletsky, V.S**. (2008). Fundamentals of chemistry and physics of combustible minerals. Part II . Donetsk. Oriental Publishing House. 640 P. Retrieved from https://uchebnik-online.net/book/769-osnovi-ximiyi-i-fiziki-goryuchix-kopalin-chastina-ii-posibnik-saranchuk-vi-ilyashov-mo-oshovskij-vv-bileckij-vs/ 6-8-torf-i-vugillya.html

4. **Semenyuk, V.V., Kucheruk, M.O**. (2020). Environmental justifications for the use of peat. Kazakhstan, Karaganda: International scientific-practical on-line conference "Integration of science, education and production - the basis for the implementation of the Plan of the Nation" (Sagin readings №12). KarSTU.P. 780-783.

5. **Kucheruk, M., Strikha, V., Kirichik, I.** (2017). Ecological prospects for the use of peat carpets in the development of peat deposits. Kryvyi Rih: II International Scientific and Technical Internet Conference "Innovative Development of the Mining Industry". P. 53.

6. **Vozniuk, S.T.,Moshinsky, V.S.andother** (2017). Peatland resource of the North-Western region of Ukraine. NUVGP, Rivne.91 P.

7. **Malanchuk, Z.R., Gavrish, V.S., Strikha, V.A., Kirichik, I. M**. (2013). Technologies of open pit mining. NUVGP, Rivne. P. 255-277.

8. **Inshekov, E. M., Chernyushok, L. M.**(2012). Peat as an alternative source for thermal energy, on the example of the paper industry. Kyiv: Sustainable energy development. Technical University of Ukraine "Kyiv Polytechnic Institute named after Igor Sikorsky". P. 240-246. Retrieved from http://en.iee.kpi.ua/files/2012/240-246.pdf

9. **Curly, V. P**. (2003). Phytomelioration: textbook. Lviv: Svit. 540P.

10. **Gray M.** Peat resources of Ukraine: current state, prospect of use. Economic and social geography. Scientific Notes № 1. pp. 88-85, (2012).

https://doi.org/10.31713/m1005

MONITORING OF THE BENCHES AND SIDES STABILITY OF THE QUARRIES

Nizametdinov F.K.
Karaganda Technical University, Professor, Doctor of Technical Sciences, Professor, Department of Mine Surveying and Geodesy, Kazakhstan

Ozhigin S.G.
Karaganda Technical University, Professor, Doctor of Technical Sciences, Vice-rector on scientific work, Kazakhstan

Nizametdinov N.F.
Karaganda Technical University, Ph.D., Candidate of Technical Sciences, Senior Lecturer, Department of Mine Surveying and Geodesy, Kazakhstan

Oralbay A.O.
Karaganda Technical University, Doctoral student, Department of Development of mineral deposits, Kazakhstan

Abstract. The increase in the volume of opencast mining is facing the main problem of ensuring the stability of the open pit slopes on the planned contour. To achieve this goal, required reliable geomechanical support of the parameters of the slopes of quarry benches and sides, then placing them on the planned contour using special technological schemes of the slopes and constant instrumental monitoring of their condition in an automated mode. The main emphasis in the work has been given to the method of instrumental monitoring of the quarry's arrays state using modern instruments with the analysis of their measurement's accuracy. The approved instrumental methods of monitoring at the open-pit mines of Kazakhstan are presented.

Introduction

Forecasting and ensuring the stability of the slopes of quarry benches and sides is one of the most important tasks in open pit mining. When taking into account the factors affecting the stability of open pit slopes, it is necessary to know: the type of deformations, the activity of the destruction process, the frequency of disturbance, the parameters of landslide or collapse, the nature of the slope destruction, the characteristics and conditions of rocks bedding, the duration of the development of deformations, the nature and configuration of the sliding surface. Information of this kind of breaches is impossible to obtain without systematic instrumental surveying monitoring, which serve as the most reliable basis for predicting the state of stability of quarry slopes [1-5].

The main requirements for the production of surveying monitoring of the condition of slopes in open pits are set out in the methodological guidelines [6,7]: systematic visual inspection of the slopes condition, simplified short-term surveying monitoring with intensive development of ledges deformations of slopes in individual sections or sides of the open pit, high-precision instrumental monitoring along profile lines along the deformations development of the open pit sides, surveying for the certification purpose of landslides and collapse of benches, systematic surveying control over compliance with the planned parameters of the benches and sides slopes.

Much work on improving the methods of instrumental monitoring in different years was carried out by Kazakhstani scientists: Popov I.I., Okatov R.P., Baklanov E.V., Nizametdinov F.K., Ozhigin S.G. [8,9] and others. It is proposed to transfer the elevation from one ledge to another by geometric leveling with an inclined sighting beam, for this E.V. Baklanov [5] developed a leveling attachment to be worn on the lens barrel. The methods of instrumental monitoring along the profile lines with the use of a light range finder, photogrammetric survey, electronic total station and a laser scanner have been tested in open pits [12-15].

Employees of the SPMU Research Center (St. Petersburg, Russia) have developed a number of laser devices that can be successfully used in mine surveying and geodetic works in open fields. An example is a small-sized laser attachment for telescopes of theodolites and levels, designed for prompt transfer of theodolite or

level to the mode of operation of a laser pointer, laser theodolite or level [3,11].

The disadvantages of the methods for the instrumental surveys production performed by traditional mine surveying tools are the laboriousness of field and office work, the inability to fully cover the monitoring of inaccessible and dangerous places on the slopes of the quarries ledges and sides, the inexpediency of setting up and carrying out work on monitoring stations on short-term existing work sites and steep slopes of working benches, the difficulty of surveying the surface of the landslide massif, as well as the large amount of time spent on observing objects with a height difference of up to 200m and more.

Based on the analysis of literary sources on instrumental control over the state of stability of the near-sides massifs of open pits, it can be concluded that in the development of deposits the organization of systematic mine surveying instrumental monitoring should be given paramount priority.

Analysis of the methods of instrumental monitoring of the quarry slopes state and the accuracy of their measurements (Table 1) shows the need for their further improvement using modern measuring instruments and their combination: an electronic total station, a laser scanner, radar interferometry, global satellites of systems and information processing technologies.

Table 1

Methods of survey with root-mean-square measurement errors

№	Mine survey method	Distance from reference to working marks, m	RMSD for determining the position of points, m	
			in plan $m_{x,y}$	in height m_z
1	Total station	100	0,250	0,020
2	Geodetic monitoring along profile lines and leveling of the III class	100	0,010	0,002
3	Phototheodolite with graphomechanical image processing	100	0,030	0,010
4	Method of convergent phototheodolite survey with differential determination of point offsets	100	0,008	0,004

5	Air stereophoto-grammetric method with graphomechanical processing	100	0,030	0,030
6	Aerial photogeodetic with analytical processing of images	100	0,007	0,011
7	Laser scanning	100	0,050	0,050
8	Interferometry: satellite ground	1 Pixel	0.500 0.001 0,050	0.500 0.001 0,050
9	GPS: static kinematics	100	0.010 0.020	0.010 0.020

1 The basics of creating automated monitoring system of the open pit slopes stability

The existing experience of instrumental mine surveying monitoring of the state of stability of the open pits near-sides massifs in the deposit fields of Kazakhstan by the Karaganda school of geomechanics and mine surveyors made it possible to develop and implement a high-performance monitoring technique using modern electronic equipment (Fig. 1).

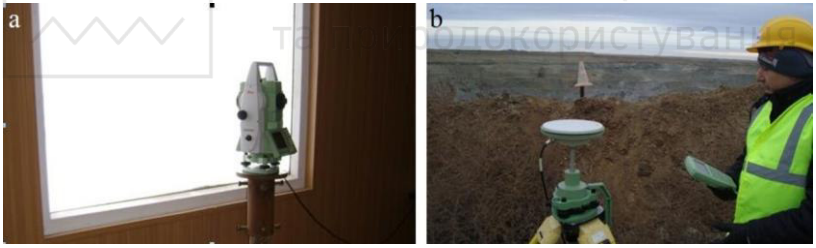

Fig. 1. Modern technologies of high-precision monitoring at quarries:
a - an automated monitoring point with an electronic total station;
b - monitoring using GNSS

To study the state of the near-sides massifs in open pits, innovative methods of instrumental monitoring using electronic total stations, GPS systems, a mining laser scanner and a ground penetrating radar were used.

Based on the tasks and functions of managing the stability of quarry slopes in the development of mineral deposits characterized by the diversity and variability of the geological structure, it is necessary to constantly conduct research aimed at obtaining reliable information about the structural features of the near-sides massif,

its strength properties, hydrogeological conditions, etc. Such studies should be carried out at all stages of the formation of slopes of open pits benches and sides (construction of a quarry, development of the planned capacity, the beginning of the design of stationary sides of a quarry on the limiting contour, completion of a quarry) within a single system. The criterion for the correctness of previously adopted technological solutions for the parameters of open pit slopes is high-precision instrumental control over the condition of the open pits and dumps sides, therefore it must also be included in the unified system of mine surveying and engineering-geological research. As a result of comprehensive studies, it is possible to assess and predict the geomechanical processes occurring in the near-sides massifs and develop recommendations on the parameters of open pit slopes in order to improve the efficiency and safety of mining operations. Based on the aforesaid, this system can be characterized by a single name - geomechanical monitoring.

Geomonitoring should include:

- obtaining complex engineering and geological characteristics of the composition and physical and mechanical properties of rocks in open pits, dumps and their foundations for calculating the stability and predicting the reliability of managing the state of the rock mass;
- study of the structural and tectonic features of the being developed deposits for calculating the stability of open pit slopes and managing the state of the near-sides massifs;
- study of the development dynamics of geomechanical processes in open pits and dumps slopes for the development of anti-deformation measures;
- engineering-geological and geomechanical complex of works for the study, forecast and control of the state and properties of open-pit and dump massifs, which makes it possible to control the parameters of open-pit slopes during the design, construction, operation and liquidation period, as well as ensuring the industrial and environmental safety of mining operations;
- substantiation and development of an effective technology and methodology for integrated monitoring of opencast mining;

- recommendations for the operational change of the technological schemes' parameters of open-pit and dump sides elaboration and their development;

- substantiation of measures and technical solutions to ensure the safety of mining operations, their technical and economic efficiency.

2 Instrumental control over the state of quarries massifs stability

The main requirements for the production of mine surveying monitoring of the slopes condition in open pits are set out in the instructions of VNIMI [6]. In accordance with it, in open pits it is necessary to carry out a full range of measures for instrumental control over the condition of the slopes of the open pits' benches and sides.

2.1 Monitoring of the open pit sides displacement using an electronic total station

The use of an electronic total station for instrumental monitoring (Fig. 2) makes it possible to determine the position of the working benchmarks in space and build a picture of the vector displacement of the benchmarks taking into account time. In this case, it becomes necessary to determine the magnitudes of errors that arise during measurements.

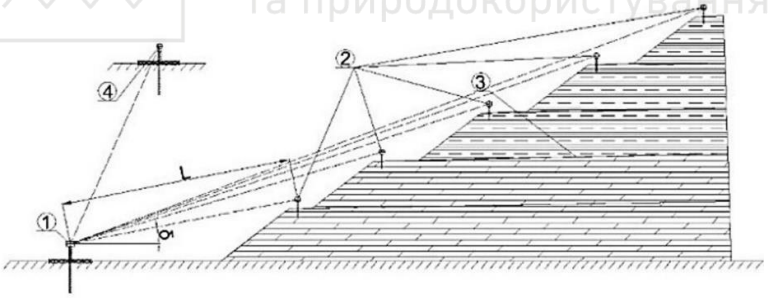

Fig. 2. Surveying the position of the working benchmarks from the support pylon: *1* - electronic total station mounted on a support pylon; *2* - working benchmarks with optical prisms; *3* - open pit side; *4* - orientable support pylon; *L* - the distance to the observed reflector; *δ* - tilt angle up to the observed working benchmark

The accuracy of the transmission of an elevation mark by an electronic total station is determined by the error in calculating the excess by trigonometric leveling according to the formula, mm

$$m_h^2 = L^2 \cos^2 \delta \frac{m_\delta^2}{\rho^2} + m_L^2 \sin^2 \delta + 2m_V^2, \quad (1)$$

where m_δ, m_L, m_V - the root mean square errors of the vertical angle, distance and height of the instrument and reflector.

The first term on the right side is the excess error due to the error in measuring the vertical angle δ not exceeding 45°. Errors in determining the excess at vertical angles of 15°, 30°, 45° have almost the same value at a distance of up to 500 m, therefore, during measurements it is necessary to maintain this value.

The error of the planned position of the working benchmarks is determined by the formula, mm

$$m_p^2 = \frac{m_\beta^2}{\rho^2} L^2 + m_L^2 + m_C^2 + m_F^2 + m_{ID}^2, \quad (2)$$

where m_β - the error in measuring the horizontal angle; m_L - the error in determining the distance; m_C - centering error; m_F - the error of fixing the reflector; m_{ID} - initial data error.

The error in fixing the reflector to the working benchmarks depends on the performer, which necessitates the use of rigid plumb lines to center the reflector over the benchmark. In this case, the reflector can be installed with an accuracy of ±0.5 mm. The laser centering error of the total station is ±0.5 mm.

The analysis of the methods for determining the benchmarks position showed that when using the method of double polar intersection and linear-angular intersection, the results are practically the same and both the first and the second methods can be used. The error in determining the position of the working benchmark by the method of polar coordinates, taking into account the influence of all components, will be equal to m_p=±4.1 mm. The calculation of the expected error was made for the working benchmark, located at a distance of 500 m from the reference one, and the angles were measured at three steps. Knowing the errors in determining the excess and the planned position of the working benchmarks, it is possible to calculate the total error of the benchmark position when measured with an electronic total station, which will be M_{tot}=±4.9 mm.

Compliance with this condition in determining the position of the initial benchmarks in current and prospective systematic monitoring allows for a unified approach and the same measurement accuracy.

2.1.1 Instrumental monitoring schemes

For high-precision instrumental monitoring using an electronic total station, schemes have been developed for conducting monitoring along a profile line for working benchmarks from reference and tie points, which allow to ensure the required accuracy under various mining and technical conditions of field development (Fig. 3,4,5).

Fig. 3. Monitoring scheme along the alignment

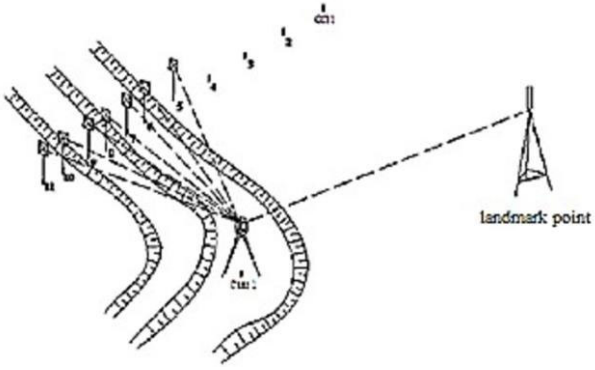

Fig. 4. Monitoring scheme from tie points

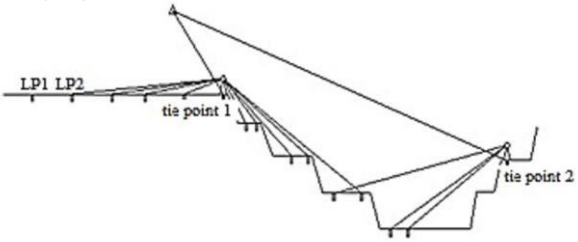

Fig. 5. Monitoring scheme from the opposite side of the quarry

When carrying out systematic instrumental monitoring in open pits, one of the important conditions for fast, accurate and error-free work is the development of a unified scheme for binding and orienting the reference and tie marks of profile lines for the operator of an electronic total station and a scheme for the location of working marks relative to reference points for mine surveyors with reflectors.

A method is proposed for monitoring the state of the quarries mass by placing a benchmark with a reflecting plate in the slope, using the technology of pulse measurements based on the reflectionless function of an electronic total station.

For this method, monitoring scheme has been developed, where the working benchmarks are located along the entire length of the profile line, and the reference benchmark at the base of the quarry or on the opposite side of the quarry in the alignment of the working benchmarks, taking into account the angle of sight on the plates not more than 30°.

It was revealed that at small angles of incidence (from 0° to 30°), the error does not exceed the permissible measurement accuracy with a reflectorless total station.

2.2 Monitoring of the quarries massif displacement using a laser scanner

The essence of terrestrial laser scanning (TLS) (Fig. 6) is to measure at a high speed the distances from the scanner to the points of the object and register the corresponding directions (vertical and horizontal angles), therefore, the measured values during terrestrial laser scanning are the same as in operation with electronic total stations. However, the principle of total shooting of an object, and

not of its individual points, characterizes the TLS as a survey system, the result of which is a three-dimensional image, the so-called scan.

Fig. 6. Mining Laser Scanner

The system for terrestrial laser scanning consists of an TLS and a field personal computer with specialized software. The TLS consists of a laser rangefinder adapted for high frequency operation and a laser beam sweep block.

The spatial coordinates of the object points in the TLS coordinate system are calculated by the formulas

$$X=R\times\cos\varphi\times\sin\theta;\ Y=R\times\sin\varphi\times\sin\theta;\ Z=R\times\cos\theta \quad (3)$$

where R - the measured distance from the point of the scanner to the object; φ - the horizontal angle of the measured direction of the laser beam R; θ - the vertical direction angle R, measured from the Z-axis to the vector R (zenith distance of the laser beam direction).

The procedure for performing measurements with a laser scanner is produced in the following sequence:

- install a laser scanner over the reference point with known coordinates;
- centered on a point using an optical plummet;
- leveling the device due to the built-in electronic compensator, which significantly increases the leveling accuracy;
- carry out the adjustment of the laser scanner using a field tablet with special software;
- input atmospheric corrections, taking into account pressure, air temperature and relative humidity (for high-precision measurements of distances, the atmospheric correction must be determined with an accuracy of 1 ppm (1 mm per 1 km), air temperature - with an

accuracy of 10°C, atmospheric pressure - up to 3 mbar, relative humidity - up to 20%).

- input name and coordinates of the scanner position, tool height, name and coordinates of the scanner orientation point;

- perform orientation of the device;

- enter the program measurement mode, where the scanning area of the device is selected and the measurement is started.

To organize instrumental monitoring at a quarry, it is necessary to decide the following:

a - select potentially unstable or landslide areas based on the analysis of engineering-geological and mining-technical conditions of development to determine the scanning sites;

b - to take out the reference points of the monitoring stations in nature and lay the benchmark;

c - to carry out the binding of reference points (determination of coordinates *X*,*Y*,*Z*) to the nearest points of the mine surveyor geodetic reference network;

d - make a laser scan of the selected area;

e - process the results of laser scanning and analyze them.

The obtained volumetric electronic version of the quarries massif is processed on a computer in order to obtain the parameters of the occurrence of cracks and discontinuous breaches: angles of incidence and strike, the sizes of structural blocks formed by cracks, as well as comparison of the digital model (Fig. 7) when scanning the same section of the quarries massif repeatedly.

The data acquisition module is responsible for collecting data in real time, monitoring measurements and measuring cycle, checking the permissible values of monitoring displacements.

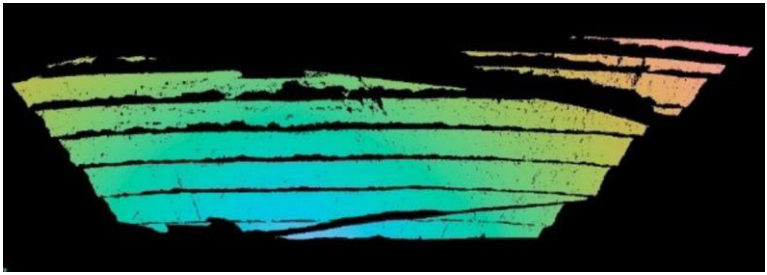

Fig. 7. Checking the presence of collapses of the investigated part of the quarry boards using a digital model

The received data analysis module is responsible for the analysis of the measured data, reporting, editing and post-processing. Results can be presented in digital and graphical form with soundtrack.

2.3 Monitoring of the quarry sides displacement using global navigation satellite systems (GNSS)

The application of methods for determining the position by GNSS signals for mine surveying and geodetic purposes in Kazakhstan began in 2000. During the period of their use, significant advantages were revealed in comparison with traditional mine surveying methods. These include a wide range of accuracy, independence from weather conditions, time of day and year, from mutual visibility between benchmarks, high automation, the ability to work continuously and in motion.

At the same time, the use of satellite methods in practice revealed a number of disadvantages: dependence on obstacles, vulnerability to radio interference, expensive equipment, but especially the need to adjust the theory and practice of mine surveying to observe the movement of slopes along profile lines.

In this regard, to improve the efficiency of the mine surveying application of GNSS in open pits, the following tasks must be solved:

- study GNSS measurement errors and develop methods for their reduction;
- to develop a methodology for monitoring the deformations of the quarry sides with modern mine surveying instruments;
- to improve the design of GNSS receivers to reduce measurement errors when observing the quarry sides.

At most mining enterprises, where deformations are measured at monitoring stations for fortified objects, there is a difficult or poor-quality reception of satellite radio signals. The main unfavorable factors in this case will be electrical noise, shadow effect from the slope and limited visibility to satellites. The unfavorable effect of electrical noise can be excluded even at the design stage of the monitoring station, in this case it is necessary to avoid laying working and reference benchmarks closer than 25-50 meters from power lines, transformer substations and the contact network of

electric transport. GNSS receiver errors depend on its installation and centering.

When observing the movement of slopes along profile lines in open pit mines, the error of the user signal can be reduced due to the correctly selected measurement technique.

The results of measurements in the "kinematics" mode to study the effect of "multipath" on the measurement accuracy at different positions in height showed that when measuring in the kinematics mode, the measurement accuracy decreases by 25% with increasing tripod height. The use of a metal disk when measuring in the kinematic mode increases the horizontal measurement accuracy by 17%, in the *X*-axis by 27%, in the *Y*-axis and in height by an average of 36%.

It should be noted that the use of a satellite geodesy complex for observing the process of displacement of the earth's surface at mining enterprises makes it possible to conduct research at a qualitatively higher level. The measurements carried out by the GNSS complex have shown high efficiency for solving the problems of geomechanics, thanks to its use, it became possible to regularly monitor deformations and stresses occurring in the earth's crust.

According to the data obtained from the study of the influence of the "shadow effect" on the accuracy of GNSS measurements, it can be concluded that the measurement error increases when moving to the slope. Knowing the height of the slope and the permissible distance from the slope, it is possible to derive the formula for the permissible position of the working benchmark for planned and altitude determination

$$m_{perm}=0{,}292\times H, \quad (4)$$

where H - the slope height, m.

This formula should be used when planning the laying of monitoring lines for the displacement of slopes using GPS systems.

2.4 Monitoring of the quarries sides displacement using the GeoMoS system

The GeoMoS system controls sensors in a fully automatic mode, at a great distance from the data collection and processing site. The automated system allows high speed measurement cycles and eliminates human error. The operator is required to conduct a qualitative analysis of the results in order to select the necessary

monitoring means, their location and connection into a single network.

Having constantly updated parameters of the observed object, it is possible with a high degree of reliability to make forecasts of its state, to prevent possible accidents.

The system consists of two software subsystems - Monitor and Analyzer. Monitor (Fig. 8) is responsible for real-time data collection, control of measurements and the measurement cycle, validation of acceptable values, monitoring of messages.

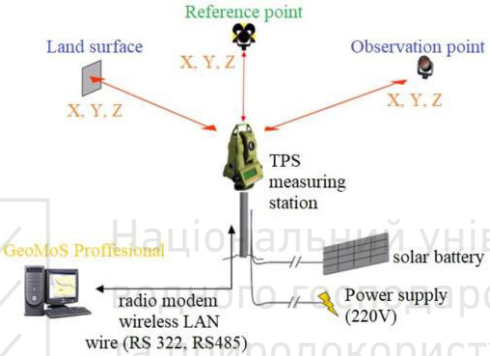

Fig. 8. Measuring cycle principle of the Monitor subsystem

The Analyzer is responsible for analyzing the measured data, reporting, editing and post-processing. Data and results can be presented numerically and graphically, as shown in Fig. 9, and exported in various standard formats.

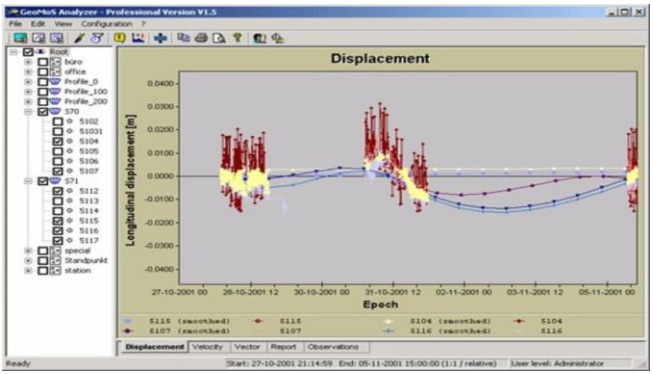

Fig. 9. Graphical and numerical presentation of measurements and results of the Analyzer subsystem

The hardware component of the GeoMoS monitoring system is various data collection devices: total stations of the TPS1200, TPS1800 and TPS2003 series; GPS System 500; meteorological sensors.

The device is located in the measuring booth, which is designed to protect the instrument (Fig. 10).

Fig. 10. GeoMoS monitoring station

The results of the Analyzer system are: displacements (longitudinal, transverse), displacement velocities, displacement vectors (in plan and height).

The measuring booth must be equipped with climate control for the smooth functioning of the system. Climate control is important to avoid extreme temperatures, humidification and condensation.

Main technical characteristics of the GeoMoS system:

- modular configuration from one to several stations;
- the ability to connect and combine a large number of measuring stations into one system;
- remote access to work and change settings;
- messages about the current state of the system (exceeding critical displacements of the object, lack of power, hacking or destruction);
- modeling the meteorological net around the measurement object;
- recording the changes made during editing and post-processing;
- parallel use of several devices (total stations, GPS, metrological and geotechnical sensors);
- automatic regulation and synchronization of data reception via cable, radio modem, LAN, WAN or via the Internet;

- the ability to measure distances over a long range (up to 5 km);
- a powerful set of tools for graphical and digital data analysis;
- transmission of messages by e-mail or digital interface;
- import-export to other systems (ASCII, DGN, WMF, Excel);
- support for large databases with an interface (SQL-Server);
- data archiving.

The position of the initial benchmarks in the created monitoring system must be determined either by a double polar intersection, or by a linear-angular intersection from the reference survey-geodetic network points. All measurements with an electronic total station, in order to improve accuracy and eliminate gross errors, should be performed in 3 steps. Acceptance of measurement includes one aiming at a reflector, in which several readings are taken. The weighted average value of the measurements is taken as the final result, while the difference between individual readings should not exceed ±2 mm.

Compliance with this method of determining the position of the initial benchmarks in the conditions of current and future systematic monitoring allows you to have a unified approach and the same accuracy of the work performed.

3 Implementation of geomonitoring systems for quarries massifs in Kazakhstan

In 2008, on the basis of geomechanical research of the quarries and dump massifs of the Sarbaiskiy (Fig. 11), Sokolovskiy and Kacharskiy open pits, projects of monitoring stations were developed for the state of stability of their quarries and dumps sides, and in 2013 monitoring stations were laid at the “Kurzhunkolskiy” open pit.

Fig. 11. Instrumental control of the western side of the “Sokolovsky” quarry

The projects consider the issues of creating a geomonitoring system based on instrumental surveying and geodetic monitoring of displacements and deformations of massifs according to the established benchmarks of the monitoring stations profile lines using an electronic total station and GPS receivers of a satellite positioning system.

The selection of sites for laying benchmarks of monitoring stations was made based on the analysis of the geomechanical situation in the open pits. The design and length of the profile lines have been determined. The design of monitoring and control points, reference and working benchmarks of profile lines has been developed.

The total number of profile lines of the "SSGPO" JSC open pits geomonitoring system is 41, including for open pit mines: Sarbaisky - 10 profiles, Sokolovsky - 15 profiles, Kacharsky - 16 profiles. The total number of benchmarks - 1728 pieces, of which reference benchmarks - 50 pieces, including for quarries: Sarbaisky - 575 benchmarks, of which reference - 14, Sokolovsky - 397, of which reference - 16, Kacharsky - 756 benchmarks, of which support -20.

The objects of Zhairem GOK include the Ushkatyn-III, Zhairem, Zhomart deposits, which are mined by open pits: Ushkatyn-III, Zapadny, Dal'zapadny open pit №1, Dal'zapadny open pit №2 and Zhomart.

Based on the analysis, in 2002, nine monitoring stations were established at the open pits of the Zhairem GOK. For example, the barite-lead part of the Ushkatyn-III open pit is currently in a state of temporary conservation. Special slope making measures were not carried out on the side of the open pit, therefore, to establish their feasibility, a monitoring station I was established. The analysis of the geomonitoring results of the quarries massifs state of the Zhairem GOK, carried out at nine monitoring stations for four years (2002-2005), showed that the deviations of the coordinates of the working benchmarks from their initial position are within the measurement accuracy. There are some local deformations of the benches slopes in the open pits, while the deformations of the sides are not generally established.

Based on the studies carried out in 2018 in certain areas of the quarries massifs of the "Vasilkovsky" open-pit mine (Fig. 12), where the mining depth reached 260 meters, the following conclusions were made: the upper clay slopes of the ledges are fairly reliably beveled,

in the weathering crust's middle part the slopes of the ledges are folded semi-rock breeds and special slopes making works were not produced (there are individual local rock falls and overhangs), and the lower slopes of the ledges, composed of rocky breeds, are set using the technological diagrams of the slopes making and look quite reliable from the point of view of stability. The concern here is caused by the quarry's massifs, complicated by tectonic faults and, according to the falling fractures, diagonal to the slope.

The stability assessment of the anisotropic slope of a 30 m high ledge with an inclination angle of 65º at 85 m horizons of the southern side of the open pit was carried out. The initial geometric base (elements of occurrence of cracks and discontinuous breaches from the mirror sliding surface) was obtained by scanning with a laser scanner. Average values of the parameters: the strike azimuth of the fault (A) 249º and the angle of inclination (δ) 43º, and the fractures A=179º and δ=87º, and the azimuth of the strike of the slope A_{slope}=285º.

Fig. 12. Laser scanning in the "Vasilkovsky" quarry with the HDS 8800 mining scanner

Knowing the geometrical parameters of the slope and calculating the parameters of the collapse prism, it became possible to determine the strength characteristics: adhesion along a fault, equal to 2.5 t/m^2 and ρ″=20º, and along a breaking crack: adhesion 5.5 t/m^2 and ρ″=23º. The obtained strength characteristics were used to assess the stability of a neighboring rock block of a similar nature, which showed that the safety factor is equal to: 5.90 at a bench slope height of 30 m and 2.90 at a bench slope height of 60 m. This indicates its stable

state, according to the methodological instructions [7]. Inspecting the slope surface according to laser survey data in this area, it can be argued that other possible weakening surfaces do not affect the stability of the rock mass, and the previously assumed crack is not detected.

Data processing of the obtained monitoring results at the Kentobe iron ore quarry, changing in the lengths of the intervals between the benchmarks, i.e. horizontal spacing *dS* between the benchmarks relative to the initial values, the offset of the benchmarks relative to the reference marks at each station (ΔL). From these displacements, one can judge the presence of displacements of the quarries massif, composed of clay deposits. The deformation of the massif is confirmed by the presence of vertical displacements at station "*A*" within -10 mm; at station "*B*" is -29 mm, and at station "*C*" within -26 mm. The array also shifts along the coordinates ΔX, ΔY relative to their original position.

Conclusions. Thus, forecasting and ensuring the stability of the benches and the sides slopes of the quarries is one of the most important tasks when conducting open pit mining. At the same time, special attention is paid to the creation of a system of integrated instrumental control over the state of the quarries massifs in open pits, and systematic monitoring allows:

- in a constant mode to receive operational information about the processes occurring in the rock mass;
- send signals about an increase in deformations to all the main services of the enterprise;
- promptly develop measures to prevent landslides and emergencies;
- to determine the frequency of instrumental surveying monitoring according to the data of the displacement of the profile lines reference marks.

Therefore, the work considers the existing digital measurement technologies to determine the displacements of the rock mass:

- the basics of creating automated systems for monitoring open pit slopes;
- instrumental control along profile lines using an electronic total station: the resulting measurement errors and the implemented monitoring schemes;
- laser scanning of the most dangerous areas of the quarries arrays with a mountain scanner and comparison of two or more digital scans;

- use global satellite systems during monitoring of benchmarks laid down along profile lines;

- implementation of the GEOMOS system complete with a robotic total station and optical prisms.

Modern methods of instrumental monitoring have been introduced and tested at the open pit of the following mining enterprises: “SSGPO” JSC, “Altaypolimetals” LLP, “Kazakhmys Corporation” LLP, “Altyntau Kokchetau” LLP, “Zhairemsky GOK” JSC, “Shubarkolkomyr” JSC, “ORKEN: Kentobe, Atansor and Lisakovsk” LLP and others.

References

1. **Fisenko, G.L**. (1965) Stability of the sides of open pits and dumps. Moscow: Nedra.

2. **Pevzner, M.E.** (1978) Fighting rock deformations in quarries. Moscow: Nedra.

3. **Galust'yan, E.L.** (1980) Management of geomechanical processes in open pits. Moscow: Nedra.

4. **Popov, I.I., Okatov, R.P.** (1980) Landslide control in quarries. Moscow: Nedra.

5. **Popov, I.I., Nizametdinov, F.K., Okatov, R.P., Dolgonosov, V.N.** (1997) Natural and man-made foundations for managing the stability of quarry benches and sides. Almaty: Gylym.

6. Rules for ensuring the stability of the sides of coal mines. (St. Petersburg, VNIMI, 1998).

7. Guidelines for observing the deformations of sides, slopes of benches and dumps in open pits and the development of measures to ensure their stability. (Approved by the MES of the RK dated 2008).

8. **Dolgonosov, V.N., Shpakov, P.S., Nizametdinov, F.K.** et al. (2009) Analytical methods for calculating the stability of quarry slopes. Karaganda: SANAT-Polygraphy.

9. **Popov, V.N., Shpakov, P.S., Yunakov, Yu.L.** (2008) Quarry slope stability management. Moscow: MGGU.

10. **Nesmeyanov, B.V., Nesmeyanova, Yu.B.** (2012) Stability of quarry walls in the course of sequential underground-open-pit development of deposits. Moscow: MGGU.

11. **Nizametdinov, F.K., Portnov, V.S., Nizametdinov, N.F.** (2007) Modern methods of instrumental monitoring of the open pit slopes state. Karaganda: SANAT-Polygraphy.

12. **Ozhigin, S.G.** (2009) Management of the stability of the rock massifs in the open pit mines of Kazakhstan. Karaganda: SANAT-Polygraphy.

13. Opportunities of Geodetic Monitoring on the Example of Current Projects in Eastern Europe. (Germany, Aachen, 2013)

14. **Nizametdinov, F.K., Ozhigin, S.G., Nizametdinov, R.F., Ozhigina, S.B., Nizametdinov, N.F., Khmyrova, Ye.N.** (XV International ISM Congress (International Society for Mine Surveying) 2013) State and prospects for the development of geomechanical support for open pit mining. (Vol. 1) Deutscher Markscheider-Verein e.V. – DMV.

15. **Galperin, A.M**. (2003) Geomechanics of open pit mining. Moscow: MGG U.

https://doi.org/10.31713/m1006

PRINCIPLES OF OPTIMIZATION OF THE FUEL AND ENERGY COMPLEX BASED ON MINIMIZING THE DESTRUCTIVE IMPACT ON THE ENVIRONMENT

Kovshun N.E.
National University of Water and Environmental Engineering, Professor, Doctor of Economic Science, Professor, Department of Finance and Economic Security, Ukraine

Moshchych S.Z.
National University of Water and Environmental Engineering, Candidate of Economic Sciences, Senior Lecturer of the Institute of Postgraduate Education, Ukraine

Malanchuk L.O.
National University of Water and Environmental Engineering, Candidate of Economic Sciences, Associate Professor, Associate Professor of the Department of Public Administration, Documentation and Information Activity, Ukraine

Kostrychenko V.M.
National University of Water and Environmental Engineering, Candidate of Economic Sciences, Associate Professor, Associate Professor of the Department of Business Economics and International Business, Ukraine

Veretin L.S.
National University of Water and Environmental Engineering, Candidate of Economic Sciences, Senior Lecturer of the Institute of Postgraduate Education, Ukraine

Summary

In the context of the social and economic crisis, the energy sector plays a strategic role in terms of Ukraine's sectorial structure: filling the budget, additional export revenues, and other economic and social benefits. However, further exploitation of existing technologies for extraction, transportation and conservation of mineral resources has a negative impact on the environment, which ultimately leads to a loss of quality of energy resources themselves.

Achieving the goals set by the Energy Strategy of Ukraine until 2035, as well as other sectorial programs, among which integration into European energy markets is important, requires large-scale modernization and reform.

The subject of the research is the methodological principles of bi-criteria substantiation of investments in energy projects, which provide for the assessment of the economic feasibility of such projects taking into account the possible environmental consequences.

The research methodology includes consideration of methodological bases of ecological regulation of national energy development in the conditions of implementation of European ecological requirements, analysis of conditions of achievement of strategic priorities of national economy development, formalization of methodical bases of substantiation of investments in energy projects using multivariate approach.

The purpose of the study is to develop an algorithm for economic and environmental justification of investments in energy projects, taking into account environmental impacts and economic interests of energy market participants.

The conducted research, in order to solve the outlined problems of the branch, requires the implementation of the proposed practical recommendations of bringing the ecological regulation of the national energy complex to the requirements of the European Energy Community.

Introduction

Ukrainian energy has significant potential for attracting investment. The investment process has an important impact on structural changes and aims to respond flexibly to changes in the volume and structure of needs and to influence the volume and structure of production in the appropriate direction [1]. However, for a long time, the industry lacked transparent, competitive and clear rules of the game for market participants, monopolies and over-regulation. This hindered the progressive development and modernization of the Ukrainian energy sector. And the system of cross-subsidization and subsidies from the budget restrained the growth of energy prices for the population, at the same time laundering huge funds, creating unequal conditions, hindering modernization and development, introduction of new technologies at fuel and energy enterprises.

The reform of the energy sector aims to bring it to a fundamentally new, high-quality level of development, bring it in line with EU norms and standards, liberalize and form full-fledged natural gas and electricity markets with transparent and competitive pricing and adequate protection of vulnerable consumers. These

actions are also designed to optimize the energy balance and increase economic, energy and environmental security.

General approaches to reforming Ukraine's energy sector have been studied by domestic scientists, international experts and institutions. At the same time, as numerous studies show, in the modern practice of diversification of sources of production and supply of natural gas from traditional and non-traditional sources, there is mostly no comprehensive approach to environmentally regulated optimization of energy projects.

The purpose of the study is to develop an algorithm for economic and environmental justification of investments in energy projects, taking into account environmental impacts and economic interests of energy market participants.

To achieve this goal, the study solved the following tasks: revealed the methodological principles of environmental regulation of national energy in the implementation of European environmental requirements, analyzed the conditions for achieving strategic priorities of the national economy, formalized the methodological principles of investment in energy projects, developed practical recommendations for bringing the environmental regulations of the national energy complex to the requirements of the European Energy Community.

The study contains elements of scientific novelty, in particular, the proposed method of environmentally regulated optimization, which is universal and is a tool for analyzing the interaction of society and nature in the implementation of production activities, which is inevitably accompanied by man-made environmental impact. The result of such an analysis is an economically and environmentally sound decision on the feasibility or inexpediency of implementing energy projects.

Environmental economic research

The rapid growth of energy consumption creates the danger of a rapid depletion of energy resources. In addition, the dynamics of world energy consumption indicates its exponential growth, which is a potential threat of increasing excessive heat emissions, which can disrupt the thermal balance of the planet and lead to catastrophic changes in its climate. Therefore, the development of national energy using the methods of environmental regulation will contribute to the

sustainable development of fuel and energy. We believe that the key element of such development is ecologically regulated optimization [2; 10].

Under the ecologically regulated optimization of the fuel and energy complex we understand its restructuring on the principles of systemic minimization of the destructive impact of energy-producing technologies on the environment and on its main element - man with the use of methods of ecological regulation.

It is clear that energy in its essence has never been and will not be completely environmentally friendly [11]. Even renewable energy sources in their large-scale application give a predictable or unpredictable, not only positive but also negative effect.

The reform of the energy sector aims to bring it to a fundamentally new, high-quality level of development, bring it in line with EU norms and standards, liberalize and form full-fledged natural gas and electricity markets with transparent and competitive pricing and adequate protection of vulnerable consumers [5; 8].

It should be emphasized that in companies that manage privatized or transferred to the management of fuel and energy enterprises, when drawing up business plans, the obligatory main section is environmental optimization, which provides a set of well-founded and certainly appropriate measures (reduction of unproductive costs, sale of non-core assets , increasing productivity, etc.). However, companies tend to ignore the increase in the cost of environmental measures, and in some cases even allow them to be reduced to reduce production costs. Therefore, the signing of Ukraine's association agreement with the EU and the long-term task of achieving full membership in it should put an end to such environmentally destructive and harmful to society approaches in public fuel and energy management and business by Ukrainian fuel and energy entities [12; 13]. Without taking into account the environmental component, it is impossible to hope for real integration with the European Union. Therefore, environmentally regulated optimization as an approach to management in the fuel and energy sector should become dominant at all levels - national, regional, level of the business entity.

Economic and environmental levers must be mutually taken into account and balanced. No effective economic solution should be

considered without taking into account the possible environmental consequences [6]. Only such an approach to the functioning and development of fuel and energy will ensure socio-economic and political stability in the country. The proposed method of environmentally regulated optimization of fuel and energy involves the use of multifactor analysis of production processes (technological, environmental, economic, socio-political) with the obligatory dominance of the environment (production, which results in irreversible negative environmental changes, have no right to exist; or liquidation in general, fundamentally new productions should not initiate the creation of new, not previously fixed and technologically uncompensated environmental problems).

The management practice of diversification of gas supply sources in the context of ensuring Ukraine's energy security and reforming its energy markets is considered on the example of the gas production market. Proven reserves of traditional gas allow keeping annual production in the range of 20-23 billion cubic meters with a tendency to insignificant growth (subject to investment). According to the United States Agency for International Development (USAID), in the case of the development of Ukraine's fuel and energy sector while maintaining current trends and government policy, moderate investment in the gas industry will increase traditional gas production to 23.5 billion cubic meters in 2025 and 25.7 billionm^3 in 2030. The main increase in natural gas production in Ukraine in the future, according to USAID, can be achieved due to non-traditional types of gas, which in Ukraine include gas of dense rocks; shale gas; methane from coal deposits. Note that the exploration of these types of gas in Ukraine is at an early stage, none of these types is still being extracted. Due to the lack of accurate geological data on the reserves of unconventional gas, there is still significant uncertainty about the possible volume and cost of unconventional gas production.

Taking into account the method of ecologically regulated optimization, we will analyze the possibility of extracting in Ukraine the most realistic in terms of available technologies varieties of unconventional gas - the so-called gas of dense rocks and shale gas. On the territory of Ukraine, two promising regions with deposits are considered: dense gas Dnieper-Donetsk (Eastern Ukraine) and shale

gas Lublin (Western Ukraine) with reserves of 1.4 trillionm^3 and 4.2 trillionm^3, respectively.

Analysis of the specifics of dense gas and shale gas in terms of technological, environmental, economic factors leads to the conclusion that there is a significant environmental risk of extracting this energy at the current technological level and the lack of convincing arguments for greater economic efficiency compared to traditional gas.

However, the curtailment of work to prepare for unconventional gas production in 2015 took place not only in Ukraine but also in other European countries, where such work was carried out: in Poland, Lithuania, Romania, Bulgaria. The list of reasons for the curtailment of work on unconventional gas in Ukraine includes the increase in 2014 of rent for gas production to 50-60%, careful public monitoring of the state of the environment [9]. However, the priority reason is the fall in world prices for energy hydrocarbons.

To formalize the understanding of attempts to transform the gas market of Ukraine, we will use the possibilities of situational analysis. Thus, the tool for transforming the gas market was investing in the production of a new energy product - unconventional gas. This process allowed meeting the needs of three parties - the government, the public, the investor. At the same time, the ecological impact on the environment was carried out, which had to be assessed in accordance with the normatively permissible levels. The end result is the extracted gas, the price of which was formed depending on the costs incurred by the investor and compared with the price level in the current market.

For formula display, enter the appropriate notation: P_v - needs of the government; P_s - the needs of society; P_i - the needs of the investor; EV_{norm} - the total environmental impact on the environment from the use of unconventional gas production technology, allowed by the standards established in Ukraine; EV_{fact} - the actual environmental impact on the environment from the use of unconventional gas production technology; C_r - the current market price for gas in the relevant market of Ukraine; These are the price of extracted unconventional gas set by the investor.

Possible options for the development of the situation with the extraction of unconventional gas are presented in the form of a matrix of situational analysis (table 1).

The study used a multivariate approach that allows you to model the layout of different situations in the process of transformation of the gas market.

And the option (optimistic) can be described as follows.

The technology of unconventional gas extraction has created an actual ecological impact on the environment not higher than the standards allowed in Ukraine ($EV_{fact} \leq EV_{norm}$).

The costs of the investor (cost of production) allow him to set a competitive price for the received unconventional gas ($C_i \leq C_r$).

The needs of the investor, the government and society regarding the extraction of unconventional gas are generally met ($P_i = P_v = P_s$).

The investor has an interest and the opportunity to plan the continuation of work on the extraction of unconventional gas and expand its market.

Table 1

Matrix of formalized situational analysis of transformation of the gas production market of Ukraine

Situation	I option (optimistic)	II option (pessimistic)	III option (unbalanced)	
			Scenario 1	Scenario 2
The technology of unconventional gas production has created an actual environmental impact on the environment	$EV_{fact} \leq EV_{norm}$	$EV_{fact} \geq EV_{norm}$	$EV_{fact} \geq EV_{norm}$	$EV_{fact} \leq EV_{norm}$
The investor's costs (production cost) allow him to set the price of unconventional gas	$C_i \leq C_r$	$C_i \geq C_r$	$C_i \leq C_r$	$C_i \geq C_r$
The needs of the investor, the government and society regarding the extraction of unconventional gas	$P_i = P_v = P_s$	$P_i \neq P_v \neq P_s$	$Ps \neq Pi$ $Ps = Pv$ $Pv \neq Ps$	$Pv \neq P_s$ $P_v = P_s$

Source: compiled by the authors

II option (pessimistic) can be described as follows.

The technology of unconventional gas extraction has created an actual ecological impact on the environment above the standards allowed in Ukraine ($EV_{fact} \geq EV_{norm}$).

The costs of the investor (cost of production) do not allow him to set a competitive price for the unconventional gas ($C_i \geq C_r$).

The needs of the investor, the government and society regarding the extraction of unconventional gas are not met ($P_i \neq P_v \neq P_s$).

The investor has no economic interest in continuing to produce unconventional gas.

Option III (unbalanced) can be described in two scenarios as follows.

Scenario 1: the technology of unconventional gas production has created an actual environmental impact on the environment above the permitted standards in Ukraine ($EV_{fact} \geq EV_{norm}$).

At the same time, the investor's costs (production cost) allow him to set a competitive price for the received unconventional gas ($C_i \geq C_r$).

The needs of the parties are in a more complex interaction:

a - $P_s \neq P_i$ - the needs of society come into conflict with the needs of the investor; in the case of $P_s = P_v$, ie the identity of the interests of society and government, the investor is forced to increase the cost of environmental measures to reduce EV_{fact}, but this automatically leads to an increase in Qi and minimize profits.

b - $P_v \neq P_s$ (which is typical for the current state of affairs in Ukraine) - the government is forced to manipulate public opinion, to ignore it, while exposing it to the threat of a social explosion, in order to interest investors in continuing work without changing technology.

Scenario 2: the technology of unconventional gas production has created an actual environmental impact on the environment below the standards allowed in Ukraine ($EV_{fact} \leq EP_{norm}$).

At the same time, the investor's costs (production cost) do not allow him to set a competitive price for the received unconventional gas ($C_i \geq C_r$).

The options for the parties may be as follows: the investor reduces the cost of environmental needs, thereby increasing EV_{fact} (without exceeding or exceeding EV_{norms}) to achieve $T_i \leq C_r$ (to ensure

a competitive price). In the case of $P_v \neq P_s$, the government will simply not control the increase in EV_{fakt} and will allow the investor to reach a competitive price under any conditions, receiving the threat of social protests. In the case of $P_v = P_s$ by constant monitoring will be provided $EV_{fact} \leq EV_{norm}$, but the authorities will have to resort to subsidizing the sale of unconventional gas under the conditions of $C_i \geq C_r$.

Immediately note that we consider the probability of scenario 2 of option III (unbalanced) to be extremely low. Analysis of the activities of unconventional gas companies in the United States, Canada, Great Britain, and West Africa confirms in almost all cases the construction of business plans according to the situational scheme of scenario 1 of option III. That is, the investor (while partially ignoring the environmental impact) achieved a competitive price for the extracted unconventional gas, ignoring, as far as possible, public protests. The authorities acted differently in each case, but in general, for global political reasons (to assist national investors in the struggle for the world gas market), they maintained, so to speak, positive neutrality.

The trend of the Central Bank to a significant decline has made it impossible for investors to produce unconventional gas. This explains the contraction of unconventional gas production in Eastern Europe, including Ukraine, which was the result of investors' forecasting of the future situation in accordance with the second option (pessimistic).

The situational analysis (according to the proposed method of environmentally regulated optimization) of attempts to transform the gas production market of Ukraine is based on a comprehensive approach to the object of study and makes it possible to reveal the degree and direction of the main factors.

The proposed method of environmentally regulated optimization is universal. It allows you to analyze the interaction of society and nature in the implementation of production activities, which is inevitably accompanied by man-made pressure on the environment. As a result of such analysis, a bi-criteria decision can be made (according to economic and environmental parameters) on the feasibility or inexpediency of implementing certain programs, business projects, etc.

Given the technological level of fuel and energy, the total need for innovative financing (according to experts) is from 8 to 12 billion UAH annually.

Businesses will not be able to obtain such financial resources on their own without targeted foreign investment. Therefore, the problem of creating an attractive investment climate in the fuel and energy sector of Ukraine to intensify innovation processes has become especially important.

As noted by the specialists of the National Institute for Strategic Studies, to increase the investment attractiveness of the innovation market of the fuel and energy complex of Ukraine, it is necessary to perform a consistent set of measures, which are summarized in Table 2.

An objective indicator of the effectiveness of innovation in the fuel and energy sector, taking into account the requirements of environmental regulations should be the achievement of certain levels of basic indicators that characterize the efficiency of the fuel and energy sector and its impact on the environment.

As an option for a possible assessment, we offer a set of parameters listed in Table 3, formed using data from the National Institute for Strategic Studies.

Achieving these levels of basic indicators requires not only the intensification of investment activities.

Ultimately, the environmental regulation of the fuel and energy sector (as well as other sectors of the economic complex) requires the construction of a new system of relationships in the chain: central government - regional government (local government) - the business entity.

However, the dominant role of the central government in the implementation of the system of environmental regulation and control over this process objectively encountered insurmountable difficulties in the current conditions, namely: the lack of effective and objective environmental monitoring; unsatisfactory control over the implementation of state environmental programs and a formal approach to monitoring the implementation of regional environmental programs.

Table 2

Measures to create an attractive investment climate in Ukraine's fuel and energy sector

Stages	Contents of the stage
I stage - until 2025	1. Formation of a system of support for the introduction of energy technologies and management systems (stimulation of the introduction of innovative technologies), creation of a system of scientific and technical centers for technology development, research and development of energy potential (grants, scholarships, funding for study abroad).
	2. Providing financial support for basic and applied research.
	3. Approval of the methodology for estimating the cost of capital, which can be taken into account for the formation of tariffs for products and services for various sectors of the fuel and energy sector.
	4. Formation of a national network of energy technology transfer, state support of technology transfer (technology purchase), localization of energy technology production.
	5. Introduction of new specialties for the energy sector and new training programs for specialists in educational institutions in order to train staff to work in energy markets.
	6. Introduction of a system of advanced training of specialists on the implementation of energy management systems, use of renewable energy equipment.
	7. Updating the material and technical base of scientific institutions and institutions of higher education, which provide training for fuel and energy
II stage - until 2030	1. Ensuring the participation of domestic research institutions in scientific and technological programs of the EU and the approximation of Ukraine to the European scientific space.
	2. Introduction of an investment risk insurance instrument within the framework of the mechanism for supporting the implementation of innovative projects in the energy sector (Energy Development Fund).
	3. Formation of a system of support for venture activity and transfer of energy technologies, development of Ukrainian engineering companies.
stage - until 2035	1. Creation of national energy companies and support for their entry into foreign markets.
	2. Implementation of pilot projects for carbon capture and storage, processing of household waste, etc.
	3. Improving training programs in accordance with the needs of competition of Ukrainian companies in European energy markets.

Source: compiled by the authors for [4]

Table 3

Basic performance indicators functioning of the fuel and energy complex and its impact on the environment

Indicators	2015	2020	2025	2030	2035
1. Energy intensity of GDP, kg.e.n / 1 $ GDP	0,33	0,27	0,23	0,20	0,17
2. Fuel consumption at TPPs for sold electricity, g.p./kWh.	396	384	367	353	334

Continuation of table 3

3. Level of residual resource of fixed assets of fuel and energy complex,%	20	30	50	60	80
4. Share of shunting capacities of FEC power generation to the total installed capacity,%	8,6	12	14	16	18
5. Share of losses in distribution power grids,%	12	11	10	9	8
6. Share of exchange trade in energy resources,% of domestic consumption, including electricity, coal, oil, gas and other fuels	10	25	50	60	70
7. The share of renewable energy sources in gross final energy consumption,%	4,5	11	15	18	20
8. Share of local alternative fuels in local fuel and energy balances,% of total consumption		10	15	18	20
9. Reduction of emissions in CO2 equivalent to final fuel consumption, %, from 2010		>5	>10	>15	>20
10. Reduction of specific emissions in CO_2 equivalent in the production of 1 kWh,%, from 2010		>5	>10	>15	>20
11. Reduction of specific emissions in CO_2 equivalent during production 1 Gcal,%, from 2010		>5	>10	>15	>20
12. The share of capacity in thermal generation that meets EU environmental requirements (emissions of SO_2, NOx, ash),%		20	40	80	100

Source: compiled by the authors for [4]

Like any reform, this process requires a system of funding. Implementation costs (according to European practice) are divided into 2 categories - public sector costs and private sector costs. The first of them rely on the budget sphere, the second - on the funds of enterprises. In the composition of both, in turn, should be calculated three main components: administrative costs; investment (capital) costs; operating costs. The main focus is on investment costs related to the construction, reconstruction and modernization of facilities.

An important problem is the need to quantify investment costs for Ukraine. In reality, in our opinion, macroeconomic comparisons and comparative approaches are really the only ones available. They are based on the analysis of European experts on the implementation of EU environmental requirements in Central and Eastern Europe. Its results (in terms of forecasting implementation costs in absolute terms and per capita) are shown in Table 4.

When evaluating the financial indicators shown in Table 4, it should be borne in mind that the timeframe for the implementation of EU environmental requirements is calculated in the range of 10 to 20 years. Among these countries, Poland and Romania are the most similar to Ukraine in terms of economic structure and population.

Table 4

Forecast of costs for the implementation of EU environmental requirements in Central and Eastern Europe

Country	Population, million people	Investment needs, million euros	Costs per person, euros
Bulgaria	7,5	8610	1148
Latvia	2,3	1480-2360	643 - 1026
Lithuania	3,6	1600	444
Poland	38,6	22100-42800	573-1109
Romania	22,3	22000	987
Slovakia	5,4	4800	889
Slovenia	2,0	2430	1215
Hungary	10,0	4100-10000	410-1000
Czech Republic	10,2	6600-9400	647-923

Source: compiled by the authors for [7]

With a certain conditionality, it is possible to estimate the projected costs of Ukraine for the implementation of EU environmental agreements in the amount of 1000-1100 euros per person and in general (for 10-20 years) - in 43000-47300 million euros. The share of Ukraine's fuel and energy sector in the total amount of harmful emissions into the atmosphere and other environments is expertly estimated at 40%. Therefore, we can predict that the investments of the Ukrainian fuel and energy complex for its adaptation to environmental Euro requirements should amount to 17.2 to 18.9 billion euros in 10-20 years.

The analysis of actual environmental costs in Ukraine [2] taking into account the deflator index showed that, starting from 2000, there is a stagnation of environmental costs. Absolute funding for

environmental protection in Ukraine is significantly less than 2 billion euros per year. This is clearly inferior to the level required to implement EU environmental requirements. Therefore, for Ukraine, especially for fuel and energy, a topical issue is (in addition to investing own funds of the budget and businesses) to attract assistance from EU funds, grants and international loans. After all, the implementation of EU environmental requirements (ie environmental clean-up and quality of life standards) is needed primarily by Ukraine, not the EU.

In general, it should be noted that at the governmental level the plans for the implementation of EU environmental requirements in terms of adaptation of domestic legal and regulatory requirements have been developed and approved in sufficient detail. However, the effectiveness of all work on the implementation of EU environmental requirements will be determined not only by the similarity of relevant regulations of Ukraine and the EU, but primarily by the increased level of investment of economic entities and budgets at all levels in environmental programs, effective control and monitoring, real dissemination of environmental management at the sectorial, regional levels and directly in economic entities. In the complex, these are the main components of the reform of environmental and regulatory means of influence to adapt the national fuel and energy sector to EU requirements.

Conclusions

1. Ecologically regulated optimization of the fuel and energy complex involves its restructuring on the principles of systemic minimization of the destructive impact of energy-producing technologies on the environment and its main element - man. Eco-regulated optimization should be a mandatory element of expert assessment of all fuel and energy projects in Ukraine. The main factors that inhibit the effective use of mechanisms of environmental regulation of the national energy complex are identified.

2. In order to ensure the sustainable development of fuel and energy, the methodological principles of substantiation of investments in energy projects are formalized, which are a tool for analyzing the interaction of society and nature in carrying out production activities, which is inevitably accompanied by man-made environmental impact. Its use will facilitate the decision on the feasibility or inexpediency of implementing investment projects in energy production technologies.

3. The level of innovation activity in the fuel and energy sector should be objectively assessed by the proposed system of so-called indicators that characterize the efficiency of the fuel and energy sector and its impact on the environment in accordance with EU requirements. The innovative model of Ukraine's fuel and energy sector development taking into account the requirements of environmental regulations requires a change in the system of government relations, strengthening the competence, activity and legal capacity of local authorities to solve environmental problems created by businesses located in the respective communities.

4. Practical recommendations for bringing the environmental regulations of the national fuel and energy sector to the requirements of the European Energy Society in terms of environmental and economic assessment of existing energy capacity and planned projects are proposed.

5. Euro-adaptation of the fuel and energy sector requires significant and consistent investment from economic entities, as well as budget support and financial assistance from the EU. Increased investment in environmental programs, effective control and monitoring, the use of environmental management at the sectorial, regional levels and directly by economic entities will ensure the process of reforming environmental regulatory tools for the European adaptation of national energy.

References

1. **Moshchych S.Z.** Organizational - managerial methods of ecological regulation and their application at the international and national levels. Global and national economic problems: electronic science. view. Mykolayiv National Univ. **V.O. Sukhomlinsky**. Mykolaiv, 2016.Issue 9. Pp. 553–558. URL: http://global-national.in.ua/issue-9-2016. (appeal date: 25.02.2021).

2. **BortnyukT.Yu., Moschich S.Z.** Ecological optimization of the fuel and energy complex of Ukraine. Modern Transformation of Economics and Management in the Era of Globalization: International Scientific Practical Conference: conference proceedings, Lithuania, Klaipeda, 29 January, 2016. Klaipeda University, 2016. R. 52–55.

3. Reports on the implementation of state (national, target) programs. Ministry of Environmental Protection and Natural Resources of Ukraine: official website.URL: http://www.mepr.gov.ua/protection/protection5/261-zvity-pro-vykonannia-derzhavnykh-tsilovykh-prohram. (appeal date: 25.02.2021).

4. Energy strategy of Ukraine for the period up to 2035. White Paper on Energy Policy of Ukraine "Security and Competitiveness". National Institute for Strategic Studies under the President of Ukraine. URL: http:

//www.niss.gov.ua/public/File/2015_table/Energy%20Snrategy.pdf. (appeal date: 25.02.2021).

5. Kovshun N.E., Melnyk O.M., Moschych S.Z. Problematic issues of national economy development in the context of sustainable development. Sustainable development - XXI century: management, technologies, models. Discussions 2017: collective monograph / Averikhina TV, Adamets TP, Anderson NV [etc.]; for science. ed. prof. Khlobystova EV; NTUU Kyiv Polytechnic. Institute named after Igor Sikorsky; Institute of Telecommunications and Global Inf. space of the National Academy of Sciences of Ukraine; Higher School of Economics and Humanities. Kyiv, 2017. P. 60–70.

6. **Kushnir N., Kostrychenko V**.Identification of the level of economic and ecological sustainability of agricultural land use in drainage conditions. 3 nd International Scientific and Technical Internet Conference "Innovative development of resource-saving technologies and sustainable use of natural resources". BookofAbstracts. - Petroșani, Romania: UNIVERSITAS Publishing, 2020. P. 256-258.

7. **Mishchenko V.** The EU "imposes" cleaner air and water on Ukraine, or the Environmental component of the Association Agreement with the EU. Mirror of the week. 2014. №12. URL: http: // gazeta.dt.ua/energy_market/yes-nav-yazuye-ukrayini-chistishi-povitrya-ta-vodu-abo-ekologichna-skladova-ugodi-pro-asociaciyu-z-yes_.html. (appeal date: 25.02.2021).

8. **Moschych SZ** Implementation of reorganization of the fuel and energy complex of Ukraine. Problems of rational use of socio-economic and natural resource potential of the region: financial policy and investment: coll. Science. wash. Kyiv: SEU; Rivne: NUVGP, 2015. №4. Pp. 89-97

9. **Moschych S.Z.** Methodology for assessing environmental risks in the system of environmental safety. Development of a new economy at the global, state and regional levels: materials International. scientific-practical Conf., Lviv, February 19-20, 2016, Part 2. Lviv: LEF, 2016. P. 51–55.

10. **Moshchych S.** International experience in the application of methods of environmental regulation. International practice of socio-economic development of the country: problems and prospects: a collection of abstracts. works of participants International. scientific-practical conf. for students, graduate students and young scientists, Kyiv, December 18-19, 2015 Part 1. Kyiv: Analytical Center "New Economy", 2015. P. 133-135.

11. **Moshchych S.** Current state and problems of development of the coal industry of Ukraine.3rd International Scientific and Technical Internet Conference Innovative development of resource-saving technologies and sustainable use of natural resources. Book of Arstracts. Romania: 2020. P. 205–208.

12. **Moshchych S, Levun O., Pylypchuk I.** Energy efficiency management of the national economy.3rd International Scientific and Technical Internet Conference Innovative development of resource-saving technologies and sustainable use of natural resources. Book of Arstracts. Romania: 2020. P. 235–236.

13. **Savina N.B., Malanchuk L.O., Ignatiuk I.,Z., Moshchych S.Z.** Institutional basis and trends of managements of the use of the subsoil in Ukraine. Topical scientific researches into resource-saving technologies of mineral mining and processing . Multi-authored monograph. Sofia: 2020.P. 51–60.

https://doi.org/10.31713/m1007

SELECTED PROBLEMS OF RHEOLOGY IN THE CONTEXT OF ROCKS BEHAVIOUR. VARIABILITY OF THE MODULUS OF ELASTICITY AS AN EXAMPLE OF THE INFLUENCE OF TIME AND STRESS FACTORS

Krzysztof TOMICZEK[1]

PhD Eng. Krzysztof Tomiczek, Department of Geomechanics and Underground Building, Faculty of Mining, Safety Engineering and Industrial Automation, Silesian University of Technology, Gliwice, Poland

Summary

Most of the solutions to the problems of rock mechanics, rock mass mechanics, but also soil mechanics and geotechnics ignore the influence of the time factor. The solutions are *here* and *now*, *at the moment*. Meanwhile, plastic-viscosity properties, when rocks are in a 3D stress state, play more and more importance in the course of time. The deformability variability is of particular importance, as measured by the modulus of elasticity *E*. This chapter analyzes the magnitude of this modulus obtained in uniaxial short-term tests and creep tests of a well-known and described, typical sandstone, at different stress values σ_0=const.

Keywords: rheology, creep of rocks, modulus of elasticity, deformability, viscosity, plastic flow, uniaxial compression test, sandstone

Introduction

The beginning of rheology dates back to 1928, when on the initiative of Professor Bingham (Lafayette College, Easton, Pa., US) the "Society of Rheology" and the "Journal of Rheology" were established. Rheology has become a branch of physics dealing with the deformation, plasticity and flow of materials (based [19], [20]).

The name "rheology" has been widely used by British scientists since 1930. In 1940 the British Rheologists Club was founded and Scott Blair announced "Introduction to Industrial Rheology."

The reasons for the emergence and development of rheology are to be found in industrial development, which resulted in the production of many new materials. These materials should have specific mechanical properties. Determining the mechanical properties of

[1] Krzysztof.Tomiczek@polsl.pl , k.tomiczek@yahoo.co.uk , https://orcid.org/0000-0001-9227-310X Researchgate: Krzysztof_Tomiczek

materials only on the basis of solutions based on the theory of elasticity and viscosity was insufficient. Also, the application of *pure* plasticity theory turned out to be insufficient. Conferences and symposia on this subject were organized by the American Chemical Society in 1924, 1926 and 1928.

Fig. 1.1. Layers of limestone and flint on the road to Jericho. "Creep in nature is a very long and probably developing process" (Reiner, 1949, 1955)

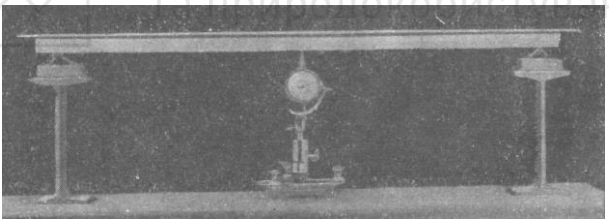

Fig. 1.2. Cement beam at the Tel-Aviv Materials Testing Laboratory showing a permanent increase in *deflection* from the horizontal line. “The creep phenomenon was observed in the laboratory within one year and is still progressing” (Reiner, 1949, 1955)

Particular attention was paid to the phenomena of plasticity and flow of materials. It was the issues of deformation and flow of materials that became the subject of research by the Society of Rheology and the adoption of the Heraclitus *pantha rhei*.

Engineers and scientists began to talk *seriously* about creep, flow, and plasticity as important, and perhaps even the most important, properties of materials.

The father of rheology is considered to be Marcus Reiner, who from the beginning cooperated with Professor Bingham, and in the years 1931-1934 he gave a series of lectures at Lafayette College and Princeton University.

Reiner in 1937 and 1941 gave a series of lectures at the Hebrew University in Jerusalem. Reiner published, in March 1949 "Twelve lectures on theoretical rheology" (North Holland Publishing Co., Amsterdam), and in 1955 “Rheologie theorique” (Dunod, Paris). At various stages of his work, he cooperated with professors: Bingham, Blair, Hatchekow and Andrad.

Basic concepts

Rheology is the study of the flow and deformation of materials. Flowing and deformation result from the movement of one body molecule in relation to another (based [9], [26], [27]).

The movement of material bodies is the subject of the field of physics called mechanics.

2.1. Basic laws of mechanics in rheology

Theoretical mechanics deals with material points, systems of material points and systems of bodies. In these problems, the properties of the material of the bodies are not analysed, e.g. in solutions to the motion of the planets, planets are treated as material points.

However, the rheological properties of the materials which are made up bodies, such as planets, are different. By analysing the movement of some parts of the body in relation to others, we observe their different behaviour.

Materials can behave differently under the impact of forces. In general, materials under the influence of forces (or load) show the following behaviour:

- elastic; the deformation reaches a certain state under the certain forces (or loads), the state of deformation disappears when we remove the forces;
- plastic, when permanent/ plastic deformations remain after removing forces;
- flow if, under the forces with a constant, limited value the deformations increase indefinitely.

Regardless of the solutions, the rules of mechanics apply in rheology:

1st principle

$$\Sigma P = a_0 \cdot m,$$

where

Σ at ΣP - means adding vectors,

ΣP - is the resultant of all forces acting on the body,

m - mass,

a_0 - acceleration of the center of gravity of the body,

wherein the mass m is a scalar.

2nd principle

Let $\Sigma M = \Sigma P_r$

where

r -force arm, distance from the line of action of the force from the centre of gravity this

$$\Sigma M = fa \cdot rdm,$$

where

f - is the integral of all particles,[2]

a - is the acceleration of a molecule with mass dm,

r - now expresses the distance of the acceleration action from the stationary point.

The above equation is also correct if the centre of gravity of the body weight is moving.

3rd principle

Newton's 1st, 2nd and 3rd law (1687) applies:

$\Sigma P = m \cdot a$ (1st and 2nd Newton's law)

$$A \leftrightarrow B$$

The action of body A on body B is equal to the reaction of body B to A (Newton's 3rd law.

4th principle

The quantity that characterizes the material of which the body is made is the density Σ. Density Σ is the *only one* material constant that occurs in mechanics.

$$\rho = \frac{dm}{dV},$$

[2] it was decided to use the word "*particle*" rather than "*molecule*" because of its mass.

where

m –body weight,

dm – particle mass,

V – body volume,

dV – volume of the particle.

In rheology, the basic equations relate strain kinematic quantities to stress dynamic quantities using parameters that are constants or material coefficients and that describe the rheological properties of various materials.

2.2. Basic rheological models of rocks

According to Kwaśniewski [13,14], the basic functions describing the *simple* creep process are (Fig. 2.1):

I. Creep equations for linear viscoelastic material with differential models:

Maxwell

$$\varepsilon(t) = \frac{\sigma_0}{E}\left(1 + \frac{E}{\lambda}t\right).$$

Features of the Maxwell model:

- has the ability to immediate elastic deformation,
- characterized by an inability to elastic after-effect,
- shows only secondary creep properties,
- simple creep describes only the 2nd stage of the generalized rock creep characteristic.

Features of the Kelvin - Voight model:

- does not have the ability to immediate elastic deformation $\square_e$=0,
- characterized by a total elastic retardation,
- shows properties of primary creep only,
- describes only the 1st stage of the generalized creep characteristic.

Zener

$$\varepsilon(t) = \frac{\sigma_0}{E_1} + \frac{\sigma_0}{E_2}\left(1 - e^{\frac{E_2}{\lambda_2}t}\right).$$

Features of the Zener model:

- has the ability to immediate elastic deformation $\square_e$,

- is characterized by a partial elastic after-effect,
- shows properties of primary creep only,
- the standard creep curve describes only the 1st stage of the generalized rock creep characteristic.

Burgers

$$\varepsilon(t) = \frac{\sigma_0}{E_1} + \frac{\sigma_0}{E_2}\left(1 - e^{\frac{E_2}{\lambda_2}t}\right) + \frac{\sigma_0}{\lambda_3}t\,.$$

Features of the Burgers model:

- has the ability to immediate elastic deformation ε_e,
- combines the properties of primary – elastic, and secondary - viscous creep,
- describes the 1st and 2nd stage of the generalized creep characteristic.

Where in the equations:

σ_0 -constant stress in the creep test,

t - time,

E, E_1 i E_2 - longitudinal elasticity coefficients,

λ, λ_1 i λ_2 - longitudinal viscosity coefficients.

II. Creep equations for linear viscoelastic media with integral model:

Abel

$$\varepsilon(t) = \frac{\sigma_0}{E}\left(1 + \frac{\delta}{1-\alpha}t^{1-\alpha}\right).$$

Features of the Abel model:

- has the ability to immediate elastic deformation ε_e,
- describes only incompletely the 1st stage of creep; according to this model, $\varepsilon(\infty)=\infty$.

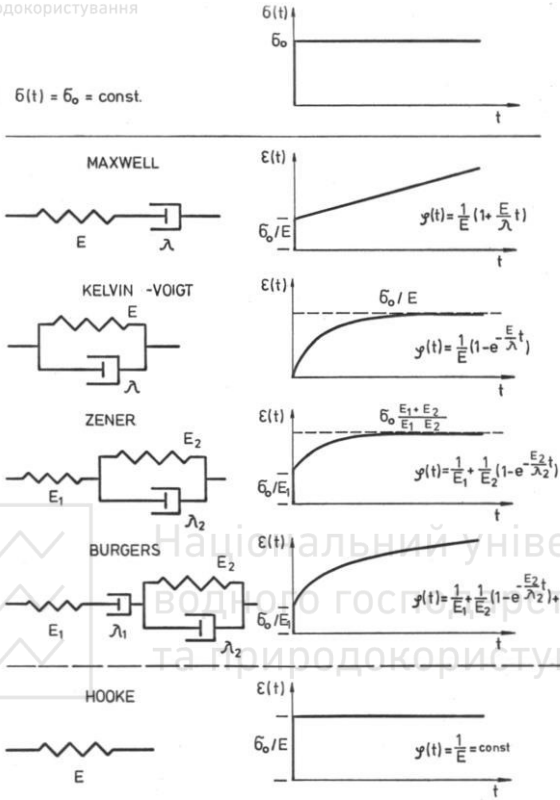

Fig. 2.1. Basic mechanical models and simple creep characteristics of viscoelastic materials after Kwaśniewski (Kwaśniewski, [13])

Rabotnov

$$\varepsilon(t) = \frac{\sigma_0}{E}\left[1 + \frac{\chi}{\beta - \chi}\left(1 - e^{(\chi-\beta)\tau^{1-\alpha}}\right)\right]$$

Features of the Rabotnov model:

- has the ability to immediate elastic deformation ε_e,
- shows properties of primary creep only,
- describes only the 1st stage of the generalized creep characteristic.

Where in the equations:

δ,α,χ i β - creep parameters (Kwaśniewski [13] after Rabotnov[18]).

3. Carbon rocks creep testing (based on Borecki et al., [1-6])

3.1. Basic assumptions

Research on the creep phenomenon requires the determination of the basic characteristics of the creep process of the rock. These features are:

- limit creep time,
- creep deformations,
- stages of the creep process,
- determination of the simple rock creep function in the air-dry state for various loading levels,
- determination of the linearity or non-linearity of simple creep.

The basic task for describing the creep phenomenon is to determine the creep characteristic, i.e. the relationship $\varepsilon_i=f(t_i)$, where ε_i is the deformation (strain) at time t_i.

The creep curve is the basis for the determination of the creep function and rheological parameters.

The creep test consists of two stages:

I. Increasing the sample load from 0 to the value of stress, at which a specific stress σ_0 induces in the sample cross-section. The stress σ_0 is part of the uniaxial compressive strength σ_C(σ_0=(0.4-0.9) σ_C). This stress corresponds to the initial deformation ε_0.

II. Maintaining a constant load σ_0=const. (Fig. 3.1) while continuously recording the deformation of the sample taking place in time $\varepsilon=f(t)$.

When testing samples with the method of constant loading, it is assumed that the sample is constantly under the conditions of a constant, unchanging load over time $\sigma=\sigma_0$=const. This assumption is not entirely factual, but admissible (Borecki et al., [5]).

Test conditions [5]:

- accuracy of maintaining a constant load value $\sigma=\sigma_0$: (0.3-1.0)%,
- force measurement: KMBM ring dynamometers, class 0.2,
- deformation measurement: a system of 3 dial gauges with an accuracy of 0.001mm,
- the samples were tested in air-dry conditions.

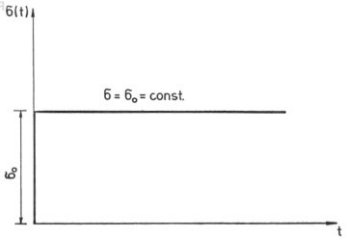

1. $t \to 0^+$ $\sigma \to 0^+$ $\varepsilon \to \varepsilon_0$
   $t = 0^+$ $\sigma = \sigma_0$ $\varepsilon = \varepsilon_0$
2. $t > 0^+$ $\sigma = \sigma_0 = \text{const.}$ $\varepsilon = f(t) = ?$

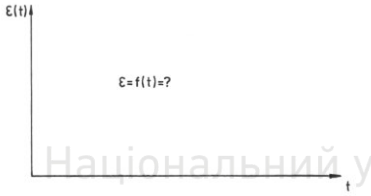

Fig. 3.1. General scheme of the creep test; ε - strain, ε_0 - immediate (initial) strain, t - time, σ - stress, σ_0 - initial stress (required, constant, σ_0=const.), lower than σ_C ($\sigma_0 < \sigma_C$), σ_C - uniaxial compressive strength [13, 5]

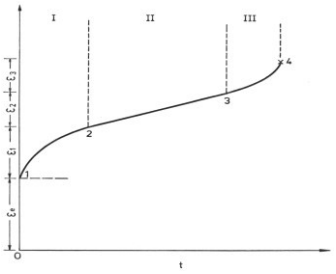

Fig. 3.2. Generalized rock creep curve. I - primary creep, transient, II - secondary creep steady, III - third degree creep, progressive, tertiary; ε - strain, ε_e - immediate deformation, ε_1, ε_2, ε_3 - deformations of individual creep stages, t – time [13, 5].

Figure 3.2 shows a *typical*, *classical* rock creep curve under constant stress σ_0=const. and constant temperature conditions. On its basis, four stages of rock deformation over time can be distinguished:

0. Elastic deformation occurring at time t=0$^+$ (0-1).

I. First Stage of Creep, primary, transient creep, called elastic creep or elastic flow. The creep speed decreases with time, reaching in point 2 the minimum value for the entire creep process (1-2).

II. Second Stage Creep - secondary, stabilized creep, also called viscous creep, pseudo-viscous flow, or plastic flow. Creep velocity maintains its minimum value from point 2 and remains constant throughout the range (2-3).

III. 3rd Degree Creep - 3rd degree creep, progressive. Short stage. A sharp increase in creep speed causing failure.

The entire rock creep process, and more precisely the total creep deformation:

$$\varepsilon(t)=\varepsilon_e+\varepsilon_1(t)+\varepsilon_2(t)+\varepsilon_3(t)$$

where:

ε_e - immediate deformation (elastic strain),

$\varepsilon_1(t)$ - primary creep strain,

$\varepsilon_2(t)=v\cdot t$ - secondary creep deformation, where $v=\varepsilon_2'=const$ is the secondary creep velocity,

$\varepsilon_3(t)$ - third degree creep strain,

t - time.

In the case of rock mechanics and rock mass, as well as underground construction, the first and second stages are particularly important, as they influence to the values of deformation pressure on the support of tunnels, chambers, underground heading, including shafts.

3.2. Apparatus

The laboratories of the Department of Geomechanics and Underground Construction are equipped with 8 PSH-400 spring-hydraulic creepers (Fig. 3.3-3.7). Creepers have a simple and reliable design. They enable loading P_{max}=480 kN and testing of hard rocks. Loading is carried out by means of 16 hydraulically tensioned steel springs; 2-3 rock samples can be tested in each creeper.

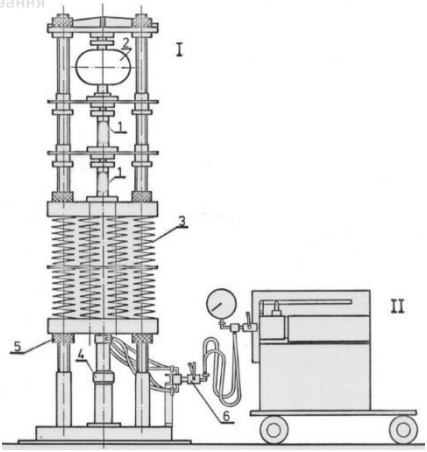

Fig. 3.3. Scheme of the PSH-400 (I) spring-hydraulic creeper with a hydraulic supply (II): *1* - rock samples (*h*:*d*=2); *2* - proving ring for measuring sample loads; *3* - set of 2×16 springs keeping constant load on the samples; *4* - hydraulic actuators tensioning the set of springs (3) and applying the preload to the samples, then keeps by the springs; *5* - four stop nuts disconnecting the set of springs (3) from the hydraulic actuator system after applying the load to the samples (stress $s=\sigma_0$); 6 - valves shutting off the actuators (4) from the hydraulic supply (II)

Fig. 3.4. Set of 9 spring-hydraulic creepers

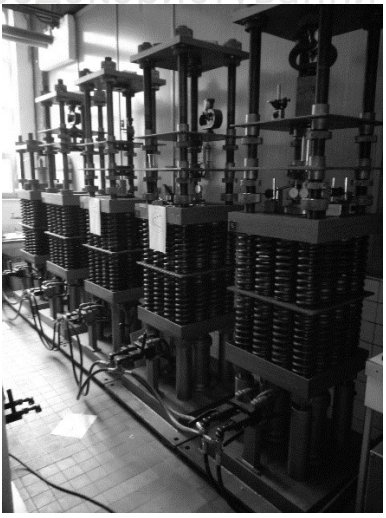

Fig. 3.5. Each creeper tests 2-3 samples simultaneously

Fig. 3.6. View of a set of spring-hydraulic creepers. The first from the left is a triaxial tes

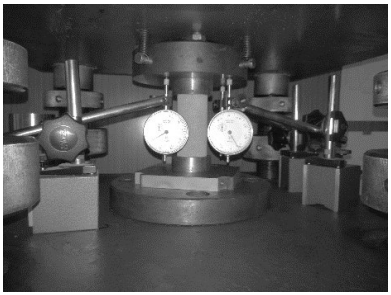

Fig. 3.7. View of the rock sample tested in the uniaxial creep

3.3. The results of research on the phenomenon of creep (based on Borecki et al., [3-6])

3.3.1. Basic rock characteristic

Five types of rocks from the upper-saddle layers were investigated. They were: clay, mudstone, sandstone (Jastrzębie) and conglomerate.

The cores were drilled from a depth of -200 m. They had a diameter of 42 mm and a slenderness (*h*:*d*) of 2. All tests were laboratory tests in which the principles of the recommendations of the International Society of Rock Mechanics were followed.

After cutting, the samples were ground with the following accuracy:

- deviation of parallelism of the frontal planes of the sample: 0.05 mm,
- longitudinal axis deviation <0.05/50mm,
- convexity of face surfaces <0.03mm.

Before starting the tests, the samples were stored under normal conditions, i.e. temperature 18-24°, humidity 60-70%, for about 6 weeks.

The basic properties of the rocks are presented in Table 3.1. Although only the behaviour of the Jastrzębie sandstone will be analysed, the table lists the constants of the remaining sedimentary rocks in order to better describe the properties of the surrounding rock mass.

Tab. 3.1

Parameters of the tested rocks

Quantity	Rock type						
	Claystone (A)	Mudstone (B)	Jastrzębie sandstone		Conglomerate (E)	Claystone (F)	Mudstone (G)
Specific gravity ∟∟∟kN/m^3	26.3	26.2	25.8	26.8	25.4	26.9	27.6
Volumetric weight ∟∟∟kN/m^3	25.8	26.0	24.4	25.5	24.5	25.4	26.0
Volumetric porosity n_o, %	2.2	0.9	5.2	4.2	3.6	5.5	5.6
Weight water absorbability n_w, %	0.8	0.3	2.1	1.6	1.5	2.1	2.1
Elastic modulus E_s, GPa	15.5	37.7	31.3	30.8	41.8	17.2	14.8
Deformation modulus E_o, GPa	16.8	41.1	32.3	30.0	34.5	17.6	16.1
Poisson's ratio ∟, -	0.17	0.23	0.16	0.17	0.15	0.17	0.17
Uniaxial compressive strength R_c ($∟_C$), MPa	90.6	106.8	83.5	111.2	83.4	76.6	79.6
Uniaxial tensile strength R_r ($∟_T$), MPa	10.0	10.0	6.0	10.3	7.2	7.7	9.2

3.3.2. Selected results of rheological tests of the Jastrzębie sandstone in the context of its deformability

Selected results of the Jastrzębie sandstone creep rheological tests, and more specifically the elasticity modulus (deformability

coefficient) E[3] for various creep models are showed in Table 3.2. The creep tests lasted from 204 to 1302 hours, depending on the value of σ_0 and the creep limits or failure of the rock samples.

Tab. 3.2

Values of the modulus of the elasticity modulus (deformability coefficient) E for different creep models and for different stress values $\sigma = \sigma_0$=const. (based Borecki et al., [2-6]).

	Load level	Zener model		Burgers model		Abel model	Robotnov model
	1	2	3	4	5	6	7
Jastrzębie sandstone	σ_0 MPa	E_1 GPa	E_2 GPa	E_1 GPa	E_2 GPa	E GPa	E_1 GPa
	41.7 ($0.50\sigma_C$)	17.6	968	16.7	1476	17.6	17.6
	50.1 ($0.60\sigma_C$)	20.3	674	20.3	1200	20.4	20.5
	58.4 ($0.70\sigma_C$)	22.8	601	23.1	760	23.2	23.1
	62.6 ($0.75\sigma_C$)	20.9	512	21.0	656	21.3	21.2
	66.7 ($0.80\sigma_C$)	18.1	112	18.5	422	18.3	18.8
	75.1 ($0.90\sigma_C$)	23.8	489	25.5	861	24.2	24.2

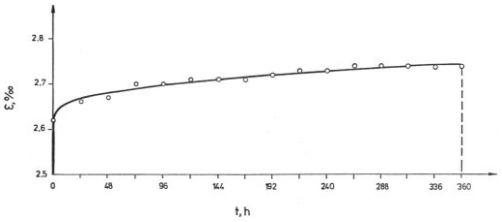

Fig. 3.8. Creep characteristic of *Jastrzębie* sandstone: $\sigma_0=0.6\cdot\sigma_C$. Abel creep function; σ_0=50.1MPa, E=19.1GPa, $\delta=0.0020\cdot h^{\cdot\alpha-1}$, δ=0.0020 [2-6]

[3] Being aware of the differences between the modulus of elasticity and the deformation coefficient, it was assumed that in accordance with the results of short-term compression tests, these coefficients can be identified.

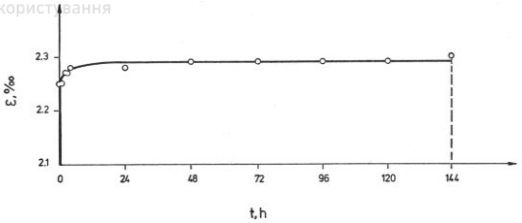

Fig. 3.9. Creep characteristic of *Jastrzebie* sandstone: σ_0=0.5·σ_C. Zener creep function; σ_0=41.7MPa, E_1=18.6GPa, E_2=9.6GPa λ_2=3266Pah [2-6].

From the point of view of the analysis, in this chapter we are interested in the analysis of the E values in columns 2, 4 and 6. The test results show that the differences in the E values for the same stress values σ_0 do not exceed 1.0MPa.

The second, more important observation is that for different values of σ_0 the *limit* values of E at time t are different. They vary depending on the creep model from 16.7 to 25.5GPa. This represents an increase of approximately 52%. Examples of creep curves for various models are shown in Figs 3.8-3.13. Most of the curves show that the creep has stabilized in shape.

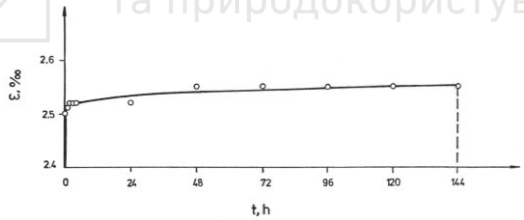

Fig. 3.10. Creep characteristic of Jastrzębie sandstone: σ_0=0.5·σ_C. Rabotnov creep function; σ_0=41.7MPa, E=16.7GPa, χ=0.0082·$h^{\cdot\alpha-1}$, β=0.1099·$h^{\cdot\alpha-1}$ [2-6]

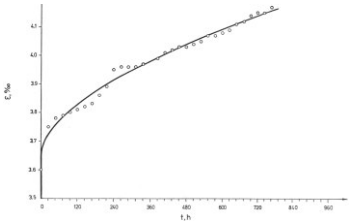

Fig. 3.11. Creep characteristic of Jastrzębie sandstone: σ_0=0.8·σ_C. Abel creep function; σ_0=66.7MPa, E=18.3GPa, σ=0.0018·$h^{\cdot\alpha-1}$, α=0.433·$h^{\cdot\alpha-1}$ [2-6]

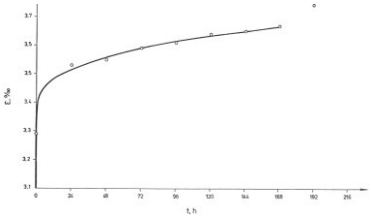

Fig. 3.12. Creep characteristic of Jastrzębie sandstone: σ_0=0.9·σ_C. Rabotnov creep function; σ_0=75.1 MPa, E=22.8GPa, χ=0.0404·$h^{\cdot\alpha-1}$, β=0.1189·$h^{\cdot\alpha-1}$ [2-6]

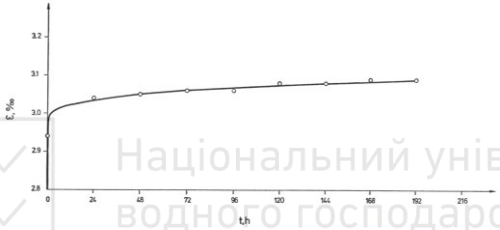

Fig. 3.13. Creep characteristic of Jastrzębie sandstone: σ_0=0.9·σ_C. Rabotnov creep function; σ_0=75.1 MPa, E=25.5GPa, d=0.0219·$h^{\cdot\alpha-1}$, α=0.2632·$h^{\cdot\alpha-1}$ [2-6]

4. Deformation properties of Jastrzębie sandstone under uniaxial short-term compression

Laboratory uniaxial compression tests were carried out in the servo-operated test laboratory. The tests were conducted in accordance with the recommendations of the ISRM. These studies have already been described in other publications (see Tomiczek, [24-27]). The diameter of the cylindrical rock samples d was equal to 42mm, and the slenderness d:h=2.

Tab. 4.1

Research results on deformation properties of Jastrzębie sandstone under the short-term uniaxial compression conditions

Rock type and sample symbol			Jastrzębie sandstone		
			220F1	220F2	220F3
Dimensions	diameter d, cm		4.13	4.14	4.16
	height h, cm		8.22	8.22	8.21
Slenderness		h:d	1.99	1.99	1.97
Cross-sectional area		S, cm^2	13.40	13.46	13.59

Short term uniaxial compression strength	σ_C MPa	136.45	102.25	87.59
Secant coefficient of axial deformability at the stress level σ_z=0.5σ_C	E_{s50} GPa	29.02	23.16	19.79
Mean axial deformation coefficient at the stress level σ_z=0.5σ_C	E_{m50} GPa	29.51	22.11	20.87
Linear axial deformation coefficient (equal to E)	E_l (E_{t50}) GPa	30.34	28.60	23.23
Poisson's ratio	ν	0.214	0.129	0.151

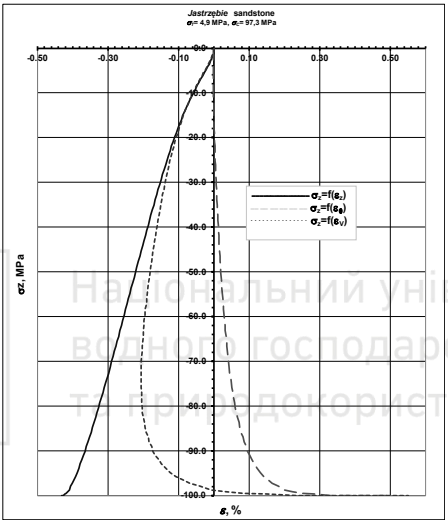

Fig. 4.1. Typical: normal stress σ_z - axial ε_z, lateral ε_θ and volumetric strain ε_V characteristics of the Jastrzębie sandstone in the uniaxial (short-term) compression test. Compressive stresses and strains are assumed to be negative in this figure

Tab. 4.2

Deformational coefficients (modulus of elasticity) in short-term and creep tests

σ_C MPa	E_s GPa	σ_0 MPa	E_{mZ} GPa	E_{mB} GPa	E_{mA} GPa	E_{mR} GPa
83.5	31.3	41.7	17.6	16.7	17.6	17.6
87.6	23.2	50.1	20.3	20.3	20.4	20.5
102.3	28.6	58.4	22.8	23.1	23.2	23.1
111.2	30.8	62.6	20.9	21.0	21.3	21.2
136.5	30.3	66.7	18.1	18.5	18.3	18.8
		75.1	23.8	25.5	24.2	24.2

where σ_C - uniaxial (short-term) compressive strength, E_s - modulus of elasticity determined on the basis of uniaxial (short-term) compression tests, σ_0 - value (constant) of stress in creep tests, E_{mz}, E_{mB}, E_{mA} and E_{mR} - modulus of elasticity of Zener, Burgers, Abel and Rabotnov models, in creep tests

Jastrzębie sandstone samples have a mid-range value of uniaxial compression strength σ_C. This strength of the Jastrzębie sandstone is approximately 109 MPa.

The average values of the deformation coefficients (modulus of elasticity) E_{t50} and E_{m50} of the Jastrzębie sandstone are approximately 27.4 GPa and 24.0 GPa, respectively.

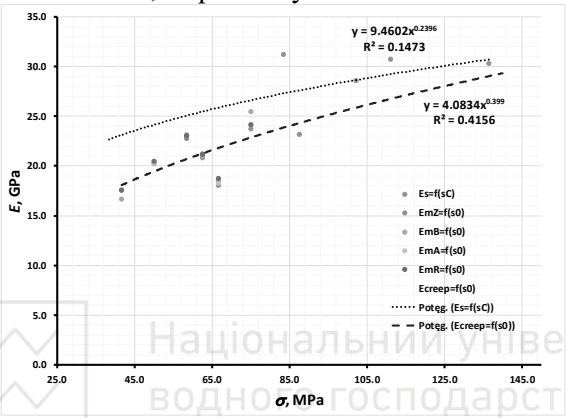

Fig. 4.2. The relationship between the stress σ and the deformation coefficient (modulus of elasticity) E. σ_C - under (short-term) uniaxial compressive strength tests, *mZ*, *mB*, *mA*, *mR* - of Zener, Burgers, Abel and Rabotnov models, *creep* - for all creep models, σ_0 – stress, σ_0=const. in creep, *Potęg.* - approximating power function

Comparison of the value of the elastic modulus (deformation coefficient) E in tab. 4.2 and in Fig. 4.2 means that the values of E strongly depend on the value of the stress σ_0 (or σ_C). The values of E, generally increase as σ_0 increases. From the value of about 16.7G Pa, at σ_0=41.7 MPa for the Burgers model to about 25.5G Pa, at σ_0=75.1 MPa, also for the Burgers model.

In addition, as shown by the results of short-term uniaxial compression tests, the E value in these tests is definitely higher than in the long-term creep tests. These differences reach 5G Pa, with values of 23.2G Pa, which is from 16 to 22%.

Figure 4.3. shows the relationship between the primary creep time (stage I, transient) t and the modulus of elasticity E, taking into account the uniaxial compression tests. The presented data show that the important factor influencing the value of E, regardless of the

value of the compressive stress σ, is the time t, especially in the Ist stage of creep, when there is an intensive closure of the micro-voids. The differences in the values of E, resulting from the load time, are large, reaching 8GPa. The E values for sandstone under short-term stress (uniaxial compression tests) are definitely higher.

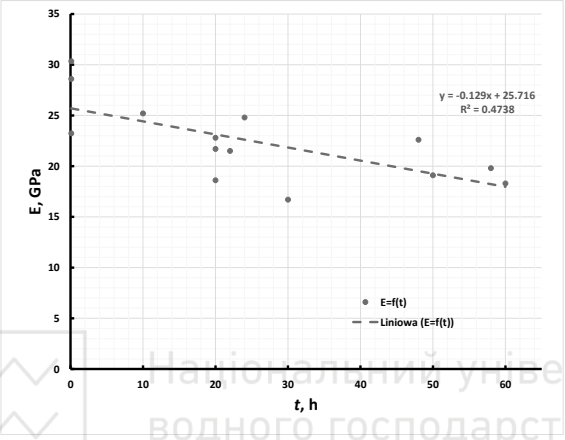

Fig. 4.3. The relationship between the primary creep time (stage I, transient) t and the modulus of elasticity E, taking into account the uniaxial (short-term) compression tests; *Liniowa* - approximating linear function

5. Summary and final remarks

The chapter highlights the neglected in recent years, effect of the time factor influence on the deformation properties of rocks. Selected results of research conducted by professors Borecki and Kwaśniewski at the Department of Geomechanics and Underground Construction (now) are presented. The well-known Jastrzębie sandstone was selected, which has been the subject of comprehensive own research in recent years. This medium-fine sandstone is *quasi*-isotropic and *qasi*-homogeneous.

Particular attention was paid to the variability of the value of the modulus of elasticity (deformation coefficient) E. As shown, the time t and the value of the (compressive) stress in the time σ_0=const. (or σ) have a strong influence on deformation properties:

1. Values of E, generally increase with increasing (long-term) stress σ_0. From the value of about 16.7 GPa for σ_0=41.7 MPa to about 25.5 GPa at σ_0=75.1 MPa.

2. As shown by the results of short-term uniaxial compression tests, the *E* value in these tests is definitely higher than in the long-term creep tests. These differences reach 5GPa, with values of 23.2GPa, which is from 16 to 22%.

3. Presented data show that the important factor influencing the value of *E*, regardless of the value of the compressive stress σ, is the time *t*, especially in the Ist stage of creep, when there is an intensive closure of the micro-voids. The differences in the values of *E*, resulting from the load time, are large, reaching 8 GPa. The *E* values for sandstone under short-term stress (uniaxial compression tests) are definitely higher.

Rocks, including those in the vicinity of underground headings, tunnels and chambers, remain under stress for long time. Rock properties are determined as standard short-time tests. It is widely recognized that there is a need for studies on rocks that creep strongly, such, as rock salt.

However, as the research shows, the variability of the properties of typical Carboniferous rocks over time is an important indicator of describing the state of the rock mass. This is the reason why this research is needed.

Sources (selected)

1. **Borecki M.:** Badania nad określeniem wskaźnika reologicznego skłonności węgla do tąpań. Research on the determination of the rheological coefficient of coal rockbursts. Zeszyty Naukowe Politechniki Śląskiej nr 571, s. Górnictwo z. 88, 3-15, 1979

2. **Borecki M., Chudek M. i Oleksy S.:** Problemy wpływu anizotropii masywu skalnego na stan naprężeniowo-deformacyjny wokół wyrobisk górniczych. Problems of the influence of anisotropy of a rock mass on the stress-deformation state around underground excavations. ZN Politechniki Śląskiej, nr 555, s. Górnictw**o, z. 85, 15-28, 1977**

3. Borecki M., Oleksy S. i Pacha J.: Aproksymacja krzywych pełzania skał jako ośrodka dziedzicznego o modelu całkowym. Approximation of creep curves of rocks as a inheritance medium with an integral model. Prace Naukowe Instytutu Geotechniki Politechniki Wrocławskiej, nr 26, s.Konferencje, nr 10, 175-185, 1978

4. Borecki M., Kwaśniewski M. i Oleksy S.: Ciśnienie deformacyjne górotworu jako ośrodka reologicznego działającego na obudowę wyrobiska korytarzowego. The deformation stress of the rock mass with rheological properties acting on the heading support. ZN Politechniki Śląskiej, nr 595, s.Górnictwo, z.96, 23-34, 1979

5. **Borecki M., Kwaśniewski M., Oleksy S., Ordysiński Z., Wojciechowski S. i Żyliński R.**: Podstawy teoretyczne i metodyczne badania własności reologicznych

skał. Fundamentals of theoretical and methodological studies on the rheological properties of rocks. Opracowanie Instytutu Projektowania, Budowy Kopalń i Ochrony Powierzchni Politechniki Śląskiej, 125/3.1.3.1, Gliwice 1976

6. **Borecki M., Kwaśniewski M., Oleksy S. i Pacha J.:** Badania nad pełzaniem skał karbońskich warstw siodłowych z kopalni Jastrzębie. Research on rock creep of Carboniferous saddle layers from the Jastrzębie coal mine. Opracowanie Instytutu Projektowania, Budowy Kopalń i Ochrony Powierzchni Politechniki Śląskiej, 115/3.3, Gliwice 1978

7. **Chudek M.** Mechanika górotworu. Rock mechanics. Skrypt centralny wyższych studiów technicznych dla pracujących, nr 956/61, Gliwice 1981

8. **Glamheden R. and Hökmark H.:** Creep in jointed rock masses. Svensk Kärnbränslehantering AB, Swedish Nuclear Fuel and Waste Management, 00R-06-94CM, 2010-2011

9. Kisiel I.: Reologia skał. Podstawy naukowe. Rock rheology. Scientific foundations. Polska Akademia Nauk, Wydawnictwo PAN, Warszawa 1973

10. **Kisiel I.:** Reologia w budownictwie. Rheology in civil engineering, Wyd. Arkady, Warszawa 1967

11. **Kłeczek Z.:** Doświadczalne kryterium doboru modelu reologicznego dla skał. Experimental criterion for selecting a rheological model of rocks. Prace Komisji Nauk Technicznych PAN, Górnictwo 5, PWN, Kraków 1968

12. **Kłeczek Z.:** Geomechanika górnicza. Mining geomechanics. Śląskie Wydawnictwo Techniczne. Katowice 1994

13. **Kwaśniewski M.**[*]: Funkcje pełzania skał. Rock creep functions. Zeszyty Problemowe Górnictwa, t.15, z.2, s. 3-50, 1977

14. **Kwaśniewski M.:** Granica stosowalności modelu lepkosprężystości liniowej do opisu reologicznych własności skał. The limit of applicability of the linear viscoelasticity model for the description of rheological properties of rocks. Prace Naukowe Instytutu Geotechniki Politechniki Wrocławskiej nr 31, Konferencje nr 12, 41-49, 1980

15. **Kwaśniewski M.:** Wpływ stanu naprężenia, temperatury i prędkości odkształcania na mechaniczne własności skał. Influence of the stress state, temperature and strain rate on the mechanical properties of rocks. Archiwum Górnictwa, t. 31, z. 2, 383-415, 1986

16. **Kwaśniewski M. and Nguyen V.H.:** Experimental studies on anisotropy of time-dependent behaviour of bedded rocks. In Proceedings of the International Symposium on Engineering in Complex Rock Formations, Beijing 1986, pp. 325-337. Pergamon Books Ltd. and Science Press, Beijing 1986

17. Mitzel A.: Reologia betonu. Concrete rheology. Arkady, Warszawa 1972

18. **Rabotnov Yu. N**.: Creep Problems in Structural Members. North-Holland Publishing Company, Amsterdam – London, 1969

19**. Reiner M.:** Twelve lectures on theoretical rheology. North Holland Publishing Co., Amsterdam 1949

20**. Reiner M**.: Rheologie theorique. Dunod, Paris 1955

21. **Sałustowicz A.**: Mechanika Górotworu. Rock mechanics. Wydawnictwo Górniczo-Hutnicze, Katowice 1955

22. **Sałustowicz A.:** Górotwór jako ośrodek sprężysto-lepki. Rock mass as an elastic-viscous medium. Archiwum Górnictwa, t.III, z.2, PWN, Warszawa 1958

23. **Singh D.P.:** A study of creep of rocks. International Journal of Rock Mechanics and Mining Sciences & Geomechanics Abstracts, Volume 12, Issue 9, pp. 271-276, September 1975

24. **Tomiczek K.:** Badanie właściwości procesu odkształcania się i kruchego pękania skał przy ściskaniu oraz przy rozciąganiu w oparciu o wykorzystanie metody elementów odrębnych. Research on the properties of the process of deformation and brittle fracture of rocks under compression and tension based on the the Distinct Element Method. Prace Katedry Geomechaniki, Budownictwa Podziemnego i Ochrony Powierzchni Politechniki Śląskiej, BW-487/RG-4/99, Gliwice 1999

25. **Tomiczek K.:** Symulacja próby jednoosiowego ściskania próbki ziarnistego materiału skalnego. Simulation of uniaxial compression test of a granular rock sample. Prace Naukowe Instytutu Geotechniki i Hydrotechniki Politechniki Wrocławskiej; nr 73 Seria: Konferencje; nr 40 1230-3100, 2002

26. **Tomiczek K.:** O własnościach wytrzymałościowych i odkształceniowych pewnego piaskowca w warunkach trójpunktowego zginania w kontekście jego zachowania się przy rozciąganiu i ściskaniu. Strength and deformation properties of certain sandstone under three-point bending conditions in the context of its tensile and compression behavior. "Górnictwo Zrównoważonego Rozwoju 2018" - konferencja naukowa, Gliwice, 28. listopada 2018

27. **Tomiczek K.:** A note on the strength and deformation properties of a some sandstone under three-point bending in the context of tension and compression behaviour. Mining of Sustainable Development IOP Conf. Series: Earth and Environmental Science 261, 012055IOP, Publishing doi:10.1088/1755-1315/261/1/012055, 2019

(*) – **Marek Kwaśniewski** (1947-2014), PhD, DSc, Professor at Silesian University of Technology, the head of the Rock Mechanics Laboratory (1975-2014, SUoT), Secretary-General of the International Bureau of Strata Mechanics (1973-1988), President of the Polish National Group of the International Society of Rock Mechanics (2007-2014), Editor-in-Chief of the Geomechanics Research Series from CRC Press/Balkema (since 1987), member of the editorial boards of Archives of Mining Sciences (since 1999) and Rock Mechanics & Rock Engineering (since 2009), Author of more than two hundred research articles and several monographs. Professor **Kwaśnieski's** special interests were: the influence of anisotropy, triaxial studies and research on the phenomenon of dilatancy as a harbinger of rock failure.

https://doi.org/10.31713/m1008

PROSPECTS OF METHANE MINING IN THE WESTERN REGION OF UKRAINE

Chukharev S.M.
National University of Water and Environmental Engineering (NUWEE), Ph.D. (Engineering), Associate Professor, Department of Development of Deposits and Mining, Ukraine

Lozynskyi V.H.
Dnipro University of Technology, Ph.D., Associate Professor, Department of Mining Engineering and Education, Ukraine

Zaiets V.V.
National University of Water and Environmental Engineering (NUWEE), Ph.D., Associate Professor, Department of Development of Deposits and Mining, Ukraine

Solvar L.M.
Chervonograd State College of Mining Technology and Economics, Director, Ukraine

Okseniuk R.R.
National University of Water and Environmental Engineering (NUWEE), Assistant, Department of Development of Deposits and Mining, Ukraine

Summary
Methane reserves of coal mines of Ukraine are analyzed, and comparisons with other coal mining countries of the world are made. It is determined that Ukraine is among the countries with the largest reserves of mine methane. Data on the need to reduce methane emissions and its negative impact as one of the main greenhouse gases on global warming and climate change are presented. The world experience of methane extraction and processing from coal mines is studied, the advantages and disadvantages of different types of methane neutralization are determined. The priority directions of this activity for Ukraine are determined.

Introduction

The problem of reducing methane emissions from coal mines into the atmosphere and its utilization, at the moment, is very acute around the world. The use and processing of methane from coal mines is an urgent scientific and applied task, the solution of which should significantly increase the environmental security of Ukraine,

reduce global warming, create economic conditions for the development and transformation of the mining industry. To solve this problem associated with the extraction and utilization of methane, it is necessary to conduct research aimed at assessing the state of the industry and prospects for its development.

General characteristics of methane from coal mines

Much of the world's primary energy production is coal. As a result, industrialized countries are somewhat dependent on energy coal resources using coal as the main energy source.

Due to the growing dependence and increasing demand for coal in many countries around the world is increasing and its production. As a result, coal has to be mined in increasingly difficult conditions, as part of the shallow reserves is declining and as a result there is a need to develop coal mines, which are located at greater depths and are richer in gas.

Coal mining on ever lower horizons and with higher gas concentrations increases the already existing danger of carrying out these works for miners and enterprises in particular. Methane present in coal seams can cause explosions and accidents in mines, which is why technologies related to methane mining and utilization, degassing of coal mines and mine ventilation should be improved.

In addition to being explosive, methane is also released into the atmosphere, making it the second most common greenhouse gas after carbon dioxide (CO_2), which is largely released into the atmosphere by humans. The largest greenhouse gas is water vapor.

Methane as a greenhouse gas has existed in the atmosphere for about 9-15 years, which is why this gas is considered a "short-term climate-forming factor." Its share of global greenhouse gas emissions is about 14 percent. Although methane enters the atmosphere in smaller quantities than CO_2 and remains in it for less time, its ability to retain heat in the atmosphere - the so-called "potential contribution to global warming" - is 21 times higher.

In addition to coal mining and transportation, methane is released during the production of natural gas and oil. In addition, it is formed in the process of decomposition of organic waste at municipal landfills, in some manure storage systems for farm animals and in a number of systems for treatment of agro-industrial and domestic wastewater. Methane emission control provides a unique opportunity not only to mitigate climate change, but also to obtain an additional

source of energy. However, unless tougher measures are taken to reduce methane emission sources, by 2030 their volume will increase by about 45 percent and reach 8,522 million metric tons of carbon dioxide equivalent (million tons of CO_2e) [1].

According to preliminary estimates, methane resources in the world are estimated at 260 trillion m^3. The largest reserves are concentrated in countries such as the United States, China, Russia, Australia, South Africa, India, Poland, Germany and Ukraine. It should be borne in mind that currently there is no single methodology that would determine the exact reserves of mine methane, so the data in different scientific or analytical sources may differ. The presence of methane in the main coal-mining countries of the world, according to one source, is given in the table. 1 [2].

Table 1

The amount of methane reserves in coal mines in major coal mining countries

Country	Methane reserves, trillion m^3
USA	60
Russia	58
China	28
Australia	22
India	18
Germany	16
PAR	thirteen
Ukraine	8
Kazakhstan	8
Poland	3
Other	26
Together in the world	260

Thus, as we see, Ukraine has significant reserves of methane concentrated in coal seams and surrounding rocks that could be used as energy. Data published in 2014 show that Donbass mines emit about 1.5 billion m3 of methane per year, and the Lviv-Volyn coal basin approximately 60 million m^3. The share of methane used as gas fuel is only 8%. All other gas is simply released into the atmosphere and pollutes the environment. In terms of the amount of carbon methane emissions into the atmosphere, Ukraine ranks fourth in the world, which is clearly demonstrated by the diagram shown in Fig. 1 [2]

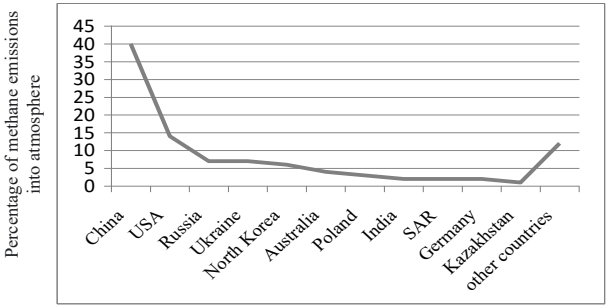

Fig. 1. The structure of mine methane emissions by major coal mining countries, %: China - 40; USA-14; Russia - 7; Ukraine - 7; North Korea - 6; Australia - 4; Poland - 3; India - 2; SAR - 2; Germany - 2; Kazakhstan - 1; other countries- 12

Since Ukraine has significant reserves of methane, its use and processing is an urgent scientific and applied task.

According to the Global Methane Initiative Table 2 (Global Methane Initiative, GMI), Ukraine also ranks 4th in the estimated amount of methane released from coal mines. In total, in 2010, about 584 million tons of CO_2e were released from the world's coal mines, or 8% of global emissions of this gas [1].

CO_2e or CO_2 equivalent is the global warming potential of a given greenhouse gas, the amount of which is equal to the amount of CO_2 with the same global warming potential.

Table 2

Estimated volume of methane released from coal mines in the countries of the top ten GMI in 2010

The country	Million tons of CO_2e
China	299.5
USA	59.0
Russia	55.2
Ukraine	27.4
Australia	26.8
India	26.5
Kazakhstan	13.5
Poland	8.3
Colombia	7.4
Vietnam	6.0

According to the Ministry of Energy and Coal Industry, in 2012, 1.4 billion m^3 of mine methane was extracted from 85.7 million tons of coal. The main amount of methane through the ventilation systems of the mines got into the atmosphere and only 370 million m^3 was captured by degassing systems, which at that time were equipped with only 44 mines out of 155. But that's not all, only 43% of the captured methane was subsequently 'utilized or burned on a torch, and the rest also entered the atmosphere.

It is also worth noting that at the moment part of the Donbass is occupied, and therefore it is impossible to provide more relevant information on methane emissions throughout Ukraine.

The problem of reducing methane emissions and its utilization is very acute at the moment. Its use and processing is an urgent scientific and applied task, the solution of which will significantly increase the ecological security of the country, will have an impact on the planet's climate, and may also have a certain economic effect. To solve this problem associated with the extraction and utilization of methane, it is necessary to conduct scientific and research work aimed at assessing the state of the industry and prospects for its development.

Problems and prospects of methane mining in the coal industry

To determine the prospects for methane extraction from coal mines, it is necessary to take into account the world experience of other countries that also have certain methane reserves in coal mining and have made certain investments and have already started mining and utilization of mine methane.

The previous section shows Table 1, where the reserves of methane from coal seams in the world's coal-mining countries should be noted that Ukraine is not a leader in world reserves: The United States - 60 trillion m^3, Russia -58 trillion m^3, China - 28 trillion m^3, Australia - 22 trillion m^3, India - 18 trillion m^3, Germany 16 - trillion m^3, South Africa - 13 trillion m^3, Ukraine - 8 trillion m^3, Kazakhstan - 8 trillion m^3, Poland - 3 trillion m^3, others - 26 trillion m^3.

Therefore, considering the experience of other countries, it is worth paying attention to the successful cases not only of leaders in stocks, but especially countries that have a similar or smaller number of stocks than ours.

In Poland, coalbed methane is concentrated in the deposits of the three Lublin Basin (which is a continuation of the Lviv-Volyn Basin), Lower Silesia and Upper Silesia, and their forecast reserves are 15 and 1.75 and 89.1 billion m^3, respectively. At the Zofiówka mine in Silesian Voivodeship, there is a thermal power plant, where the new unit installed in 2018 burns methane along with coal, which covers 10% of fuel needs and is cheaper than using natural gas. The thermal power plant produces electricity, heat and compressed air (supplied to the mine) [3].

The Czech Republic and Belgium, which have lower methane reserves than Ukraine, also produce and process this gas. In particular, in the Czech Republic, more than 50 million m^3 of degassing methane is used each year in boiler houses and coal drying plants. And in Belgium, methane is mined in deposits where coal is no longer mined. As for countries with large reserves of methane in coal seams such as the United States, China, Russia, Australia, they are actively implementing technologies aimed at degassing coal mines and methane processing, which indicates the potential for its extraction. For example, in China in 2005 production was 3-4 billion m^3, and in 2010 p. this figure was 10 billion m^3 [3].

The Energy Strategy of Ukraine until 2030 states that the extraction of 1 ton of coal emits an average of 10-12 m^3 of methane. In some deposits in the Donbass, the specific content of methane in coal reaches 500 m^3/t.

As for the Lviv-Volyn coal basin, the projected reserves of hydrocarbon gases in coal seams exceed 18.8 billion m^3, and this figure may increase with the implementation of a more thorough study [4].

The total projected methane reserves in Ukraine, which are listed in this and the previous section, indicate the prospects for methane production from coal seams.

In the mining industry of Ukraine and the world there are constant problems with methane, which complicates coal mining. Due to the fact that the depth of extraction is constantly increasing and the amount of available methane in it. Because of what they are trying to reduce these emissions.

Coal mine methane is methane that is released from coal and the surrounding layers of rocks during mining operations. During

underground coal mining, coal mine methane is explosive to miners, causing it to be removed from the mines through ventilation systems. In some cases, the ventilation system is supplemented by a degassing system, which consists of a network of wells and gas pipelines. In abandoned mines and either during opencast coal mining, methane can also be released into the atmosphere through natural cracks or other diffuse sources [5].

Methane in coal mines can be released from five sources, namely:

- in degassing systems at underground coal mines. When using these systems can use horizontal or vertical wells, as well as their combination for methane production before extracting the most mineral, this method is called "pre-mine drainage") or methane can be extracted after mining;
- together with ventilation air from underground mines, which contains a small percentage of methane;
- abandoned or closed mines. In this case, methane may be released through ventilation shafts or cracks in the ground, which arose as a result of mining or improper care of non-functioning mines;
- at open development of deposits. During this time, methane in the coal seams is directly exposed to the atmosphere;
- allocation (loss) as a result of processing and transportation of minerals. This process occurs after the mineral has been mined and coal continues to emit methane when it is stored in piles and transported.

Methods of using methane from coal mines

The availability of methane production technologies from coal mines allows us to consider a number of areas for the sale of methane and its products. There is no single specific consumer of mine methane in the world, because the directions of its use depend on a number of factors, the main of which is probably the quality of the extracted gas, the concentration of methane and the presence of other components. In addition to the quality of gas, no less important factors are the presence of certain end users and economic indicators of the project, which is aimed at the extraction and processing of methane.

There are the following ways of using and processing mine methane in the world:

- for electricity generation. For example, you can consider the construction of TPP directly near the mines;
- for central heating, as boiler fuel or city gas;
- sold to natural gas pipeline systems;
- for drying coal;
- as a heat source for mine ventilation air;
- as additional fuel for mine boilers, or possible combustion in combination with other fuels;
- as a motor fuel in the form of compressed or liquefied natural gas;
- incineration and use in production or industry. For example, as raw materials for the production of gaseous carbon black, methanol, acetylene, ammonia and other substances;
- use in the field of fertilizer production;
- oxidation of methane and obtaining useful thermal energy for heating, refrigeration or electrical installations;
- use as a raw material in the fertilizer industry;
- for the conversion of coal into a gaseous energy carrier [6,7].

Consider the advantages and disadvantages of the main methods of using methane [8]:

- electricity production. This technology is probably one of the most common and can be used in gas engines, to provide power to mines or to supply electricity to the grid. The advantages of this method of application are that this technology is tested; waste heat recovery can be used to heat mine structures, shower rooms of miners, as well as to heat and cool the air of mine shafts. The disadvantages of this method are the high capital costs at the initial stage of project implementation; unstable electricity production;
- use as pipeline gas. High quality purified mine methane is used for this technology. The advantages of this method are that as a result of methane processing the equivalent of natural gas is obtained, and the application of this method can be quite profitable at high gas prices; it is better to apply where there is a strong pipeline infrastructure. The disadvantages of this method are the expensive process of methane purification; construction of pipeline infrastructure is required if it is absent.

• use as urban or industrial gas of medium quality. These applications can be used for local district heating systems in residential areas and for industrial use, such as in industrial furnaces. The advantages of this method are to obtain a fuel source at a low price; cleaning may be minimal or non-existent. The disadvantages are the high cost of the distribution system and maintenance; uninterrupted supply; the need to build special gas storage facilities for regulation during peak needs;

• use of methane as a raw material for the chemical industry in particular. The possibility of using methane for the production of soot, synthetic fuels and other substances. The advantage of this method is the use of high-quality mine methane in difficult conditions. The disadvantages here may be the high cost of processing to obtain certain substances; the supply of certain substances on the market may not meet the demand;

• use on site of coal mining. In this way, it is possible to use methane in mine boilers, for drying coal, as a heat source for mine ventilation air, for heating houses adjacent to the mines. The advantages of this method are that methane can partially replace coal, and be environmentally friendly and cheap energy. The disadvantages of this method are that the amount of methane extracted will exceed the needs and, accordingly, not all methane will be used; may be less cost-effective to use at the location of the mine than outside it;

• use as automotive fuel in the form of compressed or liquefied natural gas. Advantages of the method there is free access to the market for gas supplies in difficult conditions; high prices for motor fuel. The disadvantages are high standards for cleaning; costs of gas processing, storage, injection and transportation.

Thus, as we see, there is a fairly wide range of uses of coalbed methane in industry for various needs of the national economy. The choice of methane use should be made taking into account the mining and geological characteristics of the extracted methane, as well as the needs of the region where the project of processing and utilization will be implemented.

And given the environmental aspect, namely that methane is a greenhouse and ozone-depleting gas, its use will have a positive effect in improving the environmental situation in Ukraine and the

world, and the establishment of a mechanism for "emissions trading" under the Kyoto Protocol to the UN Framework Convention on Climate Change, can become an additional source of foreign exchange and foreign investment in our country, in particular in industrial regions.

Analyzing all the data presented in the previous section, the extraction and processing of methane from coal seams is a promising area of development of the mining industry.

The experience of coal-producing countries, where the utilization of coalbed methane is well developed, shows that methane production is possible and appropriate at three stages of mine development:

- before the extraction of minerals;
- in an abandoned or closed mine;
- at the existing mine.

Prior to the extraction of coal, gas can be extracted only with the use of methods that stimulate its desorption - directional drilling, fracturing, pumping water.

Gas pumping in existing mines in the process of coal mining is performed by the methods of current degassing, when due to the unloading of the coal mass from the pressure is the desorption of methane from coal and its filtration from the cracks of reservoirs. This method has already been implemented in Donbass, where the extraction of methane from coal mines took place by drilling underground wells and wells from the surface in the fields of existing mines, as well as degassing works.

After the extraction of coal, methane extraction, which fills the produced spaces of spent lavas and closed mines, is carried out by drilling wells. Then the methane is pumped out by vacuum pumps.

Methane from coal seams can be extracted as a stand-alone or as an associated mineral. In Ukraine, the method of extraction of methane as an associated mineral by the method of mine degassing in the extraction of the main mineral - coal, is done mainly not for the purpose of further processing of methane but to ensure gas safety [9].

Consider the implementation of projects for the extraction and processing of methane [1].

To implement a successful mine methane emission reduction project, the mine owner needs to address a range of issues, from

project design to installation and operation. The success of the project requires a thorough examination of methane reserves and analysis of gas emissions, effective integration of degassing and utilization measures and the extraction process, as well as the availability of a market for methane. Despite the fact that in recent years there have been significant positive changes in the implementation of mine methane utilization projects, project participants may face a number of technical, economic and institutional problems that can hinder implementation. Among the important issues to consider are the following:

- methane should be seen as a useful and cost-effective product, not just a source of increased danger;
- the mine and project developers must have at their disposal modern state-of-the-art methane extraction systems, as well as the technologies and training facilities necessary for the use of this valuable resource;
- it is necessary to create an effective mechanism for collecting and disseminating reliable and unbiased information, including technical and market information;
- it is necessary to clarify the regulatory framework governing the collection and disposal of mine methane, and to address any issues related to possible violations or restrictions;
- it is necessary to provide access to the capital market.

Consider ways to process methane from coal mines in different directions.

Obtaining acetylene from coalbed methane. Acetylene can be obtained by thermal decomposition of coalbed methane at temperatures above 1500°C. Depending on the method of heat supply to the reaction zone, different technologies of acetylene production are used: electro cracking, pyrolysis in a reactor with a nozzle, oxidative pyrolysis and pyrolysis in low-temperature plasma, homogeneous pyrolysis. A substance such as acetylene is used in the manufacture of raw materials for the production of plastics, synthetic rubber fibers, etc.

Obtaining carbon black from coalbed methane. Carried out by thermal decomposition of methane without access of air at an operating temperature of 1100 °C get soot. The advantages of this process are simplicity and relative cheapness, high soot yield, the

formation of a quality by-product of gas with a high hydrogen content. The disadvantages of this method are the periodicity of the process and the heterogeneity of the resulting carbon black, which clearly reduces its quality. Soot is used in the manufacture of car tires, rubber products, printing industry, etc.

Chemical processing of methane into synthesis gas. The main direction of chemical processing of methane is currently the conversion into synthesis gas (which is a mixture of components CO and H_2) on its basis is subsequently synthesized for ammonia, methanol, higher alcohols and other chemical elements that are valuable. The most advanced technologies are methane steam conversion, partial oxidation and autothermic reforming.

Catalytic oxidative dimerization of methane. Work in this direction has been carried out for almost 30 years, the process of catalytic oxidation of methane dimerization is not currently implemented in industry, but it seems quite promising. The temperature of this process is 850-950 °C. However, the yield of the sum of the products of C_2 (Ethylene + ethane) is small. Among the disadvantages of this process is the low productivity of the catalysts.

Method of direct oxidation of methane to methanol. Currently, two main options for the implementation of this process are technologically developed: cyclic and flow. It is better to use the cyclic process to carry out the most complete conversion of hydrocarbon gas in the absence of external consumers. The flow process is simpler from a technological point of view, it allows the use of air as an oxidant, which may be more cost-effective than the cyclic process. It is advisable to use flow if there is fuel natural gas nearby (for example, it can be a thermal power plant or a gas compressor station).

Given the needs of Ukraine in the production of additional electricity, more and more news about a possible energy crisis in the country due to insufficient coal at thermal power plants should consider technologies for processing methane from coal mines for electricity production.

Gas turbines are often used to convert methane into electricity. An example of whose work in different versions is considered in the work of V.I. Kharchenko, Wu Tai Thu, O.O. Filonenko, O.S. Kucherenko, A.Yu. Voloshin "Utilization of mine methane in a gas turbine installation" [10] the scheme of a gas turbine installation with a vacuum combustion chamber is shown in Figure 2.

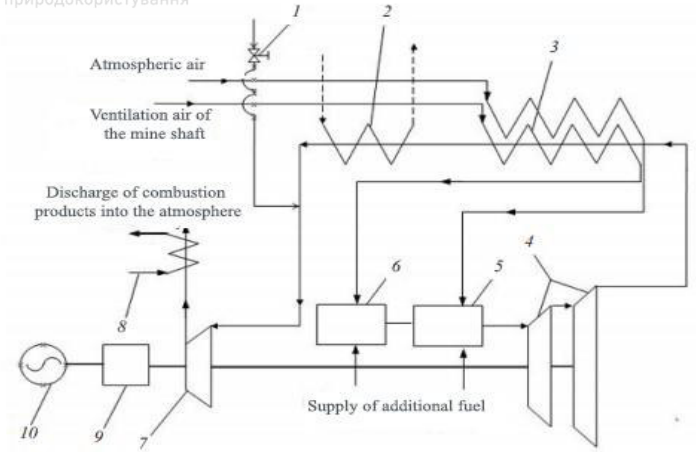

Fig.2. Gas turbine unit with vacuum combustion chamber with regenerative heating of atmospheric and ventilation air of the mine shaft

The principle of operation is that the ventilation air from the shaft of the mine is supplied to the regenerator 3 heat gases coming from the turbine. After that, the ventilation air through the concentrator 6 enters the combustion zone of the vacuum combustion chamber 5, which can be supplied with additional methane to provide the fuel concentration required for continuous combustion. In the combustion zone, combustion products are formed with a temperature that is close to stoichiometric. Atmospheric air is supplied to the regenerator 3 heat gases from the turbine. Next, the air is supplied to the mixer of the vacuum combustion chamber 5, moving with the high-temperature combustion products from the combustion zone and forming at the outlet of the vacuum combustion chamber combustion products of the desired temperature. From the vacuum combustion chamber, the combustion products are fed to the turbine 4, and then to the regenerator 3 and the low-potential boiler 2. It should be noted that the temperature of the combustion products at the entrance to the vacuum compressor 7 decreases to 40°C, while the water temperature in the low-potential boiler increases to 90°C. In the vacuum compressor there is an increase in the pressure of the combustion products to the parameters that ensure the flow of gas through the boiler 8 and the device exhaust gas into the atmosphere. The water temperature in the boiler rises to 150°C. Turbine 4 rotates

the vacuum compressor 7 and through the reducer 9 - the generator 10. In hot water boilers begins to produce thermal energy, and in the electric generator, respectively, electricity. that the temperature of the combustion products at the entrance to the vacuum compressor 7 is reduced to 40°C, while the water temperature in the low-potential boiler increases to 90°C. In the vacuum compressor there is an increase in the pressure of the combustion products to the parameters that ensure the flow of gas through the boiler 8 and the device exhaust gas into the atmosphere. The water temperature in the boiler rises to 150°C. The turbine 4 rotates the vacuum compressor 7 and through the reducer 9 - the electric generator 10. In hot water boilers begins to produce thermal energy, and in the electric generator, respectively, electric. that the temperature of the combustion products at the entrance to the vacuum compressor 7 is reduced to 40°C, while the water temperature in the low-potential boiler increases to 90°C. In the vacuum compressor there is an increase in the pressure of the combustion products to the parameters that ensure the flow of gas through the boiler 8 and the device exhaust gas into the atmosphere. The water temperature in the boiler rises to 150 °C. Turbine 4 rotates the vacuum compressor 7 and through the reducer 9 - the generator 10. In hot water boilers begins to produce thermal energy, and in the electric generator, respectively, electricity. which provide the flow of gas through the boiler 8 and the device exhaust gas into the atmosphere. The water temperature in the boiler rises to 150°C. Turbine 4 rotates the vacuum compressor 7 and through the reducer 9 - the generator 10. In hot water boilers begins to produce thermal energy, and in the electric generator, respectively, electricity. which provide the flow of gas through the boiler 8 and the device exhaust to the atmosphere. The water temperature in the boiler rises to 150°C. Turbine 4 rotates the vacuum compressor 7 and through the reducer 9 - the generator 10. In hot water boilers begins to produce thermal energy, and in the electric generator, respectively, electricity.

The procedure of formation of combustion products in the combustion chamber of the gas turbine unit is carried out in stages. The first stage assumes that in the combustion zone of the combustion chamber the fuel is burned together with the coefficient of excess air, which is close to unity, and the temperature close to

stoichiometric. To do this, use part of the air that is taken from the compressor and enters the combustion zone of the combustion chamber. This part of the air is called the primary air.

During the second stage, in the mixing zone of the combustion chamber, the combustion products are mixed with the rest of the air from the compressor (i.e. secondary air) to the desired temperature of the combustion products at the inlet to the turbine of the gas turbine unit.

The ratio of primary air $G_{ПЕРВ}$ to the amount of air at the entrance to the combustion chamber $G_{КЗ}$ can be expressed through the ratio of excess air coefficients in the combustion zone $\alpha_{ПЕРВ}$ and at the exit of the combustion chamber $\alpha_{КЗ}$. [10]

$$\frac{G_{перв}}{G_{кз}} = \frac{\alpha_{перв}}{\alpha_{кз}}. \quad (1)$$

Calculations for the formula. (1) indicate that when carrying out stoichiometric combustion of fuel in the combustion zone of the combustion chamber and the temperatures of the combustion products at the inlet to the turbine 1000-1100 °C the ratio $G_{перв}/G_{кз}$=0.28-0.33.

That is, in a gas turbine installation of the traditional scheme, it is useful to use only 28-33% of the mass of methane contained in the air of mine ventilation systems.

Taking into account the considered options of methane extraction and processing, as well as the prospects of such activities and resources of the Lviv-Volyn coal basin, we can offer a complex for degassing and processing of methane from coal mines by a gas turbine for electricity production in mines of Lviv-Volyn region.

The complex envisages methane extraction by current degassing for electricity production, and the use of ventilation methane for heat production (for the needs of the mine).

The schematic diagram of the complex can be seen in Figure 3.

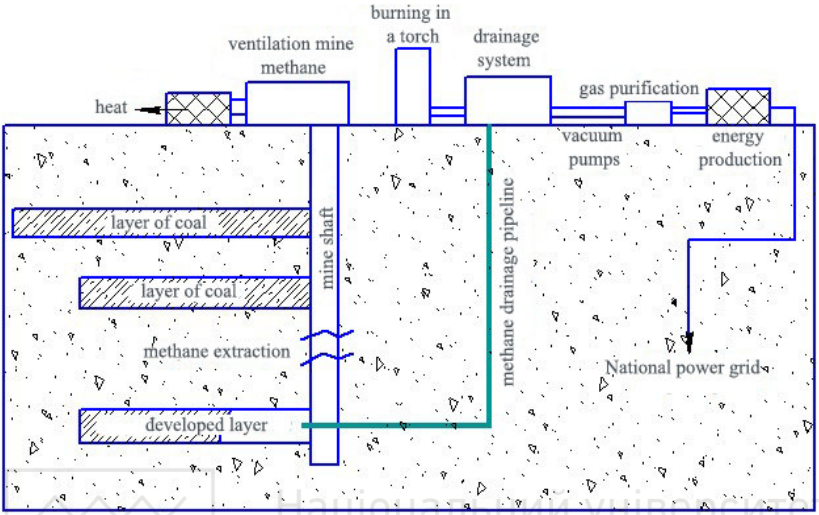

Fig. 3. Schematic diagram of the complex for degassing and methane processing of coal mines by a gas turbine unit for electricity generation

Methane extraction is envisaged by the methods of current degassing on already operating sections of the mine. For efficient extraction, a drainage system will be used from which the gas mixture will be fed to the gas purification through vacuum pumps. After that, the methane will enter the gas turbine plant in which the process of electricity production will take place, which will be supplied to the national grid.

It should be noted that this scheme does not exclude the possibility of introducing methods of methane production by pre-degassing.

In the conditions of mining operations, certain fluctuations may occur, which will relate to methane production, equipment for processing methane into electricity may malfunction or stop for maintenance of units. It is for such moments that it is proposed to burn gas in a flare, this will make it possible to minimize methane emissions.

Despite degassing during coal mining, small amounts of methane will still enter the workings and be removed by ventilation systems. Such methane will have a lower quality, so it is proposed to use it to produce heat for the needs of the enterprise.

By implementing this complex in the Rivne-Volyn coal basin of Ukraine, it is expected to significantly reduce the release of methane into the atmosphere and make coal mining safer by reducing the possibility of sudden methane emissions. Methane processing for energy generation and heat production for the needs of the mine will bring the company economic income through the sale of energy and cost savings. Also, the introduction of new technologies for the use of methane increases the cost of the enterprise by generating capital that can be reinvested in equipment and measures to ensure the safety of the mine.

Conclusions

It is determined that Ukraine has significant resources of methane, which is found in coal seams and can be used as an alternative energy resource [11]. The quantitative analysis of methane reserves of coal mines in the leading countries of the world on coal mining is carried out.

Positive aspects have been identified that will reduce the environmental risk by reducing greenhouse gas emissions into the atmosphere, which is a source of increasing global warming; increase the safety of mining operations; will allow the use of mine methane as an energy resource.

On the basis of the considered modern directions of extraction and processing of methane of coal mines it is established that this direction is perspective, especially in needs of Ukraine on energy. The experience of other countries is analyzed and a comparison with the possibilities of Ukraine is made.

The review of technologies for extraction and processing of methane from coal mines is carried out in the work.

The scheme of the complex on degassing and processing of methane by the gas turbine installation for production of the electric power at mines of the Lviv-Volyn region is offered.

The complex also provides for the separate use of ventilation methane to generate heat, which is more appropriate to use in the needs of the enterprise. And given that the amount of methane produced is unstable, whether it is possible to stop electricity production for technical reasons, the excess gas is proposed to be disposed of through flare combustion, which is also provided in the proposed complex.

References

1. Global Methane Initiative, GMI, (2011). Methane from coal mines: opportunities to reduce emissions, improve collection and disposal, September - 4 p.

2. **E.S. Sai, K.A. Ganushevich**, (2014). Utilization of mine methane and its transportation in the gas-hydrate state // Development of deposits: Coll. Science. pr .. - T. 8. - S. 299-307. - Bibliogr .: 15 titles. - Russian

3. Unconventional sources of hydrocarbons in Ukraine: a monograph. (2014). In 8 books. Book 1. Non-traditional sources of hydrocarbons: a review of the problem / [Kurovets IM etc.]; Nat. joint-stock company "Naftogaz of Ukraine", etc. - K.: Nika-Center, 2014. - 208 p. ISBN 978-966-521-654-4

4. **Kostyk I., Matrofaylo M., Korol M**. (2013). Prospects of modern natural gas potential of coal seams of deep horizons of the Lviv-Volyn basin. Geologist of Ukraine. 2013. № 3. S. 50-59

5. United States Environmental Protection Agency, Coal Mine Methane Sources, https://www.epa.gov/cmop/coal-mine-methane-sources

6. **Malanchuk Z.R., Zayets V.V., Solvar L.M., Romanchuk S.S.,** (2016). Methods of conversion of coal into gaseous energy carrier at the place of occurrence, Bulletin of NUVGP series "Technical sciences" issue 2 (74)

7. **Malanchuk Z.R., Zayets V.V., Solvar L.M., Romanchuk S.S.,** (2016). Underground gasification of coal deposits, Bulletin of NUVGP series "Technical Sciences" issue 2 (74)

8. European Economic Commission Methane - Markets Partnership (2010). Guide to Best Practices for Efficient Degassing of Methane Sources and Methane Utilization in Coal Mines, ECE Energy Series, 31, United Nations New York and Geneva

9. **Yukhimchuk S.Ya.,** (2020). Analysis of the state of methane extraction and use in Ukraine, Student Bulletin of NUVGP, vol. 2 (14)

10. **Kharchenko VI, Wu Tai Thu, Filonenko OO, Kucherenko OS, Voloshin A.Yu.**, (2011). Utilization of mine methane in a gas turbine unit, ELECTRONIC BULLETIN NUK • №1 •

11. **Oksenyuk RR, Semenyuk VV, Yukhimchuk S. Ya.,** (2020). Evaluation of methane production and use in Ukraine, International scientific-practical conference of young scientists, graduate students and applicants for higher education "Problems and prospects for the development of modern science" Rivne, Art. 136-137.

https://doi.org/10.31713/m1009

MODERNIZATION OF METALLURGICAL EQUIPMENT WITH THE DEVELOPMENT OF AN INNOVATIVE METHOD OF COILING HOT-ROLLED STRIPS

Kassym Yelemessov
Satbayev University, Candidate of Technical Sciences, Associate Professor, Director of the Institute of Metallurgy and Industrial Engineering, Republic of Kazakhstan

Kanay Rysbekov
Satbayev University, Candidate of Technical Sciences, Associate Professor, Director of the Institute of Geology, Petroleum and Mining engineering, Republic of Kazakhstan

Dinara Baskanbayeva
Satbayev University, Master of Technical Sciences, senior researcher, Republic of Kazakhstan

Akzhan Igbayeva
Satbayev University, Master of Technical Sciences, researcher, Republic of Kazakhstan

Annotation (Abstract)

The report presents the results of laboratory studies on the use of a combined (water and air) method of coiling hot-rolled strips on a coiler of a continuous broad-strip mill 1700. An innovative method of coiling strips allows to completely abandon the mechanical formation of hot-rolled coils. In order to study the hydraulic formation in laboratory conditions, a model of a coiler was created, which was structurally tied to the existing laboratory rolling mill "DUO-100". Studies carried out on the laboratory model of a coiler with hydraulic roll formation confirmed the fundamental possibility of using the proposed coiling method for working with various materials. Aluminum and lead strips were used as hot rolled strip. The results of laboratory work indicate a sufficient convergence of calculations with experimental data, which allows using the results obtained as recommendations for the creation of industrial installations. A method for calculating the flow rate and pressure of water and air is proposed. The calculation of the clamping force of the front end of the strip and the refined selection of the number of collectors and the maximum angle of rotation of the nozzle are carried out. The use of the combined principle for the formation of the first turns of the roll avoids contact between the rolled metal and the strip, expands the adjustment limits and reduces the requirements for its accuracy. The results obtained make it possible to recommend the use of a combined method of strip coiling in rolling production.

Introduction

Steel sheet production is the backbone of ferrous metallurgy. More than 80% of steel smelted at metallurgical plants is used for the manufacture of rolled products: thick and thin sheets, pipes of various diameters, bent sections from sheet metal, etc. [1,2]. Wide-strip hot rolling mills for steel strip have found wide application in the global production of rolled steel. The reason for this was the development of technologies for obtaining finished products from sheet material, such as stamping, bending of profiles, obtaining welded pipes of various sections and purposes.

Continuous wide-strip mill 1700 (CWSM) is designed for rolling steel strip with a thickness of 1.8 mm to 12 mm and a width of up to 1550 mm [3,4].

One of the main conditions for increasing production efficiency is increasing reliability, reducing downtime, extending the overhaul periods of rolling equipment, starting from the loading device and ending with the lifting-rotary tables of the mill.

From the analysis of the content of works devoted to the coiling of wide hot-rolled strips, the following conclusion can be drawn. The works of the authors of the CIS and most of the works of authors from Western countries are aimed at changing the design as a whole, improving individual units, and sometimes devoted to the problems of technology. The vast majority of Japanese works are devoted to the automation of the process, the use of various sensors in conjunction with computer systems, and the use of algorithms developed by the authors in the process of winding [5-10].

In order to study the innovative system of coiling at the Kazakh National Research Technical University named after K.I. Satbayev (Satbayev University), the authors carried out special studies to create a laboratory installation for a combined method of coiling hot-rolled strips [11].

The following tasks were solved:

- creation of the laboratory design of the coiler with the combined strip coiling system;
- development of the method for calculating the clamping of the front end of the strip;
- calculation of consumption, pressure of water and air;

The results of these studies are presented in this report.

Methods

During the research, a comprehensive methodology was used, including an analytical review of literary sources, a review of the operating experience and yield of suitable products while coiling of strips with coilers of industrial enterprises in Kazakhstan and foreign countries from reporting and statistical data. Theoretical studies of the technical parameters of a new design of coilers and experimental studies of coiling methods were also used.

This data will make it possible to evaluate and highlight the main influencing factors that will allow the creation of an innovative and efficient system for coiling hot-rolled strips. Experimental studies were carried out on a new design of coilers with reference to the laboratory rolling mill "DUO-100", and their results were processed by methods of mathematical statistics according to standard techniques. In the course of laboratory studies of the coiler model with the combined roll formation, one of the main parameters was the force from the side of a stream of water and air on the surface of the drum or on the coiled strip. The nozzles themselves used in the installation had calibrated holes, for which precisely manufactured jets from automobile carburetors were used.

Lead and aluminum strips were used as hot-rolled strip, which perfectly simulated the parameters of hot-rolled strips. This ensured a high reliability of the results obtained and made it possible to carry out calculations on the flow rate and pressure, as well as to develop a method for calculating the pressure of the front end of the strip.

Results and discussion

The development was based on a British patent [12], which proposed a device for winding thin metal strips (foil) by pressing the front end of the strip to the drum with a jet of compressed air. The air supply manifold bends around the reel drum in a circle and after the strip is captured, it can be removed from the surface of the coiled roll. The use of compressed air as a working medium limits the capabilities of this device, as the force from the side is jetted by its cross section, the speed of the working medium (air) outflow and the specific gravity of the working medium. It was proposed to form

rolls of hot-rolled steel practice in a similar way, using water in the working body [11-14].

Initially, we have completely replaced the working body of the system, i.e. air to water and calculations were carried out only for the hydraulic system. However, after a series of discussions and preliminary publications, we received comments on the problem of water residual between the turns of the rolls. Subsequently, it was decided to use a combined method of strip coiling. Hot air under pressure completely removes water between the coils, thus ensuring high quality coiled strips.

Coiler model design

The model of the coiler is designed to study the parameters of winding on model materials, to work out various modes, conditions for forming a roll. To obtain information simulating the operation of coilers in the shop, the coiler model was structurally tied in its parameters to the existing laboratory model of the "Duo-100" rolling mill (Fig. 1,2).

Diagram of the laboratory rolling mill "Duo - 100" with a reel model

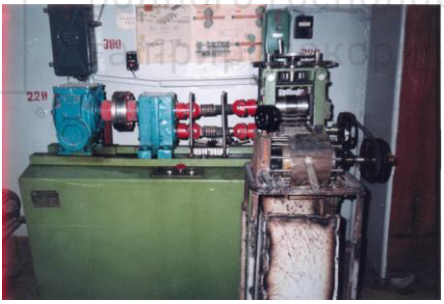

Fig. 1.

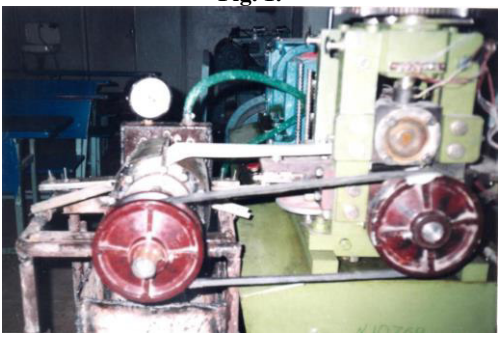

Fig. 2.

The main unit of the coiler is a drum with a diameter of 300 mm, made from a pipe. The length of the drum is 200 mm, which corresponds to the length of the roll barrel of the rolling mill. The drum is connected through trunnions to the drive shaft mounted in roller bearings. In the above calculations, for the most difficult case of winding a lead strip, the required power of the electric motor is determined. However, in order to simplify the design and at the same time to expand the possibilities of adjusting the relative speeds of the work rolls of the mill and the drum, a *V*-belt transmission was used. Were used pulleys - variators, allowing you to change their radius by changing the distance between their cones. The driving pulley is fixed coaxially with the lower roll of the mill, and the driven pulley is fixed on the axis of the reel drum.

The hydraulic forming device is mounted independently of the drum on the non-drive side (Fig. 2). It is based on a sealed steel tank with a capacity of 0.002 m^3 liters. It has two fittings for water supply and pressure gauge installation. On the side wall of the tank, perpendicular to the drum axis, collectors for supplying water and air to the winding strip are fixed.

The collectors are copper tubes with an outer diameter of 10 mm and an inner diameter of 8 mm. One end of the tubes is plugged. In each manifold, five holes are drilled along one longitudinal line, designed for screwing calibrated nozzles into them. The pipe is not plugged at the other end and the thread is cut. With the help of the thread, the collector is attached to the wall of the water tank, where, in turn, the thread is cut. Such fastening allows, by turning the collectors in the thread, to change the angle of inclination of the nozzles relative to the drum surface. Holes for mounting collectors are located radially relative to the axis of the reel drum.

The diameter of the centers of the fixing holes determines the distance from the cut of the working nozzles to the surface of the drum and the coiled strip. The holes for screwing calibrated nozzles into the manifolds are arranged in such a way that they evenly overlap the entire width of the strip wound on the drum.

The bearing housings of the drum and the tank for supplying water to the manifolds are welded to a frame mounted on the floor. The height of the frame is such that the upper level of the drum is 5 mm above the pick-up table of the rolling mill and approximately at

the upper level of the lower roll. The frame is equipped with waterproof casings that enclose the drum. The casings are made with a cut in the upper part, designed to feed the coiled strip from the rolling mill table to the drum. During the experiments, water is supplied to the reel model from the hydraulic pneumatic accumulators with a hose. The pressure in the reel tank is changed by adjusting the valve at the inlet to the tank according to the pressure gauge. Under the reel model there is a 40 liter water collection tank with a drain valve.

Research of the winder model

Calculations have shown the possibility of creating a laboratory design of a coiler designed for winding a lead strip 50 mm wide and up to 1 mm thick. In this case, the nozzle diameters of 0.7 mm, 0.9 mm and 1.1 mm were chosen as the basis for the calculation.

However, when making the current working model, it was necessary to take into account the objective reasons that limit the capabilities of the device. Thus, a check with a pressure gauge in the water supply network showed that its maximum value does not exceed 0.38 MPa. The diameter of the outlet section of the valve for water supply is 12 mm. Based on the specified pressure, we determine the force of the jet at nozzle diameters of 1 mm, 2 mm and 3 mm.

For pneumatic and hydraulic systems, in order to ensure the amount of supplied liquid or gas at the operating pressure value, it is necessary that the total cross section of the jets at the final stage be less than or equal to the supply line. Otherwise, the volume or pressure of the supplied working fluid decreases. In the current model, copper tubes with an outer diameter of 10 mm and with an inner diameter of 8 mm were used as collectors for supplying water to the nozzles. The number of nozzles with a diameter of 1 mm can be no more than 144 pieces, with a diameter of 3 mm - 16 pieces, with a diameter of 5 mm - 6 pieces. Assuming that the number of supply manifolds must be at least six, and the number of nozzles on each manifold must be at least five, then the total minimum number of nozzles will be 30 pieces.

Method for calculating the clamping force of the front end of the strip for a laboratory coiler

To determine the number of collectors (points of load application to the strip), we proceed from the following conditions:

1. The strip fed for coiling has the same width and thickness and is flat or nearly flat. This complies with the requirements for a rolled strip.

2. The task of the forming device is to provide compression of the strip to the surface of the drum along its entire generatrix (along the entire circumference). For the laboratory design of the coiler, it was decided to test the forming device without the use of additional mechanical guides.

The action of normal force to the surface of the drum, the movement of the front end of the strip can be viewed tangentially to this point.

For further winding, it is necessary that when moving, the front end must necessarily fall under the action of the next one. Consequently, the deformation of the surface of the coiled strip is less than 1%. For a laboratory coiler, this ratio will be: 1/130=0.0077. With such a small value of the total degree of deformation, the main part of the deformation will be elastic.

Since it is almost impossible to separate the plastic and elastic components of the deformation of the strip being coiled, then when determining the number of collectors, we assume that the deformation produced at the point of application of the force to the strip is mainly elastic. It follows from this that it is necessary to determine a sufficient number of points of application of force (jet), that is, it is necessary to choose the optimal number of collectors and the angles between them. To do this, we will use the graphic-analytical method and construct the intersection points of tangents and cuts of nozzles located at different distances from the drum surface.

Accordingly (Fig. 3), the number of nozzles decreases as they move away from the drum surface. The results are summarized in Table 1.

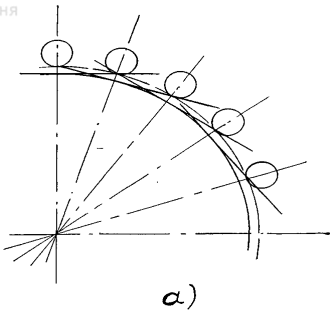

Fig. 3. Graphic-analytical method for determining the number of collectors for the coiler model

Table 1

The number of collectors and angles between them

h_0, mm	3	5	10	15	20
cos α	0,942	0,915	0,855	0,802	0,756
α^0	19,61	23,8	31,24	36,68	40,9
η	18,36	15,13	11,52	9,82	8,9
η_ϕ	18	15	12	10	9
α_ϕ^0	20	24	30	36	40

In order for the force from the side of the jet to have a pushing component, the jet must have an inclination in the direction of the movement of the strip. However, the angle of inclination cannot be greater than a certain value, since with its increase, simultaneously with the growth of the horizontal component, the normal one, which is responsible for pressing the strip to the drum and elastoplastic deformation, decreases.

The required force consists of two values - from the bending of the strip in the elastic-plastic region and from overcoming the centrifugal force. Figure 4 shows the direction of the forces acting on the strip to press it against the drum surface.

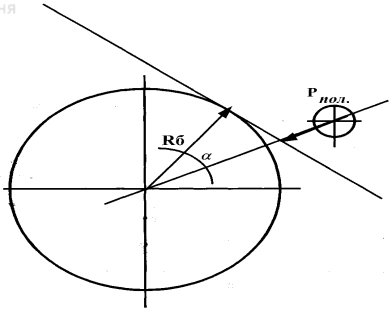

Fig. 4. The action of the forces forming the roll

The dimensions of the strips are taken constructively, based on the characteristics of rolling on a laboratory rolling mill:

width b=50 mm = 0.05 m;

thickness h=0.2; 0.5; 0.8; 1 mm = 0.0002; 0.0005; 0.0008; 0.001 m;

α is the angle between forming rollers or nozzles (in our case, α=36°).

The total force acting on the front end of the strip will be made up of static and dynamic forces

$$R_{pol}=R_{st}+R_{din}$$

The results of calculating the values of the clamping force are summarized in Table 2.

Table 2

The results of calculating the values of Pst, N

Strip width, m	0,05	0,05	0,05	0,05
Strip thickness, m	0,0002	0,0005	0,0008	0,001
Static force, N	0,4	2,6	6,9	10,7

The results of calculating the values of the mass and weight of one turn of the strip, as well as the dynamic force are shown in Table 3.

Table 3

The results of calculating the value of the mass and weight of one turn of the strip, as well as the dynamic force

Thickness, m	0,0002	0,0005	0,0008	0,001
Width, m	0,05	0,05	0,05	0,05
Mass M, kg	0,046	0,116	0,186	0,23
Weight W, N	0,46	1,16	1,86	2,3
Dynamic force, N	0,000185	0,00047	0,00075	0,00093

From the Table 3 it follows that the dynamic forces to overcome the centrifugal force are insignificant due to the low rolling speed.

Based on the dimensions of the drum, the number of hydraulic supply lines is initially assumed to be ten with an even distribution across the diameter through 36°. The arrangement and the number of nozzles on each collector are determined from the condition of winding strips of different widths. All ten hydraulic feeding lines will operate in the winding of coils up to 50 mm wide.

The total force per nozzle system when winding strips of different thicknesses and widths is shown in Table 4.

Table 4

Total force P, N

Strip width, m	0,05	0,05	0,05	0,05
Strip thickness, m	0,0002	0,0005	0,0008	0,001
Force, N	0,4	2,6	6,9	10,7

Calculation of water pressure and flow

Based on the arrangement of nozzles and the required values of the total forces on one hydraulic supply line (Table 4), dividing the latter by the number of nozzles in the line, we determine the required force of the water coming out of one nozzle. The calculated forces of the jet emerging from one nozzle are entered in Table 5.

Table 5

The force of the jet coming out of one nozzle, N

Strip width, m	0,05	0,05	0,05	0,05
Strip thickness, m	0,0002	0,0005	0,0008	0,001
Force, N	0,08	0,52	1,38	2,14

From Table 5 it follows that when bending strips with a width of 0.05 m and a thickness of 0.001 m, the force of water should be equal to 2.14 *N*. We take this value as the main one when carrying out further calculations. For the calculation, we set three nozzle diameters: 0.7 mm, 0.9 mm, 1.2 mm.

The required force of the water jet on the strip is determined by the formula

$$Q_{\text{m}} = P \cdot V \cdot S,$$

where ρ is the density of water, ρ=1000 kg/m^3;

s - nozzle section, m^2.

We get the expression for the effort of the water jet

$$P_c = \rho \cdot s \cdot v^2$$

Subsequent values of the speed of the water jet are given in Table 6.

Table 6

Estimated value of water jet speed, m/s

Section, m^2	0,08	0,52	Force, N		
				1,38	
$0{,}4 \cdot 10^{-6}$	14,14	36.1		58,74	$0{,}4 \cdot 10^{-6}$
$0{,}64 \cdot 10^{-6}$	11,2	28,5		46.4	$0{,}64 \cdot 10^{-6}$
$0{,}95 \cdot 10^{-6}$	9,2	23,4		38,1	$0{,}95 \cdot 10^{-6}$

Subsequent water flow rates are shown in Table 7.

Table 7

Estimated value of water consumption, kg / s

Section, m^2	Thickness, m			
	0,0002	0,0005	0,0008	0,001
$0{,}4 \cdot 10^{-6}$	0,006	0,014	0,023	0,03
$0{,}64 \cdot 10^{-6}$	0,007	0,02	0,03	0,04
$0{,}95 \cdot 10^{-6}$	0,009	0,02	0,04	0,045

The required water pressure in the system is determined from the expression

$$P_в = \frac{Q_m^2}{2 \cdot \mu^2 \cdot S^2 \cdot \rho},$$

where μ=0.62 (for water) is the flow coefficient for low-viscosity liquids.Subsequent water pressures are summarized in Table 8.

Table 8

Estimated value of water pressure, Pa

Section, m^2	Thickness, m			
	0,0002	0,0005	0,0008	0,001
$0{,}4 \cdot 10^{-6}$	$0{,}029 \cdot 10^6$	$0{,}17 \cdot 10^6$	$0{,}44 \cdot 10^6$	$0{,}69 \cdot 10^6$
$0{,}64 \cdot 0^{-6}$	$0{,}0163 \cdot 10^6$	$0{,}105 \cdot 10^6$	$0{,}28 \cdot 10^6$	$0{,}44 \cdot 10^6$
$0{,}95 \cdot 10^6$	$0{,}011 \cdot 10^6$	$0{,}07 \cdot 10^6$	$0{,}19 \cdot 10^6$	$0{,}29 \cdot 10^6$

Conclusion. The conducted research led to the following conclusions:

1. It has been proposed to replace the traditional roll former system with the hydraulic roll former. To test the idea of the hydraulic forming of rolls, a model of a coiler was made.

Research carried out at the Department of Technological Machines, Transport and Logistics at Satbayev University confirmed the efficiency of this proposal and made it possible to make a number of developments and recommendations for creating an industrial coiler.

2. The performed calculations showed the possibility of replacing the mechanical formation with the hydraulic one using a working medium - water and air.

3. In order to study the combined formation in laboratory conditions, a model of a coiler was created, which was structurally tied to the existing laboratory rolling mill "DUO-100".

4. Studies carried out on a laboratory model of a coiler with combined coil formation, have confirmed the fundamental possibility of using the proposed method of coiling for working with various materials.

5. The results of laboratory work indicate a sufficient convergence of calculations with experimental data, which allows using the results obtained as recommendations for the creation of industrial installations.

The use of the combined principle for the formation of the first turns of the roll allows avoiding contact between the rolled metal and the strip, eliminates the appearance of rust due to water residues, expands the adjustment range and reduces the requirements for its accuracy.

References

1. **Grudev A. P., Mashkin L. F., Khanin M. I.**, (1994). Technology of rolling production: textbook. M.: Metallurgy

2. **Rudskoy A.I., Lunev V.A**. (2005). Theory and technology of rolling production: Textbook. – SPb. Nauka

3. **Korolev A.A.** (1981). Rolling mills and equipment for rolling shops. Atlas: Textbook for universities. – 2 nd ed. - M.: Metallurgy

4. **Sverdlik G.I., Sobolev S.E.** (2013). Technological machines and equipment for metallurgical production. Methodical instructions for practical exercises. Vladikavkaz

5. **Yatunchi K, Noma Y, Shimizu R, Tanomoto S.,** (1982). Unmanned operation technology for a hot strip mill. Jron and Streel Engineer, v. 59, № 11

6. Samways №.1. (1984). Dofasco: Canada's largest tlat rolled producer. Iron and Steel Engineer, v.61, n 9, p.t.83 -t 101.

7. **Juschba R., Stanbermann H.** (1985). Hot-strip coiler process technology. – Metallurgical Plant and Technology, n 2, p. 42-47.

8. **Ogashi H., Imail I.,** (1983). New generation hot strip mill at nipon Steel, s Ywata works/ E. Toda e.s.-Iron and Steel engineer, v.60, n 12, p.53-61.

9. **Carroll W.P., Macneil P.A.** (1965). Design and start-up of the Stelco 2050 mm hot strip mill. –Iron and Steel Engineer, , v. 62, n 4, p. 39-45.

10. **Morennikov, N.V.,** (1987). Certificate of authorship № 1362528. USSR. The drum of the coiler of the strip rolling mill. Beekeeper. Publ., B.I. №. 48.

11. **Davilbekov N.Kh., Kurapov G.G., Pepelyaev I.V., Eskulov S.S., Klement'ev V.A., Mizyurin V.V., Kolynyuk E.P., Elemesov K.K.** Method of coiling on a drum of a coiler of a strip mill. Patent RK №. 6363.

12. Patent № 2096873 Great Britain. A device for threading a metal strip into a coiler. Publ. 27.10.82.

13. **Davilbekov N.Kh., Kurapov G.G., Elemesov K.K.** (1999). Improving the operation of broadband coilers. Proceedings of the International Symposium dedicated to the 100th anniversary of the birth of K.I.Satpayev. Almaty: KazNTU,.S. 268-270.

14. **Davilbekov N.Kh., Kurapov G.G., Eskulov S.S, Elemesov K.K.,** (1995). Device for coilers for coiling strips. Technology of production and processing of ferrous metals. Almaty, RIK on educational and methodological literature, pp. 61-64.

https://doi.org/10.31713/m1010

ASSESSMENT OF FORECAST ACCURACY DANGEROUS PROPERTIES OF COAL LAYERS BY THE DEGREE OF METAMORPHISM OF SOLID FOSSIL COALS

Antoshchenko Mykola
Volodymyr Dahl East Ukrainian National University,
Doctor of Engineering Sciences, Professor,
Head of the department of Mining, Ukraine

Rudniev Yevhen
Volodymyr Dahl East Ukrainian National University,
PhD, Associate Professor, Head of the Department
of Electrical Engineering, Ukraine

Filatiev Mykhailo
Volodymyr Dahl East Ukrainian National University,
Doctor of Engineering Sciences, Associate Professor Department of
Town Planning, Municipal Facilities and Materials Science, Ukraine

Filatieva Elvira
Volodymyr Dahl East Ukrainian National University, Senior
Lecturer Department of Chemical Engineering and Ecology, Ukraine

Brozhko Rostyslav
Volodymyr Dahl East Ukrainian National University,
PhD, Associate Professor, Associate Professor of the Department
of Electrical Engineering, Ukraine

Abstract

In the normative base of Ukraine for the safe mining of coal seams, only five indicators of the degree of metamorphism are used to predict the manifestation of their hazardous properties during mining operations: mass release of volatile substances during thermal decomposition of coal without air (V^{daf}) access to characterize coal; volumetric yield of volatile substances V_V^{daf} to establish the distinctive properties of anthracites; logarithm of electrical resistivity ($\lg\rho$); the thickness of the plastic layer (y) and the grade of coal (M) for predicting the outburst hazard of seams. When developing regulatory documents, it was assumed that these criteria for assessing the degree of coal metamorphism remain constant within one mine field. Their values, as mining operations show, are influenced by the location of the coal sampling site in relation to the distance from relatively large geological

disturbances or the boundaries of the gas weathering zone.

In most cases, the boundaries of mine fields are usually relatively large geological faults. The proximity of the locations of coal sampling points to them influences the obtained results of evaluating the properties of mine layers.

Adjusting indicators (V^{daf}, V_V^{daf} , lgρ, y ,M) for individual mines on the possible impact of geological disturbances, the depth of the mining robot and the distance from the zone of gas weathering, according to the requirements of regulatory documents. For this reason, it is of scientific and practical interest to establish the possible ranges of change in the indicators of the degree of metamorphism of coal within the same mine layer. The results of research in this direction are relevant, as they are necessary to improve the regulatory framework for the safe mining of coal mines.

A possible change within a separate mine field was considered using the example of the indicator V^{daf} as the most studied at present. According to a specially developed methodology, the analysis involved data on 2193 mines from different coal basins. Most of them belong to the mines of the Donetsk basin (1773). The rest of the basins account for information on 460 mine layers, including data on 46 mine layers for the Lvov-Volyn basin.

Introduction

It has been established that within the boundaries of a separate mine formation, V^{daf} remains relatively constant. Along with this, it was found that, in addition to the location of the coal sampling site, the accuracy of determining the indicator is significantly affected by the absolute value V^{daf}. Absolute standard deviation (σ_i) from the averaging straight line in separate intervals the values were 2.29-5.33%, and the relative ($\Delta\sigma$) - were in the range of 8.50-213.01%. Maximum values $\Delta\sigma$ (more than 20%) corresponds to the values In the regulatory documents, the degree of coal metamorphism is assessed, including for the range of variation V^{daf} within 2-8%, which can lead to even greater relative deviations $\Delta\sigma$ (more than 100%) and errors in predicting the hazardous properties of mine layers. Such an accuracy of V^{daf} determination V^{daf} and other indicators of thermal destruction of coal casts doubt on their use for predicting the hazardous properties of mine layers.

In essence, thermal decomposition is another artificial stage in the transformation of coals outside the Earth's interior at a higher temperature than the process of metamorphism. It does not directly reflect changes in the chemical composition, internal structure and properties of coals that have occurred in the past geological periods

of time.

To improve the regulatory documents on the safe conduct of mining operations to characterize the degree of coal metamorphism when predicting the hazardous properties of mine layers, it is necessary to use classification indicators that directly reflect the change in the composition and properties of coals in the process of geological transformations.

Main Body. During mining, in many cases, accidents occur, accompanied by the processes of gas release, gas-dynamic phenomena, spontaneous combustion of coal, increased dust formation with its tendency to explosiveness. These and some other dangerous phenomena accompanying accidents with serious consequences in mines, according to many scientists [1-5], due to the genetic properties of fossil coals. They appeared as a result of metamorphic processes of transformation of the original organic matter under the influence of increased temperature and pressure within the Earth in the past geological periods of time. In the generally recognized case, metamorphism means a variety of endogenous processes, which are associated with changes in the structure, mineral and chemical composition of coals [6].

The degree of metamorphic transformations in accordance with the requirements of the modern regulatory framework of Ukraine for the safe conduct of mining operations [7-10] is predicted, in most cases, by one indicator - a massive release volatiles during thermal decomposition of coal without air access (V^{daf}).

When developing regulatory documents, it was assumed that the indicator and some other criteria for assessing the degree of coal metamorphism are relatively constant within the same mine field. The accuracy of the prediction of the manifestation of hazardous properties of each mine layer largely depends on the reliability of the assumption. In most cases, the boundaries of mine fields are usually relatively large geological faults [11]. The proximity of coal sampling sites to them undoubtedly affects the results obtained for assessing the properties of mine layers. For example, the degassing effect of the Karlovsky and Sofievsky discharges spread over a distance of up to 680 m [12]. In close proximity to geological disturbances, the coal gas content did not exceed 10 $м^3$/tons of ash-free rock, and outside the zone of their influence, it stabilized at the

level of 30 м^3/tons of ash-free rock. The gas content of the anthracite layer also changed depending on the distance to the upper boundary of the methane zone. The methane content of coal-bearing deposits is mainly determined by the depth of the seams, the degree of coal metamorphism, the presence of cover deposits and other factors [13].

The information provided indicates a possible change in gas content depending on the location of coal sampling at different values of depth and distance to a geological fault or a zone of gas weathering. In turn, in the regulatory documents [7-10] empirical dependences of gas content and other hazardous properties of the manifestation of mine layers during mining operations on the degree of coal metamorphism are used without taking into account the influence of this factor. In almost all cases, predicting the manifestation of hazardous properties and the likelihood of emergencies is established [7-10] in relation to a separate mine layer. An individual assessment of the manifestation of the hazardous properties of each mine layer is made, in general, using five indicators of the degree of coal metamorphism. In addition to the indicator V^{daf} in some cases, in addition to characterizing the properties of anthracites, the volumetric yield of volatile substances is use (V_V^{daf}) and logarithm electrical resistivity (lgρ). In other cases, to establish the hazardous properties of mine layers, sometimes the thickness of the plasticity layer is also considered (y) and coal brands (M). They are not corrected for the possible influence of geological disturbances, the depth of mining operations and the distance from the gas weathering zone. For this reason, it is of scientific and practical interest to establish the possible boundaries of the ranges of variation of the indicators of the degree of metamorphism of coal within the same mine formation. In a number of cases, it is also necessary to substantiate the possibility of using indicators of the degree of coal metamorphism without adjusting them to establish the manifestation of the hazardous properties of mine layers in different coal basins. The research results in this direction are necessary to improve the requirements of the regulatory framework for the safe mining of coal mines, which indicates their relevance.

The idea is to use experimental data on the quantitative value of one of the main indicators of the degree of coal metamorphism,

determined by different researchers for a specific mine formation at different periods of time of its development. This allows you to analyze randomly generated databases on the current ranges of change in the classification indicator in the aggregate of the considered layers of the mine.

The goal is to establish possible absolute and relative individual errors in determining one of the main indicators of the degree of metamorphism V^{daf} within the boundaries of a separate mine formation at a random place of coal sampling.

Methodology. One of the main and most studied indicator of the degree of coal metamorphism is the release of volatile substances (V^{daf}). To predict the manifestation of hazardous properties of mine layers during mining, this indicator is used in all regulatory documents [7-10]. Sufficiently voluminous information about the values of the indicator V^{daf} contained in the "Catalog of mine plastics of the USSR on the dust factor" [10]. It provides data for 2,193 mines from different coal basins. The bulk of the data relates to the mines of the Donetsk basin (1773). The rest of the basins account for information on 460 mine layers, including data on 46 mine layers for the Lvov-Volyn basin. In parallel with the data [10], the analysis involved information on the release of volatile substances for 206 mines according to other sources [1-4, 14, 15].

To exclude possible errors in establishing the correspondence between the considered mine layers according to different sources of information, their belonging was checked by the name of the mines (mine departments), the local name of the layers and their geological symbols.

Results of statistical studies. Processing of data pairs of weight yield of volatile substances V_1^{daf} и V_2^{daf}, borrowed, respectively, from the "Catalog of Mine Plastics of the USSR on the Dust Factor" [10] and others [1-4, 14, 15] sources have shown a close correlation between them (fig. 1). The correlation coefficient (r) for the considered sample of 206 data pairs was quite high $(0{,}935)$.

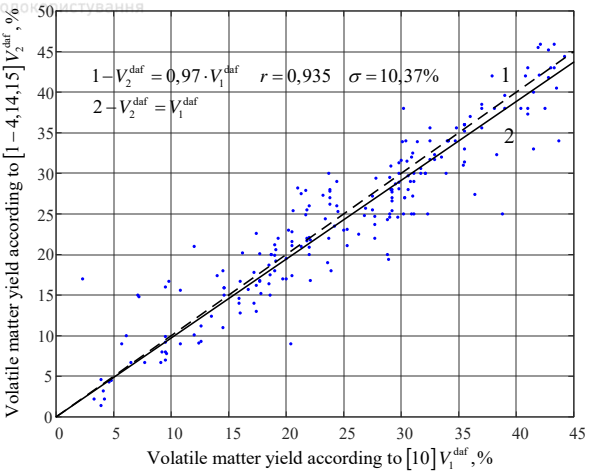

Fig. 1. Correspondence of the yield of volatile substances during thermal decomposition of coals of different coal deposits between data $\left(V_1^{daf}\right)$, catalog [10] and given in others [1–4, 14, 15] sources $\left(V_2^{daf}\right)$

1 - straight line obtained from processing results experimental data by the least squares method; *2* - bisector of the coordinate grid;

• - points defining the relationship between V_1^{daf} and V_2^{1daf};

r, *σ* - respectively the correlation coefficient and standard deviation

This indicates that within the boundaries of an individual mine formation, the value of the mass yield of volatiles during the thermal decomposition of coal remains relatively constant. Ideally, the experimental points of interdependence of the function $V_2^{daf} = f\left(V_1^{daf}\right)$ must be located on a segment of the bisector line (2) of the coordinate grid.

The resulting averaging regression line (1) slightly differs from the bisector (2). On the other hand, experimental data from different sources in a significant part of cases deviates significantly from the considered straight lines (1,2). One of the reasons for this situation may be coal sampling in different parts of the mine field and at different distances from the zones of influence of geological disturbances and gas weathering. In addition to the place of sampling of coal in the mine field for significant deviations σ=10.37%

experimental data from averaging straight lines (1, 2) could provide the accuracy of determining the yield of volatiles during thermal decomposition of coal without air access. To assess the influence of this factor, the absolute standard deviations were considered $(\bar{\sigma}_i)$ in separate ranges V^{daf} (tab. 1).

Table 1

Information about the values of standard deviations (RMS) $(\bar{\sigma}_i)$ from the averaging straight line 1 (Fig. 1) in separate ranges of variation V_i^{daf}

Ranges of change V_i^{daf}, %	0-5	5-10	10-15	15-20	20-25	25-30	30-35	35-40	40-45
Average value in the range V_i^{daf}, %	2,5	7,5	12,5	17,5	22,5	27,5	32,5	37,5	42,5
Absolute RMS in the range $\bar{\sigma}_i$,%	5,33	4,23	3,62	2,29	4,22	3,08	3,17	4,38	3,61
Relative RMS,% $\Delta\bar{\sigma}_i = \frac{\bar{\sigma}_i}{\bar{V}_i^{daf}} \cdot 100$	213,01	56,4	28,95	13,07	18,74	11,19	9,76	11,7	8,50

Absolute standard deviations (σ_i) were in the interval 2,29-5,33 % with correlation dependence (r=1) от $\bar{V}_i^{daf}$ (fig. 2*a*). Its average value (line 1) is 3,8 %.

Relative standard deviations ($\Delta\sigma_i$) defined by dependency

$$\Delta\sigma_i = \frac{\bar{\sigma}_i}{V_i^{daf}} \cdot 100, \%. \quad (1)$$

For the considered sampling possible values output volatiles V_i^{daf} were in the range 1-50%, and the absolute standard deviations $(\bar{\sigma}_i)$ in separate ranges V_i^{daf} were 2,29-5,33%. Based on possible values V_i^{daf} and $\bar{\sigma}_i$, calculated according to equation (1) the minimum expected ($\Delta\sigma_{min}$), maximum ($\Delta\sigma_{max}$) and middle ($\Delta\sigma_{cp}$) relative standard deviations.

Minimum value $\Delta\sigma_{min}$ will be observed at the maximum value

V_i^{daf} $(\approx 50\%)$ and minimal $\bar{\sigma}_i$ $(\approx 2{,}29\%)$. For this case

$$\Delta\sigma_{\min} = \frac{2{,}29 \cdot 100}{50} = 4{,}58\% .$$

Maximum value $\Delta\sigma_{\max}$ will be observed at $V_i^{\text{daf}} = 1\%$ and $\bar{\sigma}_i = 5{,}33\%$:

$$\Delta\sigma_{\max} = \frac{5{,}33 \cdot 100}{1{,}0} = 533\% .$$

Based on similar reasoning, the average value $\Delta\sigma_{\text{ср}}$ for the considered sample is determined by the average possible values $\bar{V}_i^{\text{daf}} \approx 25\%$ и $\bar{\sigma}_i = 3{,}8\%$

$$\Delta\sigma_{\text{ср}} = \frac{3{,}8 \cdot 100}{25} = 15{,}2\% .$$

Based on the above calculations and the schedule of changes $\Delta\bar{\sigma}_i$ (fig. 2) should, what $\bar{V}_i^{\text{daf}}$ more or less reliably determined when its values are higher 25%. The relative standard deviation in this case is about 15%, which is quite acceptable for technical calculations.

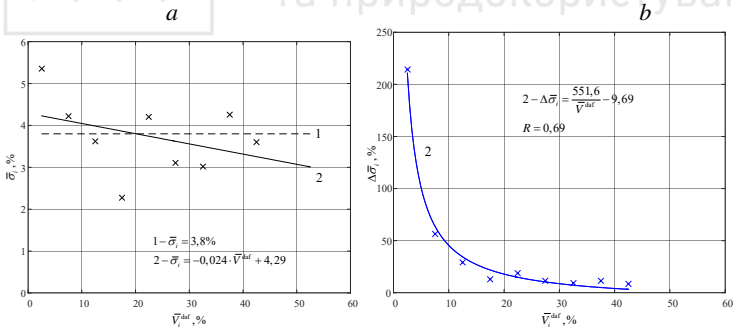

Fig. 2. Dependence of changes in absolute (a) and relative (b) $(\Delta\sigma_i)$ root-mean-square deviations from the value of the release of volatile substances in separate intervals $\bar{V}_i^{\text{daf}}$: 1(*a*) - direct dependence of the mean absolute value $\bar{\sigma}_i$; 2(*b*)- relative value curve $\Delta\bar{\sigma}_i$;

× - average values $\bar{\sigma}_i$ and $\Delta\bar{\sigma}_i$ in the respective ranges $\bar{V}_i^{\text{daf}}$;

r, *R* - correlation coefficient and correlation ratio

At values of the yield of volatile substances in the range of 25-

8%, the determination accuracy $\overline{V}_i^{daf}$, since the relative standard deviations can exceed 50%. This casts doubt on the use of the yield of volatile substances in the considered range of its change as a reliable classification indicator of the degree of metamorphism of coals when establishing the hazardous properties of mine layers.

The accuracy of determining the mass yield of volatile substances decreases even more when its values are less than 8%.

In this case, the relative standard deviations can exceed 500%. Such an accuracy in determining any parameter is unacceptable for its use in engineering calculations.

The features of the accuracy of determining the mass yield of volatile substances were taken into account when developing GOSTs for the classification of coals according to their genetic and technological parameters.

According to [16] V^{daf} used as a classification indicator for dividing fossil coal into fuels. When V^{daf}=8% and more coals are classified as stone, and when V^{daf}<8% - to anthracites. In the range and more, using this indicator, coals are divided into 21 types according to their consumer properties. The high determination error in the range of 8-25% when establishing consumer properties according to industrial classifications was compensated for by considering additional indicators characterizing the technological properties of coals. The final selection of a set of classification indicators for the coals under consideration was established empirically with subsequent verification in production conditions. Thanks to this approach, a modern industrial classification has been created [16].

It is not possible to predict the hazardous properties of coal layers in this way, due to the lack of conditions for carrying out appropriate experiments in mine conditions. For this reason, in the regulatory documents [7-10], the release of volatile substances during the thermal decomposition of coals without air access remains practically the only classification indicator of the degree of metamorphism. When establishing certain types of hazardous properties of coal layers, meaning V^{daf}≥4% [3-5], which does not exclude a relative error of up to 100% in determining this indicator. In the regulatory documents [7-8], the assessment of the degree of

metamorphism of coals is performed for the range of variation within 2-8%, which can also lead to significant errors. The above facts testify that the modern regulatory framework of Ukraine for the safe mining of coal deposits requires its improvement in terms of predicting the hazardous properties of coal layers using other indicators of the degree of coal metamorphism V^{daf}.

In addition to the place of sampling of coal in the mine field and the absolute value V^{daf} ash content also affects the error of its determination [17,18]: the higher it is, the more the value is distorted V^{daf}. With an increase in ash content, the proportion of volatile substances from mineral components increases and the proportion of organic matter decreases, which includes the total value of volatiles from the organic and mineral parts of coal, calculated on a dry ashless mass. Due to the lack of methods for complete demineralization of the sample, to obtain an accurate value laboratory is impossible, and recalculation of volatile substances per organic mass leads to an overestimation of the indicator V^{daf}. Currently the indicator only approximately characterizes the behavior of the organic mass of coals during thermal destruction and is completely unacceptable for calculations at high ash content of samples V^{daf}. In accordance with the current situation, when establishing the consumer properties of coal, their ash content should not exceed 10% [19]. Samples with a higher ash content are preliminarily enriched in organic or inorganic liquids in accordance with the developed GOSTs. Such an artificial decrease in the indicator of the content of mineral impurities in coal samples when determining does not correspond to the natural state of mine layers, which undoubtedly affects the accuracy of predicting their hazardous properties V^{daf}.

The presence of a stable connection between V_2^{daf} and V_1^{daf} (r=0,935, fig. 1) when sampling coal at different distances from the zones of gas weathering and geological disturbances, it indicates that the release of volatiles during the thermal decomposition of coal is a fairly stable indicator for separately considered mine formation regardless of the coal deposit. This is, to a degree, due to the weak correlation dependence of volatiles on the depth of the gas weathering zone (r=0.51) and its practical absence (r=0.05) and

angle of the abundance coal seam [20].

The studies carried out have confirmed some constancy of the volatile matter yield for coal of a particular mine formation, regardless of the sampling location. Along with this, taking into account the ambiguous change in the relative RMS depending on the absolute values of the indicator, it cannot be considered scientifically justified to establish the degree of metamorphic transformations of coals with the release of volatile substances less than 25%.

As it was established earlier, the relative RMS for such cases can exceed 100%, which obviously indicates the possibility of obtaining unreliable results when predicting the manifestation of hazardous properties for a significant number of mines.

The use of the volatile matter yield indicator for predicting the hazardous properties of mine layers [7-10] is borrowed, without proper scientific justification, by analogy with its application in the industrial classification [16]. To establish consumer properties, coal samples are prepared for dry or dry ashless mass [19], which does not correspond to the state of coal in mine layers during mining operations. When predicting the tendency of coal mines to manifest their hazardous properties, it is necessary to take into account the existing differences between the laboratory determination of indicators and the conditions for finding coal in production conditions. They are primarily distinguished by the presence of natural moisture and ash content during mining operations.

Also, without proper scientific substantiation in the regulatory documents [7-10], the release of volatile substances during thermal decomposition of coals is accepted as a classification indicator of the degree of coal metamorphism. The generally accepted concept of metamorphism is the transformation of brown coal sequentially into coal and anthracite as a result of changes in the chemical composition, structure and physical properties of coal in the bowels, mainly under the influence of increased temperature and pressure [6]. Volatile products during the thermal decomposition of coals cannot directly characterize changes in the chemical composition, structure and physical properties of coals, occurring in past geological periods of time. In essence, the processes of thermal decomposition are the next artificial stage in the transformation of coals at higher temperatures [21]. The processes of coal metamorphism in natural

conditions reached a certain degree of transformation of organic matter at a temperature of no more than 650 °C. Thermal decomposition, according to the requirements of chemical and technical analysis, is carried out at 900 °C or 850 °C [19].

Conclusions. The studies carried out allow us to make the following conclusion, important for improving the regulatory framework for the safe mining of coal seams:

1. The release of volatile substances during the thermal decomposition of coal is a relatively constant indicator for individual mine layers in different coal basins, which is confirmed by a high mutual correlation dependence between the results of laboratory tests of coal samples taken in different parts of the mine fields.

2. The relative error in determining the weight yield of volatile substances for all considered coal basins depends on the absolute value of the indicator. The maximum relative standard deviations of more than 100% are observed when the release of volatile substances is less than 8%, and when the release of volatile substances is more than 25%, they stabilize at the level.

3. When developing normative documents for the safe mining of coal mines, the indicator of the weight yield of volatile substances to characterize the degree of metamorphism was borrowed from industrial classifications characterizing the consumer properties of coal without sufficient scientific justification.

4. The value of the weight yield of volatile substances according to the methods for establishing consumer properties is determined in laboratory conditions with an artificial decrease in ash content of less than 10% and removal of external moisture, which does not correspond to the production conditions of the manifestation of hazardous properties of mine layers during mining.

5. In essence, thermal decomposition is another artificial stage in the transformation of coals outside the bowels of the Earth at a higher temperature compared to the processes of metamorphism. Decomposition products do not directly reflect changes in the chemical composition, internal structure and properties of coals that have occurred in the past geological periods of time.

6. To improve the regulatory documents on the safe conduct of mining operations to characterize the degree of coal metamorphism

when predicting the hazardous properties of mine layers, it is necessary to use classification indicators that directly reflect the change in the composition and properties of coals in the process of geological transformations.

Referenses

1. **Ayruni, A T.** (1981). Teoriya i praktika borbyi s rudnichnyimi gazami na bolshih glubinah. Moskva: Nedra.

2. **Ettinger, I. L., & Shulman, N. V.** (1975). Raspredelenie metana v porah iskopaemyih ugley. Moskva: Nauka.

3. **Grekov, S. P., Pashkovskiy, P. S., & Orlikova, V. P.** (2014). Teplovoy effekt okisleniya ugley i endogennaya pozharoopasnos. Ugol Ukrainyi, 10, 46-50.

4. **Akinshin, B. T.** (1985). Metamorfizm i vzaimosvyaz mikro– i makroporistoy strukturyi, vlazhnosti uglya s gazonosnostyu plastov. Ugol Ukrainyi, 3, 37-39.

5. **Medvedev, E. N., Saranchuk, V. I., & Kachan, V. N.** (1984). Otsenka pyileobrazuyuschey sposobnosti ugley v ryadu metamorfizma. Ugol Ukrainyi, 8, 32-33.

6. GOST 17070–2014. Ugli. Terminyi i opredeleniya. Mezhgosudarstvennyiy standart. (2015). Moskva: Standartinform.

7. SOU 10.7.00174088.011–2005. Pravila vedeniya gornyih rabot na plastah, sklonnyih k gazodinamicheskim yavleniyam. (2005). Kiev: Minugleprom Ukrainyi.

8. Rukovodstvo po proektirovaniyu ventilyatsii ugolnyih shaht. (1994). Kiev: Osnova.

9. Rukovodstvo po preduprezhdeniyu i tusheniyu endogennyih pozharov na ugolnyih shahtah Ukrainyi: KD 12.01.402. (2000). Donetsk: NIIGD.

10. Rukovodstvo po borbe s pyilyu v ugolnyih shahtah. (1979). Moskva: Nedra.

11. Katalog shahtoplastov Donetskogo ugolnogo basseyna s harakteristikoy gorno-geologicheskih faktorov i yavleniy/Akademiya nauk SSSR, IGD im. A.A. Skochinskogo. (1982). Moskva: MUP SSSR.

12. **Antoschenko, N. I., Okalelov, V. N., & Pavlov, V. I.** (2013). Formirovanie dinamiki metanovyideleniya iz podrabatyivaemogo massiva pri otrabotke gazonosnyih ugolnyih plastov: Monografiya. Alchevsk: DonGTU.

13. **Brizhanev, A. M., Sheyko, Y. M., & Dzhamalova, H. F.** (1982). Vliyanie tektonicheskih narusheniy na raspredelenie gazov v uglenosnyih otlozheniyah Donbassa. Ugol Ukrainyi, 2, 39-40.

14. **Butuzova, L. F., Shakir, S. M., Kulakova, V. O., & Kolbasa, V. A.** (2016). Vzaimosvyaz mezhdu tehnologicheskimi svoystvami ugley i sostavom tehnicheskogo ekstraktov. Vestnik Donetskogo Tehnicheskogo Universiteta, 1(1), 13-20.

15. **Vasilenko, T. A., Grinev, V. G., Molchanov, A. N., & Ponomarenko, D. A.** (2015). Vliyanie gorno-geologicheskih i struk-turnyih faktorov na soderzhanie metana v ugolnyih plastah. Zbirnik Naukovih Prats UkrDGRI, 1, 46-55.

16. GOST 25543-2013. Mezhgosudarstvennyiy standart. Ugli buryie, kamennyie i antratsityi. Klassifikatsiya po geneticheskim i tehrologicheskim parametram. Izdanie ofitsialnoe. (2014). Moskva: Standartinform.

17. **Zhukov, P. P., & Paschenko, V. I.** (1985). Ob otsenke vyihoda letuchih veschestv iz uglya. Ugol Ukrainyi, 9, 39-40.

18. **Vodolazskiy, V. T.** (1980). O pokazatelyah stepeni metamorfizma kamennyih ugley Donbassa. Ugol Ukrainyi, 6, 35-36.

19. **Avgushevich, I. V., Sidoruk, E. I., & Bronovets, T. M.** (2019). Standartnyie metodyi ispyitaniya ugley. Klassifikatsii ugley. Moskva: «Reklama master».

20. **Vodolazskiy, V. T.** (1980). Svyaz glubinyi gazovogo vyivetrivaniya s uglom zaleganiya plastov i ih metamorfizmom. Ugol Ukrainyi, 1, 38.

21. **Antoschenko, N. I., & Tomalak, N. V.** (2002). Vliyanie temperaturyi na stepen metamorfizma iskopaemyih ugley. Ugol Ukrainyi, 7, 36-38.

https://doi.org/10.31713/m1011

RESULTS OF PHYSICO-CHEMICAL STUDIES OF ORE ROCKS AND ELEBARATION THEWAY OF EXTRACT USEFUL COMPONENTS FROM THEM

Toktosunova B.
Kyrgyz State University of Geology, Mining and Natural Resources Exploitation named after Academician U.Asanaliev (KGGU), Doctor of Chemistry, Professor, Head of the "Natural Sciences", Kyrgyzstan

Sultankulova A.
Kyrgyz-Russian Slavic University named after B. N. Yeltsin (KRSU), Candidate of Chemical Sciences, Associate Professor, Leading Researcher, Kyrgyzstan

Kushnazarova S.Z.
Kyrgyz Institute of Mineral Resources (KIMR), Researcher, Kyrgyzstan

Aitkulov B.T.
Kyrgyz Institute of Mineral Resources (KIMR), Researcher, Kyrgyzstan

Toktosunov N.M.
Kyrgyz Institute of Mineral Resources (KIMR), Researcher, Kyrgyzstan

Annotation

This paper work determinesthe results of research on the physico-chemical properties of ore minerals from the deposits of the Sarijaz Ore Area of the Berkutsk Group of the Kyrgyz Republic.Mechanical processing of test minerals according to known method was carried out.The influence of particle dispersion in test samples on the expression of some metals in ore minerals has been studied.The effect of the

sample size on the yield of the useful components has been determined.It is shown that in a finely fragmented sample the output of the noble metal is several times higher than the control metal.

Keywords: ore, crushing, lyddite, dispersion, spectral and elemental analysis, coarse and fine fraction, raster electron microscope.

Introduction

Chemical and technological research into ore minerals, the identification of useful components therein and the search for netmethods for recovering them from ores are priorities in mining.In this context, carbon-silicon shale (UKS) and the Berkut group lyddite of the Sarijaz ore region of the Kyrgyz Republic are promising subjects for detailed study. Early studies have provided that the ores in this area contain rare (V, Mo, Bi, etc.), noble (Ag, Au, Pt, Pd), etc. Metals with signs of graphite and diamond (fullerit) particulates [1-6].

In addition, during the exploration of the facility, a number of additional non-metallic industrial products were identified, moreover to metallic components, such as elemental silicon, silicon carbide, graphite, abrasives and refractory lining materials for civil applications industrial construction; high resistance colorants , commercial decorative stones for construction and architecture. ScientificResearches have been carried out on the possibility of using Kyrgyz lyddite in the development of new types of refractory and chemically resistant material.

However, the mineral resources of the Sarijaz Ore Area remain poorly studied, so new data on their formation, distribution, feasibility and prospects for industrial platinum concentration are periodically available, palladium and other platinum metals.(PMG)However, owing to the lack of efficient processing technology, it has not been possible to fully separate the valuable components of ore rocks from tailings . Consequently, research work into the useful components of lyddite and how to extract them from it is highly relevant [7].

Consistent with *the objective set out below****the purpose of this research*** is to study the physico-chemical characteristics of the lyddite and to identify useful components therein, as well as to find ecologically renewable and clean methods of extracting them.

Examination of the structure and texture of the ore mineral under study by a raster electron microscope

Objects of research

The samples of lyddite from the Berkutsky field were taken for:

- research into the type of mineral ores;
- withdrawing the characteristics of the ore
- study of texture-morphological structures.

According to the purpose of the research, texture fragments were selected for the manufacture of polished knobs.Dimensions of the samples were: polished Anschliff - 2.5 cm, and coarsely (>0.5 cm) and finely (<0.01 cm) shredded.

Materials and methods of research

One type of ore mineral with different textures was studied: the material for analytical studies wasfine-dyspersated, large-grained and pieces of lyddite. (Figure 1.)

Figure 1. Crushed Lidite Lumps

The preparation of samples and the choice of the mode of operation of the SEM have been conducted in accordance with the known method [8].

Resultsand discussion for the research.

It is known [9] that the structure and texture of the ore give an indication of the sequence of extraction of minerals and mineral associations and subsequent changes in them.The structure of the ore and the composition of the paragenetic associations of minerals may indirectly indicate all the conditions (temperature, pressure, time of formation and starting material) at which ore was deposited or altered. Structural texture of the ore is therefore important in determining the genesis and explaining the subsequent geological history of the mineral deposit.In this work, the characteristic texture-structure characteristics of the mineral being studied are identified by SEM image analysis.

The fragment of the ore mineral in Figure 2 confirms that there is no spatial reference of the grains in any one primary direction.

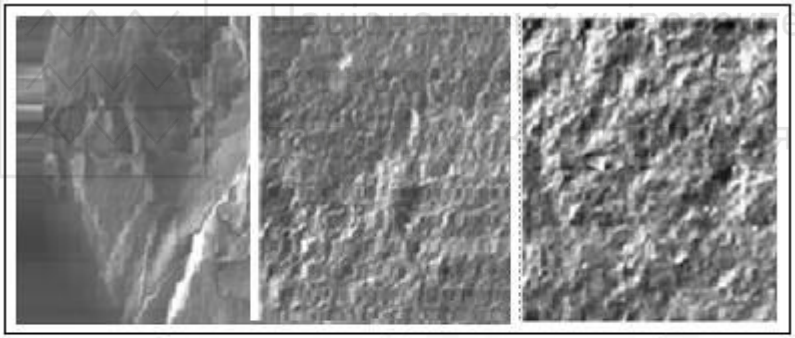

a) b) c)

Fig.2. Morphological and structural features of the studied polished section of the mineral

Ore mineral fragment

a) magnification x 46 (widch 6.23 microns)
b) magnification x 490 (widch 595 microns)
c) magnification x1020 (widch 296 microns)

The sample also shows the high density and density, no cavities and voids. Therefore, this fragment makes it possible to definitive statement aboutthat the rock consists of one mineral, i.e. it has a uniform massive and uniform structure. By increasing the same fragment, the structure of the mineral being studied shows that the

mineral is due to the shape and nature of the fusion of mineral grains (Figures ***2a,b*** and ***c***, respectively).

The following is the analysis of electronic images of ground mineral samples. It is well known that rock disintegration has different objectives.[10–11]. The fundamental objective is to release a valuable component from tailings, to uncover it. Nevertheless, the morphological-structural features of the mineral are highly dependent on the way the ore is destroyed.Because grinding fails to uncover ore minerals because of their extremely small size and thin sprouting with non-metallic minerals.Accordingly,*in the context of the above*hypotheses, the morphology of the experimental mineral after grinding has been studied.(Figures ***3a,b,c***).

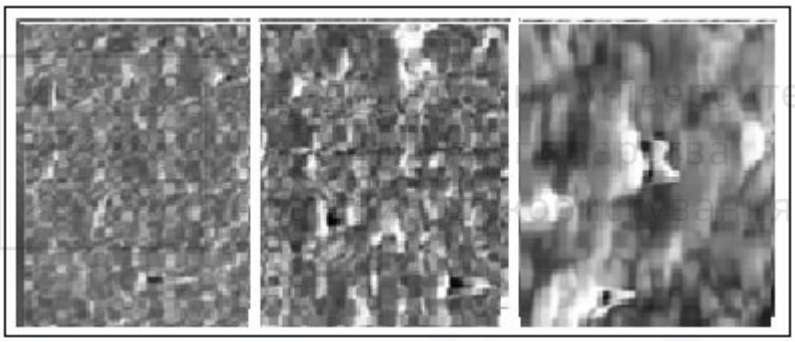

a) b) c)

Fig.3. Morphological and structural features fine fraction of the studied natural mineral
Fragment of ore mineral LT-2-SM
(fine fraction) SEM
a) magnification x 410 (widch 582 microns)
b) magnification x 1010 (widch 248 microns)
c) magnification x. 4000 (widch 61.5 microns)

The structure of the ore mineral is *homogeneity*in mass and structure. In addition, in the drawings «magnetite» inclusions are noticed, as evidenced by electrolysis of samples.

The photographs of the mineral shown in Figures **4*a*,*b*, and *c*** suggest that the mineral is characterized by a clastic structure.

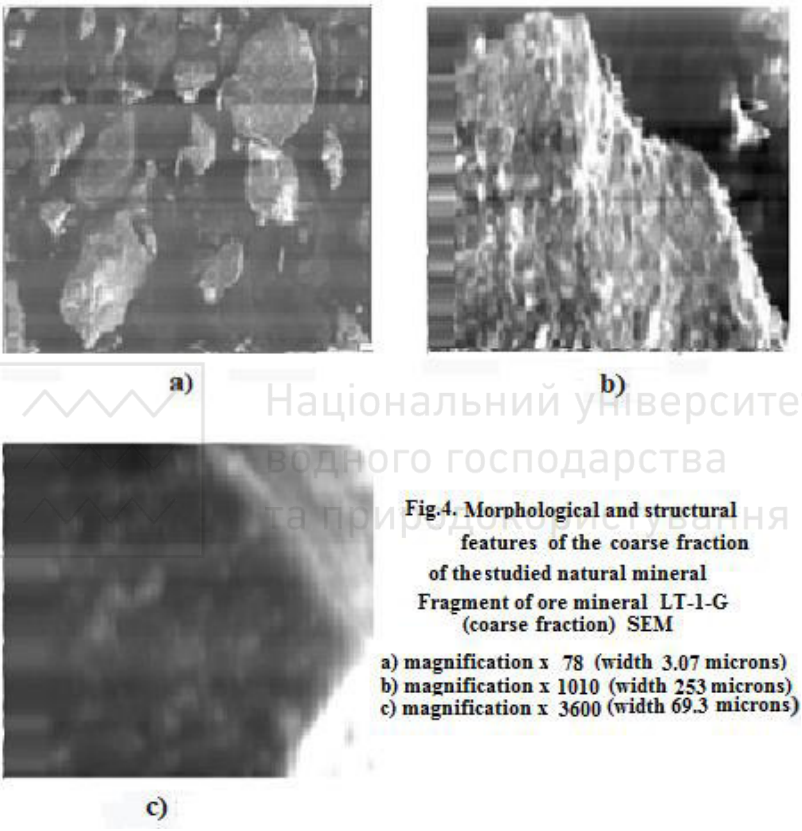

Fig.4. Morphological and structural features of the coarse fraction of the studied natural mineral Fragment of ore mineral LT-1-G (coarse fraction) SEM

a) magnification x 78 (width 3.07 microns)
b) magnification x 1010 (width 253 microns)
c) magnification x 3600 (width 69.3 microns)

The image magnification [x1010 (width 253 sm)] and [x4000 (width 61.5 sm)] indicate that the mineral is evenly grained, non-porous and does not include (figures **5*a*,*b*** and ***c***).

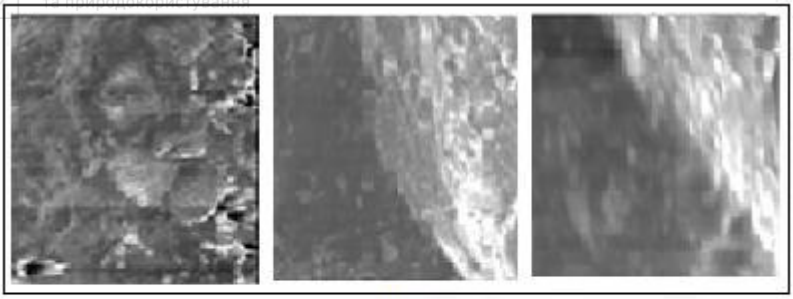

a) b) c)

Fig.5. Morphological and structural features of the coarse fraction of the studied natural mineral . Fragnent of ore mineral LT-1-G (coarse fraction) SEM

a) magnification x 99 (widch 2,5 microns)

b) magnification x 1010 (widch 246 microns)

c) magnification x 4000 (widch 60,6 microns)

Images ***6a,b*** and **c** show no layering, even microlayering, and no overlapping veins. The dark grey «pebbled surface» (fragment ***b***), i.e. the surface of the mineral looks rough - shallow (with dark spots).

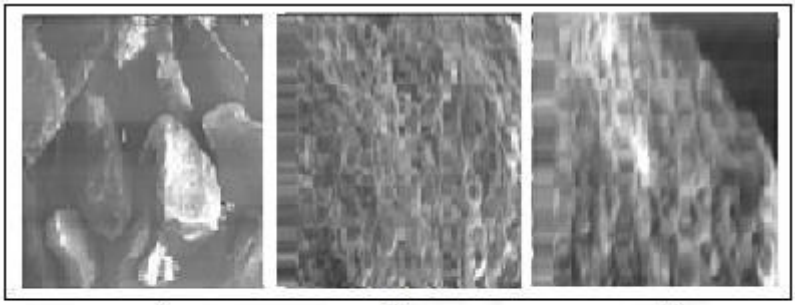

a) b) c)

Fig.6. Morphological and structural features of the coarse fraction of the studied natural mineral . Fragnent of ore mineral LT-1-G (coarse fraction) SEM

a) magnification x 41 (widch 5,67 microns)

b) magnification x 1010 (widch 252 microns)

c) magnification x. 1800 (widch 139,4 microns)

Analyses of electron-morphological images suggest that the ore studied refers to minerals of «moderate magnetism», the texture of the mineral is massive and the structure is hidden crystal.That has been proven by scientific data, specifically «The latent crystal structure is characterized by fine grained formation of minerals whose grains are indistinguishable by the eye».

Examination of chemical composition

Samples from the Sarijaz field (115-L and 116-L) were shredded and spectrally analyzed. The results are presented in table 1.

Table 1

Spectral analysis of reference samples from the Sarijaz deposit

Sam. no.	10-2 Mn	10-3 Ni	10-3 Co	10-1 Ti	10-2 V	10-3 Cr	10-3 Mo	10-2 W	10-2 Zr	10-2 Hf	10-3 Nb	10-1 Ta	10-3 Cu	10-3 Pb	10-4 Ag	10-2 Sb	10-3 Bi	10-2 As	10-2 Zn
115-I	-	0,3	-	0,12	15	3	2	-	0,4		-	-	-	0,9	-	-	-	-	3
116-L	-	0,5	-	0,07	20	3	1,2	-	0,4		-	-	9	0,5	-	-	-	-	2

Sam. no.	10-2 Cd	10-3 Sn	10-3 Ge	10-3 Ga	10-3 In	10-3 Yb	10-3 Y	10-2 La	10-1 Ce	10-1 P	10-4 Be	10-2 Sr	10-2 Ba	10-3 Li	10-2 Th	10-1 U	10-3 Pt	10-2 Au	10-2 Sc
115-L	-	-	-	0,7	-	-	-	-	-	-	-	2	-	-	-	-	-	-	-
116-L	-	-	-	0,5	-	-	-	-	-	-	-	-	-	-	-	-	-	-	-

Sam. no.	SiO_2	Al_2O_3	MgO	Fe_2O_3	CaO	Na_2O
115-L	70	0,3	0,12	4	0,3	-
116-L	70	0,3	0,12	3	0,3	-

The Table indicates that the majority of iron oxide content (Fe_2O_3) in samples (115-L) is 4% and (116-L) 3%. This quantity of iron oxide is also confirmed in the mechanical separation of Fe_2O_3.

Furthermore, to examine theeffect of the size of the dispersed particles on the metal in ores, the experimental samples were roughly grinded at a crushing plant at a pressure of 30-60 atm/cm2.Spectral analysis of the fine particle of the lyddite sample are presented in Table 2

Table 2

Spectral analysis of dispersed lyddite samples from the Sarijaz field

Sam. no.	10-2 Mn	10-3 Ni	10-3 Co	10-1 Ti	10-2 V	10-3 Cr	10-3 Mo	10-2 W	10-2 Zr	10-2 Hf	10-3 Nb	10-1 Ta	10-3 Cu	10^{-3} Pb	10-4 Ag	10-2 Sb	10-3 Bi	10-2 As	10-2 Zn
CF	0,3	2	0,3	0,2	5	5	0,9	0,3	0,4	-	2	-	9	30	15	-	-	-	1,2
SF	0,3	4	0,3	0,4	12	12	1,5	0,4	0,7	-	2	-	20	30	150	-	-	-	5

Sam. no.	10-2 Cd	10-3 Sn	10-3 Ge	10-3 Ga	10-3 In	10-3 Yb	10-3 Y	10-2 La	10-1 Ce	10-1 P	10-4 Be	10-2 Sr	10-2 Ba	10-3 Li	10-2 Th	10-1 U	10-3 Pt	10-3 Au	10-3 Sc
CF	-	0,2	-	-	-	0,4	5	-	-	-	-	2	-	-	-	-	-	-	-
SF	-	0,4	-	-	-	0,5	5	-	-	-	-	2	-	-	-	-	-	-	-

Sam. no.	SiO_2	Al_2O_3	MgO	Fe_2O_3	CaO	Na_2O	K_2O
	%						
CF	>50	0,12	-	7	0,12	0,12	-
SF	>50	0,2	0,12	7	0,2	0,12	-

In comparing data of spectral analysis, initial samples, (115-L and 116-L) (Table 1), coarse samples (LT-HF) and fine fractions (LT-CMP) (Table 2), some metals are only found in the finely dispersed sample, H: Mn, Co, W, Hb, Ag, Sn, Yb, Y.Moreover other metals (Ni, Ti, Cr, Cu, Pb, Zn.) have been shown to increase in fine milling.

Conclusion

1. The *impacts achieved suggest*tthat the electron morphological analysis suggest that the examined ore refers to moderately magnetic minerals, the mineral texture is massive and the structure is latent crystal.

2. *According to the results*of the the spectral analysis we may point out that , the size of the dispersed particles impacts the expression of some metals (Mn, Co, W, Hb, Ag, Sn, Yb,Y).

3. Provisional data assign that the metal content of fine samples is several times higher than that of coarse grinding samples.

4. The *availability of a wide range* elements shown in the lyddite sample.

References

1. Features of the formation and platinum-metal content of carbonaceous-siliceous shales, lidites of the Berkut rare metal deposits, issues of their complex use / **Dzharatov A., Baytukenova N.O., Toktosunova BB, Toktobaeva Ch.K., Batrakeeva G.E., Mukambetova G .J.** // Izvestia KSTU im. I. Razzakov. - No. 14. - Bishkek, 2008. - P.213–216**.**

2. **Dzharatov A.** Features of the geological structure, formation conditions and minerals of the Lower Paleozoic sediments of the upper reaches of the Chatkal and Saryjaz rivers (Middle Tien Shan). - Author's abstract. Cand. diss., Frunze, 1986**.**

3. Preliminary data show that the content of metals in finely dispersed samples is several times increased in comparison with coarsely ground samples.

4. **Sozinov N.A.** Platinoids in black shales [Text] / Sozinov **N.A., Ermolaev N.P., Chinyonov V.A.** et al. // Nature. 1997.– No. 8. - C.11–17.

5. Application of lidite as refractories. No. 1167. / **Vinogradov V.V., Sulaimankulov K.S**. et al. // The patent is registered in the State Register of Inventions of the Kyrgyz Republic from 30.06.2009.

6. Unconventional mineral sources of palladium and some other platinoids, problems of their complex extraction / Sulaimankulov KS, Bleshinsky SV, Dzharatov A. et al. // Modern technologies and quality management in education, science and production: experience of adaptation and implementation. Mater. int. scientific. conf. - Bishkek, 2001. – Ch.III.– P.104–109.

7. **Kozhogulov K. Ch.** Geomechanical problems of the development of ore deposits in the Kyrgyz Republic. g. Mining information and analytical bulletin (scientific and technical journal). Issue No. 12. –Vol. 9. – 2007.

8. Scanning electron microscope. Teaching aid for students of the Faculty of Physics and Technology / Compiled by **V.P. Makarov, O.N. Kanygina**. Kyrgyz-Russian Slavic University. Bishkek, 2006 .-- 25 p.

9. **Neradovsky Yu.N.** Ore Mineragraphy: Textbook for direction 130100 "Geology and Exploration of Mineral Resources" / Yu.N. Nedarovsky. Murmansk: MSTU Publishing House, 2009.- 76 p.

10. **Portnov V.S**. Optimization of refractory ore crushing process [Text] VS Portnov, VM Yurov, AK Tursunbaeva. et al. // Fundamental research. No. 9.– 2012. - pp. 167–170.

11. **Baksheeva I.I.** Development of physical and chemical methods of preparation of mineral raw materials for enrichment [Text]: dis. ... Cand. tech. Sciences: 25.00.13: Krasnoyarsk - 2014.

12. **Minkina I.I.** Logistic management of the process of extracting rare earth metals from apatite ore of the Kola Peninsula. Advancesinchemistryandchemicaltechnology. VolumeXXVII. - 2013. - N9.

https://doi.org/10.31713/m1012

STUDY OF SOLIDIFYING MIXTURES IN MINING KRYVYI RIH IRON ORE DEPOSIT "KIROV"

Serhii Pysmennyi
Kryvyi Rih National University,
Ph.D. (Engineering), Associate Professor, Ukraine

Valerii Pozdniakov,
Department of Polytechnic Institute of Gamal Abdel Nasser
University of Conakry, Professor, Republic of Guinea

Victoria Biluk
Kryvyi Rih National University,
student, Ukraine

Abstract

The work addresses the issue of selecting a solidifying mixture when mining deposits of naturally lean iron ores by open stoping systems to decrease mining costs without the concern for surface subsidence. Magnetite quartzites are mined by systems applied to mining naturally rich iron ores that provide for leaving significant reserves in pillars. In view of the above, when mining magnetite quartzites, it is reasonable to consider application of open stoping with backfilling. Application of polymer additives in the backfill instead of cement allows decreasing costs for water and binders while retaining its strength. As they are able to couple with any binders and fillers, polymers can be added to not only concretes and cement grouts. This provides opportunities to widely use mining and concentrating wastes, i.e. slag and waste rock. Advantages of applying mixtures with plasticizers are: lower labour costs, reduced risks of cracking, increased abrasion resistance, lower shrinkage, increased resistance to temperature fluctuations, backfilling without vibrations, a longer concrete mixture lifecycle. Aggregate technical and economic indicators demonstrate that with similar physical properties of the backfill, polymer-based backfilling is 2-3 times cheaper as compared with the cement-based one. Thus, when stoping with backfilling at Artem underground mine, it is advisable to use a polymer blast furnace slag backfill as a solidifying mixture.

Introduction

The iron ore deposit of Artem underground mine (the PrJSC "Central GZK") is located between property areas of underground mines "Rodina" (the PJSC "Kryvbaszalizrudkom") in the north and "Hihant" (the PJSC "Central GZK") in the south. Below the level of 1045 m of Artem u/m, rich iron ores are mined by the mine group of

the PJSC "ArcelorMittal". The underground mine's property stretches for 2.2 km from the southwest to the northeast [1].

Magnetite quartzites of the first and second ferruginous layers occur in the footwall of the mined-out areas of reach iron ore deposits. Geology of the deposit is made of granitoid rocks of Dniprovsko-Tokivska and Kirovohradsko-Zhytomirska series and the metamorphic complex of Kryvorizka series.

The ferruginous layers are made of martite, goethite-hematite-martite, silicate- carbonate-magnetite, silicate-magnetite and magnetite quartzites with schist bands. Thickness of the ferruginous layers varies from 4 to 100 m. The schist bands that are 20-100 m thick consist of quartz-sericite-chlorite schists with ore-free quartzite interlayers.

The main ore-bearing structure of the deposit is Saksahanska syncline made of magnetite-quartzite layers and rich iron ore bodies. The latter occur mainly in the fourth, fifth and sixth ferruginous layers.

Magnetite quartzites occur in the first and second ferruginous layers in the footwall of rich iron ore bodies under mining.

The quality of ferruginous quartzites of the first and second ferruginous layers varies significantly on the strike and on the dip. Difference between the maximum and minimum iron content in S_x^{1f} reaches 1.6-1.3% for Fe_{tot} and 1.68-1.23% for Fe_{mag}, in the second ferruginous layer Sx^{2f} it makes 1.9-0.8% and 4.3-3.5% respectively. On the strike, these fluctuations make 1.7-1.0% for Fe_{tot} and 2.5-2.0% for Fe_{mag} in the first ferruginous layer, and 4.1 – 2.9% and 4.6-2.5% respectively in the second layer. Exploration maturity of ferruginous quartzite reserves in the first and second ferruginous layers is given in Table 1.

Quartz-biotite-chlorite schists of the first, second and third schist layers and magnetite-carbonate-silicate quartzites of the first and second ferruginous layers [2] represent the country rocks.

At present, the area of the deposit is built up with residential structures and industrial facilities. In addition, there are caving zones resulted from mining rich iron ore deposits by the above-mentioned mining companies. Along the strike of the deposit, there is a railway

of "Ukrzaliznytsia" and a highway connecting residential areas.

Table 1

Reserves and mass fraction of iron in magnetite quartzites

Cut-off grade of Fe, %	Stratigraphic index	Quartzite reserves by categories, kt		Mass fraction of iron, %			
				C_1		C_2	
		C_1	C_2	tot	mag	tot	mag
20	S_x^{1f}	341284	62543	33.2	24.8	32.6	24.4
	S_x^{2f}	218140	52335	32.8	25.8	31.8	25.3
	Total	**559424**	**114878**	**33.0**	**25.2**	**32.2**	**24.8**
16	S_x^{1f}	505760	82339	32.2	22.2	32.0	22.2
	S_x^{2f}	241607	55189	32.5	24.5	31.8	24.9
	Total	**747367**	**137528**	**32.3**	**22.9**	**31.9**	**23.3**
10	S_x^{1f}	617895	103782	31.2	20.0	31.0	19.6
	S_x^{2f}	294966	65656	31.6	21.7	29.9	20.5
	Total	**912861**	**169438**	**31.3**	**20.5**	**30.6**	**19.9**

Thus, there are two options for mining magnetite quartzites of the deposits: by the open stoping method within the range of depths and by the system with complete backfilling.

When mining magnetite quartzites, there occur stopes of about 1.2 M m^3 annually. However, when applying systems with backfilling, voids are filled with solidifying mixtures to prevent surface subsidence.

When mining quartzites by the room-and-pillar method, despite available underground voids, there is no significant surface subsidence due to pillars left [3].

Both options provide for steps to prevent development of displacement. Thus, new aquiferous areas are not entrained to the displacement zone. Due to very low filtration parameters of both magnetite quartzites and country rocks, sizes of a depression crater caused by dewatering of naturally rich iron ores do not practically grow.

To calculate reserves of the I and II ferruginous layers within the "Kirov" leasehold, two options of mining magnetite quartzites are suggested: 1) mining the underground mine field leaving pillars and 2) mining the underground mine field by the systems with backfilling. By the considered options and with the cut-off grade change from 20% to 10%, proved reserves increase from 73723 to 116586 kt and from 228453 to 361248 kt respectively.

Application of open stoping systems (option 1) inevitably results in 2.0-2.5-fold decrease of the reserves to be mined and requires additional monitoring of the pillar state after mining main reserves and, consequently, keeping main and ventilation shafts, mail haulage levels in the working order. The mining system with backfilling using the solidifying backfill enables mining the reserves of the deposit more completely [4].

The system of mining with backfilling prevents creation of caving craters and partly obviates the necessity of monitoring the state of the mined-out space. In view of the above, further studies of mining magnetite quartzites should focus on the second option, i.e. the mining system with backfilling.

At present, at mining rich ores, the annual progress of mining operations does not exceed 17-19 m. A low rate of deepening is conditioned by hoisting capabilities of main shafts and significant mining depth of 1200-1300 m. The maximum annual progress at underground mining of ferruginous layers with backfilling is 17.5 m when traditional processes are applied [5].

From the practice of Zaporizhzhia iron ore basin (ZZRK) where self-propelled equipment is applied, the minimum annual progress of mining with backfilling makes 11.9 m with annual output of 3000 kt. According to the process design standards, the maximum progress makes 17.5 m.

The underground mine applies the open stoping system with solidifying backfilling and rhomboid stopes, Fig. 1.

Within a mining site, two stopes may be worked out simultaneously in the way that between them there is a 30 m wide ore or backfill pillar.

The backfill is prepared at a specialized facility on the surface. It is transported to backfill levels by pipes in two holes drilled from the backfill facility. The facility comprises sand, slag and cement storage areas and a building for slag mills and mixers. The designed annual output of the backfill facility is 1.5 M m^3 of the backfill mixture.

The following technical and economic indicators by mining systems with various shapes of stopes to be backfilled were obtained in mining the deposit, Table 2.

Analysis of underground mining operations enables the conclusion that open stoping systems and those with backfilling are

widely used in reserve extraction [7-9].

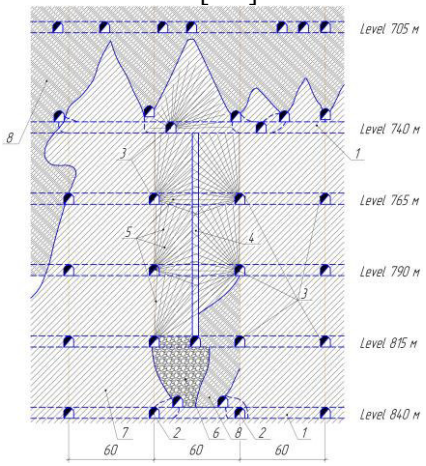

Fig. 1. Open stoping with solidifying backfill of rhomboid stopes (ZZRK):
1 - haulage drift; *2* - loading ort; *3* - drill drift; *4* - ore raise; *5* - blasthole rings; *6* - broken ore; *7* - ore massif; *8* - solidifying backfill

Table 2

Technical and economic indicators

Indicators	Stope shape	
	Rectangular	Rhomboid
U/m output, t/shift	9.6	11.6
Costs for preparatory development operations, m/kt	3-9	4-7
Broken ore losses, %	9.0	8.2
Ore dilution, %	5.6	4.0
1 m^3 of backfill cost, USD	65-82	65-82
Production costs (free at joker chute), USD/t	68-77	65-71

Methods. Backfilling technologies and the composition of solidifying backfill are studied by famous scholars, M.N. Tsyhalov, M.I. Ahoshkov, O.N. Baikonur, R.M. Bronnikov, V.V. Kulykov, K.V. Miasnykov, E.O. Shternbek, V.P. Kravchenko, A.M. Kuzmenko, H.T. Faustov, Z.R. Malanchuk, V.H. Perepelytsia, S.A. Kurnosov, K.Yu. Repp, N.F. Zamesov, A.L. Trebukov, V.P. Voloshchenko, V.I. Liashenko, Ye.P. Chystiakov being among them.

Processability (strength, transportability) and cost-effectiveness (component costs, transportation costs) are key criteria for selecting solidifying backfill. Backfilling practices show direct dependence of

backfill massif strength on binder consumption.

Scholars' contribution to increase of efficiency of mining ore deposits applying systems with backfilling focuses on issues of complete reserve extraction and development of cement-free backfill mixtures made of local materials to decrease backfilling costs.

Considerable amounts of ferrous and non-ferrous metallurgy slag in waste dumps that contaminate the environment can now be used as binders. This decreases consumption of expensive portland-cement, cement, enables even refusal of using them and provides disposal of wastes underground [14, 15].

Economic efficiency of using wastes of mining and beneficiation plants (GZK) as backfill with added polyhexamethyleneguanidine compounds is considered in [15] where reliability of the suggested backfill composition is also substantiated.

[16] substantiates deformation characteristics of the backfilling material with polymer fiber compounds. Tests of this material show promising results - application of polymer fibers increases shearing strength of concrete, thus suggesting an alternative method of designing joints between concrete and grout structure members.

The authors note that traditional mixtures used for backfilling underground voids possess great deformability and low strength that ultimately condition displacement of rock massifs after void elimination. Thus, it is expedient to use mixtures with reinforcing elements, e.g. disperse fiber of steel or polypropylene, for backfilling (or for moth-balling).

In addition, multiple researches demonstrate that PPV in the amount of 0.1% of the total volume provides residual strength, antimicrobic effects, reduced permeability as well as resistance to subsidence, concrete segregation, concrete cracking at plastic shrinkage, abrasion, freezing/thawing cycles, impacts and fire. This means that PPV can be used in all fields of concrete and grout application. Grouts with PPV demonstrate better adhesion that accelerates backfilling. A large content of longer fibrillated fibers can equate mixture strength to concrete with 25-30 kg of reinforcing steel.

To sum up the above said, it should be noted that the application area for the mentioned materials is almost limitless and will be growing in the future.

Research tasks. Thus, study and substantiation of the open

toping system in underground mining of magnetite quartzites with further alternative backfilling at Artem underground mine (the PrJSC “Central GZK”) are topical.

Material and results of research

To test the reserves of magnetite quartzite in the mine field "Kirova" it is expedient to apply a surface-chamber system of development with a bookmark of the made space. When working on the floor of 220-130 m, it is proposed to form a vaulted chamber in the upper part [10].

The essence of the proposed option is as follows. The deposit is divided into chambers of the first and second turns of 30 m with a floor height of 90 m (Fig. 2-4).

In the lower part of the block, a trench cut is formed by drilling the ore mass with rod holes from the cutting horn. Next, form a vertical compensation chamber by drilling the ascending and descending fans of deep wells. Then destroy the array of deep wells from the drilling rig, see Fig. 2-4.

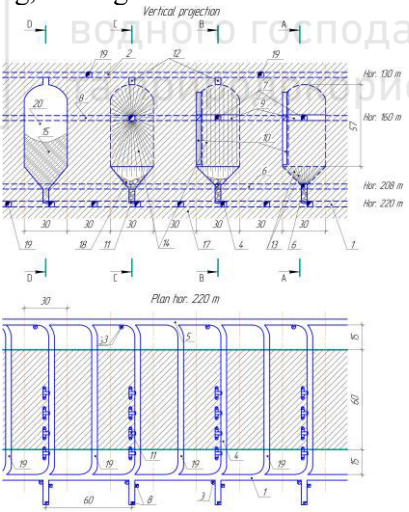

Fig. 2. Surface-chamber system of development with a bookmark of the made space at working off of stocks of mine field "Kirova": *1* - retractable drift;

2 - mortgage road; *3* - ventilating running gezenk; *4* - ort arrival; *5* - ventilated subfloor drift; *6* - cutting ort; *7* - drilling rig; *8* – material gezenk; *9* - cutting lane;

10 - detachable gezenk; *11* - paired vibrating feeder; 2 - mortgage ort; *13* - rod holes; *14* - deep wells; *15* - hardening bookmark; *16* - vertical compensation chamber; *17* - ore massif; *18* - collapsed ore; *19* - ventilation ort; *20* - mortgage chamber

After loading and blasting of deep wells the release of collapsed ore from the treatment chamber is performed.

Production and delivery of ore is carried out by means of paired vibrating feeders.

After the complete release of ore, the cleaning chamber is filled with a hardening tab, which is transported to the chambers along the embankment road.

Having worked out the chambers of the first turn of a floor of 220-130 m begin excavation of chambers of the second turn (interchamber pillars of chambers of the first turn)

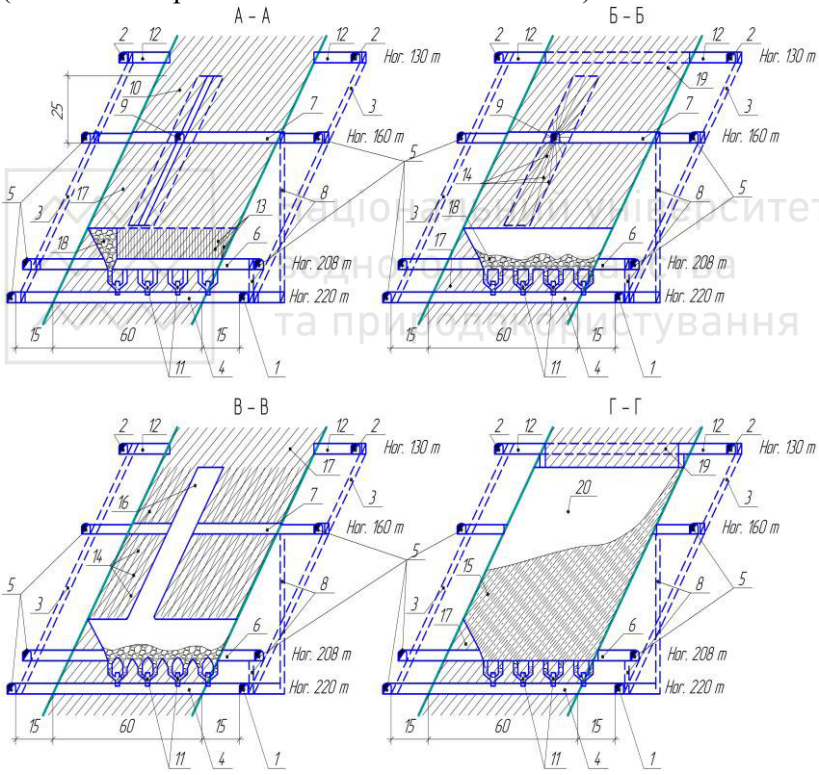

Fig. 3. Sections of the surface-chamber development system:
1-20 - symbols are shown in Fig.2

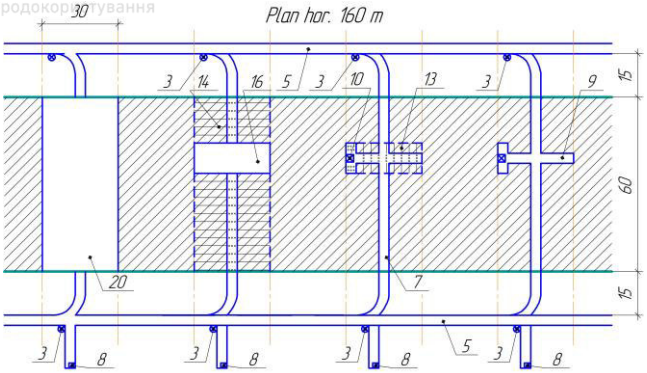

Fig.4. Plan of the surface-chamber development system:
1-20 - symbols are shown in Fig.2

It is also possible to use powerful self-propelled equipment. From the analysis of field development, loading and delivery machines are widely used.

In the laboratory of Kryvyi Rih National University were conducted studies on the stability of cameras of various shapes [11].

The results of the studies are shown in table 3.

Table 3

The results of laboratory tests

Name of indicators	The shape of the cleaning chamber		
	rectangular		vault
Parameters of the cleaning chamber, m:			
- height	90	90	90
- length	30	30	30
- width	60	60	60
Width of the interchamber whole, m	30	30	30
The ultimate strength of the whole, MPa	125	125	125
Camera behavior, months:			
- before chipping the whole	6	10	8
- chaotic chipping of the whole	1.5	0.5	-
- intensive chipping of the whole	9.0	-	-
- complete destruction	+	-	-
Strength of the whole in 28 days., MPa	30	105	118

As a result of research it is established that at working off of stocks of magnetite quartzites in a floor of mountains. 130-220 m are the most stable vaulted chambers [12,13].

The principal difference of the solidifying backfill from the dry and hydraulic ones consists in its ability to not only keep its shape and properties but also withstand various loads. These features of solidifying backfill have enabled enhancement of current stoping methods and facilitated development of new ones. This type of backfillis used to create monolithic sill pillars, enclosure retaining walls, stoppings, concrete blocks. The mining industry started to apply solidifying backfills 50-60 years ago. In fact, they are a sub-type of "lean" concretes that have been studied and used for hundreds of years. Due to high costs of solidifying materials, this type of backfill is used after a feasibility study into its application.

At depths of over 600 m, consumption of binders makes 300 kg/m^3 and more, this necessitating the search for more economical ways of enhancing strength of the backfilled massif.

Application of expensive materials stimulates the search for alternative components of the backfill and results in the idea of introducing cheaper and more modern materials to the backfill mixture. Such additives can enhance mixture properties, this not making such mixtures inferior to traditional compositions in quality.

Polymers can be added not only to concretes and cement grouts as they can be well-coupled with any binders and fillers. They enable mixtures with the required fluidity for easier backfilling and better quality of works, give a good showing at various temperature modes (frost-resisting additives) and solidify faster with a rise in temperature. While solidifying, grouts with polymer additives become 20-25% stronger, more plastic, require less water (by 20%) and binders (by 15%) and do not lose their quality.

To strengthen cohesion of components in the grout, a polypropylene fiber is used as a reinforcing additive (0.6-0.9% per 1 m^3). This enhances adhesion of the concrete grout preventing sedimentation of large and heavy particles at compaction, thus providing plasticity of the fiber mixture in a liquid form and easy pumping.

Increased plasticity after adding the fluid-plastic polypropylene fiber prevents ruptures and segregation of cement products while receiving them from the concrete mixture or the cement grout.

Advantages of mixtures with plasticizers are: economy of

cement; reduced efforts for receiving a smooth surface; reduced risks of concrete cracking; increased abrasion resistance; increased adhesion with the reinforcement cage (if available); lower shrinkage; increased resistance to temperature fluctuations; backfilling without vibrations; a longer concrete mixture lifecycle (up to 2 hours), degreased risks of segergation and early solidification.

Advantages of applying fiber are: decreased cracking; increased resistance to breaking and shrinkage; decreased segregation (peeling); decreased deterioration.

To enhance strength characteristics of mixtures currently used for backfilling, it is suggested to add polymers as plasticizers (e.g. СП-1ВП) and reinforcing polypropylene fibers to grout compositions, Table 4.

Table 4

Backfill composition

Backfill	Cement M300, kg/m^3	Cement M400, кг/м^3	River sand, kg/m^3	Broken stone (20-40mm), kg/m^3	Granulated blast furnace slag, kg/m^3	Fluxing limestone wastes, kg/m^3	Crushed dump rock, kg/m^3	СП-1ВП, kg/m^3 (%)	Polypropylene fiber (12± cm), kg/m^3 (%)	Water, l/m^3	Strength on 28th day, MPa
№1	300	-	1400	–	–	–	–	–	–	410	3-4
	255	-	1400	–	–	–	–	1.35 (0.6)	–	328	
№2	–	382	705	1080	–	–	–	–	–	220	30-32
	–	324	705	1080	–	–	–	1.94 (0.6)	–	176	
№3	–	–	–	–	400	1050	362	–	–	400	6-7
	–	–	–	–	360	50	362	2.16 (0.6)	0,6	320	

It should be noted that selection of a backfill is greatly influenced by its cost. Adding polymers to the backfill composition is not always profitable, but sometimes such backfilled massifs cost less and possess enhanced properties (Figure 5).

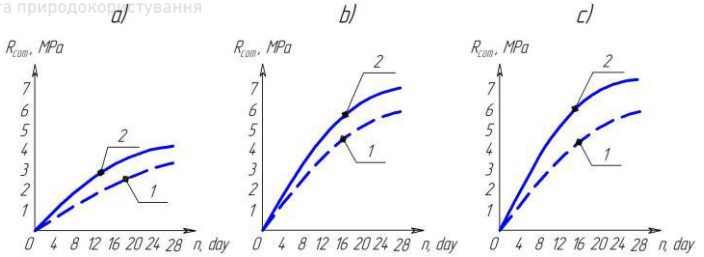

Fig. . Sample strength development in the allotted time: *a* - bookmark based on cement M300; *b* - bookmark based on cement M400; *c* - bookmark based on blast furnace slag; *1* - without the addition of polymers; *2* - on the addition of polymers

When expensive mining systems with backfilling are applied, costs for materials can be reduced through optimal selection of the mixture composition considering all requirements to a backfilled massif. Application of expensive materials will no doubt enable higher quality of grouts (normal heavy concretes) and more accurate forecast of their future behaviour.

Based on the above, strength development of samples in the allotted time can be depicted. It is reasonable to use these materials only if certain properties of mixes are required. Table 5 presents technical and economic calculations for substantiating reasonability of applying the given systems and comparing various options with different backfill compositions and shapes of stopes.

Table 5

Technical and economic indicators by stope shapes

Indicators	Stope shape	
	Rectangular	Vault
Ore reserves in block, kt	525.0	450.0
Specific costs for preparatory development operations, m/kt	4.7	3.9
Specific consumption of explosives. kg/t	0.28	0.28
Labour efficiency. t/shift:		
a) at drilling	1228.0	1296.0
b) at hauling	1025.0	1025.0
c) by mining system	195.0	223.0
Average monthly block output. kt	14.6	16.7
Time for preparatory development operations. months	5	4
Time for block mining. months	12	11
Fe_{mag} content. %:		
a) in massif	25.16	25.16

b) in mined ore mass	24.47	24.51
Ore losses. %	9.0	8.5
Ore dilution. %	5.0	4.7
Ultimate compressive strength. MPa	3–7	3–7
Backfilling costs. by composition. UAH/t:		
-№1 (Cement M300)	140.7	164.1
-№2 (Cement M400)	273.1	318.6
-№3 (Blast furnace slag)	64.4	75.1
-№1*a* (Cement M300)	136.6	159.4
-№2*a* (Cement M400)	196.7	229.5
-№3*a* (Blast furnace slag)	64.0	74.7

Analysis of the data in Table 5 shows that reserves of the rectangular stope are larger by 75 kt and difference in output by systems makes 2.1 kt/month. ore losses and dilution differ by 0.5% and 0.3%. Fe_{mag} content is lower by 0.04%.

Thus. difference in costs for mining 1t of ore with application of the cement M300-based backfill in stopes of different shapes varies within 4.1-4.7 UAH/t. with application of the cement M400-based backfill - within 76.4-89.1 UAH/t. with application of the backfill based on blast furnace slag the cost is 0.4 UAH/t.

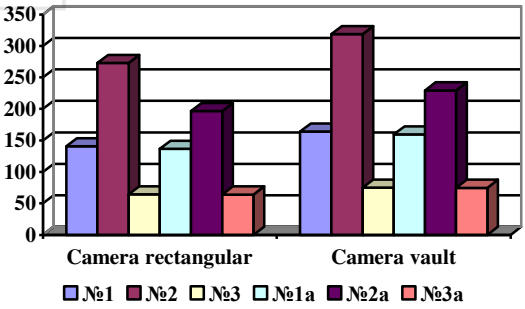

Fig. 6. Costs of mining 1t of ore with backfill of various composition in stopes of different shapes

Conclusions

The research conducted enables the following conclusions:

1. When mining magnetite quartzites. it is reasonable to apply the open stoping method with backfilling that prevents the surface from deformations and caving craters.

2. Analysis of available solidifying mixtures shows that backfills based on the cement grout possesses several disadvantages (high costs and special transportation conditions). However. polymer-based backfills do not require special conditions for transportation.

3. Aggregate technical and economic indicators demonstrate that with similar physical properties of the backfill. polymer-based backfilling is 2-3 times cheaper as compared with the cement-based one.

Thus. when stoping with backfilling at Artem underground mine. it is advisable to use a blast furnace slag backfill as a solidifying mixture.

References

1. Feasibility study of production value and substantiation of condition parameters for calculation of reserves of I and II iron layers in the mining allotment of SE "Kirov Mine". - Kryvyi Rih: Kryvbasproekt, 2005.

2. **Stupnik M.I, Pysmennyi S.V.** Parameters of floor-chamber excavation of ferruginous quartzites with inclined pillars // Mining Bulletin: Scientific and Technical Collection. - Kryvyi Rig. - 2013. - № 96. - P. 3-7.

3. **Malanchuk Z.R., Stupnik M.I., Fedko M.B., Pysmennyi S.V., Kolosov V.O., Kurnosov S.A.** Investigation of the stability of the outcrops of the chamber systems of development during the development of complex structural deposits of iron ores of the Kryvyi Rih basin // Bulletin of NUVGP: Series "Technical Sciences", 2018. - Issue 3 (83). - P. 162-175.

4. **Pysmennyi S.V.** Investigations of the stability of the pillars from the shape of the cleaning chamber during the development of magnetite quartzites in the fields of existing mines underground // Bulletin of Kryvyi Rih National University. - 2014. - № 36. - P. 9-13.

51. **Pysmennyi S.V.** Development of complex-structural deposits of rich ores by chamber development systems // Mining Bulletin: Scientific and Technical Collection. - 2014. - № 97. - P. 3-7.

6. **Stupnik N.I., Kalinichenko V.A., Kolosov V.A., Pysmennyi S.V.** Modeling of the cleaning chamber in unstable ores during the development of ore deposits / // Metallurgical and mining industry. - 2014.– No. 4. - P. 68-71.

7. **Egorochkin A.A., Ezhenov A.E.** Improving the technology of ore mining with backfilling during the development of steeply dipping ore bodies in difficult mining and geological conditions // Improving the technical level of mining: Proceedings of VNIItsvetmet. Ust-Kamenogorsk, 1988 .- P. 109-122.

8. **Pysmennyi S.V., Khivrenko V.O., Sbitnev V.A., Polukhina N.V.** Determination of the parameters of the vaulted compensation chamber //

Development of ore deposits. - Kryvyi Rih: KTU. - 2002. - Issue. 79 .- P. 48-52.

9. **Tsarikovsky V.V. Tsarikovskiy V.V., Sakovich V.V., Nedzvetskiy A.V., etc.** // Determination and control of the permissible dimensions of structural elements of development systems at the mines of Kryvbass. - Kryvyi Rih: NIGRI, 1987. - 76.

10. **Stupnik N.I., Kolosov V.A., Pysmennyi S.V., Fedko M.B.** Development of naturally poor ores of the Krivoy Rog iron ore basin with the backfill of the worked-out space / // Metallurgical and mining industry. - 2014. - No. 3. - P. 95-98.

11. Development of technology for the production of folding structured pads, which contact with overly clayey rocks: Sound about / NDR №. 30-79-09 (Conclusions) No. DR 0109U002336 // Kryvory Technical University - Kryvyi Rih, 2010.

12. **Stupnik N.I., Pysmennyi S.V.** Physical modeling of the form of compensation chambers when mining blocks at great depths // Bulletin of the Kryvorizkiy National University. - 2012. - No. 31. - P. 3-7.

13. **Pysmennyi S.V.** Methods of assigning an active zone and a crypt on the contour of an underground transport vyrobka when combining the development of gold ore genera // Bulletin of the National Technical University "KhPI". Collection of Science Works. Series: Mechanical and technological systems and complexes. - Kh .: NTU "KhPI", 2017. - No. 16 (1238). - P. 99-106.

14. **Kuzmenko A.M. Petlyovany M.V., Mustache V.Yu.** Solid bookmark during the release of steep ore loads at the folding geological-geological minds // Monograph: Ministry of Education and Science of Ukraine, Nat. girn. un-t. - D .: NSU, 2015. - 139.

15. **Gorbunova O.A.** Development of warehouses solid bookmarks on the basis of the approaches to the garnishing-zbagachuvalny virobniztva from the additional polymers of the class polyhexamethyleneguanidin // GIAB - 2010.

16. **Stradanchenko S.G., Shubin A.A.** On the use of cement-based fiber mortar polymer / Science Pratsi DonNTU. Series "Girnicho-geological" No. 7 (135). 2008. - P. 36-39.

17. **Vasil'ev V.V.** Polymeric compositions in the reference book. -M.: Nauka, 1986. - 294.

18. **Kuzmenko A.M., Petlyovany M.V.** The standpoint of the prospects for the development of mortgages in the underground mines of Ukraine // Geotechnical mechanics. - 2013. - VIP. 110. - P. 90-98.

https://doi.org/10.31713/m1013

CONTROL OF THE VIBRATION SPECTRUM IN SOILS AND ROCKS BASED ON THE MATHEMATICAL SIMULATION OF SHORT-RELEASED EXPLOSIONS

Remez N.S.
National Technical University of Ukraine "Igor Sikorsky Kyiv Polytechnic Institute", Doctor of Technical Sciences, Professor of the Department of Geoengineering, Ukraine

Boiko V.V.
Institute of Hydromechanics of the National Academy of Sciences of Ukraine
Research laboratory on seismic safety of technological explosions, Doctor of Technical Sciences, Professor, Head of the laboratory, Ukraine

Dychko A.O.
National Technical University of Ukraine "Igor Sikorsky Kyiv Polytechnic Institute", Doctor of Technical Sciences, Professor of the Department of Geoengineering, Ukraine

Hrebeniuk T.V.
National Technical University of Ukraine "Igor Sikorsky Kyiv Polytechnic Institute", Candidate of Technical Sciences, Associate Professor of the Department of Geoengineering, Ukraine

Bronytskyi V.O.
National Technical University of Ukraine "Igor Sikorsky Kyiv Polytechnic Institute", TF of the Department of Geoengineering, Ukraine

Abstract

In this work, seismic-explosive waves are investigated on the basis of mathematical simulation of short-delayed explosion of a system of charges and effective and seismic-safe schemes are calculated. Numerical simulation of the explosion of a group of charges of cylindrical symmetry in a rock mass is carried out. During the development of the explosion, two stages are distinguished. At the first stage, the explosion of a cylindrical explosive charge in an unlimited soil mass is considered. The principle of superposition of fields is used in the study of explosions of two or more charges, while the influence of the intervals of deceleration and distribution of masses of charges within a group on the parameters of seismic-explosion waves is investigated. It is established that approximately the same stress state is achieved in the soil mass in the near and middle zones of the

explosion, which is necessary for the destruction of the rock. The efficiency of application of the proposed schemes for mining in quarries is proved. At the second stage of solving the problem, an assessment of the total action of a short-delayed explosion of a system of cylindrical charges is made.

The results of theoretical studies on the determination of the optimal short-delay detonation schemes depending on the distribution of masses within the group and the deceleration intervals are presented. The development of the method for calculating seismic vibrations based on mathematical modeling of a short-delayed explosion of a system of charges, which makes it possible to calculate wave parameters depending on the distribution of masses of charges within a group of deceleration intervals, is made and proved its effectiveness.

Keywords: explosion, short-delayed blasting, deceleration interval, vibration spectrum.

Introduction

Under conditions of the constantly expanding scale of blasting operations for the needs of the national economy, it is necessary to develop new approaches to their implementation, in which it is possible to achieve both effective destruction of rocks and ensure seismic safety of protected objects. If, relatively recently, explosive technologies were used only for crushing or mining of rocky rocks, nowadays, explosive methods are gaining importance in the extraction of natural hydrocarbons, the construction of engineering structures in rocks, soil compaction, strengthening, stamping and welding of metals, etc. Variety of technological operations using the energy of the explosion is determined both by the possibility of creating high pressures and by the speed of the operating of working processes. However, along with the advantages, blasting operations have a significant disadvantage - low efficiency of the explosion (when crushing rocks, it does not exceed 10%, when stamping - 15...18%). As a result of the action of seismic and explosive loads from blasting operations, there is a disturbance and decrease of the rock mass outside the contour of the blasted area. As a result, the cohesion of rocks decreases, while the friction forces on weakened surfaces are significantly reduced, which can ultimately lead to catastrophic consequences.

A large number of studies by Ukrainian and foreign scientists are devoted to the mechanics of surface manifestation of seismic effects, but the most number of publications concerns earthquakes. The influence of the amplitude-frequency characteristics of oscillations during man-made

explosions on the foundations of protected objects, despite the expanding scope of blasting operations, is not studied sufficiently. In practice, the assessment of the impact of seismic explosive waves on protected objects is carried out on the basis of the existing regulatory documentation only for the parameter of the permissible mass vibration velocity, without taking into account the frequency characteristics in the system, which leads to a significant error in assessing the intensity of seismic vibrations during explosions.

Studies [1-6] cannot solve the problem of optimal prediction of the seismic effect of industrial explosions, since they are based on the laws of vibration propagation during the explosion of a concentrated charge, which leads to a discrepancy between the calculated and actual data. In [7, 8], the interaction of blast waves during short-delayed blasting is studied, but the amplitude-frequency characteristics of seismic vibrations are not taken into account.

The purpose of the work – is investigation of seismic explosive waves on the basis of mathematical simulation of short-delay explosion of a system of charges for the calculation of effective and seismic-safe schemes.

Material and research results

In this work, a numerical simulation of the effect of an explosion of a group of charges of cylindrical symmetry in a rock mass is carried out, while two stages are distinguished at the development of an explosion.

At the first stage, the explosion of a cylindrical explosive charge (HE) in an unlimited soil massif is considered. The movement of detonation products and soil is described by equations (1)-(5).

The problem is solved in a related formulation, while it is assumed that in the rock mass far from the free surface there is a cylindrical explosive charge (HE) with a length l and radius r_0, which detonates instantly. As a result of the instantaneous action of this pressure on the contact boundary of the "detonation products - rock" section, a shock wave is spread through the massif, the contact boundary expands, and a converging wave moves to the charge axis. In this case, an equally high pressure P_n is established throughout the entire volume of the charge. And the density of detonation products (DP) ρ_n is equal to the initial density of the explosive.

Detonation products and rock (HP) are studied within the framework of continuum mechanics, the equations of motion for cylindrical symmetry are as follows [9]

$$\frac{\partial \sigma_{rr}}{\partial z}+\frac{\partial \sigma_{rz}}{\partial r}+\frac{\tau_{rz}}{r}=\rho\frac{du}{dt},\qquad u=\frac{dz}{dt}; \tag{1}$$

$$\frac{\partial \tau_{rz}}{\partial z}+\frac{\partial \sigma_{zz}}{\partial r}+\frac{\sigma_{zz}-\sigma_{\theta\theta}}{r}=\rho\frac{dw}{dt},\qquad w=\frac{dr}{dt}; \tag{2}$$

$$\frac{1}{V}\frac{dV}{dt}=\frac{\partial u}{\partial z}+\frac{\partial W}{\partial r}+\frac{W}{r} \tag{3}$$

$$\sigma_{zz}=S_{zz}-P;\quad \sigma_{rr}=S_{rr}-P;\qquad \sigma_{\theta\theta}=S_{\theta\theta}-P \tag{4}$$

$$P=\frac{1}{3(\sigma_{rr}+\sigma_{\theta\theta}+\sigma_{zz})};\qquad V=\frac{\rho_0}{\rho}; \tag{5}$$

where z, r - coordinates;

t - time;

σ_{rr}, $\sigma_{\theta\theta}$, σ_{zz} - normal voltages;

τ_{zr} - shear stress;

S_{zz}, S_{rr}, $S_{\theta\theta}$ - stress tensor deviator components,

P - mean hydrostatic pressure;

ρ - density;

u, w- velocity components;

V - specific volume.

The expansion of detonation products occurs according to the two-term isentrope

$$P=A\times\rho^{n}+B\rho^{\gamma+1}, \tag{6}$$

where A,B,n,ρ - constants that characterize this type of explosive.

The initial conditions of the problem are as follows

$$u=0, w=0, P=P_n\rho=\rho_n \quad \text{at} \quad z<l, r<r_0 \tag{7}$$

$$u=0, w=0, P=P_0\rho=\rho_0 \quad \text{at} \quad z<l, r<r_0 \tag{8}$$

The boundary conditions are as follows

$$u_{dp}=u_s,\quad P_{dp}=P_s,\quad \rho_{dp}\neq\rho_s \qquad at \quad z=1 \tag{9}$$

$$w_{dp}=w_s,\quad P_{dp}=P_s,\quad \rho_{dp}\neq\rho_s \qquad at \quad r=r_0 \tag{10}$$

Here, the indices "DP" and "S" mean detonation products and soil, respectively.

When investigating explosions of two or more charges, the principle of superposition is used.

To approximate the system of differential equations (1)-(10), the method of finite differences is used using a finite-difference scheme of the "cross" type [10] of the second order of accuracy in spatial and temporal coordinates.

The influence of the intervals of deceleration and distribution of masses of charges within the group on the parameters of seismic-explosive waves is investigated. In this case, it is assumed that the same group mass explodes, but according to different schemes. In the case of three charges, according to the first scheme, at first a charge of a smaller mass explodes, then a larger one, and, finally, a smaller one, equal to the mass of the first charge. Let's call this pattern "triangle up". According to the second scheme, a charge of a larger mass explodes, then a smaller one, and again a larger one ("triangle down"). With an increase in the number of charges, such a mass distribution is maintained according to the two proposed schemes (Fig. 1).

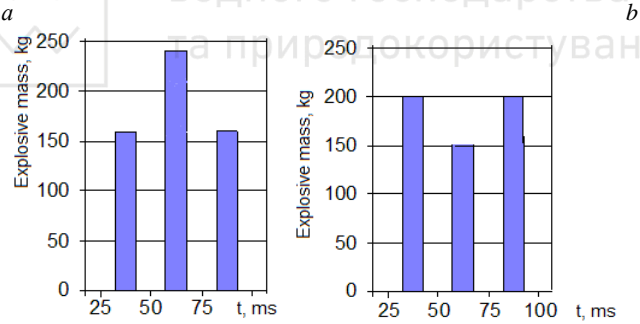

Fig. 1. Various schemes of exploding a group of cylindrical charges: *a* - "triangle up", *b* - "triangle down"

The explosion of a system of cylindrical charges of TNT in loam with a deceleration interval Δt=0,02 s is studied. The physical and mechanical characteristics of the loess are as follows: ρ_{10}=1,2, ρ_{20}=1000, ρ_{30}=2650 *kg/m*^{3} ; c_{10}=330, c_{20}=1500, c_{30}=4500 *m/s,* γ_1=*1,4*, γ_2=7, γ_3=4.

The explosive used is TNT with an initial density of ρ_m=1600 kg/m^3, which constants for the equation of state (6) have the

following values: P_n=9,6·10^9 Pa; k_n=3, k_0=1,25, n=3,123, γ=1,25, A=0,884 Pa (kg/m^3)$^{-m}$, B=0,623·10^5 Pa (kg/m^3)$^{-\gamma}$.

Various variants of mass distribution are investigated. Let's take the mass 36,0 kg as a unit charge q. Then, in the first version of calculations according to the first scheme, the masses of sequentially exploded charges are as follows Q_1=q, Q_2=1,4q, Q_3=q; to the second one - Q_1=1,2q, Q_2=q, Q_3=1,2q.

Fig. 2 and 3 show the isobars of voltages σ_{rr} (in 10^{-3} Pa) at the moment of time t=40 ms for short-delayed explosions of the system of cylindrical charges, produced according to the "triangle up" and "triangle down" schemes. From the analysis of the figures, it follows that in the soil massif in the near and middle zones of the explosion, approximately the same stress state is achieved, which is necessary for the destruction of the rock. Therefore, we can conclude about the effectiveness of the application of both schemes for the extraction of minerals in open quarries.

At the second stage of solving the problem, the dependences of the maximum displacement on the relative distance r_i during the explosion of the i-th cylindrical charge with mass Q_i are used, obtained as a result of a numerical solution in the form

$$(u_{\max})_i = k\left(\frac{Q_i}{r_i}\right)^{\mu} \qquad (11)$$

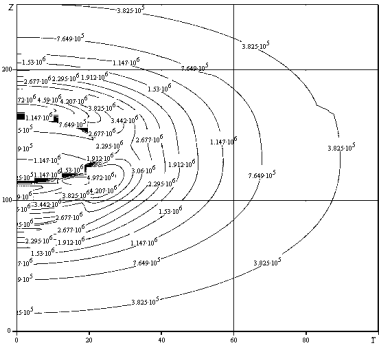

Fig. 2. Isobars of voltages σ_{rr} (in Pa) at the moment t=40 ms of the explosion of cylindrical charges according to the "triangle up" scheme

To estimate the total action of a short-delayed explosion of a system of cylindrical charges, the principle of superposition of waves

is used [9]. The disturbance in the elastic zone for the *i*-th source can be described by the following expression

$$u_i = (u_{\max})_i e^{-vt} \sin w_i t, \qquad (12)$$

where $(u_{\max})_i$ - maximum displacement amplitude for the *i*-th charge, *v* - seismic wave attenuation index, ω_i - oscillation frequency from the *i*-th source.

Then the resulting displacement in a short-delayed explosion of *n* different charges with deceleration interval Δt is determined by the formula $u = \sum_{i=1}^{n} u_i$, or, taking into account formulas (11-12), we obtain the expression

$$u = \sum_{i=1}^{n} k \left(\frac{Q_i}{r_i} \right) e^{-vt} \sin(t(i=1)\Delta t) \qquad (13)$$

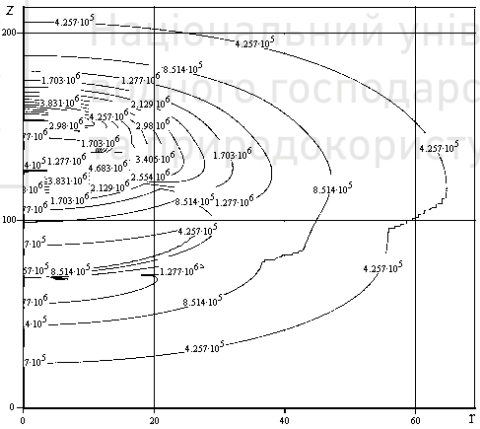

Fig. 3. Isobars of voltages σ_{rr} (in Pa) at the moment t=40 *ms* of the explosion of cylindrical charges according to the "triangle down" scheme

Let us consider the explosions of a system of cylindrical charges of TNT in loam with an interval of deceleration Δt=0,02 *s*. The total weight of the group is 112,4 kg. Various variants of mass distribution are investigated. For convenience of presentation, we denote the charge by the mass Q_1=36,0 *kg* per unit charge *q*. Then, in the first version, according to the first scheme, the masses of sequentially

exploded charges are as follows $Q_1=q$, $Q_2=1,4q$, $Q_3=q$; on the second – $Q_1=1,2q$, $Q_2=1,2q$, $Q_3=1,2q$.

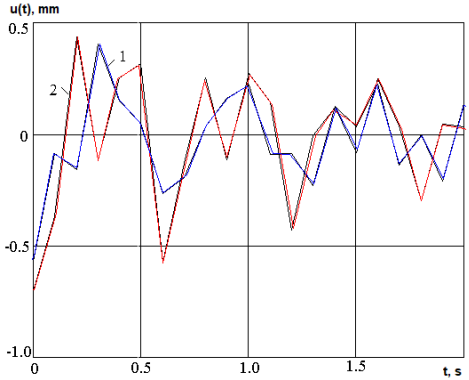

Fig. 4. Dependences of the displacement on time at a distance of 1000 m from the epicenter of the explosions: *1* - $Q_1=1,2q$, $Q_2=1,2q$, $Q_3=1,2q$; *2* - $Q_1=1,2q$, $Q_2=q$, $Q_3=1,2q$

Fig. 4 shows the time dependences of the displacement at a distance of 1000 m from the epicenter of the explosions. The numbering of the curves corresponds to the numbering of the proposed detonation schemes.

From the analysis of the figure it follows that with a slight difference in the displacement amplitudes, the frequency of oscillations during detonation of charges according to the second scheme is twice higher than according to the first, which is an unfavorable factor for the seismic resistance of protected objects.

The following variants of blasting schemes are investigated. In the second variant according to the first scheme $Q_1=0,9q$, $Q_2=1,6q$, $Q_3=0,9q$; to the second one - $Q_1=1,4q$, $Q_2=0,6q$, $Q_3=1,4q$ (Fig. 5).

In the third version according to the first scheme, the masses $Q_1=1,1q$, $Q_2=1,2q$, $Q_3=1,1q$; to the second one - $Q_1=1,2q$, $Q_2=q$, $Q_3=1,2q$ (Fig. 6).

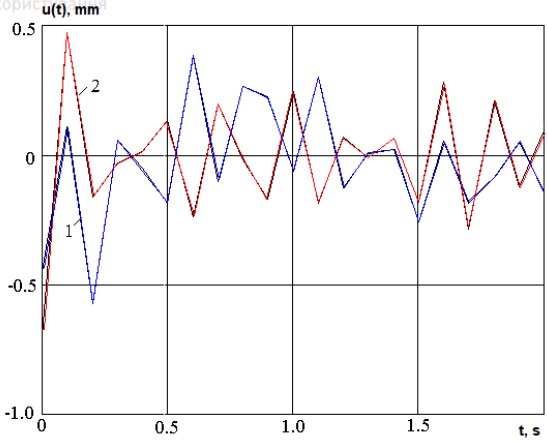

Fig. 5. Dependences of displacement in time at a distance of 1000 m from the epicenter of explosions at various blasting schemes: *1* – Q_1=0,9q, Q_2=1,6q, Q_3=0,9q; *2* – Q_1=1,4q, Q_2=0,6q, Q_3=1,4q

From the Fig. 4 it follows that with an increase in the difference in the masses of successively detonated charges in comparison with the first option, with a slight increase in the amplitude of oscillations, a significant increase in frequency occurs in both detonation schemes (1,5 times).

A decrease in the difference in charge masses (Fig. 6) does not lead to an increase in the vibration frequency compared to the first option, but leads to an increase in the amplitude at 20-25%, which also undesirably affects on the seismic resistance of protected objects.

From the analysis of Figures 4-6 it follows that for any mass distribution in the group, the "triangle up" circuits are preferable to the "triangle down" circuits because the first ones generate lower vibration frequencies.

In addition, it is found that for a specific group mass of charges and soil conditions, there is an optimal distribution of masses within the group, in our case it is scheme 1 according to the first option: a "triangle up" scheme with a mass difference of 40%.

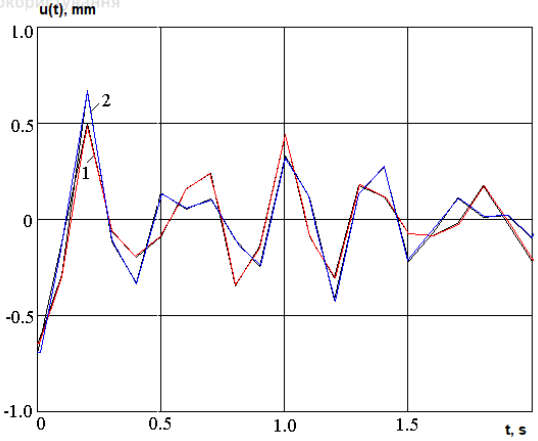

Fig.6. Dependences of displacement in time at a distance of 1000 m from the epicenter of explosions at various blasting schemes: *1* - Q_1=1,1q, Q_2=1,2q, Q_3=1,1q; *2* - Q_1=1,2q, Q_2=q, Q_3=1,2q

It should be noted that the study of explosions of the group of 4 and 5 charges obtained results are similar to those described above.

Figure 7 shows the time dependences of the displacement at a distance of 1000 m from the epicenter of explosions in explosions of a group of four charges with different mass distributions. According to the first explosion scheme Q_1=0,5q, Q_2=1,2q, Q_3=1,2q, Q_4=0,5q; to the second one – Q_1=1,2q, Q_2=0,5q, Q_3=0,5q, Q_4=1,2q.

From the comparing Fig. 6 with Fig. 4-5 it follows that with the dispersal of the explosive mass (an increase in the number of charges), the frequency of oscillations during explosions according to the "triangle up" scheme decreases. At the same time, during explosions according to the second scheme, the amplitude increases in 1.5 times and the frequency - in 1.7 times.

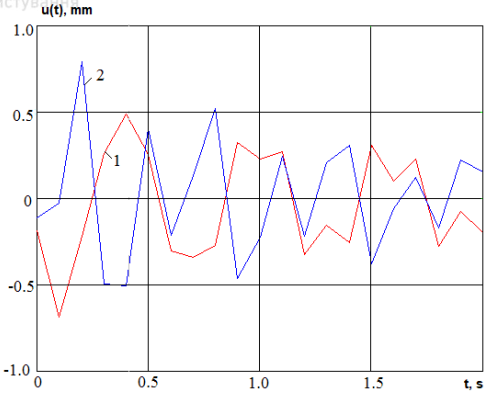

Fig.7. Dependences of displacement on time at a distance of 1000 m from the epicenter of explosions at various blasting schemes: 1 - Q_1=0,5q, Q_2=1,2q, Q_3=1,2q, Q_4=0,5q; 2 - Q_1=1,2q, Q_2=0,5q, Q_3=0,5q, Q_4=1,2q

The study of the effect of a further increase in the number of charges on the frequency-amplitude spectrum of oscillations is made. From the comparison of Fig. 7 and 8, it can be concluded that a further increase in the number of charges with the same total mass in the group leads to a significant decrease in the amplitude-frequency spectrum of ground vibrations. But just as for the cases considered above, the "triangle up" scheme gives lower values of the amplitude (2 times) and frequency (1,3 times) compared to the "triangle down" scheme).

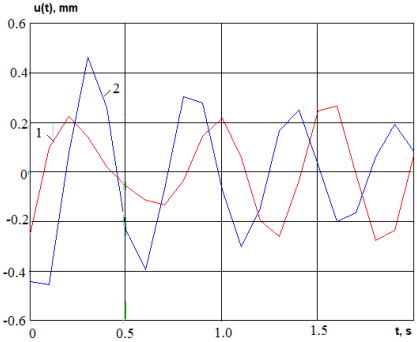

Fig. 8. Dependences of displacement in time at a distance of 1000 m from the epicenter of explosions at various blasting schemes: *1* - Q_1=0,5q, Q_2=1,7q, Q_3=1,0q, Q_4=0,7q; *2* - Q_1=0,85q, Q_2=0,7q, Q_3=0,5q, Q_4=0,7q

To study the influence of the deceleration intervals on the spectrum of seismic vibrations, studies of group explosions are carried out according to the 1st option, 1 scheme. Figure 9 shows the time dependences of the displacement for different deceleration intervals: curve *1* corresponds to Δt=0,02 s, *2* - Δt=0,04 s, *3* - Δt=0,065 s.

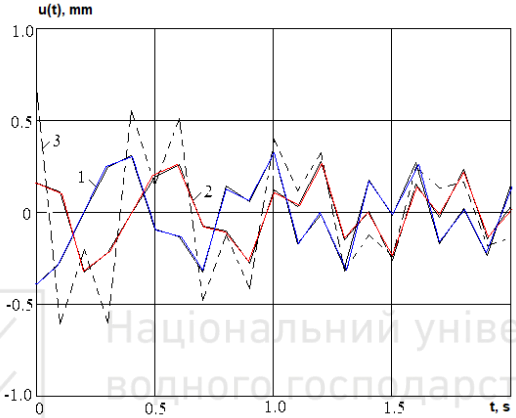

Fig. 9. - Dependences of the displacement in time at a distance of 1000 m from the epicenter of the explosions: *1* - Δt=0,02 s; *2* – Δt=0,04 s; *3* – Δt=0,065 s

It is shown in the Figure 9 that with a twice increase in the deceleration interval (curves *1* and *2*, respectively), the amplitude and frequency of oscillations decreases, which is quite an expected result. However, with a further increase in the deceleration interval (curve *3*), a significant increase in the amplitude and frequency of seismic vibrations occurs, which is undesirable for protected objects. From this analysis, it follows that there is an optimal most safe deceleration interval for group explosions.

Conclusions

An effective method of calculating seismic vibrations based on mathematical modeling of short-delayed explosion of a system of charges, allowing the calculation of wave parameters depending on the distribution of charge masses within a group of deceleration intervals, is developed.

On the basis of numerical and analytical studies, it is established that there are optimal blasting schemes (for the studied conditions -

"triangle up" with a mass difference of 40%) and optimal periods of deceleration from the point of view of seismic safety of protected objects.

The direction of further research is the study of the influence of soil conditions, parameters of charges and their mutual arrangement on the spectral characteristics of seismic vibrations.

The results of this work can be used in the design of blasting operations for the calculation of rational blasting schemes and control of the explosive spectrum of vibrations.

References

1. **Sadovskiy M.A.** Seysmicheskiy effekt vzryiva. Tr. Vses. sovesch. po buro-vzryivnyim rabotam. M.-L., Gostopizdat, 1940, s. 290-319.

2. **Bogatskiy V. F., Fridman A. G.** Ohrana inzhenernyih sooruzheniy i okruzhayuschey sredyi ot vrednogo deystviya promyishlennyih vzryivov – M. : Nedra, 1982. – 162 s.

3. **Mironov P. S.** Vzryivyi i seysmobezopasnosnost sooruzheniy – M.: Nedra, 1973. – 168 s.

4. **Safonov L. V., Kuznetsov G. V.** Seysmicheskiy effekt vzryiva skvazhinnyih zaryadov – M. : Nauka, 1967. – 102 s.

5. **Tseytlin Ya.I., Smoliy N.I.** Seysmicheskie i udarnyie vozdushnyie volnyi promyishlennyih vzryivov. – M.:, Nedra, 1981, -192 s.

6. **Kuzmenko A.A., Vorobev V.D.** Obespechenie bezopasnogo vzryivaniya v karerah stroitelnyih materialov. Institut gidromehaniki AN Ukrainyi.-Kiev, 1992.-24s.- DEP v UkrINTEI 11.08.1992 g., №1192-UK92.

7. **Melnik G.V.** Regulirovanie spektra seysmokolebaniy pri korotkozamedlennom vzryivanii. – Vzryivnoe delo. – M.: Nedra, 1983. - S.48-52.

8. **Lyashenko V.I., Melnik G.V., Shvyidko P.V.** Progresivnyie tehnologii upravleniya vzryivnyimi rabotami na gornyih predpriyatiyah. Tsvetnaya metallurgiya. Gornoe delo – M. – 2009. - №8 – S. 3-11.

9. **Luchko I.A., Plaksiy V.A., Remez N.S. i dr.** Mehanicheskiy effekt vzryiva v gruntah – Kiev: Nauk. dumka, 1989. – 232 s.

10. **Luchko I.A., Remez N.S., Luchko A.I.** Matematychne modeliuvannia dii vybukhu i gruntakh i hirskykh porodakh. Kyiv: NTUU «KPI», - 2011. – 264 s.

https://doi.org/10.31713/m1014

INFORMATION AND TECHNOLOGICAL ASPECTS OF MINE SURVEYING SUPPORT FOR THE DEVELOPMENT AND CONSERVATION OF SUBSOIL RESOURCES

Sayyidkosimov S.S.
Tashkent State Technical University after named Islam Karimov, Professor, Doctor of Technical Sciences, Professor, Department of Mine survey and Geodesy, Uzbekistan

Raximov Sh.Sh.
Tashkent State Technical University after named Islam Karimov, PhD, Senior Lecturer, Department of Mine survey and Geodesy, Uzbekistan

Nizamova A.T.
Tashkent State Technical University after named Islam Karimov, PhD, Senior Lecturer, Department of Mine survey and Geodesy, Uzbekistan

Raximova D.B.
Tashkent State Technical University after named Islam Karimov, PhD, Senior Lecturer, Department of English language, Uzbekistan

1. A monitoring of career

The current state of opencast mining, especially deep open pits of OOO «Kharanut», is reached a depth of more than 500 m, requires the organization of systematic instrumental measurements on the sides based on the laid down observation stations, in the form of metal benchmarks, taking into account the developed layouts and observations. This makes it possible to monitor and predict the state of the rock massifs in open pits.

In order to organize geomonitoring of mine surveying observations of the state of open pit slopes, the following is required:

- to take potentially unstable areas based on the analysis of engineering-geological and mining-technical conditions of development for the establishment of observation stations;
- to develop a design for an observation station for deformations of the slopes of the sides of quarries and dumps;
- to set up some benchmarks of observation stations in the quarry;

- to perform a binding of reference marks with the definition of coordinates *X*,*Y*,*Z* to the nearest points of the reference geodetic network;

- select the positions of the control points of the profile lines;

- to determine the observation point position that is being created the measuring station;

- to carry out systematic control over the invariability of the position of measuring stations using GPS receivers (satellite positioning system);

- instrumental measurements that the benchmarks of the observation station's profile lines;

- the results processing where the instrumental observations and their analysis.

The layout of the observation stations' the profile lines should be selected on the analysis that based on the state edge masses and dump slopes, the modern mining work and the prospects for their further development. To ensure the long service life reference benchmarks, control points and points of measuring stations are proposed to be installed in the form of a permanent reinforced concrete pillar.

In the created monitoring system, it is counselled to monitor the pits and dumps position made by a semi-automatic method. The semi-automatic observation system is based on the production of systematic instrumental surveying and geodetic observations of the displacements and deformations of the working benchmarks that using profile lines an electronic total station and GPS receivers to control the control points and measuring stations position invariability, and in the observation results mathematical processing.

The area is rich with useful mineral deposits: Kharanutskoe coal deposit, Burpalinskoe copper deposit, Golevskoe synnyrites deposit, Katuginskoe cryolite-rare earth-rare metal deposit, Kitemyakhtinskaya gold placer, Olondinskoe lithium deposit, Udokan copper deposit, Chineyskoe iron-titanium-vanadium deposit, Yuzhno -Sulumat iron deposit, etc.

According to the reference terms, the work requires:

- to draw up a work program;

2. Creation of digital 3D models of a pit

Fig. 1. Diagram of a site layout

- to perform instrumental observations on the Kharanutsky section with a length no more than 2500 m (Fig.1);

- to create observation stations for performing deformation instrumental observations of the cut sides;

- the work must be performed in accordance with the requirements of the current regulatory and technical documentation.

3. Reconnaissance of the work area

Topogeodetic work begins with the auxiliary information collection (diagrams, drawings, map materials) from the responsible Customer's representatives. Based on mine surveying and geodetic maps and plans, ideas were obtained about the nature of the relief, the GGS points location, connected to the work site. Further, the object reconnaissance was carried out.

At this stage, the followings are carried out: the object visual assessment; the object boundaries clarification; the ability to conduct satellite and linear-angular observations.

Based on the results of the work area reconnaissance, conclusions were drawn about the methods of conducting instrumental observations. A work program has been drawn up.

4. The work methods

In Static mode, GNSS receivers are installed simultaneously at the initial and determined points for collecting data from all satellites visible in the area. Data collection at points continues during some time, depending on the distance between the receivers, the state of the constellation of satellites, obstacles that affect the collection of data (trees, buildings, mountains, and so on, blocking part of the sky).

Satellite measurements are performed in a static mode, in sessions the duration of synchronous observations by a pair of receivers at the points that form the spatial vector, not less than thirty minutes. At the same time, special attention was paid to the selection of the most favorable time intervals, when the simultaneous visibility of 10 satellites is ensured.

The static measurement method is the most accurate of any other GNSS survey method. This is mainly due to the increased acquisition time of measurements, and, consequently, the large volume of measurements required for statics (Table 1).

Table 1

Base Station Coordinate Catalog

Names	X	Y	H
БАSE ВП	6331944.388	570488.701	1152.617
BASE Fig.2	6334744.245	572316.000	1563.127
BASE РТК	**6334169.529**	**572629.490**	**1479.784**
BASE СМ.1	6332779.008	571886.820	1371.588

Geodetic measurements were carried out in the conditional coordinate system and the Baltic 1977 height system.

5. Topographic survey of the Kharanutsky coal mine

The survey of the coal mine side was carried out using a RIEGL Z-400I ground-based laser scanning system.

The profit of the ground-based method of laser scanning over tachymetric survey and other types: portable, durable, economical; served by one person; instant three-dimensional visualization; high accuracy; incomparably more complete results; fast data collection; ensuring safety when shooting hard-to-reach and dangerous objects.

The material costs for collecting data and modeling an object that used three-dimensional ground-based laser scanning methods are comparable to traditional survey methods in small areas and objects, and lower in areas of large area or length. Even with comparable survey costs, the completeness and accuracy of the results of terrestrial laser scanning allow that avoiding additional costs at the stages of design, construction and operation of the facility.

Scanning control and transformation of the scanner coordinate system are carried out by the RISCAN PRO and MicroStation software which supplied with the scanner.

6. Scanning

A complex of field work on ground laser scanning was carried out on the work area, consisting of the following types of work:

1. Reconnaissance. Survey work using a ground-based laser scanning system which begins with the collection of auxiliary information (diagrams, drawings, map materials) and the object a reconnaissance is carried out.

2. The creation of a survey rationale determines the necessary coordinates of reference marks (elements of external orientation of the scanner). Reflective marks were temporarily fixed on the ground on special landmarks. The milestones stability was fixed with bipods.

3. Scanning was performed using a RIEGL *Z*-400*i* ground-based laser scanning system. Scanning parameters: *L*-950m, frequency range 150 kHz: *t*-24 min, fixation of the last reflection with maximum angular sweeps (Fig. 1-3). For scanning the side of the section, 4 points of the device were required. The placement of scan positions meets the following requirement: from the scanning point, all mine workings and elements to be displayed are clearly visible. Scanning at each station was carried out in 2 stages: performing high density scanning; recognition of reflective marks.

7. Coordination of reference marks

To orient the point clouds (obtained during scanning at each scan-position) between themselves in one coordinate system, reflective marks are needed, which are fixed on the ground during scanning.

Coordination of marks was carried out from survey points that using TRIMBLE R8-III GPS receivers

8. Digital data processing.

Digital data processing includes the following steps:

1. Transformation (landing) of the point cloud obtained by scanning using the GCP points coordinates files in a certain coordinate system.

Fig. 2. Installation at the Duty Point of the Scanner RIEGL Z-400I

2. Creation of a digital terrain model. The primary processing of the scan results was performed using the RISCAN PRO and MicroStation software, further processing and construction of the topographic plan were acted with using AutoCAD Civil 3D.

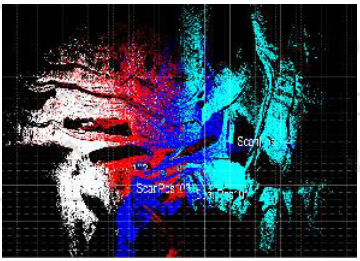

Fig. 3. Location of scan positions (october 2019y)

Fig. 4. Thick point cloud after scanning

10. Field control

Completeness control that carried out by comparing the material is ready for to transfer with the terrain. In this case, both facts of lack of information and facts of information redundancy are recorded.

The coverage object was controlled by the discharged summary file points of laser reflections from all scans.

Control is necessary in each stage of the work, since the modeling process is quite long and errors can be detected long after till the end of the survey. The accuracy of determining reference marks is also monitored.

11. Creation of a digital terrain model

In their essence, the transformed point clouds are already in a digital model with real 3D coordinates, in the accepted conditional coordinate system of the project, (Fig. 5-9).

The terrain model that built during post-processing in MicroStation, has an average density of 9 points per 1 m2. This density allows us to have a full understanding of the actual geometric parameters of relief elements.

Further processing is performed in the AutoCAD Civil 3D environment and the consists in three-dimensional modeling of the characteristic relief contours.

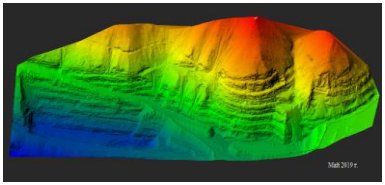

Fig. 5. 3D model of the cut side for May 2019

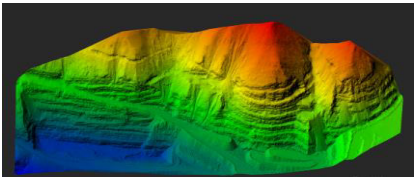

Fig. 6. 3D model of the cut side for October 2019

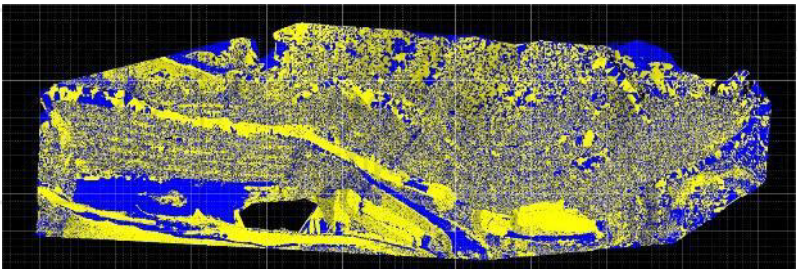

Fig: 7. Comparison of 3D models of the cut flank. View - 2: blue color –May, yellow color - October

Fig. 8. Photo report of the cut side

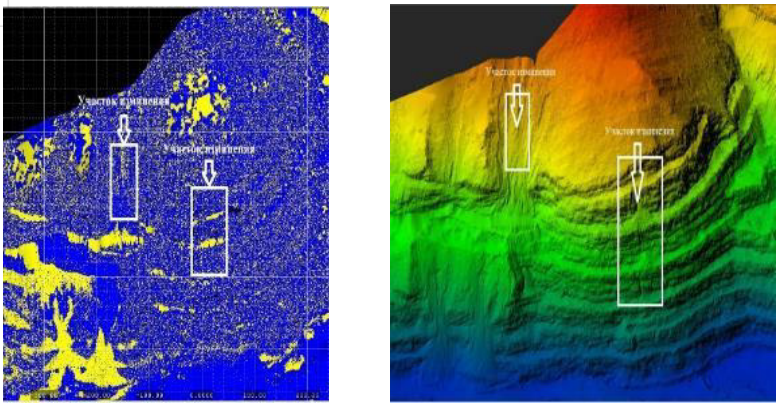

Fig. 9. Section of the Kharanutsky open-cut mine (indicating displacements and deformations)

The comparative analysis that based on the monitoring results was carried out to determine the deformations and displacements of the sides of the Kharanutsky coal mine, according to the data of ground-based laser scanning for various periods, which was carried out in the RISCAN PRO environment (Fig. 4.10). Digital elevation models (DEM) were built based on two observation cycles. DEM according to observations of the first cycle is plotted in blue, the second cycle - in yellow. The comparison results show the places where deformations and displacements are detected.

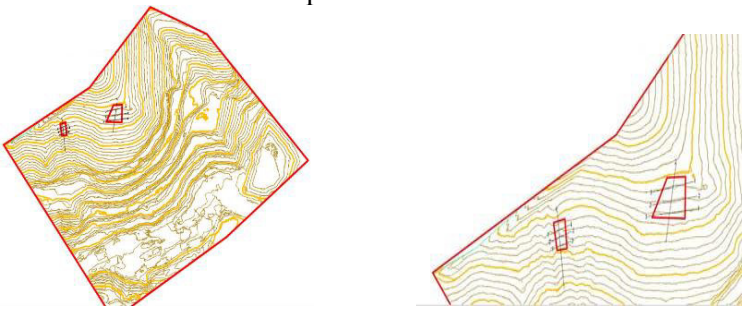

Fig. 10. A plot of debris recorded based on the results of 2 observation cycles

There are the graphs below that built according to the data in Fig. 9, which shows the dynamics of the changes in the state of the

working side of the section for two cycles of observations and the displacements identified (red - 1 cycle, green - 2 cycle) (Fig. 11-18).

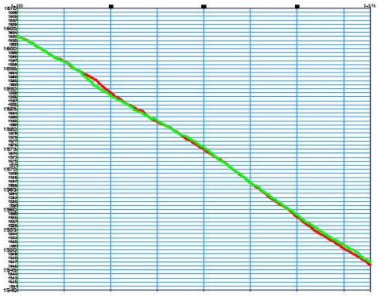

Fig. 11. Longitudinal section 1, where displacements are observed

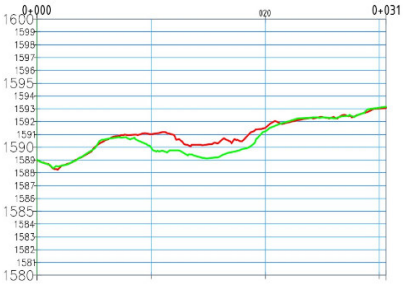

Fig. 12. Cross section 1-1

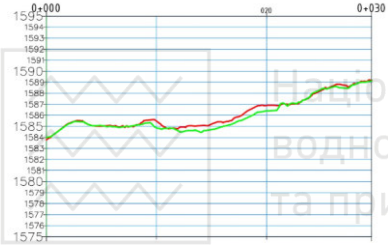

Fig. 13. Cross section 2-2

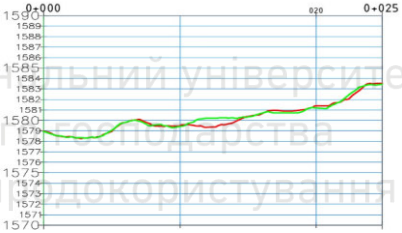

Fig. 14. Cross section 3-3

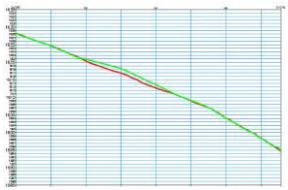

Fig. 15. Longitudinal section 2, where displacements are observed

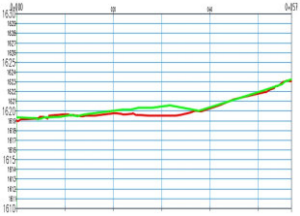

Fig. 16. Cross section 1-1

Поперечное сечение 2-2

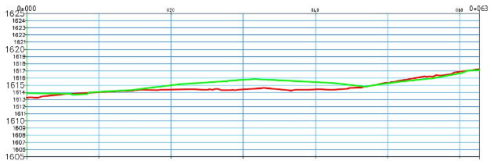

Fig. 17. Cross section 2-2

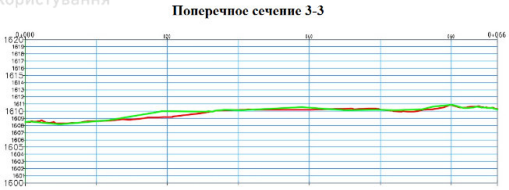

Fig. 18. Cross section 3-3

Such as the results of observations of deformation processes at the Kharanutskiy coal mine show that there no significant changes are observed on the sides and ledges of the section. Not any displacement massif mountain of a landslide nature is observed accordance to the results of the 2nd measurement cycle, however, talus was recorded in some parts of the section. Some changes recorded in the places of mining operations are due to the excavation of the rock mass and drilling and blasting operations. According to the deformation observations and side displacements of the Kharanutskiy coal mine, it can be concluded that at this stage not any critical displacements have been identified, despite of these places where small rockslides are manifested in the rock mass. Further observations are recommended.

The results of laser scanning confirm the drawn conclusions from the results of satellite observations at control points and the survey of the sides of the section. To perform work on ground-based laser scanning along the strike of the entire section, a special-purpose network (base stations, Fig. 19) was created with a high accuracy of mutual position in the WGS-84 coordinate system.

Fig. 19. Base station locations

Conducting sequential series of laser scanning and the section GPS survey with the results subsequent analysis makes it possible to solve the following set of tasks: to carry out remote areal monitoring of the propagation of deformations of the sides with the identification of areas where surface subsidence occurs (landslide areas); determine the volumes of deforming masses; identify trends in the course of the deformation process; delineate hazardous areas; assign design sections to assess the stability of the pit walls; operational surveying accounting of the volume of mining operations performed.

12. Approbation of the cycle of monitoring deformation processes on the example of a deep open pit

When developing a methodology for observing the structures settlements, primary attention should be paid to justifying the accuracy and frequency of measurements. These issues are related to the adopted measurement scheme and the method of processing the measurement results, as well as the model for predicting deformations and depend on the initial indicators used in the calculation.

To calculate the accuracy of measurements, the formula can be used

$$\sigma\Gamma = s_0 \frac{\Delta}{6} s_0 \frac{\delta}{3}, \qquad \sigma_\Gamma = s_0 \frac{\Delta}{6} = s_0 \frac{\delta}{3} \tag{1}$$

where σ_Γ is the standard deviation of the measurement from a constant parameter, which is understood as the absolute and relative total values of the displacements;

c_0 – coefficient of transition from technologically normalized tolerance to the tolerance of its measurement;

Δ – technologically standardized tolerance;

δ – technologically permissible deviation.

Coefficient c_0 varies within from 0,20 to 0,70.

In cyclic measurements, the accuracy is normalized according to the formula

$$\sigma\Gamma = \frac{\sigma\Gamma}{(n-1)}, \qquad \sigma_{\Gamma_{int}} = \frac{\sigma_\Gamma}{(n-1)} \tag{2}$$

that - standard deviation of parameter measurement in each tracking interval;

n - number of measurement cycles;

(n-1) - tracking number intervals.

The main indicators when calculating the observations accuracy should be the values of the relative ultimate deformations. The observation accuracy calculation should be made based on the values that expected final limit values of settlements and deformations.

The surveying observations' accuracy that the structures deformations can be normalized based on the values where determine the limiting state of the altitude position of the structure under study and the nature of the flow of precipitation and deformation.

To ensure the structure stability, the settlement value obtained from the measurement results of the (n+1) first cycle, and the absolute error of its determination must be less than the limiting value of the settlement, i.e.

$$S_{t_{n+1}} + \delta_{St_{n+1}} \le S, \qquad (3)$$

the $\delta_{St_{n+1}}$ - is maximum error of the true draft value;

S – design tolerance for the amount of draft.

The quantitative characteristic that serves to substantiate the method for measuring the settlement of structures, they are the marginal errors $\delta_{St_{n+1}}$. Based on condition (3) and according to the amount settlement tolerance

$$S_{ist} + \delta_{S_{ist}} \le S, \qquad (4)$$

the S_{ist} - the benchmark (mark) settlement value equalized in the (n+1) - first measurement cycle.

The deformations nature structures are determined, as known, by the magnitude and speed, i.e. change in the deformation process for the selected time interval. The accuracy and frequency of surveying measurements are prescribed in such a way that the results obtained satisfy the principle of practical confidence both in the magnitude of deformations at the time of observation and in its intensity, which allows, on the one hand, to judge the studied process invariability in time and the losing information impossibility about the nature of its change - on the other. So, the intensity value of deformations plays a more significant role than its absolute value. Following this, the

measurements accuracy and frequency should be determined from the condition

$$\Delta S = S(t_i) - S(t_{i-1}) \geq \sigma(\varepsilon), \quad (5)$$

the $S(t_i)$ - is the amount of deformations at the time t_i;

σ - standard deviation of strain determination;

ε - coefficient depending on the measurement distribution errors and the level confidence.

The required measurement accuracy depends on the coefficient ε, for the determination of which it is necessary to have and a priori decision on the form of the distribution of measurement errors and the confidence probability, which characterizes the reliability of obtaining the desired values. The distribution law of measurement errors, as a rule, is close to normal, and the confidence probability is taken within the limits $0{,}955 \leq \beta \geq 0{,}977$. In this situation ε varies in the range from 4.0 to 6.0.

Depending on the measurement results responsibility, the optimal ratio between the assignment of the error and the expected deformation measurements result is determined. In practice, this ratio is taken to be from ¼ to □. But for β=0.995÷0.997, the deformations will be within the confidence interval of the measurement errors. This means that the values taken for deformations may in fact turn out to be measurement errors. To avoid this, it is necessary to take a different relationship between the error and the expected result of strain measurement, for example, ¼-⅙, depending on the accepted confidence level.

The surveying observations accuracy of the structures deformations can be normalized based on the values that determine the altitude position's limiting state study structure and the precipitation and deformation flow nature.

Permissible errors in engineering structures determining settlement on various soils:

0,001 m - for buildings and structures erected on rocky and semi-rocky soils;

0,002 m - for buildings and structures erected on sandy and semi-sandy soils;

0,005 m - for buildings and structures erected on bulk, subsidence, peat and other highly compressible soils.

The measurement accuracy adopted in the first cycles, depending on the nature of the flow of precipitation, must be corrected. If "*n*" measurement cycles have been made, then during calculating the accuracy in the (*n*+1) - first cycle, the sediment equation obtained from the measurements results in the previous "*n*" cycles is used.

The displacement rate of the points of the array is determined by the value of the displacement of the working benchmarks of the mine surveying observation station for a certain period of time in the direction of the displacement vector. Depending on the dynamics of the process, the rate of deformation can be measured: m/hour, m/day, mm/hour, mm/day, mm/month. To characterize the degree of danger of deformations, the most indicative is the displacement rate in the initial period of the active stage of the displacement and deformation process.

The latent stage of landslide development is the period at the beginning of the development of micromovements in the massif until the appearance of visible signs of the landslide formation of (the appearance cracks on the earth's surface, bulging of rocks at the base of the pit wall, and so on). The rate of displacement of the points of the array towards the end of the latent stage is 1-10 mm/day. The stage of landslide decay is the period of displacement of the landslide masses with a decreasing speed until the displacement completely stops. The timing of repeated observation cycles is set depending on the tasks set in the project and the development of the displacement process. According to the requirements of the instructions, in the first time after the laying of the observation station, observations are carried out monthly. After 3-4 series of observations and the establishment of the rate of displacement of the technogenic massif, the frequency of observations changes. If the rate of displacement of the benchmarks does not exceed 1 mm/day and decays in time, the time intervals between the series of observations can be increased to 3-4 or more months, but observations should be carried out at least 1-2 times a year. If the rate of displacement of the benchmarks is constant and is 0.5-1.0 mm/day, observations are carried out, respectively, once every two months and monthly. When the shift process is activated, the intervals between the series of observations are reduced to several weeks or even days.

Methodological guidelines established that when observing active landslides with velocity displacements of 10 mm/day or more, a series of observations are carried out daily; if the rate of displacement of the benchmarks increases with time, then to establish the critical rate of displacement, preceding the failure of landslides, the time intervals between the series of observations are reduced to several hours, in some cases, automatic signaling devices of the rate of deformations are installed.

To calculate the speed of displacement of working benchmarks, use the formula

$$\upsilon = \frac{S_{CP}}{T}, \tag{6}$$

the S_{CP} - average displacement of working benchmarks over the observation period t, m.

so, the average value of the displacement is determined

$$S_{cp} = \frac{S_1F_1 + S_2F_2 + \ldots S_nF_n}{F_1 + F_2 + \ldots + F_n}, \tag{7}$$

the $S_1,S_2,\ldots,S_n$ - benchmarks offset 1, 2,…, n, m;

F_1, $F_2,\ldots,F_n$ - the area referred to the coverage area of the corresponding reference points. m^2.

In some cases, the working benchmarks the average displacement's structure is calculated as the arithmetic mean of the sum of the absolute displacements of all benchmarks.

In accordance with the methodology of prof. N.G. Vidueva, the standard deviation of the draft is determined by the formula

$$\sigma(\upsilon) = \frac{1}{\Delta t}\sqrt{\sigma^2(\Delta S) + \upsilon^2\sigma^2(\Delta t)}, \tag{8}$$

In this case, the relative error in determining the rate of settlement will be

$$\frac{\sigma(\upsilon)}{\upsilon} = \sqrt{\frac{\sigma^2(\Delta S)}{\Delta S^2} + \frac{\sigma^2(\Delta t)}{\Delta t^2}}. \tag{9}$$

f you set some value of the relative error $\frac{\sigma(v)}{v} \le \frac{1}{N}$, then the standard deviations $\sigma(\Delta S)$ and $\sigma(\Delta t)$ must satisfy the condition

$$\frac{\sigma^2(\Delta S)}{\Delta S^2}+\frac{\sigma^2(\Delta t)}{\Delta t^2}\le\frac{1}{N^2}. \quad (10)$$

For a preliminary calculation, you can use the principle of equal influence of sources of errors, then

$$\frac{\sigma(\Delta S)}{\Delta S}=\frac{\sigma(\Delta t)}{\Delta t}, \quad (11)$$

Here

$$\frac{\sigma(\Delta t)}{\Delta t}\le\frac{1}{N\sqrt{2}}. \quad (12)$$

Having set some standard deviation, acceptable for specific observation conditions, $\sigma(\Delta t)$, we get

$$\Delta t \ge N\sigma(\Delta t)\sqrt{2}, \quad (13)$$

the Δt - the period during which precipitation changes evenly, day.

The required accuracy of such a period will be $\sigma(\Delta t)\le\frac{\Delta t}{N\sqrt{2}}$.

Then we get

$$\frac{\sigma(\Delta S)}{\Delta S}\le\frac{1}{N\sqrt{2}}. \quad (14)$$

Considering, that $\Delta S=v\Delta t$, can write

$$\sigma(\Delta S)\le\frac{\upsilon\Delta t}{N\sqrt{2}}. \quad (15)$$

So, it becomes necessary to understand the rate of settlement [21]. When approximating the precipitation of one or another curve, an exponential curve is used, characterized by the equation

$$S_i=S_k(1-e^{-\alpha t}). \quad (16)$$

the S_k - final draft, m;

α - an empirical coefficient depending on the nature of the soil, foundation structure, load, etc.

The draft can be represented by another equation

$$S_\tau=S_k\frac{t}{d+t}, \quad (17)$$

the d - empirical coefficient ($0\le d\le 1$).

The sediment values can also be approximated by a polynomial of the form

$$S_{\pi i} = \sum_{i=1}^{p} a_i t^i \,. \tag{18}$$

Coefficient α fluctuates over a wide range $0.05<\alpha<2.5$.

When designing observations of the structure settlement, some parameter values that determine St are used, and in the process of observations, the model of settlement (the deformation process nature) is refined. For this model, the displacement rate of the working benchmarks is determined by the formula

$$v = \frac{dS}{dt} = S_k \alpha \times e^{-\alpha t} \quad . \tag{19}$$

The rate of upsetting changes over time. For a certain period of time from t_1 to t_2, the offset reaches the value

$$\Delta S = \int_{t_1}^{t_2} v \cdot dt = S_k \left(e^{-\alpha t_1} - e^{-\alpha t_2} \right). \tag{20}$$

Given some value of t, can find $\Delta t=t_2-t_1$ time interval at which the offset ΔS acquires a certain predetermined value. Determined Δt by solving the equation

$$e^{-\alpha t_2} = e^{-\alpha t_1} - \frac{\Delta S}{S_k} = a \,, \tag{21}$$

where

$$t_2 = -\frac{\ln a}{\alpha} \,. \tag{22}$$

In this case $S_k \ \dfrac{\Delta S}{S_k} = \varepsilon = \text{const}$

$$e^{-\alpha t_i} = e^{-\alpha t_{i-1}} \varepsilon = a_i \,, \tag{23}$$

then

$$t_i = -\frac{\ln a_i}{\alpha} \tag{24}$$

The calculation of the required accuracy of determining the displacement of the benchmarks can be made using the absolute error of the displacement rate. Let us introduce the condition $\sigma(v) \le \sigma_0(v)$. Then used the formula (8), we ger

$$\frac{1}{t}\sqrt{\sigma^2(\Delta S)+\upsilon^2\sigma^2(\Delta t)} \le \sigma_0(\upsilon). \quad (25)$$

We will accept $\sigma^2(\Delta S) = v^2\sigma^2(\Delta t)$.

Then the accuracy of determining the observation period will be

$$\sigma(\Delta t) = \frac{\sigma(\Delta S)}{v}. \quad (26)$$

This technique makes it possible not only to find the required accuracy of the precipitation measurement, but also to determine the observation period with an assessment of its accuracy.

When deciding on the rate of displacement of benchmarks, one proceeds from the absolute deformation critical for a given structure, which depends on the nature of the soil, foundation design, load, etc.

The degree of danger of deformations is determined from the rate of displacement and the magnitude of deformations by comparing them with the permissible deformations established for specific rocks, laboratory studies, and the deformation properties of rock samples.

At a steady rate of deformation (relative shear), the time to the collapse of the slope is determined from the expression

$$\frac{\gamma_{пр}-\gamma_{уст}}{tg\psi} = t \quad (27)$$

,

the γ_{pr} - the limiting relative shear deformation, established by laboratory tests of rocks or field observations, upon reaching which the destruction of the rock occurs;

γ_{ust} - shear deformation, upon reaching which a steady-state constant deformation rate is observed, m;

ψ - the slope of the segment of the dependence graph $\gamma=f(t)$ in the area of constant strain rate (the tan φ value numerically corresponds to the shear strain rate), degree.

Taking into account that the rate of shear deformation at the stage of decaying creep at any of its intervals is greater than the rate of deformation at the subsequent stage of steady-state creep, an approximate estimate of the time to destruction of the slope from the rate of deformation at the stage of decaying creep should be carried out by the expression

$$t \geq \frac{\gamma_{пр} - \gamma_i}{tg\,\psi_i}, \quad (28)$$

the γ_i - shear deformation at the time of this calculation, m;

$tg\ \psi_i = \upsilon_\gamma$ shear strain rate at the decaying creep stage upon reaching the total shear γ_i, mm / day.

When predicting the development of landslides of slopes of quarries and dumps in time, it is necessary to take into account, in addition to the increase in displacement rates, the development of a detachment crack outlining the landslide on the landslide flanks is also possible (the active stage of a landslide occurs when it is completely delineated by a separation crack on the flanks) According to the data of joint observations of the increase in the rates of displacement of the landslide in its central part and the development of separation cracks along the flanks of the landslide, the critical rates of displacement of the landslide are established for the given engineering-geological and mining conditions.

We will evaluate the accuracy of measurements with an electronic total station and a GPS system.

For deep quarries, it is characteristic that the length of the profile lines of the observation stations becomes significant, and the number of connecting benchmarks located on the near-belt strip and on the berms of the benches of a deep quarry also increases.

When observing the condition of the sides of deep quarries, it is necessary to substantiate the location of the reference, control and connecting benchmarks with an assessment of the accuracy of their planned-high-altitude position.

In accordance with the permissible errors in determining the planned and altitude position of the benchmarks, an assessment was made of the accuracy of the position of the tie benchmarks located on the side strip and on the berms of the benches of a deep pit.

The root-mean-square error of determining the excess by the trigonometric leveling method using an electronic total station is determined by the formula

$$m_h^2 = L^2 \cos^2\delta \frac{m_\delta^2}{\rho^2} + m_L^2 \sin^2\delta + 2m_\upsilon^2 \quad (29)$$

the m_{δ}, m_L, m_V - root mean square errors of measurement of the corresponding values (vertical angle, distance, instrument height and sighting).

The error in measuring distances with an electronic total station is determined by the expression m_L=2 mm±2 mm/km L, the L - side length in km, UPC of vertical angle measurement for high-precision Leica TCR 1201 total station is 1.5".

The dependence of the root-mean-square error in determining the excess on the angle of inclination of the sighting beam of the telescope and the distance from the connecting reference to the working one is given in Table. 2

Table. 2

The root-mean-square error of determining the excess with three measurements with the Leica TCR 1201 total station

Distance from total station to last benchmark L, m	Angle of inclination of the sighting axis, degree			
	b=5	b=10	b=15	b=20
	Mean square error in determining the excess with three measurement methods m_h, m			
50	0,00085	0,00087	0,00090	0,00094
100	0,00092	0,00094	0,00097	0,00101
150	0,00104	0,00105	0,00107	0,00111
200	0,00118	0,00119	0,00121	0,00123
300	0,00150	0,00151	0,00152	0,00153
400	0,00187	0,00187	0,00186	0,00186
500	0,00225	0,00224	0,00223	0,00216
600	0,00264	0,00263	0,00261	0,00258
800	0,00345	0,00343	0,00339	0,00334
1000	0,00427	0,00423	0,00418	0,00411

The graph of the dependence of the measurement accuracy on the angle of inclination and the distance from the binder to the working benchmark is shown in Fig. 20.

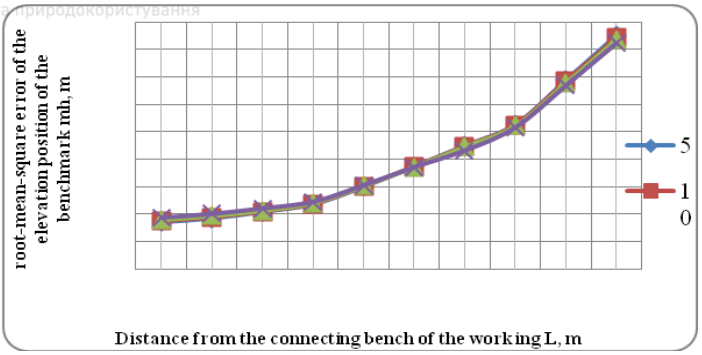

Fig. 20. measurement dependence graph of the accuracy on the angle of inclination and the distance from the working benchmark binder

The root-mean-square error of determining the position of the next linking reference will include the RMS of the first linking reference and the error of the actual method for determining the excess of the reference

$$m^2_{(n+1)_h} = \sqrt{m^2_{(n)_h} + m^2_h} \qquad (30)$$

To calculate the accuracy, the angle of inclination of the sighting axis of 20˚ was taken, which is most often found during instrumental observations along the profile lines on the side of the open pit.

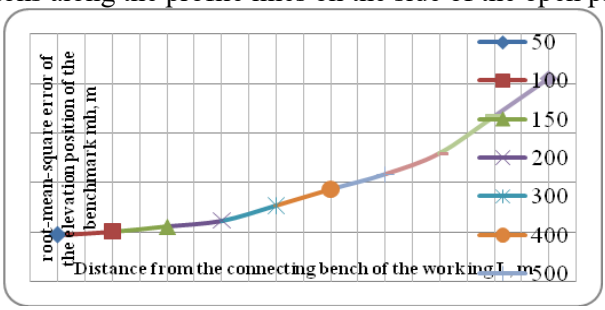

Fig. 21

The calculating results of the RMS determining the altitude position of the connecting benchmarks are summarized in Table 3.

The root-mean-square determining error of the altitude position of the connecting benchmarks with three measurement techniques

Table 3

Binder reference number	Distance between connecting benchmarks, L m					
	100	200	300	400	500	600
	RMS for the height position of the tie marks, m_h mm					
1	1,01	1,23	1,53	1,86	2,160	2,580
2	1,43	1,739	2,164	2,630	3,055	3,649
3	1,75	2,130	2,650	3,221	3,741	4,469
4	2,02	2,460	3,060	3,719	4,320	5,160

The graph of the change in the accuracy of determining the position of each next connecting benchmark is shown in Fig. 22.

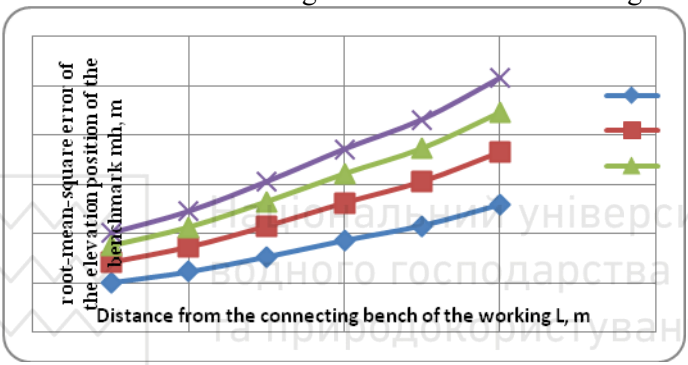

Fig. 22. Graph of changes in the accuracy of determining the position of each next linking reference

An analysis of instrumental measurements assessment accuracy determines the altitude position of tie marks shows that to ensure an admissible measurement error of 3 mm, the number of tie points should be equal to n=3 at a distance between ties of 370 m and with three measurements with a high-precision Leica TCR 1201 total station.

The following main sources of errors affect the accuracy of determining the planned position of the connecting reference marks of stations using an electronic total station: - error of the proper method of polar coordinates $m_{floor.}$, m; - initial data m_{ICX}, m; - centering the total station $m_{ts,t}$, m; - orientation of the original direction m_{orien}, m; - fixing the reflector $m_{f.r}$, m.

The average square error of determining the planned position of the first connecting reference point by the method of polar coordinates is determined by the expression

$$m_R^2 = m_{FLOOR}^2 + m_{ISX}^2 + m_{C.S}^2 + m_{ORIEN}^2 + m_{F.R}^2 \qquad (30)$$

The average square error of the actual method of polar coordinates for "n" measurement methods is determined by the formula

$$m_{FLOOR} = \frac{1}{\sqrt{n}} \sqrt{m_L^2 + \left(\frac{m_\beta}{r}\right) L^2} \qquad (31)$$

The error of orientation to the original direction is determined by the formula

$$m_{ORIENT} = \frac{m_\beta L}{r} \qquad (32)$$

The results of the calculation of the UPC for determining the planned position of the connecting reference points at three measurement methods are summarized in Table 4.

Table 4

The average square error for determining the planned position of the connecting reference points at three measurement methods

The rapper's binding number	Distance between connecting reference points, L m					
	100	200	300	400	500	600
	UPC of the planned position of the connecting reference points, mR mm					
1	2,120	2,396	2,764	30192	3,661	4,155
2	2,487	2,824	3,255	3,749	4,285	4,848
3	2,807	3,195	3,681	4,233	4,929	5,453
4	3,094	3,527	4,063	4,667	5,318	5,998

The analysis of the results of the measurement accuracy assessment showed that with three methods of measurement with the Leica TCR 1201 total station for determining the planned position of the reference points, the required accuracy of 3 mm is provided only for two connecting reference points located at a distance of 250 m from each other, which is insufficient for deep quarries.

The results of the performed calculations of the UPC for determining the planned position of the connecting reference points with six measurement methods are summarized in Table 4.10.

Table 5

The rapper's binding number	Distance between connecting reference points, L m					
	100	200	300	400	500	600
	UPC of the planned position of the connecting reference points, mR mm					
1	1,910	2,150	2,482	2,874	3,305	3,761
2	2,120	2,396	2,764	3,192	3,661	4,155
3	2,311	2,619	3,020	3,482	3,985	4,515
4	2,487	2,824	3,256	3,749	4,285	4,848

The graph of changes in the accuracy of determining the position of each subsequent connecting reference point is shown in Fig.23.

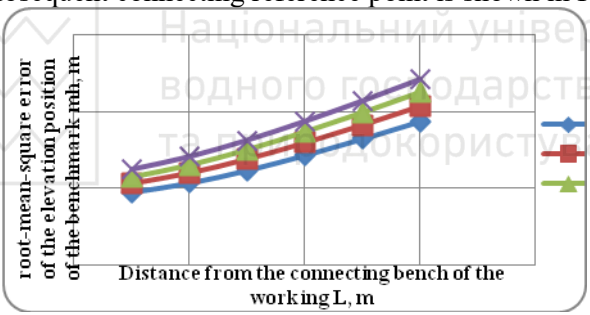

Fig. 23. Graph of changes in the accuracy of determining the position of each subsequent connecting reference point

For deep quarries with complex mining and geological conditions, a significant increase in the connecting reference points along the profile line of the observation station is characteristic. So, with an average distance between the connecting reference points equal to 300 m, the average square error of the position of the connecting reference points according to calculations on the lower horizons is: the 1st binding reference point 3,2 mm; the 2nd binding reference point 3,5 mm; the 3rd binding reference point 3,7 mm; the 4th binding reference point 3.9 mm.

The accuracy analysis shows that the positions of the reference points obtained by the UPC exceed the permissible value of 3 mm. Therefore, there is a need to improve the methods of production of instrumental observations by combining electronic total station and GPS observations.

After conducting studies of the accuracy of determining the planned altitude position of GPS reference points with GPS devices and taking into account the main factors that affect the accuracy of the work, you can express the UPC of the position with the following formula

$$m_{com-GPS} = \sqrt{m_{c.p}^2 + m_{TECHN}^2 + m_{GOR}^2 + m_{TS.A}^2} \qquad (33)$$

the $m_{ц.п}$- ошибка центрирования GPS приемника над связующим репером, мм;

$m_{TECHN-GPS}$- accuracy of GPS survey technology to determine the position of points,

m_{GOR} - GPS receiver positioning error, mm;

- error for instability of the antenna phase center, mm.

The average square error of centering for the optical centering of the total station is determined by the formula, mm

$$n_{C.T} = e\sqrt{1+\left(\frac{L}{b}\right)^2} = 0.5\sqrt{2} = 0,7 \qquad (34)$$

the e - the linear centering element, which is assumed to be equal to 0,5 mm and for $L \approx b$, b - is the length of the basis.

The accuracy of the GPS survey technology depends on the technology and the measurement time. For connecting reference points of observation stations of deep quarries, the "fast static 20-30 minutes" technology is provided at a distance of 10 km from the base receiver, then =1,0 mm.

The horizontal error of the GPS receiver depends on the accuracy of setting the axis of the round level in the vertical position and is determined by the expression

$$m_{GOR} = \frac{0.1\tau}{r} h_0 \qquad (35)$$

the τ - the price of dividing the round level of the reflector stand, seconds;

h_0 – GPS receiver installation height, m.

The GPS device has a round level, the division price of which is 10' or 600". Then the error of positioning the GPS receiver will be, mm

$$m_{GOR} = \frac{0.1 \times 600}{206265} 1500 = 0.44. \quad (36)$$

The error for the instability of the phase center of the antennas is taken on the basis of studies conducted in the "fast static" mode, which showed fluctuations of the phase center in the horizontal plane of less than 1.0 mm.

The average square error of determining the planned position of the connecting reference point using GPS survey technology will be equal to, mm

$$m_{Comm3-GPS} = \sqrt{m_{c.p}^2 + m_{Techn-GPS}^2 + m_{gor.}^2 + m_{c.A}^2} = \sqrt{0.7^2 + 1.0^2 + 0.44^2 + 1.0^2} = 1{,}64 \quad (37)$$

The conducted studies proved the feasibility of using a GPS receiver to determine the planned altitude position of the connecting reference points for the combined method of instrumental observations, where the position of the working reference points of the observation stations will be determined by an electronic total station.

Conclusion

As a result of the practical implementation of complex geomechanical studies of the state of stability of instrument arrays of deep quarries on the basis of instrumental observations using advanced geodetic instruments and technologies, the following results were obtained:

1. Projects of observation stations for the state of stability of the sides have been developed in which, depending on the mining and geological conditions of field development, based on geomechanical studies of the composition and properties, structural and tectonic features of the instrument arrays of quarries, hydrogeological conditions of fields, assessment of the state of real slopes of deep quarries, the following are made: justification of the locations and structures of observation stations; choice of a method for systematic instrumental observations; the design of reference reference points,

observation and control points of observation stations has been developed.

2. Two series of instrumental surveying and geodesic observations of the state of stability of the sides of quarries were performed using a robotic electronic total station TSA1201, GPS systems 1200, and a 3D scanner.

3. A complex method of geomechanical study of the stability state of deep quarry instrument arrays based on instrumental observations, spectral seismic and GPR profiling, laser scanning of the most dangerous areas of the quarry side is proposed, which allows us to most reliably justify the locations of observation stations based on the factor of tectonic (man-made) disturbance of the array, take into account the nature of rock deformation and predict their development in time and space.

4. A system of geomechanical monitoring of the stability state of the quarry instrument arrays has been designed, consisting of 17 observation stations (25 profile lines), including 972 reference points, 30 of them reference ones, which allows evaluating and predicting geomechanical processes occurring in the quarry instrument arrays and monitoring the correctness of decisions made on the parameters of the side slopes.

References

1. **Seredovich, A.V.** Application of three-dimensional laser scanning for determining the deformations of vertical reservoirs [Text] / **A.V. Seredovich, A.V. Ivanov** // Laser scanning and digital aerial photography. Today and tomorrow: tez. dokl. V-th International Conf. and exhibitions. – M.: XportMedia, 2005. – p. 43-46.

2. The method of calibration of ball tanks by ground-based laser scanning [Text] / **A.V. Komissarov, M. S. Kalinina, E. A. Yegorchenkova, N. S. Korotchenko** // Problems of collecting, preparing and transporting oil and petroleum products.- 2015. – №. 4 (102). – Pp. 163-170.

3. **Agarkov I. B., Konovalov A.V**. Estimation of displacements of ledges and sides of a quarry according to laser scanning data/ / https:/ /geomix.ru /blog/science /otsenka-smeshhenij-ustupov-i-bortov-karera.

4. **S. V. Tursbekov, M. G. Aituganov.** Fundamentals of creating a surveyor monitoring of the state of quarry instrument arrays// Bulletin of the KRSU. - Karaganda,2013. - Volume 13. - No. 4. - p. 85-87.

5. **Anikushkin M. N.,** Ground-based laser scanning systems. Experience of work Text. / M. N. Anikushkin/ / Geoprofi. 2005. - No. 1. - p. 49-50.

6. **Yushkin V. F**. Methods of three-dimensional modeling of rock massifs in the study of geomechanical properties and mining operations//INTEREXPO GEO-SIBERIA.- Novosibirsk, 2015. - Siberian State University of Geosystems and Technologies.- Volume 2. - No. 3. - pp. 293-297.

7. Laser scanner Z+F IMAGER 5006EX // https: / / www.gsi.ru /catalog /laser_scanner/zf_imager5006ex.

8. instruction for the production of surveying works/ Ministry of Coal Industry of the USSR. All-Union Research Institute of Mining Geomechanics and Surveying. - M.: Nedra, 1987 240 p.

9. Leica TPS400 Series Easy, quick, reliable and powerful [Electronic resource]: Leica Geosystems website. Access mode: http://www.leica-geosystems.com/common/shared/downloads/inc/downloader.asp?id=2226 LMS-Z360 Laser mirror scanner. Technical documentation and users instructions. Horn: Riegl Laser measurement systems, 2003. 92 p.

10. **Komissarov, A.V**. Research on the accuracy of constructing a digital relief model based on ground-based laser scanning data [Text] / **A.V. Komissarov**// GEO-Siberia-2006. Vol. 1. Geodesy, Афонин, Д.А. Геодезический контроль деформаций при строительстве городских подземных сооружений открытым способом: автореф. дис. ... канд. техн. наук: 25.00.32 / **Афонин Дмитрий Андреевич**. - СПб, 2013. - 22 с.

11. **Afonin, D. A.** Design of geometric parameters of ground-based laser scanning in the control of deformations of buildings and structures in conditions of dense development / **D. A. Afonin, M. Ya. Bryn, E. G. Tolstov** / / Geodesy and Cartography. - 2013. - No. 2. - p. 2-7.

12. **Bykov, A. B.** The desired and the real in geometric modeling [Electronic resource] / A. B. Bykov// CAD and Graphics. - 2002. -№ 1. Access mode: http://www.sapr.ni/Archive/SG/2002/l/7/

13. **Kanashin, H. B**. Development of technology for ground-based scanning of railway stations: dis. ... kand. tehn. nauk: 25.00.35 / **Kanashin Nikolay Vladimirovich**. - M., 2009. - 160 p.

14. **Seredovich, A. B.** Methodology for creating digital models of objects of . –2011.– No2. –C. 96–99.

15. **Seredovich, A. B.** Application of the RISCAN PRO software product for registration of scans [Electronic resource] / **A. B. Seredovich, A. B. Ivanov, O. A. Dementieva** // Interexpo Geo-Siberia. - 2011. - №2. Access mode: http://cyberleninka.m/article/n/primenenie-programmnogo-produkta-riscan-pro-dlya-registratsii-skanov.

16. Autodesc information site:http://www.autodesk.com/products/ recap/ overview.

17. **Vinogradov, K. P.** Perspective methods of processing the results of ground-based laser scanning/ **K. P. Vinogradov** / / Vestnik. Architect. 21st century. - 2011. - №2 (39).- C.80-81.

18. Autodesk AutoCAD Civil 3D/https://cad.EN/ support/bz/ archive / 82/ autodesk-autocad-civil-3d.

19. Software Rimining mining for laser scanner RIEGL VZ series/ www.riegl.ru.

20. Manual deformation of the sides of the slopes of the ledges and dumps in quarries and the development of measures to ensure their sustainability" (UTV. Gosgortekhnadzor of the USSR 21.07.1970)

21. Methodological guidelines for monitoring deformations of sides, slopes of ledges and dumps in quarries and developing measures to ensure their stability/Approved by Order

No. 39 of the Committee for State Control over Emergency Situations and Industrial Safety of the Republic of Kazakhstan dated September 22, 2008.

https://doi.org/10.31713/m1015

THEORY AND PRACTICE OF DETERMINING THE CATEGORY HAZARD OF COAL MINES BY THE GAS FACTOR

E. Filatieva
Volodymyr Dahl East Ukrainian National University, Senior Lecturer, Ukraine

A. Oleinichenko
Volodymyr Dahl East Ukrainian National University, Senior Lecturer, Ukraine

M. Filatiev
Volodymyr Dahl East Ukrainian National University, Doctor of Engineering Sciences, Associate Professor, Ukraine

V. Sokolenko
Volodymyr Dahl East Ukrainian National University, Candidate of technical science, Associate Professor, Ukraine

Annotation

A comparative analysis of the theoretical and practical definition of the category hazard of coal mines by gas factor based on experimental data obtained in real conditions of mining gas-bearing coal seams is presented. The mine's hazard category by gas factor is determined in accordance with the current regulatory document. The processing of experimental data obtained in field studies leads to contradictions in the requirements for the safe mining of gas-bearing coal seams. The necessity of changing the regulatory framework for predicting methane release and establishing the category hazard of mines by gas factor is substantiated, as well as the theoretical part of the research is experimentally confirmed and practical proposals are given to improve the requirements of regulatory documents for the safe mining of gas-bearing coal seams.

The gas release from seven possible sources, the exposed surface of the working face, the undermined adjacent seams and their enclosing rocks, the overworked adjacent seams and enclosing rocks, the worked-out space of the stopped lavas, are accepted for consideration. The studies have shown that by removal the bottom from cut and the area of the mined-out space of the operated section and the wing of the

mine field, taking into account the stopped longwalls, it is possible to predict the processes of rock displacement that determine the absolute gas release from the undermined sources.

Introduction

Establishment of the category of mines for the hazard of methane emission is carried out in accordance with the normative document [1] using the relative gas emission per one ton of mined coal. This technique was developed for the conditions of Donbass in the fifties of the last century. At that time, mines were mined at shallow and medium depths. The main source of gas release into the mine workings of extraction areas (more than 60%) was the developed seam. The gas balance in most cases was characterized by methane release from the broken coal and the exposed surface of the working face. The direct relationship of gas emission from these sources with the level of coal production suggested their direct proportional relationship. This was a theoretical justification for dividing mines according to their category using the amount of methane per ton of coal mined.

A little later, it was found that the relative gas release is not a constant parameter, but depends on the level of coal production [2]. This circumstance was not taken into account when developing a forecast of gas emission in the relevant regulatory documents, including in the current manual [3]. As a result of this, significant discrepancies were subsequently revealed between the experimental data on gas evolution and their predicted values [4]. In addition, if we proceed from the fact of a decrease in the relative gas abundance with an increase in coal production, then the category of mines should, according to [1], decrease, and with a decrease in production, it should increase. Such tendencies in the change in the relative gas abundance have led to contradictions in the determination of the mine gas hazard category. They consist in reducing the gas hazard according to [1] with an increase in coal production. This is not consistent with the practice of mining gas-bearing coal seams. It has been unequivocally established that with an increase in coal production, other things being equal conditions, an increase in gas emission is observed [4]. The real gas hazard is increasing, not

decreasing, as it follows from the definition of the category of mines according to [1].

The above facts testify to the relevance for science and the coal industry of improving the regulatory framework [1,3] in terms of forecasting methane release and establishing the categorization of coal mines by their gas hazard.

The idea of work and purpose. Substantiate the need to change the regulatory framework for forecasting methane release and establish the category hazard of mines by gas factor. Experimentally confirm the theoretical part of the research and give practical suggestions for improving the requirements of regulatory documents for the safe mining of gas-bearing coal seams.

The transition to the development of coal seams at deeper horizons caused changes in the gas balance in terms of its distribution by sources. The share of methane release from the developed seam (broken coal and the exposed surface of the working face) has significantly decreased (up to 10-20%). The main sources in the development of seams in deep horizons are undermined and overworked adjacent coal seams and their host rocks (80-90%). Changes in coal production do not equally affect methane emissions from different, by nature, sources. This led to contradictions in the requirements for the safe mining of gas-bearing coal seams.

Theoretical part. The predominant amount of gas in coal mines is emitted during cleaning works. Based on this ratio of the gas balance between mining operations, on a mine scale, the main gas release is associated with the operation of mining areas. For this reason, we considered the theoretically possible fractions that make up the total relative gas content of the excavation area q in the presence of all possible sources of gas release. Such sources are: the mined seam (broken coal I_{oy} and the exposed surface $I_{oз}$ of the working face), the undermined adjacent seams I_{cn} and their enclosing rocks I_{nn}, the overworked adjacent seams I_{cn} and the enclosing rocks $I_{нп}$. The forecast of gas release from the listed sources, without touching on its scientific validity, is made according to [3]. This normative document does not take into account the fact that with a sufficient development of cleaning work in the wing of the mine field, gas release occurs when the movement of the underworked

coal-rock strata is activated from the worked-out space $I_{вп}$ of stopped longwalls [5].

For consideration we have accepted gas release from seven possible sources. Methane release from the losses of chipped coal in the worked-out area of the operated and stopped longwalls was neglected. The approximate share of this source with ten percent coal losses does not exceed one percent of the total gas release from the developed seam, and it has no practical effect on the increase in the concentration of methane in the atmosphere of existing mine workings.

The establishment of categorization by the relative gas content of the excavation area $q_{уч}$ according to [1] and on the basis of n sources accepted for consideration can be presented in the following form, м^3/т

$$q_{уч} = \frac{\sum_{i=1}^{n} I}{A} = \frac{I_{оу}}{A} + \frac{I_{оз}}{A} + \frac{I_{сп}}{A} + \frac{I_{пп}}{A} + \frac{I_{сн}}{A} + \frac{I_{нп}}{A} + \frac{I_{вп}}{A} + \frac{I_{д}}{A}, \qquad (1)$$

where $q_{уч}$ - average monthly relative gas emission per one ton of mined coal, m^3/t; A - average monthly coal production, t; $I_{оу}$,$I_{оз}$,$I_{сп}$,$I_{пп}$,$I_{сн}$,$I_{нп}$,$I_{вп}I_{д}$ - the average monthly amount of gas released, respectively, from the broken coal, the exposed surface of the working face, adjacent undermined seams, undermined rocks, overworked adjacent seams, overworked rocks, mined-out space of stopped lavas and into degassing systems, m^3.

The ratio $I_{оу}/A$ of the right-hand side of equation (1) characterizes the outgassing from one ton of chipped coal. Its numerator $I_{оу}$ is directly related to the amount of coal mined. Broken coal is the most disturbed part of the gas-coal system, from which the rock pressure is completely removed. The parameter $I_{оу}$ has been studied quite fully back in the sixties of the last century. The studies were carried out both in laboratory and in production conditions. All other things being equal, the main factors determining the gas release from the chipped coal are its natural gas content in the mining zone, the fractional composition and the time elapsed since the coal stripping. Gas evolution occurs most intensively in the initial period of time, that is, directly in the face space of the longwall. Usually coal after its breaking is in the bottomhole space for about 10 minutes, and within the site - 30-60 minutes. For this reason, the amount of gas

released from coal while it is in the bottomhole space is at least 70% [6]. The share of the evolved gas on the conveyor is several percent [7]. The insignificant release of gas during the transportation of coal from its total amount in the excavation zone is explained by the beginning of intensive gas release from the exposed surface of the seam $I_{оз}$ a few meters ahead of the executive body of the extraction mechanism [8], a sharp increase in the intensity of gas release in the first minutes of its breaking [6,9,10] and a large residual gas content of coal discharged from the longwall [11].

The processes of gas release from the exposed surface of the seam $I_{оз}$ and chipped coal $I_{оу}$ are practically impossible to experimentally divide into two components. The relationship between them can be estimated based on the equations of external dynamics of gas release and experimental data on the numerical values of the gas-dynamic parameters of the seam and chipped coal [12]. The calculations performed [7] indicate the predominant gas release from the exposed surface of the working face. This ratio is due to the longer period of methane release from the exposed surface compared to gas release from the chipped coal. This is confirmed by the reduction in the intensity of gas emission from the exposed surface within several months after the termination of coal mining. This period of methane release from the surface of the exposed seam practically does not affect the creation of safe conditions in mine workings in terms of the gas factor. But according to the attitude $I_{оз}/A$, the mine in all cases must be attributed to the supercategory. This is explained by the fact that in the absence of coal mining (A=0), insignificant gas evolution occurs for several months $I_{оз}$. In such a situation, the ratio $I_{оз}/A$ tends to infinity, which gives a formal basis [1] to transfer the mine to the category of supercategory.

An explosive atmosphere caused by the joint release of gas from the broken coal and the exposed surface of the working face arises in the mining mechanisms during the period of their direct operation lasting, at most, several tens of minutes. This period is incommensurably small in comparison with the monthly average data, according to which the category of mines is established [1]. This indicates that the average monthly parameters $I_{оу}/A$ and $I_{оз}/A$ accepted for consideration do not reflect the real danger of gas release from the developed formation. The danger of exceeding the

methane concentration standards arises only when the extraction mechanism is operating for several minutes, and its assessment is made according to the average monthly indicators obtained during the past year.

The method for determining the relative gas content according to equation (1) assumes a proportional change in gas release from each source when the load on the working face changes. This assumption was not confirmed by the example of considering the duration of the processes of gas evolution from broken coal and an exposed surface. In addition to the different duration of these processes, they also differ in factors that determine the different mechanism of gas release from the broken coal and the exposed surface of the working face. With some assumptions, we can assume that, other things being equal conditions, and are directly proportional to coal production.

Other sources of gas release ($I_{сп}$,$I_{пп}$,$I_{сп}$,$I_{пп}$,$I_{вп}$,$I_{д}$) do not directly depend on coal mining. The level of gas emission from them, in addition to coal mining, is largely determined by other factors. The tightness of the correlation relationship between gas release from these sources and coal production was established by statistical processing of monthly average experimental data [7]. A distinctive feature of all dependencies is the absence of a direct influence of coal mining on the processes of gas emission from these sources. Depending on the type of violation of the initial natural state of the gas - coal (rock) system, each source has its own distinctive features of the gas release process. Methane release from undermined sources ($I_{сп}$,$I_{пп}$,$I_{вп}$) depends on the degree of development of treatment works both within the excavation area and in the wing of the mine field. In addition to the displacement of the underworked coal-rock massive, the initial state of methane in them affects the gas evolution from each source. In the coal of adjacent seams, gas is mainly in a sorbed state. In the host rocks, gas can be partially contained in a sorbed state, and a significant amount in a free state, filling the pores. Significant gas release from organic coal substances dispersed in the rocks is not excluded [13].

The overworked gas emission sources ($I_{сн}$,$I_{нп}$,) before the treatment are in approximately the same initial natural state as the underworked ones. The difference in the processes of gas evolution

from them is caused by the conditions of violation of the natural state of the gas - coal (rock) system during overworking.

In the overworked and underworked zones, completely different processes of rock displacement occur, due to different phenomena, which predetermines the distinctive features of gas release from these zones.

The influence of coal mining on methane release in degassing systems I_o depends, other things being equal conditions, both on the state of the source being degassed and the method used for capturing gas.

Preliminary theoretical analysis shows that the change in coal production does not proportionally affect the change in gas emission from each possible source. This is due to the distinctive features of the natural equilibrium state of gas in coal and rocks, as well as the conditions for violation of this state.

Experimental research. The work was carried out using the known experimental data obtained in the conditions of the mines "Krasnolimanskaya" [2] and them. A.F. Zasyadko [14], as well as the average monthly performance of longwalls for coal mining and methane release in the conditions of the mines named after. newspaper "Izvestia" PJSC "Donbassantratsit", them. D.F. Melnikov of PJSC Lisichanskugol and the Sukhodolskoye - Vostochnoye mine department of PJSC Krasnodonugol, which were previously used to establish the category of these facilities in terms of methane emission hazard.

The absolute and relative gas content of the extraction area of the 3rd southern face of the seam ℓ_3 of the Krasnolimanskaya mine were determined according to [2] using the number of working days. This approach is inconsistent with the outgassing process that continues in the absence of coal mining.

For this reason, using the data [2], we considered the dependences of the absolute (I) and relative (q) gas abundance using the actual periods of longwall operation (Fig. 1).

Several features of these dependencies have been identified. The increase in coal production (A) led to a nonlinear increase in the absolute gas release (Fig. 1*a*, curves *1*,*2*), and did not change in direct proportion, as indicated by the authors [2].

Sharp changes in coal production (Fig. 1*b*) several times, both upward and downward, did not have a practical effect on the closeness of the relationship between the dependencies *I* and *q* with coal production (Fig. 1*a*).

In all cases, during the period of increasing coal production, there was an increase in the absolute gas release (*I*) and a decrease in the relative *q* methane release. With a decrease in *A*, on the contrary, there was a decrease in the absolute gas release (*I*) and an increase in the relative methane release *q*.

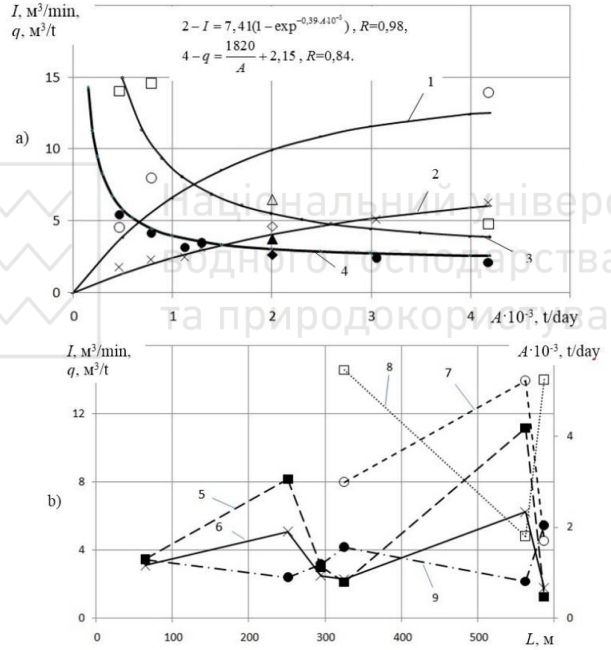

Fig. 1. Dependence of the absolute (*I*) and relative (*q*) gas abundance on the production (*A*) of coal (*a*) and movement (*L*) of the working face (b) during the development of the seam ℓ_3 by the Krasnolimanskaya mine according to [2]:

1 - averaging curve of the absolute total gas release into mine workings and degassing wells; *2* - averaging curve of absolute gas release into mine workings; *3,4* - curves of relative gas release, respectively, total and into mine workings; *5-8*; *9* - change, respectively, of coal production (5), absolute gas release in workings (6) and total (7) in workings and wells, relative total gas release (8) and relative gas release in workings (9); ■ - experimental data of changes in coal production (*A*) as the working face moves (*L*); ○, × - experimental data of absolute gas release,

respectively, total and into mine workings in certain periods of longwall operation; □, ● - experimental data on the relative gas release, respectively, of the total and into mine workings in certain periods of exploitation of the extraction area; Δ, ▲, ◊, ♦ - experimental data on the results of operation of the site for the entire observation period, respectively, the average absolute total gas release, average absolute gas release in mine workings, average relative total gas release and average relative gas release in mine workings

For the first three months, the mining area was operated without degassing any sources of methane release. In the next three months, degassing of undermined adjacent layers ℓ_4,ℓ'_4 and worked-out space by wells was used [2]. Capturing with the help of wells more than half of the amount of gas from its total release did not affect the nature of the change in the dependence of the absolute gas release in workings (2) on coal production (Fig. 1*a*). This fact indicates the absence of aerodynamic connection between the degassed sources and mine workings during the period of the cleaning work.

This situation is explained by the considerable duration of the processes of displacement of underworked rocks and the time lag behind them of gas release into mine workings [15]. Along with this, there are sources of methane release in the mining areas, which are not directly related to the processes of displacement of the undermined rocks. These include chipped coal, the exposed surfaces of the seam being mined, and the enclosing roof and soil rocks immediately adjacent to the seam. Gas release from these sources mainly depends on the intensity of development of the developed formation. In this case, the dependence of gas release in mine workings on coal production is not affected by changes in the degassing conditions by wells of remote, at some distance, adjacent layers. This is confirmed [7] by the operation of excavation areas in the conditions of the mine named after. newspapers "Izvestia" on a layer ℓ_2^a in the undeveloped and overworked zones, 70 m distant by the adjacent layer ℓ_4. The overworking did not affect the decrease in gas emission in the workings of the working areas, which was confirmed by the same dependence of methane release on the load in the overworked and undeveloped zones.

In the conditions of the Krasnolimanskaya mine, the introduction of degassing of undermined sources by wells also did not affect the

change in the dependence of gas release in production (Fig. 1*a*, curve *2*) on the average daily coal production. The above facts indicate that gas release into mine workings from some sources is characterized by a stable dependence on coal mining. This is also confirmed by the fact that the average absolute and relative gas release for the entire observation period, with an average daily coal production of 2010t, coincide with the dependencies (2,4) during the operation of the mining area in certain periods of time (Fig. 1*a*). In this case, the average indicators I and q did not depend on the duration of the considered periods of exploitation of the mining area, but were determined only by the average values of coal production during these periods.

Using similar dependencies typical for some mining-geological and mining-technical conditions, it is possible to reliably predict gas release into mine workings at any load on the working face. The proof of the legitimacy of this approach are the results obtained during the operation of the extraction areas by the Sukhodolskaya-Vostochnaya mine during the development of the seam i_3'. The seam was mined by long pillars along strike at a depth of more than 1000 m. In all areas, contiguous formations were degassed by wells drilled from underground workings. In most cases, in addition to them, wells were drilled from the earth's surface.

The mining-geological and mining-technical conditions for the development of mining areas, from the standpoint of the same dependence of gas release in mine workings on the average daily coal production, despite the differences in the methods and efficiency of degassing the undermined sources, were identical (Fig. 2). This dependence was characterized by a high correlation ratio (R=0.86) for the five mined mining areas. The change in the average daily coal production was in the range of 75-2333 tons. The root-mean-square deviation of gas release in the workings from the averaging curve was 2.2 m^3/min or 16.9%. This makes it possible to classify the considered lavas as analogous lavas according to the criterion of gas release into mine workings. When the average daily coal production reached 1.0-1.3 thousand tons, the average gas emission in the mine workings stabilized at about 18.0 m^3/min. Its actual fluctuations were in the range of 15.7-20.1 m^3/min. This indicates the stabilization of

gas emission in production at a certain level, which does not depend on a further increase in coal production [15].

In contrast to gas release into workings with an average daily coal production of more than 2 thousand tons, the maximum total gas release into workings and degassing systems was not reached (Fig. 2). This follows from a comparison of the experimental data of the maximum gas release (62.4 m^3/min) and the empirical coefficient (90.61) of the exponential equation (Fig. 2). The value of this coefficient of 90.61 indicates the possibility of reaching a maximum total gas release with the average daily coal production significantly exceeding 2.3 thousand tons. According to approximate calculations, the maximum total gas release in mine workings and degassing systems can be achieved with an average daily coal production of about 20 thousand tons. This indicates significant gas resources in the undermined coal strata. Large deviations of the experimental data (σ=4.3 m^3/min) from the averaging curve indicate a significant influence of factors other than coal mining. These include, first of all, the intensity of the processes of displacement of the undermined rocks.

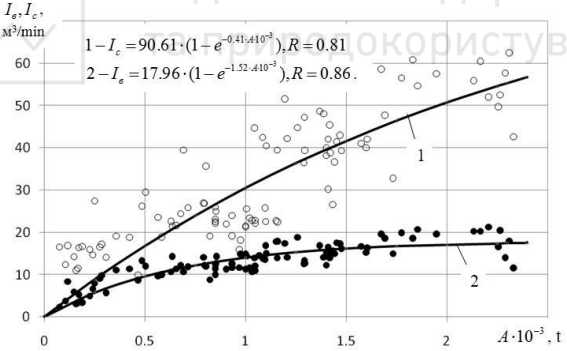

Fig. 2. Dependence of methane release (I) on the average daily coal production (A) during the operation of the excavated sections of the Sukhodolskaya-Vostochnaya mine (12th eastern unloading, 12th bis eastern, 24th eastern, 24th western and 25th I'm western lava): 1,2 - averaging curves, respectively, of the total (I_c) and methane release into mine workings ($I_в$); ●, ○ - experimental data, respectively, of total and methane release into mine workings; R is the correlation ratio

Stabilization of the level of maximum gas release in mine workings and an increase in its total methane release at the achieved loads on the production faces, indicates the capture of a significant

part of methane by degassing systems, which is not released into the mine workings.

Statistical processing of experimental data [14] obtained in the conditions of the mine. A.F. Zasyadko, indicates a significant resource of gas in the undermined coal-bearing strata. During the operation of the 16th eastern lava of the seam m_3, the undermined sources were degassed by wells drilled from underground workings and from the earth's surface. In addition, the gas mixture was removed from the worked-out space. With an average daily coal production of about 3 thousand tons, the maximum absolute gas release reached 108.5 m^3/min. The dependence of the total amount of released gas (I_c) from all sources was directly proportional to the average daily coal production (A), м^3/min

$$I_c = 0.029 \cdot A + 6.6 . \quad (2)$$

The dependence of the relative gas content was described by an isosceles hyperbola with asymptotes A=0 t and = 42.2 , м^3/t

$$q = \frac{9484}{A} + 42.2 . \quad (3)$$

The tightness of the relationship between the total absolute gas release and coal production was characterized by a high correlation coefficient (r=0.84). The relative gas abundance was less dependent on coal production (correlation ratio R=0.39).

To establish a more detailed change in the absolute and relative gas release, we considered the change in three parameters A, I and q with the distance L of the working face from the cut (Fig. 3).

The first maximum of absolute gas release was reached two months after the start of exploitation of the extraction area. When the working face moved away from the split furnace at a distance of about 200 m, the main roof apparently settled.

During this period I of longwall operation, coal production A, absolute I and relative q gas release increased in parallel. An increase in the relative gas content q, along with an increase in A, is explained by the development of the processes of displacement of the undermined coal-rock strata and an increase in absolute gas release from it.

At the next stage of exploitation of the mining area (II), the maximum coal production was reached.

For unknown reasons, during this period, with an increase in coal production from 2514 to 2824 tons/day, the total absolute gas emission decreased from 91.0 to 70.0 m^3/min. As a result, the relative gas emission also decreased from 52.1 to 35.7 m^3/t.

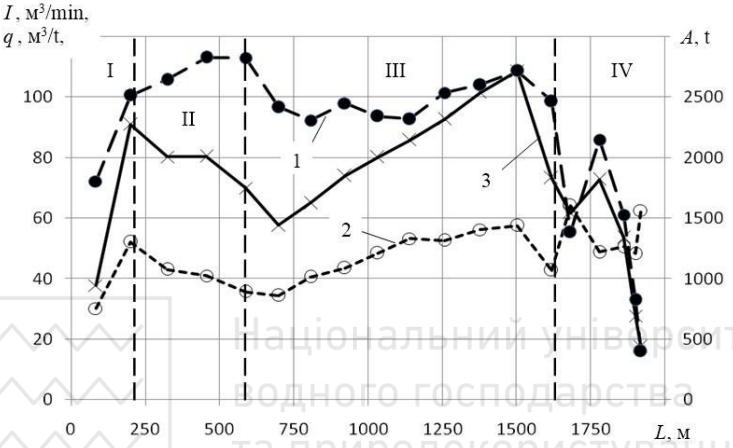

Fig. 3. Change in coal production (*A*), absolute (*I*) and relative (*q*) gas abundance at the distance (*L*) of the working face from the split furnace of the 16th eastern longwall of the seam m_3 of the mine named after I. A.F. Zasyadko according to [14]: *1*,*2*,*3* - curves of change, respectively, of coal production, relative and absolute gas release; ×, ●, ○ - experimental data; I, II, III, IV - typical periods of exploitation of the mining area

The third stage of exploitation of the mining area (Fig. 3) was distinguished by stable coal production (2320-2716 tons/day). Fluctuations in absolute gas emission occurred during this period synchronously with changes in coal production. As a result, the relative gas evolution changed in a similar way.

The fourth stage is associated with a reduction in coal production before stopping the longwall. During this period, for several months, coal production decreased to 402 tons/day. The absolute gas emission decreased to 17.5 m^3/min, and the relative one increased to 62.6 m^3/t.

Based on the results of the analysis of experimental data obtained in the conditions of the mine. A.F. Zasyadko [14], it follows that,

along with coal mining, the absolute and relative gas release is influenced by the development of cleaning operations and the associated processes of displacement of underworked rocks.

The influence of these factors was confirmed by experimental data obtained during the development of the seam ℓ_6 with the 1st northern longwall of the mine named after D.F. Melnikov. Observations were carried out for five years from 2014 to 2018 inclusive. A characteristic feature of the operation of the mining area was, with a relatively low productivity, significant fluctuations in coal production. The maximum coal production in rare cases exceeded 1000 tons/day.

Along with this, there were periods when coal mining was absent for several months. Methane emission sources were not degassed. Absolute (I) and relative (q) gas release into mine workings, depending on coal production (A), were described by nonlinear equations (Fig. 4*a*).

With the growth of coal production, the absolute gas release increased exponentially (curve *1*). On the contrary, the relative gas content decreased according to the hyperbolic dependence (curve *2*).

Significant deviations of the absolute gas release from the averaging curve (1) were observed to the smaller side when the working face moved away from the split furnace at a distance of up to 100 m.

This was caused by the insufficient development of the processes of displacement of the undermined coal-rock strata to the settlement of the main roof and, as a result, not all sources of methane release fell into the zone unloaded from rock pressure.

Deviations of the absolute gas release values from the averaging curve (*1*) towards excess were observed with a sharp decrease in coal production or its absence. This is due to the fact that even in the absence of coal mining, gas is released from some sources for several months (Fig. 4*a*).

Insignificant fluctuations in the relative gas release were observed (curve *5*) during the active cleaning work (Fig. 4*b*).

Its abnormal bursts occurred at the level of coal production, close to zero or its absence.

This nature of the change in the relative gas abundance predetermined its dependence on coal production according to the hyperbolic dependence (curve *2*, Fig. 4*a*).

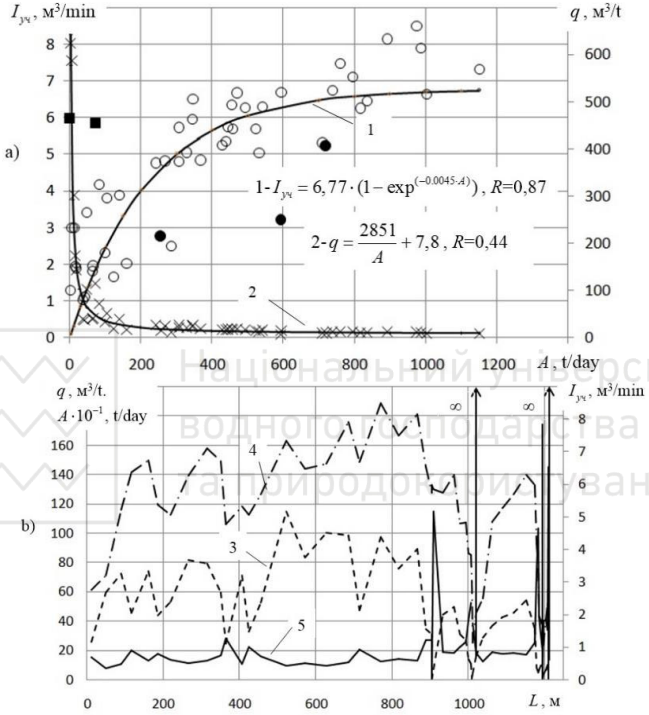

Fig. 4. Dependence of the absolute (*I*) and relative (*q*) gas abundance on the production (*A*) of coal (a) and the movement (*L*) of the working face (*b*) of the 1st northern lava of the seam ℓ_6 of the mine named after D.F. Melnikov: 1, 2 - averaging curves of changes in absolute and relative gas release, respectively; 3, 4, 5 - change, respectively, of coal production (3), absolute (4) and relative (5) gas release; ×, ○ - experimental data; ●, ■ - experimental data, respectively, in the initial period of longwall operation or a sharp decline in coal production; $\infty \nearrow$ - value of q at $A = 0$; R is the correlation ratio

Similar studies of changes in the absolute and relative gas release during the development of the extraction pillar were carried out during the operation of the 9th western face of the seam $\ell_2^в$ by the

mine named after newspaper "Izvestia". Its characteristic features were:

- the lack of cleaning works in the wing of the mine field for two months before the commissioning of the 9th western longwall;
- a smooth increase in coal production both when the stope is removed from the split furnace, and its decrease before the stopping of the longwall;
- significant development of cleaning works in the wing of the mine field. Before the start of anthracite mining in the 9th western longwall, ten longwalls were mined in the wing of the mine field;
- at the site, the undermined sources were degassed by wells. Outside the mining area, there were wells connected to the degassing system after the shutdown of previously worked longwalls.

These features of the operating conditions of the 9th western longwall made it possible to establish the patterns of gas evolution both within the mining area and beyond its boundaries with the activation of the movement of underworked rocks.

The absolute total gas release in the wing of the mine field $I_{кр}$ depended directly on coal production (Fig. 5*а*, line 1). Within the mining area, the absolute gas release $I_{уч}$ changed exponentially (curve *2*). Below this averaging curve, with significant deviations, are the experimental values of the absolute gas release, obtained before the settlement of the main roof. Previously, for the conditions of the mine. According to the Izvestia newspaper, according to the level of gas emission into the wells, it was established [5] that the sediment of the main roof occurs when the working faces are removed from the cut workings at a distance of 80-120 m.

The development of the processes of displacement of the coal-rock strata to the settlement of the main roof caused a more intense absolute gas release in the wing of the mine field compared to an increase in the absolute gas release within the mining area. Such a difference in the intensity of absolute gas release between $I_{кр}$ and $I_{уч}$ is established on the basis of the location of the corresponding averaging (1,2) on the graph (Fig. 5*а*). The relative gas content of the mine field wing from coal production changed according to the hyperbolic relationship (curve *3*). According to a similar relationship,

there was a change in the relative gas content $q_{уч}$ of the excavation area (not shown in the figure), м^3/t

$$q_{уч} = \frac{6304}{A} + 6\,. \qquad (4)$$

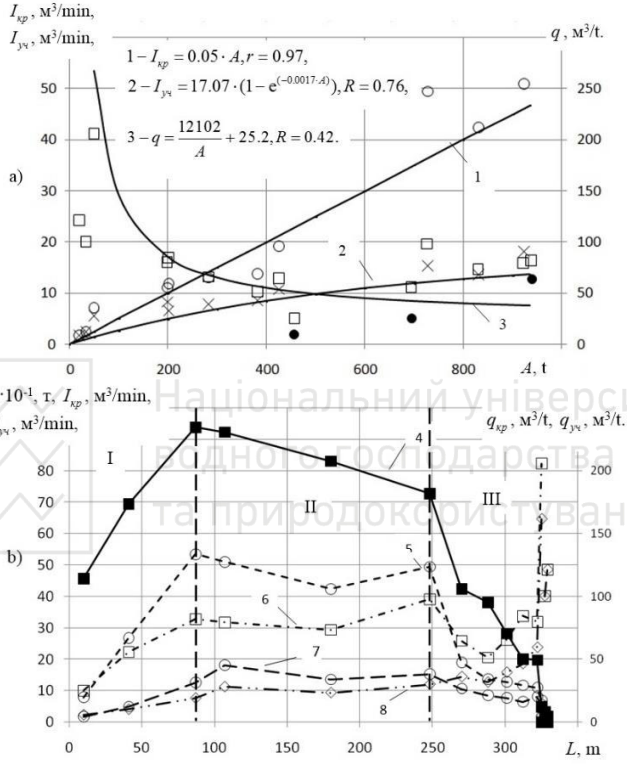

Fig. 5. Dependences of the absolute (*I*) and relative gas abundance (*q*) on the production (*A*) of coal (a) and the distance (*L*) between the stope and the split furnace (b) during the development of the 9th western face of the seam ℓ_2^6 by the mine named after newspaper "Izvestia": *1* - averaging straight line of the absolute gas release in the wing of the mine field ($I_{кр}$); 2 - averaging curve of absolute gas release within the mining area; 3 - averaging curve of the relative gas release in the wing of the mine field; 4, 5, 6, 7, 8 - change, respectively, of coal production (4), absolute (5) and relative (6) gas release in the wing of the mine field and within the excavation area (7, 8) ;, ■ - change in coal production as removal of the stope from the split furnace; ×, ○ experimental data of the absolute total gas release in the wing of the mine field and within the excavation area; □, ◊ - experimental data on the change in the relative gas release, respectively, in the wing of the mine field and

within the excavation area; ● - experimental data of absolute gas release before settlement of the main roof; *r*, *R* - correlation coefficient and correlation ratio, respectively; I, II, III - stages of exploitation of the mining area, respectively, when the planned coal production indicators are achieved, stable operation and a reduction in coal production before stopping the working face

The tightness of the correlation between $q_{уч}$ and A was characterized by a correlation ratio *R* equal to 0.75.

The features of the change in the considered parameters A,$I_{кр}$,$I_{уч}$ and $q_{кр}$ as the distance (L) of the working face from the split furnace is shown in the graph (Fig. 5*b*). According to it, three characteristic stages of exploitation of the mining area can be distinguished, due to the peculiarities of changes in coal production and gas emission. The growth of coal production (A), absolute $I_{кр}$,$I_{уч}$ and relative gas release $q_{кр}$,$q_{уч}$ before the main roof settling occurred synchronously between these parameters (stage I).

The second stage was characterized by relatively stable coal production. The absolute $I_{кр}$,$I_{уч}$ and relative gas evolution $q_{кр}$,$q_{уч}$ were subject to insignificant fluctuations during this period.

The third stage is associated with a steady decline in coal production before stopping the longwall. This led to a decrease in the absolute gas release in the wing of the mine field and within the excavation area to 1.6 m^3/min. With a decrease in coal production, a specific maximum relative methane content of the excavation area and the wing of the mine field was recorded, the value of which was determined by the real figure of 205.7 m^3/t. After stopping the working face and stopping production (A=0), the values $q_{кр}$ and $q_{уч}$ tended to infinity.

Such an increase in the relative gas abundance and a decrease in the absolute gas release leads to contradictions in the definition of the category hazard of coal mines according to [1]. In particular, they consist in reducing the real gas hazard with a decrease in the absolute gas release, and the determination of the categorization by the relative gas abundance with insignificant coal production allegedly indicates an increase in this hazard.

Scientific and practical conclusions. Long-term (from 6 months to 8 years) observations under the conditions of five mines made it possible to analyze and generalize the experimental data of absolute and relative gas release depending on the influencing factors. The

main factor that determines both absolute and relative gas release is coal production and its fluctuations throughout the entire period of operation of the mining area. Formally, in all cases, an increase in coal production led to an increase in trends in absolute (1, 2, 3) and a decrease in relative (4) gas release (Fig. 6*a*).

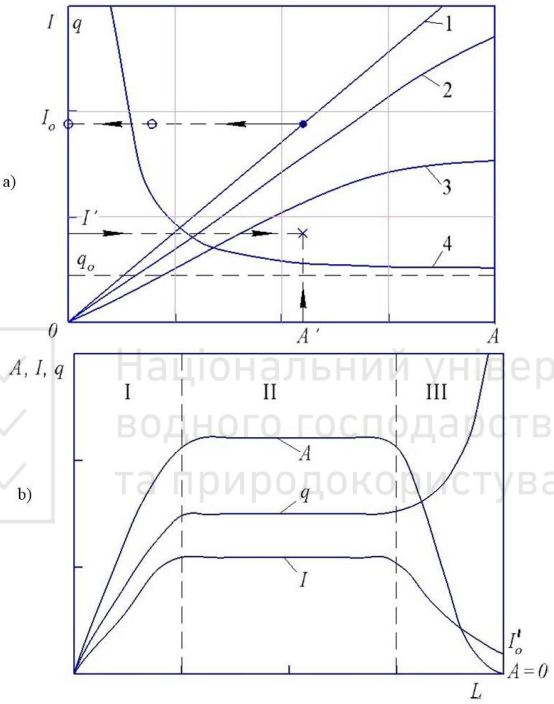

Fig. 6. The results of the analysis of the experimental data of the dependence of the absolute (*I*) and relative gas content (*q*) of mining areas on the production (*A*) of coal (*a*) and the change in these factors with the distance (*L*) of the stope from the split furnace (*b*): *1*,*2*,*3* - possible types of dependence of absolute gas release on coal production; 4 - change in the relative gas emission from coal mining; I, II, III - stages of exploitation of mining areas, respectively, in the initial period before the settlement of the main roof, stable operation and a decrease in coal production before stopping the longwall; × - experimental data (*A*',*I*') observed before settlement of the main roof at the first stage of exploitation of the mining area; ○ - experimental values of absolute gas release (I_o) with a sharp reduction in coal production or its temporary cessation; I'_o - the level of absolute gas release at the moment of stopping the longwall (A=0); q_o - the asymptote of the hyperbole of the dependence of the relative gas release on coal production

The absolute gas evolution varied according to different dependences for each observed object. In some cases, at the achieved level of coal production, it changed according to a direct proportional relationship (straight line 1, Fig. 6*a*). Such a dependence of the total absolute gas release in mine workings and degassing systems was observed in the conditions of the mines named after A.F. Zasyadko and them newspaper "Izvestia" in the development of seams with high natural gas content of coal (up to 35 m^3/t.d.a.m.). The total absolute gas release into mine workings and degassing wells, including those drilled from the surface, during the development of the seam i_3' by the Sukhodolskaya - Vostochnaya mine (curve *2*, Fig. 6*a*) was found close to a direct proportional relationship. The natural gas content of the coal in the developed seam was 33 m^3/t.d.a.m.

At a lower natural gas content (6-8 m^3/t) in the conditions of the mines "Krasnolimanskaya" and them D.F. Melnikov, the absolute gas release at the achieved level of coal production tended to a certain limiting value. In these cases, the change in the absolute gas release occurred according to a clearly pronounced exponential dependence (curve *3*, Fig. 6*a*).

According to a similar relationship, gas was released into the local mine workings of the mines named after. newspaper "Izvestia", them. D.F. Melnikov, Krasnolimanskaya and Sukhodolskaya-Vostochnaya. This confirms the stated assumption about the stabilization of the absolute gas release in the area workings at a certain level, which does not depend on a further increase in coal production.

The analysis made it possible to establish some features of the dependence of the absolute gas release on the level of coal production. In all cases, in the initial period of exploitation of the mining areas before the main roof settling, along with the increase in coal production, the absolute gas emission also increases. But all experimental points during this period are significantly below the averaging lines (Fig. 6*a*). This situation is due to the insufficient development of the processes of displacement of underworked rocks.

With a sharp decrease in coal production or its temporary cessation, the experimental points of absolute gas release are located

significantly above the averaging lines. This indicates the presence of gas emission immediately after stopping the treatment.

In all considered cases, the relative gas release q, depending on the level of coal production, changed according to the hyperbolic dependence (curve *4*, Fig. 6*a*). One asymptote of this hyperbola A=0, and the second is equal to the free term q_o of this equation.

The considered parameters A,I,q and change ambiguously with the distance L of the working face from the split furnace (Fig. 6*b*).

Working out of cut areas with long faces, as a rule, is characterized by three stages. This is due to the technological and organizational features of the treatment. After putting the excavation site into operation, the equipment is tested and the identified deficiencies and malfunctions are eliminated. For this reason, it is practically impossible from the first days of exploitation of the mining area to ensure the planned indicators of coal production. At the stage of increasing coal production (A), there is an increase in both absolute gas release (I) and relative (q) (Fig. 6*b*).

After reaching the planned indicators and the settlement of the main roof, coal production is stabilized (stage II) and its fluctuations are insignificant. As a result of this insignificant irregularities are subject to absolute and relative gas content.

At stage III, before stopping the working face, a decrease in coal production is observed, and, as a consequence, a decrease in absolute gas emission. The rate of decline in coal production outstrips the decline in absolute gas emission. For this reason, taking into account the equality $q=I/A$, there is an increase in the relative gas release, and when the cleaning work is stopped (A=0), the relative gas release tends to infinity (Fig. 6*b*).

At all three stages of the cleaning work, some fluctuations in the parameters A,I,q are possible, and in the direction of their increase or decrease, but they do not change the trend of the averaging curves (Fig. 6*b*).

At all stages of exploitation of mining areas, the averaging absolute gas release corresponds to the direction of change in coal production. The direction of the change in the relative gas release at all three stages of the treatment works occurs in different ways. At the first stage, it increases synchronously with coal production, at the second, it stabilizes at a certain level, at the third, it increases with

the reduction and termination of coal mining (Fig. 6*b*). The ambiguous direction of the change q at the stages of cleaning works predetermines its lower correlation dependence on coal production in comparison with the analogous dependence of the absolute gas release.

The tightness of the relationship between the relative gas release and coal production was characterized by the values of the correlation ratio (R), which are in the range of 0.39-0.84. The dependence of the absolute gas release was characterized by higher correlation indicators (0.81-0.97).

This testifies to the instability of the relative gas release throughout the development of mining areas, as an indicator of the category hazard of mines in terms of the gas factor. Its use does not guarantee an adequate establishment of the mine's categorization, and with it the level of hazard in terms of the gas factor.

The use of relative gas abundance as a criterion for assessing gas hazard leads to contradictions between the requirements of the regulatory document [1] and the results of the experience of mining gas-bearing coal seams.

The maximum danger in terms of the gas factor arises at the second stage of the cleaning work. During this period, stable coal production takes place and the maximums of absolute gas emission are reached. At the same time, the relative gas abundance tends to its minimum value, which supposedly indicates a minimum gas hazard.

At the final stage (III) of the cleanup, there is a decrease in coal production and a stop of the longwall. The absolute gas emission is reduced to a minimum, and consequently the hazard in terms of the gas factor is reduced. The relative gas release increases, and after the termination of cleaning work tends to infinity. This indicates an apparent increase in the gas hazard in accordance with the regulatory document [1].

The above examples indicate that the relative gas release is not a sufficiently informative indicator. According to its level, all mines in Ukraine are divided [1] into four categories ranging from zero to 15 m^3/t and more. Based on the experience of the mines, this indicator varies in a much wider range from zero to infinity, which gives grounds for almost all gas mines to be transferred to the category of supercategory. The categorization of mines in this case is not a reliable criterion for their distribution by gas hazard.

The most acceptable indicator of gas hazard is absolute methane release, since it determines the possibility of hazardous gas mixtures formation and the choice of measures to ensure safe conditions in mine workings.

The direction of the change in the trend of absolute gas release unambiguously repeats the fluctuations in coal production at all stages of exploitation of mining areas. For this reason, close correlations have been established between the parameters A and I. Substantial deviations of the experimental data on absolute gas release from the averaging functions of the dependence $I=f(A)$, other things being equal, are possible only in two cases. In the first, the experimental data were obtained in the initial period of exploitation of the excavation area before the settlement of the main roof. The experimental points of absolute gas release at this stage are located below the averaging curves. In the second, the experimental points of absolute gas release are above these curves, which is caused by a temporary sharp decrease or cessation of coal production. Other anomalous deviations of the absolute gas release from the averaging lines can occur only when the mining-geological and mining-technical conditions change. These include a change in the natural gas content of possible sources, underworking or overworking of the developed layer close to each other, the entry of the production face into the zones of influence of geological disturbances or increased rock pressure, etc. Proposed changes in mining and geological and mining technical conditions are established by the relevant services of coal mining enterprises. Changes in treatment conditions can be taken into account at the stage of preparation of technical documentation. This makes it possible to timely adjust the forecast of absolute gas release.

The tendency to change the coal production and absolute gas release occurs as the distance (L) of the working face from the split furnace to the complete mining of the extraction column.

Coal mining clearly characterizes the absolute gas release only from the chipped coal and the exposed surface of the working face. According to its values, it is not possible to analyze the absolute gas release from other sources when mining technical or mining and geological factors change.

With the prevailing methane release from the undermined coal-rock strata, the absolute gas release, all other things being equal, depends on the intensity of the displacement of the enclosing rocks. The main factor that determines the intensity of rock displacement processes is the rate of movement of the working face $\upsilon_{оч}$. The geometrical dimensions of the worked-out area functionally correspond to the monthly average values $\upsilon_{оч}$, in addition to coal mining. They give more visual information about the undermined area of the coal-rock strata in each specific case.

With all possible options for the combination of mining and geological factors, the rate of movement of the working face (c) determines the level of coal production (A). The presence of such a dependence makes it possible to consider the geometrical dimensions of the mined-out space

$$A = k \cdot \upsilon_{оч} = L_{л} \cdot m \cdot \gamma \cdot \upsilon_{оч}, \qquad (4)$$

where k - the coefficient of proportionality; $L_{л}$ - the length of the lava; m - the recoverable thickness of the developed formation; γ - the specific gravity of coal.

The combination of the parameters $L_{л}$,m,γ make it possible for each object under consideration by means of the coefficient (k) to establish a relationship between $\upsilon_{оч}$ and A. The product $L_{л}$ $\upsilon_{оч}$ characterizes the area (S) of the underworked coal-rock strata for a month. It corresponds to the absolute gas emission that is emitted from the undermined sources. With a constant face length ($L_{л}$), the parameters A,$\upsilon_{оч}$,S are functionally mutually correlated with each other. This gives grounds to use any of them to analyze the change in the absolute gas release from the undermined coal strata.

By removing the stope from the split furnace (L) and the area of the mined-out space of the exploited section and the wing of the mine field, taking into account the stopped longwalls, it is possible to predict the processes of rock displacement, which determine the absolute gas release from the undermined sources.

The performed theoretical studies and analysis of experimental data show that when determining the relative gas content of mine workings for each excavation site operated in specific mining and geological and mining conditions, according to [1], it is necessary to

preliminarily establish the absolute gas emission corresponding to a certain level of coal production.

Taking into account the results of the studies carried out and the complex interdependence of the considered parameters with an ambiguous change in the relative gas release, there is no need for its preliminary determination according to the established values of the absolute gas abundance. This indicates the advisability of developing a fundamentally new method for assessing the hazard of coal mines, based on the direct determination of the absolute gas release from the sources of its entry into mine workings and degassing systems.

References

1. Pravila bezpeki u vugil'nih shahtah (NPAOP 10.01-1.01-10, Kiev, 2010).

2. **I.F. Yarembash, V.I. Beskrovnyj, S.P. Fishchenko, A.E. Bludov**, Ugol' Ukrainy. **1**, 37-39 (1969).

3. Rukovodstvo po proektirovaniyu ventilyacii ugol'nyh shaht / Yanko S.V. i dr. K.: Osnova, 1994. 311p.

4. **M.V. Filatiev, N.I. Antoshchenko, A.I. Dubovik**, Geomekhanicheskie processy sdvizheniya podrabotannyh porod i obosnovanie metodiki prognoza gazovydeleniya v ugol'nyh shahtah (Lisichansk, DonSTU, 2017).

5. **N.I. Antoshchenko** et al., Bezopasnaya otrabotka gazonosnyh ugol'nyh plastov s uchetom geomekhanicheskih processov sdvizheniya podrabotannyh porod (Alchevsk, DonSTU, 2014).

6. **Zhupahina, E., & Ustinov, N.** (Trans.). (1967). Gazovydelenie iz otbitogo uglya. Rudnichnaya Aerologiya I Bezopasnost' Truda v Shahtah. Nauchnye Soobshcheniya. IGD Im. A.A. Skochinskogo, 26-36.

7. **Antoshchenko N.I**. et al., Geomekhanicheskie processy i prognoz dinamiki gazovydeleniya pri vedenii ochistnyh rabot v ugol'nyh shahtah (Alchevsk, DonSTU, 2010)

8. **A.S. Cyrul'nikov, I.Y. Eryomin, V.F. Mikitchenko, V.P. Ponomaryov**, Ugol' Ukrainy. **11**, 46-48 (1969)

9. **Kuz'min D.V., Mibchuani A.G., Nedviga S.N.** (1968) Prognozirovanie metanovydeleniya iz razrabatyvaemogo plasta pri vysokoj proizvoditel'nosti zaboev. Sovershenstvovanie ventilyacii i sposobov bor'by s pyl'yu i gazom v ugol'nyh shahtah. IGD im. A.A. Skochinskogo. **171**.14-18.

10. **Petrosyan A.E., Sergeev I.V., Ustinov N.I.** (1968) Gazovydelenie pri rabote uzkozahvatnyh kombajnov. Rudnichnaya aerologiya i bezopasnost' truda v shahtah. IGD im. A.A. Skochinskogo.M.: Nedra. 15-23.

11. **Fertel'mejster, Y. N**. (Trans.). (1962). Issledovanie gazoyomkosti uglej i gazonosnosti plastov. Metody Opredeleniya Gazonosnosti Plastov I Prognoz Gazoobil'nosti Shaht: Trudy Vsesoyuznogo Nauchno-tekhnicheskogo Soveshchaniya, 25-35.

12. **Klebanov, F., & Firchanek, B.** (1981). Prirodnye opasnosti v shahtah, sposoby ih kontrolya i predotvrashcheniya (E. Karpov, Trans.). M: Nedra.

13. **V.V. Lukinov, A.P. Klec, B.V. Bokij, I.A. Efremov**, Ugol' Ukrainy. **1**, 50-53 (2011)

14. **V.V. Bokij, O.I. Kasimov,** Ugol' Ukrainy. **5**, 17-21 (2005).

15. **Kryzhanovskij, Y., & Antoshchenko, N.** (2014). O maksimal'nom gazovydelenii v gornye vyrabotki pri otrabotke ugol'nyh plastov (R. Gasyuk, Ed.). Sb. Nauchnyh Trudov MakNII, 2(32), 69-76.

https://doi.org/10.31713/m1016

MODELING OF PHOSPHORUS PRODUCTION PROCESSES AND DEVELOPING A MANAGEMENT STRUCTURE BASED ON GREY SYSTEMS

Toktasynova Nigina
Satbayev University, Master of Engineering and Technology, Junior Researcher of Department “Automation and Control”, Kazakhstan

Suleimenov B. A.
Satbayev University, Doctor of Engineering Sciences, Professor of Department “Automation and Control”, Kazakhstan.
Hassen Fourati, PhD, Associate Professor of Gipsa Lab, Grenoble, France

Kulakova Ye.A.
Satbayev University, Master of Engineering and Technology, Lecturer of Department “Automation and Control”, Kazakhstan

Abstract

The agglomeration process is one of the complex, multidimensional technological processes; it takes place under conditions of a large number of disturbing influences. As a result, the amount of return during sintering reaches 40-50%.

The work is devoted to the development of a mathematical model capable of predicting and controlling the sintering point based on real-time data. As the main parameters for the construction of predictive models, data measured in real time were used – the temperature in the vacuum chambers and the gas velocity determined through the measured pressure (rarefaction) in the vacuum chambers.

This paper describes the methodology and basic algorithms for modeling agglomeration processes, starting from the ingress of the charge into the sinter machine and ending with the production of a suitable agglomerate. The obtained curves of the developed mathematical model of temperature in vacuum chambers served as the basis for testing the forecast model based on the use of the theory of gray systems and the optimization algorithm of the "swarm of particles". Based on the developed mathematical model, a system for predicting the sintering point is constructed, which is the basis for determining the quality of the agglomerate, which

will reduce the return volume during sintering. The general structure of the sinter control system based on a dynamic predictive model is also proposed.

The practical significance of the developed predictive model based on the theory of gray systems is as follows:

- forecast of the sintering point value of the agglomerate and synthesis of the control action based on the forecast;
- the algorithm for constructing a mathematical model of the forecast can be used for any process that has the character of a "gray exponential law".

Introduction

Agglomeration in metallurgy is a thermal process of sintering of a metallurgical charge consisting of granules of various metals and fuel. In terms of natural resources, agglomeration is a key technology for recycling products or dust from metallurgy. The raw materials used can vary widely from ore to recycled dust and fluxes.

The agglomeration process is a complex, multidimensional technological process; proceeds under conditions of a large number of disturbing influences: changes in the chemical-mineralogical, granulometric composition of the charge components; conditions of moistening, dosing, mixing and placing the charge on the surface of the sinter machine. The process is automated, but the control systems for the sintering process in modern production facilities do not allow ensuring the maximum productivity of sinter machines and the constancy of high quality of the output product.

Agglomeration is a nonlinear process, which makes real-time quality management of the final product challenging. In practice, the process is controlled with a delay: the operator changes the process parameters after receiving the final product, which leads to the appearance of a return, i.e. sinter, which must be returned to the initial stage for re-processing. The return can be up to 40-50% of the final sinter, which significantly increases the cost of the process, and also introduces uncertainty into the composition of the initial charge.

Improving the quality of the sinter can be achieved both by process change - optimizing the composition of the charge, the size of the granules, changing the amount of fuel, water, etc., and by process control - controlling the speed of pallet movement, discharge in vacuum chambers, and by the height of the charge.

The solution of the task of process change leads to the need to use an analytical modeling method that uses the

physicochemical 3 processes that occur during agglomeration. The advantage of the analytical method lies in the completeness of constructing a model that takes into account all the processes of agglomeration and allows research and experiments on the basis of the model. Moreover, this method is universal for modeling similar processes. The problem of using and adapting existing models for the process of agglomeration of phosphorite ores is that this process is not widespread, and the use of ready-made models for the agglomeration of iron ores is impossible due to the differences in the chemical reactions. This circumstance leads to the need to create an original model of sinter roasting of phosphorus-containing materials.

Modern methods for solving the task of process control are based on an empirical research method, which consists in collecting a large amount of data and in creation of a model based on training algorithms. This method involves performing experiments on an object to obtain a representative data sample. At the moment, models created on the basis of neural networks are increasingly used for technological processes. The disadvantage of this method is the need for a large amount of data and retraining the model when the process conditions change. This fact is critical for the agglomeration process, due to the change in the composition of the charge, which depends on both the mineralogical properties of the ore and the amount of return. In connection with the above mentioned, it becomes necessary to create a model using a small amount of information and allowing retraining the model in real time.

1 THE CURRENT STATE OF MATHEMATICAL MODELING OF THE AGLOMERATION PROCESS

1.1 Description of the agglomeration process

Agglomeration in metallurgy is a thermal process of sintering of fine materials that are constituent parts of a metallurgical charge. The agglomeration process is a complex nonlinear system with a large delay, in which many process parameters are interrelated, and the sintering process takes place with different chemical transformations

at each stage of the sinter machine operation and on different layers of the sinter.

The process of agglomeration of phosphorite ores is carried out at the Novodzhambul Phosphoric Plant (NDPP) [1], located in the south of Kazakhstan, near the Karatau deposit. Agglomeration method consists in sintering phosphorite fines on an AKM-7-312 sinter machine at temperatures up to 1623 K using crushed coke as a solid fuel. Agglomeration is the second most important process on the plant, after the production of yellow phosphorus, for which the sinter is the raw material. The technological process (Figure 1.1) begins with the initial mixing of the charge with cold and tertiary return, which is fed without dosing, which leads to significant changes in the fuel in the charge. Then the charge is sent to the moving belt, where it is ignited with natural gas or CO2, passing through the hearth. Sinter gases are sucked off through 26 vacuum chambers located under the sinter machine. Due to the vacuum created in the vacuum chambers, the heat from the combustion of the fuel gradually moves to the underlying layers, uniformly sintering a layer of 260 mm and goes to the end of the 78 m long belt. Temperature and vacuum control is provided in all vacuum chambers. The regulation of the vacuum in the vacuum chambers is carried out using dampers, which are remotely controlled from the control panel of the sinter machine. Then the sinter is cooled, crushed to the required size and, after sorting, is sent to the batching department of the furnace room No. 05, and the poor quality sinter is sent to the beginning of the process.

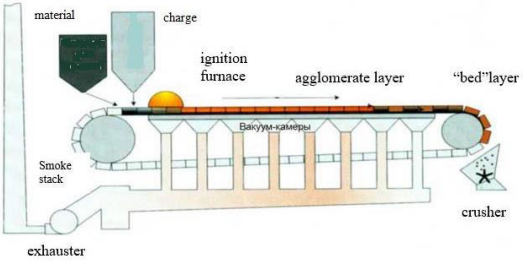

Fig. 1.1. Schematic representation of the sinter machine

1.2 Characteristic features of mathematical models of the agglomeration process

Let's highlight the main characteristic features of mathematical models of the agglomeration process:

1. Like any mathematical model, they are subdivided into one-dimensional, two-dimensional and three-dimensional in relation to the dimension of space (table 1.1).

2. During the sintering process, the charge undergoes three phase states: solid, gaseous and liquid.

3. The main mechanism of heat transfer considered during the sintering process is convection, which forms the basis of heat transfer during sintering.

4. The main equation of motion of the gas phase or the equation of moment is the Ergun equation for porous medium

$$\frac{\Delta p}{L} = \frac{150\mu u(1-\varepsilon)^2}{d^2\varepsilon^3} + \frac{1{,}75\rho u^2(1-\varepsilon)}{d\varepsilon^3},$$

where Δp - pressure drop, L - height charge, μ - viscosity, ε - porosity, ρ - density, d - granule diameter, u - air flow rate.

Table 1.1

Comparative analysis of various agglomeration models

Ref.	Objective	Type	Phase	Types of heat transfer	Combustion of coke	Chemical reactions	Gas flow equation	Condensation and Evaporation	Porosity	Result
[6]	Modeling structural changes in the sinter	1-D	Solid, gaseous	Convection	$C+O_2 \rightarrow CO_2$	Decomposition of $CaCO_3$	Unknown	Evaporation rate as a dependence from particle diameter	Changing the radius of particles due to combustion	Study of the effect of coke content and melting temperature on the sinter structure
[7]	Modeling the agglomeration process with a focus on the speed of the heat front through the layer	1-D	Solid, gaseous	Convection, Thermal conductivity	$(1+\varphi)C + \left(1+\frac{\varphi}{2}\right)O_2 \rightarrow \varphi CO + CO_2$, $CO + 1/2O_2 \rightarrow CO_2$	Decomposition of $CaCO_3$, $FeCO_3$, $MgCO_3$, $MnCO_3$. Arrhenius equation. Nonlinear regression equation for CaO and $Ca(OH)_2$	Modified Ergun Equation	Evaporation temperature equation depending on pressure	Through particle shrinkage model	The most sensitive process parameters are determined
[8]	Modeling of the process in a multilayer solid phase, taking into account porosity and shrinkage with geometric changes	1-D	Several solid, gaseous	Convection, thermal conductivity, radiation	$CO + 1/2O_2 \rightarrow CO_2$, $C + 1/2O_2 \rightarrow CO$	Decomposition of $CaCO_3$	Input air rate - function of time - 2nd order polynomial. Pressure drop not taken into account	Through reactions solid-gaseous phases	Geometric changes in the sinter associated with reactions between solid and gas	Analysis of the influence of 3 different coke contents on sinter temperature and gas composition
[14]	Model of changes in the structure of the sinter: pore ratio, mineralogical composition, quality of the sinter	3-D	Solid, gaseous, liquid	Convection, Thermal conductivity Rans-Marshall equation for heat transfer between 2 phases and Cooney-Smith equation - for thermal conductivity	$C+O_2 \rightarrow CO_2$	Decomposition of $CaCO_3$ $MgCO_3$, Fe_2CO_3	Ergun Equation	$H_2O(l) \Rightarrow H_2O(g)$	The change in porosity is represented by pseudo particles, which disappear after the equations of porosity, combustion and decarbonization	Consideration of changes in sinter quality and throughput by installing a gas flow tray
[9]	Determination of the optimal structure of the 2-level process – the hydrocarbon content at each level and determination of the layer thickness	2-D	Solid, gaseous,	Convection according to the Kuni-Suzuki equation	$C+O_2 \rightarrow CO_2$, $2C + O_2 \rightarrow 2CO$, $C+CO_2 \rightarrow 2CO$	Decomposition $CaCO_3$, Fe_2O_3	Ergun's equation	$H_2O(l) \Rightarrow H_2O(g)$, $H_2+1/2O_2 \Rightarrow H_2O$	Not considered	Obtaining a high-quality agglomerate with a min. return rate due to the genetic optimization method with a min. amount of hydrocarbon
[15]	Development of a wet iron ore agglomeration simulator	2-D	Solid, gaseous,	Unknown	$C+O_2 \rightarrow CO_2$	Decomposition $CaCO_3$	Ergun's equation	Unknown	Not considered	A model for analyzing, optimizing, and

										controlling the process. The model predicts the temperature of the agglomerate and gas, the sintering point.
[10]	3D model for modeling processes in the agglomerate	3-D	Solid, gaseous,	Convection, Thermal conductivity, radiation	$C+O_2 \rightarrow CO_2$ $C + 1/2O_2 \rightarrow CO$ $C+CO_2 \rightarrow 2CO$ $C+H_2O \rightarrow CO+H_2$	Decomposition $CaCO_3$ Fe_2O_3	Modified Ergun equation	CO_2 (g)+ H_2 (g)$\rightarrow CO$(g)+ H_2O(g) H_2O(l) $\leftrightarrow$ H_2O(g)	Consideration of volume fraction, particle diameter and size factor	Demonstration of the 3D behavior of the agglomeration front and the internal temperature distribution
[1]	Development of a model of the agglomeration process using the effects of humidity, condensation and evaporation	1-D	Solid, gaseous,	Convection	Burning of hydrocarbon	Not considered	Unknown	Balance equations for changes in moisture, evaporation, and condensation	Constant	The model predicts the temperature values in the agglomerate
[11]	Predicting agglomerate quality, inchding chemical characteristics and physical strength, performance, and fuel consumption	1-D	Solid, gaseous,	Convection	$(1+\varphi)C + \left(1+\frac{\varphi}{2}\right)O_2 \rightarrow \varphi CO + CO_2$	Decomposition $CaCO_3$ $MgCO_3$	Ergun's equation	Evaporation and condensation	Not considered	Model parameter identification by optimization using temperature measurements and a self-organizing Kohonen map
[17]	Improving the efficiency of the agglomeration process by optimizing the permeability configuration	2-D	Solid, gaseous,	Convection	$C+O_2 \rightarrow CO_2$	Decomposition $CaCO_3$, the sulfation equation	Brinkman equation, where the permeability and Forsheimer coefficients are expressed through the Ergun equation	H_2O(l) $\leftrightarrow$ H_2O(g)	Developed on the basis of measured values of air velocity in the charge and depends on the vertical and horizontal permeability bars	1 and 2-layer horizontal and vertical slats and their influence on the temperature in the agglomerate, the coke residue and the moisture content are considered
[12]	Determining the effect of the growth of granules on the duration of agglomeration and the yield of finished products	2-D	Solid, gaseous,	Convection, Thermal conductivity, radiation	$(1+\varphi)C + \left(1+\frac{\varphi}{2}\right)O_2 \rightarrow \varphi CO + CO_2$ $CO+1/2O_2 \rightarrow CO_2$	Decomposition $CaCO_3$ Fe_2O_3 oxidation Fe_3O_4	The Navier – Stokes equation, where the pressure drop is described by Darcy's law and obeys the Ergun equation in a porous medium	Patinson's model for predicting evaporation CO_2 (g)+ H_2 (g)$\rightarrow CO$(g)+ H_2O(g)	Empirical Castro Equation	Increased sinter yield and reduced thickness of the molten zone by increasing the size of iron ore, which shortens sintering time and increases productivity

Based on the analysis of modern studies of the agglomeration process (Table 1.1), the following conclusions can be drawn:

- most of the reviewed works are devoted to the agglomeration of iron ores, as the most common process, and therefore there is a gap in the study of phosphorite ores. The difference between the sintering process of iron and phosphorite ores lies in the chemical transformations that take place on the sinter machine, as well as operational variables - sintering time, temperature and discharge in vacuum chambers, cake permeability and many other parameters

- the research results are verified with laboratory experiments obtained in the "test pot", the material in which goes through the same stages as the material on the sintering belt. Therefore, the results do not take into account the influence of natural external factors encountered directly in the real process, which makes the results obtained with a laboratory setup ideal. This leads to the need for additional verification of the obtained mathematical models at the plant;

- most of the models do not take into account the effect of porosity change during sintering, which is an important characteristic of the process that affects the rate of gas movement in the charge;

- chemical reactions occurring during the process have a major effect on the temperature of the charge.

Therefore, in order to create an adequate model, it is necessary to carry out a complete analysis of the charge: the melting and solidification temperature, the properties of the components, such as density, heat capacity, viscosity, and others, to create a mathematical model for changing the sinter porosity and to verify data on real objects.

Works on the classical modeling of an object are devoted to the use of equations of temperature change in the solid, gaseous phases and to the heat transfer between them. In this case, the initial charge is a porous material, which implies the possibility of using a heat transfer model in a porous medium. This will allow taking into account both the heat change in solid and gaseous medium, and the changing model of the material porosity.

2 SYNTHESIS OF THE MATHEMATICAL MODEL OF THE AGLOMERATION PROCESS OF PHOSPHORITE ORE

2.1 Object of modeling

The object of modeling is a pallet on which the initial material - charge is supplied. A step signal (step time = 2 min) is used to simulate the gas supply to the pallet under the hearth (average time of the pallet under the hearth). These assumptions are taken on the basis of [2] depending on the speed of the sintering belt. Sinter machine length is 78 m, average speed 3.6 m/min, charge layer height 260 mm.

As can be seen from the literature review, for the agglomeration process modeling, namely, temperature changes during sintering, there are used the physical sintering laws of heat transfer between solid and gaseous medium. It is known that the charge as a result of the sinter roasting process turns into an sinter, which is a lumped material and, in fact, is a porous material.

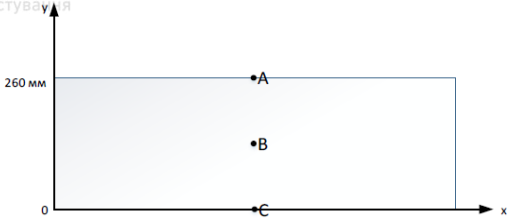

Fig. 2.1. Object of modeling

A porous material is a solid body containing free space in its volume in the form of cavities, channels or pores. The pore sizes, as a rule, are much smaller than the geometric dimensions of the solid body itself.

The initial charge can also be considered as a porous material, since the granules of the charge have a size $(3\text{-}10)\cdot10^{-3}$ m, and the distance between the granules is $(0\text{-}3)\cdot10^{-3}$ m. Therefore, to simulate the temperature change in vacuum chambers in the process of agglomeration, in this work, there is considered a model of heat transfer in a porous material, at which the temperatures of gas and solid material are considered the same. This will reduce the dimension

of the final mathematical model, and speed up the process of modeling and calculation. To determine the correctness of the created model, there will also be created a classical model of heat transfer between the solid and gaseous phases of the sintering process. The simulation results will be presented at points A, B and C (Figure 2.1).

2.2 Schematic representation of the model

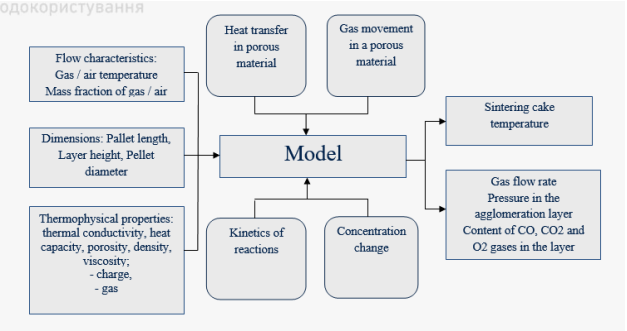

Fig. 2.1. Schematic representation of the model

2.3 Calculation of the temperature change during sintering

Heat transfer in porous material

Heat transfer through a porous medium is usually considered as combined heat fluxes [3], such as heat conduction along its solid matrix, heat radiation through internal pores, and thermal convection or thermal conduction through gases filling the pores. Regarding the last one, there is an inevitable choice between convective and conductive heat flow in pores filled with gas, convective heat transfer is suppressed in pores less than about 10 mm in size. Porous materials have applications across a wide range of engineering and scientific disciplines. The porous material is essentially a two-phase structure - a solid phase and a gaseous (liquid) phase [4]. The initial phosphorite charge, as well as the final sinter, is a porous material in which the solid and gaseous phases are considered. In this case, the temperatures of the solid and gaseous phases in the porous material are equal to $T_s = T_f = T$ and are determined by the following formula

$$\theta\rho_s c_{\rho.s} + (1-\theta)\rho Cp\frac{\partial T}{\partial t} \rho C_s u\nabla T + \nabla(-(\theta k_s + (1-\theta)k\nabla T) = Q, \quad (2.1)$$

where $k[W/(\text{m}\cdot k)]$ - thermal conductivity (gas),

ρ[кг/м^3] – density (gas),

C_p[Дж/(кг·K)] - heat capacity at constant pressure (gas),

γ - specific heat ratio (gas),

θ=(1- porosity) - volume fraction (solid),

$k_s[W/(\text{m}\cdot K)]$ - thermal conductivity (porous matrix),

ρ_s[кг/м^3] - density (porous matrix),

C_{ps} [Дж/(кг·К)] – specific heat (porous matrix) (formula 2.16),

$Q[W/m^3]$ - heat source from chemical reactions (formula 2.13) and heat source supplied from outside,

u - gas velocity in a porous medium (formula 2.7).

Calculation of heat transfer between solid and gaseous media

Heat transfer is the process of transferring heat from one point to another due to a difference in temperature. Heat transfer combines 3 main processes - thermal conductivity (conduction), convection and radiation.

When considering the process of heat transfer occurring during sintering of a charge, there is often considered a model in which two media are considered: solid (charge) and gaseous (agglomerated gases) and heat transfer between them [5].

The solid phase temperature is determined by the following formula

$$\rho_g C_{pg} \frac{\partial T_g}{\partial t} + \rho_g C_{pg} u \nabla T_g - \nabla k_g \nabla T_g = Q + Q_{sg}, \qquad (2.2)$$

where index g indicates the properties of the gaseous phase, Q_{sg} - heat transfer between solid and gaseous phases (formula 2.5). The boundary conditions of all walls correspond to the temperature T_g.

The temperature of the solid component is calculated by the formula

$$\rho_g C_{pg} \frac{\partial T_s}{\partial t} + \rho_s C_{ps} u \nabla T_s - \nabla k_s \nabla T_s = Q + Q_{sg} \qquad (2.3)$$

where index s indicates the properties of the solid phase, Qgs - heat transfer between gaseous and solid phases.

In this case, the temperature in the vacuum chamber is the temperature of the exhaust gases.

Heat transfer between phases according to [21] is calculated by the formula

$$Q_{g \to s} = (T_g - T_s) \frac{\alpha \cdot 6(1-\varepsilon)}{d}$$
$$\alpha = \frac{kg}{d}\left(2 + 0.6\sqrt{\mathrm{Re}}\sqrt[3]{\mathrm{Pr}}\right) \qquad (2.4)$$

where ε - material porosity,

Re - Reynolds number,

Pr - Prandtl number.

Due to the fact that the fraction of the solid phase is not equal to the gaseous one, we introduce this relation into formula (2.4)

$$Q_{gs} = \frac{Q_{g\to s}}{\theta};\;\; Q_{sg} = \frac{Q_{g\to s}}{1-u}. \qquad (2.5)$$

The Prandtl number is determined by the formula [22]

$$Pr = \frac{MC_p}{k}$$

where M - dynamic viscosity of the gaseous phase.

2.4 Determination of the gas movement velocity in a porous medium

Modeling the movement of a gas flow for the sintering process of phosphorite ores has the greatest influence on the speed, temperature of the sintering process and its quality.

One of the new directions for describing the movement of a gas flow during agglomeration is the use of the Ergun equation as part of other equations. The Brinkman equation appeared as a combination of Darcy's law and the Navier-Stokes equation, and describes the slow

flow movement in a porous medium and fast flow in channels. Flow in a saturated porous medium can be modeled using Darcy's law or Darcy-Brinkman model depending on the specific pore size. They allow to find the same variables as the Navier-Stokes equations, but they include terms that take into account the porosity of the medium through which the fluid flows [6]. Then the equations of movement in a porous material can be determined by the Brinkman equation

$$c\frac{\partial u}{\partial t} = \nabla\left[-pI + \text{м}\frac{1}{\in_p}(\nabla u + (\nabla u)^T\right] - \left(\text{м}\,k^{-1} + \text{в}_f|u| + \frac{c\nabla u}{\in_p^2}\right)u \quad (2.6)$$

where k[м^2] - permeability (porous matrix), T[C] - charge temperature (formula 2.1), then, taking into account the Ergun equation, layer porosity, surface roughness and, possibly, the presence of walls [7]

$$k = \left[\frac{150 mu(1-e)^2}{d^2 e^3}\right]^{-1} \cdot \frac{1}{f_p f_{pbase}}, \quad (2.7)$$

$$b_f = \frac{1{,}75 cu^2(1-e)}{de^3} \cdot \frac{1}{f_p f_{pbase}}, \quad (2.8)$$

where f_p - porosity change factor during sintering shrinkage, f_{pbase} - the global calibration constant in the Ergun equation = 3.5.

2.5 Determination of heat resulting from combustion of coke

The agglomeration process is accompanied by the release of heat due to the combustion of coke. In this case, during the combustion of coke, only part of the coke is oxidized to carbon dioxide, the other part is oxidized to carbon monoxide. The high temperature in the layer leads to the fact that most of the monoxide is oxidized to carbon dioxide [8]. When burning coke, the following chemical reactions are usually considered

$$\begin{aligned} &C + O_2 = CO_2, \\ &C + 0{,}5\,O_2 = CO, \\ &0{,}5\,C + 0{,}5\,CO_2 = CO, \\ &C + H_2O = CO + H_2. \end{aligned} \quad (2.9)$$

The kinetics of reactions according to [44] depends on the concentration of carbon monoxide, oxygen and water in gas.

$$R_j = k^f \prod c_i^j, \quad (2.10)$$

where k^f - reaction rate constant determined by the Arrhenius equation

$$k^f = A^f \exp\left(\frac{-E^f}{R_g T}\right), \quad (2.11)$$

where A^f - frequency coefficient, $E^f[j/mol]$ - activation energy, R_g - universal gas constant. The coefficients are determined according to [7].

Then the heat released by the reaction is determined by the formula

$$Q_j = -R_j H_j, \quad (2.12)$$

where H_j - enthalpy.

2.6 Change in concentration due to combustion reaction

The change in gas concentration in equation (2.12, 2.13) is determined

$$c_i = \frac{\rho\omega_i}{M_i}, \tag{2.13}$$

where ω_i - mass fraction of gas i

$$\varepsilon\rho\frac{\partial\omega_i}{\partial t} + \nabla j_i + \rho(u\cdot\nabla)\omega_i = R_i, \tag{2.14}$$

where j_i - variable containing the diffusion model of the process, R_i - reaction rate (formula 2.13).

2.7 Determination of thermo physical properties of the charge

The thermo physical properties (TPP) of ore materials require numerous experiments, since the samples differ in the multicomponent mineral and chemical composition and, at the same time, individual components undergo chemical changes at elevated temperatures. The composition of the initial charge includes carbonate phosphorites (P_2O_5 content = 18-25%) and coke. Data on heat capacity, thermal conductivity, density can be determined from various reference books [9-12]. Then the thermophysical properties of the charge (thermal conductivity k_s, heat capacity $c_{p.s}$, density ρ_s) can be determined as follows [13]

$$k_s = \sum\omega_{s.i}k_{s.i};\quad c_{\rho.s} = \sum\omega_{s.i}c_{\rho.s.i};\quad \rho_s = \sum\omega_{s.i}\rho_{s.i}, \tag{2.15}$$

where $\omega_{s.i}$ - mass fraction of charge component

The thermal conductivity of individual components in the structure of phosphorites was obtained from experimental data for a wide range of mineralogical composition of phosphorites by the method of nonlinear least squares.

2.8 Agglomeration process modeling

The possibility of using the physical law of heat transfer of a porous material for the agglomeration process is tested through standard models of heat transfer in the gaseous and solid phases, presented in many works on the study of the agglomeration process.

First of all, the form of the temperature curves at the points of the charge A, B and C (Figure 2.1) and the velocity of the gaseous phase inside the sinter is determined. Since the main parameter characterizing sintering is temperature, it is necessary to calculate the temperature for models of heat transfer between solid and gaseous media, and heat transfer in porous material at points A, B and C (Figure 2.3 - Figure 2.5). The gas velocity inside the agglomeration cake at point B is shown on Figure 2.6.

Since the temperature during the agglomeration process moves from top to bottom due to the vacuum chambers located under the sintering belt, the main parameter responsible for layer sintering is the temperature in the vacuum chamber (point C). Therefore, it is advisable to calculate the root-mean-square error between 2 models at point C

$$RMCE = \sqrt{\frac{\sum_{t=0}^{n}\left(T_g^t - T^t\right)^2}{n}} = 3{,}85C$$

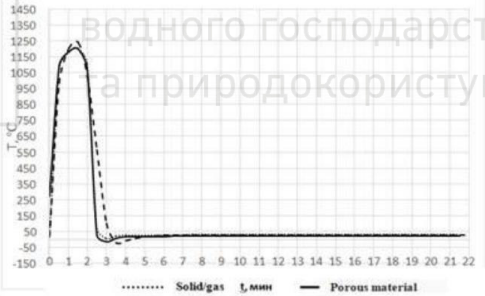

Fig. 2.3. Temperature at point A

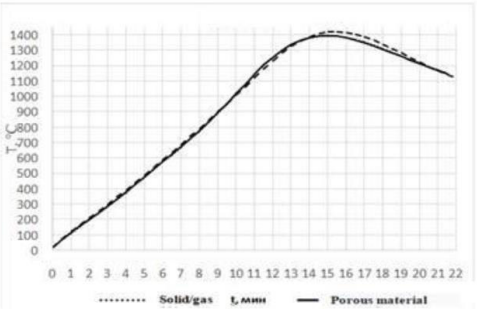

Fig. 2.4. Temperature at point B

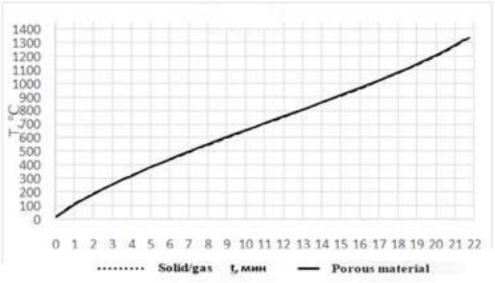

Fig. 2.5. Temperature at point C

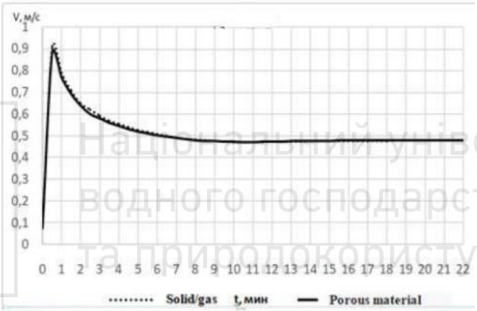

Fig. 2.6. Velocity of the gas phase at point B

As can be seen from the graphs (Fig. 2.3-Fig. 2.6), the use of the physical laws of heat transfer in a porous material for agglomeration process modeling practically does not differ from heat transfer modeling between solid and gaseous media. The root-mean-square error at a temperature of 1350 °C is less than 4 ℃ with the same initial parameters of the charge. Also, the use of a heat transfer model in porous materials makes it possible to reduce the dimension of the system of partial differential equations, which leads to a lighter model and to a reduction in modeling resources, both for setting up the model, connections with other physical processes, and resources for computing (solving) the model.

3 THE CURRENT STATE OF SYNTHESIS METHODS OF CONTROL SYSTEMS OF THE SINTERING POINT DURING SINTER ROASTING

3.1 Predictive models of the sintering point of the charge

One of the key indicators of the sintering quality is the sintering point, which indicates the end of the agglomeration process, and is the point with the highest temperature. Often the sintering point is determined by the operator and based on this prediction, the need to change the output process variables is determined. With the rapid development of prediction methods, there have appeared a huge number of systems that allow prediction the sintering point based on historical data and data from the current process, as a result of which the productivity of the process increases and the quality of the finished product improves.

The problem of predicting and controlling the sintering point has been studied in many works using various algorithms, such as neural networks, genetic algorithms and fuzzy control. Due to the development and widespread use of neural networks, a large number of works, related to prediction, use this method in various areas of research. In the problem of controlling the sintering point of the agglomeration process, *neural networks* have been assigned a huge layer of work. So, for example, in [14], the parameter introduced by the authors - the mathematical bend point of the temperature curve of sinter gases measured in the middle of the sintering belt - is fed at different times to the input of a multilayer neural network, the output of which predicts the sintering point values 5 steps ahead. The predicted error of this model was 0.15, when training the network on a sample of 600 data groups. The neural network is also used in [15], where the values of the sintering belt speed and the position of the sintering point at the previous time instants are fed to its input. The network, together with the training algorithm, is used to update the parameters of the sintering point model, thus forming the neural network identifier used in the adaptive pole (position) finding method. In [16], for intelligent control of the agglomeration process of iron ores, there are fed up data on the current position of the sintering point, the temperature in the middle and the end of the process and the sintering belt speed to the neural network input, the

result is the sintering point prediction. Fuzzy neural networks are also used to predict the sintering point in [17], where the temperatures in the vacuum chambers are selected as input variables and the sintering point as the model output. The neural networks used by the authors in [18] for the synthesis of the model of the sintering point of iron ores are trained on a set of 10,000 data. The dataset includes process parameters (sintering belt speed, ignition temperature, layer height, layer permeability, return, fuel and moisture) and ratio parameters (return, fuel and moisture, limestone, ore, etc.). The prediction result and real values of the sintering point are then fed to a multilinear regression model in order to compensate the neural network error. In this case, the maximum prediction error was 1.3 m. A neural network trained using fuzzy sets is presented in [19] for predicting the sintering point. The input of the neural network is a sample of 80 values of the temperature under the sintering belt, the speed of the sintering belt and the parameter associated with it. The first layer of the network represents inputs, the second layer is responsible for linguistic meaning and is used to calculate the membership function of each component, each node of the third layer represents fuzzy rules, the last layer is the output of the network.

Some works use 2 predictive models of the sintering point: temporal and technological. So, in order to predict the permeability of lead-zinc ores in [20], 6 previous permeability values are fed to the input of a temporary neural network, and for a technological neural network, the input is the fire temperature, humidity, sulfur, lead, silicon dioxide, and speed. In [21], the grey model GM (1,1) of the sintering point of lead-zinc ores is used as a time sequence, and the parameters of the charge permeability and pallet speed are fed to the input of the technological neural network. In [22], to predict the sintering point of iron ores, they also use the integration of the gray model and neural networks. The result of the gray model calculation (gas temperature in the vacuum chambers) is one of the inputs of the backpropagation neural network, along with the sinter machine speed and the sintering belt position at the sintering point at the current time. Authors of works with two predictive models use a fuzzy expert controller that maintains the desired position of the sintering point within the specified boundaries.

In [23], there are presented an optimization model of coke efficiency and a fuzzy controller of the sintering point. The main idea is to improve coke efficiency using an intelligent integrated sintering point control strategy. The sintering belt speed resulting from the optimization model and the output of the fuzzy sintering point controller is integrated using the fuzzy satisfaction method that calculates the final sintering belt speed. The sintering point prediction model developed in [24] also uses 2 models. The temperatures in the vacuum chambers are fed to the sintering point model (first model) to predict the sintering point position. The predictive sintering point temperature model (second model) uses the sintering point temperatures obtained in the previous steps. The results of both models - the position and temperature of the sintering point - together with the sintering belt speed are used as input variables to a robust fuzzy controller, which is based on an improved model of the Takagi-Sugeno linear parameter variation.

In addition to the standard neural network training algorithms, genetic algorithms are used to optimize the value of the neural network weights. Thus, in [25], an adaptive genetic algorithm was used for the control system of the sintering point during the sintering of iron ores, where the input layer of the neural network is the parameters of the initial material, density, sintering belt speed and ignition temperature, and the output layer is responsible for the temperature and pressure of agglomeration gases and gases in a vacuum chamber. The genetic neural network was used for the system for predicting the sintering point of iron ores and in [26], where 707 groups of data obtained as a result of *clustering* and classification of temperature and pressure vectors from 18 vacuum chambers, were fed into the input. The entire system of adaptive structural clustering used methods of spatial clustering of the initial data, a self-organizing neural network map for extracting data relevance properties and a Kohonen map for training the LVQ network.

The idea of clustering was also used in [27] to synthesize a model for predicting the sintering point of iron ores. The K-means clustering module, at the input of which the model of the permeability of the cold charge, the values of the ignition temperature and the coke residue is fed to, is used to form clusters.

The predictive model in this work *does not use neural network algorithms*, and the resulting clusters are fed to the input of the dynamic temperature and vacuum model. The dynamic model is created using a new genetic programming algorithm. An algorithm based on genetic algorithms for optimizing the prediction model of the final sintering based on the support vector machine is presented in [28].

Models that do not use neural networks to predict the sintering point are based *on equations for the temperature or sintering time change*. For example, in [29], the predicted value of the sintering time is determined by the least squares method based on historical data and, depending on the signal of the event model, which determines the time until the end of the pallet movement, the sintering belt velosity is controlled. The event-driven control model over the sintering point of iron ores is presented as a linear, time-constant discrete model in the state space, using the idea of breaking the continuous model into discrete events. The authors of [30] use a curve fitting method and present the result as a cubic curve and a 5 degree curve near the sintering point position. In [31], there is used a parabolic model of the change in the temperature of the sintering point control, compiled from the measured values in three vacuum chambers. It is used to determine the volume of sinter gases and to correct the main signal - the volume of sinter gases, calculated from the volume of oxygen, moisture, and data on the composition of the charge. In [32], there is considered a two-level hierarchical control system for the sintering point and the vertical sintering rate of the agglomeration process of iron ores. The model of the sintering point proposed by the authors is a piecewise-quadratic dependence of the temperature on the position on the sintering belt, which is used when the process is unstable. With a stable sintering process, the vertical sintering rate is calculated using historical data on sintering belt speed and charge height. In [33], the sintering point was approximated using a quadratic function of the output gas temperature. At the same time, a dynamic model of the state space is created to obtain the temperature of the output gases, which uses 6 input variables: the thickness of the charge layer, the speed of the pallets, the pressure in the vacuum chambers and the temperatures of the output gases in the three previous vacuum chambers. A grid

search algorithm optimizes variables within specified limits using a scoring function that provides more accurate temperature prediction results.

The neural network is also not used in [34], where the position control of the sintering point of iron ores is divided into 2 parts: a closed identification model and a generalized predictive control model. In the first part, on the basis of an autoregressive exogenous model, to the input of which the values of the sintering belt speed, amount of moisture, the charge height, volume of air and vacuum are supplied, the position of the sintering point is calculated. Here is used the method of a closed identification system, which serves to dynamically determination of the model parameters. In the second part, based on the transfer function obtained from the identification model, the sintering point is predicted to control the sintering belt speed. In [35], the degree of influence of 4 parameters on the sintering point - pressure in vacuum chambers, air volume, sintering belt speed and ignition temperature - is determined using the optimization algorithm of a swarm of particles.

Naturally, the current position of the sintering point depends on its previous values. This idea was used in the study [36] and analyzed the trends of the time series for the sintering point, which made it possible to use the global and local variables of the trend function. These variables were used as input to the fuzzy controller created on the basis of the operator's knowledge. The output of the controller is the speed of the sintering belt to maintain the sintering point in the required position. The position of the sintering point was also predicted using the “particle swarm” optimization algorithm [37], where the value of 4 influencing parameters: vacuum, incoming air flow, sinter machine speed and ignition temperature were determined using the algorithm.

Based on the literature review, the following conclusions can be drawn:

- in order to predict the sintering point, there are used data on (1) vertical sintering rate, determined by the volume of sinter gases, discharge, properties of the initial material, permeability, charge height, etc.; on (2) temperature in vacuum chambers or sinter gases; on (3) the speed of the sintering belt; on (4) the previous values of the sintering points;

- in order to create predictive models, a large volume of the initial sample is used to obtain accurate models;

- the sintering point is controlled by changing the speed of the sintering belt.

4 MATHEMATICAL MODEL FOR PREDICTING SINTERING POINT

4.1 Main parameters of the predictive model of the sintering point

The amount of return during sintering reaches 40-50%, since the process is controlled only at the end of the sinter machine by the operator's decision, based on a visual assessment of the sinter cut. The return rate needs to be reduced by predicting and controlling the sintering point based on real-time data. The agglomeration process includes many parameters that influence the sintering point. In the work, data measured in real time were used as the main parameters for creating predictive models - the temperature in the vacuum chambers and the gas velocity, determined through the measured value of the pressure (discharge) in the vacuum chambers.

The main predictive variable is the temperature at the bottom of the sintering belt (temperature in the vacuum chambers). Temperature curves (Figure 2.5) represent data samples taken at different times in different initial conditions: different composition of the charge, amount of coke, pressure, but at a constant speed, so they are displayed on the graph only until the desired temperature is reached to determine the actual duration of the process. Additionally, the value of the pressure drop Δp is measured (the difference between the pressure in the upper and lower parts of the charge) and according to the Ergun equation (2.6) the gas velocity u (Figure 2.7) in the upper part of the charge is calculated. The porosity value is calculated according to the method proposed in [38].

4.2 Grey systems for sintering point prediction

The creation of a data collection system with its storage, analysis and constant retraining requires huge time and financial resources. Also, collecting the initial sample, training and creating an effective system requires constant interruption of the production process, which affects its efficiency. In the process under consideration, there

is no full-fledged data collection system, therefore, in order to obtain data, additional measurement systems were used that were not included in the main control circuit. In such conditions, it becomes necessary to use models that require a small amount of the initial sample for training and creating a predictive model. Grey systems theory satisfies these requirements [39].

The grey model of a type GM (1,1) is the most widely used model in the literature and is referred to the first order grey model with one variable. The model is a temporal predictive model with time-varying coefficients. In other words, the model is updated when new data becomes available to the predictive model. Grey GM (1,1) model can only be used with non-negative original samples.

In order to create a grey model GM (1,1) based on the original sample (4.4) and 1-AGO sample (4.5), the generated mean sequence has the following form [40]

$$Z^{(1)} = \left\{Z^{(1)}(1), Z^{(1)}(2), ..., Z^{(1)}(r)\right\}, \quad (4.1)$$

where $Z^{(1)}(k)$ - mean value of adjacent data

$$Z^{(1)}(k) = 0{,}5X^{(1)}(k) - 0{,}5X^{(1)}(k-1).$$

The sequence of calculating the least squares of the grey differential equation GM (1,1) is determined as follows

$$X^{(0)}(k) + aZ^{(1)}(k) = b$$

Then, the whitening equation has the form

$$\frac{dX^{(1)}(t)}{dt} + aX^{(1)}(t) = b, \quad (4.2)$$

where $[a,b]^{\mathrm{T}}$ - a sequence of parameters which can be found as follows

$$[a,b]^T = (B^T B)^{-1} B^T Y, \quad (4.3)$$

$$Y = [X^{(0)}(2), X^{(0)}(3), ..., X^{(0)}(r)]^T$$

$$B = \begin{bmatrix} -Z^{(1)}(2) & 1 \\ -Z^{(1)}(3) & 1 \\ -Z^{(1)}(r) & 1 \end{bmatrix}.$$

The solution of equation (4.8) $X^{(1)}(t)$ at the moment of time k

$$X_p^{(1)}(k+1) = \left[X^{(0)}(1) - \frac{b}{a}\right]e^{-ak} + \frac{b}{a}.$$

To obtain predicted values at the time (k+1), there is used IAGO

$$X_p^{(0)}(k+1) = \left[X^{(0)}(1) - \frac{b}{a}\right]e^{-ak} + \frac{b}{a}(1-e^{a}).$$

Most of the systems are generalized energy systems. They will follow a grey exponential law if they are not violated by any other factors, and then they can be accurately predicted by GM's grey predictive model (1, 1). Actual systems will be more or less influenced by other factors and will never fully follow the grey exponential law, so it is important to consider grey system models that take other influencing factors into account.

The influence of several factors on the predicted value for grey models can only be considered on the basis of modifications of the GM (1,n) model, which is clearly demonstrated in [41]. The continuous integral grey convolution model GMC (1,n) [42] is one of the main models with (n-1) influencing factors. Based on this model, other continuous linear gray models with (n-1) influencers have been developed. For example, the interval model with the convolution integral IGDMC (1,n) [43] is designed to predict the interval in which the variable is located. The FGMC (1,n) model [44] was developed on the basis of the idea of independence of the prediction from the first pair of initial data in the sample. The deterministic grey model with convolution integral DGDMC (1,n) [45] differs from GMC (1,n) in the estimate of the first derivative and parameters: the first derivative is estimated numerically by the cubic spline curve and model parameters, in accordance with the deterministic convergence scheme. The error in the strength prediction considered by Thien is 0.54% for FGMC (1,n), 1.25% for GMC (1,n), 1.85% for DGDMC (1,n) and 2.4% for IGDMC (1,n). Later in [46], there was shown an optimized model GDMC (1,n) - OGDMC (1,n), in which the value of the grey derivative $dX_1^{(1)}(t)\ \ (t)/dt$ is not determined by the weighted average value $X_1^{(1)}(t)\ \ X^{(1)}(t)$ и $dX_1^{(1)}(1)dX\ dX_1^{(1)}(t-1)$, but through the weight coefficient ρ_i determined using the particle swarm algorithm [47]

$$c_i X_i^{(1)}(t) - (1-c_i)X_i^{(1)}(t) \qquad (4.4)$$

Here, the value of the root-mean-square error as a percentage to the a prior sampling period (RMSPEPR) in OGDMC (1,*n*) decreased 3.8 times - from 7.07% to 1.86%. in order to select the most accurate model for predicting the sintering point in a vacuum chamber, we will conduct experiments using the FGMC (1,*n*), GMC (1,*n*) and GDMC (1,*n*) models, which have the lowest prediction error.

4.2.1 Continuous integral gray convolution model GMC (1,2)

The gas velocity calculated from the known pressure Δp measured in real time was chosen as the influencing factor. The continuous integral gray model GMC (1,2) with one influencing factor is a linear differential model

$$\frac{dY^{(1)}(t)}{dt} + b_1 Y^{(1)}(t) = b_2 X^{(1)}(t) + u \qquad (4.5)$$

where $Y^{(1)}(t)$ and $X^{(1)}(t)$ represent 1-AGO data

The gray derivative for the AGO data of the first order in (4.12) is traditionally represented as

$$Y^{(1)}(t) = \sum_{l=1}^{t} Y^{(0)}(l), X^{(1)}(t) = \sum_{l=1}^{t} X^{(0)}(l). \qquad (4.6)$$

The gray derivative for the AGO data of the first order in (4.12) is traditionally represented as:

$$\frac{dY^{(1)}(t)}{dt} = \lim_{\Delta t \to \infty} \frac{Y^{(1)}(t+\Delta t) - Y^{(1)}(t)}{\Delta t} = Y^{(1)}(t+\Delta t) - Y^{(1)}(t), \qquad (4.7)$$

with $\Delta t \to 1$.

The parameters (4.12) are determined using the least squares method (4.9)

$$\left[b_1, b_2, u\right]^T = (B^T B)^{-1} B^T Y_R, \qquad (4.8)$$

where *t* varies from 1 to *r*, representing the volume of the initial sample to build the model in (4.12),

$$B = \begin{bmatrix} -0{,}5(Y^{(1)}(1) + Y^{(1)}(2)) & -0{,}5(X^{(1)}(1) + X^{(1)}(2)) & 1 \\ -0{,}5(Y^{(1)}(2) + Y^{(1)}(3)) & -0{,}5(X^{(1)}(2) + Y^{(1)}(3)) & 1 \\ -0{,}5(Y^{(1)}(r-\dot{1}) + Y^{(1)}(r)) & -0{,}5(X^{(1)}(r-\dot{1}) + X^{(1)}(r)) & \dot{1} \end{bmatrix} \qquad (4.9)$$

$$Y_R = \left[Y^{(1)}(2), Y^{(1)}(3), \ldots, Y^{(1)}(r)\right]. \qquad (4.10)$$

The forecast of the agglomerate temperature $\hat{0}$ is determined by the following equation

$$\hat{Y}^{(0)}(t) = \hat{Y}^{(1)}(t) - \hat{Y}^{(1)}(t-1). \quad (4.11)$$

$$\hat{Y}^{(1)}(t) = \hat{Y}^{(0)}(1)e^{-b_1(t-1)} + \tfrac{1}{2}e^{-b_1(t-1)} \times (b_2 X^{(1)}(t) + u) + \tfrac{1}{2}b_2 X^{(1)}(t) + u) + \textstyle\sum_{i=2}^{t-1} e^{-b_1(t-i)} \times (b_2 X^{(1)}(i) + u). \quad (4.12)$$

4.2.2 Continuous integral gray convolution model of the first pair of FGMC data(1,*n*)

The differential equation of the gray prediction model FGMC (1,*n*), presented in [44], is the same as for GMC(1,*n*), but is modeled by data that includes information from the first pair of source data.

The parameters (4.12) are determined by the least squares method (4.15), where

$$B = \begin{bmatrix} -0{,}5(Y^{(1)}(1) + Y^{(1)}(2)) & -0{,}5(X^{(1)}(1) + X^{(1)}(2)) & 1 \\ -0{,}5(Y^{(1)}(2) + Y^{(1)}(3)) & -0{,}5(X^{(1)}(2) + Y^{(1)}(3)) & 1 \\ -0{,}5(Y^{(1)}(r-\dot{1}) + Y^{(1)}(r)) & -0{,}5(X^{(1)}(r-\dot{1}) + X^{(1)}(r)) & \dot{1} \end{bmatrix} \quad (4.13)$$

$$Y_R = [Y^{(1)}(1), Y^{(1)}(2), \ldots, Y^{(1)}(r)]. \quad (4.14)$$

The forecast of the agglomerate temperature is determined according to the following equation

$$\hat{Y}^{(0)}(t) = Y^{(0)}(0)e^{-b_1 t} + u(t-1)\textstyle\sum_{i=1}^{t}\frac{1}{2} e^{-b_1(t-i+0{,}5)}\left(b_2(X^{(1)}(i) - X^{(1)}(i-1)\right). \quad (4.15)$$

Optimal continuous dynamic integral gray convolution model OGDMC (1,*n*)

Differential equation of the gray dynamic model with the convolution integral.

$$\frac{dY^{(1)}(t)}{dt} + b_1 Y^{(1)}(t) = b_2 + \textstyle\sum_{i=2}^{n}\left(b_{2i-1}\frac{dX^{(1)}(t)}{dt} + b_{2i}X^{(1)}(t)\right) \quad (4.16)$$

The parameters (4.23) for the continuous dynamic integral model are determined using the least squares method (4.14), the YR vector is calculated by (4.21) and

$$B = \begin{bmatrix} -0{,}5(Y^{(1)}(1) + (Y^{(1)}(2) & 1 & X^{(0)}(1) & -0{,}5(X^{(1)}(1) + (X^{(1)}(2) & 1 \\ -0{,}5(Y^{(1)}(2) + (Y^{(1)}(3) & 1 & X^{(0)}(2) & -0{,}5(X^{(1)}(2) + (X^{(1)}(3) & 1 \\ -0{,}5(Y^{(1)}(r-\dot{1}) + (Y^{(1)}(r) & \dot{1} & X^{(\dot{0})}(r) & -0{,}5(X^{(1)}(r-1) + (X^{(1)}(r) & \dot{1} \end{bmatrix} \quad (4.17)$$

To obtain the parameters of the optimal model of the gray value of the derivative dX(1)(t)/dt and dY(1)(t)/dt is not determined by the

weighted average value of X(1)(t) and dX(1)(t-1), Y(1)(t) and dY(1)(t-1), respectively , and using a weighting factor of PI, defined by using the particle swarm optimization algorithm according to equation (4.11).

Forecast of the sinter temperature is defined by (4.18), where

$$\hat{Y}^{(1)}(t) = Y^{(0)}(1)e^{-b_1(t-1)} + u(t-2)\sum_{\tau=2}^{t}\frac{1}{2}e^{-b_1(t-i+0,5+0,5\lambda_1)} \times \left[\frac{1}{2}(f(\tau)-(f(\tau-1))+\frac{1}{2}\lambda_1(f(\tau)-(f(\tau-1))\right]+\frac{1}{2}e^{-b_1(t-i+0,5+0,5\lambda_2)} \times \left[\frac{1}{2}(f(\tau)-(f(\tau-1))+\frac{1}{2}\lambda_1(f(\tau)-(f(\tau-1))\right] \quad (4.18)$$

where $\lambda_1 = -\frac{1}{\sqrt{3}}$, $\lambda_2 = -\frac{1}{\sqrt{3}}$

$$f(t) = b_2 + \sum_{i=2}^{n}(b_{2i-1}X^{(0)}(t) + b_{2i}X^{(1)}(t) \quad (4.19)$$

4.3 Results of predictive models

The root mean square error in percent (RMSPE) of predictive models for 3 samples is presented in Table 4.4, where the initial sample size *r* for building the model includes data from the beginning of the sintering process to 7.5 minutes. (15 values). The results of the predictive models for each sample are shown in Table 4.4.

Table 4.4

RMSPE gray models

№	RMSPE, %		
	GMC(1,n)	FGMC(1,*n*)	GDMC(1,*n*)
1	2.2413	4.1062	2.6575
2	1.6697	3.4544	3.6921
3	1.0952	3.8123	4.1833

The best result of prediction of the sintering point of the charge was obtained as a result of using the GMC (1,*n*) model, the largest error of which is 2.2% versus 4% for other types of models.

Predictive GMC (1,*n*) models for 3 samples are presented in Table 4.5, where the volume of the initial sample for creating the model includes data from the beginning of the sintering process to 7.5 minutes (15 values). The parameters of the grey model, which were found using equation (4.15), differ significantly for each sample. This is due to the fact that each temperature curve was obtained under different initial conditions: the content of coke,

phosphorite ore, the amount of return, moisture and other parameters of the charge, which are not directly accepted for creating a predictive model. Moreover, during production under real conditions, it is impossible to continuously monitor the composition of the charge, which makes it difficult to use a model that takes into account all factors. Therefore, it is necessary to create a predictive model that uses only the parameters measured in real time and dynamically creates a predictive model for a specific batch of sintered ore. The prediction results based on grey systems do not improve the accuracy compared to other models presented in the literature earlier, but it allows to create an adequate predictive model of the sintering point in the absence of a large amount of historical data. An additional advantage of the model is the reduction in the time spent on collecting initial data and training the model.

Table 4.5

Built GMC Models

Samsung	GMC(1,в)	RMSPE,%
1	$\frac{dY^{(1)}t}{dt} - 0{,}0011762481\ Y^{(1)}(t) = = 55.0012859\ ^{(1)}X(t) + 41.90354212$	2,2413
2	$\frac{dY^{(1)}t}{dt} - 0{,}0030327\ Y^{(1)}(t) = = 62.1579506\ X^{(1)}(t) + 41.27688268$	1,697
3	$\frac{dY^{(1)}t}{dt} - 0{,}00575793\ Y^{(1)}(t) = = 47.8204758\ X^{(1)}(t) + 36.486036$	1,0952

4.4 Optimal gray predictive model of the OGMC sintering point(1, *n*)

To improve the accuracy of the predictive model GMC (1,*n*), instead of the weighted average for determining the gray derivative, we introduce the coefficient pϵ [0; 1], then (4.16) takes the following form

$$\begin{bmatrix} -(1-\rho)Y^{(1)}(1)+\rho Y^{(1)}(2) & (1-\rho)X^{(1)}(1)+\rho X^{(1)}(2) & 1 \\ -(1-\rho)Y^{(1)}(2)+\rho Y^{(1)}(3) & (1-\rho)X^{(1)}(2)+\rho X^{(1)}(3) & 1 \\ -(1-\rho)Y^{(1)}(r-1)+\rho Y^{(1)}(r) & (1-\rho)X^{(1)}(r-1)+\rho X^{(1)}(r) & 1 \end{bmatrix} \quad (4.20)$$

The coefficient ρ is determined by the swarm of particles optimization method [62]. In 1995, J. Kennedy and R. Eberhart proposed a method for optimizing continuous nonlinear functions called the particle swarm algorithm [62]. The current state of the particle is characterized by coordinates in the space of solutions (that is, in fact, the solution associated with them), as well as the velocity vector. Both of these parameters are randomly selected during the initialization phase. In addition, each particle stores the coordinates of the best solution found for it, as well as the best solution passed by all particles - this simulates instant information exchange between birds.

At each iteration of the algorithm, the direction and length of the velocity vector of each of the particles change in accordance with the information about the found optima. The particle swarm algorithm is a system of particles that move to optimal solutions, each particle contains the coordinates of the found best solution (*pbest*) and the best solution of all particles in the swarm (*gbest*). The direction and length of the particle velocity vector is determined by the following formula

$$\vartheta_i = \vartheta_i + a_1 rnd()(pbest_i - x_i) + a_2 rnd()(gbest_i - x_i) \quad (4.21)$$

where ϑ_i - particle velocity vector, a_1, a_2 - constant accelerations, a x - particle current position. In this case, the current position of the particle determines the value of the coefficient ρ.

Minimum (4.26) is used as an optimality criterion. The resulting predictive models and *RMSPE* for the period after the training sample are presented in Table 4.6, where it can be seen that the accuracy of the grey model has improved.

In [46], the interpolation coefficients ρ_i are introduced into the values of each of the variables in GDMC (1,n). Application of this algorithm to the GMC (1,n) model will have the following changes in (4.15)

$$\begin{bmatrix} -(1-\rho_1)Y^{(1)}(1)+\rho_1 Y^{(1)}(2) & (1-\rho_2)X^{(1)}(1)+\rho_2 X^{(1)}(2) & 1 \\ -(1-\rho_1)Y^{(1)}(2)+\rho Y_1^{(1)}(3) & (1-\rho_2)X^{(1)}(2)+\rho_2 X^{(1)}(3) & 1 \\ -(1-\rho_1)Y^{(1)}(r-1)+\rho_1 Y^{(1)}(r) & (1-\rho_2)X^{(1)}(r-1)+\rho_2 X^{(1)}(r) & 1 \end{bmatrix} \quad (4.22)$$

The prediction results have changed insignificantly (Table 4.7), but the time to find the optimal values of the ρi coefficients has increased. An increase in (n-1) dependent variables leads to an optimization time that increases exponentially, and makes it difficult to use an algorithm with different coefficients for each variable in real-time control.

Therefore, in order to improve the accuracy of modeling and prediction, there is used the coefficient ρ for the control task. The prediction results for OGMC (1,n) are presented on Figures 4.7-4.9 in comparison with GMC (1,n) and the original sample.

The grey model coefficients (Table 4.7), which were found by (4.15), differ significantly for each sample.

This is due to the fact that each temperature curve was obtained under different initial conditions: the content of coke, phosphorite ore, the rate of return, moisture content and other parameters of the charge, which were not directly taken to create the predictive model.

Moreover, during production under real conditions, it is impossible to continuously monitor the composition of the charge, which makes it difficult to use a model that takes into account all factors.

Therefore, it is necessary to create a predictive model that uses only measured real-time factors and dynamically creates a predictive model for a specific batch of sinter ore.

Table 4.7

Results of the optimal GMC (1,n) model

№	Коэффициенты	GMC(1,n) ρ	RMSPE ρ, %	GMC(1,n) ρ_i	RMSPE ρ_i, %
1	ρ	0.2261	1.2120	0&0.2283	1.2110
	b_1	-0.0005		-0.0005	
	b_2	56.3769		56.3554	
	u	28.3447		28.4573	
2	ρ	0.3669	1.4266	1&0.3683	1.4249
	b_1	0.0003		0.0003	
	b_2	58.9057		58.8892	
	u	30.6943		30.7584	
3	ρ	0.4193	0.9756	1&0.4384	0.9588

b_1	0.0025		0.0023	
b_2	62.1686		61.9513	
u	37.5064		38.5224	

5 STRUCTURE OF THE CONTROL SYSTEM BASED ON PREDICTIVE MODEL

Dynamic creation of a grey model assumes the use of only actual data obtained in real time about the sintering process, while the model does not depend on historical data and allows to predict the value of the charge temperature at the end of the sintering belt. If the predicted

temperature of the charge at the extreme point does not reach the specified value, the agglomeration process must be controlled. Control can be performed by changing the amount of fuel in the initial charge, the speed of the sintering belt and the pressure created in the vacuum chambers. A change in the amount of fuel affects only the part of the charge that has not yet been fed to the sinter, therefore this effect is not taken into account in the work.

The proposed control structure for the sintering point (Figure 5.1) includes:

1 Collecting data on temperature and pressure in vacuum chambers from the beginning of the process to a certain point.

2 Creation of the optimal grey predictive model OGMC (1,n) based on the accumulated data.

3 Prediction of the temperature to the end of the sintering belt.

4 Optimization of the process control parameters (speed and pressure in the vacuum chambers) to achieve the desired temperature at the end of the process.

5 Modification of control parameters for the batch under consideration to obtain good sinter quality and minimum return.

The control structure has the following algorithm: after the charge enters the hearth, the system starts collecting data on temperature, pressure in the vacuum chambers and sintering belt speed. Based on the collected data, there is created an optimal grey predictive model OGMC (1,n), which predicts the temperature value at the end of the sintering belt. If the temperature does not correspond to the sintering

point of the sinter, then the predictive optimization algorithm calculates the required values of the sintering belt speed and pressure in the vacuum chambers. These calculations are fed to the corresponding controllers. After the charge reaches the end of the sintering belt, the cycle is repeated.

The particle swarm method is used [47] as a predictive optimization method. It is implemented as follows:

1 There are generated *m*-particles (m=2) in n-dimensional space. The position and velocity of the particle are represented as $x_i=(x_{i1}; x_{i2};...; x_{in})$ and $\vartheta_i=(\vartheta_{i1}; \vartheta_{i2};...;\_\vartheta_{in})$, where i=1;...;m. The current position of the particle x (4.27) includes two variables: the sample size, from which the duration of the agglomeration process is calculated and the gas velocity.

2 Initial position of the particle *xi* and particle velocity ϑ_i are generated randomly and within specified limits: $t_{min}\leq x_1\leq t_{max}$, $X_{min}\leq x_2\leq X_{max}$, where t - time step, X - discharge in vacuum chambers.

3 According to (4.14) x_2 is substituted into matrix B and according to (4.17) x_1 is substituted as a parameter t.

4 The fitness function (4.26) is calculated for each particle

5 The value of the fitness function of each particle is compared with the best solution of all the particles in the swarm *pbest* to correct the value, if the value is optimal, then it is taken as the best position of the particle, if not, then the transition to the next step occurs.

6 Calculation of the particle velocity and position according to equation (4.27).

7 When the criterion for the end of the algorithm is reached, the result and its fitness function are determined, which correspond to the optimal parameters and RMSPE, otherwise the transition to step 3 occurs.

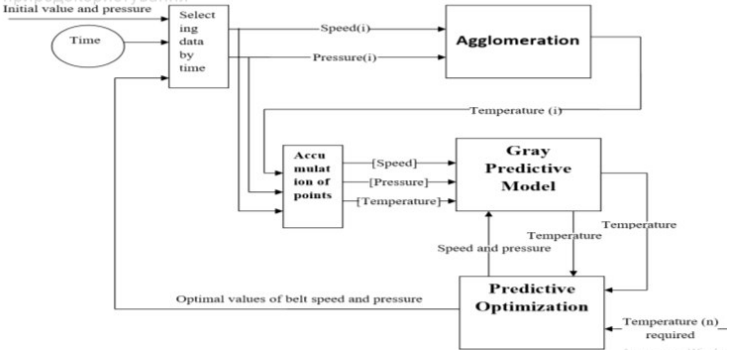

Fig. 5.1. Control system for the point of the cake

Using the obtained value of the optimal sintering process time, the speed of the sintering belt is determined, and through the optimal value of the gas valocity, the pressure in the vacuum chambers is determined, according to the Ergun equation (2.6). The simulation results of the sintering point control system for the first sample are shown on Figure 5.2. The structure of the control system looks as follows: from the beginning of the process, the system accumulates 15 values (for this example, up to 7.5 minutes of the sintering process), on the basis of which a grey model is created. The grey model predicts the temperature at the end of the sintering belt for given initial values of speed and pressure. The difference between the predicted and target value starts the prediction process. Results of prediction optimization of the 1st sample: the speed values vary from 3.5 m/min to 4.5 m/min and the pressure in the vacuum chambers from 800 mm Hg up to 760 mm Hg. Therefore, the sintering point can be reached in 17.5 minutes instead of 22 minutes, when the gas velocity changes from 0.48 m/s to 0.52 m/s.

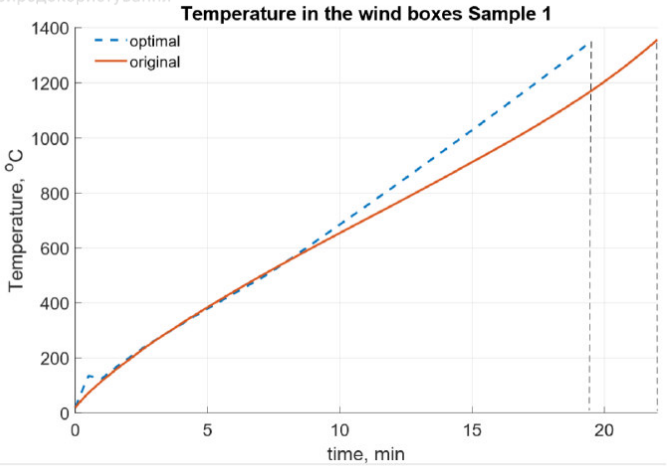

Fig. 5.2. Results of modeling the management structure for the 1st sample

Conclusion

This paper describes the methodology and basic algorithms for modeling the agglomeration processes, starting from the beginning of the charge into the sinter machine and ending with obtaining a suitable sinter. The obtained curves of the developed mathematical model of temperature in the vacuum chambers served as the basis for testing the prediction model based on the use of the theory of grey systems and the "swarm of particles" optimization algorithm. On the basis of the developed mathematical model, there is created a sintering point prediction system, which is the basis for determining the quality of the sinter. The general structure of the sinter machine control system based on a dynamic predictive model is also proposed.

The practical significance of the developed mathematical model based on physical and chemical transformations is as follows:

- in the study of the agglomeration process: changing the composition, parametric analysis and solving optimization problems, performing mathematical experiments to improve the final product;
- the mathematical model can be used as a training platform (simulator) for agglomeration processes and the use of physical laws of heat transfer in porous materials.

The practical significance of the developed predictive model based on the theory of grey systems is as follows:

- prediction of the value of the sintering point of the sinter and the synthesis of the control action based on the prediction;

- the algorithm for creating a mathematical prediction model can be used for any process that has the character of a “grey exponential law”.

The paper is written within the framework of the project entitled «Development and testing of intelligent algorithms for optimal control of the technological process of yellow phosphorus purification in the conditions of the NDFP, IRN AP08856867.

References

1. Permanent Technological Regulation No. 3 for the production of phosphorite agglomerate for the production of yellow phosphorus. // ZHF "Kazphosphate" LLP (NDFP). - 2010. - 115 p.

2. **D. A. Aznabayev**. Improvement of the theory of solid-phase chemical reactions and intensification of the agglomeration process: il RGB OD 61:85-5/4899. Website: http://www.dslib.net/cvetn-metallurgia/sovershenstvovanie-teorii-tverdofaznyh-himicheskih-reakcij-i-intensifikacija.html.

3. **L.J. Gibson, M.F. Ashby**. Thermal, electrical and acoustic properties of foams. In Cellular Solids: Structure and Properties, 2nd ed. // Cambridge University Press: Cambridge, UK. – 1997. – P. 283-308.

4. **J. Vu.** Modelling of Convective Heat Transfer in Porous Media. // Electronic Thesis and Dissertation Repository. 4852. – 2017. Сайт: https://ir.lib.uwo.ca/etd/4852.

5. **S. Majumder, P. V. Natekar, V. Runkana**. Virtual indurator: A tool for simulation of induration of wet iron ore pellets on a moving grate. // Computers and Chemical Engineering. – 2009. – №33. – P. 1141–1152.

6. Comsol: Модуль течения в грунтах. Сайт: https://www.comsol.ru/subsurface-flow-module.

7. **Y. Kaymak, T. Hauck, M. Hillers**. Iron Ore Sintering Process Model to Study Local Permeability Control. // Excerpt from the Proceedings of the 2017 COMSOL Conference in Rotterdam. –2017. – P. 1-7.

8. **N.K. Nath, A.J. Silva, N. Chakraborti**. Dynamic process modeling of iron ore sintering. // Steel Research. – 1997. - №68. – P. 285-292.

9. **A. F. Bogatyrev, S. V. Panchenko, N. A. Skuratova**. Generalization of the dependences of the thermophysical properties of solid materials with reacting

components. Retrieved from: http://www.rusnauka.com/NIO/Phisica/bogatyrev%20a.f..doc.htm.

10.Website: https://elibrary.ru/download/elibrary_29203591_49686410.PDF

11. Chemist's Handbook Retrieved from: http://chem21.info/page/100228120038234192086243212149241006093157114160/.

12. Specific heat capacities of solids, liquids and gases (gases - at a constant pressure of 1 bar abs) + reference densities. Retrieved from: http://tehtab.ru/guide/guidephysics/guidephysicsheatandtemperature/specificheat/specificheattable/.

13. **Bobkov V. I.** Models for describing the properties of phosphate raw materials. // Uspekhi sovremennoy nauki i obrazovaniya. - 2017. - Vol. 4. - No. 4-p. 73-77.

14. Q. Feng, T. Li, X. Fan, T. Jiang. Adaptive prediction system of sintering through point based on self-organize artificial neural network. // Trans. Nonferrous Met. Soc. China. – 2000. – Vol. 10. – №6. – P. 804-807.

15. **L. Peng, Z. Ji and J. Tan**. Sintering Finish Point Intelligent Control. // Proceedings of the 2005 IEEE/ASME International Conference on Advanced Intelligent Mechatronics Monterey, California, USA . – July 24-28, 2005.

16. **S. Du, M. Wu, X. Chen, X. Lai, W. Cao**. Intelligent Coordinating control between burn-through point and mixture bunker level in an iron ore sintering process. // Journal of advanced Computational Intelligence and Intelligent Informatics. – 2017. – Vol. 21. – №1.

17. **J. Wang** et al. BTP prediction of sintering process by using multiple models. // 26th Chinese Control and Decision Conference (CCDC 2014), Changsha, China. – 2014.

18. **B. Wang, Y. Fang, J. Sheng, W. Gui, Y. Sun**. BTP Prediction Model Based on ANN and Regression Analysis. // Second International Workshop on Knowledge Discovery and Data Mining. – 2009. – P.108-111

19. **J. Wang, X. Li, Y. Li, K. Wang.** BTP prediction of sintering process by using multiple models. // 26th Chinese Control and Decision Conference (CCDC) – 2014. – P.4008-4012.

20. **M. Wu, C. Xu, Y. Du**. Intelligent optimal control for lead-zinc sintering process state // Trans. Nonferrous Met. Soc. China. – 2006. – №16. – P. 975-981.

21. **M. Wu, C. Xu, J. She, W. Cao**. Neural-network-based integrated model for predicting burn-through point in lead-zinc sintering process. // Journal of Process Control. – 2012. – Vol.22. – P. 925– 934.

22. **M. Wu, P. Duan, W. Cao, J. She and J. Xiang**. An intelligent control system based on prediction of the burn-through point for the sintering process of an iron and steel plant. // Expert Systems with Applications. – 2012. – Vol.39. – №5. – P. 5971-5981.

23. **S. Du** et al. A Fuzzy Control Strategy of Burn-Through Point Based on the Feature Extraction of Time Series Trend for Iron Ore Sintering Process. // IEEE Transactions on Industrial Informatics. – 2019. – P. 1–9.

24. **X. Chen** et al. T-S Fuzzy Logic Based Modeling and Robust Control for Burning-Through Point in Sintering Process. // IEEE Transactions on Industrial Electronics. – 2017. – №64. – P. 9378–9388.

25. **W. Cheng**. An application of adaptive genetic-neural algorithm to sinter's BTP process. // Proceedings of the Third International Conference on Machine Learning and Cybernetics, Shanghai. – August 26-29, 2004.

26. **W. Cheng**. Prediction system of burning through point (BTP) based on adaptive pattern clustering and feature map. // Proceedings of the Fifth International Conference on Machine Learning and Cybernetics, Dalian. – August 13-16, 2006.

27. **X. Shang, J. Lu, Y. Sun, J. Liu, Y. Ying.** Data-Driven Prediction of Sintering Burn-Through Point Based on Novel Genetic Programming. // Journal of iron and steel research, International. – 2010. – Vol.17. – №12. – P. 1-10.

28. **D. Wang** et al. Application Research Based on GA-FWA in Prediction of Sintering Burning Through Point. // International Conference on Computer, Communications and Mechatronics

29. **W. H. Kwon, Y. H. Kim, S. J. Lee and K. Paek**. Event-Based Modeling and Control for the Burnthrough Point in Sintering Processes. // IEEE Transactions On Control Systems Technology. – 1999. – Vol. 7. – №1. – P. 31-41.

30. **B. Kim** et al. Estimation of Burn-Through Point in the Sinter Process, 14th International Conference on Control. // Automation and Systems (ICCAS 2014). – 2014 – P. 1531-1533.

31. **J. Terpak, L. Dorcak, I. Kostial, L. Pivka**. Control of burn-through point for agglomeration belt. // Metalurgia. – 2005. – Vol.44. – №4. – P.281-284.

32. **C. Wang** and M. Wu. Hierarchical Intelligent Control System and Its Application to the Sintering Process. // IEEE Transactions On Industrial Informatics. – 2013. – Vol. 9. – №1. – P. 190-196.

33. **W. Cao** et al. A dynamic subspace model for predicting burn-through point in iron sintering process. // Information Sciences. – 2018. – P. 1-12.

34. **M. Wu, C. Wang, W. Cao, X. Lai, X**. Chen. Design and application of generalized predictive control strategy with closed-loop identification for burn-through point in sintering process. // Control Engineering Practice. – 2012. – Vol.20. – P.1065-1074.

35. **J. Shi** et al. Soft sensing of the burning through point in iron-making process. // IEEE International Conference on Cognitive Informatics & Cognitive Computing (ICCI*CC 2016), Palo Alto, CA, USA. – 2016.

36. **S. Du** et al. Intelligent Integrated Control for Burn-Through Point to Carbon Efficiency Optimization in Iron Ore Sintering Process. // IEEE Transactions on Control Systems Technology. – 2019.

37. **J. Shi, Y. Wu, L. Liao, X. Yan, J. Zeng and R. Yang**. Soft sensing of the burning through point in iron-making process. // Proceedings of 2016 IEEE 15th International Conference on Cognitive Informatics and Cognitive Computing, ICCI*CC. – 2016.

39. **J. Deng**. Introduction to grey system. // Journal of Grey System – 1989. – 1. – P. 1–24.

41. **T. Tien.** A research on the grey prediction model GM(1,n). // Applied Mathematics and Computation. – 2012. – 218. – P. 4903-4916.

40. **E. Kayacan, B. Ulutas, O. Kaynak**. Grey system theory-based models in time series prediction. // Expert Systems with Applications. – 2010. – Vol.37. – 2. – P. 1784–1789.

42. T**. L. Tien**. The indirect measurement of tensile strength of material by the grey prediction model GMC(1, n). // Measurement Science and Technology. – 2005. – 16. – P.1322–1328.

43. **T. Tien.** The indirect measurement of tensile strength for a higher temperature by the new model IGDMC(1,n). // Measurement. – 2008. – 41. – P. 662-675.

44. **T. Tien**. The indirect measurement of tensile strength by the new model FGMC (1,n). // Measurement. – 2011 – 44. – P. 1884-1897.

45. **T. Tien**. The deterministic grey dynamic model with convolution integral DGDMC(1,n). // Applied Mathematical Modelling. – 2009. – 33. – P. 3498-3510.

46. **Z. X. Wang and L. L. Pei**. An optimized grey dynamic model for forecasting the output of high-tech industry in China. // Mathematical Problems in Engineering. – 2014.

47. **J. Kennedy, R. C. Eberhart**. “Particle swarm optimization”. // In Proceedings of IEEE International Conference on Neural Networks. – 1995. – P. 1942–1948.

https://doi.org/10.31713/m1017

OPTIMIZATION OF ENERGY EFFICIENCY OF A HEAT RECUPERATOR ON THE BASIS OF UNDERGROUND COAL GASIFICATION

Falshtynskyi V.S.
Dnipro University of Technology, Candidate of Technical Science, Associate Professor, Associate Professor at the Department of Mining Engineering and Education, Dnipro, Ukraine

Saik P.B.
Dnipro University of Technology, Candidate of Technical Science, Associate Professor, Associate Professor at the Department of Mining Engineering and Education, Dnipro, Ukraine

Dychkovskyi R.O.
Dnipro University of Technology, Doctor of Technical Science, Professor, Deputy Vice-rector for Scientific Affairs, Dnipro, Ukraine

Lozynskyi V.H.
Dnipro University of Technology, Candidate of Technical Science, Associate Professor, Associate Professor at the Department of Mining Engineering and Education, Dnipro, Ukraine

Abstract. Mining of the off-balanced and balanced reserves of mines, being under closure or completing their operation, required the implementation of mobile, complex, and environmentally friendly development technologies based on the processes of well underground coal gasification (WUCG) that unites mining of coal and its energy-chemical use. Environmental friendliness of the WUCG process is possible due to its controllability, hermeticity of the underground gas generator, and complex use of cogeneration technologies in the closed cycle of purification and processing of gasification products. The set engineering tasks were performed using analytical studies, bench studies and field studies. Efficiency of thermal energy generation were studies using rocks enclosing the underground gasifier and generator gases. These sources being the basic heat generating segments of energy chemical complex for coal gasification being formed at the territories of operating coal mines or mines at the stage of their closure. Prospects of coal gasification and thermal energy generation using rock disposals of coal mines have been estimated.

Introduction

The well underground coal gasification based mining of coal seams requires increased efficiency of the technology [1, 2]. Those efficiency-increasing methods include the introduction of multiple-

loop recuperators of heat energy of the “tube in tube” type with a liquid carrier of sufficient heat capacity into the rocks, enclosing the underground gas generator. That provides the possibility to remove residual heat from the rock mass during coal seam gasification and after the process completion as well as to increase the efficiency of underground coal gasification process and economic probability to gasify the coal seams of substandard thickness [3-5].

If such method is implemented, one should select the mines with a completed operating period and with substandard, overworked or underworked reserves of solid fuel [6,7]. The underground gas generator is prepared under the mine conditions with drilling of a stowing well in the seam roof, horizontal production wells throughout the seam, linkage between them, seam ignition, blow supply, coal gasification, syngas obtaining, and stowing of the deformed roof rocks and burned-out space [8-11].

Formation and functionality of the transition and reduction zones depend on the controllability and directionality of the oxidation reactions within the oxidation zones, which forms a temperature capsule in time and space around the reaction channel taking into account the fire face advance, gas generator hermeticity, and heat-capacity, thermal and temperature parameters of the rocks [12, 13]. In terms of the reduction zone, thermochemical reactions are accompanied with the absorption of heat generated in the oxidation zone [14-16]. In terms of balanced state of the zones, compensation of endothermal effect of carbon reaction with CO_2 and H_2O occurs at the expense of thermal capacity of the rocks, effecting the kinetics of the reduction zone reaction in the obtaining of fuel components of a generator gas (CO, CH_4, H_2 and others) [17-19].

Methodology

In this section the calculation of heat capacity of the loop-based heat recuperation of the rocks enclosing the underground gas generator are shown.

Use the formula to determined the convection heat exchange from the tube wall to a heat carrier

$$Nu = 0{,}021 \cdot \mathrm{Re}^{0,8} \cdot P_{rw}^{0,43} \cdot \left(\frac{P_{rw}}{P_{rc}} \right)^{0,25}, \quad (1)$$

where Nu is Nusselt number, Re is Reynolds number; P_{rw} is Prandtl number in terms of the corresponding heat carrier temperature; and P_{rc} is Prandtl number in terms of the corresponding tube wall temperature.

Determine Reynolds number from the formula

$$\mathrm{Re} = \frac{\upsilon \cdot d}{\nu_w}, \quad (2)$$

where ν_w is coefficient of viscosity (m^2/s).

Coefficient of heat capacity is found from the equation, $W/m^2 \cdot °C$

$$\alpha_2 = \frac{\lambda_w \cdot Nu}{d}, \quad (3)$$

where λ_w is coefficient of heat conductivity ($W/m \cdot °C$).

Coefficient of heat transfer from the hot rocks to a heat carrier is as follows , $W/m \cdot °C$

$$k_l = \frac{1}{\frac{1}{\alpha_2 \cdot d_2} + \frac{1}{2 \cdot \lambda_c} \cdot \ln\left(\frac{d_2}{d_1}\right)}, \quad (4)$$

where k_l is heat amount transferred from the rocks to a heat carrier through 1 l. m. of a pipe in terms of the temperature difference by 1°C; λ_c is heat conductivity of the water wall material, $W/m \cdot °C$.

The amount of heat a heat carrier obtains is as follows

$$Q_w = G \cdot C_p \cdot \Delta t, \quad (5)$$

where G is heat carrier consumption that depends on the internal diameter of a collector and heat carrier velocity in it; C_p is heat capacity of a heat carrier; and Δt is difference of temperatures while heat transferring of 1 l. m. of a pipe.

$$\Delta t = t_2 - t_1, \quad (6)$$

where t_2 is temperature of the hot rocks,°C; t_1 is temperature of a heat carrier,°C.

Results and Discussion

Technological scheme of heat recuperation of the generator-enclosing rocks as well as the heat recuperator design should take into consideration the peculiarities of thermochemical processes occurring in the reaction channel. Developed at the Department of Underground Mining and Education of the Dnipro University of Technology, the preparation method and system of the coal seam development in terms of mines (wings, walls) during WUCG with the utilization of gas generator energy heat (Fig. 1) as well as the technological scheme and the recuperator structure (Fig. 2) meet the abovementioned requirements.

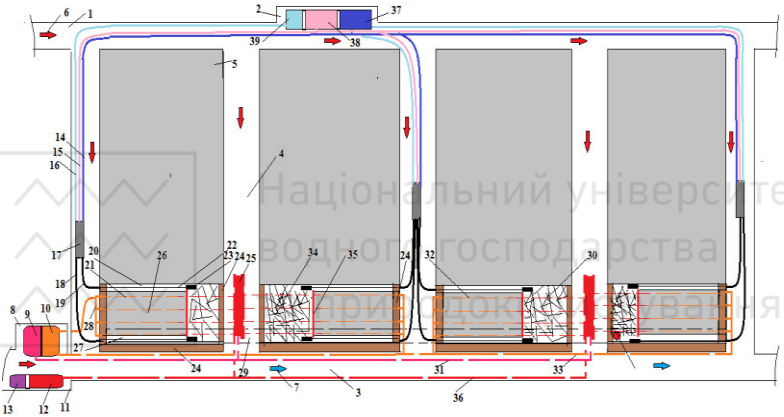

Fig. 1. Scheme of coal seam preparation and development under the mine (block) conditions in terms of WUCG is level-by-level; mining system is longwall mining to the dip; subsystem of the coal seam development being gasified is along the strike: *1* – main haulage roadway; *2* – compressor chamber; *3* – drainage roadway; *4* –ventilation pathway; *5* – extraction pillar; *6* – fresh ventilation flow; *7* – outlet ventilation flow; *8* – heat carrier chamber; *9* – cooling unit of a pump plant of a heat carrier;*10* – supplying unit of a pump plant of a heat carrier; *11* – heat turbine chamber; *12* – turbine unit; *13* – power generator; 14 – rubber air pipeline; 15 – rubber pipeline for the overheated steam; *16* – rubber oxygen pipeline; *17* – site blow mixer (SBM); *18* – flexible metal pipeline for the gas outlet well 27; *19* – flexible metal pipeline; *20* – blow well; *21* – heat recuperator pipeline with a cold heat carrier; *22* – flexible blow pipeline; *23* – perforated nozzle; *24* – heatproof phosphogypsum stopping; *25* – assembled heat recuperator with the carrier and steam separation; *26* –coal pillar being gasified; *28* – network separation of a carrier; *29* – berm of a drainage roadway in the seam floor; *30*, *34* – burned-out space; *31* – pipeline to cool down a heat carrier; *32, 33* – pipelines for a heat carrier; *34* – burned-out space; *35* – fire face of the reaction channel; *36* – steam pipeline; *37* – compressor; *38* – steam generator; *39* – oxygen generator

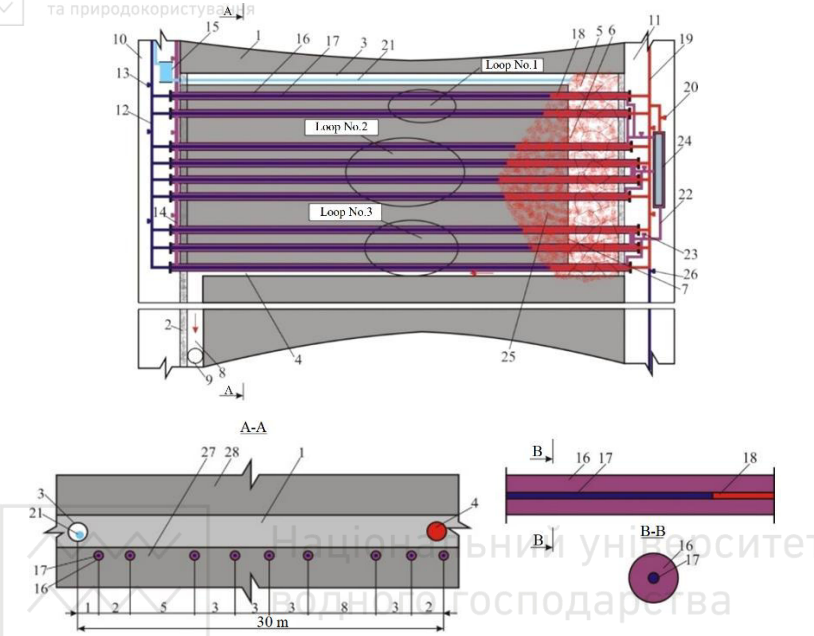

Fig. 2. Technological scheme of a three-loop recuperator of the underground gas generator heat, A-A section, and structure of a "tube in tube" recuperator with the location of Б heat carriers: *1* – coal seam; *2* – thermal insulating stopping; *3* – recuperation element; *4* – gas outlet horizontal well; *5* – burned-out space; *6* – reaction channel of a gas generator; *7* – fire face; *8* – berm of the air-supplying drift; *9* – vertical gas outlet well; *10* – air-supplying drift; *11* – heat-removing drift; *12* – pipeline with a cold heat carrier (water); *13* – controlled water distribution valves; *14* – pipeline with a heat carrier (solution of liquid alkaline metals Na or glycol); *15* – drum for a flexible air-supplying pipeline (d =32 mm); *16* – pipeline (d = 75 – 100 mm) with a heat carrier (Na or glycol); *17* – pipeline (d = 50–75 mm) with a heat carrier, water; *18* – pipeline with steam; *19* – steam pipeline (d=100–120 mm); *20* – controlled steam distribution valves; *21* – flexible air-supplying pipeline; *22* – section of the pipeline with a boiling heat carrier (Na or glycol, T_k=260–620 ºC); *23* – controlled valves for the boiling heat carrier distribution (Na or glycol); *24* – boiler-recuperator of heat; *25* – support zone; *26* – controlled pipelines distributing valves; *27* – roof of the coal seam being gasified; *28* – floor of the coal seam being gasified

According to the proposed measured, the procedure is as follows. Horizontal wells are drilled in the seam floor; three loops of the "tube in tube" system with heat carriers of different thermal and physical properties are mounted into the wells throughout the

reaction channel according to the temperature distribution. That will make it possible to remove residual heat effectively and quickly over the whole area of temperature spread in both gas generator and its enclosing rocks during the gasification process and after the gasification completion while finishing the operations with the obtaining of heat and electric energy within the underground gasification area [0]. Fig. 2 shows the developed technological scheme of a three-loop recuperator of the underground gas generator in terms of A-A section and the structure of a "tube in tube" recuperator with the location of heat carriers.

According to the calculations, 9 inclined (horizontal) wells are drilled throughout the length of the reaction channel (6) in the seam floor at the distance of 0.15-0.2 m from the coal seam from the drift (10) to the drift (11) to the extracti on pillar dip. In those wells, the pipeline (16) (d=75-100 mm) of heat recuperator with a heat carrier (Na or glycol) is mounted; the pipeline (17) of d=50-75 mm, which heat carrier is water, is inserted into the pipeline (16) of d=50-75 mm. On the drift side (10), the pipelines (12, 14) (heat carriers: water, Na or glycol) with the automatically controlled valves of heat carrier distribution (13) are laid towards the pipelines (16) and (17) from the pumps. Within the drift (11), the pipeline (17) of the heat recuperator is connected with the steam pipeline (19), d=100-120 mm; the pipeline (16) is connected with the boiler-recuperator of heat (24) from the boiling heat carrier (Na or glycol). The steam pipeline (19) is mounted towards the steam power plant to generate thermal and electric energy.

The analysis of the carried-out experimental studies within the gasified share of the underground gas generator has shown that the rock heating up to 50 ºC accounts for 62.8%, up to 100 ºC – 39%, up to 400 ºC - 17.5%, and up to 900 ºC – 6.9%. In its turn, the analysis of stand studies within the mass of temperature distribution has demonstrated that heating up to 50 ºC accounts for 36.2%; up to 400ºC - 11.4%, and up to 900 ºC – 4.4%, and distribution of temperatures in terms of WUCG along the rock stratification is by 1.4 times less than perpendicularly to the stratification [0, 0]. The studies [0, 0] have helped define that the development and stabilization of a thermochemical process of the coal seam processing (1) in the reaction channel (6) is accompanied with the temperature distribution with the formation of a temperature field around it within the rocks (Fig. 3, 4).

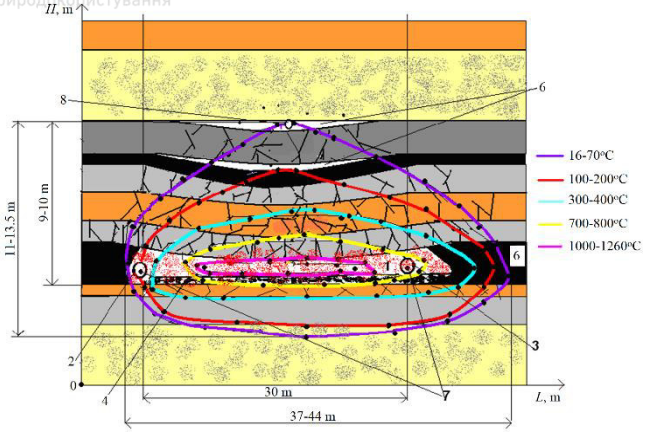

Fig. 3. Parameters of the rock coal mass heating across the stratification: *1* – reaction channel of the underground gas generator; *2* – blow inclined-horizontal well; *3* – gas outlet inclined-horizontal well; *4* – ash residue; *5* – cavity of the roof rocks stratification; *6* – coal seam; *7* – flexible pipeline; *8* – stowing pipeline

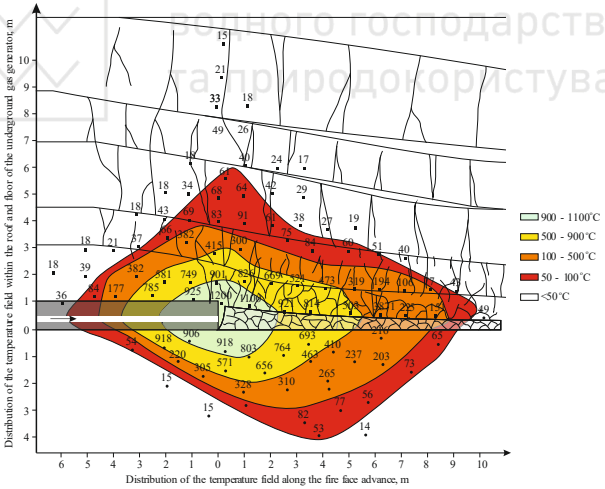

Fig. 4. Parameters of the temperature field distribution within the rocks while coal seam gasifying

According to the analysis of the experimental underground gas generators as well as laboratory, and stand studies, a graph of rock heating within the support zone within the affected area of the

underground gas generator has been developed (Fig. 5). Taking into consideration a heat flow, average coefficient of heat transfer from gas to rocks has been identified - K_n=78.2 kJ/m^{2}hour ºC. If we consider Joule Thomson effect of the rock mass enclosing the underground gas generator, then the coefficient will be K_n=43.5 kJ/hour ºC. Table 1 shows the obtained profiles of temperatures and pressures in the fire channel of the underground gas generator depending on its length.

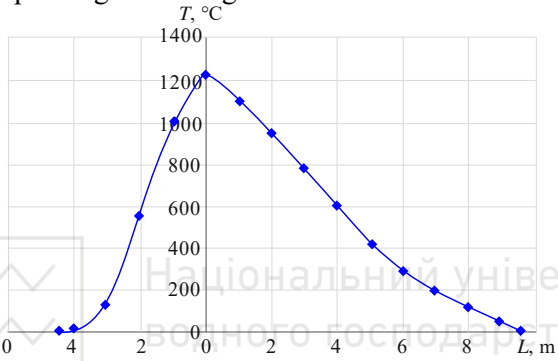

Fig. 5. Rock heating within the support zone and the affected area of the underground gas generator

Table 1

Calculation profile of the temperatures and pressures along the fire channel length

Length of the fire channel, m	Temperature profile throughout the fire channel, ºC			Pressure throughout the fire channel, MPa
	25 m	30 m	60 m	
0	200	200	200	0.60
5	565	518	505	0.58
10	882	740	610	0.57
15	1180	809	770	0.54
20	864	1240	967	0.59
25	697	911	1190	0.60
30	–	589	1007	0.60
35	–	–	926	0.54
40	–	–	819	0.54
45	–	–	755	0.57
50	–	–	641	0.57
55	–	–	537	0.58
60	–	–	459	0.58

The experiments have made is possible to specify that the temperature value of the coal seam gasification varies throughout the reaction channel (6) length. The temperature maximums (1100–1300 ºC) are observed with the transition of the oxidation zone into the reduction one (Fig. 6).

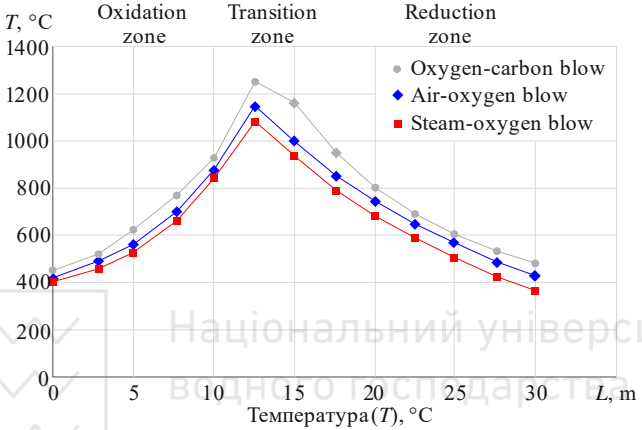

Fig. 6. Parameters of temperature distribution in the fire channel of the underground gas generator

Thus, the rocks above the fire face are subject to different thermal loading. The same situation is observed within the burned-out space. Along with the coal seam gasification and fire face advance (7), roof rocks (27) are collapsing under the effect of rock pressure and rock temperatures with the formation of a burned-out space of the gas generator. Heat and gasification products leave the gas generator through the well (4) and vertical gas outlet well (9); and a heat share (up to 30-49 %) is accumulated within the rocks enclosing the gas generator (see Fig. 2.).

The heat accumulated from the rocks within the support zone (25), fire face (7), burned-out space (5), and seam floor (28) is taken by the heat “tube in tube” recuperator according to the loop scheme and parameters of the temperature field formation in the underground gas generator involving a heat carrier with different thermophysical

properties, which provides efficiency and stability of the heat recuperation functioning irrespective of changes in heat and material balance of the processes as well as geomechanical parameters of the rock thickness enclosing the gas generator [0, 0].

The external pipeline (16) with a heat carrier (solutions of liquid metals Na, Na-K or glycol) with boiling temperature T_k=260–620 ºC transfers the heat obtained from the gas generator rocks to the external pipeline into a heat carrier (water) at the velocity of 0.1 – 0.15 m/s. Having entered the zone of temperatures being more than 100 ºC in the steam pipeline (18), water transforms into the overheated steam (loop 1 - T_1=160–190ºC with P_1=0.3-0.8MPa pressure; loop 2 - T_2=250-340 ºC with P_2=1.5-2.7

MPa pressure; and loop 3 - T_3=180-260ºC with P_3=1.1-2.2 MPa pressure) and sent further through the steam pipeline (19), equipped with the controlled steam distribution valves (20), onto the steam turbine with T=230–280ºC steam parameters with P=1.8–2.3 MPa pressure. In terms of the external heat carrier boiling with the section (22) of the pipeline (16) that can occur depending on the temperature indices in the underground gas generator within loop 2, a boiling heat carrier is discharged into the external case of the boiler-recuperator, where the internal case contains water, which transforms into steam under the temperature action and, being of T=150–260 ºC temperature and P=0.8–1.8 MPa pressure, goes into the steam pipeline (23) with the help of the controlled valves.

The heat balance equation helps determine the heat carrier velocity in the pipeline for different technological parameters: pipe diameters, heat carrier temperature in the collector pipeline at the outlet from the combustion zone, value of the combustion zone [0, 0].

The proposed method will help do the following: remove the residual heat effectively and rapidly throughout the whole area of temperature spread within the underground gas generator during the coal seam gasification as well as on the completion of the

gasification process while finishing the operations, obtaining heat and electric energy within the underground gasification area; conduct effectively the coal seam gasification under conditions of technogenic disturbance of the mass; and provide economic expediency of the gasification of low-thickness coal seams [0].

Solution of those problems requires a complex approach, which is completely in compliance with the concept of the development of WUCG technological schemes under the mine conditions elaborated in the Dnipro University of Technology at the Department of Underground Mining (Fig. 7).

a

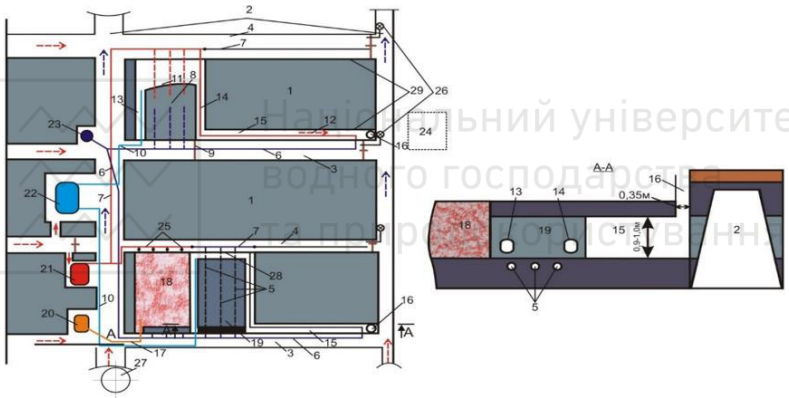

b

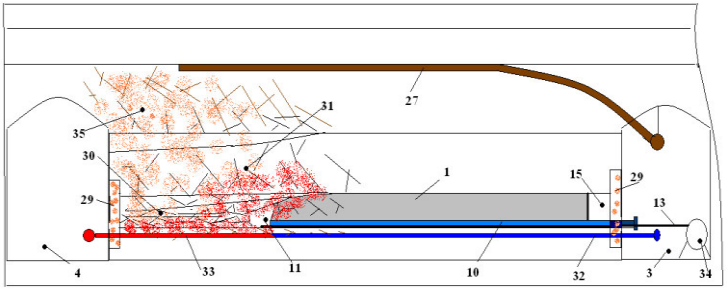

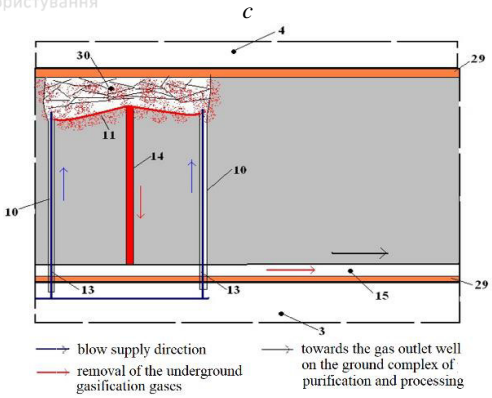

Fig. 7. Technological scheme of a mobile-modular energochemical enterprise on the basis of an operating mine while mining unbalanced coal reserves: (*a*) – top view; (*b*) – cross section of a gas generator; (*c*) – gasification of the extraction pillar by jointed gas generators (L_c = length of reaction channels being 30, 20, and 25 m); *1* –extraction pillars outlined along the strike and to the dip by the development workings; *2* – air-supplying pathway; *3* – blow drift; *4* – air drift; *5* – wells with the pipes mounted inside to supply heat carrier into the active zone; *6* – main pipeline with the heat carrier; *7* – main pipeline; *8* – sites of workings neighbouring the operating gas generator; *9* – sealed stoppings; *10* – pipeline from the compressor complex to the blow well; *11* – fire channel; *12* – gasification products; *13* – blow horizontal well; *14* – horizontal gas outlet well; *15* – berm of the blow drift; *16* – vertical gas outlet well connected with the ground complex; *17* – perforated stowing pipeline; *18* – sites of the underground workings of the extinguishing gas generator; *19* – module-gas generator; *20* – stowing complex; *21* – heat turbines; *22* – compressor complex; 23 – active zone of the heat carrier; *24* – ground complex; *25* – drift pipeline towards the turbine; *26* – pipeline of the ventilation pathway; *27* – stowing well; *28* – berm of the air drift; *29* – phosphogypsum boundary line; *30* – burned-out space; 31 – deformed roof rocks; *32* – tube recuperator with a cold heat carrier; *33* – tube recuperator with an overheated heat carrier (steam); *34* – hoisting unit for the flexible blow pipeline; *35* – stowing injection mass

Preparation of the underground gas generator involves cutting of three extraction pillars along the strike within the mine field with the modular gas generator mining to the rise (to the dip) with the utilization of heat energy of the gasification products and hot rocks, enclosing the gas generator, under the mine conditions.

The mine field area is divided into three pillars (1) outlined along the strike and to the dip by the development workings, air-supplying pathways (2), blow (3) and air (4) drifts. The extraction pillar length

is $L_{пр}$=200-400 m; its depth to the dip (rise) is $L_{п(в)}$=100 m. Chambers of heat turbines (21) and compressor complex (22) are formed within the opposite part of the extraction pillar (Fig, 7).

To remove heat from the gasification products and hot rocks, wells are drilled in the seam floor (vertical and horizontal wells – along the coal seam); then the "tube in tube" recuperators (5) with different design features and heat carriers are installed in them. That will favour uniform heat removal from the rocks taking into account nonuniformity of temperature distribution in the gas generator. Heat carrier supply into the active zone (6, 23) is performed from the blow drift (3) where the main pipeline with a heat carrier (6) is located.

Passing through the pipes (5), a heat carrier transforms into steam and travels under pressure along the main pipeline (7) located on the air drift (4) to the heat turbine (21) for electric power generation.

Flow velocity of the heat carrier in the pipes of a rock heat recuperator of the underground gas generator is 0.05-0.1 m/s depending on the stage of gas generator operation, heat capacity, heat conductivity of the floor rocks, and temperature of the UCG products.

Length of the modular gas generator is taken basing on the seam thickness and capacities of drilling facilities. Distance between the wells is determined depending on the seam thickness, geomechanical indices, hydrogeological conditions, and technological parameters of the underground gasification processes.

Further, the reaction zone is formed. A coal seam is ignited from the berm of the air drift (28) by means of hot coke and supply of the oxygen-enriched blow or with the help of binary charges on the connection with the blow well (10).

The advance pillar gasification is performed by supplying blow mixture from the blow drift (3) through the blow pipeline (10) from the compressor complex (22) into the blow horizontal well (13) of 290-250 mm diameter and further on the fire channel (11) being $l_{о.з}$=20-40 m long. Next, along with the passing of oxidation and reduction zones, gasification products (12) travel into the horizontal gas outlet well (14) with the diameter of 290-350 mm and, along the blow drift berm (15) - into the vertical gas outlet well (16) connected

with the ground complex (24) for purification and processing of gasification products for producing electric energy and chemical raw material.

Not less than two modular gas generators are under the operation. The mine field is developed in terms of a pillar, which provides safe operation of ventilation and modular gas generators.

Sites of the mine workings adjoining the operating and extinguishing gas generators (8, 18, 26) are isolated by the sealed stoppings (9); ventilation is forced with the help of fans of local ventilation (26) with warm air outburst into the air-supplying pathway (2).

On the completion of operations, the mixture is kept to be injected into the mined-out space of a modular generator through the blow well. Stowing operations are carried out along with the fire face advancing of the modular generator by injecting a mixture into the deformed thickness of the roof rocks and into the worked-out space. During the coal seam gasification, injection of the deformed roof rocks is performed along the stowing well (27) located above the coal seam.

After the pillar gasifying, there should be the operations for gas generator extinguishing related to the stowing of the burned-out space (18). Stowing material is prepared and supplied from the stowing complex (20) with the help of the perforated pipeline (17) laid within the blow well. Residual heat of the rock mass is removed by means of tube recuperators (25) and sent onto the heat turbine in the form of water steam.

During those operations, a module-generator (19) located in other extraction pillar is put into operation; when the operations in the gas-generator (19) are over, a gas generator in the first extraction pillar starts its operation. Tables 2 and 3 show the indices and technological parameters of the underground gasification of a gas coal seam under the mine conditions.

Table 2

WUCG parameters in terms of different blow type

Blow type	Blow composition, %			Composition of the outgoing gases, %							Q, MJ/m^3
	O_2	CO_2	steam	H_2	CH_4	C	N_2	H_2S	CO_2	O_2	
O_2N_2	23	–	–	9.1	6.0	18.4	55.8	0.35	9.3	1.2	5.3
O_2N_2	66	–	–	18.7	10.2	30.7	20.4	0.8	16.0	3.2	9.5
O_2N_2	61	–	–	16.5	12.4	33.8	20.0	0.7	14.1	2.5	9.6
H_2O+O_2	23	–	8.0	8.1	6.1	21.4	52.5	0.5	10.0	1.4	5.8
H_2O+O_2	56	–	19.5	15.3	10.6	37.4	8.2	1.3	23.2	4.0	10.2
	53	–	30.6	11.6	10.4	38.6	7.3	1.0	27.2	3.9	11.2
CO_2+O_2	54	42.0	–	16.5	10.1	49.6	1.3	1.3	17.8	3.4	10.8
	50	30.7	–	15.7	9.4	45.8	2.1	1.1	22.5	3.4	9.9
	50	38.5	–	15.8	9.8	49.4	2.1	1.2	18.3	3.4	11.5
CO_2+C_2+	52	34.4	15.4	16.5	11.5	47.6	2.9	0.9	17.3	3.3	11.0
$+H_2O$	44	36.9	11.0	16.0	9.5	50.3	2.6	0.9	17.5	3.2	10.7

Table 3

Technological parameters of the gasification process

Pressure in the fire channel, P, MPa	Tempe-rature of the process, T, ºC	Temperature of gases in the vertical well, T_z, ºC	Advance rate of the fire face, m/day	Adherence to the parity of the oxidation and reduction zones	Heat capacity of a gas generator, Gcal/hour	Electric capacity of a gas generator, kW/hour
1.6–3.0	1050–1250	350–6000	0.5–2.2	0.3–0.7 0.4–0.6	5–8	5760–9280

Generator gas and condensate are purified and processed in terms of the surface complex with the obtaining of electric energy and chemical raw material with the immediate utilization of the residual gasification products heat.

Taking into consideration that the coefficient of efficiency of the recuperation plants is η=53–62% and applying the commonly known principles of transferring the spatial power into the time power, calculation heat power of the loop-based recuperation of the rocks enclosing the underground gas generator will be 4.6–8.5 Gcal/hour, corresponding to 5336–9860 kW/hour.

Conclusions

The WUCG-based energy-chemical complex is a mobile module-type enterprise providing intense increment of productivity, quality, and diversity of the products of organic fuel gasification. It helps

reorient dynamically and losslessly the end-product output in the form of thermal and electric power, chemical substances, and products owing to flexibility of technological parameters and taking into consideration the conditions of dynamic changes in a mining and geotechnical situation.

Profitability and efficiency of WUCG-based energy-chemical complex are obvious as we can observe the following: growing prices for oil, gas, and coal due to the costs for extraction, transportation, processing, environmental protection, and depletion of balanced reserves of energy raw material.

The calculated heat power of the loop-based rock heat recuperation will be 4.6-8.5 Gcal/hour (5336-9860 kW/hour) with the efficiency of 53-62%. A period of the effective operation of the recuperator is from 2.2 up to 4.6 years.

References

1. **Df Maev, S., Blinderman, M.S., & Gruber, G.P.** (2018). Underground coal gasification (UCG) to products: Designs, efficiencies, and economics. Underground Coal Gasification and Combustion, 435–468. https://doi.org/10.1016/b978-0-08-100313-8.00013-x

2. **Wang, G.X., Wang, Z.T., Feng, B., Rudolph, V., & Jiao, J.L.** (2009). Semi-industrial tests on enhanced underground coal gasification at Zhong-Liang-Shan coal mine. Asia-Pacific Journal of Chemical Engineering, 4(5), 771–779. https://doi.org/10.1002/apj.337

3. **Tabachenko, M.** (2016). Substantiating parameters of stratification cavities formation in the roof rocks during underground coal gasification. Mining of Mineral Deposits, 10(1), 16-24. https://doi.org/10.15407/mining10.01.016

4. **Khan, M. S., Zhu, Z., Huang, Q., Bai, Y., & Sun, L.** (2019). Thermal hydraulic analysis of concentric recuperator of DRAGON-V loop. Fusion Engineering and Design, 142, 13-19. https://doi.org/10.1016/j.fusengdes.2019.04.042

5. **Kim, I.H., & No, H.C**. (2011). Thermal hydraulic performance analysis of a printed circuit heat exchanger using a helium–water test loop and numerical simulations. Applied Thermal Engineering, 31(17-18), 4064–4073. https://doi.org/10.1016/j.applthermaleng.2011.08.012

6. **Petlovanyi, M., Lozynskyi, V., Saik, P., & Sai, K**. (2019). Predicting the producing well stability in the place of its curving at the underground coal seams gasification. E3S Web of Conferences, (123), 01019. https://doi.org/10.1051/e3sconf/201912301019

7. **Kovalevska, I., Samusia, V., Kolosov, D., Snihur, V., & Pysmenkova, T.** (2020). Stability of the overworked slightly metamorphosed massif around mine working. Mining of Mineral Deposits, 14(2), 43–52.

8. **Dychkovskyi, R., Falshtynskyi, V., Lozynskyi, V., & Saik, P. (**2015). Development the concept of borehole underground coal gasification technology in Ukraine. New Developments in Mining Engineering 2015: Theoretical and Practical Solutions of Mineral Resources Mining, 91-95. https://doi.org/10.1201/b19901-18

9. **Lozynskyi, V.G., Dychkovskyi, R.O., Falshtynskyi, V.S., Saik, P.B., & Malanchuk Ye.Z.** (2015). Experimental study of the influence of crossing the disjunctive geological fault on thermal regime of underground gasifier. Naukovyi Visnyk Natsionalnoho Hirnychoho Universytetu, (5), 21-29.

10. **Saik, P., Falshtynskyi, V., Dychkovskyi, R., & Lozynskyi, V.** (2015). Revisiting the preservation of uniformity advance of combustible face. Mining of Mineral Deposits, 9(4), 487-492. https://doi.org/10.15407/mining09.04.487

11. **Saik, P.B., Dychkovskyi, R.O., Lozynskyi, V.G., Malanchuk, Z.R, & Malanchuk Ye.Z.** (2016). Revisiting the underground gasification of coal reserves from contiguous seams. Naukovyi Visnyk Natsionalnoho Hirnychoho Universytetu, (6), 60-66.

12. **Blinderman, M.S., & Klimenko, A.Y.** (2018). Introduction to underground coal gasification and combustion. Underground Coal Gasification and Combustion, 1-8. https://doi.org/10.1016/b978-0-08-100313-8.00001-3

13. **Klimenko, A.Y.** (2018). Early developments and inventions in underground coal gasification. Underground Coal Gasification and Combustion, 11-24. https://doi.org/10.1016/b978-0-08-100313-8.00002-5

14. **Otto, C., & Kempka, T.** (2020). Synthesis Gas Composition Prediction for Underground Coal Gasification Using a Thermochemical Equilibrium Modeling Approach. Energies, 13(5), 1171. https://doi.org/10.3390/en13051171

15. **Rosen, M.A., Reddy, B.V., & Self, S.J.** (2018). Underground coal gasification (UCG) modeling and analysis. Underground Coal Gasification and Combustion, 329-362. https://doi.org/10.1016/b978-0-08-100313-8.00011-6

16. **Sutardi, T., Paul, M.C., & Karimi, N.** (2019). Investigation of coal particle gasification processes with application leading to underground coal gasification. Fuel, (237), 1186–1202. https://doi.org/10.1016/j.fuel.2018.10.058

17. **Bondarenko, V., Lozynskyi, V., Sai, K., & Anikushyna, K.** (2015). An overview and prospectives of practical application of the biomass gasification technology in Ukraine. New Developments in Mining Engineering 2015: Theoretical and Practical Solutions of Mineral Resources Mining, 27-32. https://doi.org/10.1201/b19901-6

18. **Dychkovskyi, R., Avdiushchenko, A., & Lozynskyi, V.** (2017). Some Economic Indicators of Coal Mining from Thin Seams. Advanced Engineering Forum, 22, 13-20. https://doi.org/10.4028/www.scientific.net/aef.22.13

19. **Lozynskyi, V.H., Dychkovskyi, R.O., Falshtynskyi, V.S., & Saik, P.B.** (2015). Revisiting possibility to cross disjunctive geological faults by underground gasifier. Naukovyi Visnyk Natsionalnoho Hirnychoho Universytetu, (4), 22-27.

20. **Saik, P., Petlevanyi, M., Lozynskyi, V., Sai, K., & Merzlikin, A.** (2018). Innovative approach to the integrated use of energy resources of underground coal gasification. Solid State Phenomena, (277), 221-231. https://doi.org/10.4028/www.scientific.net/SSP.277.221

21. **Tabachenko, M.** (2016). Features of setting up a complex, combined and zero-waste gasifier plant. Mining of Mineral Deposits, 10(3), 37-45. http://dx.doi.org/10.15407/mining10.03.037

22. **Falshtynskyi, V., Saik, P., Lozynskyi, V., Dychkovskyi, R., & Petlovanyi, M.** (2018). Innovative aspects of underground coal gasification technology in mine conditions. Mining of Mineral Deposits, 12(2), 68-75. https://doi.org/10.15407/mining12.02.068

23. **Falshtyns'kyy, V., Dychkovs'kyy, R., Lozyns'kyy, V., & Saik, P.** (2013). Justification of the gasification channel length in underground gas generator. Mining of Mineral Deposits, 125-132. https://doi.org/10.1201/b16354-23

24. **Falshtynskyi, V., Dychkovskyi, R., Lozynskyi, V., & Saik, P.** (2015). Analytical, laboratory and bench test researches of underground coal gasification technology in National Mining University. New Developments in Mining Engineering 2015: Theoretical and Practical Solutions of Mineral Resources Mining, 97-106. https://doi.org/10.1201/b19901-19

25. **Falshtynskyi, V.S., Dychkovskyi, R.O., Lozynskyi, V.G., & Saik, P.B.** Some aspects of technological processes control of an in-situ gasifier during coal seam gasification. Progressive technologies of coal, coalbed methane, and ores mining, 109-112. https://doi.org/doi:10.1201/b17547-20

26. **Falsztinskij, W., Diczkowskij, E., & Łozinskij, W.** (2010). Ekonomiczne uzasadnienie celowości doszczelniania skał stropowych nad obszarem podziemnego zgazowania węgla metodą otworów wiertniczych. Prace Naukowe GIG. Górnictwo i Środowisko/Główny Instytut Górnictwa, (3), 51-59.

27. **Dychkovskyi, R.O., Lozynskyi, V.H., Saik, P.B., Petlovanyi, M.V., Malanchuk, Ye.Z., & Malanchuk, Z.R.** (2018). Modeling of the disjunctive geological fault influence on the exploitation wells stability during underground coal gasification. Archives of Civil and Mechanical Engineering, 18(4), 1183-1197. https://doi.org/10.1016/j.acme.2018.01.012

28. **Lozynskyi, V., Saik, P., Petlovanyi, M., Sai, K., Malanchuk Z., & Malanchyk, Ye**. (2018). Substantiation into mass and heat balance for underground coal gasification in faulting zones. Inzynieria Mineralna, 19(2), 289-300. http://doi.org/10.29227/IM-2018-02-36

29. **Falshtynskyi, V.S., Dychkovskyi, R.O., Lozynskyi, V.G., & Saik, P.B.** (2013). Determination of the Technological Parameters of Borehole Underground Coal Gasification for Thin Coal Seams. Journal of Sustainable Mining, 12(3), 8-16. https://doi.org/10.7424/jsm130302

https://doi.org/10.31713/m1018

STRUCTURAL BONDS DEVELOPMENT IN THE BACKFILL MASS WHEN CHANGING THE DISPERSION OF THE BINDING MATERIAL

Petlovanyi M.V.
Candidate of Technical Sciences, Associate Professor,
Dnipro University of Technology, Ukraine

Zubko S.A.
Candidate of Technical Sciences, PJSC "Zaporizhzhia Iron Ore Plant", Ukraine

Sai K.S.
Candidate of Technical Sciences, Associate Professor,
Dnipro University of Technology, Ukraine

Khalymendyk O.V.
Candidate of Technical Sciences, Associate Professor,
Dnipro University of Technology, Ukraine

Abstract

Purpose. Theoretical and experimental research on the structural and strength peculiarities of the backfill mass formation during the ore deposits development by activating the binding material of the backfill mixture using fine grinding at the stage of its preparation.

Methods. An integrated methodological approach is used, consisting of laboratory studies on determining the properties of backfill mixtures and the structural internal bonds of the backfill mass using scanning electron microscopy. Some laws of the binding material chemistry are used and systematized in the course of theoretical research.

Findings. Based on theoretical and experimental research, the interaction and the hydration products of the backfill mixture binding components with water have been studied. The use of a finely ground combined binding material made of slags and limestone improves and strengthens the structural bonds of the backfill mass through a large gap in the covalent bonds of silica and slags, the transition of ions of a weak ionic bond to the formation of other compounds and equalizing the ratio of Si and Ca ions in solution.

Originality. It has been determined that with an increase in the specific surface area of the binding material particles, the shape of structural new formations of the backfill mass improves, has high strength, and the basicity of its new formations increases.

Practical implications. Using the results, it is possible to rationally choose the binding material dispersion, obtain high strength of the backfill mass and increase the stability of its outcropping.

Keywords: structural bonds, backfill mass, strength, binding material, fine grinding.

1. Introduction

Iron-ore industry occupies an important place in the development of Ukrainian economy, providing substantial foreign exchange earnings to the state budget. Thus, according to the State Fiscal Service of Ukraine, the export of iron-ore raw materials and concentrate in 2019 amounted to $ 3.18 million [1, 2]. About 130 million tons of iron ore are mined in Ukraine annually, of which 90% is mined by open-cut mining, and 10% - by underground mining [3, 4].

Intensive iron ore mining leads to considerable changes in the environment: significant cavities are formed in the rock mass, leading to the daylight surface deformations; the natural regime of ground and surface waters is disturbed; storage of waste from the mining industry and iron-ore beneficiation occupies valuable agricultural land and is a source of their pollution. About 15 million tons of iron ore are mined by underground system of mining in 9 mines, and only 1 mine uses a highly advanced, environmentally friendly technology for the extraction of iron ore with hardening backfilling [5-9].

To prevent the consequences of engineering activity for the extraction of iron ores, the implementation of work should be provided on filling the cavities with backfill mixtures consisting of various rocks, industrial processing waste, which eventually is changed into a solid state under the influence of various factors. This is performed in the case when it is necessary to completely extract iron ores due to their high value (content of Fe>60%), and the earth's surface must be prevented from deformation.

Creating a sufficiently strong artificial mass, as close as possible to the natural strength properties of the rocks surrounding the cavity, is possible using the internal chemical transformation of the backfill mixture minerals [10]. It is important to form structural bonds in the volume of an artificially created mass to resist outcropping as a result of mining operations under the influence of impulse loads in the form of blasting operations or a stationary load from the gravitational forces of the surrounding natural rock mass. Under the influence of the forces of rock pressure and seismic loads from blasting operations, both compression and tensile stresses arise on the contour of the mined-out chamber, depending on its configuration. In this

regard, the internal structural bonds of the backfill mass must be resistant to the indicated types of stresses, especially tensile stresses, since, as for the backfilling mass, they amount to 0.05-0.1 σ_{compr} [11, 12].

Therefore, the issues of creating a strong backfill mass with internal bonds that are resistant to loads are relevant for mining enterprises that perform backfilling the underground cavities with hardening mixtures. One of the methods of significant chemical transformation and activation of hydration processes in the backfill mixture is fine grinding of the binding material, which, despite its increased energy consumption, can be cost-effective [13-15]. Moreover, some components of the backfill mixture, except for the main binding material, may have potential binding properties, improving the structure and strength of the artificial mass.

The actual influences of finely ground particles of a binding material on the properties of backfill mass are studied in this work.

2. Purpose and objectives of research

The purpose of this work is to study and identify the structural and strength peculiarities of the backfill mass formation when the binding material of the backfill mixture is activated by fine grinding.

To achieve the purpose set, the following research objectives are solved:

– preparing the test backfill mixtures with traditional and increased dispersion of the binding material;

– studying the transformation of the internal chemical bonds structure influenced by the dispersion of binding material.

3. Materials and methods of research

An integrated research method, consisting of two blocks, is used in the work: a set of laboratory studies to determine the properties of backfill mixtures, as well as physical-chemical studies of structural bonds. Some laws of the binding material chemistry are used and systematized in the course of theoretical research. This paper studies the composition of the hardening backfill mixture, which is used in the development of the Pivdenno-Bilozerske field and recommended by the Scientific-Research Mining Institute (Kryvyi Rih).

To prepare the backfill mixture, ground granulated blast-furnace slag (17%) is used as a binding material, crushed dump rocks (22%), flux limestone waste (44%) and water (17%) serve as an inert

filler [16]. Before mixing the components, granulated blast-furnace slags are ground in Ball Mills to at least 55-60% of particles with a coarseness of -0.074 mm, which is equivalent to a specific surface area of 2000 cm^2/g. This component composition has not been studied at different values of the specific surface area of the binding material. We have revealed [17] that it is expedient to jointly grind slag and flux limestone, when preparing the binding material of the backfill mixture. Moreover, the rational amount of limestone is up to 50%. Therefore, a combined binding material is considered in further research. The research objective is to study the changes in structure and strength with a 2-fold increase in the specific surface area of particles. Therefore, the backfill mass at 2000 and 4000 cm^2/g is compared.

To achieve the value of specific surface area of blast-furnace slag and flux limestone particles 4000 cm^2/g, a laboratory gas-jet unit USI-20 is used (Fig. 1). The specific surface area of particles is determined with the help of the Tovarov device. The fraction of particles fed into the gas-jet mill should be no more than 2.5 mm, therefore, using a laboratory sieve, the material is sifted through sieves of -2.5 mm.

a *b*

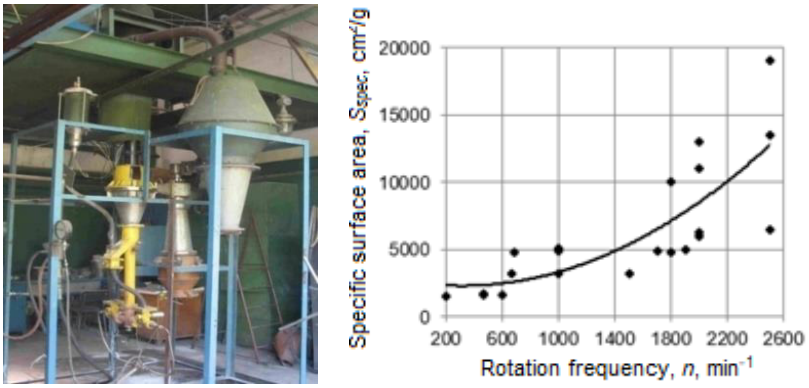

Fig. 1. Laboratory research on grinding the binding material:
(*a*) general view of the gas-jet unit USI-20; (*b*) dependence of the specific surface area on the frequency of the jet mill rotation

According to the empirical dependence [18], shown in Figure 1b, the required rotation frequency of the jet mill classifier is determined to obtain the required specific surface area. To conduct experimental research, the design basis conditions of grinding the slag and flux are given in Table 1.

Table 1

Design basis conditions of grinding the slag and limestone in a laboratory gas-jet mill

Set of tests	Material	P, MPa	n, min^{-1}	S_{spec}, cm^2/g
1	slag	0.3	1200	4000
2	limestone	0.3	1200	

Before conducting research, it is necessary to prepare the initial (traditional) backfill mixture with the specific surface area of the binding material particles, which is used in the backfilling technology. For this purpose, granulated blast-furnace slag is ground in a laboratory Ball Mill to a fineness of 55% of particles with a coarseness of 0.074 mm, which corresponds to the fineness of grinding in production mills of the backfilling complex and is also equivalent to a specific surface area of 2000 cm^2/g.

Backfill mixtures are prepared: No.1 (at S_{spec}=2000 cm^2/g), № 2 (at S_{spec}=4300 cm^2/g), and 12 samples of the hardening backfill mixture are poured in for strength testing at the hardening age of 30 and 90 days, 3 samples for each period of hardening. In the test compositions of the hardening backfill mixture, 50% of the blast-furnace slag is replaced with ground flux waste of similar dispersion.

The test backfill mixtures are prepared beginning with the calculation of the components consumption for a 9-liter container, sufficient for filling 6 cubes-samples of the backfill material per one composition. Using one mixed composition, the backfill mixture samples are made for strength testing at the age of 30, 90 and 180 days (selectively). First, crushed rock is added to the container, then – waste of flux with blast-furnace slag, and all is mixed in dry form. Then the dry mixture is tempered with water and mixed for 10 minutes. After mixing, the backfill mixtures are examined for adhesion, mobility, ultimate shearing stress.

The mixture mobility is determined using a StroyTSNIL cone device. The depth of the cone immersion in the backfill mixture is

measured. The amount of water is added to the container with dry components according to the water flow rate (350-400 l/m^3), so that the mobility is in the range 10-12 cm. The shearing stress value is determined by the Sternbek device. The effort of the moment is recorded when the pipeline section begins to displace relative to the mixture. The shearing stress value of the mixture should be no more than 1.96 MPa. The velocity of setting the mixture is determined using the Vicat apparatus. The depth of the needle immersion in the backfill mixture is measured (cm). Setting of the backfill mixture should happen no earlier than after 4 hours.

After determining the technological parameters, each composition of the backfill mixture is poured into metal moulds with size of 10×10×10 cm. The cassettes with the moulds are lubricated with technical oil in order to prevent the backfill mixture adhesion to the metal mould surface. In a day, the surfaces of the backfill mixture samples of each composition are numbered. The hardening backfill mixture is settled in the moulds for 3-4 days until complete loss of setting and complete drainage of water from the sample. Then, the moulds are dismantled, and backfill mixture samples are placed in special storage racks. The samples are placed in wet wood dust with a moisture content of about 90% and a temperature of 22-26 ºC to simulate underground conditions.

The uniaxial compression strength of the hardening backfill mixture is determined by crushing the samples in a hydraulic press at ambient temperature. The backfill mixture samples should be loaded in the press with a rate of 0.3-0.5 MPa. A press of the PSU-100 series with a strength scale of up to 10 MPa is used. And in the case, when the strength of the backfill mixture exceeds the specified value, a press of PSU-120 series of up to 50 MPa should be used. The following data are recorded: sample number; cross-sectional area S (cm), measured by vernier calliper; breaking force value F(H), which is fixed on the press scale. The sample strength is determined by dividing the breaking force value by the sample area.

The microstructure, as well as the phase and quantitative composition of the components of hardening backfill mixture and artificial stone are studied using scanning electron microscopy [19]. Using an electron microscope-microanalyzer REMMA-102-02, it becomes possible to obtain high-quality photographs of the shape of

the studied samples structure at a magnification of 50 μm (Fig. 2*a*). The built-in X-ray spectral microanalyzer makes it possible to measure the chemical composition of the hardening backfill mixture structural formations. The studied fracture surface of the hardening backfill sample is shown in Figure 2*b*.

a *b*

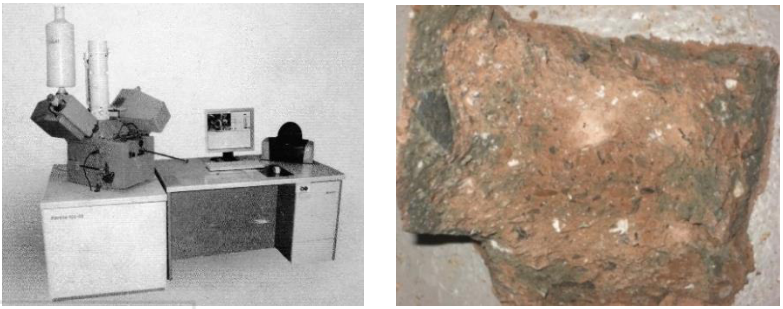

Fig. 2. Research into backfill mass microstructure: (*a*) general view of the microscope-microanalyzer REMMA-102-02; (*b*) fracture surface of the backfill mass sample

The shapes and sizes of the sample particles are studied, as well as the intergranular bonds formed during the backfill material hardening. Using the X-ray spectral microanalyzer, from 1 to 5 measurements of the quantitative composition of basic oxides CaO, SiO_2, MgO, Al_2O_3, are performed in each sample. The procedure of measuring the chemical composition consists in examining the entire field of particles in the image to detect particle of a substance with different chemical composition or oxide content.

As a result of measurements, the oxide spectra are obtained, then the microscope software calculates these spectra and displays the percentage of oxides on the computer. The method is based on the determination of the electronic image contrasts by electron diffraction.

4. Main part

4.1. Theoretical foundations of the strong hardening backfill mass formation based on the fine-dispersed particles

For a reasonable choice of the hardening high-strength backfill composition when mining the reserves of iron ores, it is necessary to

study the processes of chemical bonds structure formation under the influence of fine-dispersed fractions of a binding material. Therefore, the backfill material chemical composition is of significant importance, which either creates stable, strong bonds in the artificial mass or weakens them.

Crystallized blast-furnace slags, containing up to 4-6% MgO and up to 5-10% Al_2O_3, usually possess dicalcium silicate, rankinite and melilite with a predominant content of the helenite component. Slags are generally composed of 90% glass. In the crystalline form, the slags are not reactive, however, in the non-crystalline form, the ability to hydration is observed [20]. Blast-furnace granulated slag of the PJSC "ZaporizhzhiaStal", is in a glassy state caused by rapid cooling. It contains melilite and pseudowollastonite [21].

The main phase of the flux limestone chemical composition with a high content of CaO and low MgO is calcite, there are impurities of dolomite and wollastonite. The host rocks of the Pivdenno-Bilozerske ore field are mainly represented by quartz-chlorite-sericite shales, which are delivered to dumps. Their chemical composition contains a whole group of minerals of the mica class. At a content of 25-30% iron, hematite is present in the composition of the rocks. Hydration of backfill material minerals complies with the general laws of mineral substances hardening, the strength of which depends on the formed chemical compounds, their composition and form.

Let us study the products of hydration in the backfill mass with the fineness of binding material grinding of 55% of particles with a coarseness of -0.074 mm. Slag minerals begin to exert binding properties during hydration. Calcarenite can also exert binding properties. When producing cement, $CaCO_3$ is sometimes added as a microfiller to improve the physical and technical properties. On the other hand, limestone with a coarseness of up to 5 mm is fed to the backfill mixture, therefore, the share of fine particles is minimal, which cannot have a significant influence on strength.

Minerals of granulated blast-furnace slags, akermanite ($2CaO \cdot MgO \cdot 2SiO_2$), helenite ($2CaO \cdot Al_2O_3$), which are part of melilite, as well as pseudowollastonite (α - $CaO \cdot SiO_2$), are in a glassy state. In the natural state they practically do not exert binding properties [22]. Over time, a gel-like mass of calcium hydrosilicates

is formed on the surface of the mineral grains. When grinding the blast-furnace slag, the hydraulic activity of minerals increases. As it is noted in the work [23], with a specific surface area of 4000-6000 cm^2/g, slag minerals intensively exert hydraulic activity.

Under mechanical action on the blast-furnace slag particles, the freshly formed surface of the particle has a high reactivity caused by the surface energy accumulation. New freshly formed surfaces have significantly higher surface energy values, which leads to their increased adhesive activity. The special energetic state of the new surfaces of ground mineral materials - quartz, limestone, magnesite, gypsum, etc. – can be explained by the formation of a large number of non-saturated valence bonds. Thus, when quartz crystals are ground, as a result of breaking a significant amount of Si-O bonds, ions of Si^{4+}, O^{2-} are formed on the surface of grains [24]. Water in the backfill mixture, when coming into contact with fractures and cavities of the surface of fine-dispersed slag particles, promotes the cations transfer from the surface to the state of solution due to the breaking of silicon-oxygen bonds [25].

The main oxides of the blast-furnace slag are CaO and SiO_2, the content of which is 85% or more. In this case, in the structure of slag minerals, the predominantly ionic Ca-O and covalent Si-O bonds are destroyed. The energy of these types of bonds is 1075.6 and 1861 kJ/mol, respectively [22], which indicates a greater exposure of ionic Ca-O bonds to destruction. It can be concluded that more calcium Ca^{2+} ions are formed on the surface of ground slag particles than Si^{4+} ions. In addition, the substance solubility increases with increa-sing dispersion. The remaining silica content is in the amorphous state. It follows from this that it is necessary to transform the contained silica from an amorphous state into an active one in order to increase its content in strong crystalline formations of the backfill mass.

In the process of hydration, a hydrosilicate gel will be formed with a predominance of a weak ionic Ca-O bond in its structure. This explains the relatively low backfill mass strength of 5-6 MPa with a high consumption of blast-furnace slag 400-450 kg/m^3 and flux waste 1000-1100 kg/m^3 in the mixture composition.

As a result of melilite-like minerals hydration, a large number of gels and colloidal solutions are formed, and crystalline substances

are almost completely suppressed. With coarse grinding of slag minerals, the basicity index will be $CaO / SiO_2 \geq 1.5$. Therefore, an insufficient amount of activated silica is involved in the process of artificial mass structure formation. It can be concluded that the specific surface area of particles influences not only on an increase in the contacts number and the density of interaction between particles, but from the point of view of chemical concepts – also on the final basicity index of CaO / SiO_2, which determines the strength of crystalline formations. Under normal conditions, the hydraulically active phases of the slag slowly harden and are characterized by low strength [26].

Differences in the composition and morphology of hydrosilicate gels can be explained by unequal hydration conditions and unreacted calcium silicates, as well as by varying degrees of particle defectiveness during grinding. Consequently, with a grinding fineness of 55% of particles with a coarseness of -0.074 mm, the growth of crystal bonds will be rather slow. Due to the lower slag minerals activity, in comparison with minerals of Portland cement clinker, as well as the heterogeneity of particles after ball grinding when interacting with water, hydration will occur unevenly without oversaturation with ions. As a result, highly basic calcium hydrosilicates with a variable composition in a gel-like form are formed, which can be referred to the group C-S-H (II) (Fig. 3) [27, 28].

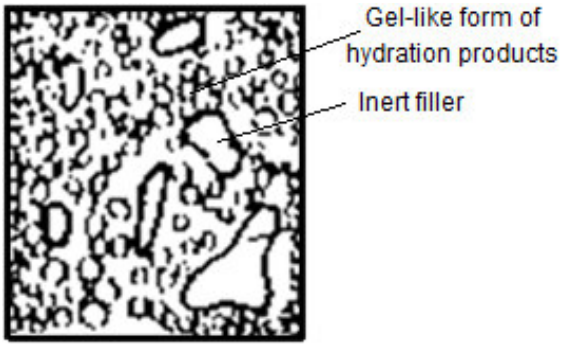

Fig. 3. Artificial stone structure containing highly basic calcium hydrosilicates

If, during the clinker minerals hydration, the hydrosilicate gel remains for several days, then during the slag minerals hydration, this process is longer. The hydration products of slag minerals are similar to cement clinker, but differ in a lower content of CaO and H_2O [25]. Gel (C-S-H) is similar in composition to tobermorite, therefore it is often called tobermorite-like.

Noticeable differences in morphology, as well as in X-ray diffraction patterns, make it possible to determine the difference between C-S-H (I) and C-S-H (II): C-S-H (I) with a ratio of $CaO / SiO_2<1.5$ is a laminate calcium hydrosilicate, and C-S-H (II) with a ratio of $CaO / SiO_2>1.5$ - is mainly fibrous calcium hydrosilicate [29, 30]. With a high ratio of $CaO / SiO_2>2$-3, calcium hydrosilicates have a round particle shape and are formed in the form of a gel. Low-basic calcium hydrosilicates are presented in the form of $(0.8\text{-}1.5)\cdot CaO\cdot SiO_2\cdot(0.5\text{-}2.5)\,H_2O$, highly basic - $(1.5\text{-}2)\cdot CaO\cdot SiO_2\cdot(1\text{-}4)H_2O$ [31].

The mineral substances represented in the slag are hydration products, but their low activity, in comparison with cements, when interacting with water, forms highly basic hydrosilicate structures. Gel (C-S-H), in addition to aluminium, iron and sulphur, may contain small amounts of magnesium, sodium, potassium, as well as remains of titanium and chlorine [30]. Therefore, as a result of slag hydration, the calcium hydrosilicates contain oxides of Al_2O_3, MgO, and FeO.

With an increase in the fineness of grinding to 100% of particles -0.074 mm, all active slag minerals take part in hydration. If the share of particles with a coarseness of -0.074 mm is 100% and flux limestone waste is added to the backfill mixture as a microfiller, then the amount of Si^{4+} ions will increase, and some of the ions of the weak Ca^{2+} bond will pass to the formation of tetracalcium monocarbonate hydroaluminate $3CaO\cdot Al_2O_3\cdot CaCO_3\cdot 11H_2O$. This will lead to equa-lizing the content of $Ca^{2+}\approx Si^{4+}$ ions in the backfill mixture and the formation during hardening of calcium hydrosilicates of fibrous and laminate types with low basicity (0.8-

1.5) $CaO \cdot (Al_2O_3, MgO, FeO) \cdot SiO_2 \cdot (0.5\text{-}2.5)H_2O$. Their structure is shown in Figure 4 [27].

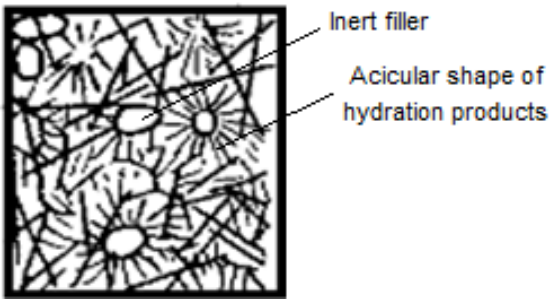

Fig. 4. Artificial stone structure containing low-basic calcium hydrosilicates

It follows from the above that for greater destruction of the Si-O bonds number, it is necessary to increase the degree of particle dispersion, which will also increase the calcium silicate particles solubility. This is facilitated by the occurrence of microfractures and defects in particles during grinding. As a result, water is in contact with all surfaces. Consequently, a strong structure of calcium hydrosilicates is formed, which are more crystallized. A finer grinding of slag minerals will release more silicon ions, which will lead to the formation of strong covalent bonds in the hydrosilicate gel. According to some data, contribution of covalent bonds to the cement stone strength is about 65% [32].

As a result, conditions are created for the growth of various forms and structures of calcium hydrosilicates, which leads to an increase in strength. The finely ground share of the limestone, which contains $CaCO_3$, exerts the ability to hydration. In this case, ground calcite will interact with water and the helenite share of melilite, which will lead to the formation of calcium hydrocarboaluminate, which helps to strengthen the artificial stone. As a result of balanced state in Ca-O and Si-O bonds due to an increase in the breaking of Si-O bonds under the action of fine grinding, calcium hydrosilicates of lower basicity $CaO / SiO_2 \leq 1.5$ are formed.

The appearance of formed crystalline structures in the backfill stone has a positive effect on the strength of the artificial mass.

Therefore, in order to increase the strength of the chamber backfill mass, it is necessary to create strong crystalline bonds in its structure by the time of mining the reserves of the second stage stope chambers. In the works [33, 34], it is indicated that the formation of low-basic calcium hydrosilicates increases the strength of the cement stone, but when highly basic hydrosilicates appear, its strength decreases.

4.2. Experimental research on the strong hardening backfill mass formation based on the fine-dispersed particles

As a result of grinding the granulated blast-furnace slag and flux limestone using the USI-20 unit, the actual value of the specific surface area of the particles is 4300 cm^2/g, with an assumed design value of 4000 cm^2/g, the deviation is 7%. The rheological properties of the backfill mixtures №1 and №.2 have been studied. The average indicators of shearing stress are 0.85 and 0.74 MPa, mobility - 11.7 and 11.4 cm, setting time - 14.5 and 13 hours. These parameters satisfy the requirements for the backfill mixture transportation.

Three samples of each test mixture № 1 and № 2 are studied for strength at the age of 30 and 90 days of hardening. Photos of the procedure for determining the strength of backfill mass for uniaxial compression of the backfill mass samples are shown in Figure 5.

Fig. 5. Strength test of hardening backfill mass samples

Analysis of the histograms in Figure 6 shows a positive tendency to an increase in the backfill mass strength with a change in the specific surface area of the particles at the age of 30 and 90 days. At the age of

30 days, the backfill mass strength increases by 2.5 times, and 90 days - 1.7 times. An intensive increase in strength after 30 days is noteworthy, since the rock mass strength actually reaches the standard strength with an indicator of 7-8MPa for a mining depth of 640-940 m.

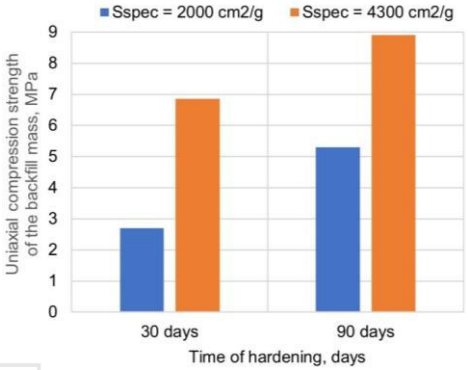

Fig. 6. Results of determining the uniaxial compression strength of the backfill mass

To confirm the theoretical assumptions of the blast-furnace slag and flux waste dispersion influence on the structure, shape and chemical composition of crystalline new formations of the backfill stone, the destroyed samples of the backfill mass with different specific surface areas of particles have been studied using scanning electron microscopy with a built-in X-ray spectral microanalyzer (Fig. 7).

a *b*

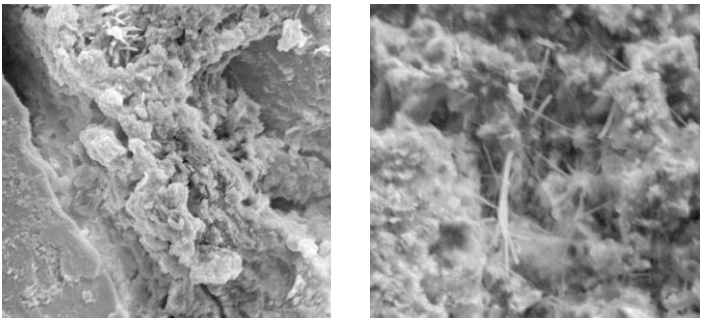

Fig. 7. Structural bonds development in the backfill mass with a change in the specific surface area: (*a*) at 2000 cm^2/g; (*b*) at 4300 cm^2/g

In the sample (Fig. 7*a*), two large filler particles are clearly observed, interconnected by weakly crystallized new formations of calcium hydrosilicate, which is in a gel-like state. Crystalline new formations have dense, round-indefinite shapes of particle with protruding disordered rare single needles and plates. Having such a structure, the mass cannot withstand tensile stresses arising on the backfill mass contour, which in practice occurs in conditions of the ore reserves development at the Pivdenno-Bilozerske field.

An increase in the specific surface area of particles of a binding material to 4300 cm^2/g has significantly influenced on the structure formation of new formation (Fig. 7*b*). Calcium hydrosilicates have an acicular-fibrous and acute-angled shape, the particles are densely distributed in relation to each other, the porosity has decreased, the inert filler grains are completely covered with hydrate formations. Artificial stone is reinforced with crystalline new formations, hence adhesion forces and resistance of internal bonds to loads increase. The structure of the new formations acquires an acute-angled shape, replacing the round shape characteristic of the samples of the first and second series. The strength properties of the backfill mixture sample significantly increase, which is shown in Figure 6. In comparison with the No. 1 mixture samples, this one clearly demonstrates the dominant influence of the bonds form and their chemical composition. Forms of bonds in Figure 7 closely correlate with the forms in Figures 3 and 4. The results of determining the structural bonds chemical composition of the mixture samples No. 1 and No. 2 are presented in Table 2.

Table 2

Results of chemical composition measurements of the hardening backfill mass structural bonds

Sample of backfill mass	S_{spec}, cm^2/g	Oxide content, %		Average value CaO / SiO_2	Form of new formations
		CaO	SiO_2		
Mixture No. 1	2000	55.12	25.14	2.63	Round, indefinite
		52.48	26.60		
		49.68	26.63		
		71.53	15.76		
Mixture No. 2	4300	45.50	22.06	1.48	Pyramidal, acute-angled, acicular-fibrous
		31.16	34.18		
		38.10	29.70		

The data in Table 2 show that with an increase in the specific surface area of the binding material particles, the basicity of the formed hydrosilicate bonds decreases, and the shape of the structural formations changes significantly. If with the basicity CaO / SiO_2=2.63, the highly basic calcium hydrosilicates with a round, pyramidal, thick- acicular structure are formed, then with CaO / SiO_2=1.48 – the low-basic calcium hydrosilicates with a pronounced acicular-fibrous structure. This also explains the significant difference in the intensity of strength growth both at 30 and 90 days of the mixture hardening.

According to the measurements of CaO and SiO_2 in the № 1 and No. 2 test backfill mixtures with various degrees of specific surface area of the binding material particles, using the positions of deriving the true formulas, the newly formed calcium hydrosilicates can be described by the following formulas

$2.63\ CaO \cdot SiO_2 \cdot H_2O$ at S_{spec}=2000 cm^2/g;

$1.44\ CaO \cdot SiO_2 \cdot 1.76H_2O$ at S_{spec}=4300 cm^2/g.

Thus, the basic principles of the structure formation of the backfill mass in relation to the strength characteristics with an increase in the dispersion of the binding material particles have been studied in the work. This makes it possible to control these parameters depending on the value of the stress field acting on the backfill mass when extracting the iron ore from the subsoil.

5. Conclusions

The issues of creating a strong backfill mass with internal bonds resistant to loads are important for mining enterprises that backfill underground cavities with hardening mixtures. The interaction and products of hydration of the backfill mixture components with water have been studied. It has been determined that with an increase in the specific surface area of the binding material particles, the new formations shape of the backfill mass improves, it has high strength, and the basicity of its new formations is capable of changing. This is caused by a large gap in the covalent bonds of silica with a more intense grinding of the binding material, as well as the transition of ions of a weak ionic bond to the formation of other compounds and equalizing the ratio of Si and Ca ions in solution.

There is a positive tendency towards an increase in the backfill mass strength with a change in the specific surface area of particles from 2000 to 4300 cm^2/g at the age of 30 and 90 days. At the age of 30 days, the backfill mass strength increases by 2.5 times, and 90 days - 1.7 times. It has been determined that with an increase in the specific surface area of the binding material particles, the basicity of the formed hydrosilicate bonds decreases, and the structural formations shape changes significantly towards their strengthening – from gel-like to acicular-fibrous.

The research data on the composition and shape of structural bonds at a certain strength of the hardening backfill mass will make it possible to rationally choose the dispersion, obtain high strength of the backfill mass and increase the stability of the artificial mass outcropping.

References

1. Derzhavna fiskalna sluzhba Ukrainy. (2019). Ofitsiinyi portal. Rezhym dostupu http://sfs.gov.ua/

2. **Shatokha, V.** (2015). The sustainability of the iron and steel industries in ukraine: challenges and opportunities. Journal of Sustainable Metallurgy, 2(2), 106-115. https://doi.org/10.1007/s40831-015-0036-2

3. **Bazaluk, O., Petlovanyi, M., Lozynskyi, V., Zubko, S., Sai, K., & Saik, P.** (2021). Sustainable underground iron ore mining in Ukraine with backfilling worked-out area. Sustainability, 13(2), 834. https://doi.org/10.3390/su13020834

4. **Pysmennyi, S.V., & Brovko, D.V.** (2018). Zberezhennia richnoi produktyvnosti shakht Kryvorizkoho zalizorudnoho baseinu pry vidpratsiuvanni zaliznykh rud na velykykh hlybynakh. Visnyk Kryvorizkoho Natsionalnoho Universytetu, (46), 164-168.

5. **Azaryan, A.A., Batareyev, O.S., Karamanits, F.I., Kolosov, V.O., & Morkun, V.S.** (2018). Ways to reduce ore losses and dilution in iron ore underground mining in Kryvbass. Science and Innovation, 14(4), 17-24. https://doi.org/10.15407/scine14.03.017

6. **Khomenko, O., Kononenko, M., & Myronova, I.** (2017). Ecological and technological aspects of iron-ore underground mining. Mining of Mineral Deposits, 11(2), 59-67. https://doi.org/10.15407/mining11.02.059

7. **Petlovanyi, M.V., & Ruskykh, V.V.** (2019). Peculiarities of the underground mining of high-grade iron ores in anomalous geological conditions. Journal of Geology, Geography and Geoecology, 28(4), 706-716. https://doi.org/10.15421/111966

8. **Hrinov, V.H., & Khorolskyi, A.O.** (2020). Studies of the basics of technology for optimal design of rational use of valuable mineral deposits. Mineral Resources of Ukraine, (2), 19-24. https://doi.org/10.31996/mru.2020.2.19-24

9. **Shashenko, O.M., Hapieiev, S.M., Shapoval, V.G., & Khalymendyk, O.V.** (2019). Analysis of calculation models while solving geomechanical problems in elastic approach. Naukovyi Visnyk Natsionalnoho Hirnychoho Universytetu, (1), 28-36. https://doi.org/10.29202/nvngu/2019-1/21

10. **Petlovanyi, M.V., Zubko, S.A., Popovych, V.V., & Sai, K.S.** (2020). Physicochemical mechanism of structure formation and strengthening in the backfill massif when filling underground cavities. Voprosy Khimii i Khimicheskoi Technologii, (6), 142-150. https://doi.org/10.32434/0321-4095-2020-133-6-142-150

11. **Bitimbaev, M.Zh., & Krupnik, L.A.** (2012). Teoriya i praktika zakladochnykh rabot pri razrabotke mestorozhdeniy poleznykh iskopaemykh. Almaty: Mir, 600 s.

12. **Kuz'menko, A.M., & Petlevanyy, M.V.** (2017). Razrushenie zakladochnogo massiva v zavisimosti ot tekhnologii ego vozvedeniya. Zbirnyk Naukovykh Prats NHU, (52), 159-166.

13. **Wu, J., Feng, M., Mao, X., Xu, J., Zhang, W., Ni, X., & Han, G.** (2018). Particle size distribution of aggregate effects on mechanical and structural properties of cemented rockfill: Experiments and modeling. Construction and Building Materials, (193), 295-311. https://doi.org/10.1016/j.conbuildmat.2018.10.208

14. **Petlovanyi, M., & Mamaikin, O.** (2019). Assessment of an expediency of binder material mechanical activation in cemented rockfill. ARPN Journal of Engineering and Applied Sciences, (14), 3492-3503.

15. **Zhang, B., Xin, J., Liu, L., Guo, L., & Song, K.-I.** (2018). An experimental study on the microstructures of cemented paste backfill during its developing process. Advances in Civil Engineering, (2018), 1-10. https://doi.org/10.1155/2018/9783046

16. **Kuz'menko, A.M., & Petlevanyy, M.V.** (2013). Formirovanie zakladochnogo massiva na osnove tonkodispersnykh chastits vyazhushchikh materialov pri podzemnoy razrabotke rudnykh mestorozhdeniy. Metallurgicheskaya i Gornorudnaya Promyshlennost', (2), 70-73.

17. **Kuz'menko, A.M., Petlevanyy, M.V., Chistyakov, E.P., & Kulish, S.A.** (2009). K voprosu podbora sostava tverdeyushchey zakladki povyshennoy prochnosti Sbornik Nauchnykh Ttrudov NAN Ukrainy, (82), 50-57.

18. **Gorobets, L.Zh., Kovalenko, V.V., & Pryadko, N.S.** (2009). Uprochnenie stroitel'nykh materialov pri obrabotke v struyakh. Dynamika ta Mitsnist Mashyn, Budivel, Sporud, 3(25), 59-66.

19. **Gouldsteyn, D., Nyuberi, D., & Echlin, P.** (1984). Rastrovaya elektronnaya mikroskopiya i rentgenovskiy mikroanaliz. Moskva: Mir, 303 s.

20. **Togobitskaya, D.N., Khamkhot'ko, A.F., & Stepanenko, D.A.** (2009). Otsenka kristallizatsionnoy sposobnosti i mineralogicheskogo sostava konechnykh domennykh shlakov v syr'yevykh i tekhnologicheskikh usloviyakh domennykh pechey zavodov Ukrainy. Fundamental'nye i Prikladnye Problemy Chernoy Metallurgii, (20), 54-60.

21. **Kulik, V.A., Saley, A.A., & Kravchenko, T.V.** (2004). Optimizatsiya sostavov zakladochnykh smesey. Analiz khimiko-mineralogicheskogo sostava i fiziko-tekhnicheskikh pokazateley shlakov Donetsko-Pridneprovskogo regiona. Voprosy Khimii i Khimicheskoy Tekhnologii, (2), 54-60.

22. **Butt, Yu.M., Sychev, M.M., & Timashev, V.V.** (1980). Khimicheskaya tekhnologiya vyazhushchikh materialov. Moskva: Vysshaya shkola, 472 s.

23. **Ramachandran, V.S.** (1988). Dobavki v beton. Moskva: Stroyizdat, 575 s.

24. **Kingeri, U.D.** (1987). Vvedenie v keramiku. Moskva: Stroyizdat, 500 s.

25. **Royak, S.M., & Royak, G.S.** (1983). Spetsial'nye tsementy. Moskva: Stroyizdat, 279 s.

26. **Dvorkin, L.I., & Dvorkin, O.L.** (2007). Stroitel'nye materialy iz otkhodov promyshlennosti. Rostov-na-Donu: Feniks, 368 s.

27. **Teylor, Kh.** (1996). Khimiya tsementa. Moskva: Mir, 560 s.

28. **Hu, C., Ruan, Y., Yao, S., Wang, F., He, Y., & Gao, Y.** (2019). Insight into the evolution of the elastic properties of calcium-silicate-hydrate (C-S-H) gel. Cement and Concrete Composites, (104), 103342. https://doi.org/10.1016/j.cemconcomp.2019.103342

29. **Kuznetsova, T.V., Kudryashov, I.V., & Timashev, V.V.** (1989). Fizicheskaya khimiya vyazhushchikh materialov. Moskva: Vysshaya shkola, 384 s.

30. **Kazanskaya, E.N.** (1990). Obrazovanie gidratnykh faz portlandtsementnogo kamnya. Leningrad: Znanie, 50 s.

31. **Gorshkov, V.S., Timashev, V.V., & Savel'yev, V.G.** (1981). Metody fiziko-khimicheskogo analiza vyazhushchikh veshchestv. Moskva: Vysshaya shkola, 335 s.

32. **Brykov, A.S.** (2008). Gidratatsiya portlandtsementa. Sankt-Peterburg: Mir, 30 s.

33. **Khayrutdinov, M.M., & Votyakov, M.V.** (2007). Vybor khimicheskikh dobavok dlya tverdeyushchey zakladki na kaliynykh rudnikakh. Gornyi Informatsionno-Analiticheskiy Byulleten', (6), 218-220.

34. **Domokeev, A.G.** (1989). Stroitel'nye materialy. Moskva: Vysshaya shkola, 494 s.

https://doi.org/10.31713/m1019

INCREASING OIL RECOVERY APPLYING ELECTRIC STIMULATION ON THE FORMATION

Akramov B.Sh.
Branch of the Russian State University of Oil and Gas (National Research University) named after I.M. Gubkin in Tashkent city (Republic of Uzbekistan), PhD, professor of the Department of Development of Oil, Gas and Gas Condensate Fields, Uzbekistan

Umedov Sh.Kh.

Tashkent State Technical University named after Islam Karimov, DSc, head of the Mining Electromechanics department, Uzbekistan

Khaitov O.G.

Tashkent State Technical University named after Islam Karimov, PhD, associate professor, head of the Mining department, Uzbekistan

Nuriddinov J.F.
Institute of Geology and Exploration of Oil and Gas Fields, engineer, Uzbekistan

Gafurov Sh.O.
Tashkent State Technical University named after Islam Karimov, assistant of the Geology of Oil and Gas department, Uzbekistan

Abstract

The work is devoted to increasing the degree of depletion of reserves of long-term exploited hydrocarbon deposits on the basis of the obtained results of theoretical and experimental studies of the application of electrodynamic technologies for stimulating the formation and bottomhole formation zone.

The electrolysis of formation fluids, water, oil-bearing rocks, is accompanied by a mass transfer, primary and secondary chemical reactions, the formation of all kinds of salts, alkalis and acids, new organic substances and all kinds of surfactants. Not only the liquid is subjected to electrolysis, but also the oil and gas bearing rocks themselves (solid electrolyte). The magnetic and electrical forces arising during the electric treatment of reservoirs make it possible to effectively drain heterogeneous reservoirs and extract residual oil from non-working layers.

The work also carried out experiments to study the effect of the electric field on the surface tension coefficient at the oil-water interface.

The circumstance of an abrupt change in the surface tension coefficient at the oil-water interface makes it possible in principle to create conditions in the reservoir that make it possible to slow down the cusping processes by applying an electric field of various magnitudes or, in other words, by regulating the amount of mass transfer.

In numerical terms, the oil recovery factor without electrophysical treatment was 52.94%. Under electrophysical impact, the oil recovery factor was 94.12%, i.e. equaled to almost complete extraction of oil from the sample. In the field, this figure, of course, will decrease by 2-3 times, but it remains quite high in comparison with other methods of increasing oil recovery.

Thus, the studies performed on samples in laboratory conditions indicate the possibility of using constant electric fields to increase oil recovery from depleted watered formations. Electrochemical treatment of the formation can significantly increase the displacement of oil from the formation. The increase in oil displacement reaches 15-20% and more.

With the help of water alone, 58% of the oil (of its total volume in the sand) was displaced from the sand, and under electric field with a voltage of 10 V and 20 V, the total amount of displaced oil, respectively, increased to 67 and 83%. Thus, the laboratory studies performed on the samples also indicate the possibility of using constant electric fields to increase oil recovery from depleted watered formations.

The carried out theoretical and experimental studies show the possibility of using the technology of electrochemical and electrothermochemical leaching of oil-saturated rocks to intensify oil production. The effectiveness of the recommended technology is especially noticeable in fields that have entered the final stage of development with a high water cut.

Introduction

Practice shows that the widespread use of traditional waterflooding technology (the main method of developing hydrocarbon deposits in Kazakhstan) does not provide effective recovery of residual reserves from low-permeability and highly watered formations. Therefore, increasing the oil recovery from producing fields applying effective methods of stimulation on water-oil-saturated formations is an important scientific and technical task facing the oilmen of the republic.

Almost all oil fields in Uzbekistan are at the late and final stages of development, which are characterized by a constant decrease in the level of oil production with a simultaneous increase in water cut (90% and more on average).

In addition, most of the residual reserves of these fields are hard-to-recover. They are concentrated in low-permeability reservoirs of small thickness with high-viscosity oil and anomalous properties,

with variable gas content and significant sizes of oil-water zones. These factors have led to the low efficiency of traditional waterflooding and create favorable preconditions for the introduction of modern EOR.

In general, for fields that are in a late stage of development, an alternative option for curbing the decline in oil production and increasing oil recovery factor may be stimulating the hard-to-recover and residual oil reserves through the expanded use of workovers, modern EOR methods and bottomhole formation zone (BHZ) treatment.

In the conditions of highly watered formations of the fields of Uzbekneftegaz JSC, which are at a late stage of development and are characterized by a high degree of reserves depletion, along with squeeze job and BHZ treatment, it is necessary to more widely use other technologies, in particular, electric stimulation (ES) on the formation and BHZ, which allows to increase oil recovery factor and reduce the cost of oil production.

The technology of ES on the formation and BHZ is based on the effects of changing the structure of the void space of a micro-heterogeneous medium and the spatial structures of filtration flows as a result of passing specially selected pulses of electric current through the productive formation. Localization of the current density in thin capillaries, that limit the rate of filtration in the medium, makes it possible to increase the cross-section of the capillaries, and thus increase the permeability in the BHZ. The use of the electrocapillary effect (change in surface tension at the phase interface under the influence of an electric field) makes it possible to shift the phase equilibrium in the medium and increase the relative permeability of oil with a simultaneous decrease in the relative permeability of water. As a result, due to a change in the spatial structure of filtration flows in the medium, the water cut of the wells can sharply decrease for a long period.

Therefore, the research focused on new energy-saving technologies that aim at reducing the residual oil reserves at a late stage of operation, especially from water flooded formations, is one of the urgent problems of the theory and practice of oil production.

Laboratory studies of electrophysical treatment

To study the effect of ES on oil-saturated rocks, we used a setup (Fig. 1), which met the following requirements: the possibility of applying an electric field; when filtering water under the pressure gradient and an electric field, the inlet end of the sample should not become contaminated, and gas in the form of a bubble should not enter it; the sample should not be heated during the experiment.

The samples were saturated with water, the flow rate of water through the sample was determined at a constant pressure gradient in all experiments, and the permeability coefficient was calculated. On the next step, the flow rate of the liquid was determined with the electric field applied.

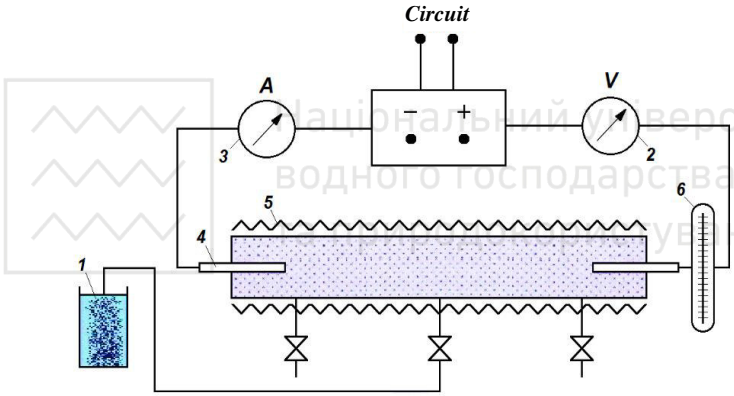

Fig. 1. Schematics of experimental setup

The studies were carried out with samples with a permeability coefficient of 2.2-0.73 D. To track the rate of advancement of the oil-water contact, an inductive control method was developed. The essence of the method lies in the fact that the dimensionless parameter of the quality factor of the inductor $Q=WZ/R$ (where W is the frequency, Z is the inductance, R is the active resistance) depends on the electrical resistivity of the core, which is the core under study or the reservoir model.

It has been theoretically and experimentally proved that the resistivity of the most liquid-saturated rocks is proportional to the resistance of the liquid saturating them. By the change in the Q-

factors of sections of the coil in time, one can also estimate the completeness of the displacement of one agent by another.

According to the electroosmotic theory, when a liquid comes into contact with solid particles, due to the electrochemical interaction of molecules, solid particles are negatively charged, and an equal positive charge is distributed over the thickness of the adjacent liquid. The density of the volumetric row of liquid decreases with an increase in the distance to the surface of the particle at a distance d and is characterized by a surface density δ. Such a system is a capacitor, the capacity of which per unit area is $C_0=EE_o/d$, and has a charge δ.

In the case of simultaneous electroosmotic and hydromechanical exposure, according to the principle of independence of action, the resulting fluid velocity will be equal to $v=v_e+v_o=k\text{grad}\,(k_2\gamma+h)$. This equation is the main one for calculating filtration processes, both in the presence and in the absence of an electric field.

The experimental setup (Fig. 1) was used to study the effect of electroosmosis on oil recovery when oil is displaced by water. Samples were saturated with aqueous solutions and the permeability of the sample was determined. Water from the sample was displaced by oil from the XIX horizon of the Parsumurun dome of the Uzen field with the following characteristics: density - 0.785 g/cm^3, dynamic viscosity - 4.19 mPa·s, paraffin content - 21.8% wt.

The amount of displaced water was used to determine the amount of oil in the sample. Then the oil was displaced from the sample with water without electroosmotic action. When the recovery of oil stopped, the amount of displaced oil was measured. Further, the displacement of oil by water was carried out at the same pressure gradient, i.e. 10^{-3} MPa/cm, but imposing electric field with a gradient of 10 V/cm. As a result, an additional amount of oil was displaced. The experiment was terminated when no more oil was releasing from the sample. In all experiments, the temperature at the outlet of the samples was maintained at a level of 20 °C.

In all cases, the use of electroosmotic treatment led to the release of an additional amount of oil from the sample, which obviously led to a decrease in the residual oil saturation. An increase in oil

recovery was obtained within a few percent of the original oil volume.

Another series of experiments was carried out using kerosene as a hydrocarbon liquid. Experiments were carried out with several samples from sandstone containing 6% montmorillonite (№ 1), 6% pealite (№ 2) and 6% kaolinite (№ 3). A control sample (№ 4) was made from pure sandstone. The magnitude of the current in the experiments varied from 5 to 15 mA. From the graph (Fig. 2) it can be seen that the most noticeable application of the electric field affected the sample № 1 and quite insignificant - on the sample of pure sandstone (№ 4). It is interesting to note that after filtration, the voltage on the sample turned out to be 2 times higher than the initial one. This suggests that, apparently, irreversible changes have occurred in the structure of montmorillonite under the influence of an electric field. As a filtrating liquid in these experiments, a solution of 0.5 wt% NaCl and 0.5% wt. CaCl was used.

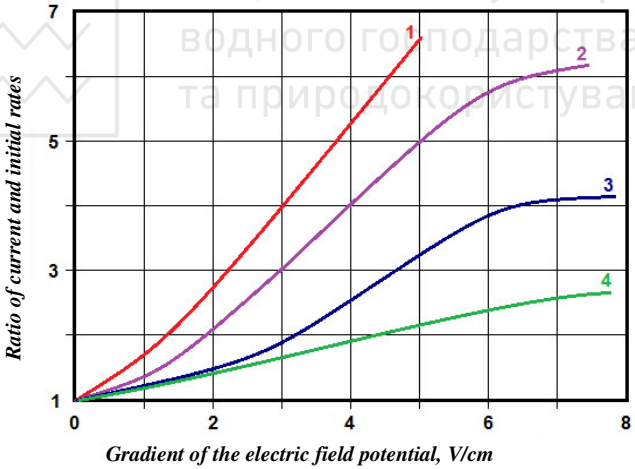

Fig. 2. Increase in the rate of water filtration (the ratio of the current rate and the rate at the beginning of the experiment q_i/q_o) through sandstone samples when a direct current is applied: *1* - montmorillonite, 6%; *2* - pealite, 6%; *3* - kaolinite, 6%; *4* - sand, 100%

Experiments on the joint flow of immiscible fluids were carried out on a sample of natural sandstone. The experiment was carried out as follows. A core sample was initially saturated with mineralized

water. Then the mixture was filtered through the sample until a steady flow of both phases was observed. Then the voltage of a direct current was applied to the electrodes. After some time, the filtration rates of the liquids were measured again, and the temperature of the liquids leaving the sample was also recorded. The current was increased from 0.5 to 3.0 mA.

In these experiments, it was found that under a constant current, the volumetric filtration rate of kerosene increased, and, consequently, increased the value of the effective permeability for kerosene depending on the voltage applied to the electrodes (Fig. 3).

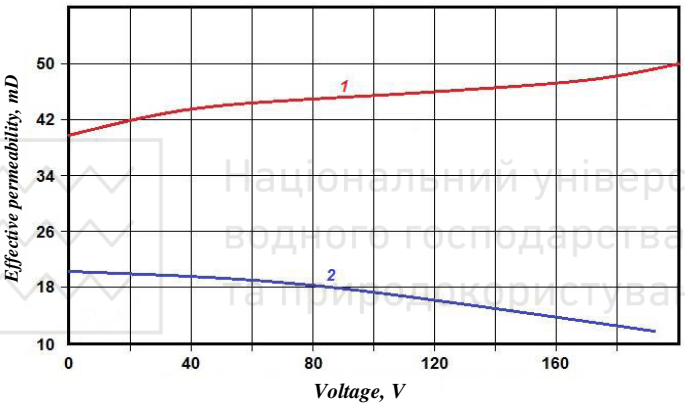

Fig. 3. Dependencies of effective permeability for kerosene (*1*) and water (*2*) from voltage

Also, experiments were carried out to study the effect of an electric field on the surface tension coefficient at the oil-water interface. In this case, a device was used in which the change in surface tension was recorded by the rate of oil flow from the capillary into the water at different voltages on the electrodes. It is established that the time between the separation of oil droplets from the capillary into the water without voltage supply practically does not change at t °C=const. When a positive potential is imposed on oil, and a negative potential on water (U=5kV), the time slightly increases, i.e. the coefficient of surface tension at the oil-water interface increases. Then, after 1.5-2.5 minutes, δ decreases and remains at that level for indefinitely long.

This abrupt change in the surface tension coefficient at the oil-water interface makes it possible to consider it fundamentally possible to create conditions in the reservoir that make it possible to slow down the processes of cusping by applying an electric field of various magnitudes or, in other words, to regulate the amount of mass transfer.

As it is known, the rate of mass transfer when extracting a liquid with a liquid is proportional to the mass transfer coefficient of the interface area (contact surface) and the driving force (pressure drop). With constant driving force, any attempt to increase the rate of mass transfer must, therefore, be aimed at increasing the other two factors. Also known the fact of a spontaneous increase in the coefficient of mass transfer due to the Maragoni effect which is a surface flow due to the appearance of a gradient of interfacial tension at the interface.

During waterflooding of oil deposits, the capillary forces manifest themselves variously. In a hydrophilic reservoir, at the front of water penetration into an oil reservoir, capillary forces contribute to the displacement of oil. In flooded zones and layers, capillary forces determine the residual oil saturation, which reduces the final recovery factor.

A direct consequence of capillary imbibition of layer-watered plays will be "mixing" of oil and water - an increase in oil saturation of the flooded layers, alignment of the phase saturation in the volume of the reservoir.

The depth of capillary imbibition naturally occurring in the formation can be determined by the formula

$$h = \sqrt{\frac{\delta \cos\theta m^{0,5} t(k_{\alpha v\cdot 0} - k^{0,5}_{\alpha v\cdot w} k^{0,5}_{\alpha v\cdot p})}{0{,}00057 \eta_w \mu_{\alpha v} \tau k^{0,5}_{\alpha v}}}$$

where δ is the coefficient of surface tension at the oil-water interface; θ - contact angle of wetting; m - porosity; t - exposure time; $k_{av.o}$ - average oil permeability coefficient; $k_{av.w}$ - average coefficient of water permeability; $k_{av.p}$ - average pore permeability coefficient; η_w - coefficient of oil displacement by water in flooded canals $\eta_w=(1–S_o–S_{or})/(1–S_o)$; μ_{av} - average viscosity of the liquid along the filtration path, $\mu_{av}=(\mu_o+\mu_w)/2$; S_o - free oil saturation; S_{or} - residual oil saturation; τ - tortuosity coefficient, $\tau=\chi/l=2\text{-}2.5$; χ - the

length of the path passed by the liquid; l is the geometric length of the porous medium.

Calculations demonstrate that an increase in surface tension at the oil-water interface due to the effect of electrostatic forces insignificantly increases the depth of capillary imbibition and, thereby, the sweep factor. However, the variability of the surface tension over time radically changes this process, increasing the rate of the capillary imbibition due to a cyclic effect on the pore space of the reservoir.

As can be seen from Fig. 4, the additional sweep factor due to the electrical effect on δ with all constant residual parameters is 0.15-0.18, which favorably affects the development parameters and, in particular, the oil recovery.

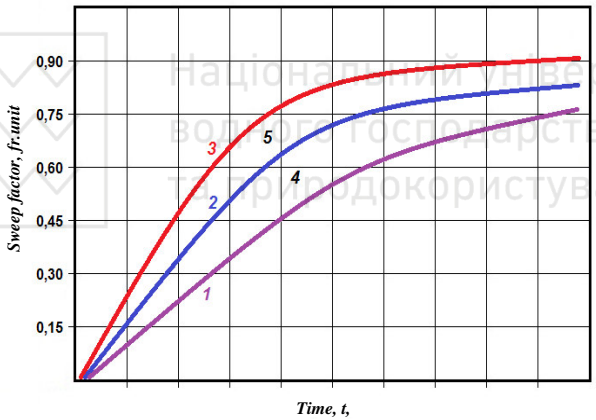

Fig. 4. Relative volume of fluid pumped through the reservoir: *1* - sweep factor without capillary imbibition; *2* - sweep factor taking into account capillary imbibition; *3* – sweep factor, taking into account capillary imbibition under the influence of an electric field; *4* - additional sweep factor due to capillary forces; *5* - additional sweep factor due to electrical impact on the surface tension coefficient at the oil-water interface

In this paper, the analysis of the displacement characteristics was carried out using the Nazarov-Sipachev method, where the dependence of $V_l/V_0=f(V_w)$ is supposed to be used to determine the initial recoverable oil reserves, where V_l, V_0, V_w is the accumulated production of liquid, oil and water, respectively. After a short period

of recovery, this relationship will become $V_l/V_0 = b+\alpha V_w$, where α is the slope of the straight line; b is the segment cut off on the axis.

Transforming the equations, at $V_w \to \infty$, we obtain $V_o \to \alpha^{-1}$, thus, the inverse of the slope α of the straight line characterizes the value of the initial recoverable oil reserves.

As can be seen from Fig. 5, the final recovery factor when oil is displaced by water without ES is significantly less than when displacing with ES. In addition, the graphs show that the curves of the dependence of K_p/K from water saturation after electric treatment shift to the right, thereby reducing the phase permeability.

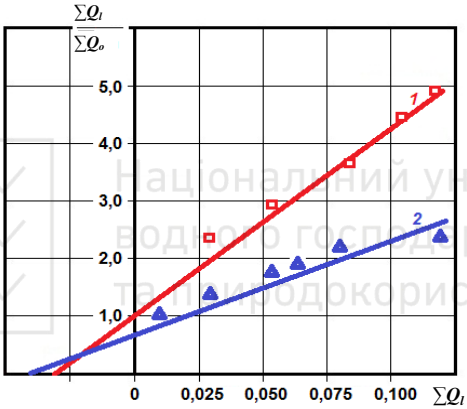

Fig. 5. Graph for the forecast of the final oil recovery: *1* - without electric stimulation; *2* - with electric stimulation

In numerical terms, the oil recovery factor without ES was 52.94%. Under E, the oil recovery factor reached 94.12%, i.e. almost complete extraction of oil from the sample. Thus, increased oil recovery amounted to 41.18%. Under field conditions, this figure, naturally, will decrease by 2-3 times, but it remains quite high compared to other methods of increasing oil recovery.

Thus, the studies performed on samples under laboratory conditions indicate the possibility of using constant electric field to increase oil recovery from depleted watered formations. Electrochemical treatment of the formation can significantly increase the displacement of oil from the formation. The increase in oil displacement reaches 15-20% and more. The increase in oil

displacement is caused by thermal and chemical effects of the current.

Studies on ES of reservoirs have shown that partially or heavily watered reservoirs are best suited for such treatment. The watered interlayers of oil reservoirs serve as conductors for current, and through them it is possible to act with heat and current on pure oil layers.

Experimental studies of electrical treatment

Experimental studies have been carried out below to study the features of electrolysis of a purely oil and water-oil (partially watered) reservoir and the effect of electric current on oil recovery (coefficient of oil displacement by water) from the reservoir. The experiments were carried out on reservoir models saturated with pure oil, water and oil. Oils used were from the Uzen field, and water - aqueous solutions of salts (NaCl) - formation and saline waters. The studies were carried out using direct current.

Based on the analysis of theoretical data on electrokinetic phenomena in capillary-porous media, we have developed several technological schemes for electrodynamic treatment of a formation in laboratory conditions, which make it possible to reveal the physical essence of electrokinetic phenomena in capillary-porous media.

To experimentally check the effectiveness of the effect of direct electric current on the change in the hydrodynamic permeability of the reservoirs, a device was used, with the help of which electroosmotic phenomena in the reservoirs were studied.

The studies were carried out using the UIK-5 unit on 2 sandstone samples taken from the well of the Uzen field.

Fig. 6 shows the results of the experiments carried out to determine $\eta=(V_1+V_2)/V_2$, where V_2 is the hydraulic filtration rate of a homogeneous liquid under the pressure drop at the ends of the sample; V_1 is the electroosmatic velocity of fluid transfer in the rock capillaries.

As follows from Figure 6, in all two studied samples during filtration of saline water with a concentration of $C = 0.1$ and NaCl (1) and kerosene (2), with each pulse of increasing the gradient of the direct current potential in compliance with the polarity, a regular increase in the filtration rate is observed. Moreover, the filtration rate under the electric forces increases tens of times compared to the

fixed filtration rate without voltage. Consequently, these results clearly show that with the help of constant electric field it is possible to intensify the inflow of fluid from the reservoirs.

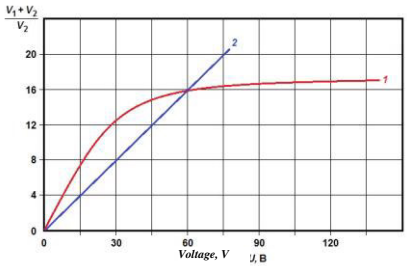

Fig. 6. Graphs of the dependence of η from the voltage value *U*. *1* - for saline water; *2* – kerosene

In addition, experiments on oil filtration through a capillary under electric field with the formation of an emulsion in a 10% aqueous solution of NaCl were carried out in a laboratory setup, and a special device was used to determine the oil recovery of sand under the influence of an electric field.

Fig. 7 shows a dependence of oil recovery of sand when it was flushed with water under the influence of electric field. As follows from the figure, 58% of the oil (of its total volume in the sand) was displaced from the sand using water alone. Under the action of an electric field with a voltage of 10 V and 20 V, the total amount of displaced oil, increased to 67 and 83%, respectively. Thus, the laboratory studies performed on the samples also indicate the possibility of using constant electric fields to increase oil recovery from depleted reservoirs producing under flooding.

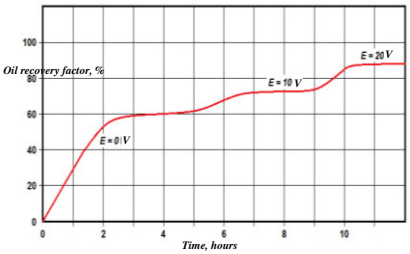

Fig. 7. Dependence of the oil displacement coefficient when flushing with water under the influence of an electric field

Laboratory studies of the process of electrical treatment (electrolysis) of an oil reservoir in static conditions containing buried water were carried out using an oil-saturated linear reservoir model equipped with graphite electrodes at both ends and connected to a DC source (Figure 1). The experiments were carried out on reservoir models filled with sand 0.5-1 mm in diameter and saturated with oil, density of which was 870 kg/m^3. The water saturation of the reservoir is 30%; buried water - formation water. Its mineralization - 120 g/l. Formation porosity 30%, permeability 200 mD, model length 75 cm, diameter 3 cm.

The results of the experiments led to the following conclusions:

- purely oil reservoirs, despite the presence of buried, saline water, have a relatively high resistivity. The resistivity of purely oil reservoirs fluctuates within 2-10 Ohm·m. However, it is several orders of magnitude less than the resistivity of oil and minerals that make up the rock skeleton. Consequently, the conductivity of a purely oil reservoir is solely due to the conductivity of electrolyte-buried saline water;

- at voltages of 50-220 V and more, the current was 20-50 mA due to the low conductivity of the formation, no noticeable heating of the formation during the period of the experiments was noted. The heating was mainly applied to the near-electrode zones.

The composition of the evolved gas in the near-electrode zones was determined according to the GOST 23781-87 method using a Kristall-5000 gas chromatograph (Russia). In this case, the cathode gas consists of homologues of methane and hydrogen, and the anode gas consists of homologues of methane, carbon dioxide, chlorine and oxygen.

To reveal the efficiency of electrical treatment of watered formations, we carried out experiments in glass formations up to 1.5 m long and 35-40 mm in diameter, filled with sand. At the same time, the permeability of the formations fluctuated within the range of 50-350 mD.

The pressure drop was determined from the condition of compliance with the parameters of the approximate simulation. In the experiments, oils with a viscosity of 15-20 mPa·s were used.

Analysis of the results of the experiments shows that in the experiments with electrical treatment, a significant (2-3 times) increase in the displacement of oil from the ionized formation was noticed. Studies on the electrical treatment of formations have shown that partially or heavily watered formations are best suited for ES. The watered interlayers of oil reservoirs serve as conductors for current, and through them it is possible to exert heat and current on pure oil layers.

Laboratory studies have shown that the electrolysis of formation water under dynamic conditions differs from the electrolysis of water under static conditions. To study this issue, we carried out special experiments on models of reservoirs filled with a porous medium and saturated with formation water.

The electrolysis was carried out at direct current at voltages of 75 and 120 V with periodic water supply and fluid withdrawal from the formation. Electrolysis was accompanied by gas formation, heating of the formation and the formation of alkaline solutions at the cathode, acid solutions at the anode. The resulting cathode solutions had a pH of more than 10, anode pH of less than 1.

Conclusion

1. Analysis of the performed theoretical and experimental studies shows the possibility of using the technology of electrochemical and electrothermochemical leaching of oil-saturated rocks to intensify oil production. The effectiveness of the recommended technology is especially noticeable in fields that have entered the final stage of development with a high water cut.

2. Experimental studies have established an increase in the rate of filtration of mineralized water and kerosene through sandstone samples, depending on the magnitude of voltage. The increase in the volume of displaced oil when exposed to electric current is 12-18% compared to that of when no voltage is applied.

3. To increase the displacing ability of the ES at the initial stage of field development, oil production should be carried out with simultaneous flooding of the oil-bearing formation, which will increase the conductivity of the electric current.

4. A calculation algorithm is proposed to determine the basic parameters of electric treatment of the formation for the resistance of

2, 3 and 4 electrode borehole systems. The calculated data are in good agreement with the results of experimental studies.

5. An analytical expression for the dependence of the temperature distribution in the reservoir for one-, two- and multi-electrode systems has been obtained, which makes it possible to plot the temperature profile in the reservoir. The calculation results and the constructed temperature profiles fully confirm the terminal thermal effects arising in the near-electrode zones, which is the basis of the electro-thermal method of impact on the bottomhole zone.

6. Methods for the implementation of electrodynamic stimulation, which differ in the technology of their implementation, are proposed: electrodynamic method for cleaning the near-wellbore part of the formation; an electrochemical method for increasing oil recovery by influencing the formation with a direct electric current.

References

1. **Akramov, B., Umedov, Sh., Nuriddinov, J., & Mirsaatova**, Sh. (2013). Electrophysical method of reservoir treatment as a method of intensifying oil production. Bulletin of TSTU, (4), 152-157.

2. **Akramov, B., Khaitov, O., Nuriddinov, J., Gafurov, S., & Joldasov, R.** (2020). Development Indicators Forecasting Issues At The Chimion Deposit. Globus, (5(51)). doi:10.31618/2658-5197-2020-51-5-4

3. **Akramov, B., Khaitov, O., & Tabylganov, M.** (2010). Methods for specifying initial and residual oil reserves based on development data at a later stage. Gorny Zhurnal, (2).

4. **Akramov, B. S., Khaitov, O. G., & Nuriddinov, J. F.** (2017). Oil displacement by water in an electric field. Austrian Journal of Technical and Natural Sciences, 20-22. doi:10.20534/ajt-17-3.4-20-22

5. **Akramov, B., Khaitov, O., Nuriddinov, J., & Mirzakulova, M.** (2019). Innovation in the development of fields with hard-to-recover reserves. International Scientific Forum "Science and Innovation - Modern Concepts", 1, 139-142.

6. **Akramov, B., Khaitov, O., & Nuriddinov, J.** (2015). Oil displacement by water in an electric field. Europaische Fach-hochschule, 11, 38

https://doi.org/10.31713/m1020

FEATURES OF FORMATION OF GROUNDWATER MASSES OF THE SIVERSKYI DONETS RIVER BASIN

Zhykalyak M.V.
State Regional Geological Enterprise "Donetskgeologiya",
Doctor of Economics, Candidate of Geological Sciences, General Director, Ukraine

Abstract

The introduction in Ukraine in 2016 of basin integrated principles in the zoning and management of water resources of the state in accordance with the Directives of the European Union was an extremely relevant and progressive measure. However, when adopting the relevant normative acts and regulations, the Siverskodonetsk river basin was unreasonably lowered to the sub-basin of the Don River.

Geomorphological and hydrological analysis of geographical maps at a scale of 1:200000-1:500000 of the south-eastern regions of Ukraine and border regions of the Russian Federation allowed to substantiate the basin status of the Siverskyi Donets River, to allocate 17 sub-basins and and their man-made changes, as well as to offer a water monitoring system.

***Keywords*.** River basin, groundwater, hydrogeology, paleohydrology.

Introduction

A well-known Ukrainian scientist - Academician V.I. Vernadskyi in his scientific works on the noosphere repeatedly emphasized that water on our planet is one of the minerals that has no equal in distribution, forms one of the earth's geospheres - the hydrosphere and determines all the chemistry of the earth's crust.

Long-term changes in the hydrological regime of surface and ecological-hydrogeological conditions of groundwater necessitate the development of program measures for effective management of river basins with the definition of surface water and groundwater masses within well-founded basins and sub-basins. That is, the basin of surface water and groundwater becomes the basic unit of integrated water resources management on a basin basis. This norm was introduced into the Water Code of Ukraine in 2016 (Law of Ukraine dated 04.10.2016 № 1641-VIII) for the development and implementation of river basin management plans. In addition, the Water Code of Ukraine is the central legislative act in the field of water law, taking into account the Code of Ukraine "About Subsoil" for groundwater. The harmonization of the Water Code of Ukraine

with the requirements of Directive 2000/60 / EC in accordance with the Association Agreement between Ukraine and the European Union (EU) has also contributed to the expansion of legal regulation of water resources on a basin basis. However, in the process of implementing the OSCE project in Ukraine "Assistance to the Ministry of Ecology and Natural Resources of Ukraine in Improving Environmental Monitoring Mechanisms" the Siverskyi Donets river basin was artificially transferred to the Don river sub-basin without taking into account established hydromorphological, geomorphological, structural-tectonic, geological, hydrogeological and paleohydrological data.

In order to restore the basin status of the Siverskyi Donets River and ensure effective management of river basins and sub-basins of surface water and groundwater of the south-eastern regions of Ukraine, we will objectively consider the hydro morphological, geomorphological, paleohydrological, structural-tectonic and hydrogeological aspects of the Siverskyi Donets River and the Don River for comprehensive substantiation of groundwater sub-basins and organization of diagnostic water monitoring.

Analytical research was carried out using a wide range of general and special scientific methods, methodology of hydrogeological research, regulations of Ukraine and published geological and geographical maps.

1. Hydrogeological Features of the Siverskodonetsk Groundwater Basin

The Siverskyi Donets River is the main waterway of the south-eastern regions of Ukraine. Together with its largest left tributary - the Oskol River - it originates on the southern slope of the Middle Russian Upland (Eastern European Platform), forms the Siverskodonetsk Plain, and flows along the northern and northeastern sides of the Donetsk Ridge (Donetsk Coal Basin). At the same time, 68.7% of the length and 55% of the intake area of the Siverskyi Donets River is located in Kharkiv, Donetsk and Luhansk Regions of Ukraine.

Within the Siverskodonetsk groundwater basin in the works of previous years, according to hydrogeological zoning and geological and structural features of this area, two hydrogeological provinces

are distinguished: Dnipro-Donetsk artesian basin and Donetsk hydrogeological folded region.

1.1. *The Dnipro-Donetsk artesian basin* is fully represented in Kharkiv region and occupies the north-western part of Donetsk and northern Luhansk regions.

The main aquifer of this artesian basin is a fractured zone of Upper Cretaceous deposits, and within the anticline and dome structures - aquifers of the Upper and Lower Triassic and Lower Permian and Upper Carbonic. The most common Upper Cretaceous aquifer is characterized by significant reserves of groundwater, mainly of drinking quality, and stable significant flow rates of operational water intakes (2-10 thousand m^3/day). Most water intakes are collective and consist of several production wells located along the riverbed on the floodplain and the first floodplain terrace. Therefore, as a result of intensive operation of these water intakes, depression funnels were formed, which are elongated along the river and have transverse dimensions of 2-4 km with a decrease in the groundwater level in the center of the funnel to 10-15 km. During the year in the definite periods of operation of natural reserves of groundwater of alluvial sands, which are replenished during floods.

A characteristic feature of the Dnipro-Donetsk artesian basin as a whole is the extremely large depth of the zone of active and significant multi-volume water exchange - up to 800-1000 m and more.

1.2. *The Donetsk hydrogeological folded region* is confined to the southern and southwestern part of the Siverskodonetsk basin and covers the peripheral areas of Donbas, Bakhmut and Kalmius-Toretsk basins covered by Mesozoic and Cenozoic deposits, and open and semi-closed basins (covered only by Cenozoic sediments) areas of the Donetsk coal basin.

Open areas of Donbas (Central, Dolzhansko-Rovenkivskyi, partially, Bokovo-Khrustalskyi and Chystiakovo-Snizhnianskyi), where cover sediments are practically absent, are characterized by intensive hydraulic connection of groundwater and surface water and precipitation filtration. For the semi-enclosed Donbas, where Cenozoic and Quaternary deposits with a thickness of 15-40 m are developed over most of the area, the hydraulic connection of groundwater and surface water and atmospheric supply of Carbonic aquifers are complicated and significantly limited [8].

The highest filtration properties of Carbonic deposits of open and semi-closed areas of Donbas are characterized by the upper weathered zone of active water exchange, with thickness from 45-60 m in the eastern part of the Donetsk basin and up to 100-150 m in its western part and within zones of tectonic disturbances [6].

Mineralization of groundwater in the zone of active water exchange of open and semi-closed areas of Donbas is 0.8-1.5 g/dm^3, and in closed - 1.5-2.2 g/dm^3. In the range of depths of 700-900 m, the mineralization of carbon groundwater on average reaches 3.0-3.5 g/dm^3, and then for every 100 m increase in depth, it increases by 0.25-0.6 g/dm^3 [6].

The closed north-western part of the Donetsk hydrogeological folded region, which partially includes the Pokrovsk coal field and completely the Bakhmut and Kalmius-Toretsk basins, is a transitional zone between the Dnipro-Donetsk artesian basin and the typical Donetsk hydrogeological folded basin. As a result of subplatform Cimmerian and Alpine tectogenesis in this area, the north-western (transitional) part of the Donetsk hydrogeological folded region is significantly complicated by linear and downfold -like synclines (Komyshuvasko-Lymanska, Kramatorsko-Chasivoyarska, Northern, Kryvolukska, Raisko-Kalynivska and Kurdiumivska), which are separated and articulated with linear (Main and Druzhkivsko-Kostiantynivska) anticlines and brachial uplifts - Bakhmutske, Sviatogirske, Kamianske, Slavianske, Bantyshevske and Toretske.

In general, depending on the geological and structural timing and openness of the main aquifers of the north-western part of the Donetsk hydrogeological region, the zone of active water exchange with fresh (less than 1.5 g/dm^3) and weakly brackish (1.5-2.5 g/dm^3) groundwater varies from 250-300m to 700-800 m [6].

Unfavorable conditions of supply and water exchange in the areas of Upper Cretaceous and Triassic overlap with Quaternary and Neogene-Peleogenic deposits cause the formation of mostly weakly brackish and brackish groundwater.

2. Geological, Paleohydrological and Geoformological Differences of the Siverskyi Donets and the Don River Basins

The main geological and tectonic megastructures of the Siverskodonetsk river basin are the Dnipro-Donetsk Rift (DDR) and Donbas, as integral components of the united Dnipro-Donetsk

avlacogenic depression, and the Don River basin - the Eastern European platform.

Within the Eastern European platform, the main continental watershed between the Baltic and Black Seas runs, and the Dnipro River megabasin and the Volga River megabasin are equivalent to the common continental megabasins of the Black Sea-Caspian continental slope. According to hydrological factors, the Don River basin in the border regions of the Russian Federation belongs to the Volga River megabasin, and the Siverskodonetsk basin valley of the Dnipro-Donetsk artesian basin together with the Middle Dnipro basin is part of the Dnipro megabasin (Fig. 1).

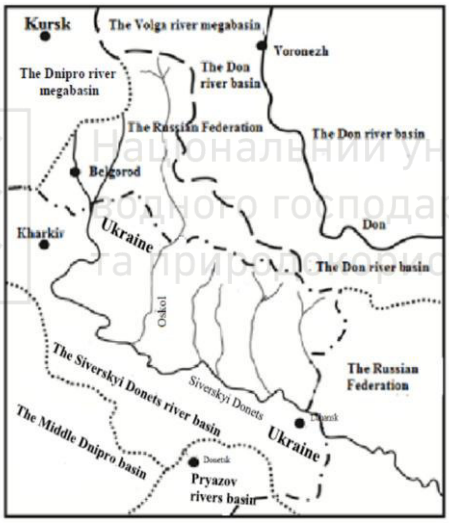

Fig. 1. Hydrographic zoning of river basins of the border regions of Ukraine and the Russian Federation

According to paleogeogeographical studies of previous years, the North Donbas Paleorica - Paleo-Donets or Pra-Donets is the largest fossil river in the Donbass, the channel valley of which is reliably isolated and well studied in the process of complex lithologic-and-facies studies of coal, Triassic Neogene and Quaternary sediments as an integral part of the watershed of the Paleo-Dnipro megabasin within the south-eastern part of the DDR and Donbas. Moreover, the

Donetsk coal basin (Donetsk Ridge) on the initiative of a domestic scientist from Slobozhan area E.P. Kovalevskyi in 1829 received its official name from the Siverskyi Donets River, not the Don River, because the Siversky Donets River receives all tributaries from the basin catchment area, washes and enriches cracked-porous groundwater on the left bank and significantly improves the water balance of open and semi-open Donbass on the right bank [5].

In the paleogeographic development of the Paleo-Don (Miocene) and Pra-Don (Late Pleistocene) Russian scientists during many years of research have established the formation of the Paleo-Don and Pra-Don joint with Pra-Manych Pryazov-Don basin and a single delta of the Pra-Don. (Fig. 2, 3).

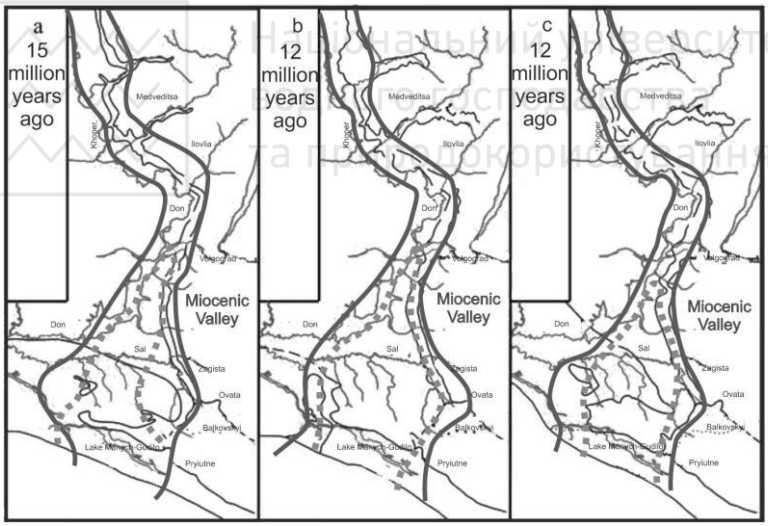

Fig. 2. Miocenic valleys of the Paleo-Don (according to M.N. Gryshchenko, 1952; A.S. Zastrozhnov, 2009; G.R. Rodzianko, 1965, 1970)

That is, Taganrog Bay then reached the meridian of the current Lake Manych [3]. However, after the Don glaciation about 600 thousand years ago and the formation of powerful moraine deposits in the Don Valley at the latitude of today's Volgograd, the course of

the Don River changed significantly in the south-western direction and occupied the submeridional valley formed by the Siverskyi Donets River, which is confined to the south-eastern confluence of the Dnipro-Donetsk depression or the Eastern Donbas.

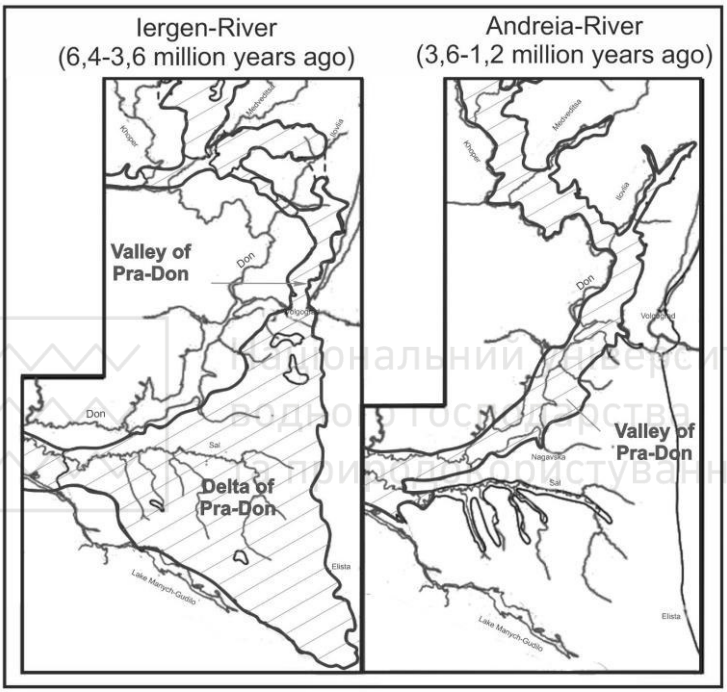

Fig. 3. The valley of the Pra-Don in the period of the Iergen River and Andeia River (M.N. Grishchenko and Y.A. Petrakovych, 1939; G.V. Kholmov, 1984)

At the same time, the independence of the Siverskyi Donets riverbed was preserved almost to the latitude of the present city of Rostov-on-Don and can be traced even now to the Taganrog Bay of the Sea of Azov called the Dry Donets River – the Aksai River – the Dead Donets River with the formation of an independent delta, separated by a strait from the delta of the Don River (Fig. 4).

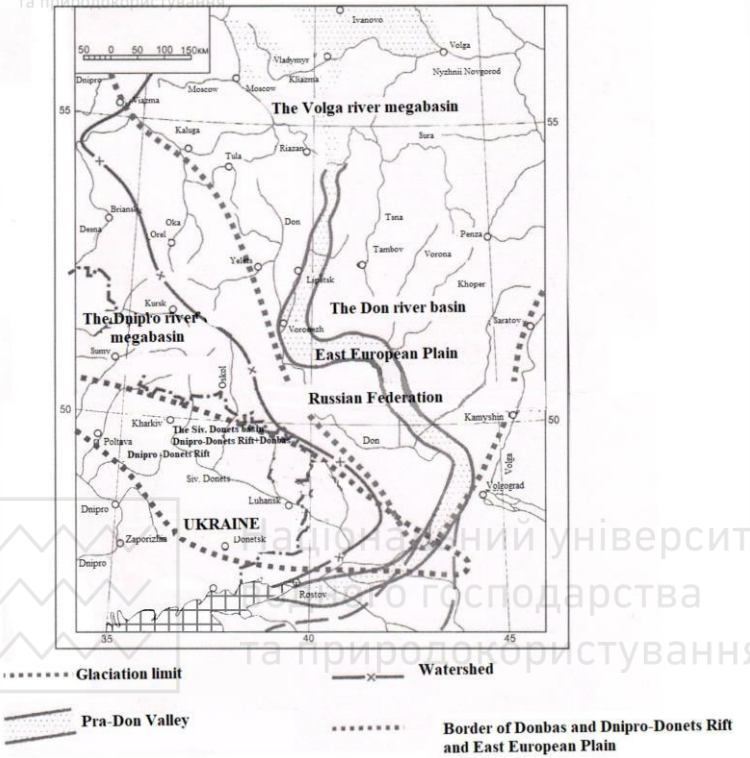

Fig. 4. Scheme of water basins in the maximum stage of glaciation between the Dnipro and Volga rivers (600 thousand years ago), according to V.A. Brymov (1984), A.S. Zastrozhnov (2009), G.I. Goretskyi (1961, 1964, 1970), M.N. Gryshchenko (1952), G.N. Rodzianko (1947, 1965, 1984)

On geographical maps of scale 1:200000-1:500000 within the Pryazov-Don lowland or the Lower Don according to geomorphological, hydrological and geological factors in Rostovregion of the Russian Federation three independent river basins of surface water and groundwater are reliably allocated: the Siverskyi Donets river basin, the Don river basin and the Pryazov rivers basin (Fig. 5).

Thus, on the territory of the south-eastern regions of Ukraine and within the border regions of the Russian Federation, the Siverskyi Donets river basin is by all signs and factors an independent river basin of both groundwater and surface water.

Fig. 5. Hydrographic zoning of river basins of the Lower Don

3. Brief Description of Sub-basins of Water Basins of the South-Eastern Regions of Ukraine

The south-eastern regions of Ukraine are represented by the Siverskodonetsk river basin, the Middle Dnipro basin of the Dnipro megabasin and the Pryazov rivers basin.

3.1. *The Siverskodonetsk basin of surface and groundwater*, taking into account hydrological, structural-tectonic and geological-hydrogeological features of the river basin, is represented by sub-basins of the left slope and sub-basins of the right slope (Fig. 6).

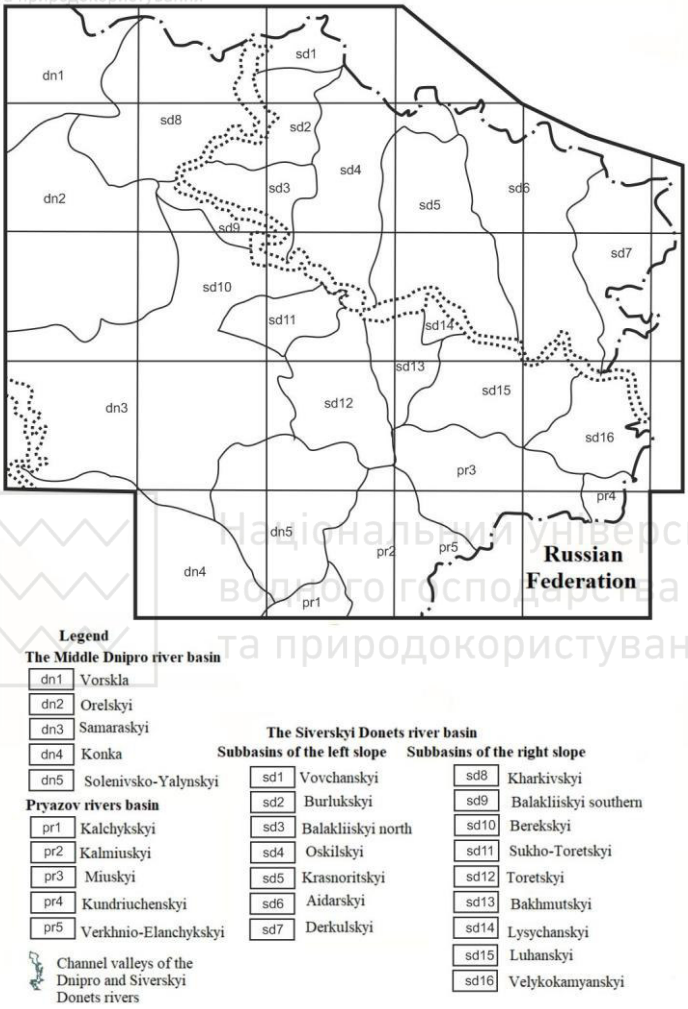

Fig. 6. Scheme of water basins and sub-basins of the south-eastern regions of Ukraine

The left slope of the Siverskyi Donets River is represented by Vovchanskyi (sd1), Burlukskyi (sd2), Pivnichno-Balakliyskyi (sd3), Oskilskyi (sd4), Krasnoritskyi (sd5), Aidarskyi (sd6) and Derkulisky (sd7) sub-basins, and the right - Kharkivskyi (sd8), South Balakliiskyi (sd9), Berekskyi (sd10), Sukho-Toretskyi (sd11),

Toretskyi (sd12), Bakhmutskyi (sd13), Lysychanskyi (sd14) Luhanskyi (sd15), Velykokamianskyi (sd16) and Kundriuchenskyi (sd17) sub-basins (Fig. 6). Aquifers and sub-basin complexes of the Siverskodonetsk River basin are traditionally distinguished in alluvial Quaternary, Neogene, Paleogene, Cretaceous, Jurassic, Triassic, Lower Permian and coal deposits, which are separated by a number of refractories. Regionally aged refractories are associated with deposits of Lower Quaternary, Neogene and Jurassic clays, clayey marls of the Paleogene Kyivan world, massive uncracked marl-Cretaceous strata of the Upper Cretaceous, chemogenic deposits of the Lower Permian and clay-shaly layers of the Lower Permian and Carbonic.

According to long-term system studies of previous years, groundwater supply of sub-basins of the Siverskodonetsk basin is carried out by infiltration and filtration of rainwater, snow melting, condensation of water vapor and film transfer of moisture with a significant impact of unloading deep waters in tectonic and tectonic zones and also the influence of natural and man-made factors in connection with the filtration losses of open canals and water mains.

3.2. *The Middle Dnipro sub-basins* are represented by the the Vorskla and the Orelka rivers sub-basins typical of the Dnipro-Donetsk Rift and the transitional sub-basins of the Samara and Konka rivers and the Solenivsko-Yalynskyi sub-basin. They are characterized mainly by medium-highly mineralized fractured waters of the Carbonic, Triassic, and Jurassic and fractured in Precambrian crystalline deposits. Weakly mineralized and fresh groundwater is associated mainly with alluvial, Neogene, and Paleogene aquifers.

3.3. *The Pryazov rivers sub-basins* are represented in the south of the south-eastern regions of Ukraine by small rivers from the Lower Dnipro basin to the eastern border of Ukraine. Groundwater masses are associated with Cretaceous and Cenozoic sediments (upper aquifers), which lie on the blurred surface of the Upper Paleozoic deposits and the Precambrian crystalline basement (pore-fractured and fractured horizons).

4. General Characteristics of Groundwater Masses of the Siverskodonetsk River Basin

Determination of geological section and pre-Quaternary surface of groundwater masses must be performed separately for each of the

17 sub-basins of the Siverskodonetsk river basin, taking into account structural-tectonic, geological-formation and hydrogeological factors and patterns. The vast majority of sub-basins are characterized by a three-layer structure of sedimentary strata in the Upper Paleozoic, Mesozoic, and Cenozoic structural-stratigraphic complexes (layers). According to the degree of openness of the Upper Paleozoic Carboniferous and Lower Permian deposits, open, semi-open and closed sub-basins are distinguished.

All sub-basins of the left slope of the Siverskyi Donets River and the Kharkivskyi, Pivdenno-Balakliiskyi, Berekskyi and Sukho-Toretskyi sub-basins of the right slope are closed sub-basins. Masses of groundwater of these sub-basins are represented by the aquifer complex of the Upper Triassic and Upper Cretaceous and Alluvial, Neogene and Paleogene sands, which are characterized by weakly mineralized and fresh hydrocarbonate, rarely sulfate-hydrocarbonate waters with a salinity from 0.3-0.8 g/ to 0-1.5 g/dm^3 [7, 8].

Intensive manifestation in these sub-basins of Cimmerian and Alpine tectogenesis has led to the formation of brachyanticline and salt dome structures and small artesian basins in synclines and downfolds with their areas of supply, transit and groundwater discharge.

In the layered systems of small artesian basins with transitional water exchange, the processes of desulfation and cation exchange are manifested, which leads to the improvement of groundwater quality mainly of chloride-hydrocarbonate-sodium composition with mineralization from 0.2-1 g/dm^3 and hardness up to 7 mmol / dm^3. However, in the watersheds in poorly permeable sediments of different ages developed processes of secondary salinization, which causes the formation of waters with increased mineralization from 1.5-3 g/dm^3 to 4-6 g/dm^3 mainly sulfate, hydrocarbonate-sulfate, sulfate-hydrocarbonate-calcium and chloride-sulfate composition [1]. In the areas of exits to the pre-Cenozoic surface of hemogenic sediments of the lower Permian within the brachyanticline and salt dome structures, groundwater mineralization increases from 2-10 g / dm^3 to 50-312 g/dm^3 of sulfate, sulfate-chloride and chloride composition [8].

Masses of groundwater of semi-enclosed sub-basins (Bakhmutskyi, Lysychanskyi and Kundryuchenskyi sub-basins) are

characterized by difficult conditions of formation of chemical composition of groundwater from fresh-slightly saline (0.5-1.9 g/dm^3) sulfate-hydrocarbonate and sodium-calcium to chloride and chloride -sodium with mineralization from 2 g/dm^3 to 7.5 g/dm^3 [6]. The effective thickness of aquifers varies from 5 m to 90 m and averages 40-50 m. Carbonic aquifers are characterized by low water enrichment and water conductivity. In the valleys, the rivers are mixed with fresh groundwater of the Middle Paleogene and Alluvium.

Masses of groundwater of open sub-basins (Toretskyi, Luhanskyi and Velykokamianskyi sub-basins are represented by porous-fissured, fissured and fissured karst groundwater, which in the near-surface weathered zone, with thickness from 46-70 m to 150-200 m, form a single aquifer). Below this zone, groundwater circulates in separate inhomogeneous aquifers, mining and man-made cavities and zones of tectonic faults with an average groundwater flow modulus of 0.5-1.5 l / sec per 1 sq. m [6].

The chemical composition of groundwater in the drainage zone of the river network corresponds to the general physical and geographical zoning: in the western part is dominated by hydrocarbonate-sulphate-sodium-calcium and sulphate-sodium-calcium water with a salinity of up to 2.5-3.5 g/dm^3, and in the east and south-east - weakly mineralized and fresh hydrocarbonate-calcium waters [8].

5. Regional Technogenic Changes and Organization of Diagnostic Monitoring of Groundwater

The territory of groundwater sub-basins of the Siverskodonetsk river basin is located in different hydromorphological, geological, structural-tectonic and hydrogeological conditions, which determines the peculiarities of the formation of groundwater masses, their resource potential, quantitative and qualitative changes of aquifers and water intakes which is necessary to take into account both groundwater and surface water in the process of organizing diagnostic monitoring [5, 9].

Indoor sub-basins are characterized by the highest protection of groundwater masses with a low level of man-made pollution associated with local impact of industrial enterprises and excessive

use of fresh groundwater of the Upper Cretaceous and hydraulically associated alluvial aquifers.

Intensive changes in hydrodynamic conditions and quality of groundwater masses of semi-enclosed sub-basins of the Siverskodonetsk river basin are associated with outdated environmentally unsanitary industrial production within Bakhmutskyi, Slovyansk-Kramatorskyi, Rubizhansko-Lysychanskyi, Siverodglovenskyi and Alchevsko-Luhanskyi industrial agglomerations with intensive pollution by metals, chemical compounds and industrial and household waste. However, given the significant reduction in recent years of the impact on the geological environment and groundwater of electricity, metallurgy, engineering and chemical industries, the greatest man-made impact are open sub-basins of the Siverskodonetsk river basin due to low protection of groundwater from industrial impact and mass closure of coal mines.

The main criterion for the protection of aquifers of the Donbas coal seam is the presence of strong (10-30 m) and sustained layers of overlapping Cenozoic and Anthropogenic waterproof deposits, but the approach of mine workings to the near-surface zone in river valleys and the presence of hundreds of sloping spatial hydraulic connection of groundwater and surface water and increase the level of man-made danger in the open sub-basins of the Siverskodonetsk river basin in the conditions of mass uncontrolled closure of coal mines [4, 6].

Currently, about 50 mines of Donbas are considered to be flooded by two thirds of the volume of the mountain massif and in the immediate vicinity of the near-surface zone of increased fracturing. At the same time, the pace and scale of changes in the ecological and hydrogeological regime of groundwater are particularly valid and significant in the territory temporarily not controlled by Ukraine, in densely populated old industrial areas and in the demarcation zone. In particular, flooding by mine waters of the near-surface zone of Bunge (Yunkom), Horlivka, Yenakiyevo, Pervomaisk, Zolote and partially Toretsk, Makiivka and Shakhtarsk led to the restoration of hydraulic connection of surface and groundwater and the formation of stable man-made systemic restoration of historical groundwater levels [4, 6].

The rise of mine water to the historical level of groundwater in areas of mass flooding of coal mines in accordance with the parabolic dependence after their rapid rise in the first 5-7 years may continue for 20-25 years from the beginning of uncontrolled flooding of mine workings depending on cyclical changes in levels and dynamic-filtration regularities of groundwater masses distribution within open and semi-open sub-basins [6].

Taking into account the above, the system of diagnostic regional and zonal monitoring of groundwater should be based on a comprehensive study of disturbed and modeling of reproducible natural regime with determination of vertical and lateral hydrogeological patterns of groundwater masses within all sub-basins of the Siverskodonetsk river basin.

The Siverskodonetsk river basin management plan for groundwater should be based on the implementation of the following mandatory structural measures (stages):

- hydromorphological, geomorphological, geological and hydrogeological description of groundwater sub-basins;
- selection and typology of groundwater masses;
- characteristics of the main factors of man-made impact on the state of groundwater;
- allocation and mapping of zones of technogenic disturbed groundwater regime in zones of industrial influence;
- determination of areas of undisturbed natural groundwater regime that are subject to protection;
- modelling and organization of the system of diagnostic monitoring of groundwater masses within the sub-basins;
- implementation of socio-economic analysis of groundwater use and preparation of recommendations to improve its efficiency.

Conclusions

The analysis of hydrogeological features of the Siverskodonetsk river basin and paleohydrological differences of the Siverskyi Donets and the Don Rivers allowed to substantiate the independent basin status of the Siverskyi Donets River on the territory of the south-eastern regions of Ukraine and border regions of the Russian Federation.

On the territory of Ukraine within the Siverskodonetsk river basin 17 water sub-basins have been identified and the hydrogeological

features of groundwater masses in closed, semi-closed and open sub-basins are briefly described.

In order to form a balanced environmentally friendly water management system of the Siverskodonetsk river basin, regional man-made changes in groundwater are considered and a system of diagnostic monitoring of groundwater is proposed.

After amendments to the Water Code of Ukraine dated 04.10.2016 № 1641-VIII on restoration of the basin status of the Siverskyi Donets River, it will be necessary to finalize regulations on the development of the Siverskodonetsk river basin management plan and allocation of sub-basins and groundwater and surface water.

References

1. **But Yu.S., Reshetov I.K.,** Drobnokhod N.I. et al. (1987). Small Artesian Basins of the North-Western Donbas. - Kiev: Naukova Dumka. – 200p.

2. **Vernadskyi V.I.** (1936). History of Minerals of the Earth's Crust//in 2 volumes/vol. 2. History of Natural Waters. - L.: ONTI Khimteoret. - Part 1, issue 3.

3. **Goretskyi G.I.** (1982). Paleopotamological Sketches of Paleo-Don and Pro-Don. - Minsk: Nauka i Tecknika. – 248p.

4. **Denisov N., Averin D., Yushchuk A.** (2017). Environmental Damage Assessment and Priorities for Environmental Restoration in Eastern Ukraine. - Kyiv: BAI.T. – 88p.

5. **Zhykalyak M.V., Kuroyedova S.V., Marynchenko M.E.** (2018). Harmonization of the Groundwater Monitoring System of Donbas with the Standards of the European Union. - Geoforum-2018. - Kyiv, UkrSGRI. - P. 119-124.

6. **Zhykalyak M.V., Kuroyedova S.V., Marynchenko M.E**. (2019). Methodical and Normative-legal Aspects of Assessment of Ecological-hydrogeological Changes as a Result of Flooding of Donbas Coal Mines/Intern. scientific-practical conf. "Modern Problems of Mining Geology and Geoecology". - SI SCMGGID NASU. Kyiv. - P. 125-133.

7. **Zastezhko Yu.S.** (1972). Characteristic Features of the Chemical Composition of Groundwater in the South-Eastern Part of the Dnipro-Donetsk Basin/Tr. of Ukrainian Research Institute for Natural Gases. Issue. 4. - Kharkiv. - P. 250-259.

8. **Suyarko O.V.** (1970). About the Connection of the Zones of Unloading of Deep Horizons of the Paleozoic with the Deep Tectonics of Donbas//Reports of AS of UkrSSR. - Ser. B. № 5. - P. 405-406.

9. **Trofanchuk S.I.** (2019). The First Steps in Developing a Management Plan for the River Sub-basin of the Siverskyi Donets and the Lower *Don Sub-basin*//Vodne Gospodarstvo Ukrayiny, № 9-10. - Kyiv. - P. 9-15.

https://doi.org/10.31713/m1021

THE ANALYSIS OF NATURE OF DAMAGE OF THE MATRIX MATERIAL, USED IN PRODUCTION OF DIAMOND DRILLING AND STONE-WORKING TOOLS DURING THE DESTRUCTION OF A ROCKS

Vynohradova O.P., Vasylchuk O.S., Zakora A.P., Petasyuk G.A. Garashchenko V.V.

N. Bakul Institute for Superhard Materials National Academy of Sciences of Ukraine,
Avtozavods'ka, 2, 04074, Kyiv, Ukraine, e-mail: vinelen@ro.ru

Abstract

In this paper are studied themechanism of matrix damage in rock cutting diamond toolswhen interacting with rock.

Earlier, in the sludge obtained during mining with a diamond tool on a block of sandstone of the Torez deposit, using a scanning electron microscope (SEM) ZEISS EVO 50 XVP, equipped with Oxford Instruments` Ultim Max 100 energy-dispersive X-ray analyzer (elemental analysis) particles were found whose chemical composition corresponded to the matrix material of the tool. According to the theory of M.V. Kirpichev, the complete correspondence of all configuration elements of the individual studied matrix particles and rock particles, which the sludge obtained as a result of work of diamond tool testifies to a single mechanism of brittle fracture of both counterbodies during dynamic interaction.

However, the nature of the matrix material indentation, remains, unexplored.

On the basis of the hypothesis that the damage to the matrix material of a diamond tool is carried out by roughness elements from the side of the rock, the goal was set to investigate the wear products of a diamond-free insert made from material, used as a matrix in a diamond rock-breaking tool with a short-term dynamic contact with cooling with a rock block

The originality of the method lies in the fact that in this study, the destructive indenters are not diamond grains, which gouge out particles of the rock, but elements of the roughness of the rock, which damage theexperimental cylindrical free-diamond element from NiSn (6%), having a density of 7.875 g/cm^3, performed by the method of intensive sintering.

The sludge obtained as a result of a short-term interaction of the experimental element and the rotating block of the rock on the bench was examined using a , using aabove-mentioned scanning electron microscope. The spectral analysis of the removed from the sludge particle of matrix material from which the experimental diamond-free element was made, confirmed the conformity of chemical composition

of particle to the chemical composition of the matrix material of the experimental diamond-free sample.Full correspondence of all configurational components of a NiSn particle (6%) obtained by the action of a rock roughness element on a diamond-free insert during their dynamic interaction with all configurational components of wear particles of a diamond tool matrix., according to the similarity theory of M.V. Kirpichev, confirms the above-mentioned hypothesis.
Key words: rock cutting diamond cutting tool, matrix, damage mechanism, matrix material particle, sludge, scanning electron microscope

Introduction

One of the main criteria when choosing the chemical composition of a diamond-containing matrix for a rock-destroying tool is the conformity of the wear resistance of the matrix to the abrasive properties of the rock.

The loss of mass of the matrix material of the drilling tool, according to works [1,2] occurs due to the simultaneous indentation of spherical particles of rock sludge, resulting in scratches on the working surface of the matrix. A similar effect of abrasive particles on existing cracks and dislocations in the metal counterbody is indicated in [3-8], and the directions of crack propagation, as the authors indicate, ultimately affect the shape of the separated particle of destruction products of the metal sample, i.e,its wear is represented by a chaotic process.

A generally accepted measure of the wear rate of functional elements of drilling tools for diamond-containing composite materials (CDM) is to measure the loss of the mass or linear dimensions, which does not reflect the mechanism of the wear of the composite material.

The efficiency of the diamond drilling tool with a high wear-resistance depends from detailed study of the mechanism of interaction of a single destructive diamond indenter with a rock

It is on the basis of the above conclusions after studying of the granulometric composition of the sludge created a model of the damage to the diamond-bearing matrix in accordance with the work of Isonkin O.M. [9] thanks to simultaneous indentation of spherical rock particles into the matrix surface, as a result, on the working surface of the matrix of the drill bit (hardness on the HRC-15 scale,), equipped with synthetic diamonds, there were scratches.

The destruction of the matrix of rock-destroying elements of the drilling tool, according to [10] is similar to the destruction of the bottom after the work of the rock -brearing tool - with formation of microgrooves on the working surface of the matrix in the form of a series of microholes, alternating with a variable step and the width –*a*, Fig.1 when chipping the products of destruction in the form of microparticles of of diamond-containing matrix of hard alloy, chipped from the element of "Slavutych" during the destruction of sandstone of the Torez deposit, Fig. 2, characterized by all components of the geometric parameters of a single particle of rock sludge: the zone of indentation 1, lateral parts 2 and the final part 3, Fig. 2,3 [11].

It is determined that the chemical composition of the particles in the selected by method of magnetic separation, the magnetic fraction of sludge (from products of destruction obtained after the turning the core of sandstone of Torez field with a cylindrical diamond rock-breaking element, corresponds to its matrix material from NiSn (6%) [12].Their geometrical parameters are similar to the geometric parameters of particles of destruction of rock, which testifies to the fragile nature of the wear of the specified matrix material

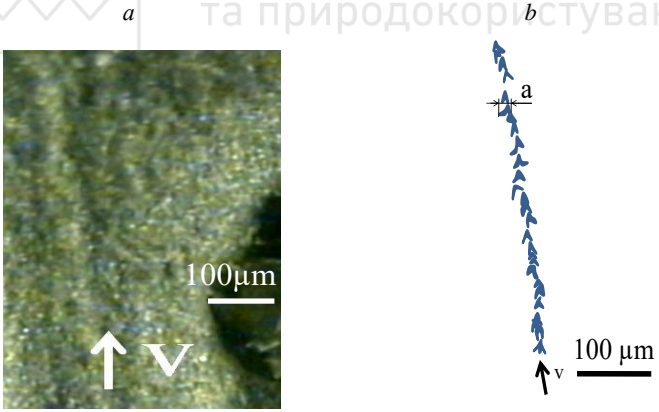

Fig. 1. The general view of: the working surface of the tungsten-cobalt matrix of the diamond rock-breaking element - *a*; *v*– the vector of the speed of breaking off of micro-particles of a matrix; schematic representation of a micro-groove consisting of microholes of hard alloy on the surface of the matrix, - *b*; *a* – the width of the microhole

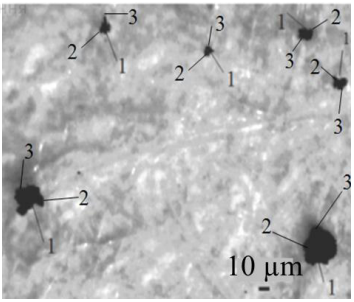

Fig. 2. The particles of fracture products of diamond-containing matrix of hard alloy, chipped from the element of "Slavutych" during the destruction of sandstone of the Torez deposit, *1* - zone of indentation (by sharp edge of quartz grain); *2* - lateral part; *3* - final part

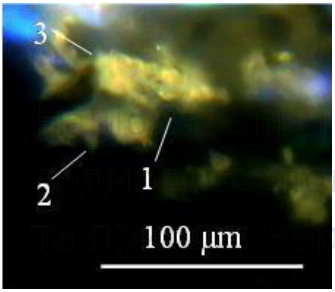

Fig. 3. The particles of sludge, chipped off from the block of sandstone of Torez field with a thickness of 40 μm: *1* - indenter penetration zone; *2*– lateral par; *3*– final part

However, the mechanism of fracture of the surface layer of the composite diamond material has not yet determined**.**

The purpose is to study of the nature of damage to the surface of a diamond-free element from NiSn (6%) by the block of sandstone of Torez field at dynamic loading.

Research methodology.

The tests to determine the nature of damage to the matrix material of experimental drilling diamond-containing elements were performed by the interaction of cylindrical block of sandstone of the Torez deposit of drilling category IX and the cylindrical free-diamond elementfrom NiSn (6%), on a special stand created on the basis of a lathe model DIP-200.The method of work on aspecial

stand created on the basis of a lathe model DIP-200.is described in detail in [13].

Before the start of the tests, a core of sandstone with a diameter of 93 mm and a length of 400 mm 1, fig.1, was drilled with a 112 mm diameter by drill bitand fixed incore holders 2 of a lathe. Cooled by the cooling system 3, the the cylindrical free-diamond element 4, fixed in a tool holder of a lathe and brought to the surface of the rock core, where longitudinal destruction of the cylindrical free-diamond element was carried out. The sludge 5 accumulated in the sludge collection bath 6 and moved through a hose for discharge of sludge 7 into the sludge receiver.

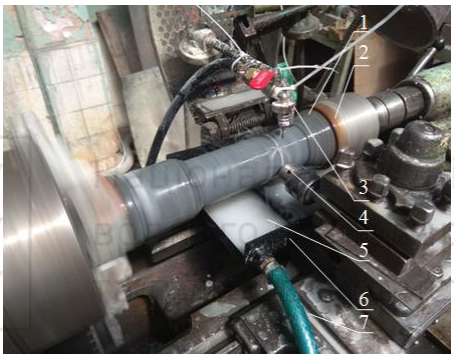

Fig. 4 The general view of a special stand in the process of research: *1* - cylindrical block of sandstone of Torez deposit; *2* - core holder; 3 - cooling system of cylindrical free-diamond element *4* - cylindrical free-diamond element; *5* - sludge; *6* - sludge collection bath; *7* - hose for discharge of sludge into the sludge receiver

The experimental cylindrical free-diamond element from NiSn (6%), having a density of 7.875 g/cm^3, was performed by the method of intensive sintering under the condition of simultaneous pressing: pressure - 300 MPa, sintering time - 14 sec amperage -1.3 kA.

The surfaces of diamond-free insertwas examined with a Bausch & Lomb, mod. Gemolite, microscope.

The sludge, in the form of a suspension, was selected, dried and examined on a microscope of the DiaInspect OSM device from VOLLSTADT DIAMANT GmbH DiaInspect OSM in order to separate rock particles and particles of the insert material, chipped off from its working surface during the dynamic action of sharp roughness elements of a rock block. The method of work on a

microscope of the DiaInspect OSM device from VOLLSTADT DIAMANT GmbH DiaInspect OSM is described in detail in [14].

Besides,at the final stage of research, the dried sludge was examined by scanning electron microscope (SEM) ZEISS EVO 50 XVP, equipped with Oxford Instruments` Ultim Max 100 energy-dispersive X-ray analyzer (elemental analysis).

Results

As a result of the short (1 min) interaction of the cylindrical element at turning with the surface of the pre-prepared by diamond tool abrasive sandstone core, at a feed rate of 0.148 mm / rev, at a feed rate of washing liquid of 5 l/min,the surface of the insert was examined with a Bausch & Lomb, mod. Gemolite microscope.

On the surface of the insert, micro-grooves were found, fig. 5*a*, identical to those formed on the surface of inserts equipped with diamond grains, that is, damage to the matrix surface occurred in both cases by roughness elements from the side of the rock block. The geometrical parameters of microholes on the surface of a free-diamond insert and microholes on the surface of inserts made of composite diamond-containing materials were identical. The width of the microholes, fig. 5*b*, reached 400 μm and the average width of the microholes creating micro-grooves 3 on the insert surface reached 200 μm.

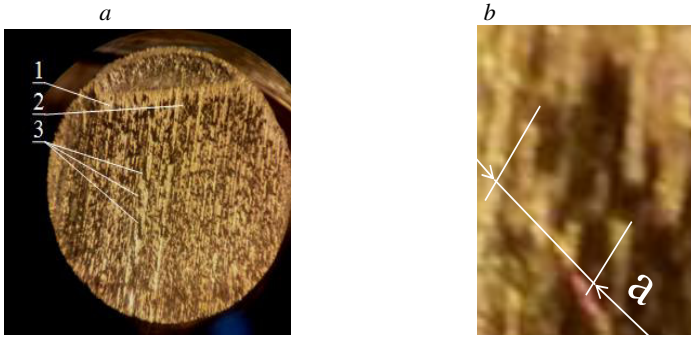

Fig. 5. The general view:ofthe surfaces of diamond-free insert: *1* - intact surface of the insert; *2* - microhole; *3* - microgrooves on the surface of insert-a, microhole 2 in Fig.5*a* (enlarged), *a* - width of microhole–*b*

The sludge, in the form of a suspension, was selected, dried and examined on a microscope of the DiaInspect OSM device from VOLLSTADT DIAMANT GmbH .

The sludge samples were examined in the field of view of a microscope of the DiaInspect OSM device from VOLLSTADT DIAMANT GmbH with penetrating lower light flux and upper illumination from a halogen light source,where the particles of sludge were located, consisting of particles of rock and the material of the insert, so, two types of particles were found, Fig. 6.

The particles of rock and, hypothetically, particles from material of the insert in the field of view look as particles light coloured and black– particles of a rock and particles of material of the experimental cylindrical free-diamond element,respectively.

An important feature of the geometric parameters of the presented particles is the presence of all the features of the configuration of rock particles when it is destroyed by a diamond tool and particles of a matrix material when a diamond-containing tool is damaged,namely, the zone of indentation (by sharp edge of quartz grain) – *1*, lateralpart – *2*, final part – *3*

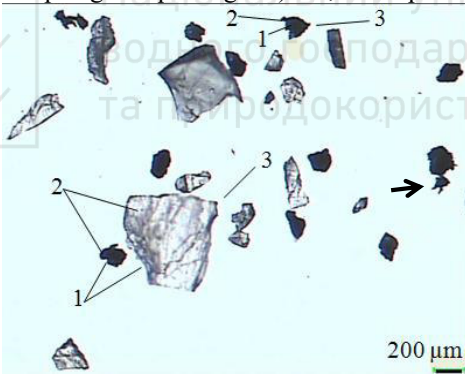

Fig.6. The particles of rock and, hypothetically. the particles of the material of the diamond-free insert in the field of view of a microscope of the DiaInspect OSM device from VOLLSTADT DIAMANT GmbH with penetrating lower light flux and upper illumination from a halogen light source: light coloured particles – particles of a rock, black particles–hypothetically, the particles of material of the experimental cylindrical free-diamond element: *1* - the zone of indentation (sharp edge of quartz grain); *2* –lateral part; *3* – final part – *b*

In order to make sure that the black particles on the microscope table are the particles of the insert material, a spectral analysis of the particles was carried out.

The dried sludge was examined by scanning electron microscope (SEM) ZEISS EVO 50 XVP, equipped with Oxford Instruments` Ultim Max 100 energy-dispersive X-ray analyzer (elemental analysis).

The study of the sludge fraction using a SEM, shows that thechemical composition of some particles, for example, presented on Fig. 7*a*, coincides with the composition of the material of the experimental element from NiSn (6%), Table 1,2 which is diamond-free.

The particle is located on the particles of the rock, as evidenced by the chemical compositions of the spectra №№ 45,46,47 with the predominant values of Silicon and Oxygen.

When moving, schematically, the detached end part 2', Fig.7*b* to the main lateral part 2, the particle take on a finished form.

The zone of penetration 1 of the particle is formed together with the residual zone of penetration 1', which, when chipping off the particles of rock with a diamond tool, is formed extremely rarely, is lost due to high fragility. With an increase in plasticity, as in the case of the studied matrix material, the residual zone 1'may not be destroyed.

The particle have an axis of symmetry; moreover,all geometrical parameters, inparticular, the introduction zone 1, the lateral parts 2, end zone 3, Fig. 6*b*, as well as overall dimensions, correspond to the relevant parameters of the particles of the wear of the element from the composite diamond-bearing material under similar conditions of their working off [12].

The geometric parameters of the particle, its overall dimensions (width and length– nearly, 90 and 150 μm, respectively), the configuration are correspond to the corresponding parameters of the particles of the matrix material, studied in the field of view of a microscope of the DiaInspect OSM device from VOLLSTADT DIAMANT GmbH with penetrating lower light flux and upper illumination from a halogen light source.

In the particle, shown by the arrow in Fig. 6, residual zone of penetration is saved. Therefore, there is reason to believe that black particles in the field of view of a microscope of the DiaInspect OSM device from VOLLSTADT DIAMANT GmbH with penetrating

lower light flux and upper illumination from a halogen light source are particles of the matrix material.

Unfortunately, the particle thickness remains undetectable for the time being.

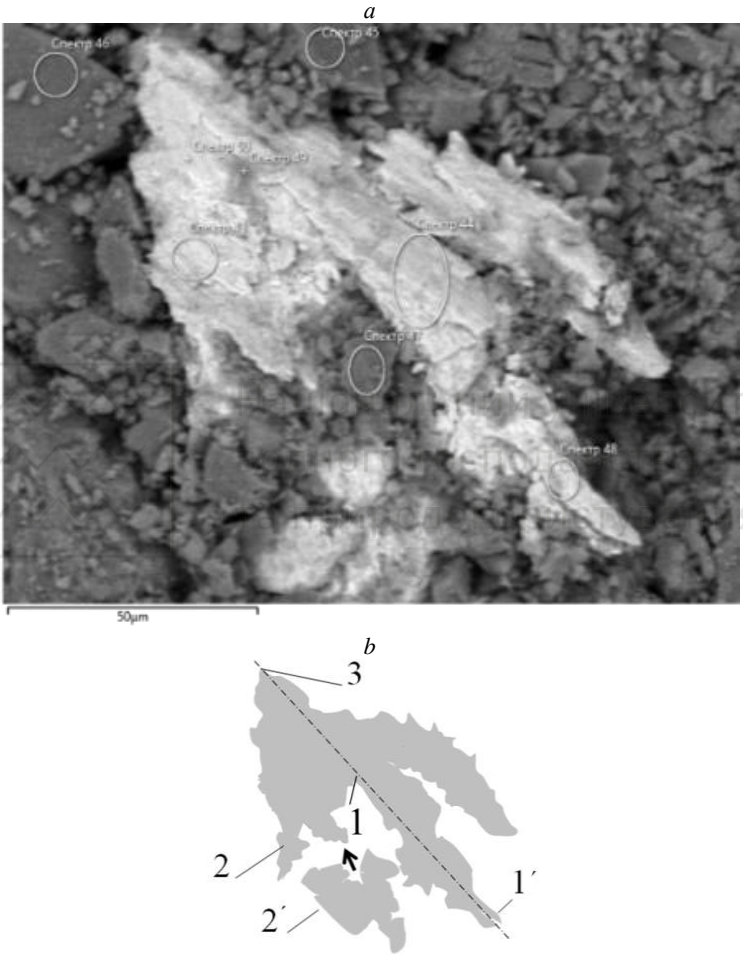

Fig. 7. The general view of the particle of wear of the diamond-free element fom NiSn (6%), against the background of abrasive sandstone sludg eparticles– image received by spectral analysis–a, schematic image of the zone of penetration 1 of the particle, residual zone of penetration 1', the main lateral part 2, the detached lateral part 2 ', final part 3–*b*

The table 1 shows, that the spectra №№43,44, 48,50 are with a predominance of Nickel in the background of sandstone particles.

The chemical composition of the sludge particle in spectrum №. 44, shown in Fig. 8, represented in Fig. 6a, in the center of the particle, namely, in the zone of indenter penetration 1 from the side of the rockby roughness element indicates on content, in addition to 71.37% Nickel , 5.42% - Stanum, which is as close as possible to the content of Stanum in the bundle - 6%, Table 1,2.

In the Spectra 50 composition, the maximum Nickel content is 84.08%, and the Stanum content is 3.74%.

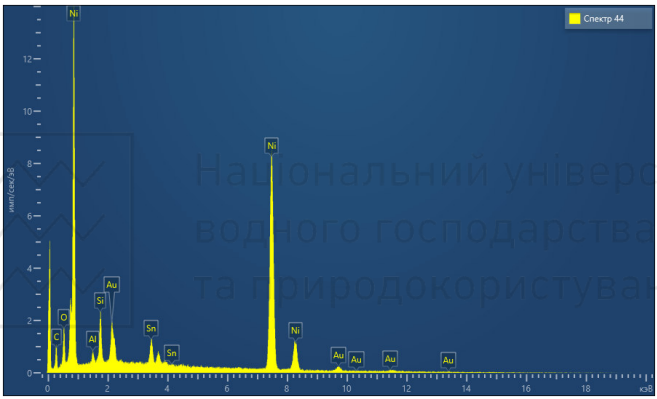

Fig. 8. The chemical composition of the sludge particle obtained by the interaction of the diamond-free experimental element with NiSn (6%) with the sandstone core of the Torez deposit, according to the results of spectral analysis - spectrum № 44

Table 1

The chemical composition of the sludge according to the results of spectral analysis

Sperc -ter tag	Spectru m 43	Spectru m 44	Spectru m 45	Spectru m 46	Spectru m 47	Spectru m 48	Spectru m 49	Spectru m 50
C	12.33	12.88	9.66	12.51	11.26	12.55	10.91	11.30
O	3.61	5.90	52.81	31.33	49.51	8.29	28.55	
Al	0.77	0.98	0.21		0.37	0.88	0.83	0.60
Si	1.78	3.46	36.73	56.15	37.20	4.80	25.05	0.29
Ni	77.06	71.37	0.57		1.65	68.73	33.07	84.08
Sn	4.45	5.42				4.75	1.58	3.74
Total	100.00	100.00	100.00	100.00	100.00	100.00	100.00	100.00

Result type-weight,%

Table 2

Statistics data of he chemical composition of the sludge according to the results of spectral analysis

Statistics	C	O	Al	Si	Ni	Sn
Max	12.88	52.81	0.98	56.15	84.08	5.42
Min	9.66	3.61	0.21	0.29	0.57	1.58
Average	11.68			20.68		
Standard deviation	1.09			21.15		

Conclusions

1. The working surface of the diamond-free experimental element is completely covered with a system of micro grooves formed by fixed indentation quartz in the form of roughness elements of the rock block.

2. Each micro-groove on the working surface of the experimental insert is formed from, separately, chipped single microholls, which indicates the fragile nature of wear of the diamond-free experimental element.

3. Geometrical parameters of a separate microholl on the surface of the diamond-free element (configuration and dimensions which reaching 400-500 μm) and micro-holes on the surface of the diamond-containing rock-destroying element based on a matrix from NiS n(6%) are identical.

4. Spectral analysis of the removed from the sludge particle of matrix material from which the experimental diamond-free element was made, which was subjected to dynamic loading from the rock block, confirmed the conformity of chemical composition of particle to the chemical composition of the matrix material of the experimental diamond-free sample.

5. The above statements confirm the hypothesis that the mechanism of wear of the matrix material of diamond-bearing rock-destroying tool consists in indentation in the surface of the matrix by "fixed" elements of rock roughness, followed by detachment from the matrix surface of individual particles of matrix material.

6. The configuration of wear particles of the matrix material of diamond rock-destroying tool, diamond-free element based on the same matrix material and particles of rock destruction is identical, which indicates the fragile nature of rock fracture and matrix from

these chemical elements,i.e.in the process of rock destruction there is mutual destruction: diamond grains in the tool chip off single particles of rock, and its elements of roughness destroy the matrix material of the tool.

7. Determination of the source of damage to the working surface of a diamond-containing rock cutting tool during rock destruction opens up new prospects in the study of the wear mechanism of the matrix material and makes it possible to develop criteria for the wear resistance of drilling and stone-working tools, which is reflected in the resource saving of the matrix material.

8. Full correspondence of all configurational components of a NiSn particle (6%) obtained by the action of a rock roughness element on a diamond-free insert during their dynamic interaction with all configurational components of wear particles of a diamond tool matrix. , according to the similarity theory of Kirpichev [14], confirms the hypothesis [15,16] that one of the sources of damage to the matrix material is the damage to the matrix material of the diamond-containing mining cutting tool occurs by fixed roughness elements from the side of the rock.

Reference

1. **Isonkin, A. M.** (2010). Kharakter i stepen vozdeisviia chastits shlama razrushennoi hornoi porody na matritsu almaznoi burovoi koronki [The character and degree of the impact of sludge particles of destroyed rock on the matrix of diamond bit]. Porodorazrushaiushchii i metalloobrabatyvaiushchii instrument – tekhnika i tekhnolohiia eho izhotovleniia i primeneniia [Rock Destruction and Metal-Working Tools –Techniques and Technology of the Tool Manufacture and applications] Vol.13, 182-187 [in Russian].

2. **Isonkin, A. M., Ilnitskaia, H. D., Tsysar, M. A.** (2015). Vliianiie mekhanoaktivirovaniia shikhty WC+Co+Cu nanoalmazami na strukturu i svoistva materiala matritsy burovykh koronok. [The effect of mechanical activation of the charge WC + Co + Cu by nanodiamonds on the structure and properties of the material of the matrix of drilling bits]. Porodorazrushaiushchii i metalloobrabatyvaiushchii instrument – tekhnika i tekhnolohiia eho izhotovleniia i primeneniia [Rock Destruction and Metal-Working Tools –Techniques and Technology of the Tool Manufacture and applications] [Rock Destruction and Metal-Working Tools –Techniques and Technology of the Tool Manufacture and applications], Vol.18, 103-109 [in Russian].

3. **Netrebko, V.V.** (2019). Naukovi ta tekhnichni osnovy pidvyshchennia mekhanichnykh i sluzhbovykh vlastyvostei vysokokhromnykh chavuniv [Scientific and technical bases of increase of mechanical and service properties of high-chromium cast iron]. Extended abstract of Doctor'sthesis. Zaporizhzhia [in Ukrainian].

4. **Chepovetskii, I.Kh.** (1978). Mekhanika kontaktnoho vzaimodeistviia pri almaznoi obrabotke [Mechanics of contact interaction in diamond processing]. Kiev: Naukova dumka [in Russian].

5. **Ohlezneva, S.A.** (2004). Almaznyi instrument s fazovymi prevrashcheniiami [Diamond tools with the phase transformations]. Treniieiiznos – Friction and wear, Vol. 25, 1, 79–84 [in Russian].

6. Zybinskii, P.V., Bogdanov, R.K., Zakora, A.P., &Isonkin, A.M. (2007). Sverkhtverdyie materialy v geologorazvedochnom burenii [Superhard materials in exploration drilling]. Donetsk: Nord-press [in Russian].

7. **Soloviev, N. V., Chikhotkin, V. F., Bogdanov, R. K., & Zakora, A. P**. (1997). Resursosberehaiushchaia tekhnolohiia almaznoho bureniia v slozhnykh heolohicheskikh usloviiakh [Resource-saving technology of diamond drilling indifficult geological conditions].Moscow: VNIIOENG [in Russian].

8. **Gorshkov, L,.K., Iakovlev, A.A., Pavlov, N.A.** (2010). Matematiko-mekhanicheskaia model razrusheniia porod pri burenii [Mathematical and mechanical model of rock destruction during drilling]. Porodorazrushaiushchii i metalloobrabatyvaiushchii instrument - tekhnika i tekhnologiia ego izgotovleniia i primeneniia [Rock-cutting and metal-working tools - equipment and technology for their manufacture and use], Vol. 13, pp. 3-7. [in Russian].

9. **Isonkin, A. M.** (2012). Formirovaniie reliefa rabochei poverkhnosti almaznoi burovoi koronki. [The formation of the relief of the working surface of the diamond drill bit]. [Rock Destruction and Metal-Working Tools – Porodorazrushaiushchii i metalloobrabatyvaiushchii instrument - tekhnika i tekhnolohiia eho izhotovleniia i primeneniia [Rock Destruction and Metal-Working Tools –Techniques and Technology of the Tool Manufacture and applications] , Vol. 15, 63–68 [in Russian].

10. **Vynohradova, O.P., Shmehera, R.S., Suprun, M.V.** (2016). Doslidzhennia kharakteru ruinuvannia almazovmisnoi matrytsi burovoho instrumentu pry zminiy ii khimichnoho skladu [Investigation of the nature of the destruction of the diamond-bearing matrix of the drilling tool by changing its chemical composition].– Porodorazrushaiushchii i metalloobrabatyvaiushchii instrument – tekhnika i tekhnolohiia eho izhotovleniia i primeneniia [Rock Destruction and Metal-Working Tools –Techniques and Technology of the Tool Manufacture and applications], Vol.19, 43–50 [in Ukrainian].

11. **Vynohradova, O.P.** (2015).Ruynuvannya girskih pored instrumentom z funktsionalnymi elementamy iz kompozitsiynyh almazovmisnyh materialiv[Destruction of rocks by the tool with functional elements from composite diamond-bearing materials].Candidate's thesis. Kyiv [in Ukrainian].

12. **Maistrenko, A.L., Shmegera, R.S., Manokhin, A.S.** (2019). Analiz produktiv znoshuvannia zviazky porodoruinivnoho elementu iz kompozytsiinoho almazovmisnoho materialu [Analysis of wear products of a rock-destroying element made of composite diamond-containing material].–Porodorazrushaiushchii i metalloobrabatyvaiushchii instrument - tekhnika i tekhnolohiia eho izhotovleniia i primeneniia [Rock Destruction and Metal-Working Tools - Techniques and Technology of the Tool Manufacture and applications],Vol. 22, pp. 93-102. [in Ukrainian].

13. **Shulzhenko, A.A., Ashkinazi, E.E., Sokolov, A.N.** (2009). Novyiultratverdyipolikristallicheskiikompozitsionnyi material [New ultrahard polycrystalline composite material]. - Porodorazrushaiushchii i metalloobrabatyvaiushchii instrument - tekhnika i tekhnolohiia eho izhotovleniia i primeneniia [Rock Destruction and Metal-Working Tools –Techniques and Technology of the Tool Manufacture and applications], Vol. 12, pp. 143–154. [in Russian].

14. **Safonova M.N., Petasyuk G.A. Syromyatnikova A.S.** (2013). Komp'yuterno-analiticheskiye metody diagnostiki ekspluatatsionnykh kharakteristik almaznykh poroshkov i kompozitsionnykh materialov na ikh osnove [Computer-analytical methods for diagnostics of operational characteristics of diamond powders and composite materials based on them].. - Novosibirsk: Iz-in SO RAN. [in Russian].

15. **Kirpichev M.V.** (1953). Teoriia podobiia [Similarity theory]. Moscow: USSR Academy of Sciences. [in Russian].

16. **Blinov G. A.** (1989). Almazosberegaiushchaia tekhnologiia bureniia [Diamond-saving drilling technology]. Lviv: Nedra. [in Russian].

17. **Vynohradova, O. P.** (2015). Kharakter vzaiemnoho ruinuvannia hirskoi porody ta almaznoho porodoruinivnoho instrumentu [The character of the mutual breaking of rocks and of diamond rock destruction tool]. Suchasni resursoenerhozberihaiuchi tekhnolohii hirnychoho vyrobnytstva. - Up-to-dateresource- andenergy- saving technologies in mining industry, issue 16(2),49-57 [in Ukrainian].

https://doi.org/10.31713/m1022

INCREASING THE EFFICIENCY OF UNDERGROUND MINING COMPLEXES APPLICATION BY IMPROVING THE POWER SUPPLY SYSTEM

Ostapchuk O.V.
Doctor of Technical Sciences (D.Sc.), (Tech.),
Associate Professor at the Department of Renewable Energy
National Technical University of Ukraine «Igor Sikorsky Kyiv Polytechnic Institute»

Bondarenko A.O.
Doctor of Technical Sciences (D.Sc.), (Tech.),
Professor of Department of engineering and design in machinery industry, Dnipro University of Technology, Dnipro, Ukraine

Kyrychenko M.S.
assistant lecturer at the Department of Power Engineering, Dnipro University of Technology, Dnipro, Ukraine

Abstract. The aim of the study is to improve the quality of electricity and reliability of power supply systems of underground mining complexes of deep-level and power-intensive mines based on determining the optimal voltage class of high-voltage power lines.

The subject of the research is the methods of quality indicators ensuring, reliability and safety of power supply systems of underground mining complexes of deep-level and power-intensive mines.

Research methods. Analytical and calculation methods were used to solve the scientific problem to assess the nature and level of electricity consumption in modern deep-level and power-intensive mines; scientific generalization was used in determining the state of development of power supply systems of underground mining complexes of modern ore and coal mines; mathematical modeling was used in the description of processes in grids.

The result of the study. The paper analyzes the current situation when choosing a rational voltage class in the underground power supply system of modern mining complexes was analyzed. Factors that have a direct impact on the efficiency of electricity consumers of deep horizons are identified. The method of power quality indicators calculation at definition of a voltage class of a certain mining horizon or the enterprise as a whole is offered. Prospects of application of voltage classes 6, 10 and 35 kV for power supply of shaft cables in the conditions of deep-level and power-intensive mines are considered.

Conclusion. According to the obtained research results, it was established that the normalized voltage levels are far from the voltage values used today for the power supply lines of the underground power supply system, namely 6 and 10 kV.

Keywords. Voltage class, underground power supply system, mining complex, mining horizons, power quality indicators, voltage deviation.

Introduction

The high degree of mechanization and electrification of modern coal and ore mines leads to an increase in the level of electrical loads and electricity consumption, which significantly exceeds the growth rate of mining in the underground way. This is due to both production and organizational factors (tendency to intensify mining, consolidation and merging of mines, increasing the daily load on the longwall, etc.) and a significant complication of mining and technological conditions in connection with the transition to deeper horizons. The need for mining in deep horizons reduces the reliability and efficiency of underground power supply systems of mining complexes by increasing the total length of high and low voltage distribution grids, imbalance of load curve and more. According to the mentioned factors, the requirements to the level of equipment and safety of power supply systems of mining complexes increase, the principles of construction and economic indicators of which depend on the production capacity of the largest electricity receivers, maximum calculated values of electric loads, consumption levels (equipment for coal-face work, transport, lifting, drainage, etc.), distribution of loads between surface consumers and underground installations, as well as from the mining and geological features of the field – gas, water inflow, etc.

Underground power supply systems of mining complexes of mining enterprises have developed and continue to develop on the basis of the principles laid down in them when designing at the initial stage of their electrification. Constant improvement of technology, mechanization and increase of power equipment in the conditions of mining works, promoted increase of capacity and increase in number of underground electric receivers, complexity of designing of underground power supply systems was grown. [1-3]. In this case, the main aspect that was taken into account in the design was compliance with, in addition to the requirements of safety rules, various standards and indicators necessary for the effective

functioning of the designed system. In some cases, some options were considered on the basis of technical and economic comparison and the most desirable of those that did not always correspond to reality was accepted. Accordingly, the quality and efficiency of design largely depend on the experience and engineering intuition of the designer.

The purpose of research is to analyze the factors influencing the choice of a rational voltage class in the conditions of changing the parameters of the underground power supply system; search for technical solutions aimed at improving the efficiency of its operation of underground mining complexes.

Presentation of the main material. When choosing the approximate voltage class at the initial stage of design, in domestic and foreign practice, the following formulas are used [4]

Germany. According to Weikert's formula, the rational voltage level (kV) is

$$U = 3\sqrt{S} + 0{,}5l, \quad (1)$$

where S is transmitted power, MVA; l is distance, km.

USA. Still's formula is used

$$U = 4{,}34\sqrt{l + 16P}, \quad (2)$$

where P is transmitted power, MW; l is distance, km.

Sweden. The formula is used

$$U = 17\sqrt{\frac{l}{16} + P}. \quad (3)$$

Expression (2) was transformed by Nikogosov and became widespread in domestic practice in the form

$$U = 16\sqrt[4]{Pl}. \quad (4)$$

These expressions allow us to determine the value of the optimal voltage, based on power and length. According to the recommendations [5], the Still-Nikogosov's formula is used in approximate calculations, when the total length of the lines is less than 250 km with a power of less than 60 MVA, which is typical for most modern mining enterprises. If the total power is known and the number of power lines is resolved, the voltage can be determined from the expression [6]

$$U_{calk} \geq 0,05\sqrt{\frac{Sl}{n}}, \quad (5)$$

where n is the number of power lines.

Underground power supply systems of mining complexes are becoming increasingly complex and take the form of a complex dynamic system that covers a set of numerous factors and objects. These factors include such as: the method of opening and preparation of the minefield, the exploitation system, the number of developed seams, their depth and angle of stratification, the level of mechanization of coal-face and preparatory work, the reliability of certain types and elements of electrical equipment, patterns formation of loads of mining machines, applied voltage in grids, quality of the electric power, operating conditions, etc. Moreover, in the technical and economic comparison of the developed power supply scheme, it is necessary to strive for a minimum of transformations and the maximum approximation of high voltage to the consumer. The choice of any general variant of the power supply system on the basis of technical and economic comparison with others is already insufficient, as well as the choice of individual variants of the general power supply system.

Currently, a voltage of 6 kV is used for underground high-voltage distribution grids. With the increase in the power of the mines under construction, and especially with the increase in the total power of electric motors in tunneling and mining areas, the shaft and underground cable grid becomes more complicated (it is necessary to increase the cross-sectional area of cable cores and lay parallel lines). into the underground power supply system and electricity losses. In the conditions of power-intensive mines it is necessary to lay a large number of parallel cables in the shaft, the number of which in some mines is up to 4-5 and more [7].

Given the existing limitations of regulations [8], the maximum cross-sectional area of the cores of laid cables (to stationary distribution points is 240 mm^2, to mobile distribution substations (DS) is 95 mm^2), power transmission at level of 5 MVA with an operating voltage of 6 kV, is up to difficult task. This is primarily due to the implementation of the requirements to ensure the necessary indicators of electricity quality for consumers of deep

horizons. These circumstances lead to the use of unreliable and dangerous in multiple sectioning operation of underground substations. According to [9], increasing the number of shaft cables to 8-14 causes difficulties not only in building reliable power supply schemes of the Main underground substation (MUS) and laying cables, but also significantly reduces the reliability of power supply and complicates operating conditions. Examples of implementation of power schemes are shown in Fig. 1.

a

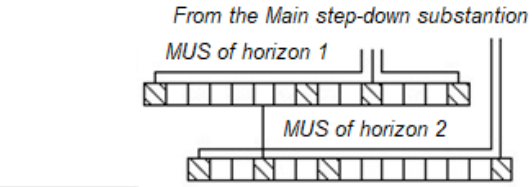

b

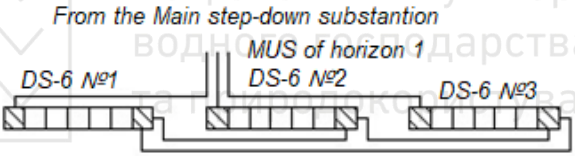

c

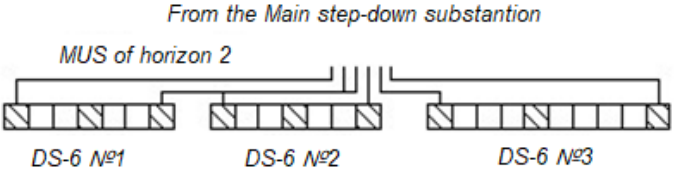

Fig. 1*a.* Power supply scheme when using three cables with a core cross-sectional area of 95 mm^2; *b* – Power supply scheme when using three cables with a cross-sectional area of 185 mm^2; *c* – Power supply scheme when using six cables with a cross-sectional area of 150 mm^2

When using three shaft cables, different variants of MUS power supply schemes are possible, which differ significantly in the number of input and sectional complete switchgears (CSG) used. When

designing MUS power supply schemes, including for deep-level mines, it is necessary to use a circuit with two inputs for each CSG. According to the requirements [10], all power cables of the Main underground substation, laid in the shaft, must be constantly under load. To supply the MUS, it is necessary to lay at least two working cables, laying of spare cables is prohibited (in case of failure one of the cables, the other cables must ensure the operation of the mine without reducing its productivity). The implementation of these requirements needs separate power supply to the sections of the MUS busbar with an even distribution of load between them. Drainage pump motors must be connected to different busbar sections, and other high-voltage consumers must be distributed between the MUS busbar sections depending on the load current. This principle of construction of the MUS scheme is expedient if we assume that the main type of damage that causes interruptions in the power supply is the failure of one of the cables.

Also in the conditions of deep-level mines, when transmitting electricity over a long distance (the length of individual lines reaches 5 km), it is necessary to take measures to increase the capacity of the grid, which should be increased in two ways: by using double cable lines and increasing the maximum cross-sectional area. The use of these methods allows to increase the transmission capacity of the lines approximately twice, to simplify the existing scheme of the MUS by reducing the number of input and section switches. The number of backup switches, which are installed at the rate of one switch for each section of busbar, is also reduced. The disadvantage of such a system is that the line is considered as one, and therefore must have 100% backup. In addition, the probability of damage to the double lines increases. The increase in transmission capacity due to the change in the cross-sectional area of the cable is limited by the types of existing complete switchgear and complicates the installation of cables in the shaft due to the growth of their weight. Due to the increase in the total length of cable lines there is a significant number of failures in the high-voltage distribution grid – the frequency of failures in a cable line with a voltage of 6-10 kV with a length of 6 km is 0.6 h^{-1} [11]. These indicators can be increased only through the development of new principles for the

construction and reconstruction of power supply systems for deep-level and power-intensive industries.

According to the requirements of [8], in the underground grid with a voltage of 6 kV at a grounding circuit resistance of 2 Ohms and a touch voltage of 30 V, the maximum allowable capacitance should not exceed 4.6 μF per phase. Therefore, the total length of the high-voltage cable grid, which is made of СБ, СБГ, ЦСКН, ЦСКл cable types under the condition of safe operation, should not exceed 24 km. Widespread recent use of the ЭВТ cable type, which has twice the capacity [11] compared to existing samples, in additional reduces the overall length of the grid.

The efficiency of supply lines transition to higher voltage rate can be explained that at the same loads, power factor, material and cross-sectional area of current-carrying cores with increasing line voltage from U_{r1} to U_{r2} the ratio of voltage losses [9] is

$$\frac{\Delta U_2}{\Delta U_1} = \frac{U_{r1}}{U_{r2}}, \quad (6)$$

and the power losses ratio

$$\frac{\Delta P_2}{\Delta P_1} = \left(\frac{U_{r1}}{U_{r2}}\right)^2, \quad (7)$$

where ΔU_1, ΔP_1 are voltage and power losses at rated voltage U_{r1}; ΔU_2, ΔP_2 are voltage and power losses at rated voltage U_{r2}.

The calculated valuesof the ratios of voltage losses and power in the mine cable grids with constant parameters of the system are given in the table.

Table

The calculated values of the ratios of voltage losses and power in the mine cable grids with constant parameters of the system

U_{r1}, kV	U_{r2}, kV	$\frac{\Delta U_2}{\Delta U_1}$, %	$\frac{\Delta P_2}{\Delta P_1}$, %
6	10	60	36
	35	17	3

From the table, we can conclude that in case of transition the 6 kV lines to higher voltage rate, particularly 10 or 35 kV, the losses

are 40 and 83% cut respectively, the power losses are 64 and 97% reduced.

Technical and economic comparative analysis of power supply options at different voltage classes should be performed taking into account quality indicators that do not have a cost estimate. Qualitative indicators of the option are better if:

- when working in the mains there are smaller voltage fluctuations;
- total voltage losses decrease;
- installation and operation of underground power supply grids simplify;
- grid reconstruction is simplified if necessary (if it is necessary to increase production capacity).

In papers [7, 13] the necessity of application of voltage class 10-20 kV for high-voltage distribution grid of mines under construction is noted. This allows to reduce the number of shaft cables, to improve the start-up conditions of powerful electric motors of stationary installations (primarily drainage), to increase the quality of voltage in the underground power supply system, efficiency and reliability of equipment. A special advantage of such a technical solution is the achievement of voltage stability even in the most remote sections of the distribution grid. The starting torque of powerful stationary motors is significantly increased (by about 20%), which does not cause a decrease in voltage when they are started under load and the associated shutdown of control and protection devices.

To date, there are design developments for the construction of a step-down transformer substation, which provides power supply to underground consumers of the unit with a voltage class of 10 kV in the conditions of PJSC " Pokrovskoye Mine Management". The total power of underground consumers of this unit is 22.8 MVA, and the total current is 1268 A, while when using a voltage class of 6 kV, it is 2194 A. Reducing current loads at a voltage of 10 kV instead of 6 kV, contributes to the corresponding reducing the voltage drop in the cables (1.73 times) [14]. The use of a voltage class of 10 kV instead of 6 kV for underground distribution grids requires the development of a complex of equipment in explosion-proof design (cables, switchgear, transformers, powerful motors, etc.). The transition to 10

kV can be effective only by increasing the allowable short-circuit power from 50-75 to 100-150 MVA, which requires a fundamentally new approach in the development of protection. Crucial in this case is the coordination of rated voltages of the power supply system of the mine and its consumers. For example, the use of 10/6 kV transformers in the pits for power supply of powerful consumers significantly reduces the field of use of the voltage class 10 kV.

The use of deep-level input of 35 kV voltage in underground mine workings also deserves additional attention, when there are no significant restrictions on the level of grid transmission capacity. The main problems are the development of underground substations in explosion-proof design and appropriate protection devices to ensure the established level of safety. Additional advantages of using this approach are the provision of independent power supply to consumers of the underground power supply system without the installation of separate transformers, as well as the transfer of the distribution boundary from the main step-down substation to the MUS, which reduces the total length of power cables by several kilometers. In addition, the use of 35/6 kV transformers at the Main underground substation will limit the short-circuit current to an acceptable level and abandon current-limiting reactors, which will increase the reliability and safety of underground grid maintenance.

When performing the relevant research, it is necessary to choose a mine with average productivity, depth of mining, water inflow, etc. When performing the analysis, it is necessary to take into account that to select the supply grid voltage, it is advisable to use the classes of the corresponding standard series: 6, 10 and 35 (110) kV. The use of a voltage class of 20 kV [15,16] is not appropriate due to the lack of necessary equipment of domestic production (primarily motors and transformers).

In the conditions of deep-level and power-intensive mines, the urgent problem is to provide the necessary indicators of electricity quality at the stage of design and development of a certain working horizon. First, the assessment of the impact of voltage quality indicators in consumers of electricity of the underground grid, the reliability of the power supply system, the analysis of the capacity of the respective distribution grids are performed [17-20]. The main indicator of the transmission capacity of cable lines is the value of

the transmitted total power at a given level of voltage losses and rated voltage. The voltage losses in the line is determined by the expression, *V*

$$\Delta U = \sqrt{3} I \left(R \cdot \cos\varphi + X \cdot \sin\varphi \right), \tag{8}$$

where *I* is current in line, A; f is phase shift angle between current and voltage; *R* and *X* are active and inductive resistance of cable cores respectively, Ohm.

More often the allowable voltage losses are expressed in %

$$\Delta u = \frac{\Delta U}{U_r} 100, \tag{9}$$

where U_r is rated voltage, V.

Taking into account (9), and assuming that the total power transmitted is equal to $S = \sqrt{3} I U_r$, the expression will take the form

$$\Delta u = \frac{S\left(R \cdot \cos\varphi + X \cdot \sin\varphi \right)}{10 U_r^2}, \tag{10}$$

then total power *S*, MVA is

$$S = \frac{\Delta u U_r^2}{\left(R \cdot \cos\varphi + X \cdot \sin\varphi \right)} \cdot 10^{-2}. \tag{11}$$

Based on expressions (10-11), the appropriate voltage depending on the grid parameters and the allowable level of losses is determined by the formula

$$U = \sqrt{\frac{100 S \left(R \cdot \cos\varphi + X \cdot \sin\varphi \right)}{\Delta u}}, \tag{12}$$

Δu is set voltage deviation level, c.u.

The proposed expression allows the analysis of the allowable voltage level, with appropriate restrictions on its deviation (up to 5%). When performing the calculation, the parameters of real deep-level and power-intensive mines with a working load of S = 2..10 MVA and a horizon depth of 1000 m were used. The best operating conditions are considered: power factor is 0.95; 4 cable lines with the maximum possible cross-sectional area of cable cores of 240 mm^2.

The results of the calculation are shown in Figure 2. From the above graph it can be concluded that according to the established criteria, the normalized voltage levels are far from those used today

for the voltage values for power lines of the underground power supply system, namely 6 and 10 kV.

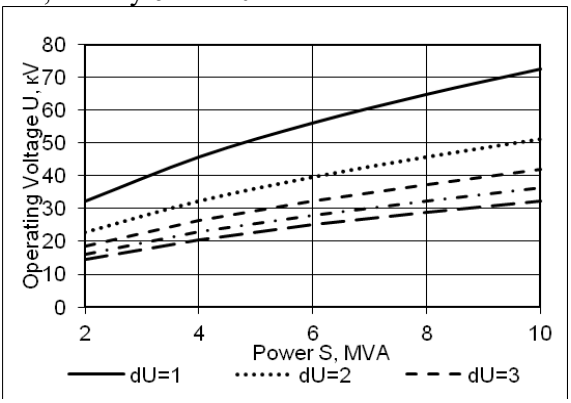

Fig. 2 Rational voltage classes in deep-level mines at restrictions on the allowable voltage deviation at the end of the line

Conclusion. These indicators clearly show the technical efficiency of the use of underground mining complexes by increasing the voltage class for distribution grids in conditions of insufficient transmission capacity of underground cable lines. Therefore, it is advisable to use voltage deviation indicators to assess its prospective class. This measure allows you to plan in advance the use of a certain voltage class in terms of changes in the cost of electrical equipment and electricity.

References

1. **Bondarenko, A.A. & Naumenko, R. P.** (2019) Comprehensive solution of recycling waste from stone processing industry. Naukovyi Visnyk Natsionalnoho Hirnychoho Universytetu, (4), 96-102.

2. **Bondarenko, A.O., Maliarenko, P.O., Zapara, I. & Bliskun, S.P**. (2020). Testing of the complex for gravitational washing of sand. Naukovyi Visnyk Natsionalnoho Hirnychoho Universytetu, (5), 53-59. https://doi.org/10.29202/nvngu/2020-5/14.

3. **Bondarenko, A.O.** (2017). Mining machines for opencast mining (in Ukrainian): Textbook. Dnipro, Ukraine: National Mining University.

4. **Fedorov, A.A.** (1972). Fundamentals of power supply of industrial enterprises (in Russian): Textbook. Moscow: Energy.

5. **Plashchansky, L.A.** (2006). Fundamentals of power supply of mining enterprises (in Russian): Textbook. Moscow: Publishing house of the Moscow State Mining University.

6. About power industry (in Ukrainian): Law of Ukraine 1997, № 575/97-ВР with changes and additions dated (01.01.2017). Retrieved from http://zakon2.rada.gov.ua/laws/show/575/97-%D0%B2%D1%80.

7. **Pivnyak, G. G., Razumnyy, Y. T., & Rukhlov, A. V.** (2008). Prospects for increasing the rated voltage of the electrical grid in the power supply system of coal mines (in Russian). Energy Saving, (3), 9-11.

8. Safety Rules in Coal Mines (in Ukrainian) / NPAOP 10.0-1.01-10. № 62 dated 22.03.10, with changes № 661 dated 24.09.2014. Retrieved from: http://sop.zp.ua/norm_npaop_10_0-1_01-10_02_ua.php

9. **Vinogradov, V.S.** (1983). Electrical equipment and power supply of mining enterprises (in Russian). Moscow: Subsoil Assets.

10. **Prakhovnik, A.V. Rozen, V.P. & Degtyarev, V.V.** (1985). Energy-saving modes of power supply of mining enterprises (in Russian): textbook. Moscow: Subsoil Assets.

11. **Shkrabets, F.P.** (2009). Ways to improve the fail-safety of distribution grids of mining enterprises (in Russian). Naukovyi Visnyk Natsionalnoho Hirnychoho Universytetu, (1), 59-65.

12. **Shishkin, N.F. & Antonov, V.F**. (1981). The main directions of electrification of modern mines (in Russian): monograph. Moscow: Science.

13. **Razumnyy, Yu.T. & Shkrabets, F.P**. (1984). Improving the efficiency of power supply of coal mines (in Russian): monograph. Kyiv, Ukraine: Technique.

14. **Basov, N.M., Dzyuban, V.S., Rymar, M.I. & Matsegora, A.A**. (2013). Directions of improvement of underground power supply systems of mines (in Russian). The Coal of Ukraine, (5), 28-31: http://www.irbis-nbuv.gov.ua/cgi-bin/irbis_nbuv/cgiirbis_64.exe?C21COM=2&I21DBN=UJRN&P21DBN=UJRN&IMAGE_FILE_DOWNLOAD=1&Image_file_name=PDF/ugukr_2013_5_7.pdf.

15. **Degtyarev, V.V. & Serov V.V.** (1988). Handbook of electrical installations of coal enterprises. Electrical installations of coal mines (in Russian). Moscow: Subsoil Assets.

16. **Vaneev B.N.** (2001). Handbook of a coal mine power engineer: in 2 volumes (in Russian). Donetsk: LLC «Southeast, Ltd».

17. **Pivniak, G.G., Beshta, O.S., Pilov, P.I., Kuzmenko, O.M., Shkrabets, F.P.** (2011). Ecological and economic components of the use of geotechnical systems of Ukraine (in Ukrainian): monograph. Dnipropetrovsk, Ukraine: National Mining University.

18. **Shkrabets, F.P., Bezruchko, Yu.N. & Ostapchuk, A.V.** (2010). Deep-level input voltage 35 kV for powering consumers of deep horizons of the Zaporizkyi Iron-ore Plant PJSC (in Russian). Mining electromechanics and automatics, (84), 69 – 76.

19. **Shkrabets, F.P. & Ostapchuk, A.V** (2013). Application of 35 kilovolt voltage for underground power consumers supply systems of deep power-intensive mines. Naukovyi Visnyk Natsionalnoho Hirnychoho Universytetu, (1), 83–90.

20. **Shkrabets, F.P. & Ostapchuk, O.V.** (2014). Power supply of deep-level and power-intensive ore and coal mines (in Ukrainian): monograph. Dnipro, Ukraine: National Mining University.

https://doi.org/10.31713/m1023

THE STUDY OF ORE BREAKAGE IN BALL MILL TO ASSESS THE ENERGY EFFICIENCY OF ITS GRINDING

Kondratets V.
Central Ukrainian National Technical University, Doctor of Technical Sciences, Professor, Professor of the Department of Automation of Production Processes, Ukraine

Matsui A.
Central Ukrainian National Technical University, Ph.D., Associate professor, Associate Professor of the Department of Production Process Automation, Ukraine

Pikilniak A.
Kryvyi Rih National University, Ph.D., Acting Dean of the Faculty of Mechanical Engineering and Transport, Ukraine

Artiukhov A.
Central Ukrainian National Technical University, Ph.D., Associate professor, Associate Professor of the Department of Mechanical Engineering Technology, Ukraine

Abstract

The results of mathematical modelling of ore breakage by a ball mill based on mathematical models of loaded and unloaded elastic elements are presented. The property of the arrangement of balls in the drum due to segregation is used, under the influence of which they are distributed with increasing size from the loading to the unloading throat, and in the cross-sections from the lining to the axis. It is shown that it is advisable to use the balls in the cross-section of the drum, where their size is 50 mm. The more the volume of ore is destroyed, the more the ball's energy is spent on this, the less energy will be converted into deformation of the elastic element. Consequently, the value of the deformation of the elastic element corresponds to the volume of the destroyed ore, as well as the energy efficiency of its grinding. The approach of interaction of balls with an elastic element from the point of view of mass phenomena will be more effective. The average value of deformations by all balls that have passed through the elastic element, arbitrarily accurately characterizes the average value of the destroyed volume of ore, that is, the energy efficiency of its grinding. The controlled parameter is found in accordance with the proposed relationship with the measured average deformation value of the elastic element. The deviation of certain values from the reference values is within 1%, which meets the requirements of the technological process.

Keywords: energy efficiency**,** mathematical modelling, ball mill, an elastic element, deformation

1. Introduction

Today, the reserves of rich iron ores are almost exhausted. Therefore a steady transition to the development of low-grade reserves with an iron content of 20-35% is taking place, with an increase in the content of the useful component to 65% in the beneficiation process. This trend, in particular, is noted in the priority areas outlined in [1]. Poor iron ores are crushed in several stages before enrichment. This process requires a large amount of electricity, grinding media, and lining. Especially high costs fall on the first grinding stage, which is carried out in ball mills. As a result, the cost of magnetite concentrate is growing, which is a problem of iron ore industries.

2. Actuality of the paper

This problem can be solved in various ways, one of the most effective is the grinding of the initial ore of the beneficiation plants in conditions of high energy efficiency of its grinding in ball mills. Under the highest energy efficiency of the grinding of the material should be understood the best use of the energy of the falling ball. If there is not enough material at the moment of impact under the ball, then a part of the acquired energy will not be useful. Besides, excess energy will be spent on the destruction of both the grinder and the lining. With an excess of ore under a falling ball, its breakage will not be effective. The technological unit will enter the emergency state of overload, which is not permissible. For any technological type of ore, it is possible to select such a volume of ore, which is subject to grinding, when the energy of the falling ball practically corresponds to the required energy for breakage. A specific small excess of the energy of the ball after the breakage of the ore can be an indicator of the energy efficiency of grinding. In these conditions, there is no waste of electricity, balls and lining. Scientists and practitioners have been working on solving this problem for a long time. As a result of the complexity of the processes in the ball mill, indirect methods of controlling technological parameters were used in the studies. For example, in [2], it is noted that the average power of the electric motor and the noise of the mill are used as a criterion for automatic optimization in extreme systems supporting the operating point on the static characteristic of the average power or intensity of the acoustic signal as a function of filling the drum near the

extremum. The control action is the flow of the initial ore into the mill. In industry, such systems are not widely used, because the maximum performance by the finished product does not correspond to the operating point in the area of extremum. In this regard, the problem of automatic optimization of ore preparation is solved by compensating of disturbing influences of initial feed (which is problematic) or the search and justification of technological parameters, which are automatically controlled and directly characterize the energy efficiency of the breakage process in the mill drum.

Thus, [3] showed that there is a definite relationship between power consumption and filling of a ball mill drum with pulp. However, it is still difficult to use such a relationship. The work of [4], is also based on measuring the energy used for crushing a ton of ore. A more sustainable approach to assessing the effectiveness of ore grinding is considered in [5]. Here, in addition to power accounting of the mill electric drive, it is proposed to consider indirect energy consumption - for ore extraction, the manufacturing of the ball, etc. In this case, the implementation of these approaches does not reveal anything new in measuring technological parameters by power, their disadvantages remain and do not provide the necessary accuracy. The results of the studies outlined in [6] expand the understanding of the relationship between the power consumed by the ball mill and the technological parameters, but this data cannot be used to improve the mill load control with an assessment of the energy efficiency of ore grinding. In [7], the calculation of the grindability indices is made. These indices allow quantifying the work expended on grinding in ball mills over the area of the newly created surface, considering all size classes. The work establishes the necessary links, but the parameters cannot be controlled automatically. To reduce the influence of various factors on the measurement of the mill filling level and to increase the accuracy of its measurement, a new variable was proposed [8].

Using theoretical calculations and experiments, the relationship between the mill filling level and the angular position of the maximum vibration point on the ball mill housing was established. Vibration signals were measured with an accelerometer mounted on the mill shell to establish a correlation between the mill filling level and the angular position. It has been established that the position of

the maximum vibration point on the mill housing changes to a lower angular position when the drum filling level is increased. The new variable proposed in this paper is more stable. However, the filling level of the mill is determined approximately by an indirect method. It was proved in [9] that the total collision energy of a grinding media per unit time significantly increases with optimal parameters of a ball mill operation. However, the energy efficiency of ore breakage cannot be determined due to the influence on the process of the ball load amount in the drum, the characteristics of its size, lining state and other factors. Despite this, the task of the energy efficiency control, improving ore grinding in ball mills of the first stage is relevant and requires further study. It is more efficient to control the energy efficiency of ore grinding in ball mills by direct energy loss during the destruction of material in the drum, i.e., to perform direct measurement of losses, since the strain analytical dependencies of the unloaded and loaded elastic element are obtained upon the ball's impact.

3. Unresolved parts of a common problem

Based on the obtained dependencies, it was concluded that it is possible to directly measure the energy efficiency of ore grinding, directly in a ball mill. This approach provides an objective assessment of the ore grinding state. However, the effect of a possible change in the balls mass on the results of automatic control of the material destruction energy efficiency has not been studied.

4. Aim of the research

The aim of the research is the mathematical modelling of the ore breakage in a ball mill with the accuracy characteristics determination of the grinding energy efficiency automatic control under conditions of a possible change in the ball mass.

5. Method

At the first stages of ore grinding at concentrating plants, the powerful ball mills are used, in which it is expedient to process a specific technological type of ore and maintain the ball load at a given level and characteristic of ore size, which can provide the highest productivity. Such a constant in time ball load is distributed along with the drum by size due to longitudinal segregation. At the end of the feed are the smallest balls, and at the end of the drum - the

largest. Their size changes gradually, creating zones along with the drum with approximately the same size of balls. In each of these zones, due to transverse segregation, the largest balls are located closer to the drum axis, and the smallest ones are at the lining. So, the outer layer of balls of a certain zone will be represented by balls of almost the same size due to two types of segregation. The analysis shows that it is convenient to organize the control in the zone where the size of the balls is 50 mm. The diameter of the balls, and accordingly their mass may differ slightly from the average value. The effect of changes in the mass of balls on the results of automatic control of the energy efficiency of ore grinding can be set in accordance with mathematical models

$$x_1 = \frac{mg + \sqrt{mg(mg + 2ch)}}{c}, \quad (1)$$

$$x_2 = \frac{mg + \sqrt{mg(mg + 2ch) - 2ckk_1V_p}}{c}, \quad (2)$$

where x_1, x_2 - are the deformation of the unloaded and loaded elastic element; m - is the weight of the falling ball; g - is the gravitational acceleration; c - stiffness of the elastic element; h - is the height from which the ball falls - the equivalent of its speed; k - is the proportionality coefficient depending on the strength of the ore; k_1 - is the constant characterizing the relationship between the total and the deformed volume of the ore piece; V_P - is the volume of the ore piece.

The dependence determines the separation angle α of the outer layer balls from the lining

$$\alpha = arc\cos\frac{\pi^2 n^2 R}{900g}, \quad (3)$$

where π=3,14; n - is the number of rounds of the ball mill drum per unit time, rpm.; R - is the inner radius of the mill drum.

The speed of falling of the outer layer balls at the point of collision with the lining is equal to

$$\upsilon_p = \upsilon\sqrt{1 + 8\sin^2\alpha}, \quad (4)$$

where $\upsilon=\pi Rn/30$, m/s.

From (3) and (4) it is seen that the speed of falling balls in the mill is a constant value. Therefore, it is possible to use mathematical models and (2) for h=const. The speed of the balls falling does not depend on their mass, and the deformation of the elastic element depends on the mass.

In (1) and (2), the parameters c and h are constant. If the ore pieces are not large enough, and the crushed ore type is specific, then k, k_1 are also constant. Then, at a particular ball mass m, it is possible to determine the volume of the ground ore V_p by the deformation value x_2 of the elastic element, which corresponds to the energy efficiency of its grinding.

Considering that the change in the mass of the balls affects the deformation of the elastic element, we should expect an error of automatic control of the energy efficiency of ore grinding from this factor. The analysis shows that in this case, the compensation of the error mentioned above can be used. If the control is carried out with the use of (2), then at a constant value of the ground ore volume V_p, a change in the mass of the ball m will lead to an error.

If we also use (1), then we will have at our disposal two strain values x_1 and x_2, caused by a specific mass. The difference in these deformations $\Delta x=x_1-x_2$ to a certain extent compensates for the effect of changes in the mass of the ball, but not quite, since kinetic energy must be spent on the grinding of the ore, which also depends on the mass of the grinding body moving at a constant speed.

Specific dependencies can be obtained in the process of modelling. Let's take h=4,0872 m for the non-weared up lining of a ball mill, k=3.2 kgm/cm^3, k_1=0.3, V_p=1 cm^3, s=35555555.5 N/m. The simulation results are shown in Fig. 1, where the mass of the balls was changed by ±10%. From Fig. 1 it follows that with a constant diameter (mass) of the balls, the measurement of the ore grinding energy efficiency in a ball mill is carried out without error (curve *2*). If the mass of the balls is increased by 10%, then a measurement error occurs, which depends on the mass of the balls, which are used in the measurement (curve *3*). The largest error will appear in the measurement for balls with a diameter of 40 mm. It is impossible to measure such a high error. The error rapidly decreases for d_k=50 mm and more, depending on the growth of the size of the balls. A decrease in the mass of the ball relative to the normative mass (curve

1) also leads to a measurement error with the same features. Hence, it is possible to effectively control the energy-efficient ore grinding by balls with a diameter of 50 mm, in this case, the error is relatively small, and the size of the ore pieces is also small. It is not advisable to use large ball diameters, especially after d_k=60 mm, since large delays occur and too small pieces of ore are found. From the dependencies obtained, it also follows that the error is compensated - with a 10% deviation of the mass, the measurement error is almost half as much, but it is too large. The errors are almost symmetrical in sign. In the beneficiation processes, they should be significantly less, within 5% [10], even in separate processes. Therefore, it is advisable to focus on the total error in measuring the technological parameters of beneficiation, which should not exceed 3.0%, given that this technological parameter is new. Ensuring the required accuracy of information tools in the management of beneficiation processes is mentioned in [11]. Given this requirement, it is necessary to improve the accuracy of measuring the energy efficiency of ore grinding by ball mills.

The obtained measurement errors of this technological parameter are shown in Fig. 1 and correspond to 1 cm^3 of broken ore. Currently, there is a clear tendency to reduce the coarseness in the crushing department and certain unloading of ball mills by reducing the size of the initial ore. Under these conditions, considering the kinetics of grinding, a smaller product will be produced by a ⅓-½ of the ball mill drum length, which will make it possible to grind a much smaller volume of ore in certain sections of the drum V_p. To destroy a specific volume of ore with a ball, it is necessary to expend a certain amount of kinetic energy. The reduced ball loss of kinetic energy will increase the effect of compensation by determining $\Delta x=x_1-x_2$, which will be aimed at improving the accuracy of measuring the technological parameter. Let's simulate ore grinding under the same conditions, but with reduced volumes of destroyed material V_p to clarify the possibilities of these changes effect compensation in the mass of the balls on the measurement results. We will change the mass of the ball in the same range ±10%. The simulation results are presented in Tab. 1.

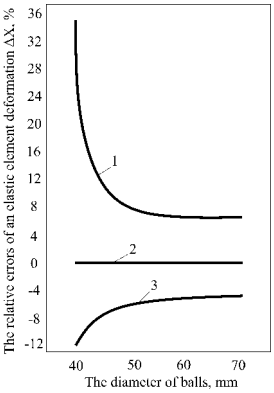

Fig. 1. Change of relative errors of an elastic element deformation with a deviation of balls mass by ±10% in the process of breakage of 1 cm^3 of ore:
1 - reduced; *2* - constant; *3* - increased

From the data of Tab. 1, it can be seen that with an increase in the size of the ball, the measurement errors decrease. They also decrease with a decrease in the volume of broken ore. At the minimum value of the ball mass, an error with a positive sign is formed, and at the maximum value of the mass - with a negative sign. With the same normative values of the ball diameter, the errors are arranged symmetrically and have almost the same values. Despite the reduction of errors in the small volumes of destroyed ore, they remain relatively large and require a reduction.

Tab. 1

Relative deformation errors of the elastic element caused by changes in the mass of the balls (%) at their nominal diameters, mm

The volume of broken ore, V_p, cm^3	Nominal and deviated ball mass	Relative deformation errors of the elastic element caused by changes in the mass of the balls (%) at their nominal diameters, mm			
		40	50	60	70
0.75	min	10.321	6.831	6.108	5.845
	nominal	0	0	0	0
	max	-7.674	-5.654	-5.160	-4.961
0.5	min	8.095	6.258	5.847	5.643
	nominal	0	0	0	0
	max	-7.633	-5.236	-4.972	-4.856
0.25	min	6.217	5.777	5.615	5.410
	nominal	0	0	0	0
	max	-5.234	-4.933	-4.810	-4.696

In a ball mill at the same time, there is a considerable number of balls of different sizes. During operation of the mill, the mass phenomena occur. In particular, it is known that as a result of longitudinal segregation, they are arranged by size when it increases from feed to discharge throat. Segregation is carried out in the cross-sections of the drum when the smallest balls are located at the lining, and larger balls are closer to the drum axis. It is shown that zones of a certain width with the distribution of one-dimensional balls in the outer layer of a ball load are established along with the drum of a ball mill. In the central part of such a zone, there will be, for example, balls with a diameter of 50 mm. However, they cannot exactly correspond to this size. A change in size (mass) within certain limits will lead to errors in measuring the energy efficiency of ore grinding, if the elastic element, as a sensitive device, is installed at a certain point of the drum lining. The interaction of the elastic element with the balls in the process of the mill will be a mass phenomenon.

It is known that mass phenomena have the property of stability, which is the physical content of the "law of large numbers", which in the narrow concept of this word is represented by a number of mathematical theorems. These theorems establish the fact and conditions of convergence in the probability of certain random variables to stable, non-random variables. There is another group of limit theorems, which concerns not the limit values of random variables, but the limit distribution laws. It is also a group of theorems, known as the "central limit theorem".

The general idea of the type of theorem of large numbers law can be formulated as follows. Let a sequence of random variables be given as

$$\xi_1, \xi_2, \dots, \xi_n, \dots . \tag{5}$$

Consider the random variables ξ_n, which are some predetermined symmetric functions of the first n values of a sequence (5)

$$\xi_n = f_n(\xi_1, \xi_2, \dots, \xi_n)$$

If there is such a sequence of constants $a_1, a_2, \dots, a_n, \dots$, which at any $\varepsilon > 0$ are

$$\lim_{n\to\infty} p\left[\left|\xi_n - a_n\right| < \varepsilon\right] = 1, \tag{6}$$

then the sequence (5) is subjected to the law of large numbers with given functions f_n.

The concept of the large numbers law has a much more specific meaning. Namely, they are limited to the case when fn is the arithmetic mean of the values ($\xi_1,\xi_2,...,\xi_n$). Averaging a sufficiently large number of independent and equally distributed random variables, we obtain a value with a probability arbitrarily close to unity. This value arbitrarily small differs from the general mathematical expectation of values [12].

During the operation of a ball mill, a large number of factors affect the grinding bodies - the interaction of a separate ball with a lining, with ground material, with pulp, with a wide size spectrum of balls, complex ball movements in different layers in a ball mill drum during its rotation, movement along with the drum, in cross-sections of the drum before the lining, etc. Lyapunov showed that if a random variable can be considered as the sum of a large number of small components, then under fairly general conditions, the distribution law of this random variable is close to normal, no matter what the distribution laws of individual components. So, the random variable – the diameter of the balls in a particular standard cross-section of a ball mill drum can be approximately considered as distributed according to normal law.

Let's suppose that when a ball mill is operating, the volume of ore under the balls will not change. However, the deformation of the elastic element will be variable, but considering, for example, all the balls, which are in the normal cross-section of the drum. As a result, we obtain the average value of deformations, corresponding to the mathematical expectation of the ball impact with a diameter of 50 mm, respectively. This value will characterize the volume of ore break under the balls. The mass phenomena here will also respond broken ore volume under the balls, which relates to the average size of the ball of 50 mm. The broken ore volume may occasionally change randomly. However, if we determine the mean deformation value under all balls, which have passed through the elastic element, then with arbitrary accuracy it will characterize the average value of the broken ore volume, i.e., energy efficiency of ore crushing. Let's simulate this process on a simplified mathematical model.

Mathematical modelling will be performed using a ball with a diameter of 50 mm on the same elastic element with c=35555555.5 N/m, ore with k=3.2 kgm/cm^3 and with k=0.3, h=4.0872. The mass of balls in the experiments will be taken as nominal, reduced by 10% and increased by 10%, and the broken ore volumes, respectively – 1.25; 1.0; 0.75; 0.5 and 0.25 cm^3. We will determine the elastic element deformation without ore x_1, with ore x_2 and the difference of these deformations Δx. For each ore volume V_p, we conduct three experiments with balls of different masses, by determining the value x_1,x_2 and x by the averaged data, according to three measurements. The simulation data are presented in Tab. 2.

Tab. 2

Results of mathematical modelling of ore breakage in a ball mill using a simplified mathematical mode

Nominal and deviated ball mass	Deformation of the elastic element without ore x_1, mm	Deformation of the elastic element with ore x_2, mm	Average deformation of an elastic element without ore x_{1c}, mm	Average deformation of an elastic element with ore x_{2c}, mm	The difference of deformations of the elastic element $\Delta x = x_1 - x_2$, mm	The volume of broken ore V_p , cm^3
min	1.01758	0.61090	1.07173	0.69560	0.37620	1.25
nominal	1.07263	0.69916				
max	1.12499	0.77674				
min	1.01758	0.71109	1.07173	0.78570	0.28605	1.0
nominal	1.07263	0.78822				
max	1.12499	0.85778				
min	1.01758	0.79882	1.07173	0.86616	0.20559	0.75
nominal	1.07263	0.86786				
max	1.12499	0.93180				
min	1.01758	0.87782	1.07173	0.93976	0.13199	0.5
nominal	1.07263	0.94110				
max	1.12499	1.00035				
min	1.01758	0.95027	1.07173	1.00792	0.06383	0.25
nominal	1.07263	1.00900				
max	1.12499	1.06450				

The data of the three measurements in Tab. 2 for each value of V_p completely characterize the array of measurements, also considering the intermediate values of the balls mass, since the average value,

which corresponding to the nominal one is stable. That is, if all the balls with a variable mass, which are contained in the normal cross-section of the drum, a constant volume of broken ore, for example, V_p=1.25 cm^3, then the mean deformation value x_{2c}, determined by the measured x_2, completely characterizes the volume of the broken material V_p=1.25 cm^3. In a simplified mathematical model, x_{2c} was determined by three values - two limit and one average. The value of the elastic element deformation x_2 at the nominal mass is true. As the analysis shows, deviations of values x_{2c} from x_2 at a nominal mass of the ball is insignificant and depends on the value of the broken ore volume. The values x_{2c} are less then x_2 with the nominal ball mass and change accordingly - 0.51% (with V_p=1.25 cm^3); 0.32% (V_p=1.0 cm^3); 0.20% (V_p=0.75 cm^3); 0.14% (V_p=0.5 cm^3); 0.11% (V_p=0.25 cm^3).

Average deformation of the unloaded elastic element x_{1c} less than x_1 by a constant value - 0.084% with the nominal ball mass. Since the real and experimentally determined values of the elastic element deformation almost coincide, according to Tab. 2, it is possible to build the dependency curves of x_2 (designate as x) and Δx on the value of the broken ore volume, which are presented in Fig. 2. From Fig. 2, it is clear that the curves are non-linear.

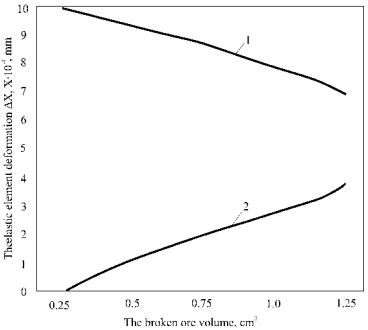

Fig. 2. The dependence of elastic element deformations on the broken ore volume: *1* - deformation of the elastic element with ore; *2* - the deformation difference of the loaded and unloaded elastic element

The graphs obtained in Fig. 2, allowing continue the mathematical modelling of the ore destruction process in a ball mill. If for a specific time the balls in the mill broke all the ore volumes, which are shown in the Tab. 2 and all the deformations were

determined, then the mean x_{2c}, which corresponds to all measurements can be determined by data x_{2c} from the table. It is equal to 0.859028, which corresponds to the mean value of the broken volume of 0.75 cm^3. According to curve 1 in Fig. 2 by ordinate 0.859, we determine the value of the broken ore volume of 0.75 cm^3. Thus, for example, according to curve 1 in Fig. 2, it is possible to determine the volume of the broken solid by the measured average strain value of the loaded elastic element, which corresponds to the energy efficiency of ore breakage.

By fitting curve 1 in Fig. 2, the equation for the dependence of the broken ore volume on the expectation of the deformation of the elastic element x_{2c} is obtained

$$V_p = -1{,}9118x_{2c}^2 + 0{,}0546x_{2c} + 2{,}1371 . \qquad (7)$$

This equation allows us to find the average value of the broken ore volume, which characterizes the energy efficiency of its grinding in a ball mill for a certain mathematical expectation of the loaded elastic element deformations.

Let's simulate the process of controlling the energy efficiency of ore breakage in a ball mill in accordance with (7). We will use the data of complete ore grinding cycles for volumes of 1.25; 1.0; 0.75; 0.5 and 0,25 cm^3 described in Table 2. Since the volumes of 0.5 and 0.25 cm^3 are rather small, and the ball mill should work at the overload limit, the cycles for 1.25; 1.0; 0.75 cm^3 most fully characterize the work of the technological unit. In the process of modelling, we use various combinations of ore grinding cycles. The simulation results are listed in Tab. 3.

Tab. 3

The mathematical modelling results of the energy-efficient control of ore grinding in a ball mill by a combination of different grinding cycles

Combination of ore crushing cycles with specific volumes V_p, cm^3	Average deformation of an elastic element with ore x_{2c}, mm	The reference value of the destroyed ore volume determined according to Table 2, V_{pe}, cm^3	The volume of broken ore, determined by (7) V_p, cm^3	Relative error of control of broken ore volume δ, %
1.25; 1.0; 0.75	0.782487	1.0	1.009256	0.926
1.0; 0.75; 0.5	0.86387	0.75	0.757546	1.006

0.75; 0.5; 0.25	0.93795	0.5	0.506406	1.280
1.25; 1.25; 1.0; 0.75	0.76076	1.0625	1.072158	0.910
1.25; 1.0; 1.0; 0.75	0.78329	1.0	1.006896	0.690
1.25; 1.0; 0.75; 0.75	0.803405	0.9375	0.946976	1.011

From Table 3 it is clear that when measuring mass and using various combinations of the mass of the ball and broken ore volumes it is possible to determine the averaged value of the broken ore volume, which characterizes the grinding energy efficiency by the measured mean deformations of the loaded elastic element x_{2c} and the resulting analytical dependence.

6. Results and discussion

The proposed mathematical models (1) and (2) can be applied in a ball mill for h=const, since the balls movement speed therein unchanged and independent of their mass. As a result of segregation, the balls are located along with the drum of the mill with an increase in their size (mass) from the load to the throat neck. It is advisable to carry out the measurements with a ball diameter of 50 mm, where the delays are small, and the size of ore pieces is significant. The dependence of the loaded elastic element deformation on a variable within certain limits of the mass of the ball leads to measurement error. This error can be offset by using (1) of an unloaded elastic element. At the same time, in the conditions of 10% deviation of the ball mass, the error of measurement is almost twice less, remaining significant, slightly more than 5%. Reducing the volume of material, which is broken by the falling ball contributes to increasing the direct measurement accuracy of the ore crushing energy efficiency. However, the error practically does not exceed 5%, and this leads to the delay increase. In terms of mass phenomena, a more effective approach may be the interaction of the elastic element with the falling balls. The random values here will be a change in the mass of the balls within certain limits and the broken ore volumes. As the analysis showed, the average value of deformations under all the balls, which passed through the elastic element, also characterizes the average value of the broken ore volume, i.e., the energy efficiency of its grinding.

As a result of the mathematical modelling of this process, the dependences of the elastic element deformation, the difference in the

deformations of the unloaded and loaded elastic element on the volume of the broken ore are obtained. They are practically consistent with each other. Considering the insignificant final result of compensation and the strong influence of averaging features on it, it is advisable to consider (1) in Figure 2 and its approximation equation (7). Equation (7) according to the mathematical expectations of the loaded elastic element deformations, allows finding the averaged value of the broken ore volume, which characterizes the energy efficiency of its milling in a ball mill. Mathematical modelling has confirmed the validity of such a conclusion for the random arrangement of ore volumes on an elastic element. The average values of the broken ore volumes (see Tab. 3) determined by (7) are slightly higher than the reference ones. The mismatch of values is basically in the range of 0.690-1.011%. A slightly higher deviation value of 1.28% can be disregarded since it refers to the smallest loads, which can hardly occur during ore grinding. Thus, the deviation of the measured averaged volumes of the broken ore from the reference value does not exceed 1%. The resulting accuracy of the average volume determination meets the requirements of the process.

7. Conclusions

For the first time, the approach of the direct control of ore grinding energy efficiency in ball mills by measuring the mathematical expectation of the elastic element deformation, which interacts with balls and ore in the cross-section of the drum, followed by determination of the broken material volume, which characterizes the measured parameter in accordance with the proposed dependency is proposed. The deviation of the measured averaged volumes of the broken ore from the reference value does not exceed 1%, which satisfies the requirements of the technological process. Automatic control of this technological parameter forms the prerequisites for a significant reduction in energy and material overspending in the first stage of ore grinding at the beneficiation plants.

The prospect of further research is the development of tools for direct measurement of the energy efficiency of ore destruction in ball mills of the first grinding stages at the ore-dressing plants.

References

1. (DGRI) Directorate-General for Research and Innovation (European Commission). (2013), Sustainable process industry. EU publications. http://dx.doi.org/10.2777/30452.

2. **Pivnyak G., Weisberg L., Kirichenko V., Pilov P., Kirichenko V.** (2007), Grinding. Energy and technology, Ore and Metals., Moscow.

3. **Soleymani M., Fooladi M., Rezaeizadeh M.** (2016), Effect of slurry pool formation on the load orientation, power draw, and impact force in tumbling mills, Powder Technology, Vol. 287, 160–168. http://dx.doi.org/10.1016/j.powtec.2015.10.009.

4. **Duroudier J.P.** Grinding Energy. (2016), Size Reduction of Divided Solids, 53-72. https://doi.org/10.1016/B978-1-78548-185-7.50002-3.

5. **Musa F., Morrison R.** (2009), A more sustainable approach to assessing comminution efficiency. Minerals Engineering, **22**(7-8), 593-601. https://doi.org/10.1016/j.mineng.2009.04.004.

6. **Rezaeizadeh M., Fooladi M., Powell M., Mansouri S.** (2010), Experimental observations of lifter parameters and mill operation on power draw and liner impact loading, Minerals Engineering, **23**(15), 1182–1191. http://dx.doi.org/10.1016/j.mineng.2010.07.017.

7. **Malyarov P., Soldatov G., Kaitmazov N., Baskaev P., Ivanov V., Kotenev D.** (2008), Intensification of grinding processes under conditions of the Talnakh concentrator, Ore dressing, **6**, 6–10.

8. **Huang P., Jia M., Zhong B.** (2009), Investigation on measuring the fill level of an industrial ball mill based on the vibration characteristics of the mill shell. Minerals Engineering, **22(14)**, 1200–1208,. http://dx.doi.org/10.1016/j.mineng.2009.06.008.

9. **Hu G., Otak H., Watanuki K.** (2000), Motion analysis of a tumbling ball mill based on non-linear optimization, Minerals Engineering, **13(8)**, 933-947.

10. **Morozov V., Topchayev V., Ulitenko K., Ganbaatar Z., Delgerbat L.** (2013), Development and application of automated control systems for mineral processing, Ore and Metals., Moscow.

11. **Kupin A.** (2008), Intellektualna identyficatsiia ta keruvannia v umovakh protsessiv zbahachuvalnoi tekhnolohii [Intelligent Identification and Control of Process in Concentration Technologies], KTU, Kryvyi Rih, Ukraine.

12. **Sevastyanov B.A.** (2012), The course of the theory of probability and mathematical statistics, Ed. "Book on demand", Moscow.

https://doi.org/10.31713/m1024

COMPARISON OF THE STRUCTURAL PROPERTIES OF CONCRETE BEAMS WITH COMPOSITE BASALT AND STEEL REINFORCEMENT

Sakhno S.
Kryvyi Rih National University, Ph. D., Assoc. Prof., Ukraine

Yanova L.
Kryvyi Rih National University, Ph. D., Assoc. Prof, Ukraine

Pischikova O.
Kryvyi Rih National University, Ph. D., Assoc. Prof, Ukraine

Abstract

The subject of the study. The work investigated the deformative, strength, and cost parameters of concrete beams with various reinforcement types. The nature of the behavior under a load of beams reinforced with steel reinforcement and beams with basalt reinforcement of multiple diameters has been studied.

A research methodology is the studying of finite element models of the reinforced concrete beam. The Drucker-Prager model was used to simulate concrete behavior. For steel reinforcement, a bilinear isotropic hardening model, a linear orthotropic model was used for composite reinforcement.

The goal is to reveal the advantages and disadvantages of using basalt composite reinforcement in reinforced concrete.

Conclusion of the study.

The paper considers the behavior of four models of reinforced beams. In the first model, a control one, steel reinforcement, is used. In the second, the composite reinforcement diameter is equal to the diameter of the steel one. In the third model, the diameters of the composite reinforcement are taken from the conditions of its similar bearing capacity with the steel one. The fourth model's composite reinforcement diameters have been taken from the requirements of its equal deformation with the steel one. The paper presents a method for calculating the corresponding diameters of reinforcement. The model in which the diameters of the composite reinforcement are taken from the conditions of its equal deformation with the steel reinforcement has the beam's best operation. In this case, the deformations and stresses in concrete practically do not differ from the corresponding stresses in the model with steel reinforcement. However, the utilization factor of the bearing capacity of the reinforcement in this model is deficient, and the cost of reinforcing elements is almost three times the cost of steel rods. The model in which the diameters of composite reinforcement are taken based on its equal bearing capacity with steel reduces the cost of reinforcement almost three times. However, such a beam's deformation and strength properties are significantly worse than in the control sample. The model with composite reinforcement diameters equal to the

steel reinforcement diameters has no advantages over the model with steel reinforcement.

Introduction

Composite materials are increasingly used in mining, automotive, aerospace, construction, and other industries. Compared with metal, composite materials have a lower specific gravity, high specific strength, high corrosion resistance [1, 2]. In construction, composite materials are used in the restoration and repair [1] of such structural elements as beams [3] and walls [4].

Composite materials are used relatively recently as bar reinforcement. The most widely used are fiberglass, this is due to its low cost and availability in the market [5, 6]. Still, carbon fibers have excellent prospects [7]. They are much tougher than glass fibers and have a modulus of elasticity, like steel [5].

Since the beginning of the century, basalt fiber has been increasingly used [6-10]. The primary basalt deposits are in Ukraine [6]. Compared to steel, basalt composite rebar has a higher tensile strength – 1000-1300 MPa, but a much lower Young's modulus – about 70 GPa.

Currently, there are many disputes about the effectiveness of basalt rebar. Supporters of this building material note the high bearing capacity, corrosion resistance, and cheapness of the material [2]. Opponents point to a low modulus of elasticity of the material and, accordingly, a more significant deformation under load and more extensive cracking in reinforced concrete [12,13,18].

This work aims to identify the advantages and disadvantages of using basalt rebar in reinforced concrete by analyzing the behavior of digital models of reinforced concrete beams. The deformation and strength characteristics of the models and some cost indicators were used as analysis parameters.

The modeling of these structural elements' operations with different reinforcement options was carried out to compare the behavior of concrete beams reinforced with steel and basalt reinforcement. The simulation was carried out by the finite element method in the ANSYS Student software package.

The geometrical parameters

The geometric parameters of the numerical model of the reinforced beam shown in Fig. 1. A concrete beam measuring

2080×220×120 mm mounted on two supports with a span of 1800 mm. Both supports have a rotational degree of freedom around the *Z*-axis. One of the supports rigidly fixed along the *X*,*Y*,*Z* axes; the other moves freely along the *X*-axis. The concentrated loads on the beam's upper chord transmitted through prismatic pads installed at a distance of 600 mm from the supports axes.

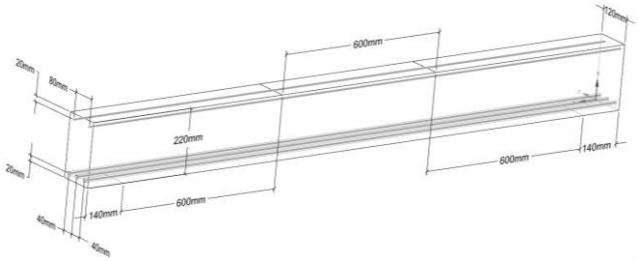

Fig. 1 The geometrical parameters of the numerical model of a reinforced concrete beam

There are some rebars in the upper and lower chord of the beam. In the lower zone - three rods with an interval of 40 mm along the axes, in the upper location - two rods with a gap of 80 mm along the axes. The distance from the rods' axes to the beams' surface is assumed to be 20 mm.

Material properties

The work investigated the nonlinear behavior of materials. The Drucker-Prager model was used to model the concrete behavior. The concrete parameters for the Drucker-Prager model investigated in the works. [15-16]. The concrete mechanical and physical properties used in the numerical model shown in Table 1.

Table 1

Physical and mechanical properties of concrete

Density	2,3e-06	kg/mm³
Isotropic Elasticity Derive from	Young's Modulus and Poisson's Ratio	
Young's Modulus	32500	MPa
Poisson's Ratio	0,2000	
Bulk Modulus	18056	MPa
Shear Modulus	13542	MPa
Drucker-Prager Base		
Uniaxial Compressive Strength	38,350	MPa
Uniaxial Tensile Strength	3,4100	MPa
Biaxial Compressive Strength	59,780	MPa

A model with bilinear isotropic strengthening was used to simulate the behavior of steel reinforcement. The steel's mechanical characteristics were taken from compliance with the AIII reinforcement and shown in Table 2.

Table 2

Physical and mechanical properties of steel rebar

Density	7,75e-06	kg/mm³
Isotropic Elasticity Derive from	Young's Modulus and Poisson's Ratio	
Young's Modulus	2,1e+05	MPa
Poisson's Ratio	0,31000	
Bulk Modulus	1,8421e+05	MPa
Shear Modulus	80153	MPa
Bilinear Isotropic Hardening	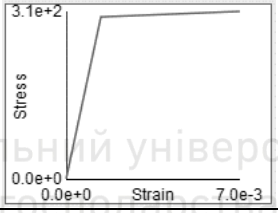	

For composite reinforcement, a linear orthotropic behavior model is adopted, and its characteristics showed in Table 3.

Table 3

Physical and mechanical properties of composite rebar

Density	1,8e-06	kg/mm³
Orthotropic Elasticity		
Young's Modulus X direction	71000	MPa
Young's Modulus Y direction	71000	MPa
Young's Modulus Z direction	71000	MPa
Poisson's Ratio XY	0,20	
Poisson's Ratio YZ	0,40	
Poisson's Ratio XZ	0,20	
Shear Modulus XY	9000,0	MPa
Shear Modulus YZ	8214,3	MPa
Shear Modulus XZ	9000,0	MPa
Compressive Ultimate Strength	0	MPa
Compressive Yield Strength	1200,0	MPa
Tensile Ultimate Strength	1200,0	MPa
Tensile Yield Strength	1200,0	MPa

Numerical model

The original simulation was done on a steel rebar model (St). The diameter of the upper rods is 6 mm, and the lower ones are 12 mm. For models with composite rebar, three options for bar diameters accepted:

diameters of composite and steel rebars are equal (C_eqv_D);

the diameters of composite rebar were calculated based on conditions of equal bearing capacity with steel rebar (C_eqv_F);

The composite rebar's diameters are calculated from the conditions of equal strain with steel rebar (C_eqv_e).

The methods for calculating the corresponding diameters of composite rebar are discussed below.

For all four models, meshes with a cell size of 20 mm were created (Fig. 2).

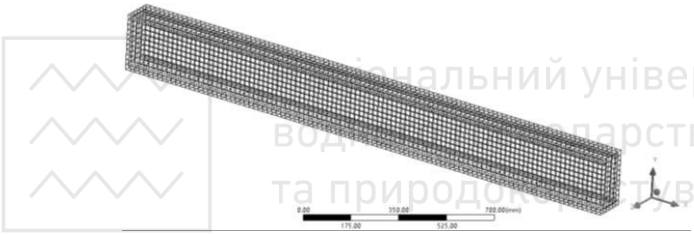

Fig. 2. Mesh of the numerical model of a reinforced beam

In all models, loading performs by applying a concentrated load to the upper chord of the beam. The load was applied in ten steps with a maximum value of 5000 N for each of the two concentrated loads (Fig. 3). The load values for each stage give in table 4. In addition to concentrated loads, gravity acts on the beam.

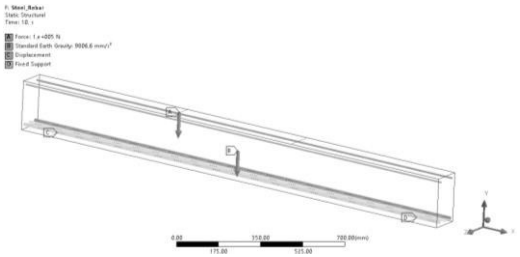

Fig. 3. Scheme of fixing the beam and distribution of loads

Table 4

Amount of load at each step of loading

Steps	Time [s]	X [N]	Y [N]	Z [N]
1	0	0	0	0
1	1	0	0	0
2	2	0	-11111	0
3	3	0	-22222	0
4	4	0	-33334	0
5	5	0	-44444	0
6	6	0	-55556	0
7	7	0	-66666	0
8	8	0	-77778	0
9	9	0	-88888	0
10	10	0	-100000	0

Method for calculating the diameters of composite rebars

As mentioned earlier, the work considers four numerical models of a concrete beam, differing in material and diameters of rebars: St, C_eqv_D, C_eqv_F, C_eqv_e. In the first two models (St and C_eqv_D), the diameters of the rebars are equal.

For the third model – C_eqv_F, the composite rebar diameter was selected based on the conditions for ensuring elastic deformation stages the same bearing capacity as steel rebar. The bearing capacity of the rebar F is

$$F = \sigma \pi r^2 .$$

In equal bearing capacity rebar made of steel and basalt, the condition must be met

$$\sigma_{k,st} \pi r_{st}^2 = \sigma_{k,cpz} \pi r_{cpz}^2 .$$

Hence

$$r_{cpz,\sigma} = r_{st} \sqrt{\frac{\sigma_{k,st}}{\sigma_{k,cpz}}} .$$

where F – rebar load

σ – rebar stress

$\sigma_{k,st}$ – characteristic strength of steel rebar

$\sigma_{k,cpz}$ – characteristic strength of composite rebar

r_{st} – steel rebar radius

r_{cpz} – composite rebar radius

$r_{cpz,\sigma}$ – radius of composite rebar that provides the same bearing capacity as steel rebar.

For the considered model $\sigma_{k,st}$=295 MPa, $\sigma_{k,cpz}$=1200 MPa. Therefore, the radius of the lower belt rebar takes:

$$6 \cdot \sqrt{\frac{295}{1200}} = 2{,}97 \ [mm]$$

Similarly, the upper chord's composite rebar' radius was calculated, which is 1.48 mm.

In the fourth model – C_eqv_e, the diameters of the composite rebar were calculated from the conditions for ensuring the same strain of the composite and steel bars at the stage of elastic deformations. The following was considered

$$E = \frac{\Delta\sigma}{\Delta\varepsilon},$$

where

$$\varepsilon = \frac{\Delta l}{l} \text{ and } \sigma = \frac{F}{A}$$

For the round section

$$A = \pi \cdot r^2.$$

Thus, for a circular section

$$\sigma = \frac{F}{\pi r^2}, \text{ a } \Delta\sigma = \frac{F_2 - F_1}{\pi r^2} = \frac{\Delta F}{\pi r^2}.$$

Hence

$$E = \frac{\Delta F \cdot l}{\Delta l \cdot \pi \cdot r^2}.$$

Let us denote Young's modulus of steel rebar through E_{st}, composite through $E_{cpz,}$ and the cross-sectional radii of the steel rebar, respectively, through r_{st}, and the composite – r_{cpz}. For the rods to have the same relative elongation $\Delta l_{cpz} = \Delta l_{st}$ at the same ΔF, the condition must be met

$$\frac{\Delta F \cdot l}{E_{cpz} \cdot \pi \cdot r^2} = \frac{\Delta F \cdot l}{E_{st} \cdot \pi \cdot r^2}.$$

Removing the components with equal values from equality, we obtain

$$\frac{1}{E_{cpz} \cdot r_{cpz}^2} = \frac{1}{E_{st} \cdot r_{st}^2} \cdot$$

Hence

$$r_{cpz,\varepsilon} = r_{st} \sqrt{\frac{E_{st}}{E_{cpz}}},$$

where $r_{cpz,\varepsilon}$ - the composite rebar radius that provides the same strain as steel rebar.

For the considered model E_s=2,1e+05 MPa, E_{cpz}=7,1e+04 MPa. The radius of the bars of the lower chord

$$6 \cdot \sqrt{\frac{2,1e+05}{7,1e+04}} = 10,32 \ [mm]$$

Similarly, the radius of the composite rods of the upper chord is calculated as 5.16 mm.

The diameters of the rebar of all numerical models are seen in table 5.

Table 5

Diameters of bar reinforcement of beam models

Top/bottom beam chord	Model code			
	St	C_eqv_D	C_eqv_F	C_eqv_e
The diameter of rods of the upper belt [mm]	6.0	6.0	2.96	10,32
The diameter of rods of the bottom belt [mm]	12.0	12.0	5.94	20.64

Research results

Based on the simulation results for different models, the beam's deflections, relative deformations of concrete, axial compressive and tensile stresses in the concrete, axial stresses in the upper and lower chords' rods, and the degree of utilization of the rod material were compared.

The dependence of the beam deflections on the load is shown in Fig. 4.

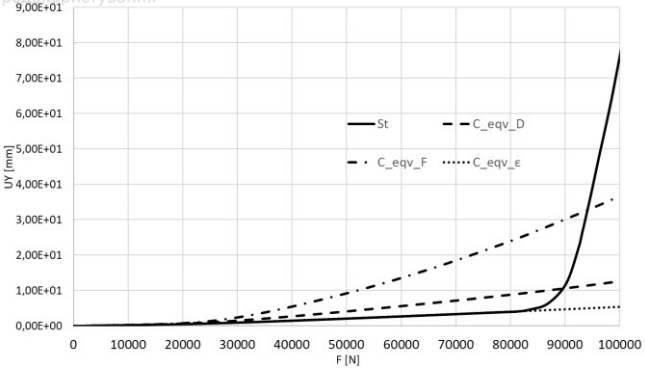

Fig. 4. Vertical deflections of reinforced concrete beams

It can be seen from the graph that the nonlinear deflection of the beam in the St model begins at a load of 85.6 kN. The most considerable deflections are observed in the C_eqv_F model. As expected, the smallest deflections are in the C_eqv_ε model. Simultaneously, until the onset of plastic deformations in steel rebar, the deflections in the model St and C_eqv_ε are practically equal. With the onset of plastic deformations in steel rebar at a load of 85.6 kN, the St model's deflections increase sharply, while in the C_eqv_ε model, they only slightly increase.

The deflections in the C_eqv_F model significantly exceed the deflections in the St model at all loads. Nevertheless, with a load of 93.3 kN, the deflections in the steel rebar plastic deformations zone in both models are equalized. Further increase in the load, the deflections in the C_eqv_F model are significantly lower than in the St.

As the load increases, the ratio of the deflection values in the steel rebars elastic work zone for models St and C_eqv_F changes from 1.15 to 4.69, and models St and C_eqv_D from 1.11 to 2.02. The models' maximum strain was determined in the lower belt seat central part (Fig. 5).

The simulation results are shown in Fig. 6. The patterns of manifestation of relative deformations of all models are practically similar to the manifestation of deflections. However, the ratio of the relative deformations of different models is somewhat less.

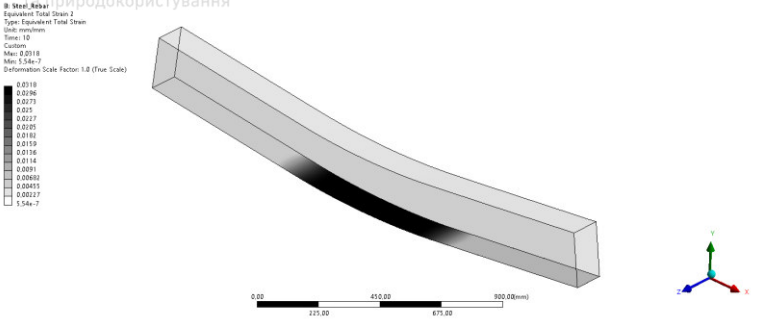

Fig. 5. Concrete strain in the lower chord of the model with steel rebar (St) at maximum load

The strain values ratio in the zone of steel reinforcement elastic work for models St and C_eqv_F varies from 1.00 to 4.28, and for models St and C_eqv_D from 1.00 to 1.62. The lowers values of the relative deformations' ratios compared with the deflections are explained by the fact that the deformations of the lower chord of the beam and the upper one take part in deflections.

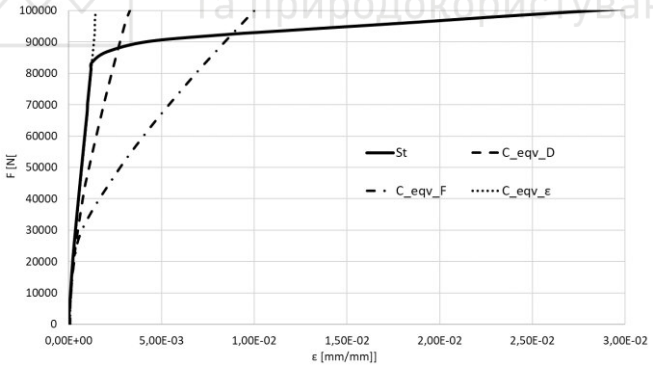

Fig. 6. Strains of numerical models of reinforced concrete beams

Per [17], the tensile strain of concrete, at which cracking begins, is determined by the formula

$$\varepsilon_{btR} = \frac{1}{15}\sqrt[3]{\left(\frac{R_{bt}}{E_{bn}}\right)^2}$$

For the concrete used in the model, the limiting strain of concrete after which cracking occurs ε_{btR}=1,48E-04 [mm/mm].

A detailed examination of the relative deformations in the load zone that corresponds to the moment of crack initiation (Fig. 7) shows that crack formation occurs earlier in all models with composite rebars. In the C_eqv_F model, cracking begins at a load of 18.5%, in C_eqv_D – by 13.1%, C_eqv_ε – by 7.0% lower than in the St.

The distribution of strain in the beam models St and C_eqv_D showed in Figs 8 and 9. The relative deformations in the figure are determined at a load of 83.57 kN, at which plastic deformations of steel rebars begin in model St.

The C_eqv_D model, in comparison with the St model, has significantly larger relative deformations both in value and in length along the lower chord of the beam.

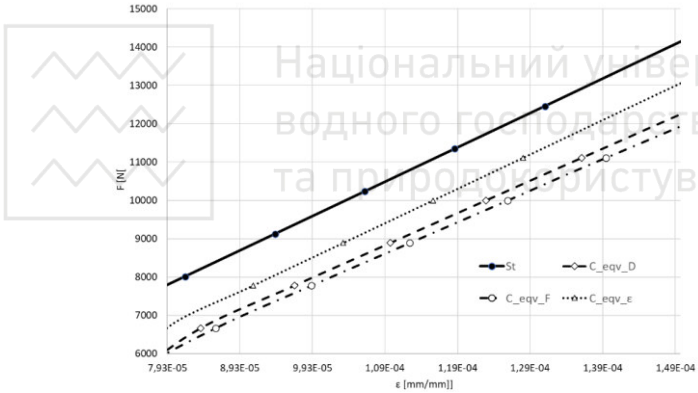

Fig. 7. Relative deformations of numerical models of reinforced concrete beams in the load zone that corresponds to the beginning of cracking

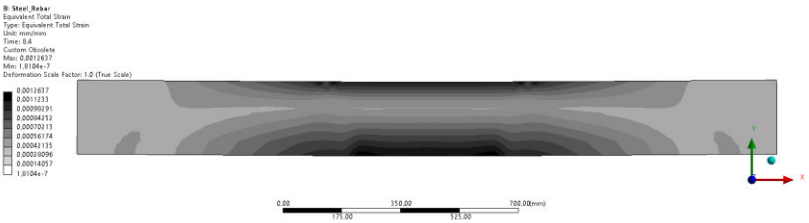

Fig. 8. Equivalent total strain in model St under a load that is corresponding to the onset of plastic deformations of steel reinforcement (83.57 kN)

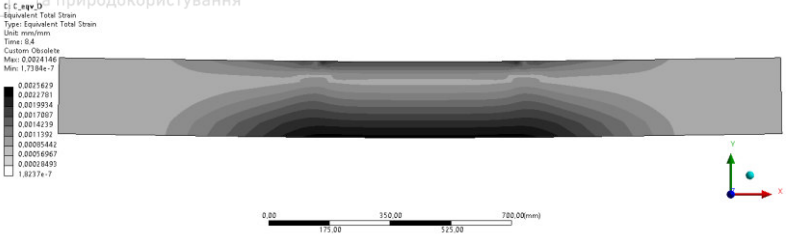

Fig. 9. Equivalent total strain in model C_eqv_D under a load that is corresponding to the onset of plastic deformations of steel reinforcement (83.57 kN)

Cracking limits all models' lower chords' maximum stresses to concrete's ultimate tensile strength (Figure 10). Therefore, after the onset of crack formation, the nature of stress growth in the lower belt for all models does not differ significantly.

The growth rate of stresses in the upper belt for different models has significant differences. With increasing load, compressive stresses increase the fastest in the model C_eqv_F. The higher rate of growth of compression stresses in the upper belt of the C_eqv_F and C_eqv_D models is associated with a decrease in the compressed zone's size (Fig. 11).

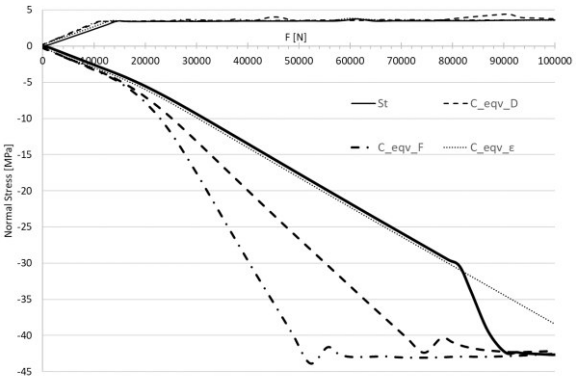

Fig. 10. Maximum stresses in the upper and lower chord of various beam models

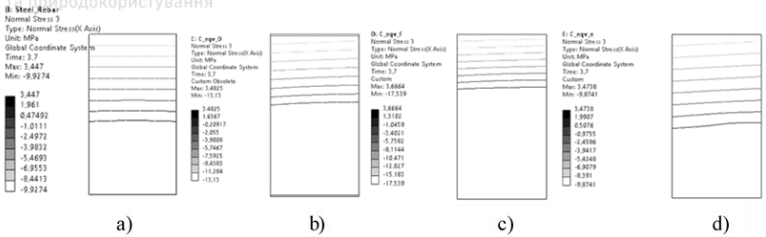

Fig. 11. Distribution of normal stresses along with height in the central part of various beam models. *a* – St; *b* – C_eqv_D; *c* – C_eqv_F; *d* – C_eqv_e. Load 30 kN

In the model with steel rebar (St), a significant increase in stresses in the beam's upper chord occurs when plastic deformations appear in the lower chord rebar. The loss of the upper chord's bearing capacity in models St, C_eqv_D, and C_eqv_F occurs at tensile stresses of about 42 MPa. This value is higher than the ultimate strength of concrete under uniaxial compression (38.5 MPa) but lower than the biaxial compressive strength (59.78 MPa). The loss of concrete bearing capacity in the compressed zone in the C_eqv_F model occurs at a load of 52.2 kN, C_eqv_D – a load of 74.4 kN, St – 88.8 kN, C_eqv_e – at a load of more than 100 kN. If we assume that the loss of the bearing capacity of a beam with steel rebars occurs not when the ultimate strength of concrete in compression is reached but at the beginning of plastic deformations of the reinforcement, then the bearing capacity of the St model not will be 88.8 kN, but 81.2 kN.

Figures 12 and 13 show the nature of stress changes of the upper and lower chords rebars. The fastest increase in stresses in the reinforcement of the lower chord is observed in the C_eqv_F model. In models St and C_eqv_F, almost the same voltages occur with increasing load.

The stresses in the lower chord rebars of the C_eqv_e model at any loading level are significantly less than in the St and C_eqv_F models. The distribution of stresses in the reinforcement of the upper chord has other dependencies (Fig. 13).

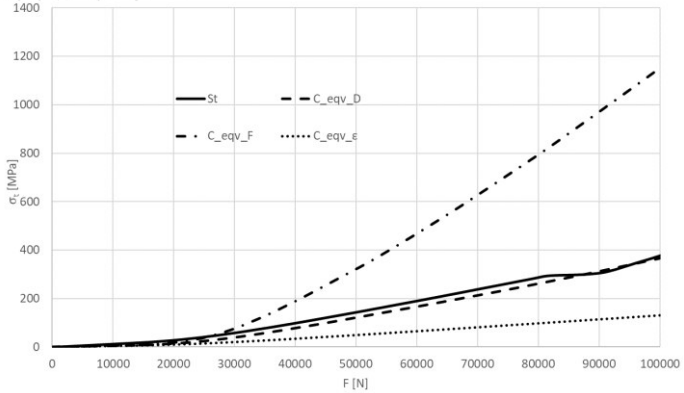

Fig. 12. Normal stresses in the lower chord rebar

The highest compressive stresses are observed in the St. The voltage is slightly lower in the C_eqv_F model, even lower in the C_eqv_D model. Model C_eqv_e has the lowest stresses in the top chord reinforcement.

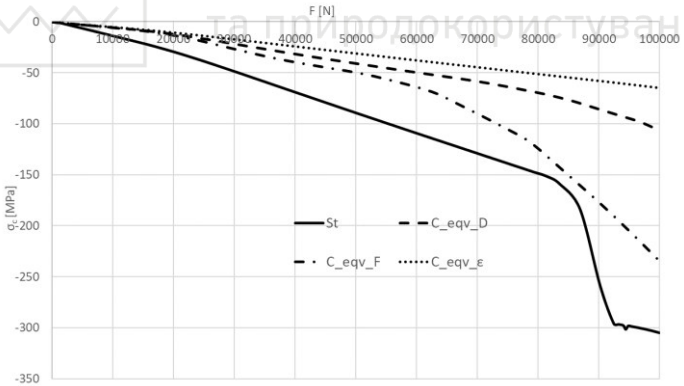

Fig. 13. Normal stresses in the upper chord rebar

Figures 14 and 15 show the coefficients of using the bearing capacity of the reinforce of the models.

The steel reinforcement bearing capacity's utilization factor was determined as the reinforcement's stress ratio to its yield point. For composite reinforcement, this is the ratio of stress to the ultimate

strength of the reinforcement. At the same loads, the maximum utilization factor for steel reinforcement of the St model, the minimum for the C_eqv_e model. At a load of 80 kN, the utilization factors of the bearing capacity of the lower reinforcement are: St – 0,99; C_eqv_D – 0,22; C_eqv_F – 0,66; C_eqv_e – 0,08. For the upper reinforcement, these indicators are: St – 0.51; C_eqv_D – 0.058; C_eqv_F 0.10; C_eqv_e – 0.04. Thus, underutilization of the bearing capacity of the material is observed for all models of composite reinforcement.

In the production of reinforced concrete, the price of both the concrete itself and the reinforcement elements is essential. Since the concrete volume in the models under consideration does not change significantly, only steel and composite rebar will be considered when calculating the cost indicators.

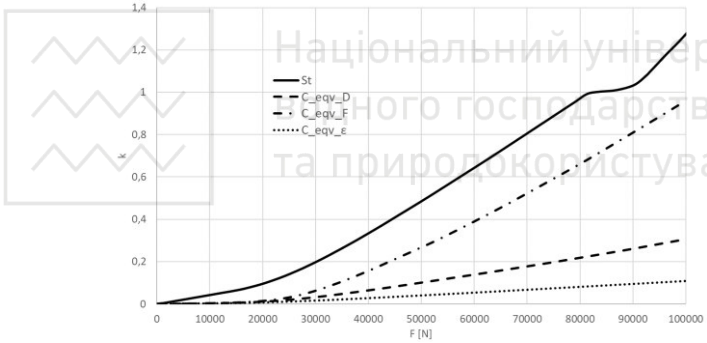

Fig. 14. Utilization factors of the bearing capacity of the bottom reinforcement

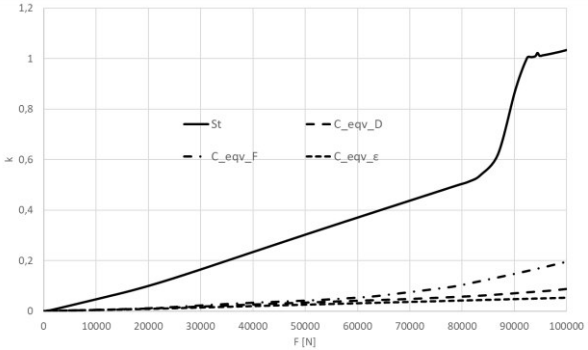

Fig. 15. Utilization factors of the bearing capacity of the upper reinforcement

Prices are obtained from open sources: [18], [19] (as of 12/01/2021). Prices for one running meter of steel and composite reinforcement of various diameters showed in Table 6. At the time of this writing, one hryvnia corresponded to USD 0.035 and EUR 0.029.

Table 6

Price of one running meter steel and composite rebar

Item No.	Diameter [mm]	Rebar type	Price [UAH]
1	6	steel	6,5
2	12	steel	17
3	3	composite	2,5
4	6	composite	4,5
	10	composite	13,7
5	12	composite	18
6	20	composite	52,7

The models under consideration use three rods with a total length of 6.24 m in the lower chord and two rods with a total length of 4.16 m in the beam's upper chord. The calculation of the cost of reinforcement showed in table 7.

Table 7

Calculation of the cost of reinforcing elements

Top/bottom beam chord	Parameter	Model code			
		St	C_eqv_D	C_eqv_F	C_eqv_e
Upper	Diameter [mm]	6	6	3	10
	Price of one running meter [UAH]	6,5	4,5	2,5	13,7
	Amount	4,16	4,16	4,16	4,16
	Total [UAH]	27,04	18,72	10,4	56,992
Lower	Diameter [mm]	12	12	6	20
	Price of one running meter [UAH]	17	18	4,5	52,7
	Amount	6,24	6,24	6,24	6,24
	Total [UAH]	106,08	112,32	28,08	328,848
In total		133,12	131,04	38,48	385,84
K		1	0,98	0,29	2,9

The last line of the table shows the relationship between the cost of composite reinforcement of the corresponding models and the cost of steel reinforcement. Calculations show that the C_eqv_F model has the lowest cost of reinforcement, with the bearing capacity of the composite reinforcement being equal to the bearing capacity of the

steel reinforcement. The cost of the reinforcement model C_eqv_D differs slightly from the cost of steel reinforcement, and the cost of the reinforcement model C_eqv_e is almost three times the cost of steel reinforcement.

Conclusions

The results obtained in work allow making a comparative analysis of various models of using composite reinforcement. All parameters of the composite model are compared with the corresponding parameters of the steel rebar model. The analysis results are summarized in Table 8.

Table 8

Summary indicators of models with steel and composite reinforcement

Parameter	Determined at load [kN]	Model code						
		St		C_eqv_D		C_eqv_F	C_eqv_e	
		value	value	deviation [%]	value	deviation [%]	value	deviation [%]
Vertical deflection [mm]	80	3,96	8,89	+124	24,01	+506	4,05	+2
Maximum concrete stresses in the lower chord of the beam [MPa]	80	3,53	3,79	+7	3,61	+2	3,54	0
Maximum concrete stresses in the upper chord of the beam [MPa]	80	29,54	40,9	+39	42,96	+4	30,38	+3
Crack initiation load [kN]	–	14,0	12,1	-14	11,8	-16	12,9	-8
Strain [mm/mm $\times 10^{-3}$]	80	1,17	2,32	+98	6,86	+486	1,20	+3
Stresses in the upper chord rebar [MPa]	80	147,1	69,6	-53	124,3	-15	51,16	-65
Stresses in the lower chord rebar [MPa]	80	282,0	262,4	-7	793,7	+181	98,12	-65
Utilization factor of the upper chord rebar	80	0,50	0,06	-88	0,10	-79	0,04	-91
Utilization factor of the lower chord rebar	80	0,96	0,22	-77	0,66	-31	0,08	-91
Rebar cost	–	133,12	131,04	-2	38,48	-71	385,8	190

The C_eqv_e model provides the best beam performance. In this case, deformations are provided at the level of deformations of the beam with steel reinforcement, and the stresses in concrete practically do not differ from the corresponding stresses in the model St. The calculation obtained lower loads at which cracks begin to form. However, the utilization factor of the bearing capacity of the reinforcement in this model is shallow. The cost of reinforcing elements is almost three times the cost of steel rods. The model also showed lower loading values at which cracks start to form.

The C_eqv_F model can significantly reduce the cost of purchasing reinforcement. The advantage of a model with reinforcement of the same bearing capacity with steel reinforcement on this ended. The deformation of the model is 5-6 times greater than in control. The upper and lower chords' concrete stresses are higher than in a beam with steel rebar. Cracking begins at loads 16% lower, and the loss of the beam's bearing capacity occurs at 35% lower loads (Fig. 10) than in the model St.

Model C_eqv_F has reinforcement diameters equal to corresponding diameters of steel reinforcement of control model St. This model, in comparison with the control (St), has only disadvantages. At the same loads, the deformation in it is more significant, the stresses in the concrete are higher, cracking and loss of bearing capacity begins earlier than in a beam with steel reinforcement. The utilization factors of the bearing capacity of the reinforcement are also insignificant.

The analysis carried out in this work at this stage of research did not reveal the significant advantages of composite rod reinforcement compared to steel. Benefits can be obtained with a significant reduction in the cost of composite reinforcement.

The high creep values of amorphous vitreous substances can significantly affect the deformation and bearing capacity of structures over long periods. Therefore, further research should be aimed at studying the creep parameters of composite reinforcement.

Bibliography

1. **Masuelli, M.** (2013). Fiber Reinforced Polymers – The Technology Applied for Concrete Repair. Rijeka, Croatia: InTech.

2. **Lapko, A, Urbański, M.** (2015). Experimental and theoretical analysis of deflections of concrete beams reinforced with basalt rebar. Arch Civ Mech Eng,15, 223-30.

3. **Kim, H.S, Shin, Y.S**. (2011). Flexural behavior of reinforced concrete (RC) beams retrofitted with hybrid fiber-reinforced polymers (FRPs) under sustaining loads. Compos Struct, 93, 802-11.

4. **Luccioni, B., Rougier, V.C.** (2013) Numerical analysis of fibre reinforced polymer retrofitted masonry panels. Engineering Structures, 49, 360-72.

5. **Campbell, F.C.** (2010) Structural Composite Materials. ASM International.

6. **Pico, D., Steinmann, W.** (2016) Synthetic fibers for composite applications. Fibrous and Textile Materials for Composite Applications, Singapore: Springer, 135-170.

7. **Holmes, M.** (2014) Global carbon fibre market remains on upward trend. Reinf Plast, 58, 38-45.

8. **Wang, X., Shi, J., Liu, J., Yang, L., Wu, Z**. (2014) Creep behavior of basalt fiber reinforced polymer tendons for prestressing application. Mater Des, 59, 558-64.

9. **Elgabbas, F., Vincent, P., Ahmed, E.A., Benmokrane, B.** (2016) Experimental testing of basalt-fiber-reinforced polymer bars in concrete beams. Compos Part B-Eng, 91, 205-18.

10. **Fiore, V., Scalici, T., Di Bella, G., Valenza, A.** (2015) A review on basalt fibre and its composites. Compos Part B-Eng, 74, 74-94.

11. **Ramakrishnanm V., Panchalan, R.** (2005) A new construction material – non-corrosive basalt bar reinforced concrete. ACI, 229, 253-270

12. **Thorhallsson, E.R., Snaebjornsson, J.T.** (2016) Basalt Fibers as New Material for Reinforcement and Confinement of Concrete. Solid State Phenomena, 249. DOI:10.4028/www.scientific.net/SSP.249.79

13. **Gunnarsson, A., Thorhallsson, E.R., Snæbjornsson, J.T.** (2014) Simulation of experimental research of concrete beams prestressed with BFRP tendons. In proceedings of the XXII Nordic Concrete Research Symposium Reykjavik, Vodskov, 153-156.

14. **Thorhallsson, E.R., Gudmundsson, S.H.** (2013) Test of prestressed basalt FRP concrete beams with and without external stirrups. In: Dancygier AV, editor. Proceedings of Fib symposium Engineering a Concrete future: Technology, modelling & Construction, Tel Aviv, 393-396

15. **Sakhno, S., Liulchenko, Y., Chyrva, T., Yanova, L., Pischikova O.** (2020) Determination of bearing capacity and calculation of the gain of the damaged span of a railway overpass by the finite element method. Topical scientific researches into resource-saving technologies of mineral mining and processing. — Sofia Publishing house "St.Ivan Rilski", 326-339

16. **Sakhno, S., Liulchenko, Y., Bilashenko K.** (2020) Investigation of the applicability of nonlinear numerical models of concrete strength for modeling the destruction of concrete prisms Hirnychyy visnyk, 107 68-73

17. **Nikulin, A.I.** (2014) To determining the limiting relative deformation of concrete in the extended area of a bended reinforced concrete element. Sovremennyye problemy nauki i obrazovaniya, 6. Retrieved from http://www.science-education.ru/ru/article/view?id=16844

18. Price list "Price for metal rolling". Retrieved from https://riber.com.ua/g397304-armatura-stalnaya (as of 12/01/2021)

19. Price list "Price for Composite Reinforcement". https://dp.dnproekt.com/kompozitnaya-armatura-na-sklade-kupit-stekloplastikovuyu-armaturu-v-krivom-roge (as of 12/01/2021)

https://doi.org/10.31713/m1025

STABILITY PROBLEMS OF LARGE SIZED MULTI ELEMENTS ROD STRUCTURES

Ivanova H. P.
National Technical University "Dnipro Polytechnic" (NTU DP"),
Ph. D. (Candidate of Technical Sciences), Associate Professor,
Department of Construction, Geotechnics and Geomechanics

Hapieiev S. M.
National Technical University "Dnipro Polytechnic" (NTU DP"),
Doctor of Technical Sciences, Professor,
Department of Construction, Geotechnics and Geomechanics

Shapoval V. H.
National Technical University "Dnipro Polytechnic" (NTU DP"),
Doctor of Technical Sciences, Associate Professor,
Department of Construction, Geotechnics and Geomechanics

Zhabchyk K. S.
National Technical University "Dnipro Polytechnic" (NTU DP"),
Ph. D. (Candidate of Technical Sciences), Associate Professor,
Department of Construction, Geotechnics and Geomechanics

Zhylinska S.R.
National Technical University "Dnipro Polytechnic" (NTU DP"),
Postgraduate student, Department of Construction, Geotechnics and Geomechanics

Abstract

Recently, process of complicating buildings and structures, which is so-called "architectural trend", as well as market competition leads to the construction of insufficiently approved structure forms. The situation is aggravated by the "lagging behind" regulatory framework, unsatisfactory skills of the construction process participants, contravention of the constructed objects operation rules and other negative factors, on the one hand. On the other hand, a number of documents are of a recommendatory nature. Thus, current above-described situation determined the relevance of this publication. There were made the following in order to correctly predict the trouble-free operation of multi-element metal structures:

- concepts, principles, qualitative and quantitative indicators of operational efficiency (survivability) and its categories related to nodes, structural elements and technical systems in general were formulated;

- a large-scale effect both in the designing and in the operation of large-sized and multi-element metal structures was considered;
- emergency metal structures destruction data were analyzed;
- reasons for characteristic defects and rod metal structures damage are considered, including the modeling of damage formation processes, the identification of random physical regularities of the sizes scattering and defects location.

Introduction

The ultimate goal of designing building structures is to ensure their reliability during construction and operation.

The behavior of building structures during their operation is mainly random. Modern standards of the building structures design take into account the probabilistic nature of loads and bearing capacity only in terms of processing the initial data. Limit states method, which is put down in the current design regulations, is semi-probabilistic. Thus, the designing structure reliability is ensured using the specific safety factors: safety factors for loads, for materials, operating conditions factors, reliability factors according to purpose and these values do not have sufficient theoretical and experimental substantiation.

At structures design according to existing standards the actual level of their reliability remains unknown. Modern regulations allow to design structures with a sufficient level of safety in most cases, what is confirmed by the long-term practice of their operation [1,2]. However, in some cases, structures reliability level can be overestimated, and causes excessive materials consumption, or it can be insufficient (rarely), which leads to unnecessary expenses for eliminating the failures consequences during operation.

The building structures calculation, reflecting their real operation behavior, should be fully based on the theory of reliability, based on probabilistic methods, which allow to give a more objective assessment of the normal operation structure suitability. The reliability theory methods provide a theoretical basis for the correct organization of the collecting and processing statistical data related to the effects on a structure, materials characteristics and its structures and other design parameters. These methods most accurately reflect the design values randomness and the relationship between external influences and structure strength.

The main obstacle in the development of the building structures reliability theory at the present time is the absence or insufficient development of probabilistic methods for assessing the complex multi-element systems reliability, which are designed buildings and structures. This is related to the building structures features: the complexity of deterministic solutions, their high reliability and complex relationships between elements. All this leads to methodological and mathematical issues [3,4].

1. Basic concepts, principles, qualitative and quantitative indicators of the operational efficiency of technical systems

The human society activity is inextricably connected with the creation of various technical systems (machines and mechanisms, buildings and structures). United by purpose and organizational structure they create the so-called organizational and technical systems, for example, geotechnical, environmental, economic systems, etc.

Technical systems are characterized by qualitative and quantitative features. The quantitative features include such features as "small", "medium", "large", the qualitative ones - "simple", "complex", "supercomplex" (Fig. 1).

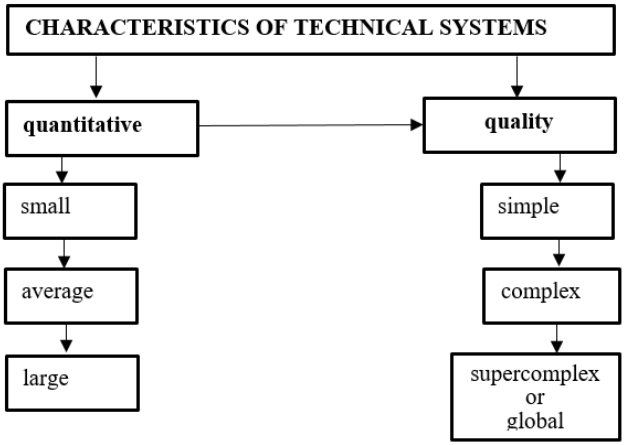

Fig. 1. Technical systems' characteristics

There is a close relationship between quantitative and qualitative characteristics.

Quantitative characteristics are more related to the geometric systems dimensions and number of homogeneous structure elements included. They can be divided into:

- small $a \cdot 10^0$ of maximum indivisible smallest sizes elements;
- average $a \cdot 10^1$;
- large $a \cdot 10^2$,

where a - is a maximum indivisible smallest sizes element of structure.

Qualitative characteristics are more related to the system structure in general, its levels number and complex mostly nonlinear relationships between them.

Systems can be divided into simple, complex and supercomplex (or global) depending on the complexity technical.

Simple systems are one level systems with a minimum number of components and connections between them, when their initial parameters are known. The study and description of such systems does not cause difficulties due to the small number of variables, and the possible states of these systems consequently.

Complex systems consist of several levels, they are distinguished by an increased number of components and connections between them, possible incompleteness of the initial information. The study and description of such systems causes certain difficulties due to the large number of variables. Additional external influences also appear and this leads to increasing the number of these systems possible states.

Supercomplex or global systems are multilevel and multicomponent systems with a big number of connections and a complex heterogeneous structure. Such systems are usually multi-parameter. Initial information about them is often incomplete. Their study and description cause serious difficulties due to a wide variety of external influences and their probabilistic nature, and due to additionally arising internal factors, consequently, which leads to the increase of these systems' possible states number. They have well developed communications and are automatically equipped. As they

develop, their sensitivity to various external damaging influences increases.

Damaging impacts can be emergency and catastrophic and the difference between them depends on only these damages scale and consequences.

Catastrophic cases are phenomena which appear in multiparameter dynamic, nonlinearly developing systems (natural, technical, humanitarian), when under the influence of slowly accumulating quantitative changes in control parameters they suddenly lose stability and enter a different qualitative state. This state is characterized by a new information field. Control parameters of complex structures mean time-varying external influences (force influence, chemical, radiation, etc.) on system and its internal (physical) properties [5].

Failure (destruction) of one or several system's elements does not mean the stopping system functioning. Therefore, the "survivability" concept is now widely used [6-9]. That means the property of a structure to maintain its overall bearing capacity in case of local destructions.

N. Streletskyi was one of the first who mentioned the problem of survivability in construction [10]. In the future, the survivability concept was introduced by V. Bolotin [11] and G. Geniiev [12]. At present, building structures survivability problems are considered in the works of A. Perelmuter [7,8], V. Kuliabko[13], Yu.Kudyshyn, D. Drobot [9,14] etc. The "survivability" concept was established in the construction regulations of Ukraine in 2009 (DBN B.1.2-14: 2009).

Generally, the survivability (stability) of load-bearing structures is their ability to keep the operation capacity for a given time in the presence of developing defects and various damages. Survivability sources are the following: physical and mechanical properties of materials, their destruction resist ability; strength reserves, which determine the stress-strain state and the degradation intensity; structural redundancy and element redundancy.

"Progressive" (or "avalanche-like") destruction is meant a fairly rapid "consistent destruction of bearing structures and bases, which leads to the collapse of the entire structure or its parts" [15,16].

There are design, maximum design and beyond design loads.

Design loads are impacts which are established by the current technical regulations.

Maximum design loads are impacts for which initial events and final states are defined, safety systems are provided. These loads consequences can be as much as possible, but within the limits established by the project.

Beyond project loads are the impacts caused by unaccounted initial events, erroneous staff decisions. These loads cause additional failures of system elements.

In construction design regulations and standards for checking metal structures strength the elasticity condition for nominal stresses is used (condition of no achieving plastic deformations according to Mises or Saint-Venan) as well as the strength criterion which limits the absolute values of main stresses by the yield strength limit. The influence of defects and stress concentrators on the strength and durability of structures is not considered. The bearing capacity reduction due to the development of macro-cracks caused by defects is not taken into account. It means that the concept of "no damages operation" is implicitly included in the technical regulations and according to it there should not be cracks in the design sections during the total service life of the structure, including fatigue cracks [17, 18]. But the requirement of total zero defectiveness of metal and welded joints of building metal structures is not provided by modern non-destructive testing techniques. Such structures are operated with the presence of cracks, due to inaccurate calculated determination of the fatigue cracks and fragile cracks appearance moment as well. Moreover, there are defects and cracks of limiting dimensions which do not reduce the strength of metal structures elements [19]. The construction regulations' calculation methods make it difficult to determine the durability, structural safety and survivability of metal structures, because they do not take into account clearly the time factor as the main parameter in the calculations according to the limit states [20].

2.The concept of reliability and durability of multi-element bar structures. Scale effect

The fundamental aspects of materials destruction over the past decades have been sufficiently investigated for simple idealized force

schemes [11], but the process of real structures destruction is more complex and requires the study of the stress-strain state under specific operating conditions, taking into account all the destruction mechanisms factors. Thus, there is a need to evaluate mechanisms, structures, technological processes and other technical systems based on their operation stability and reliability.

The answer has been found in the mathematical concept of reliability, in which reliability is considered as the probability of a trouble-free operation of a technical object.

Object reliability is a property of this object to perform its functions in a given mode for a given period of time with a given probability. A quantitative reliability assessment is the object probability to realize its functions - "*P*".

The reliability concept is inextricably related with the durability concept. Durability is the property to maintain performance for a certain time *T*. The difference between reliability and durability is in the following: in the first case probability *P* is determined, time *T* is a parameter, and in the second case the time *T* is determined at a given probability *R*.

The failure concept is associated with the concept of reliability and durability. Failure is a random event corresponds to the object operation capacity trouble. The failure probability is determined by the value

$$q=1-P.$$

There are many classifications of failure types. The most interesting and important classification for building structures has two categories:

- sudden failure;
- gradual failure.

Sudden failure is a failure (in fact, local or global stability loss), characterized by an abrupt changing values of one or more object's parameters.

Gradual failure is a failure resulting from values gradual change of one or more object's parameters. Gradual failure can finally cause the sudden failure, for example, structure failure as a result of the fatigue damages accumulation.

It should be taken into account that on the set of reliability failure conditions of structure, the durability states can be defined and its further sufficient operation efficiency is possible at these states (Fig. 2).

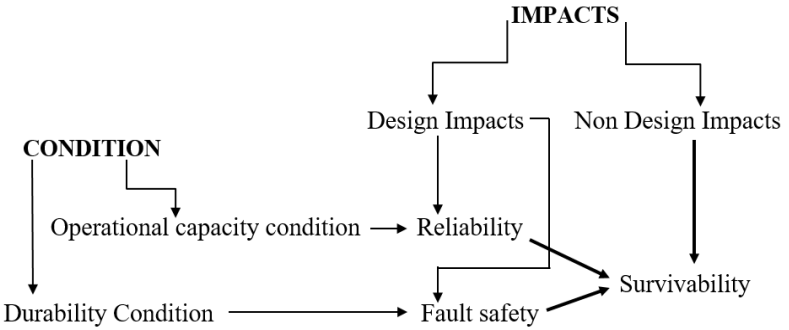

Fig. 2. Differentiation of the reliability and survivability properties depending on the system state

Fail safety is an indicator of the survivability property at normal operation. Durability, including the fail-safety concept is the system survivability in before critical operation area under the external nonregulated influences [14,21].

All technical objects are complex systems consisting of many elements. There are systems with a series elements connection, parallel elements connection and mixed elements connection.

A system with a series elements connection is a system when different elements failures are independent of each other, and the failure of one element at least leads to the failure of the entire system. The reliability of such a system is defined as the probability of failure-free operation of all its elements. If we have a system S, consistyв of n independent elements and the reliability of the i-th element is P_i, then according to the probability theory the reliability of the entire system is determined using the formula

$$P_s = P_1 \cdot P_2 \cdots P_n$$

It should be noted that the system reliability in the case of a series elements connection is less than the reliability of any individual element.

A parallel elements connection system is a system whose elements duplicate each other, and the failure of one of them does not cause the failure of the entire system. For example, let us consider a rope made of parallel wires. In this case the system remains operation capacity as long as at least one element is functioning, that means one wire at least.

The reliability of the system S, consisting of n parallel elements with the reliability P_i, where i is the element number, is determined as follows.The system S reliability, which consists of n parallel elements with a reliability P_i, where i - is the element number, is determined in the following way.

Probability of the i-th element failure

$$q_i=1-P_i$$

Probability of all elements simultaneous failure

$$q_s = q_1 \cdot q_2 \cdots q_n$$

Therefore, the system reliability is

$$P_s = 1-q_s = 1-q_1 \cdot q_2 \cdots q_n$$

can be seen from this formula that at parallel elements connection the system reliability is higher than the reliability of any of the individual elements.

In fact, as a rule, if one of the parallel elements fails, the reliability of the system's remaining elements decreases. In addition, building structures are multi-element systems with a mixed elements connection, that must be taken into account at reliability calculation.

It should be noted that as technical systems develop a scale effect assessment becomes more and more important. This is another dangerous and unpredictable factor leading to the destruction of multi-element structures.

The scale effect phenomenology is the following: any materials strength decreases when the sizes of these materials products or samples increase.

In 1938 based on statistical data Weibull suggested, that the causes of the scale effect are critical size internal defects, which become more probable in big size samples.

Regarding the technical systems, the following types of scale effect can be distinguished: volumetric type, areal type and linear type.

Volumetric scale effect is more characteristic for the geomechanical systems. Concerning this direction there are numerous studies by M. Protodiakonov, M. Koifman, S. Chyrkov, O. Shashenko [22] and other scientists. Analyzing the results of his own experiments and others known in the literature, M.Koifman proposed to distinguish the following scale effects at determinating the rocks strength:

- first kind scale effect or volumetric scale effect, associated with the structural heterogeneity of the tested material and the presence of defects randomly distributed over the volume;
- second kind scale effect or surface scale effect, associated with the quality of the samples processing and a surface layer destruction degree.

At transfering from a sample to an array the volumetric scale effect is the main, according to M. Koifman.

The areal scale effect associated with the samples transverse dimensions is characterized for the mechanical engineering and metallurgy, aircraft engineering and shipbuilding [23]. Extensive studies on the relationship between the metals strength characteristics and the sizes of tested samples are contained in the work of B. Chechulin [24]. S. Serensen and V. Kogaiev using the "weakest link" theory and the Weibull distribution function described the scale effect taking into account the nonuniform stresses distribution in the body intersection [25].

Regarding the action of variable loads, it was found that the fatigue limit decrease of samples and details at their dimensions increase has two aspects: metallurgical and mechanical. In the first case the large-scale effect is caused by the relatively high degree of material structure imperfection in large castings or forgings used for the manufacturing large-sized details. In the second case the scale effect appears at strength decrease of geometrically similar samples with their absolute dimensions increase and when these samples are cut from the same body [26].

In modern construction many structures consist of bar elements which have length which is much greater than the transverse dimensions, therefore, a linear scale effect is characteristic for bar structures especially. The linear scale effect is the least studied, although it can be observed in rod structures: bridges, overpasses,

mine headframes, masts, trusses, cable-stayed rod and mixed systems, large-span structures of stadiums. There are a number of works where it is indirectly present [27,28,29], however, these studies are clearly insufficient.

The problem of survivability and linear scale effect is especially urgent for multi-element steel structures. Steel is a good structural material; moreover, a great experience in designing and operating metal structures has been accumulated in engineering practice. But despite the development of the analytical apparatus, computer technologies and modeling methods, scientists and engineers face with the problems of designing, creating and operating complex large-sized and multi-element rod systems. Metal structures (in contrast to reinforced concrete and stone structures) have a relatively small reserve in the redistribution of efforts. For example, local damage (failure of one of the elements or one connection) sometimes can be the reason for the bearing capacity loss of the entire structure, and if the element is basic and bearing, then the entire object can be even destroyed [30].

3. Reasons for the operational operation capacity loss

Recently there has been a tendency towards the structural complication of buildings and structures in the construction industry. This is expressed in an increase of spans lengths, the height marks dimensions, structural elements number, in the use of new materials etc.

The accumulation of damage, appearance and development of defects reduces the structures bearing capacity, therefore, for large-size and multi-element systems the probability of bearing capacity loss and a service life reduction increase.

Rod metal structures take a special place among building structures. They are widely used in various industries (overpasses, mine headframes, galleries, towers, masts, bridges). These structures are affected by quasi-static, cyclic, dynamic and random loads. They are operated in corrosive environments and are affected by temperature differences [31, 32]. As mentioned above, the building regulations used in the design of buildings and structures do not give the calculation of structures with developing defects and do not allow to predict the behavior of an object in emergency situations, which can be caused by many technogenic and natural factors in a highly industrialized region.

Analysis of the catastrophic failure cases of large-sized metal structures at stresses significantly below the yield limit shows that calculation methods based on the continuum mechanics classical approaches are often insufficient [33].

In metal structures there are always defects of various origins: metallurgical, technological, operational defects, which, lead to the appearance of cracks and fragile destruction of the structure under certain conditions, [11,19,34]. The speed of initiation and propagation of cracks is determined by the features of the structure, structural parameters, loads nature, aggressiveness and temperature of the operating environment. Elements of systems in the supercritical area of operation consistently fail, redistributing the load to other elements, and thus generate negative influences internal to the system itself [35]. External and internal influences lead to further failure of the elements, and the system goes into an emergency state. How quickly the emergency state of the system occurs will also depend on the degree of its static indeterminacy.

Failure (destruction) of one or several elements of the system does not mean the termination of its functioning. Studying the structure behavior in case of failure of its constituent parts and identifying additional reserves, for example, due to alternative (spare) ways of redistributing external influences, is an important practical task.

Structural damages according to the nature of the impact on the bearing capacity can be divided into changing:

- geometric characteristics of intersections;
- nature of the stress-strain state of structural elements;
- a constructive scheme due to a connectivity disturbance between the elements.

Assembling defects or manufacture defects, corrosion, the use of metal with characteristics below design values, design mistakes, incomplete accounting possible loads and an insufficient system of structural connections can lead to the destruction of rod metal structures. Data processing on emergency destruction of metal structures is presented in Table 1.

Table 1

Operating conditions influence,%	60
Human factor influence,% .	19
Destruction of individual structural elements,%	10
Sudden impacts,%	8
The reason is undefined,% .	3

Regarding to metal structures, corrosion is one of the most significant factors causing destructions. Unlike the classical tasks, many constants characterizing the element properties in a neutral environment are functions if the element is operated in an aggressive environment. Moreover, the degree of their change is not the same for different points of the structure. Thus, an aggressive environment impact leads to the appearance of an induced (time-varying) inhomogeneity of geometric and, in some cases, structure mechanical [36, 37].

The safety problem solution of any design structure comes down to ensuring its main properties: reliability and durability. Conventionally, structure operation period before its destruction can be represented by three phases (Fig. 3):

the first - corresponds to the normal operation mode of the structure, it is the longest in time (0-t_1);

the second - corresponds to the limited operation capacity of the structure with accumulated defects, damages, failures of some elements, that is "survivability" (t_1-t_2);

the third - corresponds to the complete destruction of the structure, which occurs suddenly in a short period of time (t_2-t_3).

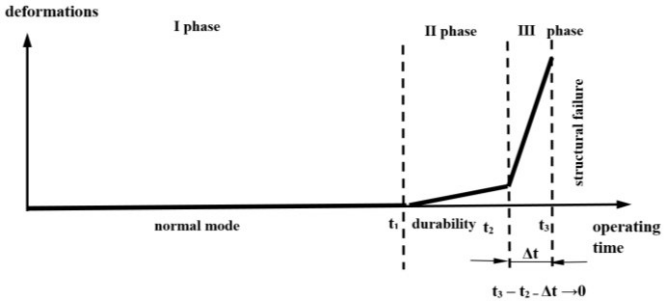

Fig. 3. The period of a structure operation

Often the assessment of the technical condition of long-term operating metal structures does not contain the main quantitative characteristic (the reliability of the structure). This is caused by the fact that, as a rule, in practice, there are no reliable and complete statistical data on the input and output parameters of the structure. Such limited information creates certain difficulties for forecasting the structure trouble-free operation. At the operational reliability assessment of a structure it is necessary to take into account the actual duration (section 0-t_2 in Fig. 3) of its operation, that means to identify the reserve (section t_1-t_2 in Fig. 3) of its bearing capacity [5,37].

4. Survivability (stability) of damaged structures

Within the framework of the developing theory of technical systems safety, the process of forming a system of quantitative indicators of survivability and safety is currently in process. The survivability quantitative characteristics of are the closest to engineering practice and can be most quickly introduced into design calculations. This requires clear qualitative definitions and quantification algorithms. In this regard, a number of survivability characteristics and methods for their assessment are proposed.

Let us consider the survivability indicators for the following structure operation mode outside the nominal operating conditions:

1 - emergency initiation mode. This is a short-term duration mode, when the design parameters of the structure go beyond the permissible values.

2 - emergency development mode. This is a free operation mode, when the structure degrades until it completely loses its strength, bearing capacity, and structural integrity.

The most common survivability indicators for these two modes belong to one of the following groups:

1 - system safety reserve;

2 - compensation characteristics;

3 - degradation intensity characteristics.

We will consider that a structure has a systemic safety reserve in the case when because of structural redundancy and increased classical safety reserves of individual elements the structure turns out to be weakly sensitive to the occurrence of local damages and destruction. In this case the damage occurrence and the loss of the

individual elements' bearing capacity leads to a such redistribution of internal force factors that classical safety reserves in all the remaining structural elements are within acceptable limits and as a result the emergency situation does not arise. A quantitative assessment of the system safety reserve can be performed using finite element technologies in one of the following positions:

1 - the structural material depending on its properties and environmental factors can be destroyed mainly according to a fragile or viscous scenario;

2 - a structural material is considered as a continuous or stochastically defective medium.

Under the assumption of a predominantly fragile state of the material the task of assessing the system safety reserve is reduced to modeling the destruction of individual load-bearing elements of the system, which is ensured by removing them from the model. In this case, a search is performed for the most loaded element with the smallest reserve relative to the ultimate strength, which can be considered a system reserve.

Considering the predominantly viscous state of the material, a series of computational experiments is performed decreasing in the stiffness characteristics of the material in the forecasted destroyed structural elements. Then, force characteristics (reserve ratios related to the yield limit in overloaded elements) or geometric characteristics (the ratio between the area or volume of the entire structure to the area or volume of elements in a state of plastic flow) can be considered as a systeme strength reserve.

Taking into account a randomly distributed defectiveness is performed in the following way. If a priori information on the probabilistic characteristics of defectiveness is absent, a crack-like defect (the maximum permissible according to the current of **crack detection** standards) is introduced into the most loaded zones of the structure. If probability distribution of defectiveness parameters is known, randomly distributed defectiveness is generated in accordance with this distribution. In this case the systemic strength reserve is determined taking into account the stresses concentration in the defects area.

The compensatory survivability characteristics are proposed to understand as structure properties to resist the transfer from the

initiation mode to the emergency development mode. In fact, they characterize the complex stability of the tress-strain state parameters. Their deviations appear in the conditions of the emergency initiation. Compensation characteristics are functions of the structure system properties. Compensation characteristics are provided by the flexibility of the structure and its elements, by redundancy, limits conditions.

The compensation characteristics can be characterized quantitatively in the following way. Firstly, temporary compensation characteristics are considered as period of time when adaptive effects appear in the structure and stress state parameters are stabilized. Secondly, force compensation characteristic can be determined as parameters of the wave processes of the spreading deformations and stresses in case of structure damage and compensation effects occurrence. Thirdly, energy compensation characteristics can be considered also. They are estimated as positive if the level of accumulated elastic energy decreases during the damage compensation, and as negative otherwise.

The degradation intensity characteristics as survivability indicators can be characterized as follows. In the emergency development mode the survivability indicators characterize both the bearing capacity fall speed and its time derivative, that means the conditions for the acceleration or deceleration of the ongoing degradation processes. In this case quantitative estimates are: crack growth speed and corrosion damage speed, changes of these speeds, the total length of the growing cracks system, indirect characteristics of the degradation processes intensity (acoustic emission intensity, local temperature increases in damage zones, etc.).

As for the special survivability indicators, they must be differentiated according to the types of structural forms and operating conditions.

The following types of structural forms are considered:

- rod three-dimensional structures;
- frame structures;
- three-dimensional plate structures;
- shell structures, including reinforced and multilayer ones;
- volumetric details and structures.

Design survivability calculations are closely related to a design case concept. The design cases choice plays a special role in the designing large three-dimensional structures. It is related to the fact that not taking into account different combinations of support conditions and loads can have catastrophic consequences, expressed in the sequential destruction of the total system. Thus, it is advisable to expand the design case concept. And in this case it is assumed to include in the design case not only the so-called emergency combinations of loads, but also to consider the destruction of one bearing element (one by one) as a probable situation. It makes it possible to analyze possible emergency scenarios at design calculation stage and exclude the "domino effect", which means uncontrolled catastrophic development destruction of the entire system.

Determining the parameters and ensuring the survivability (stability) of load-bearing structures require an complex formulation and research on various aspects of the design, construction, production, installation and operation of technical systems. Currently survivability field research is carried out in the following directions.

1. Substantiation and formulation of basic concepts, principles, qualitative and quantitative indicators of survivability and related categories regarding parts and elements of structures, joints, bearing structures and technical systems in general.

2. Analysis and change of load-bearing structures design calculations, development of computational algorithms for survivability indicators calculation, regulation of calculations and development of regulations documents drafts.

3. Studying survivability of typical structural forms of load-bearing structures, the development of increased survivability structural forms and developing the theory of such structural forms construction.

4. The comprehensive modeling of emergency situations of technical systems structures, including both the study of external causes and conditions of accidents and catastrophes and study of the internal force processes, deformation, energy, wave processes of structures.

5. Research of technological and operational defectiveness of technical systems, including probabilistic modeling of technological defectiveness processes, identification of random nature physical

regularities of scattering sizes and defects location, statistical analysis of non-destructive testing data.

6. Modeling the stress state in local zones of technological and operational defectiveness, including the development of computational technologies for modeling the damaged zones stress state and the creation of probabilistic stress state models in local zones of defectiveness.

7. Development of structural and force methods complex for survivability ensure, which implies the formulation of bearing structures shaping algorithms according to requirements of survivability, optimal structural elements design according to survivability criteria, resource management and survivability management models in the presence of local damage.

8. Development and design of a complex of technical devices, instruments, equipment which increase the operation safety of technical systems and their survivability in emergency situations.

5. Failure protecting methods of multi-element metal structures.

5.1. Reliability improvement techniques

All methods of increasing and maintaining reliability are divided into three large groups: design methods, manufacture methods and operation methods.

Design reliability improvement methods:

- reservation;
- system simplification;
- the most reliable elements selection;
- creation of schemes with limited consequences of element failures;
- facilitation of electrical, mechanical, thermal and other modes of elements operation;
- standardization and unification of elements and joints;
- built-in control;
- checking procedure automation.

The effectiveness of these methods lies in the fact that they allow to build reliable systems from unreliable elements. These methods can reduce the system failure rate, reduce the average recovery time and system constant work.

Manufacture reliability maintenance methods.

At manufacturing elements reliability can be increased by improving the production technology, by automating production processes, using statistical product quality control, training elements and systems. All these methods make it possible to reduce the failure rate of system elements.

Operation reliability maintenance methods

It is extremely difficult to improve the reliability of the system during its operation. It happens because the system reliability is created mainly at its design step, is ensured during manufacture, and it is only consumed during operation. Its consumption speed depends primarily on the operation methods and conditions.

The task of ensuring the safe structures operation is both to increase the system reliability and to save this reliability for as long as possible in the process of its design and manufacture.

Scientific operation methods include scientifically based methods of carrying out preventive measures and repairs: frequency and depth of checks, time regulation of the continuous system operation etc.

It should be noted, however, that reliability is not only consumed during the operation. At correct operation it is also possible to increase the reliability of systems. Indeed, if preventive measures prevent failures, then this is analogous to reducing the system failures rate. The only difference is that at this stage the reliability of the elements does not actually increase, as it can be realized in design and manufacture, but timely renovation or repair of elements realize. These elements are not yet failed, but their failure probability has greatly increased.

Operation has a very strong influence on the design and manufacture of a newly developed system. It happens because data regarding failures of elements and systems obtained during its operation fully characterize its reliability and therefore are often used as the initial data for the designing highly reliable systems.

Collection, scientific processing and generalization of statistical data concerning the systems elements failures is one of the important functions of technical operation.

5.2. Comparison of different methods of reliability improvement

The effectiveness of a particular method can be assessed by comparing the quantitative characteristics of the reliability of

systems which are identical in design and principle of operation, but different in methods of increasing reliability.

It is convenient to take the reliability gain as an efficiency criterion for all or most of the quantitative reliability indicators. Evaluation based on the most important indicators is necessary because the effectiveness of a method significantly depends on the criterion that is chosen to assess the reliability. Analysis results are often contradictory. For example, if reliability is estimated by the average time of zero failures work, then the most effective way is reducing system failures rate. But if we estimate the probability of zero failures work, the best option will be to choose the redundancy. At assessing the system reliability by the availability ratio, it may happen that the best way is to reduce the average recovery time.

It is possible to rationally choose one or another method of reliability increase only when the system operating conditions and the methods effectiveness are known.

Conclusions

The analysis of publications shows that currently a sufficiently coordinated interpretation of the construction objects properties which characterize their operational capability has not yet been achieved.

Some scientists base on the analysis of the sources of operational capability fails, others analyze their consequences. It is explained by fact that the theory of the systems survivability of is at the stage of formation and formalization into an independent scientific discipline.

It is necessary to distinguish between general survivability indicators, which are universal for all types of bearing structures, and specific ones, which differ from each other for various types of structural forms. These characteristics follow from the consideration the structure as a unit, as a system of interacting elements. Thus, in this case the structure of the system is one of the most important factors in its survivability formation, which is not limited by a set of individual elements' characteristics.

Operating experience should always be used in the design and manufacture of reliable systems, and the results of design and manufacture should always be used to improve operating methods.

Reliability improvement methods allow to design the highly reliable systems. The choice of method is determined by the properties of the designed system. Very often it is not possible to design a highly reliable system using only one method of increasing reliability. It is needed to use all the methods or most of the methods discussed.

The above methods of reliability increase are not required for any system. Some methods can be used to improve the reliability of one class system, other methods for another. It all depends on the system type and its operation conditions.

References

1. Steel constructions (2014). DBN.2.6-198: 2014. Kyiv/ Ukraine: Derzhstandart Ukrainy.

2. System for ensuring the reliability and safety of construction sites. General principles of ensuring the reliability and structural safety of buildings and structures (2018). DBN B.1.2-14: 2018. Kyiv/Ukraine: Derzhstandart Ukrainy.

3. **Mkrtychev O. V.** (2000). Reliability of multi-element rod systems of engineering structures. - Dis. Dr. tech. sciences. (Doctor`s thesis). Moscow/Russia,.2000, 343 p.

4. **Vostrov V.K**. (2009). Strength, crack resistance and constructive safety of building metal structures based on the development of linear fracture mechanics. (Extended abstract Doctor`s thesis). TsNIIPSK them Melnikov. Moscow/Russia, 2009 .50 p.

5. **Ivanova A.P.** (2013). Vitality and destruction of multi-element structures, Technological disasters, models, forecast, prognosis (Proceeding of the 3rd International Science and Technology Conference). Dnipropetrovsk/Ukraine: NGU 22-24 May 2013, P. 64-73.

6. **Tur V.V**.. Design strategies for the protection of structural systems from progressive collapse within the framework of the requirements of international regulatory documents. Modern metal and wooden structures (regulation, design and construction). (Sat. scientific. proceedings of International symposium). Brest/ Belarusian: 2009. P. 302 - 314.

7. **Perelmuter A.V.** (2007). Selected problems of reliability and safety of building structures. Moscow/Russia: ASV, 2007, 256 p.

8. **Perelmuter A.V.** (1995). On the assessment of the survivability of supporting structures: Metal structures. The works of school of Professor N.S. Streletsky, Moscow/Russia: MGSU, 1995. P. 62 - 68.

9. **Kudishin Yu. I.** (2009) The survivability of building structures is an important factor in reducing losses during accidents. Metal structures, 1, Yu. I. Kudishin D. Yu. Drobot,. Makeevka/Ukraine: DonNACA, 2009, P. 61 - 72.

10. **Streletsky N.S.** (1947). .Analysis of the process of destruction of the elastoplastic system [proceedings No. 5]. Moscow/Russia: MISI,1947.

11. **Bolotin V.V.** (1981). Methods of the theory of probability and the theory of reliability in the calculations of structures. Moscow/Russia: Stroyizdat, 2nd ed., rev. and add. P.351.

12. **Geniev G.A.** (1992). On the assessment of dynamic effects in rod systems from brittle materials / G.A. Geniev. Concrete and reinforced concrete. No. 9. Moscow/Russia:1992 - P. 25 - 27.

13. **Kulyabko V.V.** (2009). Modeling of dynamic processes of progressive destruction of structures. Features of design and calculation of spatial structures for strength, stability and progressive collapse. Abstracts of Papers. Moscow/Russia: 2009. P.50 - 51.

14. **Kudishin Yu.I., Drobot D.Yu**. (2008). The survivability of structures in emergency situations. Metal buildings. 2008. - No. 4 (8). P. 20 - 22.

15. **Bogdanova E.N.** (1991). Analysis of the causes of the collapse of buildings and structures. Moscow/Russia: VNIINSHI, 1991. P - 72.

16. **Kushchenko V.N**. (2009). Basic principles of ensuring the safety of building structures. Metal structures. Makeevka/Ukraine: DonNACA, 2009. № 2. P. 147 - 155.

17. **Zlochevsky A.B.** (1971). On the issue of establishing design criteria for brittle fracture as the third limiting state of structural elements : Development of calculation methods for limiting states. Moscow/Russia: Publishing letter. on building.,1971. P. 140-147.

18. **Kaminsky A.A.** (1982). Brittle fracture near holes. Kiev/Ukraine: Naukova Dumka, 1982. P -158.

19. **Vostrov V.K.** (2007). Brittle fracture of metal structures with an internal crack under complex loading. Promyshlennoe i grazhdanskoe stroitel'stvo, №4, 2007. P.32-35.

20. **Tetelman A., Bezuner P.** (1980). Application of risk analysis to the study of brittle fracture and fatigue of steel structures. Destruction of structures. Moscow/Russia: Mir, 1980. P. 7-30.

21. **Nikitin A.I.** (1987). Fault tolerance of distributed systems. Control systems and machines., No. 5. 1987. P. 25 - 30.

22. **Shashenko A.N,, Sdvizhkova E.A. & Gapeev S.N.** (2008). Deformability and strength of rock massifs. Monograph. Dnipropetrovsk/Ukraine : NGU, 2008.P. 224.

23. **Zabirov T.A.** (1994). Survivability of a surface ship. Moscow/Russia: Military Publishing, 1994. P - 360.

24. **Chechulin B.B.** (1963). The scale factor and the statistical nature of the strength of metals. Moscow/Russia: Metallurgizdat, 1963. P - 120.

25. **Serensen S.V., Kogaev V.P. & Shneiderovich R.M.** (1975). Carrying capacity and strength calculations of machine parts. Manual and reference manual. Moscow/Russia: Mashinostroenie, 1975. P - 488.

26. **Uzhik G.V.** (1948). Methods of endurance testing of metals and machine parts. Moscow/Russia.: Ed. Academy of Sciences of the USSR, 1948. P - 264.

27**. Kezin A.S.** (2003). Numerical modeling in problems of reliability and stability of rod systems under influences in the form of random processes. Extended abstract of candidate's thesis. Moscow/Russia, 2003. 212 p.

28. **Oding I.A.** (1959). Theory of dislocation in metals and its application. Moscow/Russia: Publishing house of the Academy of Sciences of the USSR, 1959. P - 84.

29. **Strunin B.M. (**1960). Theory of the scale effect in tension, Zavodskaya laboratory.1960. No. 9. P. 1123 - 1128.

30. **Doronin S.V., Lepikhin A.M., Moskvichev V.V., & Shokin Yu.I.** (2005). Modeling of strength and destruction of bearing structures of technical systems. – Novosibirsk/Russia: Nauka, 2005. P.- 250.

31. **Ivanova A.P.** (2013). Investigation of the durability of centrally compressed rods with varying geometric characteristics. Dnepropetrovsk/Ukraine: Naukoviy visnik. NGU № 3. 2013. P. 87 - 93.

32. **Ivanova A. Feskova L.** (2015). The temporary criterion account in the metal beam-rod structure design. New develop-ments in mining engineering 2015: Theoretical and practical solutions of mineral resources mining. Netherlands: CRC Press/Balkema. 2015. P. 411-414.

33. **Augusti Ya., Shledzevsky E.** (1978). Steel structures accidents. Moscow/Russia: Stroyizdat, 1978. P 180.

34. **Polipov A.N.** (1984). Explanation of the scale effect on the basis of the energy criterion of destruction. Mechanics of a rigid body, 1984. №1. P.106 - 110.

35. **Aleksandrov A. V.** (2001). The role of individual elements of the rod system at loss of stability. Moscow/Russia: Vestnik. MIIT (5). 2001. P. 46 - 50.

36. **Zelentsov, D., & Ivanova, A**. (2015). Application of neuronetwork models for solvingtasks of durability prediction of corrodible beam constructions. Naukovyi Visnyk Natsionalnoho Hirnychoho Universytetu, (4), 51-56.

37. **Ivanova A.P., Feskova L.V., Trufanova O.I.** (2015). Increasing the efficiency of solving the problems of stress-strain state and durability of corrosive block elements of metal structures. Book of Science Works "Bulletin of the Kryvyi Rih National University" Kryvyi Rih/Ukraine. 2015. P. 86-90.

https://doi.org/10.31713/m1026

MOBILE AUTONOMOUS DUST-REMOVAL INSTALLATION

Victor Shapovalov [a]*

[a]*Department of Labor Protection and Civil Safety, Kryvyi Rih National University, Kryvyi Rih, Ukraine*

*Corresponding author Victor Shapovalov, email: vash231@meta.ua

The aim of this work is to solve the actual problem of dust removal in industrial shops of processing enterprises. Technological processes for the bulk materials processing are accompanied by intense dust emission, as a result of which the air dustiness at workplaces considerably exceeds the maximum permissible values. Known methods of dust suppression do not fully localize numerous sources of dust emission. The released dust spreads over the entire volume of the production area and is deposited on various surfaces and forms the layers of different thickness. Under the influence of various factors, the settled dust can again become aerosol, which in turn, increases the air dustiness in the workplace, which may contribute to the emergence of occupational diseases among workers in processing plants. To prevent secondary dust emission and cleaning of various surfaces from the settled dust, the mobile autonomous dust-removal installation, which can autonomously move to the necessary cleaning object within the limits of the given enterprise, has been developed.

Keywords: dust emission, dust removal, dust removal installation, pipeline system

Introduction

Most industrial enterprises, which use bulk materials are forced to solve the problem associated with the release of dust and its removal. Technological processes for the bulk materials processing (crushing, sorting, reloading, etc.) are accompanied by intense dust emission, as a result of which the air dustiness at workplaces considerably exceeds the maximum permissible values. The most promising ways of dust emissions prevention are the improvement of technological processes and the introduction of waste-free energy-saving technologies. However, for most enterprises, the introduction of such technologies is not always technologically possible or economically feasible. Known methods of dust suppression, such as aspiration, room ventilation, dust binding by moistening the processed material, sealing of the transfer points, etc., do not fully localize numerous sources of dust emission [1-3]. The released dust spreads over the entire volume of the production area and is deposited on various

surfaces (building structures, pipelines, cable lines, elements of equipment, etc.), and forms the layers of different thickness. Under the influence of various factors (the operation of the technological equipment, vibration created by equipment, the movement of the bridge cranes, the production of repair works, the presence of aeration streams, etc.), the settled dust can again become aerosol. This increases the air dustiness in the workplace, which may contribute to the emergence of occupational diseases among workers in processing plants.

At the same time, the dust accumulated on various surfaces complicates the maintenance and repair of technological equipment and communications, accelerates the wear of individual units and parts, reduces the time needed for overhaul maintenance, disables control and measuring equipment and weighing equipment. In a number of industries, the settled dust causes explosions or fires [4,5]. For many enterprises (woodworking, cement, for the production of dry building mixtures, sintering, foundry, etc.), the dust settled on various surfaces is considered as a valuable resource in solving problems of energy saving and energy efficiency, due to utilization and recycling [3,6,7].

Therefore, for most industrial enterprises, which use bulk materials, dust removal is an urgent problem, the solution of which allows to improve working conditions, reduce occupational diseases, reduce equipment wear, and reduce the amount of waste due to disposal of the collected material.

To prevent secondary dust emission and cleaning of various surfaces from the settled dust, pneumatic dust-collecting installations are used, which have found wide application in various industries. There are portable, mobile and stationary dust-collecting installations depending on the performance of the main equipment and the length of the pipelines.

Materials and methods

The bulk raw material processing technologies are characterized by an abundance of intensive dust extraction sources and significant areas of dust deposits, which are subjected to dust removal. The most effective way of dust removal for such conditions is the use of

centralized dust collectors (CDC) or industrial stationary vacuum systems [8].

In the works of most authors, there was a positive experience of using the CDC in industrial conditions [9-12]. Cleaning of industrial premises using the CDC provides productive cleaning of surfaces using several dust-removal nozzles simultaneously, a high degree of cleaning in dust-collecting devices and convenient unloading of the collected material, removal of dust deposits from various surfaces located at different heights. The CDC has a high sanitary and hygienic efficiency since all the dust is removed from the premises. The considerable length of the pipeline system of the CDC allows the use of such installations in premises with a large accumulation of process equipment. At the same time, the thrust booster and dust collection devices may be located outside the cleaned premises.

Operating experience of the CDC showed their prospects, therefore, they were developed in various industrial sectors. Thus, the CDC is used in the textile and printing industries, in the shops of crushed stone and engineering plants, railway transport enterprises and other industrial enterprises [8,10-12].

However, it should be noted that CDCs are mounted permanently and fitted for cleaning only one room. The stationary pipeline system, during long-term operation, is prone to clogging and requires cleaning or dismantling. Due to dust deposits in the pipelines, the amount of air pumped through the dust nozzles is significantly reduced, as a result of which the aerodynamic parameters and the overall performance of the vacuum system change.

Technological processes for the processing of bulk materials include the use of a large number of main and auxiliary equipment. The considerable length of pipelines of stationary vacuum systems is due to the significant areas for cleaning, as well as a significant amount of equipment located in these areas. Therefore, in the working conditions of processing plants, it is necessary to use several CDCs or several separately installed stationary pipeline systems. The significant length of pipelines may contribute to the disruption of the stable operation of the vacuum system and includes the selection of high-performance thrust boosters, which consume large amounts of electricity.

Along with stationary installed main equipment, the attempts to use the CDC with equipment mounted on a mobile base were made [7]. In this case, the pipeline system is mounted stationary, and the main equipment, which is mounted on the cart, moves through the shop and alternately connects to the risers. The main disadvantages of this modification are lack of the main equipment manoeuvrability, due to the large dimensions; returning the air cleaned in dust-collecting devices back to the room, which is not recommended in highly dusty premises.

Thus, the most significant disadvantage of all modifications of the CDC is a stationary mounted pipeline system of considerable length. It should also be noted that one installation serves one production facility. For large enterprises, it is necessary to use several installations of the same type, each of which will have a stationary installed pipeline system. This complicates the control of pipelines clogging and is associated with an increase in maintenance costs and service of an extended pipeline system within one enterprise.

The accumulation of dust on the surfaces of industrial buildings and equipment is not the same. The amount of dust and the intensity of its deposition on surfaces located in the upper part of the production area is significantly less than at the dust sources. Therefore, the frequency of pneumatic dust removal in each separately taken room will depend on the intensity of deposition and accumulation of dust on the elements of this object. This will allow enterprises to "keep clean" production facilities using a mobile autonomous dust-removal installation (MADRI), which after cleaning a single object, can move to the next object, etc.

Results

The design of the MADRI uses standard typical units of aspiration and dust collection systems. The scheme of MADRI is presented in Fig.1.

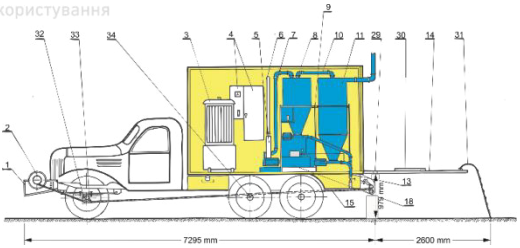

Fig.1*a*

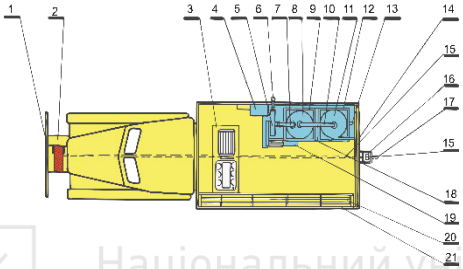

Fig. 1*b*

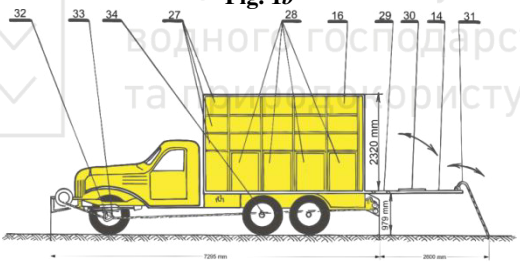

Fig. 1*c*

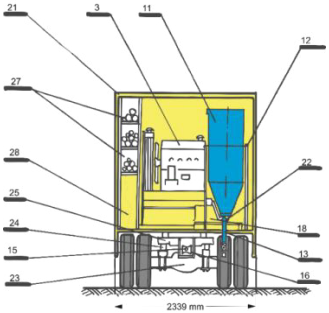

Fig. 1*d*

Fig. 1. Scheme of mobile autonomous dust removal installation

The main equipment of the MADRI is located in the back of a cargo van. Dust collecting devices are presented in the form of a two-stage cleaning system consisting of a cyclone 11 and a fabric filter 8. The cyclone and the filter are mounted on the support frames 12 and 9, respectively, and interconnected by a pipeline 10.

An air baghouse and a cyclone have discharge pressing installations 22 interconnected by a pipeline system with a lock-up valve 13. This allows the discharge of collected dust using a screw discharge device. A binder liquid (humidifier) is fed to the pressing devices from the tank 18, in order to prevent dust emission during the dust discharge.

The vacuum in the system is provided by the thrust booster 5, which pulls the dusty air through the dust collecting device and connected with it by a pipeline 7. Turning on and off the thrust booster is carried out using the control box 19. The purified air is released into the environment through pipe 6, which is brought out through the wall of the cargo body. The MADRI is supplied with electricity by means of a diesel generator 3, controlled by an electric switchboard 4.

In the cargo body, in addition to the main equipment, there are racks 27 for storing the required number of pipes of different diameters and fittings (pipe branches, tee-joints, etc.), as well as ladders and stepladders. Under the racks, there are boxes 28 for storing equipment and inventory (clamps, carabiners, ropes, nozzles, handles, etc.).

In the front part of the van, which protected by a buffer frame 1, there is a winch truck 2, on the drum of which a cable 15 is wound. The cable is laid under the bottom of the van through the front bypass roller 32, the intermediate bypass roller 34 and trough the rear bypass rollers 16. The front bypass roller is mounted on the front bridge girder of the van using a clamp 33 (Fig. 1*c*).

Assembling the pipeline vertical section, as well as the supply of fittings and elements of the pipeline horizontal section at a given height of the building, is carried out using a winch truck. The vertical section of the pipeline is located outside or inside the building (for example, a mounting aperture) and is also mounted as a horizontal section, but only for the period of premises cleaning.

The rear part of cargo body is covered with mounting plate 14. In working condition, the mounting plate is in a horizontal position, with the possibility of vertical movement and serves as a platform for conducting the installation works of the pipeline vertical section. The

opening 29 for passing the cable of the winch truck is located at the bottom of the shield. After work, the opening is closed by a cover 30. The mounting plate is also equipped with a folding ladder 31.

MADRI is serviced by three people, one of which is simultaneously a driver and MADRI operator, and two others are dust collectors. The MADRI operator controls the operation of the main equipment, and the dust collectors clean the premises, moreover, the cleaning of high-level surfaces and hard-to-reach places is carried out by two dust collectors. The first dust collector cleans up the high-level surfaces, and the second ensures the operator working on the stepladder, and also switches the flexible hose from one nozzle to another, supplies the necessary nozzles, etc.

Before starting the MADRI, it is necessary to perform installation work connected with the installation of vertical and horizontal sections of the pipeline. Since the dust removal installation is autonomous and mobile, this type of installation work will be carried out continuously when it is moved to a new place of cleaning. Before assembling the vertical section of the pipeline, the van is located near the building in the place where the pipeline system will be supplied into the premises at a given mark (Fig. 2).

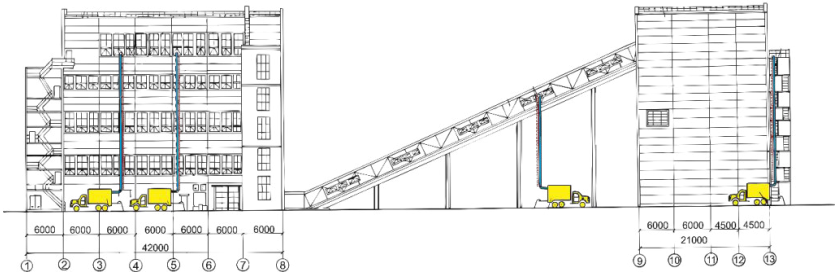

Fig.2. Location of MADRI in the process of the pipeline vertical section assembly

An important element of the equipment, which is required for installation work is a block clamp (Fig. 3).

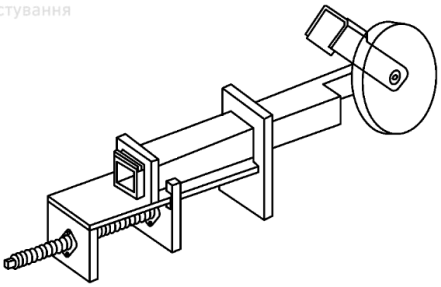

Fig. 3. Block clamp

The block clamp is used for mounting the vertical section of pipelines. One of the operators select a place for the pipeline vertical section, secures the clamp and passes the cable of the winch truck through the bypass roller. As a selected place for a clamp mounting, there can be mounting or window openings at a given elevation of a building, through which the piping system will be supplied into the premises (Fig. 2).

The rings are fixed over a certain distance on the winch truck cable. The pipe sections of the vertical section are mounted on these rings using carbines. The connection of two pieces of the pipe is made using a ring clamp (Fig. 4).

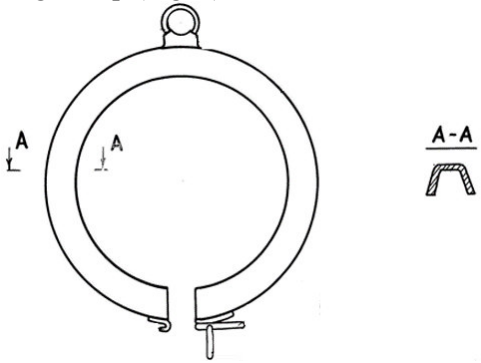

Fig. 4. Ring clamp

The ring on the clamp (Fig. 4) serves to hang the pipes on the winch truck cable, and then the pipeline is lifted to the required height, with gradually increasing of the pipeline length (height). In case of discrepancy between the rings fixed on the cable and on the

clamps, then the additional floating clamps are installed for hanging the pipes, the diameter of which is equal to the pipeline outer diameter. Two pieces of pipe are joint to each other by the ends, and then the clamp is put on and locked with a bracket (Fig. 5).

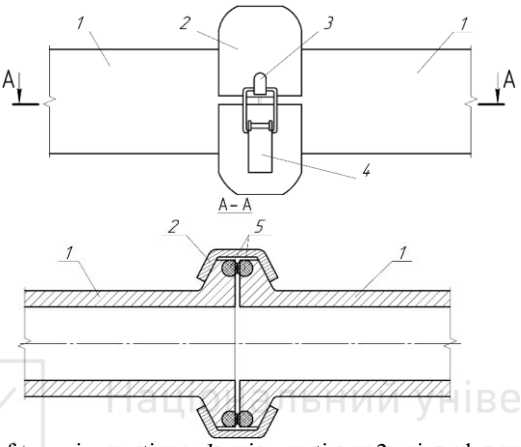

Fig. 5. Joint of two pipe sections: *1* - pipe sections; *2* - ring clamp; *3* - hook; *4* - locking bracket; *5* - rubber sealing rings

The cross-section of the ring clamp has the shape of a truncated trapezoid (Fig. 4), while the cross-section of the pipe ends when joining has the shape of rectangular truncated triangles, in which rubber sealing rings are inserted (Fig. 5). This solution of two pipe sections joining eliminates air inflow, provides tightness and rigidity of the mounted section, allows quick and efficient installation of the vertical and horizontal pipeline sections of the vacuum system.

The vertical section of the pipeline must be assembled in such a way, that a drain is located opposite each floor, which is closed by a plug. This allows moving from one level of the building to another during a shift.

After reaching the required height of the pipeline vertical section, it is joined to the cyclone from one end, and a pipe branch or tee-joint is installed on the other end to supply the pipeline into the room. After that, the horizontal branching of the main pipeline is mounted (Fig. 6).

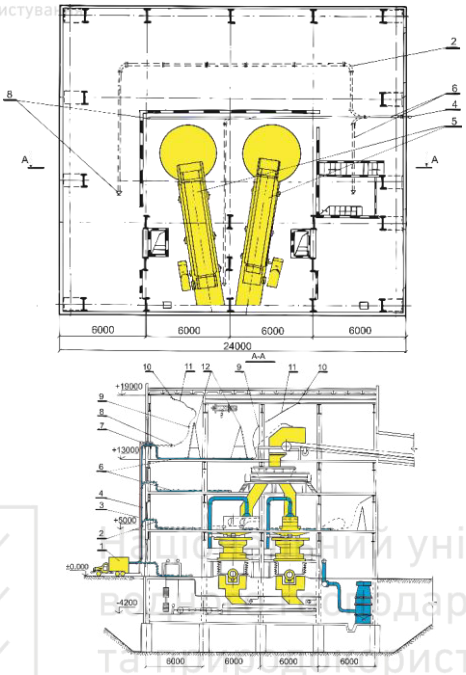

Fig. 6. Scheme of MADRI pipelines arrangement within the production premises: *1* - MADRI; *2* - pipeline elements (elbows, tee-joints, etc.); *3* - winch cable; *4* - vertical pipeline; *5* - loading conveyor; *6* - horizontal pipeline; *7* - block clamp; *8* - tapered adapter; *9* - flexible hose; *10* - nozzle; *11* - the handle; *12* - ladders

The use of quick-disconnect coupling of two pipe sections allows installation of horizontal sections not over the entire area, but only for cleaning a specific section, using for this purpose the minimum required number of pipe segments and fittings. This allows significantly reduce the length of the pipeline system.

The vertical branches in certain places on the pipeline horizontal section (if necessary) are located. Their length depends on the height of the room. The connection of the flexible hose to the fittings located at the end of the vertical branches makes it possible to clean the upper area of the production room from the building structures, bridge cranes, crane runways, etc. There are fittings for connecting a flexible hose at the length of the pipeline horizontal section (Fig. 7).

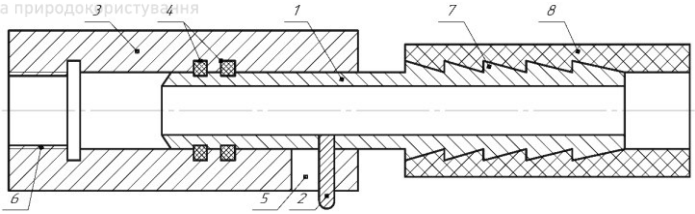

Fig. 7. Quick disconnect fitting for connecting a flexible hose: *1* - mouthpiece; *2* - pin; *3* - sleeve; *4* - rubber rings; *5* - locking slot; *8* - thread; *9* - ruff; *10* - flexible hose

The number of fittings is assumed such to allow all surfaces to be accessible when connecting a flexible hose.

Conclusions

The developed autonomous mobile dust-removal installation can autonomously move to the necessary cleaning object within the limits of the given enterprise, since the thrust booster and dust collecting devices are located in a mobile van, and the required remote system of pipelines with nozzles is mounted from separate units during the cleaning period. This reduces the overall length of the pipelines of the vacuum system and eliminates clogging of pipelines during long-term operation. The location of MADRI outside the object excludes the possibility of air recirculation in highly dusty premises. The absence of a stationary pipeline system, the ability to locate the installation at the most convenient points around the perimeter of an industrial facility, the speed of pipelines assembly and disassembly, the reuse of collected material and the high cleaning performance make it possible to solve the problem of dust collection with minimal costs. Thus, the use of mobile autonomous dust-removal installations at processing enterprises, together with the existing methods of dust suppression and dust collection, will allow “to keep clean” the production premises and to improve working conditions.

Funding

The research has no funding

Disclosure Statement

Authors have no competing financial, professional, or personal interests from other parties.

References

1. **Haponyuk O.Y., Honcharuk A.A., Lapyn A.P.** Problemy funktsyonyrovanyya aspyratsyonnykh ustanovok y puty ykh sovershenstvovanyya [Problems of functioning of aspiration facilities and ways of their improvement]. Naukovi pratsi Odes′koyi natsional′noyi akademiyi kharchovykh tekhnolohiy.2014;46(1):201-204.

2. **Golyshev A.M., Zadorozhniy S.I., Gerasimchuk A.V**. et al. Obespecheniye effektivnykh rabochikh rezhimov aspiratsionnykh sistem fabrik okomkovaniya GOKov v usloviyakh dlitel'noy ekspluatatsii [Ensuring effective working conditions of the aspiration systems of the GOKs pelletizing plants under conditions of long-term operation]. Razrabotka rudnykh mestorozhdeniy.2007; 91:232-236. Russian

3. **Sitnikov E.A.** Nauka sobirat. Investitsii v nashe budushcheye. [Science to collect. Investing in our future]. Berg-Collegium: Mass analytical research and production journal. 2005;6:28-29. Russian

4. **Sitnikov E.A.** Nauka sobirat [Science to collect] Part II. Berg-Collegium: Mass analytical research and production journal. 2004;4:12-13. Russian

5. **Ryazhin A.A.** Pylevoy resurs. Rezervy effektivnosti ugolnykh TETS [Dust resource. Efficiency reserves of coal-fired power plants]. Berg-Collegium: Mass analytical research and production journal. 2005;2:21. Russian

6. **Sitnikov E.A.** Vakuumnyye tekhnologii Wieland Lufttechnik: ekonomiya - ekologiya – effektivnost [Vacuum technologies Wieland Lufttechnik: savings - ecology – efficiency]. Proceedings of the BALTIMIX-2004. Available at http://www.baltimix.ru/confer_archive/reports/doclad04/index.php

7. **Kurnikov A.A., Kurnikov V.A.** Pnevmaticheskaya pyleuborka tsekhov mashinostroitel'nykh zavodov [Pneumatic dust cleaning of machine-building factories]. Moscow: Mechanical Engineering; 1983. Russian

8. Department of Health and Human Services. Handbook for Dust Control in Mining.Rev. Ed. Fred N. Kissell). National Institute for Occupational Safety and Health: Pittsburgh Research Laboratory; 2003. Available at https://www.osmre.gov/resources/blasting/docs/MineGasesDust/2003NIOSHDust.pdf

9. **Cecala A.B., O'Brien A.D., Schall J.,** et al. Dust control handbook for industrial minerals mining and processing. Pittsburgh, PA, Spokane, WA: Centers for disease control and prevention, National institute for occupational safety and health, office of mine safety and health research. 2012 (Report no. 9689). Available at https://www.spray.com/pdf/Dust_Control_Hanbook_RI9689.pdf

10. **Borrmann M.** Industrial vacuum systems for cement industry. Introduction and overview. Proceedings of AICCE22 – International Congress Center; 2017 Nov 15; Sharm el Sheikh: Wieland GmbH & Co; 2017

11. **Wen Nie, Wenle Wei, Peng Cai**, et al. Simulation experiments on the controllability of dust diffusion by means of multi-radial vortex airflow. Advanced Powder Technology. 2018;29(3):835-847, DOI: 10.1016/j.apt.2017.12.027.

12. **Wanxing Ren, Deming Wang, Qing Guo**, et al. Application of foam technology for dust control in underground coal mine. International Journal of Mining Science and Technology. 2014;24(1):13-16. DOI: 10.1016/j.ijmst.2013.12.003.

https://doi.org/10.31713/m1027

THE USE OF SLOPE HOISTING PLANTS TO CREATE THE CONDITIONS FOR CIRCULAR TRAFFIC OF DUMP TRUCKS

Slobodyanyuk V.K.
The National University of Kryvyi Rih, PhD (Engineering),
Associate Professor, the Department
of Open Pit Mining Operations, Ukraine

Slobodyanyuk R.V.
ROTATE, Co-Founder

Abstract

The purpose of this article is to develop and substantiate rational designs of slope hoisting systems for dump trucks in the open pit mines. In order to reduce the time losses associated with idle mileage in the transport cycle, it is proposed to use the slope hoisting plants only for hauling down the empty trucks. The basic arrangements of slope hoisting systems have been analyzed. A rational field of using them has been determined. The lack of experience in operation of slope hoisting systems with multi-rope friction winders, the possibility of reducing a friction ratio due to freezing and wetting the rope leave no chance to recognize this technical solution to be reliable. The article presents the results of the design study and determination of parameters of a hoister with a reeving system of suspension of one platform to haul down the 130-ton trucks. The developed hoisting plant consists of the main parts as follows: two 1-6×5.6/0.8 single-drum hoisters; a platform for transporting the truck; a headframe for placing the deflection sheaves; two deflection sheaves; two inclined rail tracks to move the platform. The article proposes the new technical solutions for hoisting plants with two platforms, which are alternately used for hauling down the empty trucks. The developed technology promotes improvement of the operational performance of dump trucks in the open pit mines.

Key words: slope hoisting plant, idle mileage of dump trucks, drum hoister, reeving system of vehicles, resource-saving technology

Introduction

The design depth of the Krivbas iron ore open pit mines reaches upwards of 500 m. Pre-feasibility studies providing for an increase in the depth of open pits up to 700-1000 m are known. Under such conditions, the efficiency of open pit mining operations depends on the level of transport sophistication.

A feature of open-pit transport is one-way cargo traffic. In the transport cycle, half of the distance covered by a dump truck is

associated with idle mileage. In the 80-90s of the last century, a circular truck traffic arrangement with collecting the cargo en route was proposed to use at the open pits [1, 2]. In order to use the circular truck traffic, it is necessary to create favorable conditions as follows: the sum of distances driven by a laden truck should be greater than or equal to the sum of distances driven by an empty truck. These conditions are created while in-pit dumping: the waste unloading stations are located on the dump not far from the ore faces.

The efficiency of the circular truck traffic is provided by reducing the time share associated with the run of an empty truck in its total running time. However, in the proposed version [1, 2], the circular truck traffic has a very limited area of application. The circular traffic route of open pit transport is possible with a special location of faces and delivery points for adjacent cargo flows: the loading and unloading stations for adjacent cargo flows should be located closer to each other than the loading and unloading stations for each cargo flow separately.

Another feature of deep open pits is that the mining faces are located lower than the stripping ones, and the ore unloading stations (combined transport transfer stations) are mostly located lower than the waste unloading stations. This feature of the mutual location of mining and stripping areas of the open pit and rock mass delivery points can be used as a necessary condition for the formation of an “open” (partial) circular route: mining face - ore delivery point – stripping face - dump. To complete the circular route, the truck should be lowered on the working area of the open pit using equipment for hauling down the trucks [3].

The main objective of the study is to create a technology that makes it possible, when developing steeply dipping deposits, to expand the use of circular truck traffic and reduce the time share associated with the run of an empty truck in the transport cycle.

The main idea of the developed technology is to use the principle of circular truck traffic. To apply this method of truck traffic arrangement, it is proposed to use the equipment for hauling down the empty trucks into the open pit (Fig. 1). This equipment is constructed on the non-mining pit wall to haul down the empty trucks into the open pit; after hauling down, the trucks drive as follows: ore face - ore unloading station – stripping face – waste

dump – equipment for hauling down the empty trucks into the open pit. In Fig. 1, the arrows show the direction of truck traffic during the cycle of their operation.

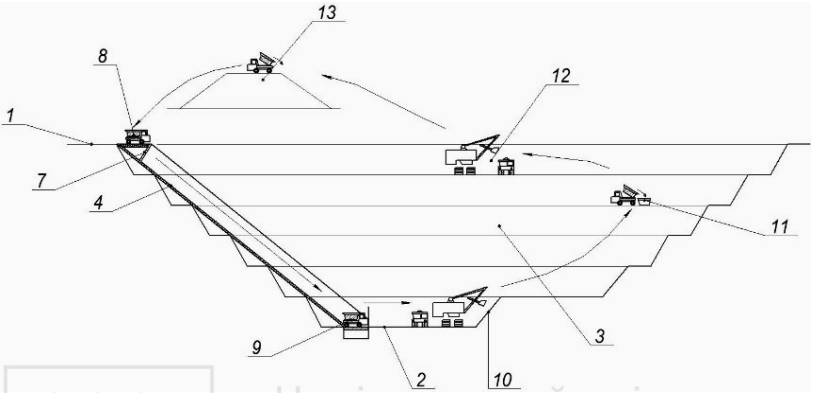

Fig. 1. The use of an equipment for hauling down the empty trucks to form a circular truck traffic in the open pit mine (*1* - day surface; *2* – open pit bottom; *3* - working benches; *4* - inclined trench; *7* – equipment for hauling down the trucks; *8*, *9* - upper and the lower positions of the platform with a dump truck; *10* - ore face; *11* - ore delivery point; *12* – stripping face; *13* – waste delivery point) [3]

Experience in the use of slope hoisting plants

By the end of the 20th century, considerable progress had been made in the development and implementation of heavy hoisting plants in the underground mines. There are examples of mines with a depth exceeding 2000 m, the lifting capacity of hoisting plants has reached over 50-60 tons. Advances in the development of mine hoisting plants have awaken fresh interest in the use of steep-slope hoisting plants in deep open pit mines [4-12]. In the 60 s, in the US, South America and China, more than 10 projects of slope skip hoisting plants were implemented [4-6]. In 1972, Siemag, the West German company, built the only in the USSR slope skip hoisting plant in the Sibaisky Open Pit Mine [7]. Along with the development and implementation of slope skip hoisting plants, a number of teams of authors elaborated an idea of using a slope hoisting plant to haul down the empty and lift the laden dump trucks in the open pit mines [8-10,12]. However, numerous projects in this regard have not been implemented. The reason for this is not only the technical complexity of slope hoisting plants, which should conform to the pit dump trucks

in their parameters, but also the doubts about the economic efficiency of such plants at a state-of-the-art open pit. The systems designed for hauling down the empty and lifting the laden trucks are distinguished by high metal consumption and complexity of technical solutions on multi-rope hoisting.

The results of simulation of an open pit operation with a slope hoisting plant for hauling the empty and lifting the laden trucks show that two streams of trucks are formed at the open pit: the flow of empty trucks from the lower unloading station of the hoisting plant to the excavating faces, and the flow of laden trucks from excavating faces to the lower loading station of the hoisting plant. The main process feature of this flowchart is a high probability of queues of empty trucks waiting for hauling down, and laden trucks waiting for lifting out of the open pit mine. The hoisting plant acts as a limiting section of the road. A few articles [5], which have analyzed the efficiency of this type of transport, note that it is difficult to achieve and maintain the open pit capacity required. The use of the hoisting plant with only one platform to haul down alternately the empty or laden trucks initially makes a bottleneck in the transport cycle and causes the queues. It is possible to improve the technological parameters of mining operations by construction of two hoisting plants, but this will require twice as much investments. The use of this plant in an open pit mine of low capacity and with pit walls located in strong monolithic rocks can be considered as efficient. In such an open pit mine, a system of haulage roads distributed on the pit wall will be a factor that increases the amount of waste rock at the final pit.

Progress in mining machinery manufacturing has increased reliability of pit dump trucks and led to an increase in the reasonable distance of rock mass haulage. There are examples when the rock haulage by trucks reaches over 10 km. In these conditions, the main negative factor that needs to be solved is the idle run of trucks. One-way traffic, equality of loaded and idle runs of trucks are the main features of truck haulage at the open pit; elimination of idle runs can be considered as the key method for improvement of truck haulage efficiency.

Analysis of arrangements of slope hoisting plants

A great contribution to the development of the theory of slope hoisting systems was made by V.I. Belobrov [8]. His work deals with

multi-rope slope hoisting plants designed to haul down and lift the trucks, as well as to lift the skips of over 120 ton capacity. However, the main orientation of researches was focused on lifting the cargo to the surface. In order to solve the problem, we used a multi-rope hoisting system with a large angle of the drive sheave contact (α=3π). With increasing α, the lifting capacity of the hoister is increased

$$S_2 = S_1 e^{\alpha f},$$

where S_2 is the tension of the rope lifting the laden vehicle; S_1 is the same from the side of the empty vehicle; f is an adhesion (friction) factor between the rope and the lining of drive sheaves (0.2-0.3).

The hoisting plants with several drive sheaves of friction have the lifting capacity by 3-6 times greater than single-drive machines. A weak point of this plant [8] is that the hoisting ropes are subjected to multiple (up to 8-9 times) kinking on the sheaves during a lifting cycle, half of them bends in different directions, that will lead to a short lifespan of the ropes.

Siemag has developed a project for a slope hoisting plant for laden trucks, which is equipped with a single platform with a counterweight [14]. In this project, a multi-rope hoisting system with a large angle of the drive sheave contact is also used.

In the world, there are several examples of using the hoisting plants for dump trucks in the mining operations under extreme conditions - in the construction of hydraulic structures in the highlands (Nant de Drance, Tokuyama, Tateyama, Miyagase, Kaprun, etc.). The capacity of these plants does not exceed 40 tons.

The main idea of this study is to increase the truck capacity by reducing the downtime associated with idle mileage in the transport cycle using the slope hoisting plants to haul down the empty trucks to the open pit [3]. Obviously, the hoisting systems equipped with two lifting platforms alternately used for hauling down the trucks can achieve maximum economic effect.

It is known that when lifting vertically using drum winders or hoisters with friction sheaves, the vehicles move in two mutually perpendicular vertical planes: in plane, where the head sheave is located, and in plane being tangential to the sheave circle (the point, where the rope leaves the sheave). The line of intersection of these

planes coincides with the axis of the hoisting rope. When lifting vertically there are no critical difficulties with creating conditions for movement of two skips in the shaft. The skips used for vertical lifting are structurally adapted to move within a limited section of the shaft (the height of the skip is greater than its dimensions in plan).

This principle is maintained even at slope hoisting – the vehicle moves along the line of intersection of two mutually perpendicular planes, but one of them (tangent to the sheave) is located at an angle to the horizon. In this case, the design solution to arrange the movement of two vehicles (skips or platforms) associated with one or more hoisters is more complex, especially when the trucks are lowered on the platform (the length of 130-ton truck is about 12 m, the width is 6 m, the weight is 105 t, the weight of lifting platform is 50 t). In most of proposed slope hoisting systems for dump trucks, this has led to placing the deflection sheaves on the headframes or in the hoist house that makes these hoisting plants complex and unreliable.

A great contribution to the development of the theory of slope hoisting systems was made by B.A.Nosyrev. In his work [13], eight basic arrangements of slope hoisting plants are defined, the estimation is given and the rational application area is specified. Fig. 2 shows the schematic diagrams of slope hoisting plants in the open pit mines, the analysis of these plants is given in Table 1.

The absolute lack of experience in operation of slope hoisting systems with multi-rope friction winders in the open pit environment does not optimize the possible increase in the calculated friction factor and even more than this, the friction factor may be reduced due to rope freezing and wetting during the periods of rain and snow melt [13].

Engineering study of a single platform hoister

In order to determine the main technical characteristics of the plant for hauling down the empty trucks (Fig. 3), the design was elaborated for the mining conditions as follows: type of the hoisting plant is single-end; lifting height, H_n=400 m; a slope angle of the lifting way, α=40°; lifting length, L_H=622.48 m; type of vehicle is a platform; capacity of the platform is Q_{gr}=105000 kgf; mass of the platform, Q_{pl}=50000 kg; the purpose of a hoisting plant is for men and cargo hoisting.

The maximum static load of the slope hoisting plant is 155 t. At present, the mine hoisters manufactured by the industry have no capacity required to meet a target. The hoisting plant with two synchronized hoisters and a reeving system of suspension of the cargo platform is proposed, that will allow reducing the suspended load in the hoisting ropes. The suspended load is,

$$Q_0 = \frac{Q_{cm}}{n \times i_n \times \eta_n} = \frac{155000}{2 \times 2 \times 0.99} = 39142, \text{ kgf}$$

where n=2 - number of hoisting ropes;

i_n =2 - mechanical advantage of a tackle block (number of ropes);

η_n=0.99 - efficiency of a tackle block on the roller bearings

The hoisters are divided on the principle of operation into drum hoisters and hoisters with friction sheaves. The parameters of large hoisters with a drum diameter from 4 to 6 m were classified as per GOST 18 115-72 standard in the Soviet mining industry. The basic drum parameters (diameter and length), the gear ratio of reducers, the maximum rope tension and static rope tension difference were subjected to standardization.

The large hoisters are designed to be installed only on the surface indoors. Fig. 4 shows the results of hoister parameter statistics as specified in GOST 18 115-72. The dependence of maximum static rope tension (T_{CT}, тс) and the maximum static rope tension difference (F_{CT}, тс) on the hoister weight without a gear and electrical equipment (M, t) is determined.

The analysis (Fig. 4) shows that a parametric series of large hoisters is represented by those with a suspended load and a static tension difference upwards of 40 tons.

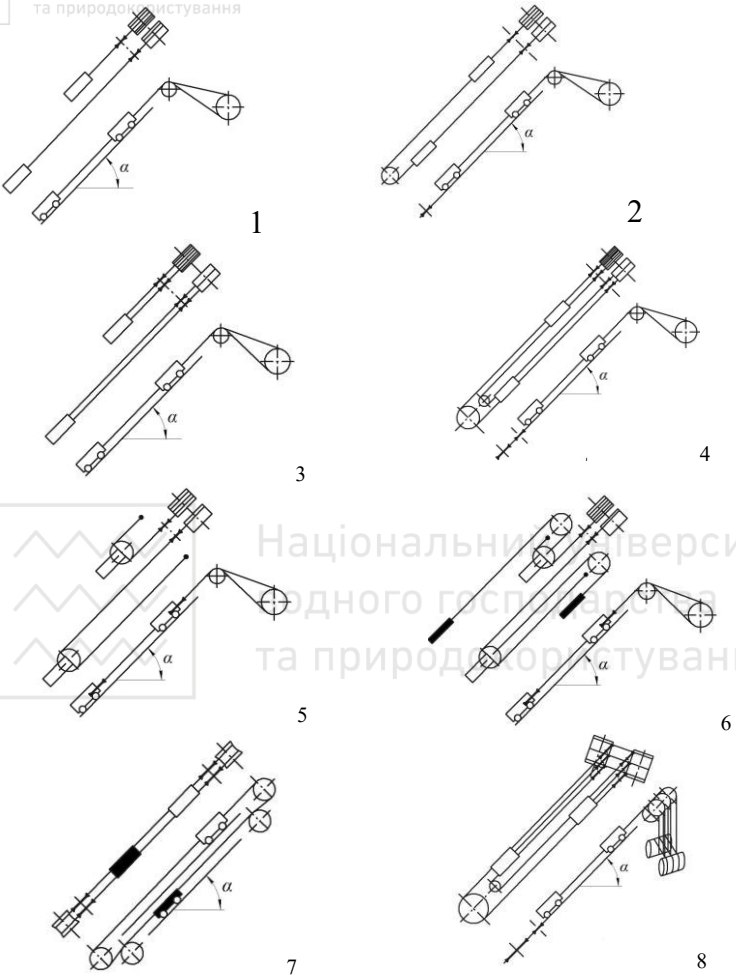

Fig. 2. Diagrams of hoisting plants [13]

Table 1

Analysis of arrangements of slope hoisting plants

Design features	Advantages	Disadvantages
A single-rope hoisting plant with multilayer rope winding on a cylindrical hoist drum (Fig. 2.1, 2.2), (drum hoist). Capacity is up to 40 t.	Simplicity and reliability of the plant; the possibility of using the lubricated ropes.	The use of this plant is limited by traction properties of the rope, the static tension of the rope line and the greatest static unbalanced circumferential force. With a greater unbalanced circumferential force, it is necessary to balance the hoisting system.
A multi-rope hoisting plant with multilayer rope winding on the section of cylindrical drums (Fig. 2.3), (Blair hoist). Capacity is over 40t, lifting height is over 400m.	Simplicity and reliability of the plant; the possibility of using the lubricated ropes, the use of a winding reel of smaller diameter than in the case of friction sheaves.	When lifting cargo from deep levels, the improvement of energy effect may be achieved by using lower balancing ropes (Fig. 2.4).
The hoisting plants with a reeving system of suspended vehicles (Fig. 2.5, 2.6).	The harmful phenomenon of uneven force distribution along the rope lines has been eliminated; due to the high speed of the rope, it is possible to use gearless drives. The use of block hoisting arrangements is reasonable for cage hoisting plants with a low lifting speed of the cage (platform).	Complication of the vehicle construction due to placing the circumferential sheave on its frame, an increase in the vehicle weight by 10-15 tons; increased wear of the rope, because of the doubled speed of its movement and additional bending on the by-pass sheave; the use of double-length ropes.
A multi-rope hoisting plant with friction sheaves (Fig. 2.7, 2.8), (Koepe hoists). Capacity is over 40 t, lifting height is over 400 m. A hoister with one driving friction sheave provides no high traction and requires the	It can be used with long ropes; decrease in inertial masses of the winding reel; increase in efficiency of the hoisting plant; rope rupture hazard prevention when the vehicle is derailed	Limited use due to the rope stress ratios; increase in wear and corrosion of the rope due to the lack of protective lubrication; reduction of the friction factor due to rope freezing and wetting during the periods of rain and snow melt; constructive complexity of two-vehicle slope

balancing ropes. In the hoisters with several driving friction sheaves, the angle of the drive sheave contact is 3π.	(jammed) and re-lifted.	hoisting plants; the low balance ropes considerably complicate the design and reduce the reliability of the hoisting plant.

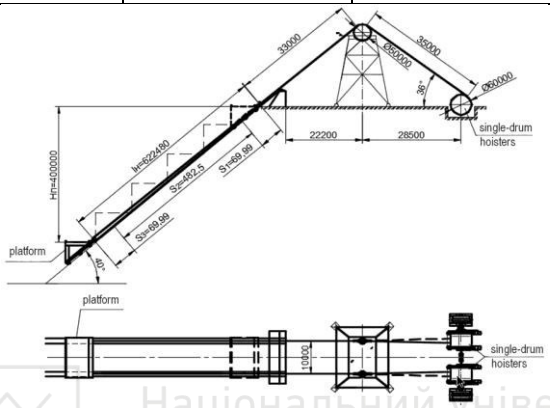

Fig.3. Diagram of a hoisting plant

As a hoister, it is rational to use the mine hoister with one cylindrical drum that has been developed by NKMZ. Based on the dimensions of the winding reel and suspended loads, the 1-6×5.6/0.8 mine hoister fits good having the parameters as follows: 6000 mm drum diameter; 5600 mm drum width; 560 kN static rope tension; 400 kN difference in static rope tension and 11200 kNm^2 flywheel effect.

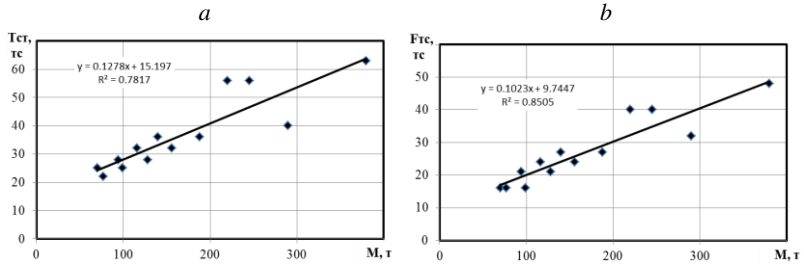

Fig. 4. Dependence of the maximum static rope tension (a) and the maximum static rope tension difference (b) on the hoister weight

The developed hoisting plant consists of the following parts:

- two 1-6×5.6/0.8 single-drum hoisters;
- platform for transporting the truck;
- a headframe for placing the deflection sheaves;
- two deflection sheaves (Ø 5 000 mm);
- two inclined rail tracks to move the platform.

In order to reduce the suspended load on the hoisting ropes, provision is made for two hoisters with fixing the ropes via a tackle block to the platform frame. This type of arrangement makes it possible to use commercially available hoisters. In order to distribute an even load, the operation of hoisters should be synchronized in terms of rope speed and tension. The parameters of the hoisting plant are determined by calculation as follows: the hoisting speed is 9.9 m/s, one cycle time is 214.2 s, the time for a truck to drive on and off the platform is 60 s, number of cycles per hour is 12-15. Fig. 5 shows the diagrams of acceleration, speed and force.

When the loaded platform is lowered, 1÷3 periods (Fig. 5), the values of driving forces on the circumference of the rope winders have negative values, i.e. the engines operate in a dynamic braking mode. When the platform is lifted, the drive motors operate in a traction mode, overcoming the static resistance of the hoisting system and at the same time ensuring the actual linear speed with the proper acceleration and deceleration adopted according to the requirements of design standards.

The hoisting plant is equipped with two P2-800-217-8SUHL4 electric motors of 3 150 kW nominal.

Study of slope hoisting plants with two platforms

The efficiency of mining operations with the use of a developed system for hauling down the trucks on the working area depends on the number of downward trips per hour. The performance of the hoisting plant with one platform is sufficient to provide operation of one shovel with a 12-15 m^3 bucket capacity. In order to provide a working area of the open pit with twice as many trucks, it is necessary to build two similar single-rope hoisting plants or to develop a hoisting plant with two platforms. The main idea that needs to be implemented in the hoisting plant with two platforms is

to balance the hoisting system and haul down the trucks while engines are operating in a regeneration mode.

The arrangements can be classified as per location of tracks with respect to the longitudinal hoister and as per position of tracks relative to each other. We will compare the advantages and disadvantages of alternative arrangements of hoisting plants having two platforms with two independent hoisting plants having one platform.

Analysis of possible kinematic diagrams allowed the following solutions to be called competitive. From the position relative to the hoister, both tracks can be located either on one side (Fig.6, 7) or on opposite sides of the hoister (Fig.8). When the tracks are located on opposite sides of the hoister, they are located in the same vertical plane, but not parallel to each other (Fig.8). In order to ensure mining technical conditions for this track location, it is necessary to provide a site for the hoister on a rock pillar, protruding in plan from the general strike trend of the pit wall. With this design of the hoisting plant, it becomes possible to haul down the trucks at two different sections of the working area. The distance between in-pit sites of the hoisting plant can reach 600-800 m. When the tracks are located on one side of the hoisting plant, they are also located in the same plane, in general, parallel to each other, but this plane can be either parallel to the pit wall plane (Fig.6), or be vertical and pass through the hoisting sheaves of the hoisting plant (Fig.7).

Fig.7 shows a general view of the hoisting plant with one-sided arrangement in vertical plane of two parallel tracks (the top and bottom tracks), where 1,2 - platforms; 3 - dump truck; 4,5 - inclined rail tracks; 6,12 - hoisting ropes; 7,13 - headframes; 8,14 – top headframe sheaves; 11,17 - bottom headframe sheaves; 9,15 – rope winding reel; 10,16 - electric motors; 18 - a hoist house (deflection sheaves on the platforms and a reeving system are not shown in the figure).

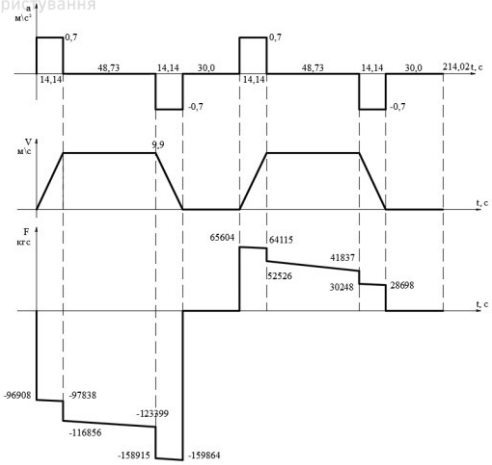

Fig. 5. Diagrams of acceleration, speed and force

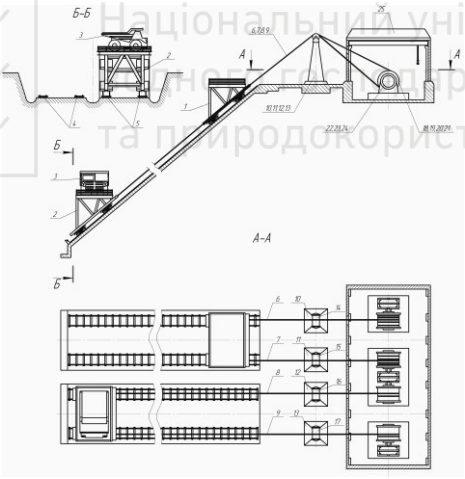

Fig. 6. General view of a hoisting plant with a single-sided arrangement of two parallel tracks in plane of a pit wall

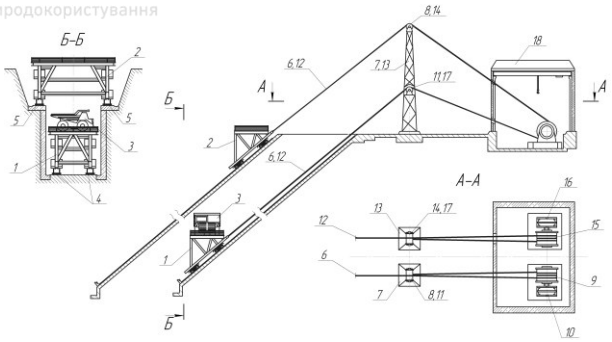

Fig. 7. General view of a single-sided hoisting plant in vertical plane of two parallel tracks

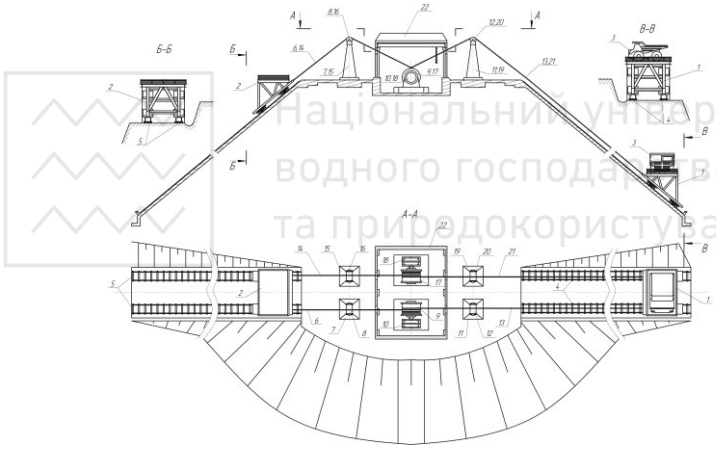

Fig. 8. General view of a hoisting plant with an opposite-sided arrangement of two parallel tracks in vertical plane

Fig.8 shows a general view of the hoisting plant with an opposite-sided arrangement (in relation to vertical plane passing through the longitudinal axis of the drum) in vertical plane of two tracks (conditionally applied to Fig.8, left and right tracks), where 1 is platform of the right track; 2 - platform of the left track; 3 - dump truck; 4,5 - inclined rail tracks; 6,14,13,21 - hoisting ropes; 7,15,11,19 - headframes; 8,16,12,20 - headframe sheaves; 9,17 – rope winding reels; 10,18 - electric motors; 22 - a hoist house (deflection sheaves on the platforms and a reeving system are not shown in the figure).

The arrangement shown in Fig.6 differs from two independent, side-by-side located hoisting plants with one platform in that the adjacent single-drum hoisters are replaced by one double-drum hoister. The double-drum hoister serves both tracks and operates all the time in a regeneration mode, the single-drum hoisters operate alternately. In this case, the hoisting plant is equipped with three hoisters. One of the main drawbacks of this arrangement is that there is no possibility to provide a through movement of trucks, that is, when driving on or off the platform, the truck drives in reverse.

The diagram in Fig. 7 differs from the diagram in Fig. 6 in that the hoisters are statically more balanced; the ropes are pairwise wound on the cylindrical drums: when one rope reels in, another one reels out. Two hoisting plants provide hauling two platforms up and down, and operate all the time in a regeneration mode. The location of tracks in section of one step-shaped trench allows the trucks to arrive and depart without additional maneuvers. The drawback of this arrangement is the need to construct a special trench with the rail tracks at two levels. The upper platform is structurally more complex than the lower one.

The diagram shown in Fig. 8, in terms of arrangement of hoister operation is substantially similar to the diagram in Fig.7. However, in this case, two tracks of the hoisting plant are located in diametrically opposite directions. This design is characterized by a safer arrangement of the truck movement on the upper loading station and provides driving the trucks off the platform in the lower position without additional maneuvers. This arrangement is characterized by a large amount of mining and capital work to prepare the construction sites for a hoist house and a track and can be used at the open pits with a long-distance haulage.

Conclusions

The article presents the results of researches on the development and substantiation of rational designs of slope hoisting systems for hauling down the empty dump trucks in the open pit mines, the use of which will reduce the idle runs. Decrease in idle runs in the transport cycle of trucks is one of the most promising ways to maintain and increase the open-pit transport capacity.

The basic arrangements of slope hoisting plants using drum hoisters and hoisters with friction sheaves have been analyzed. The design complexity of slope hoisting plants with friction sheaves, the rope exposure to atmospheric precipitation (wetting and frosting), increased rope wear due to friction against the supporting rollers and sheaves cause the low reliability of this hoisting plant. The hoisters with cylindrical drums are free from above drawbacks. The issue of providing the required hauling ability of the hoisting plant is proposed to be solved by using several drum-type hoisters in its construction.

The results of design study of the hoisting plant for hauling down the empty trucks of 130-ton capacity are presented. The arrangement of the hoisting plant with two synchronized drum hoisters and a reeving system of suspension of one cargo platform that allows reducing the suspended load in the hoisting ropes is considered. The developed hoisting plant consists of the main parts as follows: two 1-6x5.6/0.8 single-drum hoisters (manufactured by NKMZ); a platform for transporting the truck; a headframe for deflection sheaves; two deflection sheaves; two inclined rail tracks for moving the platform. When lowering the dump trucks, the hoisters operate in generator mode that allows for electrical energy regeneration.

The efficiency of mining operations with the use of a developed system for hauling down the trucks on the working area depends on the number of downward trips per hour. In order to provide a working area of the open pit with more trucks, it is necessary to build two similar hoisting plants or to develop a hoister with two platforms. The article proposes the new technical solutions for hoisters with two platforms, which are alternately used for hauling down the empty trucks. The developed technology promotes improvement of the operational performance of trucks in the open pit mines.

References

1. **Astafiev J.P.** (1991). Model marshrutizatsii avtosamosvalov pri rabote s vnutrikaryernymi punktami razgruzki [Model of dump truck routing when working with in-pit unloading stations], Razvitie teorii otkrytyh gornyh rabot. Moscow [in Russian].

2. **Astafiev J.P., Maksimov A.V.** (1992). Organizatsiya avtotransportnykh potokov v glubokikh kar'yerakh po printsipu kol'tsa [Arrangement of circular-based truck traffic flows in the deep open pit mines]. Razrabotka rudnyh mestorojdeniy:

nauchno-tehnicheskiy sbornik - Development of ore deposits: scientific and technical collection. Kiev [in Russian].

3. Sposib rozkryttya krutospadnykh rodovyshch pry vidkrytiy rozrobtsi korysnykh kopalyn: patent No. 117930 Ukraina - The open pit mining method of steeply dipping deposits: the patent of Ukraine (20 years) No. 117930 [in Ukrainian].

4. **Shilling R., Adams B.** (1971). Naklonnye skipovye pod"emniki [The inclined skip hoists]. Nauchn. tr. amerikanskogo instituta gornyh inzhenerov, inzhenerov–metallurgov i neftyanikov. Moscow: Nedra [in Russian]

5. Build Unique Truck Skip Hoist in Belgian Congo. Mining World. 1959. №6.

6. **Novozhilov M.G., Selyanin V.G., Trop A.E**. (1962). Glubokie kar'ery [Deep open pit mines]. – M: Gosgortekhizdat [in Russian]

7. **Vasil'ev M.V**. (1975) Ustrojstvo, opyt ekspluatacii i perspektivy kar'ernogo skipovogo pod"ema [Arrangement, operating experience and prospects of skip hoisting] . Tr. IGD MChM SSSR. Vyp. 46. [in Russian].

8. **Belobrov V.I., Belobrova E.A**. (2002). Mnogokanatnye naklonnye pod"emnye ustanovki dlya kar'erov i shaht [Multi-rope slope hoisting systems for open pits and underground mines]. Nauk.-tekhn. zb. «Girnicha elektromekhanika ta avtomatika». №69. [in Russian].

9. **Bondariev S.V., Horbatenko Yu.P.**(2011). Zastosuvannia pidiimachiv dlia peremishchennia avtomobiliv po krutykh skhylakh [The use of hoists to relocate the trucks on steep slopes] . Budivnytstvo Ukrainy. № 1. [in Ukrainian].

10. **Dremin A.I., Perepelicyn A.I., Krutikov N.N.** (1993). Pod"emnik dlya dostavki gruzhenyh avtosamosvalov so dna kar'era na poverhnost'. [A hoist for delivery of laden dump trucks from the open pit bottom to the surface] . Gornyj zhurnal. № 7. [in Russian].

11. **Kul'bida P.B., Rojzen V.V., Serbin V.I.** (1981). Bol'shegruznye skipovye pod"emniki dlya otrabotki glubokih kar'erov [Heavy-duty skip hoists for deep open pit mines]. Gornyj zhurnal. № 7. [in Russian].

12. **Listopad G.G.** (2001). Naklonnye pod"emniki kar'ernogo avtotransporta [The slope hoisters for dump trucks in the open pit mines]. Gornaya promyshlennost'. № 2. [in Russian].

13. **Nosyrev B.A**. (1972). Skhemy kar'ernyh naklonnyh pod"emnyh ustanovok, ih ocenka i oblasti primeneniya [Arrangement of slope hoisting plants in the open pit mines, assessment and application]. Trudy Sverdlovskogo gornogo instituta. Vyp. 97 [in Russian].

14. Trucklift System. Innovative transport technology for open pit mines. URL:http://www.siemag-tecberg.com/infocentre/ technical-information/ti_27-trucklift.html (accessed 25 May 201

https://doi.org/10.31713/m1028

MODELING THE PROCESS OF DISINTEGRATION OF SOLID MATERIALS BY ASYMMETRIC LOADING IN CRUSHING MACHINES IN ORDER TO FIND WAYS TO REDUCE ENERGY COSTS

Vasiliev L.M.
Institute of Geotechnical Mechanics. M.S. Polyakov National Academy of Sciences of Ukraine, Dnipro, doc. tech. sciences, professor, led. scientific. sotr, Ukraine

Vasiliev D.L.
Institute of Geotechnical Mechanics named after M.S. Polyakov National Academy of Sciences of Ukraine, Dnipro, doc. tech. Sciences, Art. scientific. sotr, Ukraine

Malich M.G.
National Metallurgical Academy of Ukraine, Dnipro, Cand. tech. Sci., Associate Professor, Associate Professor, Ukraine

Annotation

Subject of study. the processes of cracking and destruction of rocks under the action of the working bodies of machines for disintegration.

Methodology. A complex method of generalizing the laws of the theory of elasticity and plasticity was used; theoretical and experimental confirmation of the regularities of the distribution of contact normal and tangential stresses, equations of the limiting state of materials based on the Coulomb strength criterion; slip line theory; comparison of theoretical results with experimental diagrams "normal stress-longitudinal deformation" of samples; facts and phenomena of destruction of rocks; generalization of the theoretical regularities arising from the power contact of the tool with the rock in crushers.

Purpose. Reducing energy consumption and increasing the efficiency of rock disintegration by controlling its stress-strain state in crushers on the basis of mathematical modeling and using the established regularities of stresses and deformations in rocks when interacting with a working tool.

Output. In the contact area, with an increase in the tangential load, the zone of uniform compression of the material decreases, the depth of the most stressed point approaches the contact surface. There is a significant zone of shear deformations, which are the decisive factor in crack initiation. The development of the crack in depth and complete destruction occurs along the shear lines. Such conditions of rock loading are observed in jaw crushers with complex jaw movement, in cone crushers, in roller crushers with different roll rotation speeds and correspond to the model of the most effective sliding compression. The creation of asymmetric loading conditions using the forces of contact friction, frictional and strength characteristics of the destroyed material can reduce the energy consumption of disintegration.

Introduction

The dynamics of changes in the quality of mining ores of non-ferrous and ferrous metals, coal, mining and chemical raw materials and other solid minerals over the past twenty-five years shows that the content of useful components in them has sharply decreased. It is known that enrichment is carried out by separating mineral associations with certain technological properties in terms of mineral composition.

The existing mass disintegration technologies have low efficiency (primarily energy efficiency): even the most advanced of them "use" less than 1% of the supplied energy for useful work. And this despite the fact that energy costs for crushing and crushing rocks, already today account for a tenth of all electricity produced in the country, continue to grow [1].

If we take into account that, in addition to the processing of mineral raw materials, the processes of destruction of solid materials are widely used in construction, pulp and paper production, for the preparation of wood, in the food industry, the production of medicines, in the processing of household and industrial waste and in a number of other industries, then we can conclude that they are one of the most widespread and at the same time energy-, metal-, capital- and labor-intensive technological processes in the industrial economy. Along with this, the existing methods of disintegration do not meet a number of requirements of industrial production.

First, traditional degradation processes are characterized by low selectivity. This is expressed in the fact that when separating multicomponent materials, it is necessary to violate the integrity of the components themselves, which adversely affects their technical and technological properties.

Secondly, traditional crushing and grinding processes are not suitable for the destruction of all solid materials: especially strong materials (metals, hard alloys, raw materials for powder metallurgy, abrasive, ceramic, etc.) are destroyed ineffectively or not at all by known methods. At the same time, the need for the disintegration of such materials is beyond doubt.

Thirdly, for some technologies, in particular, in the enrichment of minerals and in the preparation of mining, metallurgical and

chemical raw materials, equipment for disintegration, which is serially produced, does not provide the necessary disintegration efficiency.

In this regard, there is a need to control the processes of disintegration and the key to this is the assessment of the bearing capacity of the rock under various types of impact of working tools.

Researchers [2] to assess the bearing capacity of the rock use diagrams "normal stress - longitudinal deformation", which are built on special presses with increased rigidity under uniaxial and volumetric compression of samples. However, the use in practical calculations of the ultimate strength and residual fracture strength of samples obtained on the basis of these diagrams are relative values due to the influence of the scale effect, which is observed not only on fractured, but also on samples without cracks and depends on their size. In addition, it was revealed that, for unknown reasons, under uniaxial compression, five forms of fracture of samples are formed, which have a different character of these diagrams.

As a result of the above, it follows that the mechanism of crack initiation and subsequent destruction of a deformable body has not yet been fully disclosed. In this case, internal and contact friction is not always taken into account, analytical methods for calculating and constructing diagrams "normal stress - longitudinal deformation" with the use of indices of rock properties available for experimental determination, which make it possible to determine the stress-strain state of rock pieces under the action of a working body to find ways of the most effective destruction.

Therefore, the development of mathematical models of the deformation of bodies when a working tool collides with a rock, the appearance of the first cracks, their development in a brittle body to control their stress-strain state in disintegration processes for the preparation of charge materials is an urgent scientific problem, which is of great practical importance for mining and metallurgical complex of the country.

Interactions of the tool with the hole under normal and tangential loading

Let us consider the interaction of working tools - elements of corrugation of armor plates in the case of external forces Q, along the normal to the line of contact of corrugation with destructible material

with a uniform distribution along the line of contact of tangential forces Q_1 (Fig. 1) [3].

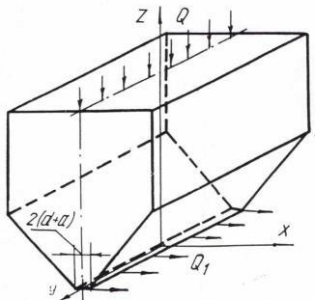

Pict. 1. Design scheme for applying loads

The solution to this problem is associated with significant mathematical difficulties [4]. The authors of [1,3] obtained an approximate solution to such a problem, taking into account the following assumptions: contact pressure is distributed over an ellipse in the zone of contact of surfaces; shear loads are proportional to normal

$$\frac{Q_1}{Q} = \frac{q_{\max}}{p^{\max}} = \varphi = \text{const}.$$

The stress state of the rock was determined by the values of the stress components

$$\sigma_x = q_{\max}\left(2e^{-\alpha}\cos\beta_0 - Sha\sin\beta_0\frac{\sin 2\beta_0}{Ch2\alpha - \cos 2\beta_0}\right);$$

$$\sigma y = 2\mu q_{\max}e^{-\alpha}\cos\beta_0; \qquad (1)$$

$$\sigma_x = q_{\max}Sha\sin\beta_0\frac{\sin 2\beta_0}{Ch2\alpha - \cos 2\beta_0}.$$

$$\tau_{xz} = q_{\max}\left(e^{-\alpha}\cos\beta_0 - Sha\sin\beta_0\left(1 - \frac{Sh2\beta_0}{Ch2\alpha - \cos 2\beta_0}\right)\right).$$

Here σ_y is found from the plane strain equation: $\sigma_y = \mu\,(\sigma_x + \sigma_z)$.

μ - is Poisson's ratio; α and β - are elliptic coordinates, the link of which with rectangular coordinates x and y using hyperbolic circular functions is determined as follows

$$x = (a+d)\text{Chacos}\beta_0, \quad z = (a+d)\text{Shasin}\beta_0 \qquad (2)$$

Graphical interpretation of the solution obtained by the authors [1], which describes the stress state of the elements of the tool and the rock in the zone of their joint contact in the form of a diagram of the distribution of σ over the contact zone, obtained at μ=0.2, are shown in Fig. 2.

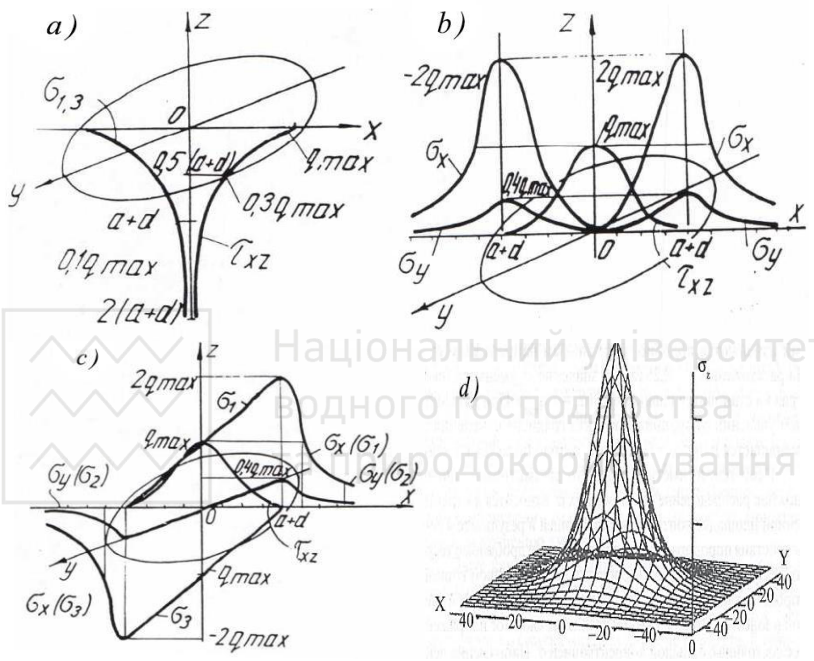

Fig. 2. Distribution of stresses over the contact zone: *a* - vertical plane; *b* - horizontal plane - normal and shear stresses; *c* - horizontal plane - principal and shear stresses. *d* - diagram of normal stresses from a concentrated force in an elastic half-space

In the vertical plane passing through the middle of the contact, σ_1, σ_2, τ_{xy} act (Fig. 2). The nature of the separation of these stresses in the vertical plane is similar. Their maximum values, equal to Q_{max}, take place on the contact surface (z=0).

In the depths of a piece of rock, the values of σ decrease intensively. Already at a distance z=0.5(a+d) from the surface, the

acting stresses decrease by about 3 times and amount to $0.3q_{max}$. At a depth of $z=a+d$ they decrease by a factor of 10, and at a distance $z=2(a+d)$ from the contact zone, the values of σ and τ tend to zero.

In the horizontal plane, including the contact zone, the main, normal and shear stresses act (Fig. 3).The normal stress σ_x within the contact area varies from $\sigma_x=2q_{max}$ at the boundary of the area to 0 at its center. When going from the center to the periphery of the contact, σ_x intensively expands and change sign to the opposite. At the opposite boundary of the contact, they again increase to $\sigma_x=-2q_{max}$.

Beyond the boundary of the contact zone (to the left and to the right of it), σ_x first sharply decreases, but then the diagram calms down and tends to zero at $x>1.5$ $(a+d)$. The distribution of stresses σ_y over the horizontal plane is similar to that considered above with the only difference that the absolute value of σ_y is less than σ_x by μ. The nature of the change in stresses σ_x and σ_y is the same both within the contact plane and outside it. Shear stresses have maximum values $\tau_{max}=q_{max}$ in the center of the contact area. To the boundary of the contact zone, they decrease and take zero values.

The main stresses are σ_1, σ_2, σ_3. The stress σ_1 along the contact area changes from $\sigma_1=2q_{max}$ to 0. Zero values of σ_1 have on the side of the action of the force Q_1. On the opposite side, at the contact boundary, σ_1 reach maximum values, outside the site, they decrease intensively and, at $x>1.5$ $(a+d)$, approach zero values. In this case, σ_2 are distributed over the contact area in full accordance with the stresses σ_y, both in terms of the values of the acting stresses and the nature of their distribution. For σ_3 in the horizontal plane, the character of change in stresses σ_1 is inherent, but has an inverted (mirror) reflection. From the side of the application of the load Q_1 at the contact boundary σ_3 has a maximum value of $\sigma_3=2q_{max}$ then they intensively decrease along the contact area and reach zero values on the opposite contact contour. Outside the contact area, σ_3 of their maximum values change like the normal stress σ_x. At a distance of $x=0.25$ $(a+d)$, the value of σ_3 decreases by 2 times and becomes equal to q_{max} $(\sigma_x=q_{max})$. With further distance from the contact boundary, the stress gradient decreases and at $x>1.5(a+d)$ σ_3

approaches zero. Such a complex distribution of acting stresses occurs over a small contact surface (units of mm).

Knowing the stress state of the working elements and a piece of rock in the zone of their contact from the action of the normal load and from the tangential forces Q_1, it becomes possible to obtain the general stress state by the superposition method (for example, by the total value of σ_{eq}). The maximum values of contact stresses, in absolute value, increase with the growth of both normal and tangential loads. In the presence of Q_1, the values of σ and τ increase significantly, a zone of shear deformations arises, which are the decisive factor in the initiation of a crack. Thus, it has been shown that, in the fracture mechanism, it is these stresses that determine the zone of crack initiation, through which fracture and displacement of the rock occur, which leads to its further destruction.

Fracture of a prismatic specimen by normal and shear stresses.

The development of destruction deep into the rock is different. To describe this process, the diagrams "longitudinal stress - longitudinal deformation" obtained for prismatic specimens under uniaxial compression are used. [5.6]. Analytical constructions of such diagrams are also used [2,7]. In real conditions of disintegration, there may be other conditions, for example, in millstones or in cone crushers where, in addition to normal, oppositely directed contact shear stresses act.

Based on the parameters of the diagrams mentioned, it is possible to determine the specific fracture energy of the sample according to the well-known formula

$$E_d = \frac{p^2}{2E}, \tag{3}$$

where p - is the specific force on the bearing area; E - is the modulus of elasticity of the material.

Let us take one [8] of the five known [9], the simplest form of destruction of prismatic rock samples - truncated-wedge (Fig. 3).

Fig. 3. Experimental truncated-wedge fracture

The truncated-wedge form of fracture of rock samples is characterized by the absence of intersection of the crack with the vertical line of symmetry (Fig. 4). When the specimen is compressed, symmetric contact shear stresses τ_c against transverse deformation arise. The sign of the contact shear stresses in the upper part of the left half of the specimen is taken with a "plus", for the lower part - with a "minus". For the right half of the sample, the signs of τ_c are assumed to be opposite. Since the lateral surfaces of the specimen acquire a convex shape due to deformation, we apply the rule of pairing of tangential stresses at the corner points. The condition for the limiting state at the crack tip is the equality of the ultimate shear strength of the material to the active shear stress minus losses for internal and contact friction according to the Coulomb criterion

$$k_n = |\tau_\alpha| - \mu\sigma_\alpha, \tag{4}$$

where k_n - is the ultimate shear strength of the rock at the crack tip at the TEMECN (trajectory of the maximum effective shear stresses) ξ; $|\tau_\alpha|$ - active shear stress on TMEKN; μ and ρ=arctgμ - coefficient and angle of internal friction; σ_α - is the normal stress on the TMECN ξ. We assume that cracks (Fig. 4) develop according to TMЭКН: - to the left according to TMЭКН ξ_l, - to the right along TMЭКН ξ_r. Since the TMEDS are symmetric, we give a description of the left TMEDN ξ_l. The angle of inclination of TMEKN ξ_l. according to the Coulomb strength criterion is determined by the formula.

$$\alpha_л = \frac{\pi}{4} + \frac{\rho}{2} + \beta_{\xi_1} \tag{5}$$

As the crack develops, part of the material comes out of the load (Fig. 4).

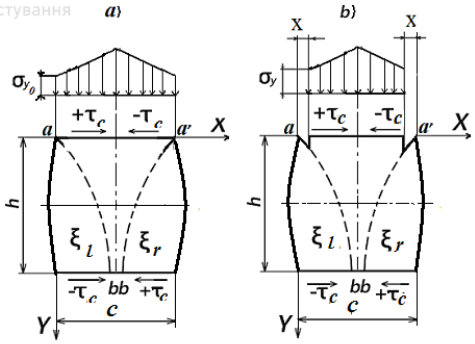

Fig. 4. Diagrams of diagrams of contact normal loads and crack propagation according to TMEKN ξ with a symmetric distribution of shear stresses: *a* - in an elastic state; *b* - at the time of crack development

Knowing the values of the coordinates of the crack tip on the TMECN ξ_l at each moment of its development, it is possible to determine the bearing part of the sample material area, equal to the initial unit length of the latter minus the part that came out from under the load. Then a single bearing area of the specimen with the development of two symmetric cracks will be

$$a_2 = c - 2x. \tag{6}$$

On the load-bearing part of the specimen with cracks emerging from under the load, the distribution of the contact load and the specific force change, the values of which we need to calculate the specific energy of destruction according to formula (3). To determine the specific force, it is necessary to know the regularity of the distribution of contact normal stresses. Regularities of the distribution of contact normal and tangential stresses are taken according to *L*. Prandtl [10]: tangential stresses are constant, and normal stresses are linear (Fig. 4), the distribution of which is described by the formula

$$\sigma_{yi} = \sigma_y \left(1 + \frac{2f \cdot x}{h}\right), \tag{7}$$

where σ_y - is the normal stress at the crack tip; f - is the coefficient of contact friction; h - is the height of the sample; x - is the abscissa of the crack tip. The specific force according to the scheme (Fig. 4*b*),

taking into account the yield of a part of the sample by the value of $2x$ on the basis of formula (6) with the use of (5), is determined as

$$p = \frac{2\sigma_y}{c - 2x_\xi} \int_0^L \left(1 + \frac{2f \cdot L}{h}\right) dL = \sigma_y \left(1 + \frac{f \cdot (0{,}5c - x_\xi)}{h}\right), \qquad (8)$$

where L=0.5c-x_ξ

The work [2] describes a method for determining the normal stress $\sigma_{\xi\gamma}$ at the crack tip as applied to the failure of specimens under uniaxial compression. The stress $\sigma_{\xi\gamma}$ at the crack tip at the TMECN ξ_1 is determined by the system of equations

$$\begin{cases} \sigma_{\gamma\xi} = \dfrac{1}{\mu}\left[\dfrac{\left(k_n\left(1 + \sin\rho\sqrt{1 - b_\xi^2}\right)\right)\exp\left(2\mu\left(\beta_\xi + \beta_b\right)\right)}{1 - \sin\rho\sqrt{1 - b_\xi^2}} - k_b\right]; \qquad (9) \\ k_b = \dfrac{\left(k_n + \mu\sigma_{\lambda\xi}\right)\left(1 + \sin\rho\sqrt{1 - b_\xi^2}\right)}{\left(1 - \sin\rho\sqrt{1 - b_\xi^2}\right)\exp\left(-4\mu\beta_b\right)}; \qquad (10) \end{cases}$$

where k_b - is the effective shear stress at the point b of the TMEKN ξ_1 on the contact bottom surface (Fig. 4)

$b_\xi = \dfrac{\tau_{xy}}{\mathbf{k}_n + \mu\sigma_{y_\xi}} = \dfrac{f\sigma_{y_\xi}\left(1 - \dfrac{2y}{h}\right)}{\mathbf{k}_n + \mu\sigma_{y_\xi}}$; β_ξ - the angle of rotation of TMEKN ξ_1 at the crack tip, equal to

$$\beta_{\xi_1} = \frac{1}{2}\operatorname{arctg}\frac{f\sigma_{y_\xi}\left(1 - \dfrac{2y}{h}\right)_\xi \cos\rho}{\left(\mathbf{k}_n + \mu\sigma_{y_\xi}\right)\left(\sin\rho - \sqrt{1 - b_{\xi_1}{}^2}\right)}; \qquad (11)$$

$$b_b = -\frac{\tau_c}{\mathbf{k}_b + \mu\sigma_{y_b}} = -\frac{f\sigma_{y_b}}{\mathbf{k}_b + \mu\sigma_{y_b}}; \qquad (12)$$

$\sigma_{y_b} = \sigma_y\left(1+\frac{2fx_b}{h}\right)$ - normal stress at point b; x_b - abscissa of the crack tip at point b; β_b - is the angle of rotation of TMEKN ξ_1 at point b, equal to

$$\beta_b = \frac{1}{2}\text{arctg}\frac{b_b\cdot\cos\rho}{\left(\sin\rho-\sqrt{1-b_b^2}\right)} = -\frac{1}{2}\text{arctg}\frac{f\sigma_{y_b}\cdot\cos\rho}{\left(\mathbf{k}_b+\mu\sigma_{y_b}\right)\left(\sin\rho-\sqrt{1-b_b^2}\right)}; \quad (13)$$

By formula (8) using formulas (9) - (13), we determine the specific force p by the iteration method. Specific force ρ on TMECN ξ_1 (Fig. 5, curve *1*) increases from the ordinate of the crack tip (as the tip moves away from the upper contact plane).

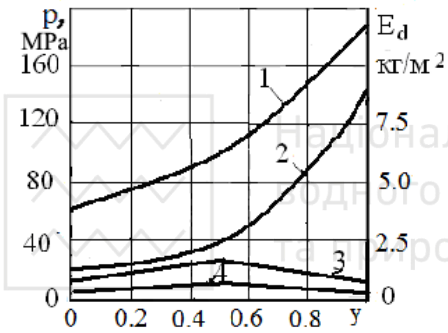

Fig. 5. Dependences of specific force and fracture energy on the ordinate of the crack tip at k_n=10 MPa, ρ=45 °, f=0.3, E=2000 MPa

Using formula (8) from dependence (3), we determine the specific fracture energy of the sample (Fig. 5, curve *2*). As can be seen, the specific energy of resolution at symmetric shear stresses is increasing all the time.

Now let us determine the specific force and specific energy of destruction from the ordinate of the crack tip at asymmetric directions of contact tangential stresses (Fig. 6). In this case, we have positive signs on the contact planes with the development of cracks from top to bottom along TMEDN ξ and from bottom to top along TMEDN η.

The formula for the distribution of contact normal stresses in this case has a different form

$$\sigma_{yi} = \sigma_y\left(1+\frac{f\cdot x}{h}\right). \quad (14)$$

Nevertheless, the formula (13) of the specific force remains the same. But in this case, the minus sign should be removed in formulas

(12) and (13), and a minus should be introduced in formula (11) for $y>0.5\ h$.

Then, in the exponential of expression (9), the parameters β_ξ and β_b will have negative signs and will significantly reduce the stress value at the crack tip σ_y.

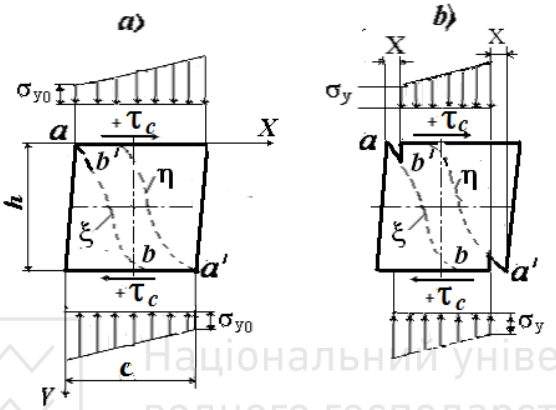

Fig. 6. Schemes of distribution of contact normal stresses and crack propagation under asymmetric contact shear stresses: *a* - in an elastic state; *b* - at the time of crack development

This, with asymmetrically directed contact tangential stresses, in comparison with symmetrically directed stresses during fracture of the sample, leads to a decrease in the specific force by up to 12 times (Fig. 5, curve *3*). To calculate the specific energy of destruction, we use the well-known formula [11], which takes into account the energy consumption during oblique shear,

$$Ed = 1/(2E)\cdot(p^2+2(1+\nu)f^2\ p^2). \qquad (15)$$

The specific energy of destruction under asymmetric loading decreases 40-45 times (Fig. 5, curve *4*).

Let us confirm this conclusion by constructing a diagram "longitudinal stress - longitudinal deformation" for this type of load and compare the latter with the diagram for symmetric loading. Let us first describe the method of constructing a diagram "longitudinal stress - longitudinal deformation" for a truncated-wedge fracture, which is also suitable for asymmetrically directed contact shear stresses. Knowing the values of stress σ_c c and longitudinal deformation ε at each moment of the position of the crack tip in the

sample, it is possible to construct an analytical dependence $\sigma_c\ \psi(\varepsilon)$. To do this, you need to determine the current value of the normal pressure on the branches of the conventional diagram. This pressure is

$$\sigma_c = pS = p(c-2x)/c \tag{16}$$

where S - is the ratio of the carrier to the starting site.

Now we need to define the second parameter of the diagram - longitudinal deformation. We assume that at the crack tip the brittle rock material obeys Hooke's law. With knowledge of the values of the specific forces on the bearing part of the sample, the value of the longitudinal deformation can be determined according to Hooke's law

$$\varepsilon = \frac{p}{E}. \tag{17}$$

где E – модуль упругости.

where E - is the modulus of elasticity.

Now we build diagrams "stress - strain" for symmetric loading (Fig. 7, curve *1*) and asymmetric directional contact shear stresses (Fig. 7, curve *2*).

Comparing curves *1* and *2*, one can confirm the conclusion already made. In addition, with asymmetric directional contact shear stresses after the entry of cracks into the opposite horizontal half of the specimen, self-sustaining failure occurs, that is, failure due to the previously accumulated elastic energy (Fig. 7, curve *2*).

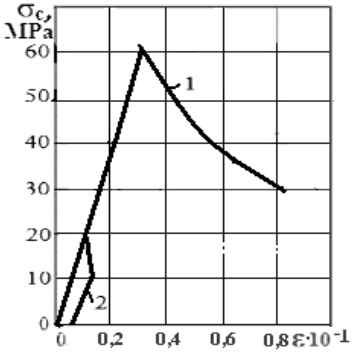

Fig. 7. Diagrams "stress - strain": with k_n=10 MPa; ρ=45 °; f=0.3; E=2000 Pa

The conditions for loading rock pieces with asymmetric directional contact shear stresses (Fig. 7) are favorable from the point of view of energy consumption for destruction during crushing of brittle bodies.

These conditions, in our opinion, are partially realized in millstones and certain types of crushers.

Features of disintegration in crushers under normal and tangential loading

Consider the features of disintegration in crushers (Fig. 8).

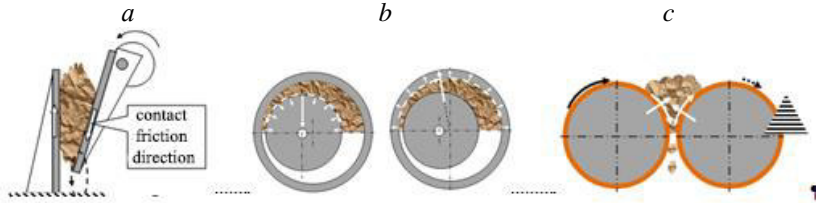

Pict. 8. Direction of friction forces in crushers: *a* - in the cheek with a complex cheek movement; *b* - in a cone; c) - in the roll.

In jaw crushers, the main difference between the crushing of material with a complex and simple movement of the jaw lies in the different orientation of the friction forces. Friction forces at the contact of the mass to be crushed with the cheeks are directed in one direction with a simple movement, and with a complex movement - in different directions

With a simple movement of the cheek, the crushed mass is in conditions of uniaxial compression, and with a complex movement of the cheek - in conditions of sliding compression [12].

A cone crusher can be considered as a result of the development of a jaw crusher associated with the transition from flat to spatial motion of the crushing body (Fig. 8*b*). In a cone crusher, frictional forces in the vertical plane arise at the contact of the rock with both the outer and inner cones. They are oriented in the same way as in a jaw crusher with a simple jaw movement. In the horizontal plane, the total projection of friction forces at the contact with the crushed ore along the arc of the crushing cone is equal to 0. Friction forces at the contact with the crushing cone are distributed in the same way as under the plate of a flat press - in different directions (Fig. 8*b*). The total projection of the friction forces at the contact with the crushed

ore along the circular arc of the stationary cone is not equal to 0 [12]. Thus, as in a jaw crusher with a complex jaw movement, the rotation of the crushing cone provides crushing in an efficient sliding compression mode.

An increase in the efficiency of destruction in a two-roll crusher is carried out due to the transition from conventional to sliding compression by choosing a different speed of rotation of the rolls (Fig. 8*c*), as suggested, for example, by the Artyomovsk Machine-Building Plant. According to [12], crushers with different (by 14-20%) roll rotation speeds are used in the asbestos industry.

Creation of a more efficient mode of using friction characteristics provides a lower energy consumption of crushing [12]. Better energy intensity, along with other technological and operational advantages, the main one of which is the ability to work under a blockage, has led to the almost complete displacement of jaw crushers by cone crushers in the iron ore industry. Jaw crushers continue to be used in the building materials industry, such as crushing pieces of concrete structures.

Output

As a result of the development of mathematical models and analysis of the tension of the zone of interaction of the elements of the crusher with a piece of solid rock, it is established:

1. At the contact between the rock and the tool, two most stressed zones are noted: the contact surface, where the maximum principal stresses act, and the zone of maximum tangential stresses under the contact surface at a depth less than the dimensions of the contact area. At the boundary of the contact zone, an almost pure shear occurs, and ultimate deformations gradually accumulate in the material, which lead to the initial development of cracks.

2. Deformations arising during the action of the tool lead to a change in the shape of the surface even with a high hardness of the material and the actual dimensions of the contact pads increase. With an increase in the tangential load, the zone of uniform compression of the material decreases, the depth of the most stressed point approaches the contact surface. There is a zone of action of shear deformations, which are the decisive factor in the initiation of a crack.

3. As the cracks develop, the specific force at symmetric contact tangential stresses increases all the time, and at asymmetrically

directed contact tangential stresses increases from the ordinate of the crack tip to the horizontal axis of symmetry, then decreases, while the maximum value of the specific force in the first case is 8-10 times higher than in the second case.

4. Specific fracture energy (by the example of a sample) at asymmetrically directed contact shear stresses in comparison with symmetric loading is reduced by up to 40-45 times.

5. The conditions of asymmetrically directed contact shear stresses during crushing of brittle bodies are more favorable from the point of view of energy consumption for fracture in comparison with symmetric contact shear stresses.

6. The above examples of the use of contact friction forces to create the so-called sliding compression in crushers confirm the effectiveness of the destruction of fragile bodies by asymmetrically directed contact shear stresses and show the way to reduce the energy intensity of disintegration when creating appropriate machines.

References

1. **V.S. Blohin, V.I. Bolshakov, N.G.** Malich Osnovnye parametry tehnologicheskih mashin. Mashiny dlya dezintegracii tverdyh materialov: Uchebnoe posobie ch.1 – Dne-propetrovsk; IMA - press.- 2006. - 404s.

2. **Vasilev L.M., Vasilev D.L., Malich N.G., Angelovskij A.A.** Mehanika obrazovaniya form razrusheniya obrazcov gornyh porod: Monografiya.- Dnipro, IMA-press.-2018-172s.

3. **N.G. Malich** Nauchnye osnovy razvitiya rascheta parametrov mashin dlya zemlyanyh rabot v gorno-metallurgicheskom komplekse. Monografiya-Dnepropetrovsk, IMA-pres.-2010 -380s.

4. **Lejbenzon L.S.** Kurs teorii uprugosti.-M.-L.:Gosizdat,1977.

5. **Vinogradov V.V.** Geomehanika upravleniya sostoyaniem massiva vblizi gornyh vyrabotok / **V.V. Vinogradov**. – K.: Naukova dumka, 1989. – 192 s.

6. **Kirnichanskij G.T.** Elementy teorii deformirovaniya i razrusheniya gornyh porod / **G.T. Kirnichanskij**. – K.: Naukova dumka, 1989. – 184 s.

7. **Vasilev, L.M.** Uchet kontaktnogo treniya v zadache o razrushenii gornyh porod szhatiem /**L.M. Vasilev, D.L. Vasilev** // FTPRPI. – 2015. – № 3. – S. 48- 56.

8. **Zorin A.N.** Mehanika i fizika dinamicheskih yavlenij v shahtah / **A.N. Zorin, V.G. Kolesnikov, K.K. Sofijskij**. – K.: Naukova dumka, 1979. – 169 s.

9. **Baron A.I**. Gornotehnical porodovedenie / **L.I. Baron**. – M.: Nauka, 1977. – 324 s.

10. **Panasyuk, V.V.** Predelnoe ravnovesie hrupkih tel s treshinami / V**.V. Panasyuk.** – K.: Naukova dumka, 1968. – 246 s.

11. **Storozhev M.V.** Teoriya obrabotki davleniem / **M.V. Storozhev, E.A. Popov – M.**: Mashinostroenie. 1967 – 423 s.

12. **N.G. Malich , L.M. Vasilev, O.A.** Usov Issledovanie vliyaniya parametrov nagruzheniya na raspredelenie napryazhenij, dejstvuyushih pri razrushenii shihtovyh materialov v drobilkah // Metallurg. i gor-norudn. prom-st.-2015.-№7.-S.99-106.

https://doi.org/10.31713/m1029

RESEARCH OF THE POSSIBILITIES OF USING URBAN GREEN SPACES IN DONBASS CITIES TO RECREATE THE RESOURCE STATE OF THE MINING REGION

V. Sokolenko
Volodymyr Dahl East Ukrainian National University, Candidate of technical science, Associate Professor, Ukraine

M. Filatiev
Volodymyr Dahl East Ukrainian National University, Doctor of Engineering Sciences, Associate Professor, Ukraine

K. Sokolenko
Volodymyr Dahl East Ukrainian National University, Postgraduate student, Ukraine

S. Piddubnyi
Volodymyr Dahl East Ukrainian National University, Senior Lecturer, Ukraine

Annotation

Ukrainian Donbass has crossed the peak of extensive growth. Today this industrialized urbanized region has faced with a complex of problems. Sustainable urban development cannot be based only on the exploitation of natural raw materials. The task is to build a balanced model for the development of an industrial region, when the criteria for success are the quality of the environment, urban development, human potential. The exploitation of the resource base must be compensated for by the preservation of the environment. The natural landscapes of Donbass have been partially destroyed, partially changed by economic and industrial activities. There is a need to reproduce adapted green landscapes of cities in order to improve the ecological situation and restore the landscape and recreational potential of the territories. Alchevsk is in many ways the median city of Donbass. The subject of the study has chosen the green spaces of the city of general use, limited and special purpose for a period of more than 25 years, that is, the duration of the General Plan. **The goal of research** is to determine the species composition of green spaces typical for the cities of the Luhansk region and the establishment of a group of plants that are maximally adapted to independent growth in the urban landscape. The geographical, climatic and orographic characteristics of the city are considered,

the analysis of the quantitative and qualitative state of the city's green spaces is carried out. The sample also covers areas of disturbed territories of waste heaps, industrial zones, landfills. Analyzed the retrospective and prospective urban planning policy in the development of green spaces, and the overall results. The actual species composition of trees and shrubs growing in the city areas has been determined. There are 44 species of trees and 20 species of shrubs registered in the city. It is desirable to spread the species composition of trees and shrubs that are used for landscaping at the expense of species that feel good in the city.

The results of the study can be taken into account in the development of measures for the greening of urban areas and the restoration of ecologically disturbed urban areas of industrial cities of the Luhansk region.

Introduction

Ukrainian Donbass is an industrial region formed on the basis of the development of the mining and metallurgical complex. A set of conditions and factors contributed to the rapid development of the region, primarily through the exploitation of natural resources. At the initial stage, these were raw material deposits, primarily coal. The metallurgical industry needs a wide range of materials and raw materials - mainly mineral. The industry produces huge volumes of industrial waste and environmentally harmful emissions. According to historical standards, a region instantly emerged, in size and population, on an industrial scale larger than individual European states [1]. But we can note the imbalance in the growth of the region, the colonial type of use of its raw materials, which led to a complex of problems: socio-political, economic, environmental [2]. At this time, the situation is complicated by an armed conflict with external intervention. Suppose that if there is political will, an armed conflict can be resolved in a short time. Unfortunately, however, environmental issues are not solved with paper-based solutions. Considering Donbass as a mining region focused on an exclusively industrial character of industrial development means its rapid decline. It is necessary to focus on the sustainable development of territories, human potential, preservation and restoration of the ecological state of the environment as the main factors of development and the resource base of the region. Industrial development should ensure the ecological balance of the territory. Now the agglomerations of Luhansk and Donetsk regions form a continuous network of settlements and industrial zones, cut natural landscapes, destroy and displace them [3, 4].

A decrease in industrial potential, the decline of mono-industrial cities are recorded. The violated territories are increasing. A paradox is created when there are large areas of abandoned territories, and a shortage of reserve territories for the development of populated areas. The task is to preserve the urban green landscapes of urbanized agglomerations, the reproduction and development of adapted green spaces. The forestry of the region is predominantly artificial, but there is accumulated experience, the goals and objectives of functioning have been determined. In cities, full-fledged scientific observations are episodic. In many cases, local authorities provide planting of flower beds and sanitary pruning of trees.

The goal of research is to determine the species composition of green spaces characteristic of the cities of the Luhansk region and to establish a group of plants that are maximally adapted to independent growth in the urban landscape.

To achieve the goal, it is necessary to solve the following tasks:

Analyze the quantitative and species composition of public green spaces in the city;

Calculate the compliance of green areas with the state buildings code requirements on the general plan of the city of Alchevsk;

Determine the species of trees and shrubs that normally grow and reproduce on the territory of the city without additional guardianship;

Develop general recommendations for improving the quantitative and species composition of green spaces in the city to improve the ecological state of the urban area.

The methodology provides for the analysis of the compliance of the number of green spaces in urban areas of general use with the requirements of state building codes. Based on long-term observations of city areas that are not subject to sanitary cleaning or the cultural influence of urban utilities, the species of trees and shrubs that grow and reproduce independently are determined. The article analyzes the existing and design solutions of the general plan of the city of Alchevsk in the current state and perspective urban planning forecast. Typical elements of the urban planning structure were selected for the study. This is one of the city's microdistricts, areas of green spaces within sanitary protection zones, separate

public gardens and public parks, green spaces of schools and kindergartens, green spaces of streets. Thus, a high representativeness of the observation sample was achieved in terms of time span and in terms of the quantitative and species composition of green spaces.

Main Body.

Ukrainian Donbass today - an industrial tired region, overloaded with the problems of unbalanced growth, has gone into decline. Historically, within a short period of time, the former Wild Field turned into an urbanized industrial region [1].

It can be considered that the development of the region took place in a colonial way, when the territorial resource was used to the maximum, without reservations for future development / state.

The history of the development of Donbass, factors, circumstances, prerequisites for its existence have been studied by many scientists [1,5,6,7]. The territory of the region is 53.2 thousand sq. km., the population of the Luhansk and Donetsk regions is 6,260,000 people together, which is comparable to the size of individual European states. Among 47 European countries, 27 have a population of less than 6 mln. person [4].

The level of urbanization in Luhansk and Donetsk regions is the largest in Ukraine. As of 2014, the percentage of the urban population of the regions reached 80-90%.

Accordingly, in the modern period, Donbass is faced with a complex of severe environmental problems, which include general pollution of the territory, pollution of water resources, degradation of small rivers and reservoirs, a large volume of territories occupied by heaps, dumps, landfills for storing industrial waste, solid waste. In the cities of Donbass, the curtailment of the industrial base is recorded, caused by objective factors. The industrial zones of the cities were formed according to the redundant principle. Similar enterprises in developed countries occupy territories that are several times smaller [6]. Since most of the enterprises during the Soviet era were focused on the production of military products, or had a narrow specialization in the national economic balance, now such enterprises have been stopped. Plots of cities are turning into wastelands. A paradoxical situation is created - there is not enough territorial

resource for sustainable development, but there are large territories that are unusable or abandoned.

An example is the general plan of Alchevsk, which provides for development at the expense of a residential zone, partly a green zone, despite the fact that there are large areas of the so-called inconvenient industrial areas. Unfortunately, capital has the ability to influence decision-making, and chooses not an environmentally friendly option, but a profitable option, when the city's territory is used, green zones that are most convenient for quick development. [8]

The territory of the Luhansk and Donetsk regions is predominantly steppe, 70% of the forests here were planted artificially. The main function of plantations in the Donbass is to protect the land from dust storms and erosion. Some of the Soviet plantations still need to be updated, another part, mainly oak and pine plantations, is drying up. There are no industrial forests in the region, which means that the Donbass forest needs full state funding. Local administrative forestry enterprises are able to sell wood mainly from sanitary felling, which is cheap firewood. According to the estimates of the State Forestry Agency in Donbass, over the past three years there have been 1,068 fires on an area of more than 16,000 hectares, which is about 15% of all forest plantations in the region.

Most of them cannot be restored yet due to mined areas. Losses from forest fires amount to almost 50 million hryvnias. The forest fires of summer 2020 were especially dangerous. However, the greatest harm from fires is not material, but environmental, because the forests of Donbass, first of all, should perform an environmental function.

In 2020, tens of thousands of hectares of forests burned down as a result of anomalous causes, which were probably artificially used in the context of an armed conflict. It also damaged the nature and ecology of the region.

The Donbass region has always belonged to the zone of risky agricultural use.

The steppe zone, poor in water resources in the conditions of archaic agriculture, could not provide a large number of the population. The borderland at the intersection of trade routes and zones of influence of several state formations - the Ukrainian

hetmanate, the Crimean Khanate, Moscovia, the Caucasus caused the absence of a centralized power with cities, consolidated the status of the territory.

Human civilizational activity has changed the natural climatic landscape of Donbass. For a century and a half, instead of a sparsely populated rocky steppe, an urbanized industrial region was formed. Natural flora and fauna partially adapted, partially transformed (Fig. 1).

The task is to assess the prevailing conditions and determine the most adapted types of green spaces that are able to reproduce local natural landscapes.

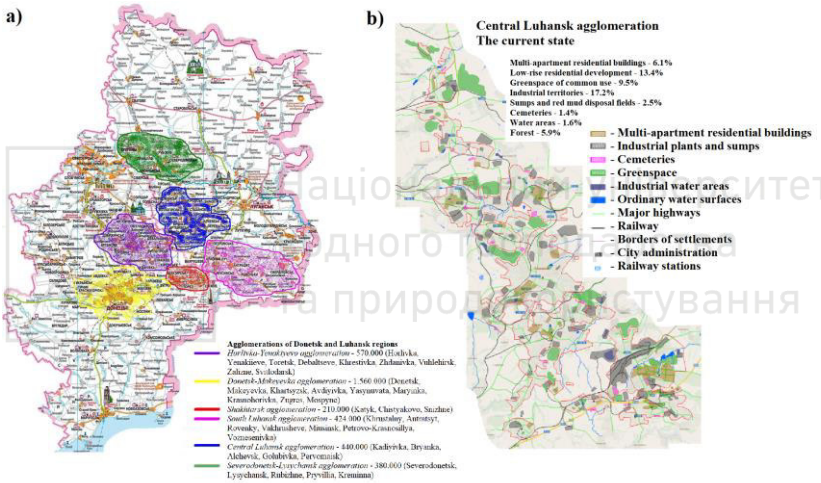

Fig. 1. *a* - the agglomerations of Donetsk and Luhansk regions; *b* - the scheme of the division of the Central Luhansk agglomeration

Changes in the natural landscape due to the nature of the industry prevailing in the Donbas. The mining and metallurgical complex was characterized by large volumes of consumption of mineral resources, huge volumes of industrial waste. The basic mode of transport for industrial needs is the railroad. The landscape has acquired the characteristic features of human activity. The visiting card of the region is waste heaps. Now their number reaches 1200. Large areas are occupied by rock and slag dumps, sludge collectors, landfills, dumps. It can be argued that the territories suitable for urban planning activities are generally used. There are no significant

reserve territories left. That is, the stage of extensive development should be changed to rational, economical and careful use of the existing territories of urban and rural settlements with the aim of their sustainable development [7,9,10]. There are two options, the first is artificial. With the availability of modern technologies, it is possible, conditionally, to grow any types of plants. For example, exotic palms. But this comes at a fixed cost. The second option is to determine the types of plants, green spaces that feel comfortable in the prevailing conditions and are able to provide a green balance of the territory at minimal cost.

Analysis of experimental data. At present, no work has been carried out in the city of Alchevsk to determine the species composition of existing greenery, their distribution by age and suitability for further use.

This paper presents the results of research to determine the species composition of existing greenery, their distribution by age and suitability for further use. Surveys of green areas were conducted in the city of Alchevsk in the period from 2010 to 2014. The period of existence and formation of the studied green areas began in 1990.

Alchevsk is a city of regional subordination, located in the west of Luhansk region, 46 km from Luhansk on the line Rodakove - Debaltseve and the highway M 04 Znamyanka-Donetsk-Izvaryne.

The territory of the city within the existing city boundary is 4901.0 ha, according to the reference plan - 5170 ha [11].

The economic complex of the city is multi-branch. The structure of the economy is formed by the following industries: industry, construction, external transport, services. As of 01.01.2008, about 52.3 thousand people were employed in all types of economic activity on the territory of the city, according to the regional statistics department [11].

Alchevsk is a significant cultural center that serves not only the population of the city itself, but also nearby settlements. The city has a number of research and design institutes, universities and special educational institutions, cinemas, palaces and houses of culture, cultural and leisure centers. The city has a stadium, sports facilities and complexes.

The city borders on the south - with the city of Perevalsk, on the north, east and west - with the lands of Perevalsk district.

Alchevsk is part of the Alchevsk-Stakhanov settlement system, which is formed in one of the most urbanized regions of Donbass - the south-western part of Luhansk region.

The population of Alchevsk is one of the medium-sized cities of Ukraine.

The current population of the city at the beginning of 2014 - 110 thousand people.

The housing stock of the city of Alchevsk is 2689.1 thousand m2 of the total area, including multi-apartment - 80.7%, manor-type - 19.3%.

The average housing supply in the city of Alchevsk is 23.2 m^2 per capita.

The main industries of the city are metallurgy and coke industry. The main enterprises of the city are PJSC "Alchevsk Metallurgical Plant" and PJSC "Alchevskkoks".

The area of existing parks and public gardens in the city is 84.0 hectares. Taking into account the approximate level of landscaping of 80% of the existing plantations, the area of landscaped public areas is 67.0 hectares.

Provision of the city population with green areas of common use - 5.7 m^2 / inhabitant.

The territory of Alchevsk is located in the northern part of the steppe Donetsk physical-geographical region, on the northern slope of the Donetsk ridge, in the basin of the White and Lozova rivers (both are right tributaries of the Luhanka River), on their watershed divided by a ravine system. Most of the city is located in the Lozova River basin.

Orographic conditions of the territory are as follows. The surface of the territory is characterized by a very rugged relief (the depth of intersection reaches 180 m) and a developed ravine network, which led to its significant erosion. In the submeridional direction, the city is crossed by a large branched Dovzhik gully with a watercourse regulated by a cascade of ponds - Yashchykivska, Likarnyany, Shkilny, Vasylivsky, Pershiy and Druhy Orlov. Temporary and permanent flows are observed in the thalwegs of other gullies. Absolute marks of the territory within the city are 122 - 290 m, with a decrease to the bottom of the gullies and the minimum values in the water cut of the ponds.

Within the city there are significant areas occupied by eroded steep slopes (with surface slopes of 15% or more) of a natural nature. As a result of intensive economic activity, the natural landscape has undergone radical changes and the manifestation of man-made landforms in the city (dumps, accumulating spoil tip, etc.).

Hydrological features. The territory of the city of Alchevsk is located on the watershed between the rivers Lozova and Bila, which are right tributaries of the river Lugan. An unnamed stream flows through the town from southwest to east in the Dovzhik gully, which flows into the Bila River near the village of Mykhailivka. In the north of the city there is a Kalinov gully, which flows into the river Lozova.

The main source of water for watercourses and reservoirs is atmospheric and groundwater. Therefore, their hydrological regime is characterized by spring level rise during floods and prolonged low-water lows with individual torrential floods. The peak of spring floods is observed in the second and third decades of March. The limit is set in April and lasts 6-7 months (the lowest levels are observed in summer - in July - September, in winter - in December - January).

The surface waters of the city are supplemented by a network of ponds: Yashchykivska, Likarnyany, Shkilny, Vasylivsky, Pershiy and Druhy Orlov. Reservoirs of the First and Second Eagle Ponds are promising for recreational use, but have unsatisfactory sanitary condition, partially silted and swampy shores and need rehabilitation.

The only place for recreation of locals is Isakovskoe reservoir. It was created by blocking the White Dam in order to provide technical water supply for industrial enterprises of the city.

The reservoir stretches from north to south along a length of 6.95 km. The length of its shoreline is 15.2 km (excluding the shore of the mouth of the White River). The average depth of the reservoir is 5.75 m, the maximum is 16.7 m. With a normal supporting horizon (110.04 m), the area of the reservoir is 2.64 km^2, the capacity is 20 million m^3 of water. It is fed by meltwater, stormwater and river runoff. Precipitation does not have a significant effect on nutritional conditions, as very large losses on evaporation and filtration. The level of filling of the reservoir depends on the water content of the year, in this regard, the provision of depths is different. The bowl is

located in Carboniferous deposits and is hydrogeologically characterized by a low level of underground supply.

Climatic conditions of the district are characterized by greater continentality (compared to other steppe regions of Ukraine) and aridity.

A brief description of climatic conditions is given by the average annual data of long-term observations of the main meteorological indicators at the meteorological stations Debaltseve and Popasna.

The air temperature is 6.7 °C. The absolute maximum temperature is 39°C. The absolute minimum temperature is minus 38°C. The duration of the frost-free period is 166 days.

Estimated temperatures: the coldest 5-day - minus 26°C - winter ventilation - minus 11.7°C.

The heating period is 189 days.

Its average temperature is minus 2.3°C. Depth of soil freezing avg./max. - 60 cm / 105 cm. Relative humidity - 75%. Precipitation (including during the warm period) - 525 mm (338 mm). The maximum height of snow cover is 30-35 cm. Dominant winds, their frequency:

eastern - 17.3%;
northeastern - 15.8%;
south-eastern - 14.6%.

The wind speed is 5.1 m/s. The largest winds are possible: annually - 25 m/s; 1 time in 5-10 years - 29-31 m/s; 1 time in 15 - 20 years - 32 m/s. Special atmospheric phenomena (average / maximum number of days) from:

fog - 106/143;
blizzard - 22/42;
thunderstorm - 29/40.

It should be noted that the wind regime in the city is relatively favorable in terms of conditions for the transfer of emissions from sources of pollution - the main sources are located west of housing in the city, in the same direction and dominated by the transfer of pollution of the main industrial zone.

The area has a high natural potential for air pollution and is characterized by unfavorable meteorological conditions for dissipation of emissions into the atmosphere.

In accordance with the zoning of climatic and construction purposes the territory belongs to III B of the climatic zone of the eastern steppe [1].

The complex geological structure and intersection of the relief, different conditions of humidification of the region have led to the heterogeneity of the soil cover of the city. The heterogeneity of soil formation conditions led to the formation of a large number of soil varieties, among which about 90% belong to chernozem.

According to the agro-climatic zoning of Ukraine, the territory of the city is located in the Donetsk steppe province, which is characterized by chernozems and sod gravelly soils formed on the eluvium of sandstones and shales. The soil cover is dominated by chernozems of medium and low humus, mainly on forest rocks, sod gravelly on the eluvium of non-carbonate rocks and chernozems gravelly on the eluvium of sandstones, sandy-clay and clay shales.

The mechanical composition of soils, which largely determines the level of their fertility, varies from light loam to light clay varieties, heavy loamy and sandy-medium loamy, gravelly soils predominate.

Soils on the slopes are eroded; soil erosion is 48-80%.

Their level of natural fertility is high, but due to the intersection of the terrain the soils are very eroded. In addition, the specialization of the economy has led to extreme disturbance of soils (dumps, settling tanks, heaps, etc.).

Highly fertile meadow and meadow-chernozem soils were formed in the floodplain and in the bottoms of watercourses.

In accordance with the geological structure of mineral resources of the region are represented by building limestone, brick and tile raw materials, coal deposits. However, there are no mineral resources of industrial significance within the city.

According to the economic service of PJSC "AMK", the metallurgical complex of the city works mainly on imported raw materials: Kryvyi Rih iron ores, Nikopol manganese ores, Chasovyarsky sand, etc.

The results of experimental data processing. The main parameters of the territories occupied by green plantations of different types within the settlements are regulated by the state building code[12].

According to Table 5.1 [12], the area of green areas per inhabitant of the city should be 12 m^2.

The share of green areas for various purposes within the city development (the level of landscaping) must be at least 45% for district III-B. In the city there are enterprises of the I class of harmfulness therefore according to appendix 1 to table 5.1 it is necessary to increase the resulted norms of city-wide green areas by 15-20 percent.

Thus, for the city of Alchevsk, the area of green areas per capita should be 12 $m^2 \times 1.15 = 13.8$ m^2.

The nomenclature of structural elements of the territory of the complex green zone of the city is determined according to appendix. [12]

City gardens, parks, squares, boulevards, forests within the city are public greenery.

Green areas of city streets and roads, streets of local significance, squares, transport interchanges and parking lots are green areas of special purpose.

Greenery in the city is divided into:

- urban forests green areas of common use area of 602.6 hectares;
- public green spaces - parks, forest parks, squares, boulevards;
- green areas in residential area and microdistrict without driveways, playgrounds and sports grounds are green areas of limited use;
- green spaces of limited use and special purpose on the territories of preschool and school educational institutions, higher educational institutions, medical institutions, sports and sports facilities, cultural institutions, trade enterprises, public catering and household services, nurseries, cemeteries;
- green spaces of limited use and special purpose in industrial, communal and warehouse territories in sanitary protection zones of enterprises of protective purpose.

The territory of public parks and squares located in the city of Alchevsk is 118.812 hectares.

There are 276 streets and alleys in the city of Alchevsk. It is not possible to survey green areas on all city streets. But, most likely, it is not necessary.

Elements of the planning structure typical for the city were selected for the survey. This is one of the city's 400 microdistricts, which is typical in its territory, timing and type of development.

For the survey of the streets, typical building streets were selected, which cover the entire territory of the city.

These are streets that cross from east to west and from north to south of the city and form a continuous line.

From east to west Metallurg Avenue - Lipovenka Street - Leningradskaya Street. Lenin Street is also Frunze Street.

From north to south of Hmyria and Gorky streets in the area from the transport tunnel to Zaporizhzhya, Kalinin and Kirov streets.

In the area of typical buildings of the 50-60s of the last century, three more intersecting streets were taken. These are Lenin Avenue, Belinsky Street and Moskovskaya Street.

Thus, by conducting a survey of 12 streets of the city, it is possible to get an idea of the quantitative and qualitative state of greenery of the street network of the city.

For the streets of the city of Alchevsk per 1 km of the street there are 0.9799 hectares of green areas for general and special purposes.

The area of the residential district 400 is 22.6754 hectares.

In addition, for the analysis of green areas of general use and special purpose were used materials of inventory of green areas, made to order KP "Alchevsk road maintenance site" in 2013 for the following objects:

- Square on the square of the 30th anniversary of the Victory;
- Belinskoho Street;
- Lenin street;
- Lenin Avenue;
- Lipovenka Street.

Materials of field surveys of green areas, conducted in 2011 in the neighborhood 400.

Green areas of limited use and special purpose on the territories of preschool and school educational institutions, out-of-school institutions, higher and special educational institutions, medical institutions, cemeteries of Alchevsk were surveyed with the help of inventory documents for land use and topographic survey of 1: 2000 scale. Acts of inspection of green plantations on the territories of

objects for which they were performed were also used. The total area of greenery is 63.8592 hectares.

The composition of green plantations of limited use and special purpose is determined.

A significant part of green areas in residential areas and public facilities, in recreational areas, along city streets, in enterprises and adjacent areas, as well as green areas for special use, are in satisfactory condition.

In total, 44 species of trees and 20 species of shrubs were registered in the surveyed area [13].

Trees near residential buildings, along the city streets have such a species composition (the order of change in the breed of the breed, the number of which is 2%):

- Acer platanoides - 14.54%;
- The horse chestnut (Aesculus hippocastanum) - 12.37%;
- The black poplar (Populus nigra) - 9.31%;
- European ash (Fraxinus exceisior) - 9.06%;
- small-leaved lime (Tilia cordata) - 6.88%;
- black locust (Robinia pseudoacacia) - 5.11%;
- Armenian plum (Prunus armeniaca) - 4.85%;
- Chinese elm (Ulmus parvifolia) - 4.8%;
- Poplar Bolle (Populus bolleana Louche) - 3.2%;
- Robinia (Robinia pceudoacacia f. umbraculifera) - 3.12%;
- Ash-leaved maple (Acer negundo) - 2.88%;
- Poplar canadian (Populus canadesis) - 2.27%.

By breed composition, the largest groups, more than 5%, are, maple (6 varieties) - 18.4%, poplar (5 varieties) - 17.56%, ash-tree (2 varieties) - 9.22%, locusts (2 varieties) - 8.23%, lime - 6.88% and elm (2 varieties) - 5.43%.

In total, the above 12 species of trees 27.27% of the number of species occupy 78.39% of the total number of trees.

Shrubs near residential buildings and along city streets have the following breed composition (listed in descending order of the proportion of the breed, the number of which exceeds 2%):

- Ligustrum vuigare - 89.61%;
- Sirsnga vulgaris - 3.29%.

The number of these shrubs changes from 1.88% to 0.01%.

Two types of shrubs store 92.9% of the total number.

The general condition of the trees is as follows:

- in the norm - 57.1%;
- require sanitary pruning - 24%;
- need rejuvenation - 11.5%;
- trees need to be removed - 7.4%

Most of the black poplar trees (more than 15% of the structural composition) are over 40 years old. Poplars are short-lived plants that are allergens (poplar down is a strong allergen). Also, these trees are largely damaged by the crown, skeletal branches and central conductor. Plants of this group should be gradually replaced by trees of another group.

Robinia and maple have damage to the crown and skeletal branches due to freezing, but much less than poplars. This requires sanitary pruning.

Other trees generally withstand the climatic conditions of the city of Alchevsk, do not have significant damage and need only appropriate sanitary pruning and rejuvenation.

To determine the species of trees and shrubs that reproduce in the city without human assistance, three sites were identified on which no economic activity was carried out. In 2016, a survey of green areas grown there was conducted at these sites. In the city of Alchevsk, elm, small-leaved, pinnate-branched and ash-shaped maple grow independently, which literally fill free areas (black elder), sharp-leaved maple (Canadian), robinia (white acacia), pyramidal poplar and black poplar, prickly dog rose [13].

To create new greenery and reconstruction of existing ones, it is desirable to expand the species composition of trees and shrubs. More to plant ailanthus, aronia, bitter cherry, gentian, walnut, mountain ash, pole, catalpa, silver sucker, Crimean pine, here, thuja, barberry, elderberry, hawthorn, viburnum, rose hips, dog rose shrubs. Additionally, introduce trees and shrubs that feel great in the city and are already used in forest plantations. These are buckthorn, buckthorn, pedunculate oak, Scots pine.

The number of green areas in the city does not meet the standards, it would be necessary to create additional ones. [8] The area of green areas for public use in the city is 118.8120 ha, 84 ha according to the Master Plan. According to the Master Plan, there is 5.7 m^2 per one inhabitant of the city, according to the materials of the survey 10.75

m^2, according to the standards there should be 19.5 m^2, or 220.3 ha of public green areas.

For the city of Alchevsk, the development of the Master Plans of the city has been carried out since 1946. The Kyiv Institute of Urban Design "Dipromisto" for the city Master plans were developed in 1968, 1993, 2011. [8] All these Master Plans pursued a single urban policy, including the placement of greenery.

The approved Master Plan of the city [8] provided for increasing the number of green areas for public use to 19.5 m^2 per capita. Based on the prospective population, which was provided for in the master plan at the end of the calculation period, the area under public greenery was to be 347.4 hectares.

The master plan provided:

- creation of large-scale territories of green zones of 78.8 and 64.8 hectares in new areas of multi-storey buildings (Eastern 1 and Eastern 2);
- the central city park was planned to be created on the basis of Victory Park, with the expansion of its territory by 90 hectares;
- other green areas (parks, squares and boulevards).

The organization of the parks, which were outlined in the master plan, was not carried out.

To provide the residents of Alchevsk with the required number of green areas for public use, it is necessary to create additional green areas in the middle or near residential buildings so that in each residential area there is a park within walking distance. It is desirable to arrange the areas of squares within the neighborhoods in such a way that the green areas of schools, kindergartens and squares are united in one massif.

To organize new parks and gardens, use the existing green areas of the Sarmatian beam, located along the eastern border of districts 58 and 59.

Within the recreational zone, create a Forest Park around the Orlovykh Ponds, which will be at a distance of pedestrian accessibility from the multi-storey residential buildings of the district's 58, 59, 399, 400, 401 of the eastern part of the city.

In the northern part of the city to increase the territory of existing forests around the villages of Administrative and Briquetting. Additionally, plant 40 hectares of forest north of the slag dump of the

metallurgical plant on Pivnichna Street in the free area between the forest tract and the Kalinov beam.

The zone of green plantations, both existing and projected, unites practically all functional zones of the city. It is formed from the existing green areas around the Hospital, School, Eagle ponds, areas that are planned to be transformed into meadows, parks, boulevards, green beams within the city. Landscaping of sanitary protection zones, organization of green passages along the streets, which together with large green spaces of parks, forests, meadows create a single system, a kind of ecological framework of the city.

The main green areas are planned to be located along the Eagle Ponds and in the northern part of the city.

Taking into account the approximate level of landscaping of existing parks and squares by 80%, the area of green public areas is 95.0 hectares.

There is 8.6 m^2 of green areas per capita, which is much lower than the norm [12].

The calculation of the required area of public green areas is performed for the population of the city in the future in accordance with the state building code [12]. The calculation is performed for the prospective population of the city within the existing and prospective limits for the calculation and urban planning forecast.

Given the existing green areas of public use - 95.0 hectares, it is necessary to organize new green areas of public use:

- for the settlement period - 162 hectares;
- on the town-planning forecast - 166 hectares.

Thus, according to the decisions of the master plan, the territory of parks, squares, boulevards of public use in the city will be about 368 hectares, including green areas of public use - 278 hectares.

Per 1 inhabitant, in the future, green areas of common use will be 22.2 m^2 (against 20.8 hectares according to the standard).

Conclusions.

Based on the results of this work, it is possible to draw the following conclusions.

The actual area of green areas for public use in parks, gardens, boulevards, forests within the city, which is 602.6 hectares of forests and 95.0 hectares of parks, gardens, boulevards.

The actual area of green plantations of limited use and special purpose in the territories of preschool and school educational institutions, higher educational institutions, medical institutions, cemeteries are determined.

On the territory of schools' green plantations occupy 10.0680 hectares - 31.1% of the territory. The average area of land per school is 1.9038 hectares, green areas 0.5922 hectares.

On the territory of out-of-school institutions green plantations occupy 3.3047 ha - 35.4% of the territory. The average area of land per out-of-school institution is 1.0376 ha, green areas 0.3672 ha.

On the territory of preschool educational institutions green plantations occupy 5.9639 hectares - 32.0% of the territory. The average area of land per preschool is 0.7159 hectares, green areas 0.2294 hectares.

On the territory of higher educational institutions green plantations occupy 7.6991 ha - 34.0% of the territory.

On the territory of medical institutions green plantations occupy 18.6160 ha - 59.1% of the territory.

On the territory of cemeteries 101.1695 green plantations occupy 18.2075 ha - 18.0% of the territory.

We consider it possible to use certain areas of greenery for a school, preschool educational institution, out-of-school educational institution when calculating the balance of the territory for cities with a population of 100-150 thousand inhabitants [13, 14].

For the city streets, the average area of greenery per 1 km of street length is determined, which is 0.9799 ha of green spaces for general and special purposes. The actual non-compliance of the total areas of green plantations with the standards established by the DBN can be considered a constant trend. Normative values of the number of areas of green plantations in accordance with DBN -13.8 m^2 and the General Plan of the city - 19.5 m^2 per capita were not achieved.

In the city there are enterprises of the I class of harmfulness therefore it is necessary to increase the resulted norms of city-wide green territories by 15-20 percent. Given the existing green areas of public use - 95.0 hectares, it is necessary to organize new green areas of public use: - for the calculation period - 162 hectares (increase by 70%); - urban forecast - 166 hectares (increase by 75%) [8,13].

The actual species composition of trees and shrubs growing on the city streets and on the territory of the typical city district has been determined. There are 44 species of trees and 20 species of shrubs registered in the city. The species composition of trees and shrubs used for landscaping is desirable to expand due to species that feel good in the city.

The results of the study can be taken into account in the development of measures for landscaping of urban areas and restoration of ecologically disturbed urban areas of industrial cities of Luhansk region.

References

1. **V. B. Molchanov**, Ukrai'ns'kyj Donbas – ekonomichne dyvo drugoi' polovyny XIX – pochatku XX st., Grani istorii': zb. nauk. prac'. Special'nyj vypusk – materialy II Vseukrai'ns'koi' naukovo-praktychnoi' konferencii' «Bahmuts'ka starovyna: krajeznavchi doslidzhennja – 2018», 1(9), 103-113 (HIFL, Bahmut, 2018)

2. **V. Zh. Popov**, Pasynky proletars'koi' revoljucii': robochi mista Ukrai'ny v umovah gumanitarnoi' katastrofy 1917–1920 rr., Grani istorii': zb. nauk. prac'. Special'nyj vypusk – materialy II Vseukrai'ns'koi' naukovo-praktychnoi' konferencii' «Bahmuts'ka starovyna: krajeznavchi doslidzhennja – 2018» 1(9), 121-126 (HIFL, Bahmut, 2018)

3. **N.M. Demyn**, Gorodskye aglomeracyy v kontekste yssledovanyja fenomena form y system rasselenyja, Mistobuduvannja ta terytorial'ne planuvannja: Nauk. - tehn. zbirnyk, 45(1), 3-15 (KNUCA, Kyiv, 2005)

4. Mis'ki aglomeracii' Ukrai'ny, https://uk.wikipedia.org/wiki/Міські_агломерації_України Accessed 25 October 2020

5. **S. Kul'chyc'kyj, L. Jakubova, Donechchyna i Luganshhyna** u XVII-XXI st..: istorychni faktory j politychni tehnologii' formuvannja osoblyvogo ta zagal'nogo u regional'nomu prostori (NASU Institute of History of Ukraine, Kyiv, 2015)

6. **A.P. Ositnjanko**, Planuvannja rozvytku mista (KNUCA, Kyiv, 2001)

7. **V. A. Jacenko**, Teoreticheskie i prakticheskie idei novogo gradostroitel'stva Donbassa: ikh proshloe, nastoyashchee i budushchee, Mistobuduvannja ta terytorial'ne planuvannja: nauk.-tehn. zb., 21, 359-366 (KNUCA, Kyiv, 2005)

8. Alchevs'k Lugans'koi' oblasti. General'nyj plan. Derzhavne pidpryjemstvo Ukrai'ns'kyj derzhavnyj naukovo-doslidnyj instytut proektuvannja mist «Dypromisto». 2010 r.

9. **Ye.Ye. Klyushnychenko**, Rekonstruktsiya zhytlovoyi zabudovy (KNUCA, Kyiv, 2000)

10. The Law of Ukraine "On the Complex Reconstruction of Quarters (Microdistricts) of an Outdated Housing Fund"

11. Lugans'ka oblast' u cyfrah. Statystychnyj zbirnyk. Derzhavnyj komitet statystyky Ukrai'ny. Golovne upravlinnja statystyky u Lugans'kij oblasti. Lugans'k 2006-2012 rr.

12. DBN B.2.2-12:2019, Planning and building of territories (Ministry for Communities and Territories Development of Ukraine, Kyiv, 2019)

13.**V.M. Sokolenko, O.E.** Podljevs'kyj, analiz kolichestvennogo i kachestvennogo sostojanija zelenyh nasazhdenij na territorii zhiloj zastrojki goroda Alchevska Luganskoj oblasti, Zbirnyk naukovyh prac' Donbas'kogo derzhavnogo tehnichnogo universytetu, 1(46), 94-101 (DonSTU, Lysychans'k, 2017)

14. **Yu.N. Belokon'** Regional'noye planirovaniye - teoriya i praktika. (Logos, Kyiv, 2003)

https://doi.org/10.31713/m1030

HYPOCHLORITE GOLD LEACHING AN ALTERNATIVE TO CYANIDE TECHNOLOGY

Prokopenko V.A.
F.D. Ovcharenko Institute of Biocolloidal Chemistry NAS of Ukraine, Kyiv, Ukraine; doctor of technical sci., director

Chernenko V.Yu.
National Technical University “Igor Sikorsky Kyiv Polytechnic Institute”, Kyiv, Ukraine; cand. med. sci., professor assistant of Chemical Technology Faculty

Vorotytsky P.V.
F.D. Ovcharenko Institute of Biocolloidal Chemistry NAS of Ukraine, Kyiv, Ukraine; graduate student

Tsyganovich O.A.
F.D. Ovcharenko Institute of Biocolloidal Chemistry NAS of Ukraine, Kyiv, Ukraine; PhD, deputy director on scientific work

Volobaiev I.I.
F.D. Ovcharenko Institute of Biocolloidal Chemistry NAS of Ukraine, Kyiv, Ukraine; PhD, researcher

Abstract

Traditional technologies of gold mining are exhausted due to the depletion of stocks of conditioned raw materials at functioning gold mining enterprises, in addition, the preservation or disposal of large-scale waste of these technologies requires significant financial costs for environmental protection measures.

Recently, the search for alternative methods of gold leaching, which involve the use of non-toxic factors, but which in their physicochemical properties can compete with traditional levels, and especially with cyanides.

The authors of this work investigated the mechanism and kinetics of the process of dissolving metallic gold in chloride-hypochlorite solutions and believe that alkali metal hypochlorites (first of all, sodium hypochlorite NaOCl, which is easily obtained by electrolysis from a solution of food's salt NaCl, or from sea water) are a very promising replacement for cyanide-containing leachates. Two series of experiments were carried out to study sodium hypochlorite as a gold leaching agent using a traditional gold disk and finely dispersed native gold as dissolution objects. Found fundamental differences in methodological techniques when working with a traditional model object and native gold.

The dependences of the dissolution rate on the solution pH, sodium hypochlorite concentration, and temperature are determined. Conditions of the gold surface passivation during its dissolution are discussed. The first-order rate constant of the gold dissolution $k_i = 0{,}079 - 0{,}4030\ h^{-1}$ at temperatures from 277 K to 304 K and others are calculated. The activation energy from the temperature dependence of the rate constants (40,3 kJ/mol) evidences a diffusion-kinetic control of the gold dissolution.

Electron microscopy (using electron probe scanning on an energy dispersive spectrometer) of native gold particles revealed foreign inclusions - adsorbed mineral particles of calcite ($CaCO_3$) and, presumably, a surface film consisting of aluminum oxide (Al_2O_3), which create a significant obstacle to the contact of leaching agents with the surface of the target gold grains.

Quantitative data on the composition of surface adsorption films, formed by model gold electrode dissolution products, are obtained using atomic adsorption spectroscopy.

Introduction

Cyanidation is still the dominant process for dissolving gold in the mining industry. Despite its high efficiency for gold leaching, it suffers from some major drawbacks including high toxicity and low dissolution rate [1]. The large-scale application of the cyanide solutions poses environmental problems in large areas. Therefore, new alternative solvents for gold are searched for, such as thiourea [2], thiosulfates, polysulfides, halide-derivatives and hypochlorites [1], etc. Leaching of metallic gold is based on a voltage-dependent redox reaction, in which gold acts as an electron donor (anode), and chlorine, which is part of sodium hypochlorite, is an electron acceptor (cathode). The activity of the leaching process depends on many factors, however, the *pH* of the medium and the solvent are of fundamental importance, which ensures the proper strength of electrolytes and the electrical conductivity of solutions, as well as allows you to control the direction of the chemical reaction and the yield of final products [3]. A thorough study of the mechanism and kinetics

of the process of interaction of the surface of metallic gold with sodium hypochlorite NaOCl solutions at different *pH* values of the medium and in different solvents is of fundamental importance for the industrial use of hypochlorite technology as an alternative to the cyanide process.

Experimental

In a series of experiments to study the kinetics of the leaching process of a model gold electrode, gold plate (99,999%) with a size of 15 by 10 by 1 mm were used, and they were rotated at a speed of 80 rpm; reproducible hydrodynamic conditions of intensified reactant supply to the dissolving gold surface were thus set up. Working hypochlorite solutions were prepared by diluting a standard solution (containing 18,4% of NaOCl and 14,1% of NaCl) with twice-distilled water. The studies were carried out in a hermetically sealed thermostatically controlled (to an accuracy of ±0,5°C) electrolytic cell. For each experiment, fresh chloride-hypochlorite solution of present composition and pH was taken. The dissolution kinetic curves were plotted from the data on the amount of gold passed into the solution for a specified time interval. The amount of dissolved gold was determined by gravimetric or atomic-adsorption method. The surface films constituted by the gold oxidation products (AuCl, AuOH, $AuCl(OH)^-$)≈200 μm thick were studied with the use of a JAMP-10S Auger electron-spectrometer (JEOL, Japan). The studied solution in the cell has a volume of 40 cm^3.

The second series of experiments was devoted to the study of the processes of leaching by sodium hypochlorite of native gold obtained by gravitational sedimentation on industrial dredges at one of the polymetallic deposits in Ghana (Africa, the mount of the Volta River). Native gold is rounded grains of irregular shape with a size from 5 to 2500 microns, on the surface of which fine particles of accompanying minerals are adsorbed – quartz (SiO_2), calcium carbonate ($CaCO_3$), aluminum oxide (Al_2O_3) and others. It is assumed that alumina is located on the surface of gold grains not in the form of separate conglomerates, but in the form of a carbon-aluminosilicate film tightly adsorbed ("intergrown") with the gold surface, which creates a serious technological problem in gold leaching. The chemical composition of the surface layer of native gold are shown in table 1.

Table 1

Chemical composition of the surface layer of native gold from a polymetallic deposit (Ghana, equatorial Africa, the mouth of the Victoria River)*

Element	Sample 1		Sample 2		Average values	
	mass %	atomic%	mass %	atomic%	mass %	atomic%
C	7,62	37,38	7,16	32,59	7,39	35,6
O	9,46	34,86	11,23	38,41	10,34	37,0
Al	0,54	1,18	0,47	0,95	0,505	1,1
Ca	1,65	2,42	0,93	1,27	1,29	1,9
Si	-	-	2,69	5,24	1,345	1,4
Au	80,73	24,16	77,53	21,54	79,13	23,0
c	100,00	100,00	100,00	100,00	100,00	100,00

*- elemental composition according to computer analysis data INCA Energy SEM "Oxford Instruments"

Result and discussion

In Fig. 1 we give a dependence of the rate of the redox leaching of the rotating model gold plate in hypochlorite solutions (6,0% NaCl, n*M* HCl) on the *pH* of the solution at 298 *K*. The results are shown after contact of the plate with the leach solution for 5 min. When diluting the solution, the chloride ion concentration was decreased to 4,71% (47,1 g/dm^3); the *pH* value was controlled by adding HCl. According to the graph, the rate of redox leaching of gold (v_{Au}) in chloride-hypochlorite solutions has a non-linear dependence on the *pH* of the medium. At extremely low *pH* (pH -1,8), gold undergo leaching at a rate of 600 $g \cdot m^{-2} \cdot h^{-1}$. This indicator is almost two times inferior to the rate of dissolution of gold in aqua regia, which is 1320 $g \cdot m^{-2} \cdot h^{-1}$ at room temperature [4].

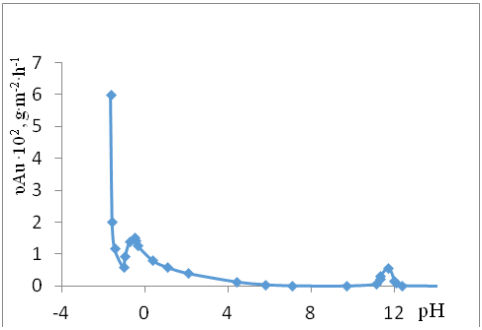

Fig.1. The solution pH dependence of gold leaching rate v_{Au} in sodium hypochlorite (6,0% NaCl, nM HCl) at 298 *K*

With an increase in *pH*, the dissolution rate drops down abruptly to a sharp minimum ($\approx 60\ g \cdot m^{-2} \cdot h^{-1}$ at pH -1,0). Further, it equally abruptly grows up, coming to 154 $g \cdot m^{-2} \cdot h^{-1}$ at *pH* - 0,2. With a further increase in *pH*, the dissolution rate gradually drops down to a flat minimum (110 to 120 $g \cdot m^{-2} \cdot h^{-1}$) in a *pH* range from 9 to 12. In a range of *pH* 12,5-14,5 the dissolution rate v_{Au} again passes a maximum: 5,6 $g \cdot m^{-2} \cdot h^{-1}$ at *pH* 13,5.

The initial sharply descending segment of the graph in Fig. 1 (in a *pH* range from -1,8 to -1,0) is of no interest for practical workers because of too high concentration of hydrochloric acid and, hence, the corrosivity of the solution approaching aqua regia in its acting components and their properties. The next sharply ascending segment is of equally low interest, because the range of dissolution rates demonstrated here is covered backward in the successive descending segment, where the acid concentration appears appropriate.

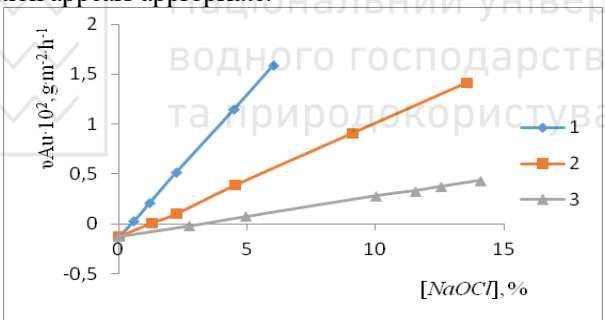

Fig. 2. Dependence of gold leaching rate v_{Au} in hypochlorite solutions on the hypochlorite concentration [NaJCl] at 298 K. The solution pH: (*1*) 1,06, (*2*) 4,15 and (*3*) 6,65

The effect of hypochlorite-concentration on the gold leaching rate at different *pH* is shown in Fig. 2. The dependence is visualized as a bunch of straight lines with a common *Y*-intercept below the origin and can be described by a general equation

$$v_{Au} = -0{,}12 + tg\alpha \cdot [\mathrm{NaOCl}],\ g \cdot m^{-2} \cdot h^{-1}, \qquad (1)$$

where tgα - the tangent of the slope of the curve in Fig. 2; [NaJCl] - concentration of sodium hypochlorite in solution (%); "-0,12" - the point of intersection of the ordinate (*Y*) by the curves of the graph at zero concentration of NaCl.

The slope of the curves at different *pH* values of solutions characterizes the change in the rate of gold leaching v_{Au}. The tgαat *pH* of 1,06, 4,15, and 6,65 equals 0,267, 0,107, and 0,025, respectively, that is, decreases by more than order of magnitude. The given data indicate that in a solution containing 6% of sodium hypochlorite and 4,71% of sodium chloride, with a decrease in pH from 6,65 to 1,06, the gold leaching rate v_{Au} increases by a factor of 26,7.

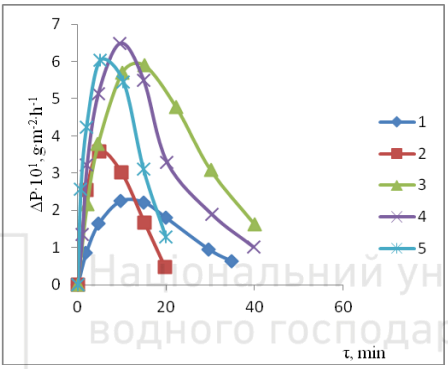

Fig. 3. Kinetic curves of the gold leaching rate in chloride-hypochlorite solutions (6,0% NaOCl, 0,1 *M* NCl, *pH* 1,06 -1,12) at different temperatures (*K*): (*1*) 289, (*2*) 297, (3) 304, (*4*) 313, and (*5*) 333

Shown in Fig. 3 data are kinetic dissolution curves (ΔP-τ_i) for a gold electrode (plate) with surface area *S*=1,0 cm^2 at temperatures 277, 289, 304, and 333 *K*. It's obvious that the kinetic curves are composite functions of time. For example, at 277 and 289 *K*, the sample mass losses ΔP-τ_i during the initial period abruptly increase, reaching their maxima (ΔP_{max}) of 22,5 and 58,5 $g \cdot m^{-2}$, respectively, after a lapse of τ_i=15 min. At temperature of 304, 313, or 333 *K*, the ΔP_{max} values: 65, 60,5, and 36 $g \cdot m^{-2}$ were reached for 10, 6, and 5 min, respectively. Figure 3 shows that the sample mass loss decreased significantly (down to ΔP=5 to $16\, g \cdot m^{-2}$), due to the gold passivation.

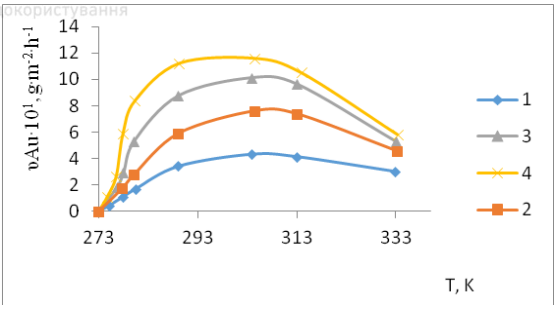

Fig. 4. Dependence of gold dissolution rate in hypochlorite solutions (6,0% NaOCl, 0,1 *M* HCl, *pH* 1,06 -1,12) on the temperature and the gold exposure time (τ, min): (*1*) 5, (2) 10, (3) 15, (4) 20

Shown in Fig. 4 data are temperature dependence of the gold leaching rate in 6,0% NaOCl, 0,1 *M* HCl (4,06% of NaCl) solution with *pH* 1,06-1,12. We see that the "v_{Au}-T" curves pass a maximum; the decay of v_{Au} is more strongly pronounced at higher temperatures. In the initial segment of the dissolution curves, at $\tau_i < \tau_{max}$, that is, before the passivation, the gold ion concentration C_{max} can be described by the equation

$$C = C_{max}(1 - e^{-k\tau}), \qquad (2)$$

which corresponds to the first-order kinetic equation [1]. Therefore, in determining the rate constants $k_i$of the gold leaching, we used the initial period, i.e., until the concentration changed at the electrode surface.

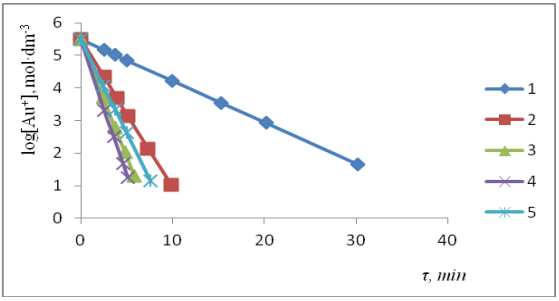

Fig. 5. Dependence of the logarithm of concentration of gold (I) ions formed during the gold leaching in chloride-hypochlorite solutions (5.3% NaClO, 0.1 M HCl, pH 1.06-1.12) on the gold exposure time at different temperatures (K): (1) 277, (2) 289, (3) 304, (4) 313, and (5) 333

All experimental curves taken during the initial period of gold dissolution in the studied chloride-hypochlorite solutions clearly can be linearized in an a "log[Au]=$f(\tau_i)$" (Fig. 5), which corresponds to the equation (2).

The rate constants $k_i$were calculated from the slopes of the initial segments of the lines; they equal 0,0790, 0,2695, and 0,4030 $h^{-1}$for temperatures 277, 298, and 304 *K*, respectively. The temperature dependence of the rate constants "$\log k_i = f\left(\frac{1}{T}\right)$"", calculated in a temperature range from 277 to 304 *K*, as well as the apparent activation energy E_a=40,3 kJ/mol, evidences a diffusion-kinetic control of the gold leaching. From the slopes of the "log[Au]=$f(\tau_i)$" we calculated the rate constants. For temperature of 313 and 333 *K*, they equal 0,2510 and 0,3293 h^{-1}, respectively. The values are lower than those found at temperatures of 289 and 304 *K*.

The results of our research indicate that the maximum gold leaching rate is achieved at 304 *K*, with a further increase in temperature, up to 313 and 333 *K*, it decreases. Such a run of the kinetic curves cannot be ascribed to a loss of the chloride-hypochlorite solution reactivity. I each experiment, fresh chemicals were used. Special experiment showed that at pH -1,8, -1,0, -0,5, 0,0, and 1,0, the molecular chlorine losses according to equations came to 3,1, 2,6, 1,7, 0,6, and 0,01 vol.%, respectively (for τ_{max}=40 min). The gold leaching efficiency (calculated by the hypochlorite consumed) was 96-99% over the entire *pH* range studied (from -1,8 to 1,0).

$$\mathrm{Na}\overset{+1}{\mathrm{O}}\mathrm{Cl} + \mathrm{Cl}^- + \mathrm{H}^+ \xleftrightarrow{\pm e^-} \overset{0}{\mathrm{Cl}_2}\uparrow + \mathrm{OH}^- + \mathrm{Na}^+, \qquad (3)$$

$$\mathrm{H}\overset{+1}{\mathrm{O}}\mathrm{Cl} + \mathrm{Cl}^- + \mathrm{H}^+ \xleftrightarrow{\pm e^-} \overset{0}{Cl_2}\uparrow + \mathrm{H_2O}, \qquad (4)$$

When studying the processes of leaching native gold with sodium hypochlorite NaOCl, a mixture of reagents was used, which, in terms of their physicochemical properties, can simultaneously function as both oxidizing agents and reducing agents.

Depending on the pH of the medium, the type of solvent and the strength of the electrolyte, the direction of the voltage-dependent redox reaction can change and the final products from the same initial components can be completely different [3]. Therefore, for the processing of native gold, methodological techniques were used that

fundamentally differed from the technology of leaching a model gold disk, consisting of exclusively pure gold (99.999%). Taking into account the fact that on the surface of native gold, we also discovered other chemical elements (except for gold), the nature of the interaction of which with the gold surface is rather complicated and ambiguous, therefore, the method of leaching the target element was modified. For this, the technological process was divided into three stages:

Stage 1: mechanical activation of the gold surface (complex chemical and mechanical destruction of the surface carbon-aluminosilicate film) using sodium hypochlorite solution with an extremely alkaline *pH* value (*pH*>12,0).

Stage 2: leaching of the target element with sodium hypochlorite dissolved in glacial acetic acid CH_3COOH (*pH*=6,8-7,0), with the addition of hydrogen peroxide (H_2O_2).

Stage 3: reduction of the target element to the metallic state by acidifying the leaching solution to *pH*<2,0 (growing hexagonal lamellar gold crystals).

At the first stage - complex mechanical activation, reactions occur that free the gold surface from the oxide film:

$$Al_2O_3 + 2\,NaOH = 2\,NaAlO_2 + H_2O, \quad (5)$$

$$NaAlO_2 + 2\,H_2O = Al(OH)_3 + NaOH; pH > 7,0. \quad (6)$$

In this case, water-soluble complex salts are formed - sodium aluminate and aluminum hydroxide hydrolysable in an aqueous medium.

At the second stage, in fact, the leaching of metallic gold occurs, which is a reducing agent for the chlorine ion ($-\overset{+1}{Cl}-$), which is part of hypochlorite, (i.e., gold is an electron donor (anode), and an electron acceptor is a chlorine ion (cathode) included in composition of sodium hypochlorite):

$$\overset{0}{Au} + NaOH + 1\frac{1}{2}\,NaO\overset{+1}{Cl} \xrightarrow{-3e^-} Na[\overset{+3}{Au}O_2] + 1\frac{1}{2}\,Na\overset{-1}{Cl} + \frac{1}{2}\,H_2O. \quad (7)$$

In this case, sodium aurate is formed - a complex oxide of sodium and gold (crystalline hydrate), easily soluble in water.

At the third stage, gold is restored from salt - sodium aurat $Na[\overset{+3}{Au}O_2]$; hydrogen peroxide (H_2O_3) is used as a reducing agent in the presence of dehydrated organic acid (CH_3COOH)

$$Na[\overset{+3}{Au}O_2] + 1\frac{1}{2}H_2\overset{-1}{O}_2 + CH_3COOH \xrightarrow{+3e^-} \overset{0}{Au}\downarrow + CH_3COONa + 1\frac{1}{2}\overset{0}{O}_2\uparrow + 2H_2O. \quad (8)$$

In this reaction, the electron donor is oxygen ($-\overset{-1}{O}$) (anode), which is part of hydrogen peroxide, and the electron acceptor is the gold atom ($[=\overset{+3}{Au}-]$) (cathode), which is part of sodium aurate. The fundamental condition for an effective one-sided transition of the reaction (irreversibility of the reaction) is a moderately acidic *pH* value (~2,0), the presence of a "weak" organic acid, which ensures the irreversibility of the reaction, as well as the unhindered removal of oxygen outside the reaction medium. In this case, in a reaction vessel (quartz, heat-resistant glass), after cooling the medium to room temperature for 16-18 hours, triangular shapes, plate-like up to 163×163 μm in size (Fig. 8). The latter are easily separated from gold crystals by washing the precipitate with warm distilled water.

It is quite remarkable that the active growth of crystals of reduced metallic gold under these conditions does not depend on the presence of biopolymer or other gel-forming matrices, which are traditionally used in the growth of gold crystals [7, 8].

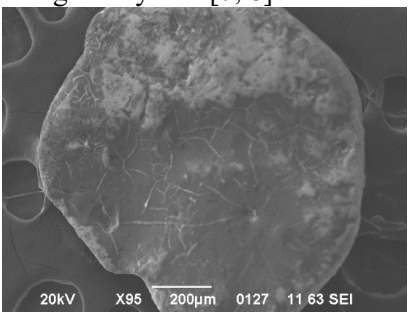

Fig. 6. Electron micrograph of native gold grain 1,35 by 1,1 *mm* in size (scanning electron microscopy, magnification x95)

On the surface of native gold, accompanying elements were found - carbon (C), oxygen (O), silicon (Si), calcium (Ca), and aluminum (Al), the presence of which is due to adsorbed microdispersed or nanodispersed particles of calcite ($CaCO_3$), quartz

(SiO_2) and aluminum oxide (Al_2O_3). On the surface of the gold (in the lower part, on the right), a small "crater" is visible - the point of a short (3-4 minutes) exposure to the scanning beam of an electron microscope. At this point, a local overheating of the surface occurred (up to several hundred degrees), as a result of which a fairly stable carbon-aluminosilicate film began to collapse. In this case, the emerging cracks are clearly visible, diverging radially from the "crater". This phenomenon indicates the real presence of a protective oxide film, which complicates the leaching of native gold.

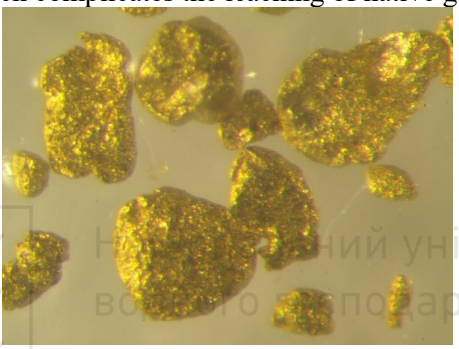

Fig. 7. Monomineral fraction of native goldfinches from an alluvial polymetallic deposit (Ghana, equatorial Africa). Dimensions of gold coins from 0,1×0,2 mm to 1,5×2,0 mm (stereomicroscopy, magnification x56)

On native gold grains, even when using a light microscope, it is not possible to detect a protective oxide film - it is quite thin and does not differ in color from the matrix.

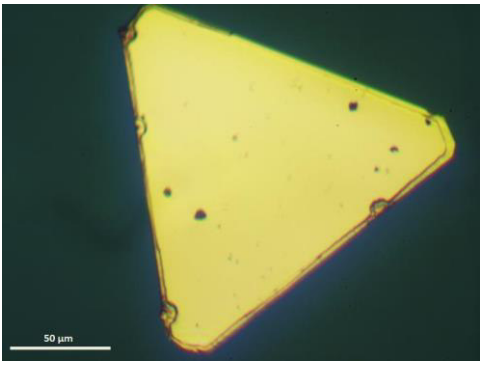

Fig. 8. The characteristic triangular shape of a crystal of metallic gold grown from a solution of gold grains, shown in Fig. 7, underwent a processing cycle according to reactions (5), (6),

(7), and (8). Crystal shape and size of extremely correct symmetry (163×163×163 microns). Polarizing microscopy (magnification x320) "Karl Zeiss", Jena

Conclusions

Working on this problem - the development of a hypochlorite method of gold leaching, the authors of this article saw for themselves - how important it is for scientists to work with safe, non-toxic, environmentally friendly reagents.

Work on this topic began in the 90s of the twentieth century. And thanks to our predecessors, our older colleagues, most of whom are no longer near the banner, we were able to complete this development, the results of which would be satisfied by our older friends.

Over time, this development will be improved by our successors - however, what we have managed to do, allows us to say that it is not in vain that we went to science and not in vain learned something.

References

1. **Kozin L.F.** Kinetics and mechanism of the gold corrosion dissolution in hypochlorite solutions / **L.F. Kozin, V.A. Prokopenko, A.K. Bogdanova** // Protection of Metals. - 2005. - V.41, N1. - P.22-29. Translated from Zashchita Metallov (Russia). - 2005. - V.41, N1. - P.26-33.

2. **Habashi F.** Kinetics and mechanism of gold and silver dissolution in cyanide solution / Bureau of Mines and Geology. State of Montana / Bulletin 59. - 1967. - 42 p.

3. Solvent as a means of controlling the chemical process / **Yu.Ya. Fialkov**. - Leningrad: Chemistry, 1990. - 240 p.

4. **Salimi H.** Gold leaching in organic solvents: simple and mild reaction conditions for fast gold dissolution / COM 2015. The conference of metallurgists // America's conference on aluminum alloys. - 2015. (Published by the Canadian Institute of Mining, Metallurgy and Petroleum / www.metsoc.org).

5. **Crundwell F.K.** A mathematical model of the leaching of gold in cyanide solutions / **F.K. Crundwell, S.A. Godorr** // Hydrometallurgy. - 1997. - V.44. - P.147-162.

6. **Jeffrey M.I.** A kinetic study that compares the leaching of gold in the cyanide, thiosulfate and chloride systems / **M.I. Jeffrey, P.L. Breuer, W.L. Choo** // Metallurgical and Materials Transactions. - 2001. - B. - 32B. - P.979 - 986.

7. **Kratochvil P.** Growth of gold single crystals in gels / **P. Kratochvil, B. Sprusil** // J. Crystal Growth. - 1968. - V.3, 4. - P. 360-362.

8. **Estrela-Llopis V.R.** Extracellular mineralization and synthesis of microcrystallites of gold and platinum in aqueous solutions of polysaccharides / **V.R. Estrela-Llopis, T.I. Borodinova, I.N. Yurkova** in the book: Colloidal-

chemical foundations of nanoscience / **Shpak A.P., Z.R**. Ullberg (ed.). - Kiev: Akademperiodika, 2005 . - P. 271-297

9. **Chernenko V.Yu.** Thermodynamic basis of environmentally-friendly technology of dissolution of carbonic polyminerals by biogenic agents / **V.Yu. Chernenko, I.M. Astrelin I.M.** // Research bulletin of the National Technical University of Ukraine “Kyiv Polytechnic Institute”. - 2010. - №5 (73). - P. 145-152.

Scientific edition

ENERGY- AND RESOURCE-SAVING TECHNOLOGIES OF DEVELOPING THE RAW-MATERIAL BASE OF MINING REGIONS

Multi-authored monograph

First publication

Co-editor **Zinovii MALANCHUK,**
Doctor of Sciences (Engineering), Professor, Director Institute of Postgraduate Education, National University of Water and Environmental Engineering, Ukraine.

Co-editor . **Maria LAZAR** - Professor, Ph.D., Research Vice-Rector University of Petroșani, Romania.

Deputy editor **Serhii CHUKHAREV,**
PhD (Engineering), Associate Professor.

Technical editor **Elena SAMOILUK**

Signed to print 29.03.21. Format A5.
30 conventional printed sheets.
The printing run is 300 copies.

UNIVERSITAS Publishing, Petroșani,
University of Petroșani Str. Universității nr. 20, 332006,
Petroșani, jud. Hunedoara, Romania